JOURNAL OF THE MECHANICS AND PHYSICS OF SOLIDS

EDITORIAL ADVISORY BOARD

J. F. BAKER—Cambridge W. M. BALDWIN—Cleveland
E. BRANDENBERGER—Zürich G. BUSCH—Zürich
A. H. COTTRELL—Birmingham C. CRUSSARD—Paris M. J. DRUYVESTEYN—Delft
A. KOCHENDÖRFER—Düsseldorf N. F. MOTT—Bristol A. NADAI—Pittsburgh, Pa.
G. SACHS—Syracuse, N.Y. E. SIEBEL—Stuttgart H. W. SWIFT—Sheffield

1.
/54

EDITOR-IN-CHIEF

R. HILL
University of Nottingham

Volume 2
1953 — 54

PERGAMON PRESS LTD · LONDON

Vol
2
1953

Contents of Volume 2

Number 1

	Page
H. G. Hopkins and W. Prager: The load carrying capacities of circular plates	1
D. S. Dugdale: Wedge indentation experiments with cold-worked metals	14
B. Crossland and R. Hill: On the plastic behaviour of thick tubes under combined torsion and internal pressure	27
J. F. W. Bishop: Calculations on sheet-drawing under back tension through a rough wedge-shaped die	39
J. F. W. Bishop: On the complete solution to problems of deformation of a plastic-rigid material	43
J. G. Davidson: Buckling of struts under dynamic loading	54
D. G. B. Thomas: Corrigenda: The autofrettage of thick tubes with free ends	67
Book reviews	69

Vol. 2 53/54

Number 2

A. P. Green: On the use of hodographs in problems of plane plastic strain	73
J. Grunzweig, I. M. Longman and N. J. Petch: Calculations and measurements in wedge-indentation	81
R. Hill: The plastic torsion of anisotropic bars	87
P. S. Symonds and C. F. A. Leth: Impact of finite beams of ductile metal	92
R. E. D. Bishop and J. N. Goodier: On eulerian co-ordinates in elastic wave propagation	103
R. Hill: Inoue's hydrodynamical analogy for the state of stress in a plastic solid	110
M. R. Horne: Shells with zero bending stresses	117
H. Fessler and R. T. Rose: On the stress distribution in the walls of pressure vessels	127
Book reviews	137
Notice of meetings	140

Number 3

K. R. Peattie and R. W. Sparrow: The fundamental action of earth pressure cells	141
F. A. Gaydon and A. W. McCrum: A theoretical investigation of the yield point loading of a square plate with a central circular hole	156
F. A. Gaydon: On the yield-point loading of a square plate with concentric circular hole	170

NUMBER 3 (*Cont.*)

Page

P. H. MORTON, R. TREON and W. M. BALDWIN, JR.: Low temperature embrittlement mechanics deduced from zinc single crystal fracture studies.. 176

A. P. GREEN: The plastic yielding of metal junctions due to combined shear and pressure 197

Book reviews 212

NUMBER 4

D. G. CHRISTOPHERSON and G. R. HIGGINSON: The strength of short cylinders under internal pressure 217

Y. G. ATTIA, D. FITZGEORGE and J. A. POPE: An experimental investigation of residual stresses in hollow cylinders due to the creep produced by thermal stresses 238

D. A. BARLOW: Yield criteria and the bending of wide beams 259

D. S. DUGDALE: Cone indentation experiments 265

R. HILL: On the limits set by plastic yielding to the intensity of singularities of stress 278

J. W. CRAGGS: Wave motion in plastic-elastic strings 286

A. P. GREEN: Hodographs in problems if plane plastic stress 296

Vol
2
1953

Author Index

(B) denotes a book review

ATTIA, Y. G. p. 238.
BALDWIN, W. M., JR. pp. 138 (B), 176.
BARLOW, D. A. p. 259.
BISHOP, J. F. W. pp. 39, 43, 137 (B).
BISHOP, R. E. D. p. 103.
CHRISTOPHERSON, D. G. p. 217.
CRAGGS, J. W. p. 286.
CROSSLAND, B. p. 27.
DAVIDSON, J. G. p. 54.
DUGDALE, D. S. pp. 14, 265.
FESSLER, H. p. 127.
FITZGEORGE, D. p. 238.
FLINT, A. R. p. 71 (B).
FOX, L. p. 216 (B).
GAYDON, F. A. pp. 156, 170.
GOODIER, J. N. p. 103.
GREEN, A. P. pp 73, 197, 296
GREENOUGH, G. B. p. 69 (B).
GRUNZWEIG, J. p. 81.
HIGGINSON, G. R. p. 217.
HILL, R. pp. 27, 72 (B), 87, 110, 138 (B). 213 (B), 214 (B), 278
HORNE, M. R. pp. 117
HOPKINS, H. G. p. 1.
LETH, C. F. A. p. 92.
LONGMAN, I. M. p. 81.
MCCRUM, A. W. p. 156.
MORRISON, J. L. M. p. 139 (B).
MORTON, P. H. p. 176.
PEATTIE, K. R. p. 141.
PETCH, N. J. p. 81.
POPE, J. A. p. 238.
PRAGER, W. p. 1.
RAYNOR, G. V. p. 212 (B).
ROSE, R. T. p. 127.
SPARROW, R. W. p. 141.
STANDLEY, K J. p. 213 (B).
SYMONDS, P. S. p. 92.
THOMAS, D. G. B. p. 67.
TREON, R. p. 176.
WISTREICH, J. G. pp. 70 (B), 215 (B).

Journal of the Mechanics and Physics of Solids, 1953, Vol. 2, pp. 1 to 18. Pergamon Press Ltd., London.

THE LOAD CARRYING CAPACITIES OF CIRCULAR PLATES

By H. G. Hopkins and W. Prager
Graduate Division of Applied Mathematics, Brown University

(*Received 25th June*, 1953)

Summary

This paper is concerned with the load carrying capacities of circular plates made of a perfectly plastic material that obeys the yield condition of Tresca and the associated flow rule. Various conditions of rotationally symmetric loading and support are discussed.

Vol. 2 53/54

1. Introduction

The concept of limit analysis was introduced by structural engineers in connection with problems concerning beams and frames (see, for instance, Kist 1920; Van den Broek 1948; Baker 1949). Only recently has the general theory of limit analysis been developed (Hill 1951; Drucker, Prager and Greenberg 1952; Prager 1952) as a chapter of the mathematical theory of perfectly plastic solids. This development has led not only to new methods for the limit analysis of beams and frames (see, for instance, Symonds and Neal 1951) but also to the application of limit analysis to other fields (Heyman 1951; Weiss, Prager and Hodge 1952; Onat and Prager 1953; Pell and Prager 1951).

As Hill (1951) has pointed out, the principles of limit analysis are most conveniently formulated for a perfectly plastic material that is rigid whenever the stress is below the yield limit. Fig. 1 shows the relation between the bending moment M and the curvature κ of a beam made of such a plastic-rigid material: the beam bends only where the absolute value of the bending moment equals the "limit moment" M_0 (> 0); wherever $|M| < M_0$, the beam remains straight. As a rule, the limit moment is reached only at isolated cross sections, and bending is therefore concentrated at these "yield hinges." Since the beam segments between yield hinges must remain straight, deformation of a statically indeterminate beam becomes possible only when yield hinges have formed in a number sufficient to transform the beam into a mechanism. The "flow limit" at which the plastic-rigid beam begins to deform is therefore distinct from the "elastic limit" at which the limit moment is first reached at some cross section.

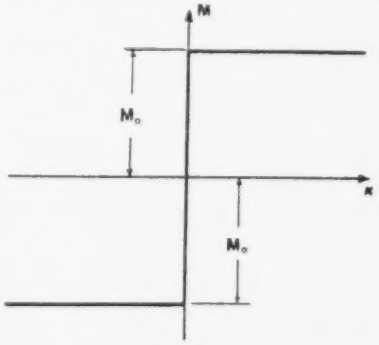

Fig. 1.

The general problem of limit analysis is the determination of the flow limit for a given structure under given types of loading; the load intensity at the flow limit is called the "load carrying capacity" of the structure. This paper is concerned with the determination of the load carrying capacity of thin circular plates made of a plastic-rigid material that obeys TRESCA's yield condition and the associated flow rule. The discussion is restricted to rotationally symmetric types of loading and edge support: both simply supported and built-in plates are considered, and the load is supposed to be uniformly distributed over either a central circular region or an annular region that extends up to the edge. For conciseness, the detailed analysis is presented only in certain typical cases, and otherwise only the final results are given.

The problems studied in this paper are, of course, only particular cases of the general problem of determining the load carrying capacity of a plate of arbitrary shape under an arbitrary type of loading. However, it is felt that from the study of such particular cases experience can be gained that will suggest ways of attacking the general problem.

2. Equation of Equilibrium. Yield Condition and Flow Rule

Let r, ϕ, z be cylindrical coordinates, the z axis being vertical and pointing downwards, and let the considered plate be bounded by the planes $z = \pm h$ and the cylinder $r = R$. In this Section, the intensity p of the distributed transverse load is assumed to be an arbitrary function of r only; the specialization to piecewise continuous loads p will be made later. The plate is either simply supported or built-in along its entire edge.

On account of the rotational symmetry of loading and support, the shearing stresses $\tau_{r\phi}$ and $\tau_{\phi z}$ vanish indentically. Furthermore, if the plate thickness $2h$ is small compared to the radius R, then, on the whole, the vertical stress σ_z and the shearing stress τ_{rz} may be regarded as small when compared to the bending stresses σ_r and σ_ϕ. The state of stress at a generic point of the plate therefore is essentially two-dimensional, and σ_r and σ_ϕ are the relevant principal stresses. These stresses give rise to the principal bending moments

$$M_r = \int_{-h}^{h} \sigma_r \, dzz, \qquad M_\phi = \int_{-h}^{h} \sigma_\phi \, zdz, \tag{1}$$

and the shearing stress τ_{rz} gives rise to the shear force

$$Q_r = \int_{-h}^{h} \tau_{rz} \, dz. \tag{2}$$

The twisting moment $M_{r\phi}$ and the shear force Q_ϕ resulting from the stresses $\tau_{r\phi}$ and $\tau_{\phi z}$, respectively, vanish indentically on account of the rotational symmetry. Note that the choice of the positive z direction and the usual sign conventions for stresses lead to the following sign conventions for the moments (1) and the shear force (2): the bending moments are positive if they produce tension in the bottom layer of the plate; the shear force transmitted across a cylinder $r = \text{const.}$, from the side of larger values of r to the side of smaller r values, is positive if it is directed downwards.

The reader should note that, inasmuch as the analysis of this paper refers

only to the initiation of motion of the plate, bending action always predominates over membrane action. Shearing deformation of the plate is completely neglected. Of course, if the ratio of plate thickness to plate radius is relatively small, then, in order for the plastic deformation once initiated to continue, presumably some increase in applied load would soon be required, this effect being due to membrane action. However, this problem is beyond our present scope.

The theory of thin plates is approximate in so far as the three-dimensional conditions of equilibrium for the local stresses are replaced by two-dimensional conditions of equilibrium for the stress resultants, i.e., the bending and twisting moments and the shear forces. For the case of rotational symmetry considered here, there are two such equations of equilibrium :

$$\frac{d}{dr}(rQ_r) + rp = 0, \tag{3}$$

$$\frac{d}{dr}(rM_r) - M_\phi - rQ_r = 0. \tag{4}$$

Except for the case of a concentrated load at the centre, which will be discussed later, the shear force Q_r must vanish for $r = 0$. Equation (3) therefore leads to

$$rQ_r = -\int_0^r r\,p\,dr, \tag{5}$$

and substitution of this expression into (4) yields

$$\frac{d}{dr}(rM_r) - M_\phi = -\int_0^r r\,p\,dr. \tag{6}$$

The equations of equilibrium are independent of the mechanical properties of the plate material. The perfectly plastic material considered in this paper is supposed to obey TRESCA's yield condition. For the case of plane stress, this yield condition is indicated in Fig. 2 : combinations of the principal stresses σ_r and σ_ϕ that produce plastic flow are represented by points on the hexagon ABCDEF. The points F and B, for instance, correspond to uniaxial tension in the radial or circumferential direction, respectively, the yield stress in uniaxial tension being $\sigma_0\,(> 0)$. All points on the yield hexagon in Fig. 2 represent states of stress for which the maximum shearing stress has the constant value $\sigma_0/2$.

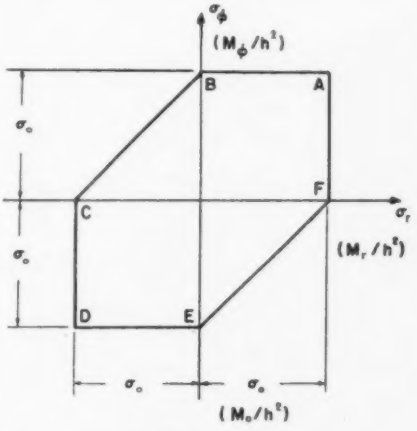

Fig. 2.

It will be convenient to speak of the set of plastic states represented by interior points of the segment AB as the plastic regime AB, and so on ; similarly, the plastic state represented by the vertex A of the yield hexagon will be called the plastic regime A, and so on.

The flow rule associated with a yield condition is concerned with the ratios between the principal strain-rates e_r, e_ϕ, e_z. For states of stress represented by points other than the vertices of the hexagon, the flow rule associated with TRESCA's yield condition predicts that the flow mechanism is pure shear (see, for instance, PRAGER 1952). In particular,

$$e_\phi \geqslant 0,\ e_r : e_\phi : e_z = \begin{cases} 0 : 1 : -1 \text{ for regime AB,} & (7) \\ -1 : 1 : 0 \text{ for regime BC.} & (8) \end{cases}$$

At the vertices of the hexagon, the flow rule admits any linear combination (with positive coefficients) of the flow mechanisms corresponding to the adjacent sides of the hexagon. Thus, with $0 \leqslant \lambda \leqslant 1$,

$$e_\phi \geqslant 0,\ e_r : e_\phi : e_z = \begin{cases} (1-\lambda) : \lambda : -1 \text{ for regime A,} & (9) \\ -\lambda : 1 : -(1-\lambda) \text{ for regime B,} & (10) \\ -1 : (1-\lambda) : \lambda \text{ for regime C.} & (11) \end{cases}$$

If an element of the plastic-rigid plate is to bend, the yield condition must be fulfilled in each horizontal layer. If, moreover, the bending of the plate transforms the material normal of the initially plane middle surface into the normal of the bent middle surface, the ratio $e_r : e_\phi$ remains constant along each normal. Both conditions are satisfied if, along a given normal, the state of stress is represented by a fixed point of the yield hexagon for positive values of z and by the diametrically opposite point for negative values of z. This assumption involves a discontinuity of stress at the middle surface, but this is clearly permissible within the framework of the plastic-rigid theory. The principal bending moments resulting from this type of distribution of the stresses σ_r and σ_ϕ along a normal are

$$M_r = \sigma_r h^2, \qquad M_\phi = \sigma_\phi h^2, \tag{12}$$

where σ_r and σ_ϕ are now used to indicate constant values of these stresses for positive values of z. It follows from (12) that the hexagon in Fig. 2 also represents the yield condition for the bending moments of the plate, provided that the coordinate axes in Fig. 2 are relabelled M_r/h^2 and M_ϕ/h^2. In his work on the load carrying capacities of reinforced concrete plates JOHANSEN (1943) has used a yield condition that would be represented in Fig. 2 by the square with the diagonal AD. For a discussion of the relation of JOHANSEN's work to the general theory of limit design, the reader is referred to PRAGER (1952).

The flow rule for the plate (see PRAGER 1952) is concerned with the ratio between the principal rates of curvature

$$\kappa_r = -\frac{d^2 w}{dr^2}, \qquad \kappa_\phi = -\frac{1}{r}\frac{dw}{dr}, \tag{13}$$

where w denotes the rate of deflection (in the positive z direction). The values of $\kappa_r : \kappa_\phi$ corresponding to the sides and vertices of the yield hexagon are readily obtained from the strain-rate ratios (7) to (11). With

$$M_0 = \sigma_0 h^2, \tag{14}$$

the following relations are obtained for the plastic regimes relevant to the subsequent analysis ($0 \leqslant \lambda \leqslant 1$; $\kappa_\phi \geqslant 0$) :

$M_r = M_\phi = M_0$; $\kappa_r : \kappa_\phi = (1 - \lambda) : \lambda$ for regime A ; (15)

$0 < M_r < M_0$, $M_\phi = M_0$; $\kappa_r : \kappa_\phi = 0 : 1$ for regime AB ; (16)

$M_r = 0$, $M_\phi = M_0$; $\kappa_r : \kappa_\phi = -\lambda : 1$ for regime B ; (17)

$-M_0 < M_r < 0$, $M_\phi = M_0 + M_r$; $\kappa_r : \kappa_\phi = -1 : 1$ for regime BC ; (18)

$M_r = -M_0$, $M_\phi = 0$; $\kappa_r : \kappa_\phi = -1 : (1 - \lambda)$ for regime C. (19)

There is the possibility, however, that a part of the plate is not yielding though the remainder of the plate deforms plastically. Since elastic deformations are neglected in the present analysis, such a part of the plate must remain plane. In view of the rotational symmetry, such a part can therefore have, at most, a uniform vertical velocity.

3. Circles Separating Different Plastic Regimes — Hinge Circles

At first sight, Tresca's yield condition would not seem to hold out any hope for mathematical simplicity because of the necessity of distinguishing various regimes each of which is governed by a separate set of relations. For each of these regimes, however, very simple relations are obtained : for the regimes corresponding to the vertices of the hexagon M_r and M_ϕ are completely specified while there is some latitude regarding the ratio $\kappa_r : \kappa_\phi$; for the regimes corresponding to the sides, on the other hand, the ratio $\kappa_r : \kappa_\phi$ is completely specified while there is some latitude regarding M_r and M_ϕ. If the entire plate were in the same regime, the determination of the bending moments and the rates of deflection at the flow limit would not constitute a difficult problem. As a rule, however, the plate is divided into a central circular region and surrounding annular regions, and each of these regions is in a different regime. Accordingly, it is necessary to discuss the relations between the various mechanical quantities on the two sides of a circle separating two regimes. First, equilibrium requires M_r and Q_r to be continuous across such a circle, but M_ϕ may be discontinuous. Second, the cohesion of the plate requires w to be continuous across such a circle, but κ_r and κ_ϕ may be discontinuous.

A circle across which $\kappa_\phi = -(1/r)\ dw/dr$ and hence dw/dr is discontinuous is called a hinge circle. For the case of circular symmetry considered here, this concept of the hinge circle replaces the concept of the yield hinge familiar from the plastic analysis of beams and frames. A hinge circle may be considered as the limiting case of a very narrow annulus across which dw/dr varies rapidly though in a continuous manner. As the width of this annulus tends towards zero, the ratio $\kappa_r : \kappa_\phi$ in the annulus becomes infinite. Accordingly, the regime at a hinge circle must be one of the following : A, C, D, F, CD or FA. It follows that dw/dr must be continuous except, at most, at circles where $|M_r| = M_0$.

The mathematical problem may now be formulated. The intensity of the distributed transverse load $p = p(r)$ is prescribed to within an arbitrary constant factor f. It is required to determine the largest value of f for which functions $M_r(r)$, $M_\phi(r)$, and $w(r)$ can be found satisfying the following conditions throughout $0 \leqslant r \leqslant R$:

(1) M_r is continuous and has piecewise continuous first derivatives; M_ϕ is piecewise continuous; w is continuous and has piecewise continuous first and second derivatives;

(2) M_r and M_ϕ satisfy the equation of equilibrium (6) in which p must be replaced by fp; at the centre of the plate, $M_r = M_\phi$;

(3) the point M_r, M_ϕ lies inside or on the yield hexagon of Fig. 2; in the first case, dw/dr must vanish; in the second case, $\kappa_r : \kappa_\phi = r\,(d^2w/dr^2)/(dw/dr)$ must be related to the state of stress M_r, M_ϕ by the flow rule, equations (15)—(19);

(4) dw/dr can be discontinuous only where $|M_r| = M_0$;

(5) at a simply supported edge, $M_r = 0$ and $w = 0$; at a built-in edge, $w = 0$ and either $dw/dr = 0$ or $|M_r| = M_0$ (in which case the edge is a hinge circle).

According to the general theory of limit design (HILL 1951; PRAGER and HODGE 1951) the value of f determined in this manner represents the factor with which the given load must be multiplied to bring the plate to the flow limit.

4. SOLUTION OF SPECIFIC PROBLEMS

In this Section, four problems are discussed involving two types of loading (circular or annular) and two types of edge support (simply supported or built-in). The complete analysis is presented only for circular loading; for annular loading only the final results are given.

For the types of loading considered here, the plate cannot reach the flow limit without becoming plastic at the centre, and the bending moments $M_r = M_\phi$ at the centre will be positive. Thus, $M_r = M_\phi = M_0$ at the centre, and the plastic regime near the centre must be AF, A, or AB. It is easy to prove that the regime AF cannot apply if p is positive as it is assumed to be. Indeed, if the regime AF did apply, then $M_r = M_0$ and $M_\phi < M_0$; for positive p this is not compatible with the equation of equilibrium (6). Similarly, it can be shown that the regime A cannot apply if p is different from zero near the centre as it must be in the case of circular loading considered here. It follows that, near the centre, the plate with circular loading must be in the regime AB. According to the flow rule, equation (16), this means that $\kappa_r = -d^2w/dr^2$ vanishes indentically in this central region. The rate of deflection w in this region therefore corresponds to the transition from the plane plate to an obtuse cone.

As r increases, the point representing the state of stress in Fig. 2 moves from A towards B. This means that M_r decreases with increasing r. For a simply supported plate, $M_r = 0$ at the edge. The state of stress at the edge is therefore represented by the point B, and the entire plate is in the regime AB. For a built-in plate, on the other hand, the regime AB applies only up to a certain radius $\rho < R$. For $r > \rho$ the plate is in the regime BC. According to the flow rule, equation (18), the rates of curvature in this part of the plate satisfy the relation $\kappa_r + \kappa_\phi = 0$. In view of the definition (13) of the rates of curvature this means that

$$\frac{d^2w}{dr^2} + \frac{1}{r}\frac{dw}{dr} = 0. \qquad (20)$$

Since w must vanish for $r = R$, the differential equation (20) implies that the rate of deflection is proportional to $\log (R/r)$. Thus, dw/dr does not vanish at the built-in edge which must therefore be a hinge circle. Accordingly, $M_r = -M_0$ at the edge. The state of stress at the edge is therefore represented by the point C in Fig. 2.

(a) *Circular loading, simply supported edge.* Here $p(r) = p = \text{const.}$ for $0 \leqslant r < a$ and $p(r) = 0$ for $a < r \leqslant R$. Since the entire plate is in the regime AB, $M_\phi = M_0$. With this value of M_ϕ and with the initial condition that $M_r = M_0$ for $r = 0$, the equation of equilibrium for the load fp at the flow limit furnishes

$$M_r = \begin{cases} M_0 - \tfrac{1}{6} fpr^2 & \text{for } 0 \leqslant r \leqslant a, \quad (21) \\ M_0 - \tfrac{1}{2} fpa^2 + \tfrac{1}{3} fp \dfrac{a^3}{r} & \text{for } a \leqslant r \leqslant R. \quad (22) \end{cases}$$

Since $M_r = 0$ for $r = R$, equation (22) yields the load factor

$$f = \frac{6M_0 R}{pa^2 (3R - 2a)}. \quad (23)$$

The rate of deflection associated with the bending moments (21), (22) is

$$w = w_0 \left(1 - \frac{r}{R}\right) \quad (24)$$

where w_0 (> 0) denotes the rate of deflection at the centre of the plate. Since the plate material is inviscid, the rate of deflection is determined only to within the factor w_0.

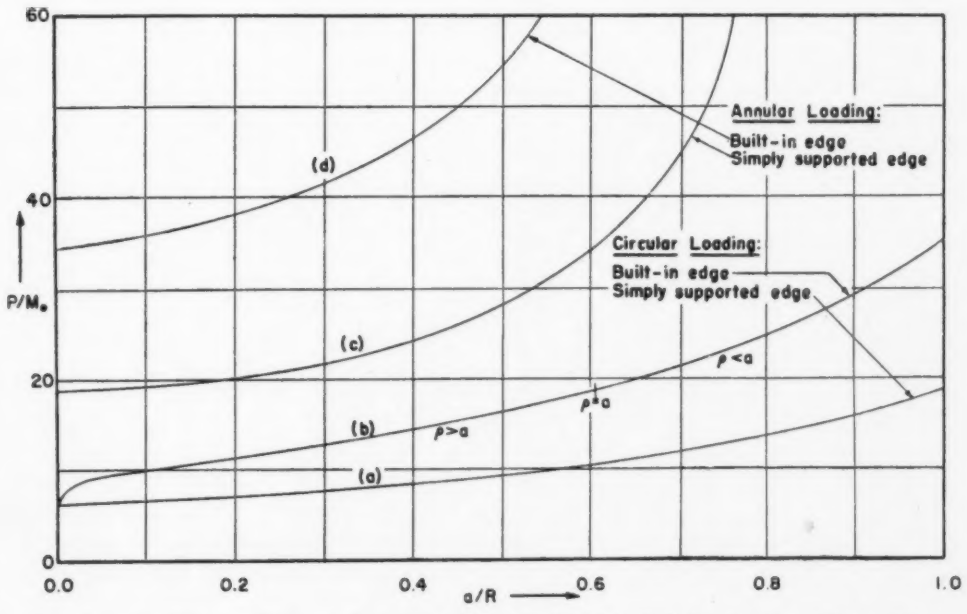

Fig. 3. Variation of total load P at flow limit with size of loaded circular or annular region.

Let $P = \pi f p a^2$ denote the total load at the flow limit. According to (23),

$$P = \frac{6\pi M_0}{3 - 2\,(a/R)}. \tag{25}$$

This variation of P with a/R is shown by curve (a) in Fig. 3. In particular,

$$P = 6\pi M_0 \tag{26}$$

for the uniformly loaded plate ($a = R$), and

$$P = 2\pi M_0 \tag{27}$$

for the plate subjected to a concentrated load at the centre. The results (25) to (27) are particularly interesting because they show that, for the considered types of loading, the dependence of the total load at the flow limit on the plate radius enters only through the ratio a/R.

This result is sufficiently startling to warrant the following discussion. Consider the case of a concentrated load P at the centre. The rate at which mechanical energy is dissipated in the plastic flow of regime AB is $M_0\,\kappa_\phi = (M_0/r)\,|dw/dr|$ per unit area of the plate's middle surface. The total rate of energy dissipation in the plate is therefore given by

$$\int_0^R \frac{M_0}{r}\,\frac{w_0}{R}\,2\pi r\,dr = 2\pi M_0\,w_0. \tag{28}$$

This rate of energy dissipation must equal the rate at which the load P does work on the velocity (24). When this rate of work, Pw_0, is set equal to the right-hand side of (28), the result (27) is obtained once more. A study of the left-hand side of (28) reveals how several factors combine to render the integral independent of the plate radius R. Equations (25) and (26) may be discussed in a similar manner.

It should be noted that the application of the present theory to the case of a concentrated load at the centre is not quite legitimate, because it has been assumed that the shearing stress τ_{rz} is small when compared to the bending stresses σ_r and σ_ϕ which, in the plastic portion of the plate, equal the yield stress σ_0 in absolute value. This assumption is justified if the load is distributed over a central circular area of a diameter which is large when compared to the plate thickness. Thus, (27) should be considered as a limiting case of (25), the radius a of the loaded area being much larger than the plate thickness, and the radius R of the plate being much larger than a.

(b) *Circular loading, built-in edge : case* $\rho < a$. As has been explained at the beginning of Section 4, in a built-in plate regime AB applies only up to a certain radius $\rho < R$. If $\rho < a$, (21) applies for $0 \leqslant r \leqslant \rho$. Since the state of stress for $r = \rho$ must be represented by the point B in Fig. 2, M_r as given by (21) must vanish for $r = \rho$. Thus,

$$\rho^2 = \frac{6M_0}{fp}. \tag{29}$$

For $r > \rho$ either regime B or regime BC must apply. It is readily shown that the equation of equilibrium rules out regime B. Accordingly, regime BC applies for $r > \rho$ and

$$M_\phi = M_0 + M_r \text{ for } \rho \leqslant r \leqslant R. \tag{30}$$

When this is substituted into the equation of equilibrium, there results a differential equation for M_r in which $p(r) = fp$ for $\rho \leqslant r < a$ and $p(r) = 0$ for $a < r \leqslant R$. This differential equation must be integrated with the initial condition that $M_r = 0$ for $r = \rho$. Thus,

$$M_r = \begin{cases} M_0 \log \frac{r}{\rho} - \frac{1}{4} fp\,(r^2 - \rho^2) & \text{for } \rho \leqslant r \leqslant a, \quad (31) \\ M_0 \log \frac{r}{\rho} - \frac{1}{2} fpa^2 \log \frac{r}{a} - \frac{1}{4} fp\,(a^2 - \rho^2) & \text{for } a \leqslant r \leqslant R. \quad (32) \end{cases}$$

It has already been shown that $M_r = -M_0$ at the built-in edge $r = R$. When fp is substituted from (29), (32) therefore yields the relation

$$1 + \log \frac{R}{\rho} = 3 \frac{a^2}{\rho^2} \log \frac{R}{a} + \tfrac{3}{2} \left(\frac{a^2}{\rho^2} - 1 \right). \quad (33)$$

Since R and a are known, (33) is a transcendental equation for ρ. In particular, $\rho = a$ if $a = R/\sqrt{e} \doteq 0{\cdot}606R$, and $\rho < a$, as has been assumed here, if $a > 0{\cdot}606R$. Once ρ has been found from (33), the load factor is determined from (29). The part of curve (b) in Fig. 3 that corresponds to $a/R > 0{\cdot}606$ shows the resulting relation between the total load $P = \pi fpa^2$ and a/R. Curve (a) of Fig. 4 shows ρ *v.* a/R according to (33).

Vol. 2 53/54

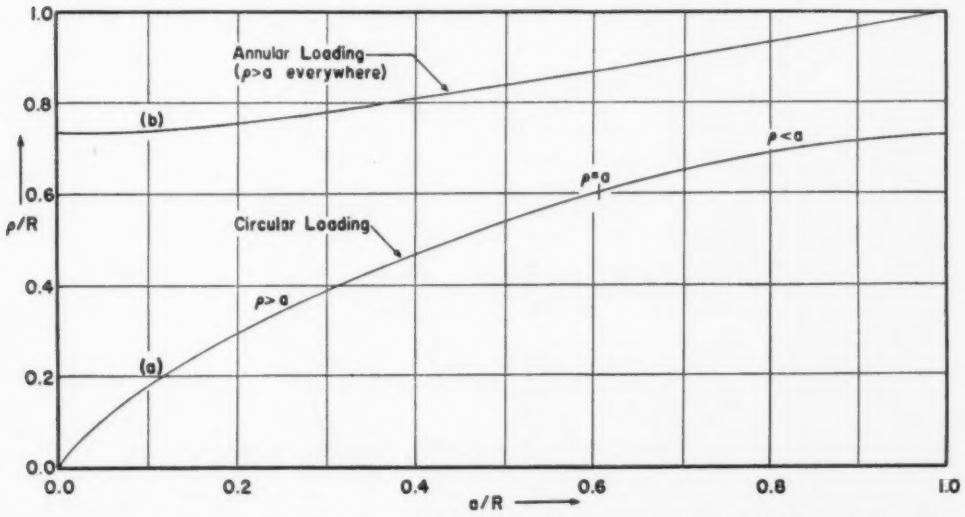

Fig. 4. Variation of position of boundary between plastic regimes AB and BC with size of loaded circular or annular region for built-in edge.

Before these results can be accepted, however, it must be shown that the bending moments (21), (31), (32) are associated with a velocity distribution $w(r)$ that fulfils the requirements established above: the function $w(r)$ satisfies $d^2w/dr^2 = 0$ for $0 < r < \rho$ and (20) for $\rho < r < R$; dw/dr is continuous except where

$|M_r| = M_0$, and $w = 0$ for $r = R$. The function $w(r)$ satisfying these conditions is found to be

$$w = \begin{cases} w_0 \left\{1 - \left(\frac{r}{\rho}\right) \Big/ \left(1 + \log \frac{R}{\rho}\right)\right\} & \text{for } 0 \leqslant r \leqslant \rho, \\ w_0 \left(\log \frac{R}{r}\right) \Big/ \left(1 + \log \frac{R}{\rho}\right) & \text{for } \rho \leqslant r \leqslant R. \end{cases} \tag{34}$$

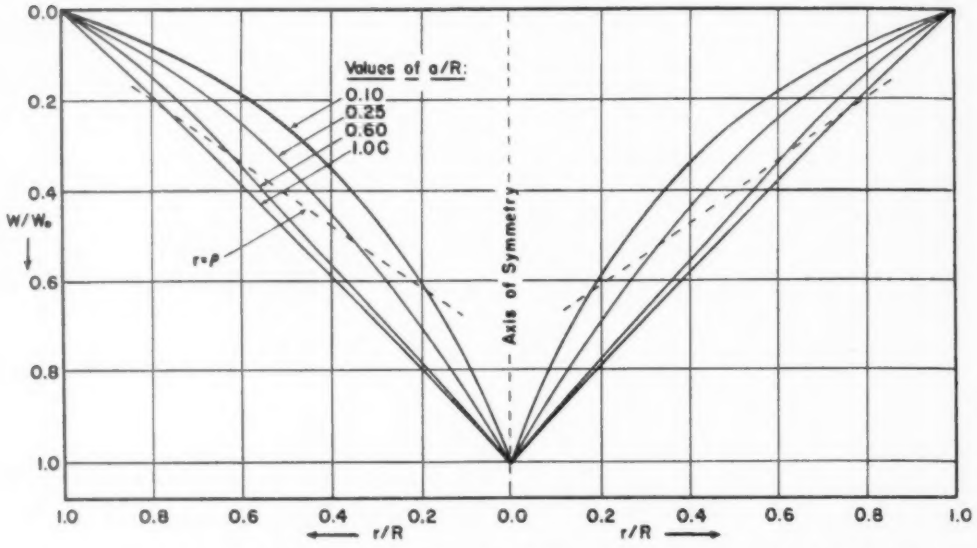

Fig. 5. Variation of normal velocity with size of loaded circular region for built-in edge.

Fig. 5 shows w/w_0 *v.* r/R for various values of a/R; the dotted line separates the logarithmic branches from the straight line branches of w/w_0.

(c) *Circular loading, built-in edge : case* $\rho > a$. Here, (21) holds for $0 \leqslant r \leqslant a$, and (22) for $a \leqslant r \leqslant \rho$. For $r = \rho$ the bending moment M_r as computed from (22) must vanish. Thus,

$$M_0 = \tfrac{1}{2} fpa^2 \left(1 - \tfrac{2}{3} \frac{a}{\rho}\right). \tag{35}$$

In the same manner as under (b) it is found that

$$M_r = (M_0 - \tfrac{1}{2} fpa^2) \log \frac{r}{\rho} \text{ for } \rho \leqslant r \leqslant R. \tag{36}$$

As before, the condition that $M_r = -M_0$ for $r = R$ furnishes a transcendental equation for ρ :

$$1 - \tfrac{2}{3} \frac{a}{\rho} \left(1 + \log \frac{R}{\rho}\right) = 0. \tag{37}$$

This yields $\rho > a$, as has been assumed here, for $a < 0{\cdot}606\, R$. When ρ has been determined from (37), the load factor f is found from (35). The part of curve (b)

in Fig. 3 that corresponds to $a/R < 0{\cdot}606$ shows the resulting relation between the total load $p = \pi fpa^2$ and a/R.

Again, it is necessary to investigate whether the bending moments (21), (22), (36) are associated with a velocity distribution $w(r)$ that satisfies all requirements. It is found that this is so, and that (34) still applies though, of course, ρ is now defined by (37).

(d) *Uniformly loaded built-in plate.* The results for this special case are obtained from the formulas in (b) by setting $a/R = 1$. Equation (33) simplifies to

$$5 + \log \frac{R^2}{\rho^2} = 3 \frac{R^2}{\rho^2}, \tag{38}$$

yielding $\rho/R \simeq 0{\cdot}730$. The load factor f is then obtained from (29):

$$f \simeq 11{\cdot}26 \frac{M_0}{pR^2}. \tag{39}$$

The total load at the flow limit is

$$P \simeq 35{\cdot}4\, M_0. \tag{40}$$

Comparison of (26) and (40) reveals that the total load at the flow limit is increased by about 88 per cent. by changing from the simply supported edge to a built-in edge.

The simplification achieved by the use of TRESCA's yield condition is worth noting. In an earlier paper (PELL and PRAGER 1951) the simply supported circular plate under uniformly distributed loading was discussed under the assumption that the plate material obeys the yield condition and flow rule of v. MISES. The mathemathical work was so much more complex in this case that an exact evaluation of the load carrying capacity proved too difficult. The best result that could then be achieved bounded this capacity to within $\pm$ 5·3 per cent. about $6{\cdot}33\, \pi M_0$, and it is of considerable interest that this value does not differ greatly from the exact value (26) obtained above for the yield condition of TRESCA and the associated flow rule. A general theorem which affords a means of comparing the load carrying capacity according to the MISES and TRESCA yield conditions has been given by HILL (1952).

(e). *Concentrated central load on built-in plate.* In the sense discussed under (a), the results obtained in (c) may be extrapolated to the case of a concentrated central load P. With $P = \pi fpa^2$, (35) may be written as

$$\rho = \frac{2Pa}{3P - 6\pi M_0}. \tag{41}$$

Similarly, the condition that (36) must furnish $M_r = -M_0$ for $r = R$ may be written in the form

$$\rho = R \exp \frac{2\pi M_0}{2\pi M_0 - P}. \tag{42}$$

Equations (41) and (42) show that, with $a \to 0$,

$$\rho \to 0, \quad P \to 2\pi M_0. \tag{43}$$

Vol. 2 53/54

Thus, the central load P at the flow limit of a circular plate is independent of the radius R. Indeed, since P has the same value $2\pi M_0$ for the simply-supported and the built-in plates, it may now be safely conjectured that this value applies also to plates which are clamped elastically along their edges.

The result (43) can be obtained independently by energy considerations similar to those presented in connection with (27).

(f). *Annular loading.* Here, $p(r) = 0$ for $0 \leqslant r < a$, and $p(r) = p = \text{const.}$ for $a < r \leqslant R$. For conciseness, the details of the analysis of a simply supported or built-in circular plate under annular loading will be omitted. The total load P at the flow limit can be read off Fig. 3, where the curve (c) corresponds to a simply-supported plate, and curve (d) to a built-in plate, under annular loading. The radius ρ of the circular boundary between the regimes AB and BC can be read off curve (b) in Fig. 4.

On the whole, the analysis for annular loading closely resembles that for circular loading. The following distinctive feature deserves mention, however. Because the region $0 \leqslant r < a$ is free from load, the regime A is no longer restricted to the centre of the plate. Indeed, with $p(r) = 0$ and $M_\phi = M_0$, integration of the equation of equilibrium under the initial condition that $M_r = M_0$ for $r = 0$ shows that $M_r = M_0$. Thus, the plate is in regime A for $0 \leqslant r < a$. The flow rule (15) then requires only that $\kappa_r = -d^2w/dr^2$ and $\kappa_\phi = -(1/r)\,dw/dr$ are non-negative, but does not furnish a differential equation for w as in the case of circular loading. Though this indeterminacy in the rate of deflection $w(r)$ may be surprising at first, it is actually quite typical of the mechanical behaviour of a perfectly plastic structural member under homogeneous stress. A perfectly plastic cylindrical rod in uniaxial tension at the elastic limit, for instance, need not deform uniformly even though the state of stress is homogeneous. In the present case, the fact that M_r and M_ϕ equal M_0 over a finite region creates a similar condition of homogeneous stressing. To remove the resulting indeterminacy in the rate of deflection $w(r)$, the work-hardening of the plate material would have to be considered.

ACKNOWLEDGMENT

The authors are indebted to the authorities of the Ballistic Research Laboratories, Aberdeen Proving Ground, for the permission to publish this paper which reports research work performed under Contract DA-19-020-ORD-798.

REFERENCES

BAKER, J. F.	1949	*J. Inst. Civ. Engrs.*, **32**, 188.
DRUCKER, D. C., PRAGER, W. and GREENBERG, H. J.	1952	*Qu. Appl. Math.*, **9**, 381.
HEYMAN, J.	1951	*J. Appl. Mech.*, **18**, 157.
HILL, R.	1951	*Phil. Mag.*, **42**, 868.
	1952	*Phil. Mag.*, **43**, 353.
JOHANSEN, K. W.	1943	*Brudlinieteorier* (J. Gjellerup, Copenhagen).
KIST, N. C.	1920	*Eisenbau*, **11**, 425.
ONAT, E. T. and PRAGER, W.	1953	*J. Mech. Phys. Solids*, **1**, 77.

PELL, W. H. and PRAGER, W. 1951 *Proc. 1st U.S. Nat. Cong. Appl. Mech.* (Chicago), 547.

PRAGER, W. 1952 *8th Inter. Cong. Th. and Appl. Mech.* (Istanbul), Sectional Address.

PRAGER, W. and HODGE, P. G. 1951 *Theory of Perfectly Plastic Solids* (John Wiley and Sons Inc., New York).

SYMONDS, P. S. and NEAL, B. G. 1951 *J. Franklin Inst.*, **252**, 383.

VAN DEN BROEK, J. A. 1948 *Theory of Limit Design* (John Wiley and Sons Inc. New York).

WEISS, H. J., PRAGER, W. and HODGE, P. G. 1952 *J. Appl. Mech.*, **19**, 397.

Vol.
2
53/54

Journal of the Mechanics and Physics of Solids, 1953, Vol. 2, pp. 14 to 26. Pergamon Press Ltd., London.

WEDGE INDENTATION EXPERIMENTS WITH COLD-WORKED METALS

By D. S. Dugdale
Department of Mechanical Engineering, University of Bristol

(*Received 15th July*, 1953)

Summary

Wedge-shape indenting tools have been used for producing plane-strain indentations in three cold-worked metals : mild steel, copper and aluminium. It was found that if the block of metal indented was larger than a certain critical size, the measured hardnesses were independent of size. These critical dimensions are given. The shear yield stress deduced from indentation tests has been compared with that obtained from torsion tests. Fair agreement was found. Precautions were taken to avoid errors that might arise from non-uniformity and anisotropy, and the effects of friction were taken into account, the friction coefficient being maintained at a small known value by suitable lubrication. The displaced metal formed a lip whose shape differed slightly from the theoretical shape for the ideal plastic-rigid material.

1. Introduction

The indentation test provides a convenient measure of the hardness of metals, and it is natural to enquire how the results of such tests can be related to the material strength as determined by tension and torsion tests. It is unfortunate that the ball and pyramid indenters in current use in engineering practice present plastic flow problems that are mathematically difficult. The large amount of empirical work that has been done on these hardness testing methods has been summarized recently by Tabor (1951). However, an indentation made by a wedge can be treated as a two-dimensional problem, provided the length is many times greater than the width, so that end effects are negligible.

Unwin, a pioneer of scientific testing of materials, suggested that the wedge indentation test could be used to provide a hardness index. His experiments (Unwin 1899) were carried out on specimens that were too small in relation to the indentation size, and his results show how important this matter is. A very different approach to the indentation problem was made by Hill, Lee and Tupper (1947), who analysed the flow around a frictionless wedge as it penetrated into a plastic-rigid material (i.e. a material for which Young's modulus is indefinitely large). They found that the surface of the displaced material remained straight, and that, in consequence of this, the geometry of the flow was very simple.

Cold-worked materials were used for the experiments to be described, for the reason that their behaviour approximates to that of a non-hardening or " ideal " plastic-rigid material ; that is, a material which flows at a constant stress after yielding. With these materials, results can be analysed by established methods (extended where necessary), and critical sizes of specimens can be precisely defined.

2. Experimental Basis of the Method

It was decided not to constrain the sides of the specimen because of the doubtful efficiency of such constraints due to their elasticity and because of possible friction at the ends of the wedge. It was, therefore, a necessary preliminary to find the critical impression width w in relation to all three dimensions of the block (Fig. 1). This was done by arranging that the dimension which was being examined was kept small, while the other two dimensions were made very large. The impression size was then found at which the measured hardness ceased to be constant due to some new mode of flow governed by this small dimension.

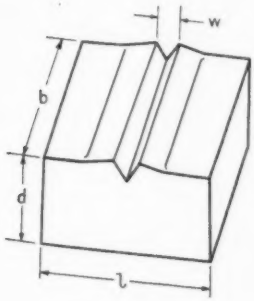

Fig. 1.
Dimensions of specimens used for wedge indentation tests.

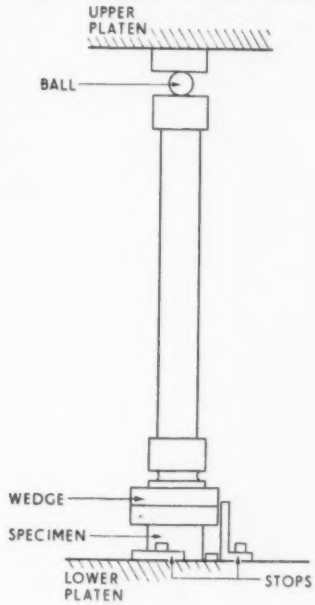

Fig. 2.
Diagram of wedge indenting tool.

A 15-ton Buckton testing machine fitted up for compression tests was used for making the indentations. The hardened steel wedge was attached to a ball-ended column 13 inches long to ensure that no lateral force was applied to the wedge. Care was taken that the wedge axes were maintained parallel to the axes of the block by making small adjustments to the stops controlling the position of the wedge and specimen (Fig. 2). It would have been more convenient to use a rigidly guided indenting tool, but guides and their associated friction effects were purposely avoided. The impression width w was measured by means of a travelling microscope at three points along the length of the impression, and an average was taken. It was found that the edges of the impression were always clearly defined.

First, the critical ratio w/b was determined for various wedge angles, using specimens 1 inch square and length $l = 3$ inches. For all the tests described in this paper calcium oleate was used as a lubricant, and the impression was filled with lubricant before applying each new load. About 13 loading cycles were found to be sufficient, the load being increased in equal increments. For each wedge a graph of impression width against applied load was plotted and in all cases this gave a straight-line relation over a certain range of load. All the present work depends on this simple experimental result. Hardness can now be defined

as the gradient of the graph of load per unit width b plotted against impression width w (Fig. 3).

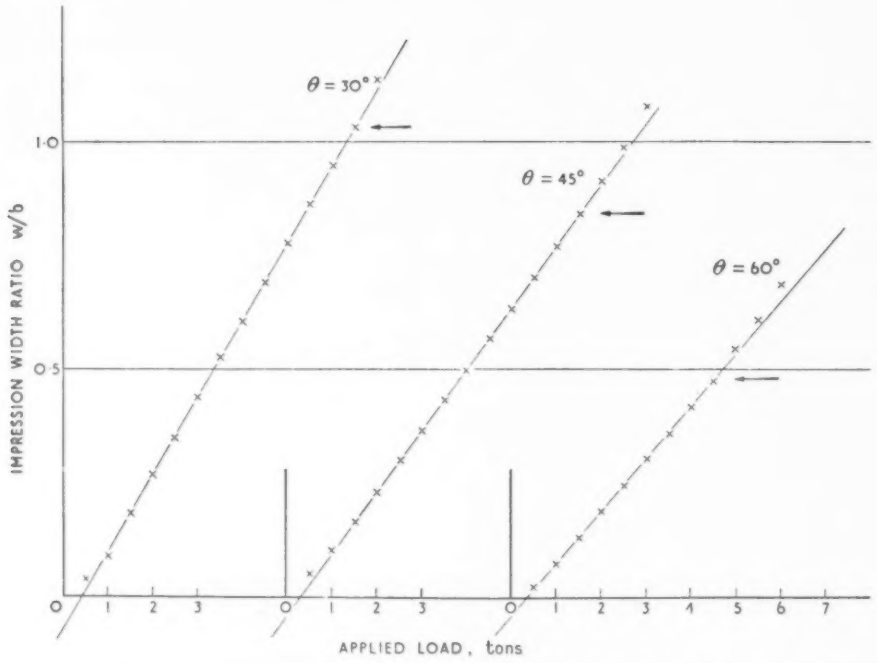

Fig. 3. Load-impression width curves. The arrow indicates the limit of the straight-line relation.

It was found that this straight line when produced back did not pass through the origin. To explain this, it is suggested that the current increment of penetration creates bare unlubricated surfaces which support a proportionately greater load than the previously made part of the impression which is fully lubricated. With small equal load increments, and with lubrication between each application of load, this excess force requires a small constant additional load to be applied to the wedge at each stage of the penetration. Therefore, by taking the gradient of the straight line, and having no regard for this small additional force, we obtain the stress acting on the fully lubricated surface. A small radius on the edge of the wedge may also introduce a small constant additional force, but this is likewise of no account. The edge radius was found to remain constant and of the order 0·002 inches when indentations were being made in steel.

At a certain value of impression width w, the relation between width and load ceases to be linear due to conditions at the ends of the impression coming into prominence (Fig. 3). UNWIN continued his tests much beyond this critical stage and showed that by plotting logarithms of penetration and load the resulting line was straight and of gradient 1·2. The writer has confirmed this, but it is of no fundamental significance. The limiting w/b ratios for a linear load-width relation are shown in Fig. 4. The parameter $h = \frac{1}{2} w \operatorname{cosec} \theta$ has been used for plotting; the significance of h can be seen in Fig. 7a.

3. Further Critical Dimensions of the Specimen

When the length l of the specimen (Fig. 1) is not sufficiently large, a certain value of impression width w is eventually reached when the forces applied by the wedge become great enough to initiate a new mode of deformation in which the length (measured in the upper surface of the specimen) increases. Similarly when the depth d is unduly small, a new field of flow underneath the wedge tip comes into existence, and the length of the specimen again increases. These cases have been discussed by Hill (1950a and 1953) for a non-hardening plastic-rigid material. However, when the material strain-hardens, the stresses in the material around the wedge exceed the yield stress of the unstrained material remote from the wedge, so it may be expected that the critical impression size is reduced below the theoretical value. This was found to be so.

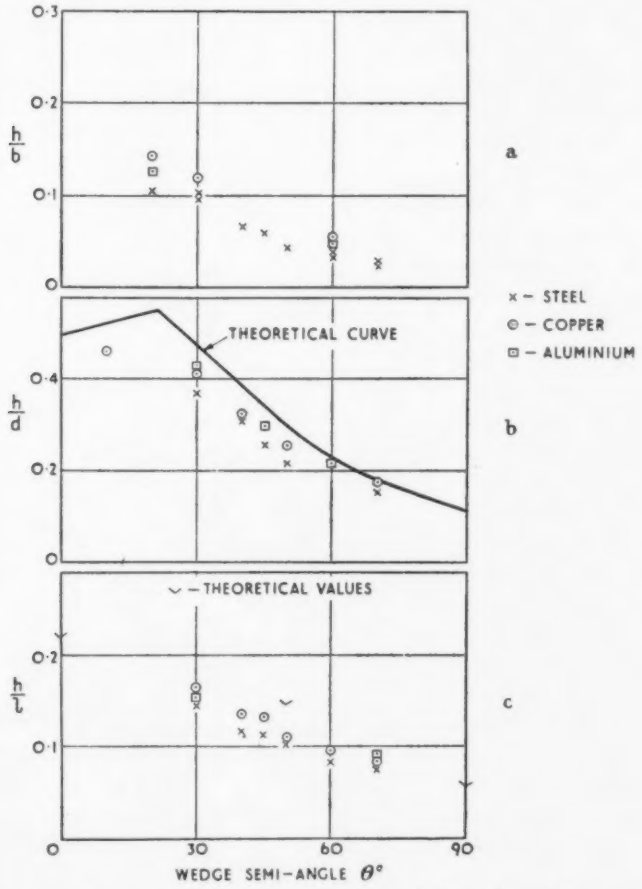

Fig. 4. Critical ratios of impression width to each dimension of the specimen.

The specimens used measured 0·2 inches in the critical direction and 1 inch or more in the other two directions. The specimens of small depth were greased underneath to reduce friction. Applied load and impression width were plotted

in the manner already described and the point at which the first perceptible deviation from the straight line occurred gave the critical proportions (Fig. 4). Measurements taken with a micrometer showed that in any particular case the length l started to increase at the same instant as the apparent hardness started to decrease, to within the experimental margin of error. It can be seen that the values for the three materials depart from the theoretical values (which are those given by HILL) by amounts roughly in proportion to their rates of strain-hardening (quoted later). In these tests no account was taken of non-unformity or anisotropy of the materials.

4. PRELIMINARY TESTS ON MATERIALS

It is usual to find that cold-worked materials are neither uniform nor isotropic, so it is necessary to investigate these matters in order to perform the tests intelligently and to assess the validity of the results.

A mild-steel bar 9 feet long and 1 × 1⅛ inches section was selected. It had been "bright-drawn," i.e. the hot-rolled bar had been given a small reduction in area by drawing through a die when cold. All tests were carried out on one half of this bar, after the ends had been discarded. From the ends of this portion sections were prepared and about a hundred Vickers Diamond Hardness readings were taken on each. The contour diagrams prepared from these readings were found to be similar, so one only need be shown (Fig. 5). It appeared that there was a hard stratum of material running along the bar, and to avoid this the wedge indentations were made on the side indicated, and torsion specimens were cut with their axes longitudinal as shown. Further Vickers readings taken along the length of the bar did not show any significant variation. A slab of electrolytic copper was used, of section 5 × 1½ inches, 3 feet long, cold-rolled from a 4½ × 2¼ inches section. The aluminium (nominally pure) had been reduced by cold-rolling from a section 8 × 2 inches to 8½ × 1½ inches, though its previous hot-working history was not

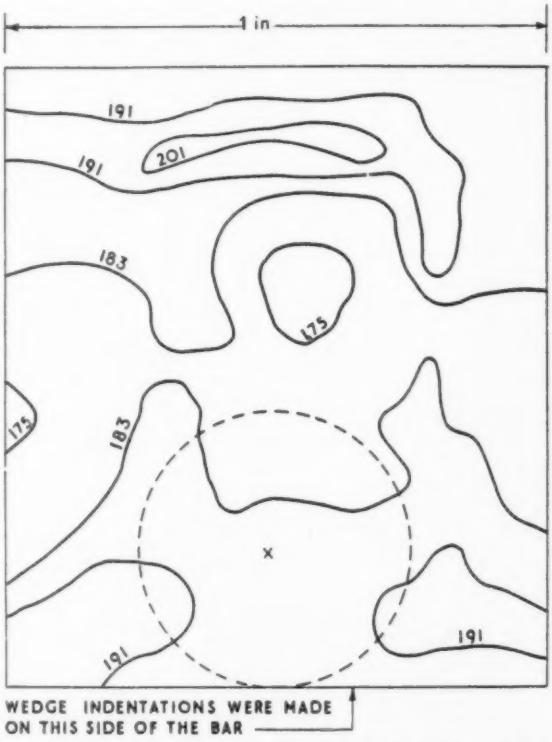

Fig. 5. Hardness contours over section of steel bar, from Vickers Pyramid hardness readings. The dotted line shows where the torsion specimens were taken from the bar.

known. One section was prepared from each of these slabs, and about 250 Vickers Diamond readings were taken on each. The result may be summarized by saying that the copper section showed irregular hard and soft areas of Vickers hardness numbers 101 to 106 and the aluminium section showed similar areas, hardness numbers 37 to 39. It was decided, on this evidence, not to select any special parts of these sections for the specimens, though half an inch of material at the ends of the sections was rejected, as this seemed softer than average. There were no significant hardness variations along the slabs.

The state of anisotropy of these materials was investigated by carrying out compression tests on specimens whose axes were respectively parallel to the three principal axes of the slab or bar. The specimens, whose ends were lubricated, were $\frac{1}{2}$ inch diameter by 1 inch long, and the diametral expansions were measured with a micrometer. When one logarithmic strain was plotted against another for each specimen, up to diametral strains of about 0·1, approximately straight curves were obtained, so the results can be conveniently shown in a Table. These values are uncertain to the extent of $\pm$ 0·05. The axes are defined in Fig. 6, x being the longer dimension of the cross-section of the slab or bar.

Vol. 2 53/54

SPECIMEN AXIS : DIAMETRAL STRAIN RATIO :	x ϵ_y/ϵ_z	y ϵ_z/ϵ_x	z ϵ_x/ϵ_y
STEEL	1·14	0·90	0·98
COPPER	1·53	1·08	0·58
ALUMINIUM	1·91	1·55	0·33

It was thought reasonable to assume that the steel was isotropic, and to carry out indentation tests in one arbitrarily chosen direction only. However, for the copper and aluminium, indentations were made with all six possible orientations of the wedge axes relative to the slab axes. The convention used for describing these orientations is explained in Fig. 6.

The aluminium crystals measured about 1 millimetre across : the steel and copper grains were much smaller than this.

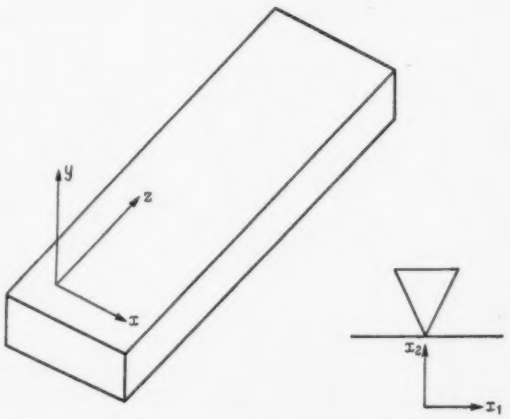

Fig. 6. Definition of axes in copper and aluminium slabs, and convention for specifying relation of wedge axes to slab axes. The wedge orientation is quoted $x_1\,x_2$ where x_1 and x_2 represent x, y or z.

5. Torsion Testing Technique

Solid specimens were used, of diameter 0·3 inches along the gauge length, which was $1\frac{1}{4}$ inches except for the through-thickness specimens which had a gauge

length of $\frac{1}{2}$ inch. A description of the torsion testing machine may be found in a paper by MORRISON (1940). The specimen was held in grips which applied the torque through hardened steel balls bearing on hardened pads. These grips offered no resistance to longitudinal expansion of the specimen, except for a small friction force. The twist over the gauge length was indicated by pointers clamped to the specimen by knife-edges, moving over a scale graduated in degrees. In view of the creep properties of the materials, it was necessary to arrange that there was some sort of similarity between the time of application of the load to the wedge indenter, and the rate of straining in the torsion test. All indentation loads were applied for 2 minutes, while the torsion specimen was subjected to a fairly large strain increment (about 0·2) and the torque reading then taken after waiting 2 minutes. NADAI's construction was used to derive the true stress.

It is well known that torsion and compression tests do not agree very closely at large strains when Mises-Hencky stress functions and their strain equivalents are plotted. The torsion test was chosen for comparison with the indentation tests because of the parallelism which exists between their modes of straining. In the case of a plane-strain indentation, a large part of the total strain which an element undergoes takes place at a surface which in a real material corresponds to the plastic-rigid boundary, where the velocity falls rapidly to zero. (This is demonstrated in the next section). Consequently the direction of the principal shear strain-increment remains unaltered, while the element of material rotates, as it does in the torsion test.

6. STRESS AND STRAIN RELATED TO MEASURED QUANTITIES

If we write down the equation of vertical equilibrium of the wedge (Fig. 7a) and put $\tau = \mu\,\sigma$ where μ is the coefficient of friction and τ and σ the tangential and normal stresses (assumed uniform), we find

$$\sigma = p/(1 + \mu \cot \theta).$$

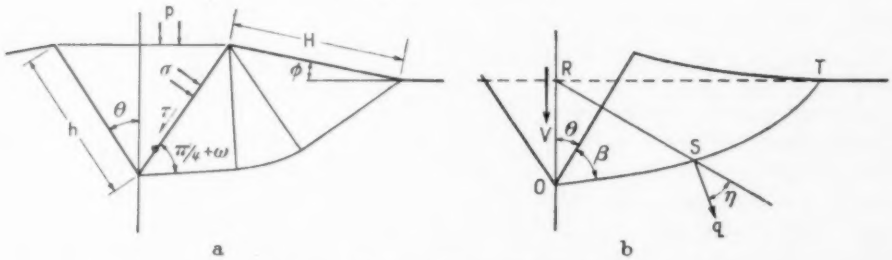

Fig. 7. Stress and strain in the distorted region.
(a) Stresses at the wedge surface. (b) Strain at the plastic-rigid boundary.

Due to friction at the wedge surface, a typical slip-line rotates from its position when there is no friction, by amount ω. By constructing the Mohr stress diagram for an element of material in contact with the wedge (Fig. 8),

$$\tau = k_i \sin 2\,\omega$$

$$\sigma_1 = \sigma + k_i\,(1 - \cos 2\,\omega),$$

where k_i is the mean yield stress in shear in the deformed material around the wedge (the subscript standing for indentation) and σ_1 is the greater principal compressive stress. From Hencky's theorem,

$$\sigma_1 = 2k_i(1 + \theta + \omega - \phi)$$

where ϕ is the angle of the raised lip. When μ is small we can write

$$\omega \doteq \mu p/2k_i, \qquad \sigma \doteq \sigma_1,$$

and hence

$$k_i = \frac{p}{2(1 + \theta - \phi)} \cdot \frac{1 - \mu}{1 + \mu \cot \theta} \qquad (1)$$

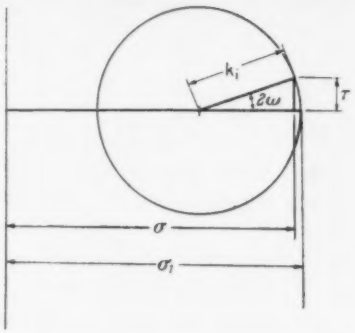

Fig. 8. Mohr stress diagram for material in contact with wedge.

To examine the state of strain in the material just inside some extreme slip-line OST (Fig. 7b) let the velocity parallel to this line at any chosen point be u. Then by GEIRINGER's equations (HILL 1950b, p. 136) u has the same value at all points on this boundary. If geometrical similarity is maintained as the penetration increases, the speed q of the boundary perpendicular to itself is

$$q = V \frac{\mathrm{R\,S}}{\mathrm{RO}} \cos \eta$$

where V is the speed of penetration and η is the angle between the normal and the line R S. The shear strain in an element that has just cross the boundary is

$$\gamma = u/q.$$

For the type of deformation caused by a smooth wedge, $\beta = \pi/4$ and $u = \sqrt{2}\,V \sin \theta$. Hence the mean strain on the boundary can be computed for an ideal plastic-rigid material. When this value was compared with the average strain over the whole area of flow (determined below) it was found that for small wedge angles the ratio between these two strains was nearly unity, falling to 0·9 for an included wedge angle of 120°. This means that an element of material undergoes only a small further strain after the large initial straining at the plastic-rigid boundary, and therefore the gradient of yield stress in any direction normal to this boundary must be small for the materials of small strain-hardening considered here. For this reason it is legitimate to apply Hencky's theorem in the deformed region.

The coefficient of friction μ was measured by the method described by HILL (1950c) using hardened steel compression platens whose surface finish was the same as that of the wedges (about $\pm$ 3 micro-inches). The values found were : steel 0·031, copper 0·020, aluminium 0·026. The same lubricant was of course used. In applying these values, it was assumed that they did not vary with pressure.

In order to compare the shear stress from the indentation tests with that from the torsion test it is necessary to estimate the mean plastic strain in the derformed material. The shear stresses thus found ought to be equal if the hydrostatic component of stress has no effect. The force acting on half the wedge (Fig. 7a) is $p\,h \sin \theta$ per unit length. The penetration below the original surface is

$h \cos \theta - H \sin \phi$ where H is the length of the raised lip. Hence the work done is

$$\frac{ph^2}{2} \sin \theta \left(\cos \theta - \frac{H}{h} \sin \phi\right).$$

But the work required for the plastic distortion is $A k_i \bar{\gamma}$ where $\bar{\gamma}$ is a mean shear strain, thus defined, and A is the distorted area. However, the experimental results suggest that it is not reasonable to use the area appropriate to the ideal plastic-rigid case (where $H = h$). The area of flow is certainly much greater than this with a work-hardening material and an approximation must be made which, although it may seem crude, brings us nearer to the true state of affairs. Suppose that this area is that of a triangle with hypotenuse H, a sector of radius $(H + h)/2\sqrt{2}$, and another triangle with hypotenuse h. It follows that

$$\bar{\gamma} = \frac{2p}{k_i} \cdot \frac{\sin \theta \left(\cos \theta - \frac{H}{h} \sin \phi\right)}{1 + \left(\frac{H}{h}\right)^2 + \frac{\theta - \phi}{4}\left(1 + \frac{H}{h}\right)^2}. \tag{2}$$

A small amount of work must be dissipated in friction at the wedge surface, but this is ignored.

It follows from the geometry of the impression (Fig. 7a) that, if the deformation takes place at constant volume,

$$\left(\frac{H}{h}\right)^2 \sin \phi \cos \phi + 2 \frac{H}{h} \sin \theta \sin \phi - \sin \theta \cos \theta = 0.$$

Experimental values of ϕ were inserted into this equation, and the values of H/h thus obtained were compared with the observed values. Reasonable agreement was found, which showed that there was, indeed, no significant change in volume.

7. Results of Torsion Tests

Specimens were taken from each of the three principal directions of the copper and aluminium slabs, each test being duplicated. The stress-strain curves for the cold-worked materials tested were almost straight after a strain of about 0·05 so the results are given in tabular form. The units of the torsion shear stress k_i in Table 1 are tons per square inch.

8. Results of Indentation Tests

The angle of the wedge was measured with a vernier protractor (reliable to within 3 minutes of arc) to give the semi-angle θ. For the tests on steel, the bar was cut into blocks 2 inches long which were ground on all sides, and the indentations were made transversely (see Fig. 5). The specimens of copper and aluminium were about 1·3 inches long in the direction of the impression and 1 inch square section. Thus in all cases the critical specimen dimensions were greatly exceeded. After indenting, the specimen was cut away to leave a section of the impression about 0·05 inches thick suitable for determing the profile by means of a toolmaker's projector, this section being in the middle of the plane-strain section of the

TABLE 1.

	Direction of specimen axis	Natural shear strain 0·2	0·5	0·7	1·0	1·5
STEEL	z	19·7	20·6	21·0	21·6	22·3
		19·5	20·3	20·8	21·2	—
		19·6	20·3	21·0	21·8	—
		19·6	20·6	21·1	21·6	22·5
	Average :	19·6	20·4	21·0	21·5	22·4
COPPER	x	10·05	10·40	10·65	10·90	11·00
		10·30	10·65	10·85	10·95	11·00
	y	9·90	10·20	10·30	10·50	—
		9·90	10·45	10·55	10·75	—
	z	9·95	10·15	10·25	10·35	10·50
		9·90	10·15	10·20	10·35	10·50
	Average :	10·00	10·33	10·47	10·63	10·75
ALUMINIUM	x	3·38	3·57	3·65	3·68	3·68
		3·42	3·63	3·71	3·72	3·74
	y	3·42	3·49	3·54	3·61	3·68
		3·41	3·54	3·62	3·68	3·76
	z	3·32	3·41	3·46	3·49	3·48
		3·37	3·50	3·55	3·58	3·56
	Average :	3·39	3·52	3·59	3·63	3·65

Vol. 2 53/54

impression. The parts of the raised lip adjacent to both the wedge and the undeformed metal (i.e. around points A and B in Fig. 9b) were slightly rounded, but there was always a well-defined straight portion which enabled the angle ϕ to be measured from a tracing taken from the projector image. Values of H (Fig. 7a) were measured by producing this straight portion to meet the surface of the wedge and the original surface of the specimen. The magnification factor was about 50. Two images were traced from each impression and average values were taken to reduce experimental error. Indentations for each wedge angle in steel and for each direction in aluminium were duplicated (Table 2). The wedges were reground between the tests on each material. A small correction obtained from a dead-weight calibration of the testing machine has been applied to the observed loads.

9. Comparison of Shear Stresses Deduced from Indentation and Torsion Tests

By substituting values from Table 2 into equation (1) the shear stress k_i for each indentation was found. These shear stresses were then averaged for each wedge angle (Table 3). To find the mean strain $\bar{\gamma}$ in the deformed material of the indentation, mean values of the stresses and of ϕ and H/h were used in equation (2). Hence the corresponding stress k_t in torsion could be found from Table 1.

TABLE 2.

	Nominal included angle of wedge	$\theta°$	Orientation	p, tons per sq. in.	$\phi°$	$\frac{H}{h}$
STEEL	40	19·70	—	52·9	9·5	1·12
				54·6	9·7	1·11
	60	30·35	—	63·1	9·6	1·15
				60·1	9·4	1·20
	80	40·00	—	71·2	8·4	1·32
				68·3	8·8	1·24
	90	45·15	—	71·5	8·8	1·26
				74·6	7·5	1·40
	100	49·80	—	77·7	6·8	1·62
				77·5	6·3	1·40
	120	60·25	—	87·7	4·6	1·43
				89·3	5·0	1·53
	140	69·60	—	90·9	2·3	2·21
				93·8	2·2	2·54
COPPER	60	30·15	xy	30·6	10·9	1·13
			yz	30·1	11·2	1·09
			zx	32·3	10·6	1·16
			zy	30·7	10·1	1·18
			yx	29·7	12·1	1·05
			xz	31·1	12·0	1·07
	90	44·85	xy	38·1	9·0	1·24
			yz	36·1	11·3	1·05
			zx	38·4	10·0	1·16
			zy	36·8	9·5	1·22
			yx	36·4	11·7	1·02
			xz	37·6	11·0	1·08
	120	60·25	xy	42·0	6·8	1·23
			yz	41·9	7·1	1·16
			zx	43·5	7·1	1·18
			zy	43·0	6·8	1·17
			yx	41·7	7·5	1·17
			xz	43·6	7·9	1·07
ALUMINIUM	60	30·30	xy	10·65	9·2	1·27
				10·15	8·4	1·32
			yz	10·60	8·8	1·30
				10·25	8·9	1·23
			zx	11·60	10·8	1·03
				11·80	10·6	1·17
			zy	10·00	10·9	1·11
				10·00	9·9	1·13
			yx	11·30	10·8	1·14
				10·70	10·5	1·19
			xz	11·15	13·4	0·94
				11·50	12·4	1·02

Vol 2 1953

TABLE 3.

	Nominal wedge angle	Mean strain $\bar{\gamma}$	Shear stresses tons/sq. in. k_i	k_t
STEEL	40	0·57	20·3	20·6
	60	0·72	20·8	21·0
	80	0·73	21·0	21·1
	90	0·71	20·7	21·0
	100	0·64	20·8	20·8
	120	0·57	21·4	20·6
	140	0·22	20·4	19·7
COPPER	60	0·72	10·9	10·5
	90	0·80	11·1	10·5
	120	0·71	10·7	10·5
ALUMINIUM	60	0·71	3·74	3·59

Vol. 2 53/54

It can be seen that the greatest discrepancy is about 6 per cent and that the torsion stress tends to be lower than the indentation stress. Many small errors may contribute to this difference and in view of the non-uniformity of these materials, caution is urged in making any deductions. However, a few possible sources of error may be enumerated. SWIFT (1948) pointed out that when a torsion specimen is prevented from expanding axially, the stress at large strains may be lower, but in the tests described above the axial force sustained by the specimen was certainly very small. The arithmetical mean of the hardnesses and torsion strengths of these anisotropic materials has been used without justification, except that it seemed reasonable to do this. There is a fundamental difficulty in specifying the effective rate of strain in a solid torsion specimen as the rate of strain varies from zero at the centre to its nominal value at the outside. There is a further difficulty in relating this strain-rate in a rigorous manner to the time of application of load to the wedge. The torsion tests showed that torque readings taken 1 minute and 2 minutes after applying the strain increment differed by roughly 1 per cent for copper and 2 per cent for aluminium.

It is thought that elastic deformation of the wedge and specimen can have no appreciable effect on these results.

10. EFFECT OF STRAIN-HARDENING ON IMPRESSION SHAPE

When the lip angles ϕ were averaged for each wedge and plotted (Fig. 9a) they were found in all cases to be less than the angles for the ideal plastic-rigid material. The graph shows that this effect is greatest for the material (steel) that has the greatest rate of strain-hardening (see Table 1). From this evidence alone it appears to be safe to infer that this reduction of the angle is a function of the rate of strain-hardening, since no other property of these materials seems to be relevant. It will be observed that friction at the wedge surface can only bring about an increase of the lip length of fraction ω (see Fig. 7a).

The proportionate reduction of the lip angle is greater for large wedge angles, but it is difficult to construct an explanation for this without introducing *ad hoc* assumptions. However, let us suppose that the position of the slip-line segment OD (Fig. 9b) remains unchanged when the ideal plastic-rigid material is endowed with a small degree of strain-hardening. Now in the ideal case it can be calculated,

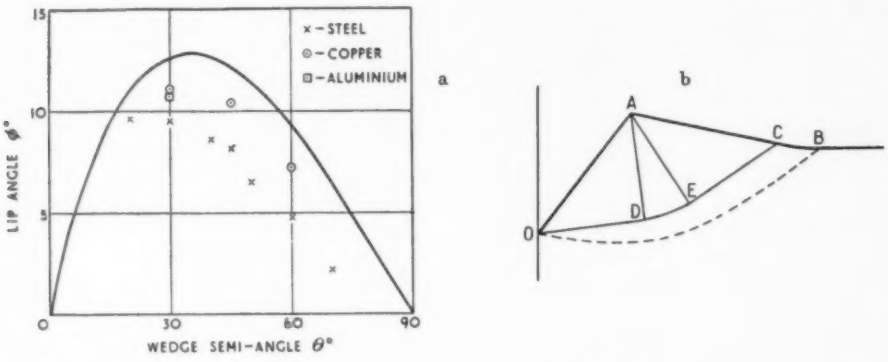

Fig. 9. Profile of impression. (a) Experimental values of lip angle. The curve shows the theoretical values for an ideal non-hardening material. (b) The possible effect of strain-hardening.

by the method described above, that the strain in the material which has just crossed the line OD increases steadily with the wedge angle, e.g. 1·0 for $\theta = \pi/4$ and 2·0 for $\theta = \pi/2$. The strain along EC is much smaller in these cases, so it is unimportant in this discussion. It is necessary therefore, when the strain-hardening is not zero, that there should be an additional area of flow ODECB so that the shear stress may be equal to the initial yield value along OB. This can only have the effect of increasing the length AB of the raised lip.

Acknowledgments

The author is grateful to Professor J. L. M. Morrison and Dr. R. Hill for a great deal of helpful criticism.

References

Hill, R.	1950a	*Phil. Mag.*, **41**, 745.
	1950b	*Mathematical Theory of Plasticity* (Clarendon Press).
	1950c	*Phil. Mag.*, **41**, 733.
	1953	*J. Mech. Phys. Solids* **1**, 265.
Hill, R., Lee, E. H. and Tupper, S. J.	1947	*Proc. Roy. Soc.*, A., **188**, 273.
Morrison, J. L. M.	1940	*Proc. Inst. Mech. Eng.* **142**, 193.
Swift, H. W.	1948	*Proc. Inst. Mech. Eng.* **159**, 109.
Tabor, D.	1951	*The Hardness of Metals* (Clarendon Press).
Unwin, W. C.	1899	*The Testing of Materials of Construction* (Longmans & Co.).

Journal of the Mechanics and Physics of Solids, 1953, Vol. 2, pp. 27 to 38. Pergamon Press Ltd., London.

ON THE PLASTIC BEHAVIOUR OF THICK TUBES UNDER COMBINED TORSION AND INTERNAL PRESSURE

B. CROSSLAND* and R. HILL**
* Department of Mechanical Engineering, University of Bristol
** Department of Theoretical Mechanics, University of Bristol

(*Received 25th July*, 1953)

SUMMARY

IN the method of plastic design of engineering structures it is necessary to be able to calculate the loads that cause collapse, and to estimate the amount of permanent deformation caused by safe loads. If work-hardening is negligible, the collapse loads are theoretically independent of any initial residual stresses, but the amount of deformation is not. The present paper describes some relevant experimental data obtained from overstraining autofrettaged steel tubes by combined torsion and internal pressure. In particular, the observed collapse loads agree closely with values calculated for the yield point of a tube of hypothetical plastic-rigid material.

Vol. 2 53/54

1. OBJECTS OF THE INVESTIGATION

THE method of plastic design of engineering structures depends on the possibility of determining the combinations of loads under which collapse begins (see, for example, BAKER 1949). In the so-called limit theorems recently applied to this problem (GREENBERG and PRAGER 1951 ; SYMONDS and NEAL 1951), the collapse loads are calculated, in effect, as those under which deformation would first begin if the structure were made of hypothetical material with an infinitely great rigidity modulus (HILL 1951, 1952). We shall refer to the instant of initial deformation in such a plastic-rigid material as the yield point. In the real structure one would normally expect that strains only of an elastic order of magnitude would be produced during monotonic loading very nearly up to the yield point of the similar plastic-rigid structure ; further small increases in load would, in the absence of work-hardening* and passive constraints, produce comparatively large distortions. These expectations are confirmed by experiments on, for example, pure torsion or bending of bars, and on combined bending and twisting of hollow and solid cylinders (SIEBEL 1953 ; HILL and SIEBEL 1953). Further confirmation is afforded by analytic solutions to plastic-elastic problems, e.g. autofrettage of thick tubes (HILL 1950, pp. 114-125 ; torsion and tension of solid cylinders (GAYDON 1952) ; combined bending and twisting of thin tubes (HILL and SIEBEL 1951). In these solutions, as a consequence of neglecting dimensional changes, the yield point loads are approached *asymptotically* with increasing strain. In very special circumstances, such as the torsion of a hollow circular cylinder, the load on a non-hardening

* The ideas and practical methods of plastic design are at present only well developed for materials such as mild steel which do not harden appreciably in the relevant range of strain.

plastic-elastic body actually *attains* the yield point of the similar plastic-rigid body in a finite strain and subsequently retains this value ; in such circumstances the internal state of stress also remains invariable, as would naturally be expected (PRAGER and HODGE 1951, pp. 217-9). If dimensional changes were to be taken into account in these solutions, the representative load-distortion relation would pass through a momentary maximum, the collapse value (somewhat below the plastic-rigid yield point), and then steadily decrease. In some structures unacceptably large displacements can occur during a strain of elastic order, well before the actual collapse load is reached (see, for example, SYMONDS and NEAL 1952).

It is clear, then, that the precise significance of the plastic-rigid yield point for plastic design depends on the particular structure or continuum. Moreover, while the yield point loads are unaffected by initial internal stresses or, more generally, by the loading path up to the final load-ratios (HILL 1951), the shape of the actual load-distortion relation depends sensitively on these factors. Very little comparative data is, however, available at present (cf. HILL and SIEBEL 1951 and ONAT and SHIELD 1953 ; also GAYDON, op.cit., and PRAGER and HODGE, op.cit., pp. 86-91).

In the present paper we examine some of these matters in relation to closed tubes subjected to combined torsion and internal pressure. This particular loading system was originally selected to provide data for designing a tubular torque-bar for experiments on the effect of hydrostatic pressure on torsional properties (CROSSLAND 1953). To see whether a worthwhile improvement could be effected in the elastic range of such a torque-bar under combined torsion and internal pressure, the tubes were autofrettaged beforehand. The subsequent combined stress tests on these autofrettaged tubes were carried beyond the elastic limit and up to the fully plastic state. It is these tests that are reported here for their intrinsic interest, both in illustrating the approach to the collapse loads and in providing evidence in support of the theoretical prediction that this load does not depend on the initial residual stresses and can be calculated as the plastic-rigid yield point when the material is non-hardening.

2. THE ELASTIC LIMIT

Consider a long uniform circular tube with closed ends, internal radius a and external radius b. Let k be the yield stress in pure shear. Then the elastic limits of the tube under internal pressure alone, and under torsion alone, are respectively

$$p_0 = k\left(1 - \frac{a^2}{b^2}\right), \qquad t_0 = \tfrac{1}{2}\pi k b^3\left(1 - \frac{a^4}{b^4}\right). \tag{1}$$

If the tube is autofrettaged to pressure p_a, the radius c of the plastic-elastic interface is given by

$$p_a = k\left(\log\frac{c^2}{a^2} + 1 - \frac{c^2}{b^2}\right). \tag{2}$$

This is exact if the material is incompressible, and an excellent approximation for ordinary values of Poisson's ratio, no matter what the yield criterion (cf. HILL 1950, p. 119). If the pressure is now reduced from p_a to p, the tube always unloads elastically if $p_a < 2p_0$, and the distribution of the residual maximum shear stress is given by

$$\frac{\sigma_\theta - \sigma_r}{2k} = \begin{cases} \left(1 - \dfrac{p_a - p}{p_0} \cdot \dfrac{a^2}{c^2}\right) \dfrac{c^2}{r^2}, & c \leqslant r \leqslant b\,; \\ 1 - \dfrac{p_a - p}{p_0} \cdot \dfrac{a^2}{r^2}, & a \leqslant r \leqslant c\,; \end{cases} \tag{3}$$

where σ_r, σ_θ are the radial and hoop stresses. The residual axial stress is approximately $\frac{1}{2}(\sigma_r + \sigma_\theta)$, since σ_z has very nearly this value during autofrettage and the change in σ_z is exactly equal to the change in $\frac{1}{2}(\sigma_r + \sigma_\theta)$ during unloading.

Suppose, now, that a torque t is superimposed. The shear stress is $\tau = krt/bt_0$ so long as the further changes of strain are elastic, which is so provided that

$$\left(\frac{\sigma_\theta - \sigma_r}{2k}\right)^2 + \left(\frac{\tau}{k}\right)^2 \leqslant 1$$

throughout the tube; here and henceforward we assume the MAXWELL-MISES yield criterion. It is not difficult to show that yielding first occurs at either the bore, the former plastic-elastic interface, or the external surface. Thus, from (3), the elastic range of the autofrettaged tube under combined torsion and pressure is to be obtained by varying p and t so that the inequalities

$$\left(1 - \frac{p_a - p}{p_0}\right)^2 + \left(\frac{at}{bt_0}\right)^2 < 1 \qquad \text{(no yielding on } r = \text{a)}$$

$$\left(1 - \frac{p_a - p}{p_0} \cdot \frac{a^2}{c^2}\right)^2 + \left(\frac{ct}{bt_0}\right)^2 < 1 \qquad \text{(no yielding on } r = \text{c)}$$

$$\left[\left(1 - \frac{p_a - p}{p_0} \cdot \frac{a^2}{c^2}\right)\frac{c^2}{b^2}\right]^2 + \left(\frac{t}{t_0}\right)^2 < 1 \qquad \text{(no yielding on } r = \text{b)}$$

are simultaneously satisfied.

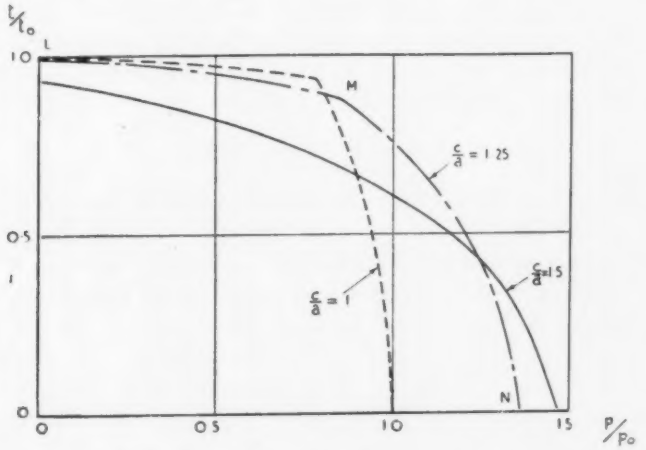

Fig. 1. Theoretical elastic limits for autofrettaged cylinders under combined torsion and pressure.

In the experiments to be described, b/a has the nominal value 1·5. For this wall-ratio we show in Fig. 1 the calculated relations between p and t at the elastic limit for $c/a = 1$ (no autofrettage), $c/a = 1{\cdot}25$, and $c/a = 1{\cdot}5$ (maximum auto-

frettage). In the present case, yielding occurs first either at the external surface (represented by LM in Fig. 1) or at the former plastic-elastic interface (represented by MN); for sufficiently thick tubes yielding occurs first at the bore for a certain range of small pressures. It will be seen from Fig. 1 that a moderate amount of autofrettage is beneficial in that a torsional elastic range not much less than t_0 can be obtained for tubes under any internal pressure up to almost p_0.

A calculation of the deformation for load combinations exceeding the elastic limit has not been undertaken. It may, however, be noted that the collapse load under torsion alone is reached after a shear strain at the external surface equal to $b/a \times k/G$, where G is the modulus of rigidity, while the collapse load under pressure alone is reached after an external circumferential strain of approximately $(1 - \frac{1}{2}\nu)/(1 + \nu) \times k/G$ where ν is Poisson's ratio. The external surface strains to collapse under combined pressure and torsion are therefore presumably also of order k/G for tubes of moderate thickness.

We now proceed directly to a calculation of the plastic-rigid yield point.

3. The Yield Point and Ensuing Strain Ratios

At a sufficient distance from the ends of the tube the stress and strain-rate in the fully plastic state are functions only of the radius r. It follows that the rz and $r\theta$ components of shear stress vanish by virtue of the equations of equilibrium and the fact that they are zero on the external surfaces. The remaining equation of equilibrium reduces to

$$\frac{d\sigma_r}{dr} = \frac{\sigma_\theta - \sigma_r}{r}. \tag{4}$$

We assume the MISES plastic potential (i.e. the LÉVY-MISES relations between stress ratios and strain-rate ratios). It may be verified *a posteriori* that the axial strain-rate vanishes and that $\sigma_z = \frac{1}{2}(\sigma_r + \sigma_\theta)$, so satisfying the closed-end condition. It follows from the MISES yield condition that

$$\tfrac{1}{4}(\sigma_\theta - \sigma_r)^2 + \tau^2 = k^2 \tag{5}$$

where τ denotes the θz shear stress component. Further, there is no warping of a transverse section and the $r\theta$ and rz components of shear strain-rate vanish. Hence the radial and circumferential components of velocity must be $b\dot{b}/r$ and $\dot{\phi}\, rz$, respectively, where ϕ is the twist per unit length. The remaining LÉVY-MISES equation is then

$$\tau / \tfrac{1}{2}(\sigma_\theta - \sigma_r) = \tfrac{1}{2} r\dot{\phi} \Big/ \frac{b\dot{b}}{r^2}. \tag{6}$$

Combining (5) and (6):

$$\frac{\sigma_\theta - \sigma_r}{2k} = \left(1 + \frac{r^6\,\dot{\phi}^2}{4b^2\,\dot{b}^2}\right)^{-\frac{1}{2}}, \qquad \frac{\tau}{k} = \frac{r^3\,\dot{\phi}}{2b\dot{b}}\left(1 + \frac{r^6\,\dot{\phi}^2}{4b^2\,\dot{b}^2}\right)^{-\frac{1}{2}}. \tag{7}$$

On integrating (4) and the second of (7) through the tube, we find the following expressions for the internal pressure P and torque T at the yield point:

$$\left.\begin{aligned} \frac{P}{P_0} &= \frac{\sinh^{-1}(\lambda n) - \sinh^{-1}\lambda}{\log n}, \\ \frac{T}{T_0} &= \frac{n\sqrt{(1+\lambda^2)} - \sqrt{(1+\lambda^2 n^2)}}{n-1}, \end{aligned}\right\} \tag{8}$$

where $n = b^3/a^3$ and $\frac{1}{2}\lambda = \dot{b}/b^2\dot{\phi}$ = (circumferential strain-rate)/(shear strain-rate) on the outer surface. P_0 is the yield point pressure in the absence of torque ($\lambda = \infty$) and T_0 is the yield point torque in the absence of pressure ($\lambda = 0$):

$$P_0 = 2k \log \frac{b}{a}, \qquad T_0 = \tfrac{2}{3}\pi k (b^3 - a^3). \tag{9}$$

The relation between P and T is shown in Table 1 for the case $b/a = 1{\cdot}5$. For this value of b/a, $P_0/p_0 = 1{\cdot}460$ and $T_0/t_0 = 1{\cdot}169$.

The fourth column reveals that the $(P/P_0, T/T_0)$ curve differs very little from a quadrant of a circle (which corresponds to a very thin tube); the radius vector exceeds unity by not more than $1\frac{1}{2}\%$, the greatest value occurring near $\lambda = 0{\cdot}6$. When $b/a = 2$, the greatest radius vector exceeds unity by about 4% and occurs near $\lambda = 0{\cdot}4$. It may be shown that, as n increases, the $(P/P_0, T/T_0)$ relation approaches two sides of a square, and that, in the limit,

$$T/T_0 = \sqrt{(1+\lambda^2)} - \lambda, \qquad P/P_0 = 1, \qquad \lambda \neq 0;$$
$$T/T_0 = 1, \qquad 0 \leqslant P/P_0 < 1, \qquad \lambda = 0.$$

TABLE 1

λ	$\frac{P}{P_0}$	$\frac{T}{T_0}$	$\sqrt{\left(\frac{P^2}{P_0^2} + \frac{T^2}{T_0^2}\right)}$	$\frac{T}{T_0}\Big/\frac{P}{P_0}$	$\frac{\lambda T}{T_0}\Big/\frac{P}{P_0}$
0	0	1	1	∞	0·512
0·2	0·356	0·935	1·000	2·625	0·525
0·4	0·591	0·818	1·009	1·382	0·553
0·6	0·729	0·708	1·016	0·971	0·583
0·8	0·811	0·610	1·015	0·750	0·600
1·0	0·863	0·527	1·011	0·610	0·611
1·2	0·897	0·464	1·009	0·517	0·620
∞	1	0	1	0	0·648

From the last column of Table 1 the strain-ratio may conveniently be found by interpolation when the load-ratio is assigned. The entries corresponding to $\lambda = 0$ and $\lambda = \infty$ may be shown from (8) to be respectively

$$\frac{\log n}{n-1} \qquad \text{and} \qquad \frac{n+1}{2n}.$$

The reason for the comparatively small difference between these extremes may be understood as follows. The rate of work of the applied loads is $\dot{W} = P\dot{v} + Tl\dot{\phi}$ where v is the internal volume of a length l of the tube. By the maximum work principle, which is valid when the yield function and plastic potential are indentical

(HILL 1951), $d\dot{W} = 0$ for infinitesimal variations of P and T along the (P, T) curve, $\dot{v}$ and $\dot{\phi}$ being regarded as prescribed. Thus

$$\dot{v}/l\dot{\phi} = -dT/dP.$$

The axial strain-rate happens to be zero for the MISES yield function and potential, and then $\dot{v}/l\dot{\phi} = 2\pi aa/\phi = 2\pi b\dot{b}/\dot{\phi}$ since the tube material is incompressible. Therefore,

$$\lambda = -\frac{1}{\pi b^3} \cdot \frac{dT}{dP}, \tag{10}$$

which may, indeed, be derived direct from (8). When the (P, T) curve differs little from the circle

$$\left(\frac{P}{P_0}\right)^2 + \left(\frac{T}{T_0}\right)^2 = 1,$$

if follows from (9) and (10) that

$$\frac{\lambda T}{T_0} \Big/ \frac{P}{P_0} \sim \frac{T_0}{\pi b^3 P_0} = \frac{n-1}{n \log n}. \tag{11}$$

When $b/a = 1{\cdot}5$, the right-hand side is equal to 0·578, approximately midway between the above extremes.

4. MATERIAL, HEAT TREATMENT AND SPECIMENS

The material used was steel, part of a batch given by the English Steel Corporation to the University of Bristol. The steel had been rolled to a 2½in. diameter bar from a single ingot. Samples of steel from the rolled bar showed little variation from the following composition :

C	Ni	Cr	Mo	Mn	Si	S	P
0·30%	2·55%	0·58%	0·59%	0·65%	0·15%	0·012%	0·013%

The bar was cut into lengths of 13½ ins., which were individually heat-treated by oil quenching from 850°C and tempering at 660°C.

From each of three lengths of 6½ ins., five specimens were taken, giving fifteen in all. Three of these were solid torsion specimens, one from each length, having a diameter of 0·500 ins. in a 2 in. gauge length and a transition radius of 1½ins. The enlarged ends, of 0·875 in. diameter, were ground to fit torsion couplings which ensure that a pure torque is applied. The tubular specimens (Fig. 2) had an approximate bore diameter of 9/32 ins. over a gauge length of 1·625 ins., and a transition radius of 1½ ins. The nominal wall-ratio b/a was 1·5, but the actual values were slightly less (Table 2). Set screws in the ends supported the high-pressure Poulter seals. At one end a longer enlarged portion accommodated a collar taking the high-pressure pipe connection.

The tubes were particularly difficult to produce as the bore was small and rather long, while the toughness of the material made it difficult to prevent the drill from wandering. A method was finally developed which enabled the axes of the bore and external surface to be made coincident to a high degree of accuracy (sections of a tube chosen at random showed no variation in wall thickness greater

Vol 2 1953/

than 0·0005 in.). After machining, all specimens were stress-relieved by heat treatment at 600°C. for one hour (in a high vacuum furnace described by MORRISON 1939).

5. APPARATUS AND TESTING TECHNIQUE

The general arrangement of the combined torsion and internal pressure machine is shown in Fig. 2. The specimen is arranged in tandem with a calibrated torque bar, the free end of which is attached to the fixed head of the torsion machine through a self-aligning torsion coupling. One end of the specimen is keyed to the torque bar; the other is connected to the moving head of the torsion machine through another self-aligning coupling. These couplings consist of an inner member keyed to the specimen or torque bar respectively, and an outer member fixed to the moving or stationary heads. The torque is transmitted through two steel balls in the outer member; these are symmetrically disposed about the centre line and bear on two hardened steel inserts in the inner member. With this form of coupling only a pure torque about the axis of the specimen can be transmitted.

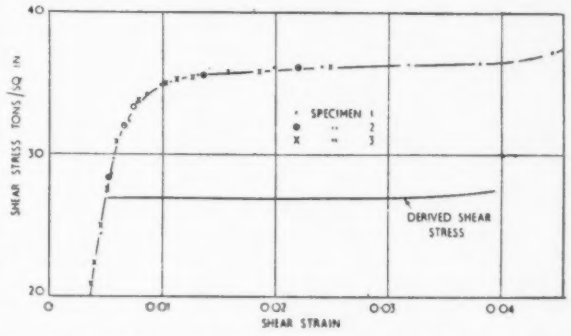

Fig. 2. Derived shear stress-strain curve from torsion tests.

The specimen is connected to a high-pressure hand-operated intensifier by a long tube arranged parallel to the axis of the torsion machine. The intensifier consists of a high-pressure cylinder fitted with inlet and outlet ball valves into which can be pushed a ram. Pressures up to 6 tons/sq.in. are obtained by reciprocating the ram with a hand-operated lever mechanism; pressures up to 30 tons/sq.in. are obtained by pushing the ram into the cylinder with a 10 ton hydraulic jack. A special seal prevents leakage round the ram, and an oil that does not freeze at these pressures is used in the high-pressure system.

The pressure could be observed on a Bourdon-type gauge, but for greater accuracy a thick cylinder fitted with a diametral extensometer was used. This cylinder and extensometer were calibrated against two dead-weight testers, one at Messrs. Budenberg Gauge Co. and the other at Messrs. I.C.I. (Winnington), with very good agreement.

To minimize the effects of possible eccentricity or non-uniform material properties, an average diametral dilatation was obtained from a double extensometer on two perpendicular diameters (Fig. 3). This is a considerably modified version of one used by COOK (1934). A change δ in the diameter BF causes the knife-edge to rotate through $Y\delta/XZ$ radians, where the distances X, Y, Z are as indicated in the Figure. This rotation is obtained from the relative movement of two mirrors, one attached to the knife-edge and the other to the arm AGE. The torsional twist is determined by observing the relative movement of two other mirrors attached

Vol. 2 53/54

to clips fixed at each end of the gauge length. The torque is derived from the optically-measured twist in the torque bar.

In the pure torsion tests the load was raised in smaller increments as the point of yielding was approached. After yield, waits of three minutes were made to allow each reading to become reasonably steady.

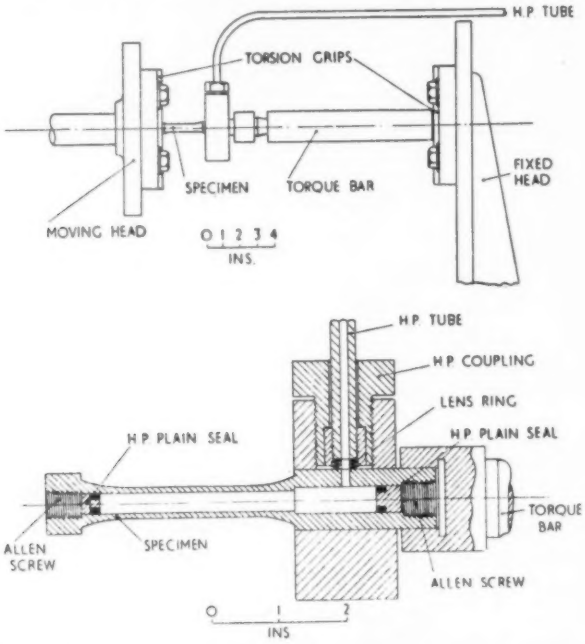

Fig. 3. Apparatus for tests on thick cylinders subjected to internal pressure and torsion.

All the tubes except No. 7 were autofrettaged to an extent such that $c/a = 1{\cdot}25$. The pressure was applied in small increments; since each additional compression caused the oil temperature to rise slightly, readings were not taken until five minutes had elapsed. The pressure was increased until the external diametral strain was $c^2/a^2 \times$ its value at the elastic limit, which was calculated from data derived from the pure torsion test. After autofrettage the tubes were subjected to a low-temperature heat treatment at 250°C in an oil bath for three hours.

The procedure in the combined stress experiments was as follows. Each tube was first twisted elastically with no pressure tube fitted, and then with the tube connected but no pressure applied; in this way the proportion of the torque carried by the tube was determined and a correction applied in the subsequent experiments. The pressure was next raised to the desired value and thereafter kept constant. Then the torque was applied incrementally and monotonically until a strain was reached where the effects of strain hardening became apparent.

5. Material Properties

The results of the torsion tests on the three solid specimens are shown in Fig. 4, where $2T/\pi R^3$ is plotted as the ordinate (T = torque, R = radius). There is

evidently no significant variation in properties along the length of the bar. The mean shear stress-strain curve has been derived by NADAI's method and is also shown. No drop in stress at the yield point could be detected; the shear stress remain sat the steady value $k = 27$ tons/sq.in. up to a shear strain of about 0·03. The mean rigidity modulus G is 5220 tons/sq.in.

Tension tests gave a mean Young's modulus of 13340 tons/sq.in.; the derived Poisson's ratio is thus $\nu = 0{\cdot}280$. The upper yield point in tension is about 51·7 tons/sq.in. and the lower yield point 49·8 tons/sq.in. The ratio of the latter value to k is 1·84, which may be compared with the value 1·73 that would be implied by the MISES yield criterion assumed in Section 3. Much better agreement with this criterion is, however, implied by the combined stress tests.

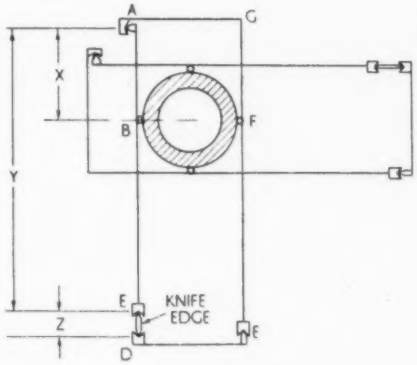

Fig. 4. Double diametral extensometer.

With these values of k, G and ν the pressure-expansion relation during autofrettage can be calculated. In terms of the radius c of the plastic zone the pressure is given by equation (2), and the external circumferential strain by

$$\frac{1 - \frac{1}{2}\nu}{1 + \nu} \cdot \frac{k}{G} \cdot \frac{c^2}{b^2} \tag{12}$$

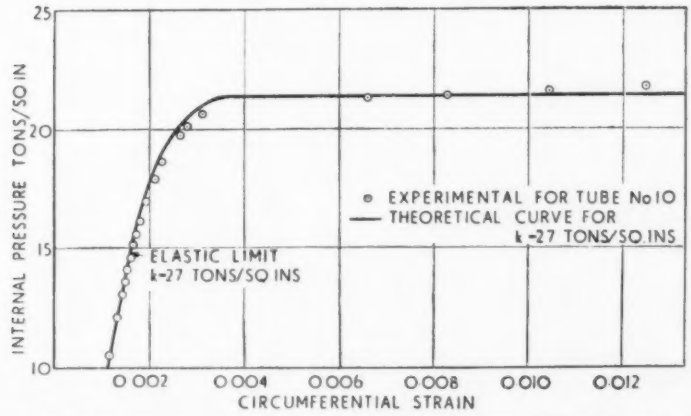

Fig. 5. Comparison of experimental and theoretical pressure v. expansion relations in autofrettage

to a close approximation (HILL 1950, p. 120). In Fig. 5 the experimental pressure-expansion relation for tube No. 10 ($b/a = 1{\cdot}484$, $b = 0{\cdot}220$in.) is compared with the calculated one for the above values of k, G and ν. Theoretically the tube should be completely plastic after a circumferential strain of amount $3{\cdot}5 \times 10^{-3}$, while, according to Fig. 2 and a rough estimate of the maximum shear strain at the bore (HILL 1950, p. 123), the tube begins to harden after a circumferential strain

of about 9×10^{-3}. The agreement with the theoretical maximum pressure is thus entirely satisfactory.

The agreement while the tube is partially plastic is less good, however. It is believed that this is due to the testing technique. After the pressure had been raised to some desired value it was necessary to release the pressure in the intensifier. During this release there was a measurable fall in pressure while the ball valve on the delivery side of the intensifier was closing, and subsequently a further fall as the temperature returned to normal. The pressure finally read was therefore lower than the maximum pressure actually reached, and the plastic strain greater than predicted. A similar discrepancy occurred during the autofrettaging of the tubes used in the main tests.

6. Results of Combined Stress Experiments

TABLE 2

No. of tube	b/a	b in.	P tons/sq.in.	T tons-in.	P/P_0	T/T_0	$\sqrt{(P^2/P_0^2 + T^2/T_0^2)}$ Experimental	$\frac{1}{2}\lambda$ Theory
4	1·492	0·211	0	0·370	0	1·000	1·000	1	0
5	1·477	0·218	8·7	0·368	0·411	0·902	0·991	1·001	0·125
6	1·499	0·212	11·9	0·320	0·543	0·848	1·007	1·008	0·176
7	1·498	0·222	15·4	0·323	0·705	0·735	1·018	1·014	0·277
8	1·483	0·209	17·3	0·213	0·812	0·588	1·002	1·015	0·420
9	1·494	0·211	20·1	0·158	0·926	0·422	1·017	1·005	0·679

Note: All tubes except No. 7 were autofrettaged to $c/a = 1{\cdot}25$.

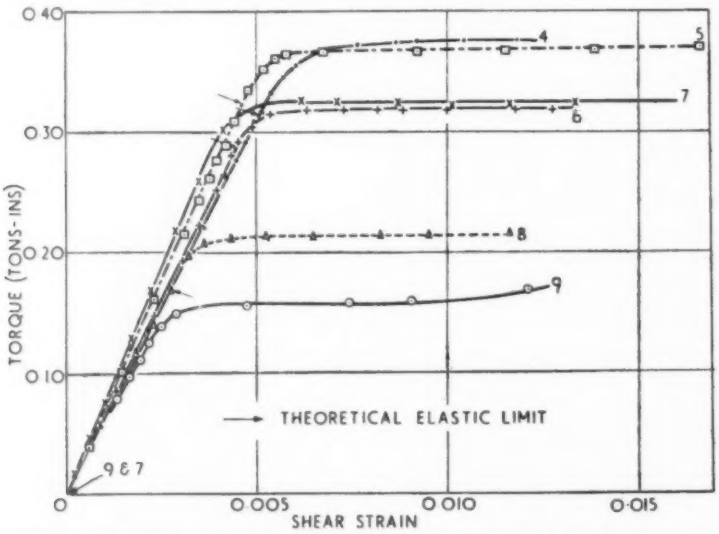

Fig. 6. Torque *v.* shear strain curves for tubes under various pressures.

The torque-twist relations for tubes under various constant internal pressures P are shown in Fig. 6, and the pressures themselves in Table 2. All of these tubes, with the exception of No. 7, were previously autofrettaged to an extent such that

$c/a = 1{\cdot}25$. The elastic limits, calculated as in Section 2, are indicated by arrows in the Figure. For tube No. 10 the final pressure was greater than the autofrettage pressure, while for tube No. 7, which was not autofrettaged, the pressure slightly exceeded p_0 (equation (1)); in both cases the elastic limit was exceeded as soon as the first increment of torque was applied. The rigidity moduli deduced from the slopes of the linear portions agree within 1% of the value measured with a solid specimen.

It will be observed that the torque reaches a steady value which is maintained for an appreciable range of strain before the effects of work hardening and changes in geometry become noticeable. More refined technique would no doubt show, in accordance with the discussion in Section 1, that a strictly steady value is not actually attained. However, within the present experimental error, we may take the ordinate T of the horizontal part of the torque-twist curve as the proper quantity to compare with the theoretical yield point of a plastic-rigid material. The experimental values of T for the various pressures P are shown in Table 2.

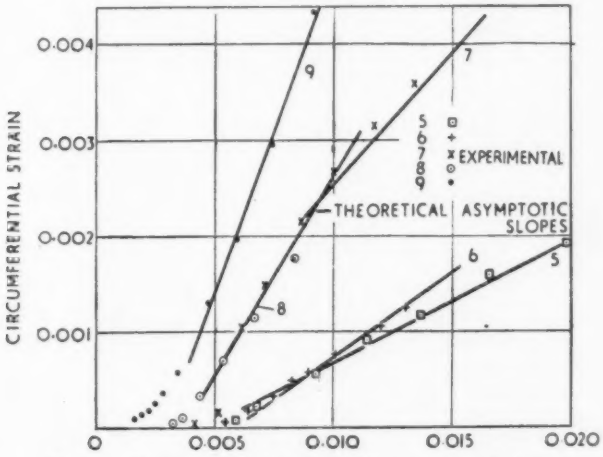

Fig. 7. Circumferential strain v. shear strain relations.

Then follow columns for P/P_c and T/T_0, where P_0 and T_0 are calculated from equations (9) with $k = 27$ tons/sq.in. and the actual values of a and b for each tube. Subsequent columns compare the theoretical and experimental values of $\sqrt{(P^2/P_0^2 + T^2/T_0^2)}$ for each of the actual non-dimensional load-ratios $(P/P_0)/(T/T_0)$.

The general agreement is excellent and virtually within experimental error. We conclude, first, that the behaviour of this material is substantially in accord with the Mises yield function and potential; second, that the relation between the applied loads at collapse is not dependent on the initial residual stresses (in this case those remaining after autofrettage); third, that the collapse values can be calculated to sufficient accuracy as those at the yield point of a plastic-rigid material. Although the outcome seems reasonably certain, it would evidently be desirable to examine whether the conclusions hold also for other distributions of residual stresses and for other subsequent loading-paths; i.e. by initially over-

straining the tubes under arbitrary combinations of pressure and torsion, and then loading with different combinations of these. It is hoped to continue the investigations further on these lines, and also to obtain more data on the rapidity of approach to the collapse values.

In Fig. 7 the relations between the external circumferential and shear strains are shown (the somewhat erratic curve No. 7 is attributed to an abnormal eccentricity in this tube discovered after the test). Theoretically (work-hardening and dimensional changes apart), the slope of each curve should approach asymptotically to a constant value. This should be comparable with the quantity $\frac{1}{2}\lambda$ defined in (8) and given in the last column of Table 2. This was obtained by interpolation of the last column in Table 1, with slight adjustments to allow for the difference of the actual values of b/a from 1·5. Lines with slopes $\frac{1}{2}\lambda$ are drawn on Fig. 7 in arbitrary positions of best fit to the experimental points. The overall agreement is satisfactory and there is no obvious indication that it could be improved by choosing a slightly different plastic potential. An indication that the Mises potential might be slightly in error for this steel was, however, provided by some measurements of the permanent axial extension which appeared to be increasing at a small non-zero rate throughout the latter stages of the tests.

REFERENCES

BAKER, J. F.	1949	*J. Inst. Civ. Eng.*, **27**, 188.
COOK, G.	1934	*Proc. Inst. Mech. Eng.*, **126**, 407.
CROSSLAND, B.	1953	*Dissertation* (University of Bristol).
GAYDON, F. A.	1952	*Qu. J. Mech. Appl. Math.*, **5**, 29.
GREENBERG, H. J. and PRAGER, W.	1951	*Proc. Amer. Soc. Civ. Eng.*, **77**, Separate No. 59.
HILL, R.	1950	*Mathematical Theory of Plasticity* (Clarendon Press).
	1951	*Phil. Mag.*, **42**, 868.
	1952	*Phil. Mag.*, **43**, 560.
HILL, R. and SIEBEL, M. P. L.	1951	*Phil. Mag.*, **42**, 722.
	1953	*J. Mech. Phys. Solids*, **1**, 207.
MORRISON, J. L. M.	1939	*Proc. Inst. Mech. Eng.* **142**, 193.
ONAT, E. T. and SHIELD, R. T.	1953	*J. Appl. Mech.*, in press.
PRAGER, W. and HODGE, P. G.	1951	*Theory of Perfectly Plastic Solids* (Wiley and Sons).
SIEBEL, M. P. L.	1953	*J. Mech. Phys. Solids*, **1**, 189.
SYMONDS, P. S. and NEAL, B. G.	1951	*J. Franklin Inst.*, **252**, 383 and 469.
	1952	*J. Aero. Sci.*, **19**, 15.

Journal of the Mechanics and Physics of Solids, 1953, Vol. 2, pp. 39 to 42. Pergamon Press Ltd., London.

CALCULATIONS ON SHEET-DRAWING UNDER BACK TENSION THROUGH A ROUGH WEDGE-SHAPED DIE

By J. F. W. Bishop
Mechanical Engineering Research Laboratory, D.S.I.R.

(*Received 30th July*, 1953)

Summary

Calculations of the drawing stress based on the Hill-Tupper theory of sheet-drawing are reported. In the range of reductions considered, the plastically deforming region extends over a finite length of the axis. The results are summarized in terms of a single empirical formula which expresses the drawing stress as a function of die semi-angle, coefficient of friction, reduction and back-tension.

Vol. 2 53/54

1. Introduction

In a recent paper Green and Hill (1952) have considered the problem of sheet-drawing through smooth and rough wedge-shaped dies without back-tension. Their calculations are based on the slip-line field theory of Hill and Tupper (1948) and the limit load theorems of Hill (1951) for a plastic-rigid material. For a smooth die, they consider reductions of thickness ranging from the bulge-limit to cases where the plastically-deforming region extends over a finite portion of the axis of symmetry : with rough dies, their calculations are limited to the range in which this region intersects the axis in a single point. In this latter case Hill (1953) has given formulae for the influence of back-tension. The present calculations, based on the slip-line field theory of Hill and Tupper, extend this range to reductions for which the plastically deforming region extends over a finite portion of the axis, and where the velocity discontinuity along the arrowed slip-lines terminates at the die exit (Fig. 1).

2. The Slip-Line Field

In the present calculations it is assumed that the coefficient of friction μ is constant on the die face. If the mean tensile stress t in the drawn sheet is regarded as known, the details of the slip-line field may be found as follows. The hydrostatic pressure p_0 on OA is given by $p_0 = k - t$, where k is the yield stress in pure shear. It can be shown by an application of Hencky's theorem that if θ is the inclination of OB to the die face and α is the semi-angle of the die,

$$\mu = \frac{\cos 2\theta}{p_0/k + 2(\pi/4 + \alpha - \theta) + \sin 2\theta},$$

$$\text{i.e. } p_0/k + 2(\pi/4 + \alpha) = \frac{1}{\mu}\cos 2\theta + 2\theta - \sin 2\theta.$$

From a graph of θ against $\frac{1}{\mu}\cos 2\theta + 2\theta - \sin 2\theta$ for a given μ, the value of θ corresponding to a given α and p_0 is read off. Iteration in

$$\theta = \tfrac{1}{2}\cos^{-1}\left[\mu\{p_0/k + 2(\pi/4 + \alpha - \theta) + \sin 2\theta\}\right]$$

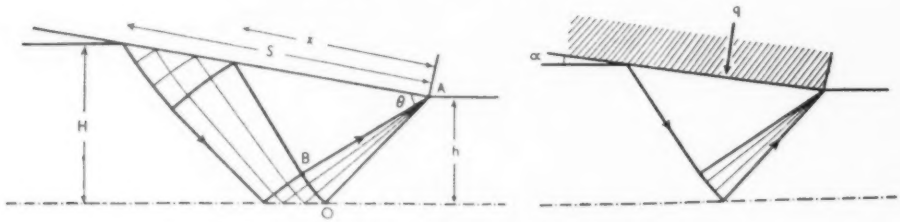

Fig. 1. Slip-line fields for the limits of reduction considered.

quickly leads to an accurate determination of θ. The angles at which the slip-lines meet the die face in the remainder of the field are found from a slight modification of these equations. The distribution of die pressure is readily found from these angles and an application of Hencky's theorem, and the back tension is obtained from the die pressure by integration along the die face.

The slip-line fields have been constructed graphically using a 5° net for coefficients of friction 0·05, 0·10 and 1·15 with die semi-angles 5°, 10° and 15° for each value of μ. The method used is that described by HILL (1950, p. 141) in which the arcs

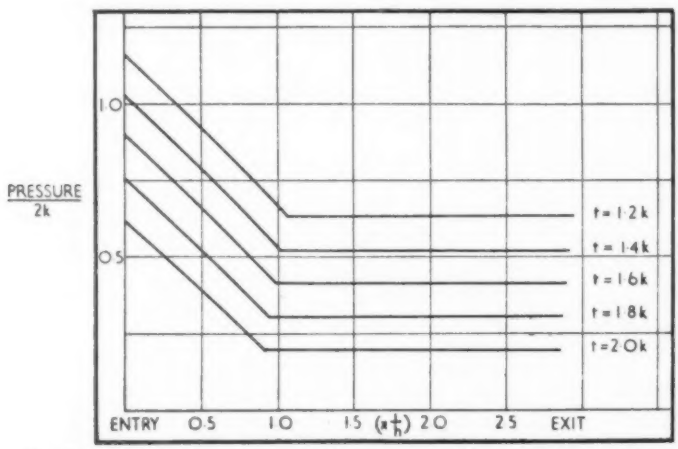

Fig. 2. Distribution of normal die pressure with $\alpha = 10°$, $\mu = 0{\cdot}10$.

of the slip-lines are replaced by chords having an inclination which is the mean of the terminal slopes. Values of p_0 were taken for each pair of values of α and μ to provide reasonable coverage between the upper limit at which the drawn sheet is just at the yield point, and the lower where the back-tension is zero. A typical set of results is shown in Fig. 2 for given α and μ and varying drawing stress.

The drawing stress may be regarded as a function of the die semi-angle, the coefficient of friction, the reduction and the back-tension. Since graphical or

tabular presentation of the data would require a prohibitive amount of space, the results have been fitted by an empirical formula.

3. Empirical Formula

It will be assumed that distribution along the die of the normal die pressure is composed of a constant part and a linearly increasing part. The typical results given in Fig. 2 show that the departure from linearity in the region in which the die pressure is not constant is very small. In order to construct an empirical formula it is therefore necessary only to find the magnitude q of the constant pressure and the length of die x over which it acts, and the rate of increase of the rising pressure. This is conveniently expressed by the slope γ of the inclined portion of the graph plotted as in Fig. 2.

If $p_0 = -nk$, it is found that the normal pressure q and the slope γ are given empirically by

$$q = k \exp \mu (1 + 2\alpha - n),$$

$$\gamma = \tfrac{1}{2} (1 - \tan \alpha + 3/2\, \mu),$$

and the length x is expressed analytically by

$$x = 2h (1 + \mu q/k)^{-\frac{1}{4}},$$

where h is the semi-thickness of the drawn sheet. If s is the total contact length on the die face, the axial component of the die load acting on one face of the die is found to be

$$Q = (\sin \alpha + \mu \cos \alpha) \left\{ qs + \frac{k\gamma (s - x)^2}{h} \right\}. \tag{1}$$

The back-tension σ can be shown to be

$$\sigma = \{k (1 + n) - Q/h\} (1 - r), \tag{2}$$

where r, the reduction is defined by $r = (H - h)/H$ being the semi-thickness of the undrawn sheet. In order to express the drawing stress as a function of the die semi-angle, the coefficient of friction, the reduction and the back-tension, this expression must be inverted. This can be effected by using a suitable power series expansion, and in terms of

$$\lambda = \mu \cot \alpha,$$

$$\tau = (1 + \lambda) \exp \mu \{r + 2\mu\gamma (r - 2 \sqrt{1 - r} \sin \alpha)\},$$

$$\nu = k\gamma (1 + \lambda) \{r - 2 \sqrt{1 - r} \sin \alpha\}^2/(1 - r) \sin \alpha,$$

the drawing stress is given by

$$t = \frac{\sigma + 2k\tau (1 + \alpha) + \nu}{1 - r + \tau}. \tag{3}$$

The back-pull factor, defined by

$$b = -\frac{1}{H} \frac{dQ}{d\sigma}$$

is found to be

$$b = \frac{\tau}{1 - r + \tau}. \tag{4}$$

In the special case of a smooth die with $r = \dfrac{2 \sin \alpha}{1 + 2 \sin \alpha}$, the expression for t reduces to $t = \sigma + 2kr\,(1 + \alpha)$, which is analytically correct. The values computed from formula (3) agree very closely with the relevant values given by Green and Hill in their Table 1 for a smooth die, and the values given by Hill and Tupper for rough dies at specific reductions. The error involved in (3) is thought not to exceed $\pm\ 0{\cdot}005k$ in the range $0 \leqslant \alpha \leqslant 15°$, $0 \leqslant \mu \leqslant 0{\cdot}15$.

4. Discussion

The back-pull factor given by (4) is a function of μ, r and α. From a more accurate determination based on (1) and (2), it can be shown to be a function also of the back-tension. It will be recalled that Hill (1953) has remarked that the die load is not strictly proportional to the back-pull in the range that he considered. Again, however, the departure from linearity is not marked, and formula (4) is in error by a negligible amount.

Consideration of typical cases shows that MacLellan's (1948) formula

$$b = 1 - (1 - r)^{1 + \lambda}$$

based on Sachs' theory of homogeneous deformation is a good approximation from below to the value derived here. For example, when $r = 0{\cdot}3$, $\mu = 0{\cdot}10$, and $\alpha = 10°$, both the exact value of b and the value obtained from (4) are 0·431 for all possible values of the back-tension. MacLellan's formula gives the value 0·428.

Acknowledgment

The author wishes to thank the Director of the Mechanical Engineering Research Laboratory, D.S.I.R. for permission to publish this paper.

References

Green, A. P. and Hill, R.	1952	*J. Mech. Phys. Solids*, **1**, 31.
Hill, R.	1951	*Phil. Mag.*, **42**, 868.
	1953	*J. Mech. Phys. Solids*, **1**, 142.
Hill, R. and Tupper, S. J.	1948	*J. Iron and Steel Inst.*, **159**, 353.
MacLellan, G. D. S.	1948	*J. Iron and Steel Inst.*, **158**, 347.

Journal of the Mechanics and Physics of Solids, 1953, Vol. 2, pp. 43 to 53. Pergamon Press Ltd., London.

ON THE COMPLETE SOLUTION TO PROBLEMS OF DEFORMATION OF A PLASTIC-RIGID MATERIAL

By J. F. W. Bishop
Mechanical Engineering Research Laboratory, D.S.I.R.

(*Received 30th July*, 1953)

Summary

The problem of finding an equilibrium distribution of stress not exceeding the yield point in the assumed rigid regions of a deforming body is considered. Theorems, based on the limit-load theorems of Hill, are given for determining whether such a stress distribution exists. A method is given for constructing a stress solution in the rigid region, and illustrated by consideration of the yielding of notched bars in plane strain and plane stress, and extrusion under plane strain conditions.

Vol.
2
53/54

1. Introduction

Three groups of differential equations describe the mechanics of deformation of a non-hardening plastic-rigid material, namely the stress equilibrium equations, the stress-strain relations and the equations relating strain and displacement. In general an infinity of stress states will satisfy the stress boundary conditions, the equilibrium equations and the yield criterion *alone*, and an infinite number of displacement modes will be compatible with a continuous distortion satisfying the displacement boundary conditions. As in the classical theory of elasticity, use has to be made of the stress-strain relations to determine whether given stress and displacement states correspond. In contradistinction to elasticity theory, however, there is no unique solution for the material under consideration. This lack of uniqueness will be considered later. With a few exceptions, the majority of solutions so far obtained have been to problems in plane stress or plane strain. The solutions normally presented consist of a deformation mode valid for the entire body considered, and a compatible stress solution for the region containing the plastically deforming material. The acceptability of such a solution depends on whether it is possible to find a stress solution, satisfying the boundary conditions and equilibrium equations for the region assumed to be rigid, that does not violate the yield conditions (see Hill, 1950a, pp. 161-163). These " partial " solutions will be called *incomplete* solutions, and ones for which the stress solution has been extended to the whole body concerned, *complete* solutions. The present paper contains a method for completing partial solutions, and discusses the significance of the complete solutions.

2. Limit Theorems

Before proceeding to a general formulation of the problem, it is helpful to consider the meaning of the incomplete solutions in the light of the limit theorems

for yield-point loads. These are the loads at which a body subjected to some given loading sequence first deforms. The theorems relevant to a plastic-rigid material are due to Hill (1951). Since they are required specifically later, they will be enunciated here in a restricted form.

Consider a plastic-rigid body subjected to loads in given ratios.

(i) *Lower bound.* The yield-point loads determined from a distribution of stress that satisfies the equilibrium equations and stress boundary conditions and which nowhere violates the yield criterion, are *not greater* than the actual yield-point loads.

(ii) *Upper bound.* The yield-point loads, determined by equating the external work to the internal work done in a deformation mode satisfying the displacement boundary conditions by that stress distribution needed to enforce it at each point, are *not less* than the actual yield-point loads. The stress distribution need not be in equilibrium and is only defined where the strain-rate is non-zero.

Steady state problems can of course be considered under this formalism by treating them as instantaneous yield-point problems. The partial stress field obtained in an incomplete solution does not meet the requirements of the lower bound theorem since it is not demonstrated that an equilibrium stress distribution satisfying the boundary conditions and not exceeding the yield point exists in the assumed rigid region. The velocity or displacement solution, however, is precisely that required by the second theorem. Hence incomplete solutions are strictly only upper bound solutions.

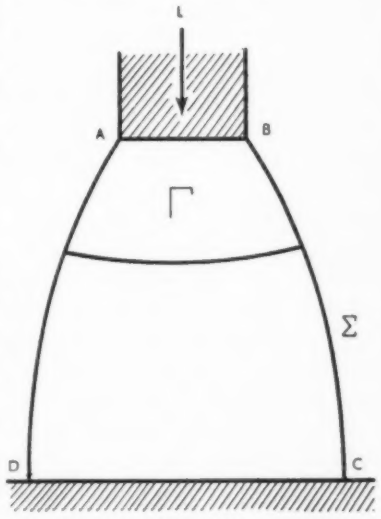

Fig. 1.

Suppose, however, that the partial stress distribution in the incomplete solution can be extended to the entire body, satisfying the equilibrium equations, the yield criterion and the boundary conditions. It is now acceptable as a lower bound solution. But the yield-point loads determined from the upper and lower bound solutions are the same since the solutions are compatible in the region in which deformation is occurring. Hence the actual yield-point loads will have been found. A further theorem due to Hill (1951) states that where deformation is actually occurring in any mode, the stress found is the actual state. The particular deformation mode obtained is *not* necessarily the actual one however.

3. Formulation of the Problem

In this section, the problem involved in extending a partial stress solution will be examined. Consider a body bounded by the surface Σ (Fig. 1). Suppose a partial stress distribution in equilibrium with the load L is known in the region Γ. Over the remainder of the surface (which may extend to infinity) it is assumed that either the surface forces or the areas supporting forces in statical equilibrium

with the applied loads are known. Thus in Fig. 1, it is assumed that the surface CD supports the load L applied at AB, and that the remainder of the surface Σ is stress-free. If a valid deformation mode has been found such that all the deformation occurs in Γ, the following problem arises : given the forces acting at each point of portions S_F of the surface of a body, and the loads applied over the remaining area S_L, find a stress distribution satisfying these boundary conditions and the equilibrium equations which does not violate the yield criterion. (It is assumed that the forces acting at *each point* of S_L are not known).

The *two*-dimensional problem may be stated in rather different terms. If a function Φ is defined by

$$\sigma_x = \frac{\partial^2 \Phi}{\partial y^2}, \qquad \sigma_y = \frac{\partial^2 \Phi}{\partial x^2}, \qquad \tau_{xy} = -\frac{\partial^2 \Phi}{\partial x \, \partial y},$$

where σ_x, σ_y and τ_{xy} are the stress components, it is required to find a twice differentiable function whose second derivatives satisfy certain relations at the boundaries, and an inequality (expressing the yield criterion) everywhere. Geometrically this may be interpreted as finding a surface in x, y, Φ space with restrictions on the curvature round some locus in the x, y plane (i.e. the boundaries) and such that some function of the curvature satisfies a given inequality. It is clear that a unique solution is not to be expected. This lack of uniqueness is a serious drawback to expanding Φ in a power series form since the coefficients cannot be determined uniquely by inserting the boundary conditions. In any event, this approach is open to the criticism that no statement as to the possible existence of a complete solution can be made unless one of the functions Φ provides a solution for which the yield criterion is nowhere exceeded. Moreover, even disregarding the inequality expressing the yield conditions, it is not usually found possible to find a function Φ satisfying the boundary conditions. It seems that these weaknesses are inherent in any method which incorporates the boundary conditions as given in the problem. As will become clear later, this difficulty may be avoided by using an inverse method of approach in which boundaries related to the partial stress solution are used.

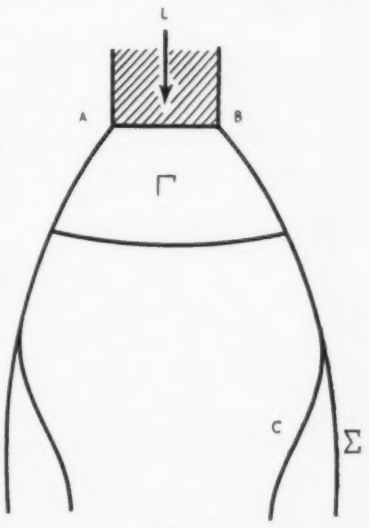

Fig. 2.

4. General Method

Since the incorporation of an inequality as a limiting condition is difficult to handle mathematically, it is easier to work with fully plastic stress states than with ones that merely do not violate the yield criterion.

Consider first the problem of a body with a stress free surface Σ apart from areas over which prescribed loads and statical equilibrium loads are applied

(Fig. 2). Let Γ be a (known) fully plastic region in equilibrium with the load L and containing a compatible deformation mode. A fully plastic continuation of the stress solution in Γ will define a stress free surface C. (Methods for doing this are discussed later). Σ and C may either terminate at a supporting surface as in Fig. 1, or extend to infinity as, for example, in the notched bar problems discussed later.

Theorem 1. If C lies wholly within or upon Σ, a complete solution exists, and the actual yield-point load has been found.

The stress solution obtained in C constitutes a valid lower bound for Σ since the region intervening can be regarded as stress free. But the upper bound must coincide with this lower bound since it is obtained from a compatible deformation mode, and hence the exact yield-point load has been found. If C lies outside Σ wholly or in part, the deformation mode contained in Γ must be extended in C until deformation can occur in a region lying outside Σ. This mode must be compatible with the stress solution in C.

Theorem 2. If C lies outside Σ wholly or in part so as to include a region in which deformation can occur, a complete solution does not exist and the yield-point load has been exceeded.

The deformation mode, extending to include a region between C and Σ in which deformation can occur, gives an upper bound to the yield-point load for C which has the same value as that determined from the partial stress solution. This is so since the extended deformation solution is compatible with the stress solution in C. An upper bound for Σ can be obtained from that part of this deformation mode which it contains. Since deformation occurs in the region lying outside Σ, this upper bound is *less* than that for C. But the upper bound for C corresponded to the load obtained from the partial stress solution. Hence a complete solution does not exist for that load applied to Σ.

It is obvious that it is not *essential* to continue the partial stress solution as a *fully* plastic state. Examples are given later in which use is made of partially non-plastic stress distributions.

If the surface Σ is not stress free (e.g. the material in an extrusion chamber does not have such a surface), these theorems are not directly applicable to the whole problem. The following theorem is valid for fixed rigid constraints at which no relative motion occurs.

Theorem 3. If an incomplete solution exists to the actual problem, and a complete solution can be shown to exist where all stress boundary conditions except those at the specified constraints are satisfied, then a complete solution exists for the actual boundary conditions.

To prove the theorem, use is made of a lemma which is an immediate derivation from Hill's (1948) maximum work principle.

Lemma : Consider a stress distribution satisfying the stress boundary conditions, the equilibrium equations and the yield criterion, and a compatible deformation mode satisfying the displacement boundary conditions. This distribution of stress does not do less work in the given displacements than a distribution of stress that satisfies only the equilibrium equations and the yield criterion.

The application of this lemma to the problem under consideration shows that a yield point load derived from the external work done under the modified boundary

conditions in the specified displacements can be used as a lower bound for the actual problem. This lower bound will coincide with the upper bound obtained from the deformation mode, since the bounds are derived from a complete solution. Further, since no work is done at the constraints, this upper bound is valid for both problems. Hence the yield point load for the actual problem has been found, and the theorem is established. This theorem can be used for moving rough constraints at which no relative motion occurs, or for smooth ones where there is relative motion, if the conditions of the theorem can be attained by imposing suitable velocities on the constraints and the material without modifying the problem.

If the contour C lies partly inside and partly outside Σ, a modified form of Theorem 2 must be employed. Suppose the deformation mode can be extended in C such that it is compatible with the stress solution and such that those portions of Σ lying outside it remain rigid, with deformation possible in portions of C lying outside Σ. An analogous argument to the proof of Theorem 2 shows that a complete solution does not exist.

To illustrate the use of these theorems, consider the plane strain systems shown in Fig. 3. In (a), (b) and (c) the platens are smooth, while the frictional conditions in (d) are unspecified. Incomplete solutions consist of a compressive stress $2k$ in ABF, k being the yield stress in pure shear, with a velocity discontinuity along AB. The dotted lines in (a), (b) and (c) show the fully plastic surfaces obtained from continuing the partial stress solutions as a uniaxial compression of amount $2k$. Use of Theorem 1 shows that the yield point stress of (a) is $2k$ and that a complete solution exists. To apply Theorem 2 to (b) and (c), the velocity discontinuity CD is used. It follows that the average applied stress $2k$ exceeds the yield point loading. For (d), the use of a stress distribution consisting of a simple compressive stress $2k$ throughout in conjunction with Theorem 3 shows that the average yield point stress is $2k$.

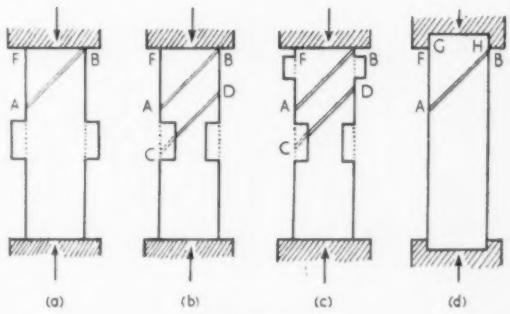

Fig. 3.

5. Stress Discontinuities

In the examples to be considered, use is made of curved stress discontinuities, and a short discussion is given here. For a consideration of straight discontinuities and the relevant literature, see Prager and Hodge (1951, p. 154 et seq.). This part of the discussion is limited to plane strain conditions, since the extension to general deformations is not required for the purpose in hand. Reference will be made to the notation used by Hill (1950a, p. 132 et seq. and p. 157 et seq.).

If p is the mean compressive stress, Hill shows that

$$|p - p'| = 2k \sin 2\theta, \tag{1}$$

where p, p' and θ are as in Fig. 4a. If Δp is the increment in p on crossing the discontinuity, and $\Delta\phi$ the angle turned through in a counterclockwise direction by a slip-line on crossing the discontinuity, the following relations can be derived from (1).

$$\begin{aligned} \Delta p + 2k \sin \Delta\phi &= 0 \text{ on an } \alpha \text{ line,} \\ \Delta p - 2k \sin \Delta\phi &= 0 \text{ on a } \beta \text{ line.} \end{aligned} \tag{2}$$

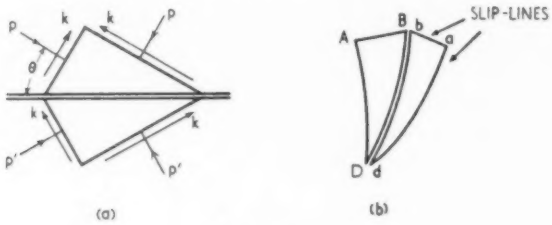

(a) (b)

Fig. 4.

It will be remarked that when the discontinuity becomes vanishingly weak, the normal slip-line field relations are recovered, namely,

$$\begin{aligned} dp + 2k\, d\phi &= 0 \text{ on an } \alpha \text{ line,} \\ dp - 2k\, d\phi &= 0 \text{ on a } \beta \text{ line.} \end{aligned}$$

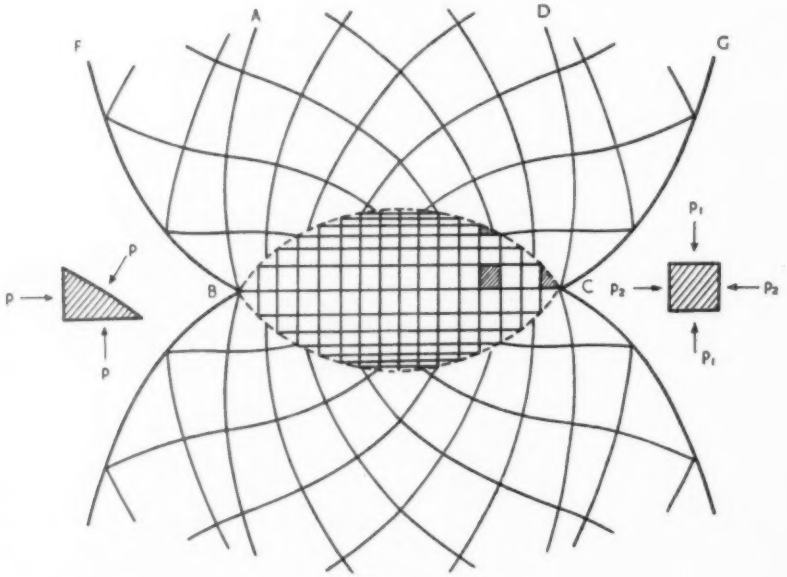

Fig. 5.

If the relations (2) are applied to the discontinuity shown in Fig. 4b, elimination of p leads to

$$2\phi_a = \phi_d - \phi_D - \sin \phi_{Dd} + \phi_b - \phi_B - \sin \phi_{Bb} + 2\phi_A,$$

where the angles ϕ_n are measured from some fixed, arbitrary direction. ϕ_{Dd} and ϕ_{Bb} are the angles turned through in a counterclockwise direction in proceeding along $ABba$, $ADda$ respectively.

Finally a specific plastic-rigid interface will be examined. Suppose two symmetrical slip-lines AB, DC have been obtained (Fig. 5). Let BF, CG be a stress free surface. The value of the normal stress acting across the principal stress trajectory terminating in B and C, and shown dotted, will have some determinate value. For convenience, the boundary BC has been resolved into a series of line elements over which the pressure is approximately constant. Consider a stress field consisting of a hydrostatic stress in the triangular regions illustrated, and an equilibrium biaxial stress in the rectangular portions. The values of the stress components at any point will have the same values as the normal pressure transmitted across BC at the points in which the horizontal and vertical columns containing the point terminate. If the number of line elements is made infinite, an equilibrium stress field has been found to support the stress transmitted across BC. Provided the maximum difference in the normal stress does not exceed $2k$, the yield criterion will not be violated, and the stress solution above BC may be reproduced as a mirror image below it. Alternatively, in this example, the straight line BC can be taken as a further discontinuity with material in a parallel-sided column below it stressed uniaxially perpendicular to BC. In the examples, both this discontinuity and a variant of it will be employed.

Vol. 2 53/54

6. Yielding of V-Notched Bars

As an example of the use of the theorems given, consider the yielding of symmetrically notched bars in tension under plane strain conditions. The incomplete solution to this problem is due to Hill (1949). In Fig. 6 one half of a bar of notch semi-angle $\pi/2 - \alpha$ is shown with CC' the transverse axis of symmetry. The slip-line OA and the condition of symmetry uniquely determines the fully plastic region OAB (in the absence of stress discontinuities). AB determines the stress free surface $AFGHK$ (see Hill 1950a, p. 147), and the solution can be continued until BJ is reached where the slip-lines of one family run together. This configuration is termed a limit line by Prager and Hodge (1951, p. 149). It is possible

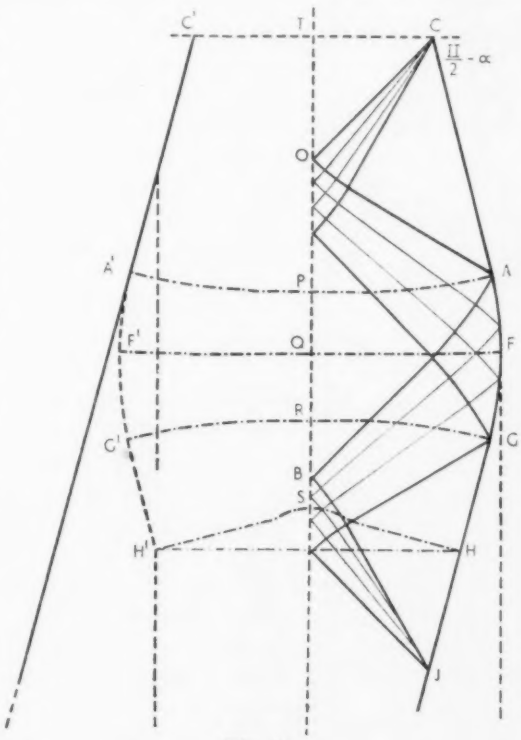

Fig. 6.

to continue the solution beyond BJ by inserting a stress discontinuity ahead of it, and an example is given later. For the case illustrated there are several alternative methods of procedure.

(i) If the specimen sides are considered to diverge indefinitely, (a situation more relevant to the analogous example of indentation), the principal stress trajectory APA' can be constructed. If this is regarded as a stress discontinuity, it can be shown that a normal uniaxial stress not exceeding the yield stress is transmitted across it for all possible notches. Consider the principal stress trajectory divided into a series of line elements over which the normal stress is approximately constant. The force on each element could be supported by a tensile column in the direction of the outward normal at the element, which, as has been stated, would not be stressed beyond the yield point. Since the trajectory is concave to the notch, an equilibrium distribution of stress could be constructed consisting of a radial fan of tensile columns with unstressed material lying between them. In the limit as the length of each line element becomes vanishingly small, the number of columns becomes infinite. This distribution satisfies Theorem 1.

(ii) If the fully plastic solution is continued as far as F where the surface is parallel to the axis of the specimen, a discontinuity line FQF'' can be constructed as shown, with the material below it stressed uniaxially parallel to the axis and satisfying the yield conditions. Again this distribution satisfies Theorem 1.

(iii) An alternative solution can be constructed by quoting the lemma given in Section 5. The discontinuity GRG' corresponds to this solution and the stress field can be extended to infinity either by alternating the solution in $CGG'C'$ and its mirror image, or by using a uniaxial tensile column terminating in GG' as stated in the lemma.

(iv) The load per unit area determined from the partial stress solution is found to be $2k\ (1 + \alpha)$, where $\pi/2 - \alpha$ is the semi-angle of the notch. This stress could be just supported by a plane strain tensile column of $1 + \alpha$ times the width at the root. The discontinuities HSH' and HH' can be constructed quite simply such that the material below HH' is stressed to the yield point in tension parallel to the axis of the bar, with the material in HSH' under biaxial stress, with one principal direction HH', and satisfying the yield criterion. If the width of the bar is not less than FF', a complete solution exists and the yield point load per unit area is $2k\ (1 + \alpha)$.

The methods detailed above can be used to examine bars with other notch shapes. The precise details of the field will be determined by the notch geometry The case of a V-notched bar with zero included angle is treated briefly since it employs the curved discontinuity line discussed in Section 5. The slip-line field shown in Fig. 7 with OA as the notch semi-width can be constructed quite straightforwardly* with the stress free surface shown, until the slip-lines of one family begin to intersect at P. The discontinuity PP' can be constructed reasonably simply using the relations given in Section 5. The strength of the discontinuity is determined by the requirement that the slip-line field immediately to the right of the discontinuity is consistent with the slip-line PQ. The discontinuity $RP'Q$ is determined from the requirement that the stress below it should be a uniaxial tension parallel to the axis ; it is found that the yield point is not exceeded in this

* I am indebted to my colleague Mr. A. C. RAPIER for drawing to my attention the ease and rapidity with which slip-line fields can be constructed using a draughting machine.

region. The minimum width of bar for which this solution is valid is the width at Q. It is found to be 8·67 times the width at the root. Thus a bar with a width not less than 8·67 times the width at the root will support the yield point load per unit area of $2k(1 + \alpha)$. HILL (1950b) has considered the problem of the minimum width of bar that will support this load. His solution, based on a rigid rotation of the corners of the bar gives a width of 8·6 times the root width. Since it is an incomplete solution, it follows that the actual critical width lies in the bracket 8·6 to 8·67.

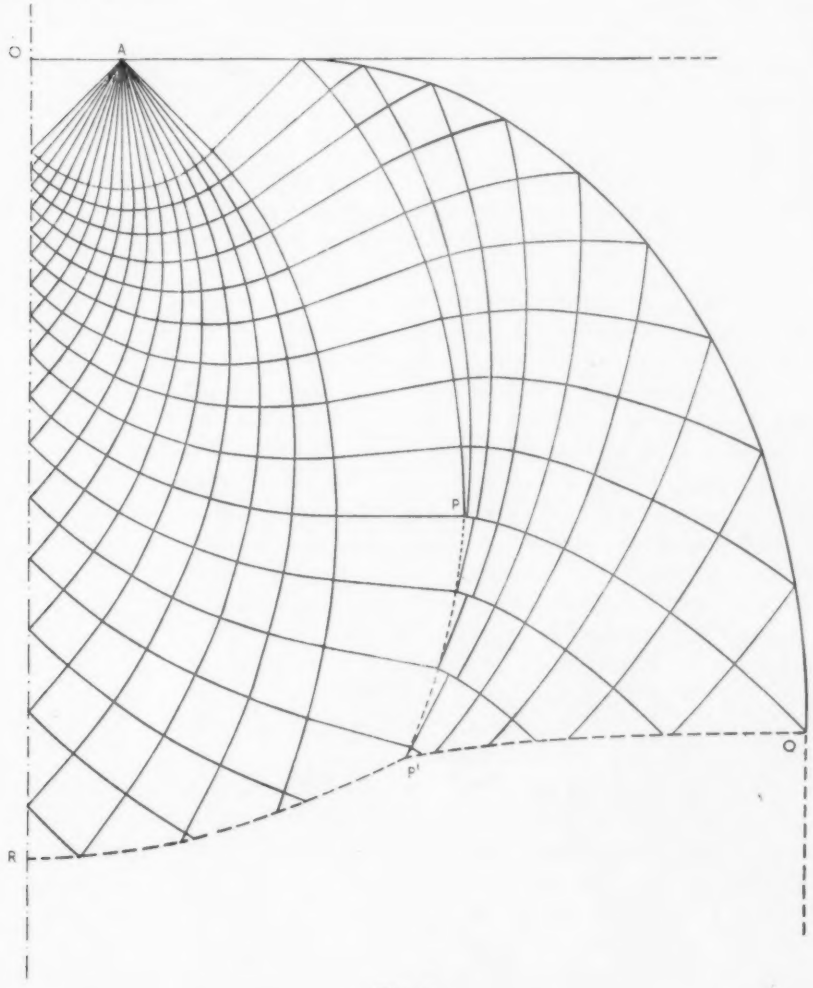

Fig. 7.

The problem of the symmetrical indentation of a bar by flat rigid dies has also been solved by HILL (1947). He finds that the critical ratio of width to indenter breadth which separates the deformation modes in which the ends of the bar separate from those in which material is forced out at the surface is 8·75. This ratio should be the same as that of OR to OA in Fig. 7, namely 8·74. These

results are felt to be striking verification of the arguments used by HILL in arriving at his results.

As an illustration of the use of Theorem 3, it is proposed to examine a particular case of direct extrusion. The incomplete solution shown in Fig. 8 consisting of the slip-line field $OACD$ is again due to HILL (1948b). Both the die face and the chamber walls are assumed to be frictionless. The deformation mode consists of velocity discontinuities along ACD and OA with AOC undergoing a continuous deformation. There is a constant relative velocity at the walls and hence the conditions of Theorem 3 can be attained. A stress distribution which satisfies the stress boundary conditions for the extruded material is shown in the figure. OAB is stressed to the yield point in uniaxial compression parallel to OB, and the material to the right of OB is unstressed. Since the conditions of Theorem 3 are attainable, it is necessary only to find a continuation of the field $OACD$ in the chamber which satisfies the equilibrium equations and the yield criterion but not the boundary conditions. The slip-line field shown satisfies these requirements. The slip-line CE is determined by AC and the axis of symmetry. CE and CD determine the field $CEFD$. If the straight line EF is continued to G, the remainder of the field is determined. The stress boundary conditions on GD are not satisfied. Thus a complete solution for the relaxed boundary conditions exists, and hence according to Theorem 3 a complete solution with the same yield point load exists to the actual problem.

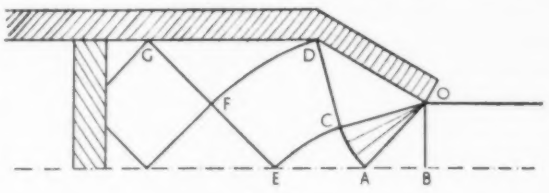

Fig. 8.

Finally an example in the yielding of a notched bar under *plane stress* conditions is considered. The solution to this problem has been given by HILL (1952a) for a material obeying the von Mises yield criterion. The reader is referred to that paper for the possible deformation modes and the details of the characteristic networks. Fig. 9 illustrates the results. The angle β is $\tan^{-1}\sqrt{2}$ and ϕ is given by $2\tan\phi + \tan 2(\alpha + 2\beta - \phi) = 0$. The stress field of the incomplete solution is bounded by the characteristic BCD. When $\alpha = 70° 32'$, the field shrinks to a pair of coincident characteristics across the neck OA.

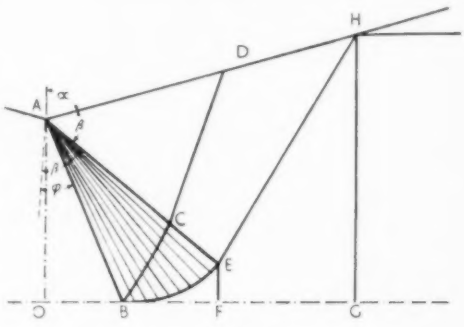

Fig. 9.

Consider a solution in which the tensile load is ultimately supported by a simple tensile column parallel to the tension axis continue the slip-line field to BEH. The discontinuities BEH, HG are determined as follows. Let $EFGH$ be stressed to the yield point with principal axes in the directions FG, GH. This determines

the principal stress component in the direction FG. The tensile stress to the right of GH has this same value, the transverse component being discontinuous across GH. The location of H is determined from the requirement of statical equilibrium of the forces acting on OA and GH. The discontinuity BE is determined by the known stress in ABE and the known horizontal stress component in BEF (which is equal to the tensile stress to the right of GH). It can be shown that the yield point is not exceeded in BEF for all possible notches. When $\alpha = 70^\circ\,32'$, B coincides with O. For smaller angles, the stress across OA remains the same as the value when $\alpha = 70^\circ\,32'$. Hence the solution for $\alpha < 70^\circ\,32'$ is the same as that for $\alpha = 70^\circ\,32'$, the material between the two boundaries being considered as stress free. Thus a complete solution exists to the plane stress problem for all possible V-notches. An analogous solution is valid under plane strain conditions, but the solution is limited to $\alpha \geqslant 26^\circ\,38'$. Thus a solution of this type cannot be used to treat the case of indentation by a flat rigid punch. R. T. Shield* has pointed out that this problem can be solved by using a curved discontinuity of the type BE but without the requirement that the load is ultimately supported by a simple compressive column.

7. Discussion

It is clear from the discussion and the examples given that there is an infinity of both stress and velocity solutions to a yield point problem in a plastic-rigid, non-hardening material. If the stress distribution in the rigid region is obtained without reference to a continuous displacement (as it has been here), it clearly cannot be regarded as the limit to the solution for a real material whose rigidity constants have become infinite. Nevertheless, the yield point loads as conceived here are the actual yield point loads for an elastic material with infinite moduli. For the significance of these loads in relation to the load-distortion curve for an actual plastic-elastic material, the reader is referred to the remarks of Hill (1951, 1952b). What relation the deformation modes obtained in the complete solutions bear to those for a plastic-elastic material is a subject for further research.

Vol. 2 53/54

Acknowledgments

The author wishes to thank Dr. R. Hill of Bristol University for valuable discussions and criticisms of the present work. Acknowledgment is made of the permission of the Director of the Mechanical Engineering Research Laboratory, D.S.I.R. to publish this paper.

References

Hill, R. 1947 *J. Iron and Steel Inst.*, **156**, 513.
1948a *Qu. J. Math. Appl. Mech.*, **1**, 18.
1948b *J. Iron and Steel Inst.*, **158**, 177.
1949 *Qu. J. Math. Appl. Mech.*, **2**, 40.
1950a *The Mathematical Theory of Plasticity* (Clarendon Press).
1950b *Phil. Mag.*, **41**, 745.
1951 *Phil. Mag.*, **42**, 868.
1952a *J. Mech. Phys. Solids*, **1**, 19.
1952b *Phil. Mag.*, **43**, 560.
Prager, W. and Hodge, P. G. 1951 *Theory of Perfectly Plastic Solids* (Chapman and Hall).

* Private communication.

Journal of the Mechanics and Physics of Solids, 1953, Vol. 2, pp. 54 to 66. Pergamon Press Ltd., London.

BUCKLING OF STRUTS UNDER DYNAMIC LOADING

By J. F. Davidson
Engineering Laboratory, University of Cambridge

(*Received 7th July*, 1953)

Summary

This paper deals with an initially curved, pin ended, strut having one end fixed in position, the other end being struck once, via a spring, by a mass, so that an impulsive axial load is applied. Two aspects of this problem have been investigated. First, simple calculations based on a theory given by Koning and Taub (1934) suggest that in practical cases stress wave and lateral bending effects are never simultaneously important. Second, complete solutions of the equations of motion suggest that, in a wide range of practical cases, strut shortening due to lateral movement does not appreciably affect strut load. These solutions were obtained on the calculating machine Edsac and have been verified by experiment. This second result gives a load time graph which is approximately a half sine wave of known period. Design curves have been drawn which use a constant strut axial load equal to the peak value of the sine wave and acting for the same period, following Koning and Taub. These curves, which err on the safe side, show that a briefly applied load may exceed the safe static load, agreeing with the conclusions of Pian and Siddall (1950). The curves also show that the allowable dynamic load is never much less than the safe static load.

1. Introduction

(i) *Historical*

The behaviour of a strut under a dynamic axial load has been treated by numerous writers. The first of these were Koning and Taub (1934), who considered, theoretically, a pin ended strut, initially curved in the form of a half sine wave, and subjected to a constant axial load P for a specified period. They showed that if $P > P_E$, the Euler load, the strut will deflect exponentially while the load is applied, and be left in a state of free oscillation after the load has been removed, the amplitude of the free oscillation being the maximum deflexion. When $P < P_E$, the maximum deflexion occurs after removal of the load only if $t_i < \pi/\omega_L (1 - P/P_E)^{\frac{1}{2}}$, t_i being the time of application of the load, and ω_L the first circular frequency. When the form of the initial curvature contains higher harmonics, these are excited by the axial load, so that when the load is removed the strut vibrates in as many harmonics as were originally present in the initial curvature. In a second paper Taub (1934) considered the same problem when the end fixings were not pinned. In this case the mode shape varies with the axial load, so that if the initial curvature is chosen so that only the first mode is excited by a given load, when that load is released the resulting free vibration will contain higher modes.

Meier (1945), using an analysis similar to that of Koning and Taub, considered the longitudinal impact of two equal bars. The axial load and time of

impact were calculated from a stress wave analysis, so that the impact time was $2l\sqrt{(\rho/E)}$ and the stress $\frac{1}{2}V\sqrt{(E\rho)}$, giving an axial load of 10·8 P_E with the values used (E denotes Young's modulus, ρ the bar density, l its length, V the relative velocity between the bars). Under these conditions the energy of lateral bending was shown to be negligible, a result which was confirmed qualitatively by DAVIDSON and MEIER (1946) who experimented with a long bar which fell on to a soft spring.

LAVRENTIEV and ISHLINSKY (1949), and ŌI (1949), independently considered the relative rates with which the modes are propagated in an initially curved bar of arbitrary form under a suddenly applied and constant axial load. They showed that the lateral deflexion takes the form

$$u = \sum_{n=1}^{\infty} f_n(t) \sin n\pi x/l,$$

t being time, x the distance measured along the bar, and l its length. Then for values of $n < \sqrt{(P/P_E)}$, $f_n(t)$ is proportional to $\exp(\alpha_n t)$, where $\alpha_n = n\omega_L\sqrt{(P/P_E - n^2)}$. If n is varied, α_n is maximum when $n^2 = P/2P_E$, suggesting that the most rapidly propagated mode is that whose critical load is nearest to half the applied load. In support of this result, LAVRENTIEV and ISHLINSKY showed photographs of a strut and a tube which had been subjected to explosion pressures and had buckled into a number of waves.

PIAN and SIDDALL (1950) carried out a very full investigation of the behaviour of a strut under eccentric axial loading of an impact type, but varying arbitrarily, in a known manner, during the impact period. To deal with this variation theoretically, the load was considered as a series of steps, each of which could be treated by the method of the previous investigators. The results were compared with experiments on a 5ft. strut having $l/k = 1110$, k being the radius of gyration. Loading was by means of a mass swung as a pendulum, striking one pinned end via a spring, the other pinned end being fixed. Loads up to 7·3 P_E were applied, the amplitudes of modes containing one and three half waves being in good agreement with theory. Some theoretical attention was also given to the case of an initially curved strut under an axial load whose variation with time was given by a single half sine wave, the best method of solution being by numerical integration. In conclusion it was suggested that a load much greater than the Euler load could be applied to a strut if the period of application were much less than the first natural period of the strut.

Similar phenomena have been investigated by HOFF (1949, 1950, 1951) and by HOFF, NARDO and ERICKSON (1951) who considered an initially curved strut whose pinned ends were made to approach each other with constant velocity. The purpose of this work was to discover the effect of inertia in an ordinary laboratory strut test, so that the rates of loading were small.

(ii) *Scope of present work*

The present investigation has been concerned with a pin ended, initially curved, strut having one end fixed in position, and the other end struck by a mass, via a spring of arbitrary stiffness. Simple calculations using the theory of KONING and TAUB (1934) suggest that, in practical cases, stress waves and lateral bending

are never simultaneously important. Thus the axial load in the strut may be regarded as constant along its length.

When calculating the axial load it is necessary to allow for the shortening of the strut due to its lateral motion, and, since the shortening is proportional to the square of the lateral movement, the problem is non-linear. Complete solutions of the resulting equations have been calculated on the electronic machine Edsac. The results have been checked by experiment, and suggest that in practical cases the shortening effect does not much affect the load. The load time graph is, then, a half sine wave, since the coupling effect is negligible.

With the sine wave loading, it is still difficult to find the strut deflexion, since Mathieu functions are required and are not fully tabulated. The analysis of KONING and TAUB (1934) has therefore been used to provide design curves, the constant axial load in the strut being taken as the peak value of the half sine wave. The curves are therefore very conservative, and suggest that the allowable impact load is only slightly less than the allowable static load, in the worst cases. When the impact load is applied for a period of the same order or less than the first lateral period of the bar, the allowable impact load is greater than the static one, agreeing with the conclusion of PIAN and SIDDALL (1950).

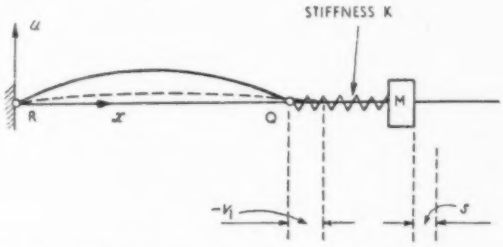

Fig. 1. Initially curved pin-ended strut struck at one end by mass M.

2. THEORY OF THE INITIALLY CURVED STRUT STRUCK BY A MASS

(i) We consider an initially curved pin ended strut and a mass M travelling along the line joining the pins, RQ in Fig. 1. The pin R is fixed in position, while Q is free to slide along RQ and carries a spring of stiffness K which is struck by the mass. The equation of lateral motion of the strut has been given by HOFF (1951):

$$B\frac{\partial^4}{\partial x^4}(u-z)+\frac{\partial}{\partial x}\left[P\frac{\partial u}{\partial x}\right]+\rho A\frac{\partial^2 u}{\partial t^2}=0. \tag{1}$$

x is distance measured from R, u the total lateral shift at any point and z the initial lateral shift, both measured from the x axis. P is the axial thrust in the strut whose sectional area is A, flexural rigidity B and density ρ. t is time.

In deriving the equations of longitudinal motion, we consider the relative magnitudes of u, v and z where v is the shift from the curved position (z), in direction Rx, of a point on the strut. dv/dx is of order e, and du/dx of order $e\,l/h$, e being the strain in the material, l the length of the strut, and h the distance from centroid to outer fibre. dz/dx is of the same order as dv/dx (about 0·002), both being smaller than du/dx since l/h is large (about 100). The longitudinal strain in the strut is then

$$\frac{\partial v}{\partial x}+\tfrac{1}{2}\left(\frac{\partial u}{\partial x}\right)^2-\tfrac{1}{2}\left(\frac{\partial z}{\partial x}\right)^2=-\frac{P}{AE}. \tag{2}$$

For longitudinal equilibrium,

$$-\frac{\partial P}{\partial x} = \rho A \frac{\partial^2 v}{\partial t^2}. \tag{3}$$

We now follow previous investigators and neglect $\rho A \partial^2 v/\partial t^2$ in (3), and from the resulting solution of (1), (2) and (3), we calculate $\rho A \partial^2 v/\partial t^2$ to see whether its neglect is justified. From (2) we see that, neglecting $(\partial z/\partial x)^2$, $\partial v/\partial x$ is always negative, so that $|v|$ is a maximum at Q (Fig. 1) where $v = v_1$, say. Thus in considering the magnitude of the term $\rho A \partial^2 v/\partial t^2$ we need consider only v_1 which can be calculated from the equation of equilibrium for M,

$$P = -Ms'' = K(v_1 + s), \tag{4}$$

dashes denoting differentiation with respect to time, and s the shift of the mass, K the stiffness of the spring. We then calculate $d^2 v_1/dt^2$ from (4), giving

$$\frac{\rho A l}{P_E}\frac{d^2 v_1}{dt^2} = \frac{m}{M}\left[\frac{d^2 p}{dT^2}(1-\mu) + p\right], \tag{5}$$

where $p = P/P_E$, $T = \omega_s t$, $\omega_s^2 = \mu AE/Ml$, $\mu = 1/[1 + AE/Kl]$, and $m = \rho Al$ is the strut mass. If the initial curvature is $z = \sum_1^\infty c_n \sin n\pi x/l$, then since the strut is pin ended,

$$u = \sum_1^\infty f_n(t) \sin n\pi x/l, \tag{6}$$

from (1), and using (6) with (2) and (4), we get

$$\frac{d^2 p}{dT^2} + p = -G \sum_1^\infty n^2 \frac{d^2}{dT^2}(F_n^2), \tag{7}$$

$$\text{where } G = \frac{\mu c_1^2}{4k^2}, \text{ and } F_n = f_n/c_1, \tag{8}$$

k being the radius of gyration of the strut section. Then, if there is no coupling between the lateral movements of the strut and the spring mass combination, the right hand side of (7) is zero, and using this result with (3) and (5) we get $l(\partial p/\partial x)_l = -\mu mp/M$. Note that this gives the maximum $\partial p/\partial x$ since (5) gives the maximum v''. Then the total variation of p with x, Δp, is limited by the relation

$$\left|\frac{\Delta p}{p}\right| < \frac{\mu m}{M}, \tag{9}$$

in the absence of coupling. If coupling occurs, so that from (7) $d^2 p/dT^2 + p$ is of order p, then from (3) and (5) $\partial p/\partial x$ and hence $\Delta p/p$ are small only if m/M is small.

(ii) *Values of $\mu m/M$*

To get some idea of the values likely to be encountered in practice, we begin by neglecting coupling, so that from (7), the axial load is a half sine wave applied for time π/ω_s. Next, we use the method of Koning and Taub (1934) and consider a constant load, given by $q = P/P_E$, P being the amplitude of the sine wave. The "load" q, if applied for time π/ω_s will then give greater deflexions than the sinusoidal loading. If the strut has initial curvature $z = c_1 \sin \pi x/l$, and $q > 1$, the maximum deflexion will be the amplitude a_1 of the oscillations which remain after the load has been removed. We use (1) to get a_1, so that

$$\frac{a_1}{c_1} = \frac{q}{q-1}\left\{\left[\cosh(\pi j\sqrt{q-1}) - 1\right]^2 + (q-1)\sinh^2 \pi j\sqrt{q-1}\right\}, \tag{10}$$

and $j = \omega_L/\omega_s$ is given by

$$j = \pi^2 \frac{k}{l}\left(\frac{M}{\mu m}\right)^{\frac{1}{2}}. \tag{11}$$

If $q < 1$, we use cos and sin in place of cosh and sinh and also use $|q - 1|$, unless $j > 1/(1 - q)^{\frac{1}{2}}$ when the maximum deflexion is

$$a_1/c_1 = 2q/(1 - q). \tag{12}$$

If a_1/c_1 is to be such that the bending stress r in the strut reaches some limiting value, say 10 tons/sq. in., and we take $E = 4550$ tons/sq. in., and $c_1/l = 0{\cdot}002$, then since $r/E = \pi^2 ha_1/l^2$,

$$a_1/c_1 = 0{\cdot}0643\, l/k, \tag{13}$$

taking $k/h = 0{\cdot}578$ as for a rectangular section. To get an upper limit for q we take the direct stress $P/A = 10$ tons/sq. in. so that

$$q = 2{\cdot}23\,(l/100k)^2. \tag{14}$$

Then eliminating $j, q, a_1/c_1$, from (11), (13), (14) and (10) or (12), we get a relation between $M/\mu m$ and l/k, plotted in Fig. 2, and giving the condition for bending and direct stresses in the bar to be both equal to the limiting value. In fact, the bending stress will be smaller, owing to the actual shape of the load-time graph being sinusoidal rather than rectangular. Hence we should expect greater values of $M/\mu m$ to be required, at any particular l/k, than those given in Fig. 2.

Fig. 2 also shows the relationship for a naturally straight strut, in which $z = 0$. In this case, the strut is held by stops in the form of a half sine wave, until the axial load P, produced by the striking mass, is the Euler load. The stops are then removed, and the motion continues freely. If we assume a constant impact load, as before, there is no motion if $q \leqslant 1$; if $q > 1$, the equivalent of (10) is

$$a_1/d = [q \sinh^2 \pi j \sqrt{q - 1} + 1]^{\frac{1}{2}}, \tag{15}$$

the initial lateral deflexion being $u_0 = d \sin \pi x/l$. d/l is taken as 0·002. This case was considered because it is easier to manufacture a straight strut than one bent in a half sine wave.

Fig. 2 shows that in practical cases, $M/\mu m > 20$, so that the maximum variation of axial load p with x, given by (9), is 5 per cent. This result is derived from the fact that longitudinal strut vibrations are always more rapid than lateral ones. For appreciable lateral movements to occur, the frequency of the axial load must be of the same order as the lateral frequency, so that although stress waves would cause the load to build up in a series of steps, each step would be small compared with the final load.

Remembering that (9) was derived on the assumption of no coupling between strut and spring mass combination, we now consider the effect of this coupling.

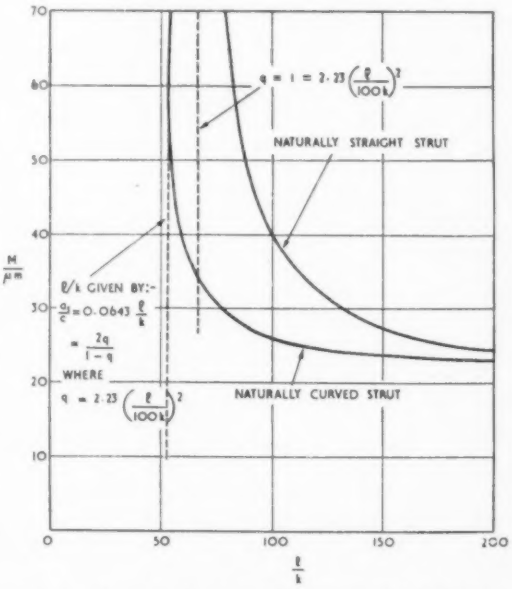

Fig. 2. Curves giving conditions at which direct stress P/A and bending stress due to impact buckling are both 10 tons/sq. in.

(iii) *Complete equations of motion for sinusoidal initial curvature*

When the bar is initially curved in the form of a half sine wave, and $z = c_1 \sin \pi x/l$, (1) becomes

$$d^2 F_1/dT^2 + j^2 F_1 (1 - p) = j^2, \tag{16}$$

where $F_1 = f_1/c_1$. F_1 is thus the ratio of the total central deflexion to its initial value c_1. (2) and (4) can be combined to give

$$p = y - GF_1^2, \tag{17}$$

where $y = \mu AEs/lP_E + G$. We then simplify (7) with the aid of (17), so that

$$d^2y/dT^2 + y - GF_1^2 = 0. \tag{18}$$

The conditions at $T = 0$ are that $F_1 = 1$, $F_1' \equiv dF_1/dT = 0$, $y = G$, $y' = Q \equiv M\omega_s V/P_E$. V is the striking velocity of the mass, and Q gives the maximum value of P/P_E which would be obtained if the strut were held straight.

When the bar is naturally straight, $z = 0$ and (1) becomes

$$d^2F_1/dT^2 + j^2F_1(1 - p) = 0. \tag{19}$$

(17) and (18) are unaltered in form, but y is replaced by $y_s = \mu AEw/lP_E$, w being the shift of the mass from the position in which the strut is straight. G is replaced by $G_s = \mu d^2/4k^2$, and the initial conditions are $F_1 = 1$, $F_1' = 0$, $y_s = 1 + G_s$, $y_s' = Q_s \equiv \dfrac{M\omega_s V_s}{P_E}$. V_s is the mass velocity when the strut load reaches the Euler load, and its relation to the striking velocity V is given by

$$Q^2 = Q_s^2 + 1. \tag{20}$$

(iv) *Values of the independent variables*

The independent variables are then G (the non-dimensional initial curvature), j (the frequency ratio), and Q (the effective applied load). We have to find Q so that the maximum deflexion shall not exceed the value given by (13).

In fixing G and j, the limiting values shown in Table I were employed.

TABLE I. LIMITATIONS ON INDEPENDENT VARIABLES FOR EDSAC SOLUTIONS

l/k	μ	$c_1/l = d/l$	M/m
< 200	< 1	0·002	< 50

The choice of M/m is somewhat arbitrary. Using the values of Table I with (8) and (11), we obtain

$$\left.\begin{aligned} G &= 97{\cdot}4 \times 10^{-6}\, M/mj^2 \\ &= 10^{-6}\, \mu l^2/k^2. \end{aligned}\right\} \quad \begin{matrix} \text{(i)} \\ \text{(ii)} \end{matrix} \tag{21}$$

j in equation (11) can be given any value by suitable choice of μ and M/m.

(v) *Edsac results*

The equations (16) to (19) were solved on the electronic machine Edsac at the Mathematical Laboratory Cambridge, the programming being done by Mr. S. GILL. Four simultaneous first order equations were used in place of (16) to (19), and the Runge-Kutta method could then be applied.

Most of the work was done with the equations for a naturally straight strut since the results could be compared with experiment. A typical results sheet from the machine teleprinter is shown in Table II.

TABLE II. NATURALLY STRAIGHT BAR $G = 0{\cdot}00122$, $j = 2$, $Q_s = 2{\cdot}0$

T	F_1	dF_1/dT	y	dy/dT	p	U
0	1·00000	0·00000	1·00122	2·00000	1·00000	4·000000
	1·01040	0·15478	1·37863	1·76147	1·37738	
	1·08169	0·60799	1·70112	1·45272	1·69969	
	1·27518	1·38785	1·95585	1·08614	1·95387	
	1·66602	2·60893	2·13270	0·67643	2·12931	
1·0	2·36232	4·48666	2·22465	0·24021	2·21785	3·999980
	3·52442	7·32100	2·22821	− 0·20449	2·21306	
	5·37466	11·40686	2·14358	− 0·63836	2·10834	
	8·17421	16·77165	1·97498	− 1·04049	1·89346	
	12·11714	22·58238	1·73106	− 1·38730	1·55193	
2·0	17·06522	26·17324	1·42554	− 1·65183	1·07025	3·999992
	22·10496	22·52781	1·07759	− 1·80798	0·48146	
	25·26499	6·96964	0·71027	− 1·84679	− 0·06849	
	24·23542	− 18·11148	0·34482	− 1·79750	− 0·37175	
	18·08584	− 42·31781	− 0·00670	− 1·71677	− 0·40576	
3·0	7·94705	− 57·17775	− 0·34206	− 1·63659	− 0·41911	4·000001

The interval of T used by the machine for integration was 0·04 while the printing interval was 0·2. The accuracy of the method is shown by the constancy of U the total energy of the system, which, for a naturally straight strut is given from (18) and (19):

$$2U\mu\, l/\pi^2\, P_E\, k^2 - 1 = Q_s^2$$
$$= (y_s')^2 + 2G_s\,(F_1')^2/j^2 + (y_s - G_s\, F_1^2)^2 - 1 + 2G_s\,(F_1^2 - 1). \qquad (22)$$

TABLE III. PEAK LOADS AND IMPACT TIMES FROM EDSAC RESULTS COMPARED WITH VALUES FOR NO COUPLING (SINE WAVE LOAD)

Case No.	G_s from	G_s	j	Max. deflexion a_1/d or F_{1m}	p_A	δp	$\pi - T_i$	$\dfrac{G_s F_{1m}^2}{p_A}$
1	(21 (ii))	0·0398	0·2	12·9	19·92	0·10	0·024	0·0405
2		0·00122	2·0	3·5	1·413	0·001	0·004	0·0105
3	(21 (i))	0·00122	2·0	11·2	1·799	0·004	0·061	0·0844
4		0·00122	2·0	25·2	2·225	0·011	0·303	0·342
5		0·005	2·0	9·5	1·790	0·013	0·189	0·245
6		0·010	2·0	3·33	1·408	0·006	0·024	0·0783
7		0·010	2·0	13·2	2·179	0·057	0·705	0·767
8	Arbitrary	0·020	2·0	10·2	2·137	0·099	0·827	0·955
9		0·00304	4·0	11·2	1·402	0·012	0·053	0·257
10		0·00304	4·0	21·6	1·742	0·061	0·022	0·786

Note that the machine continues the calculation when the load is negative, while in actual fact the striking mass will spring clear. The final strut amplitude a_1/d is calculated from the displacement and velocity at zero load. The values of Table II are plotted in Fig. 3 which shows that the load-time graph is nearly sinusoidal, indicating a small degree of coupling between the lateral movements and the spring motion.

Table III gives the peak load p_A, from points like A (Fig. 3), in a variety of cases. Also given are $\delta p = (1 + Q_s^2)^{\frac{1}{2}} - p_A$, and $\pi - T_i$. $(1 + Q_s^2)^{\frac{1}{2}}$ would be the peak load without coupling. $T_i = T_B + \tan^{-1}(1/Q_s)$ is the impact time, where T_B is the time from $p = 1$ to point B (Fig. 3). F_{1m} is the maximum value of F_1 during the time of loading.

It will be seen that the non-dimensional peak load p_A is in all cases quite close to $(1 + Q_s^2)^{\frac{1}{2}}$, and that the difference δp corresponds quite well with $G_s F_{1m}^2/p_A$. This latter is obtained from the coupling term in equations (17) and (18), and until it becomes almost unity the loading is approximately sinusoidal. This rather surprising result is due to the fact that most of the strut movement takes place during the latter part of the loading period. The result is further reflected in the difference $\pi - T_i$, which becomes large at smaller values of $G_s F_{1m}^2/p_A$, except in cases 9 and 10 where the small value of $\pi - T_i$ is fortuitous as illustrated in Fig. 4. In these latter cases the loading is only very approximately sinusoidal, owing to the large value of $G_s = 0{\cdot}00304$, corresponding to $M/m = 499$ from (21 (i)). In case 10, there is a second impact between the mass and the strut after separation at point B (Fig. 4). This phenomena is further analysed in the Appendix.

(vi) *Criterion of coupling*

It would be convenient to have a simple criterion of coupling, from which to decide whether the loading is sinusoidal in any particular case. The results of Table III suggest that

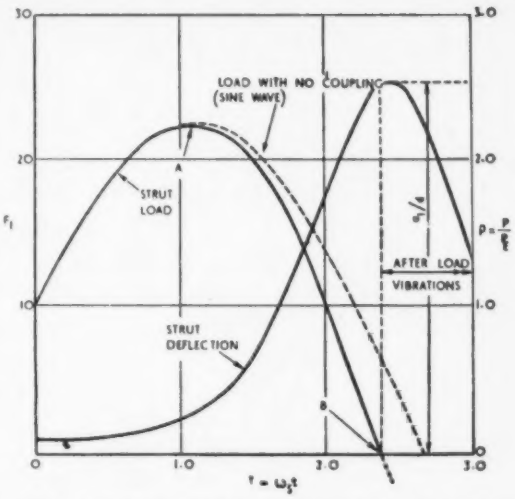

Fig. 3. Non-dimensional values of strut central displacement F_1 and axial load p. "Curvature" $G_s = 0{\cdot}00122$. "Load" $Q_s = 2{\cdot}0$. Frequency ratio $j = 2$. Strut naturally straight. See also Table II. There is no motion until the strut load reaches the Euler load.

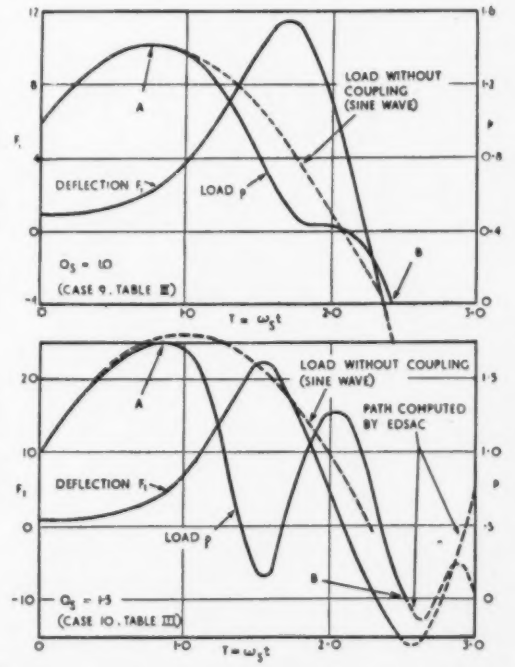

Fig. 4. Strut central deflexion F_1 and load p in cases of high coupling. Initially straight strut, $j = 4$, $G_s = 0{\cdot}00304$, corresponding to $M/m = 499$.

$G_s F_{1m}^2/p_A < 0{\cdot}2$ might give the necessary criterion. This would give a maximum error in peak load p_A of about 1 per cent, and a maximum error in impact time of about 10 per cent. In case 1 (Table III), $G_s = 0{\cdot}0398$ which is the maximum obtainable if $l/k < 200$, from (21 (ii)). The final amplitude $a_1/d = 12{\cdot}9$ is also the maximum allowable from (13), but the coupling is small, suggesting that when $j < 2$ the large value of p required for lateral deflexion makes the coupling negligible.

When $j > 2$, the peak load p_A is of order 1, so that our criterion becomes $G_s F_{1m}^2 < 0{\cdot}2$, and with (21 (i)), and using (13) as an upper limit for F_{1m}, the criterion is

$$M/m < 12{\cdot}4\, j^2 \tag{23}$$

This suggests that with the values of Table I, coupling can always be neglected.

It must be emphasized that (23) is a tentative relation, further calculations for large values of j and for a naturally curved bar being required.

3. EXPERIMENTS

(i) *Design of apparatus*

The following had to be borne in mind :

(*a*) A rectangular section strut was to be used, with electric strain gauges measuring bending stresses, and in case two gauges should be required side by side the minimum strut width was 1 inch. The length, while being as small as possible, had to be large in comparison with the strain gauge, and was decided as 24 ins.

(*b*) To keep the buckling stress and load moderate, the strut thickness was made 0·2 in. giving $l/k = 416$ and $P_E = 120$ lbs. with $E = 10{\cdot}5 \times 10^6$ lbs./sq. in. The first natural frequency was then about 32 c.p.s.

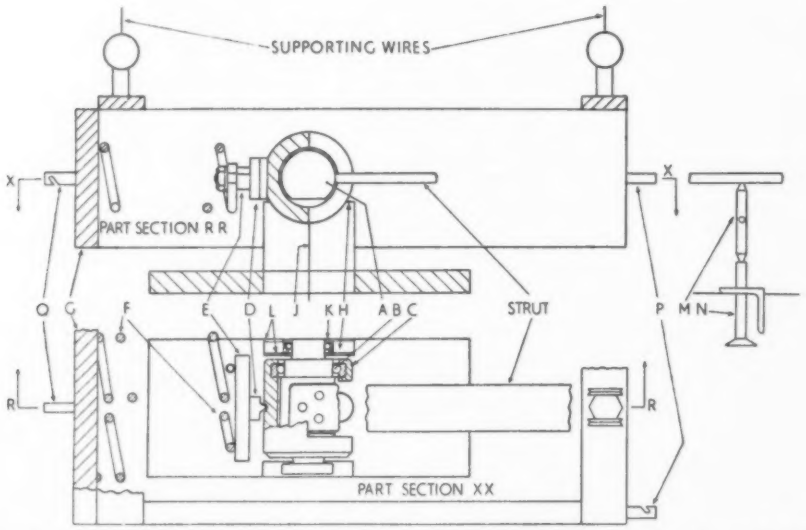

Fig. 5. Details of moving end of strut with bearings to give pin ended condition and striking mass and springs.

(*c*) It was decided to use $j = 2$, for comparison with the results of Table III, and as a basis for the design of the spring-mass combination to strike the end of the strut. A compromise had to be made between a stiff spring with a large mass and consequent low striking velocity, and a large mass with a soft spring, the latter having to be long enough to reach the Euler load of the strut.

The apparatus resulting from these considerations is shown in Fig. 5 which gives a sectional elevation and plan at one end of the strut. The axis of the strut, and its minor axis, are both horizontal, and each end carries ball bearings allowing free rotation about the minor axis. One end of the strut is fixed in position, the other end, shown in Fig. 5, being free to slide towards the fixed end on a horizontal table. The conditions of Fig. 1 are thereby realized.

Each end of the strut is bolted to an axle *A* carrying two ball bearings *B*. These transmit the axial thrust from the cage *C* which is rigidly clamped at the fixed end. At the moving end a knife edge *D* is held in a groove in the cage *C* by elastic bands. Impact takes place between the knife edge *D* and the crossbar *E* which joins two helical springs *F* in parallel. The springs are in turn fixed to a cage weight *G* suspended on four wires. The wires are arranged in two pairs, each forming a *V* having its apex on the axis *XX* when the weight *G* is in the position shown in Fig. 5. The weight swings as a pendulum in the vertical plane containing the strut axis, the planes of the two *V*s always remaining parallel, and each wire carrying a small ball bearing for free rotation. Thus when the weight strikes the end of the strut it is moving along the axis *XX* with a velocity calculable from the drop height. The weight *G* is made in the cage form so that its centre of gravity should be ahead of the knife edge *D* during impact, giving stability of motion.

To guide the free end of the strut, the horizontal table *H* was provided, the surfaces on each side of the strut being ground in one setting. Ball bearings *K*, concentric with *B* on the axle *A* were kept in contact with the table *H* by the spring loaded wire *J* pulling downwards on the cage *C*. At one side, raised lips *L* guided the bearing *K*, preventing lateral movement of the strut.

The strut was made as flat as possible (within 0·0015 in.), and an initial curvature provided by means of the stop *M*. The stop rested in a pop mark near the middle of the strut to which a known deflexion could then be applied by means of the screw *N*. A taut elastic band was applied to the stop *M* so that it was removed directly the axial load in the strut exceeded the Euler load.

Hooks *P* were attached to each side of the cage weight *G*, so that a static axial load could be applied to the strut by an arrangement of wires and pulleys carrying a dead weight, and the hook *Q* enabled the cage weight *G* to be held back prior to release.

Vol. 2 53/54

(ii) *Measurements*

Electric strain gauges were fixed to the centre section of the strut, and arranged so as to give the curvature, with no response to axial load. This load was measured by a gauge on the back of the crossbar *E* (Fig. 5). The readings were fed on to a Kelvin and Hughes paper recorder giving linear response up to 80 c.p.s. which was adequate, the first natural frequency of the strut being about 32 c.p.s. The calibration of the instrument varied rather rapidly, and the maximum strut movement was therefore measured by a pointer which deflected an oscilloscope spot on making contact with the centre section of the strut. The position of the pointer was adjusted by trial and error so that contact was just made at each velocity of the striking mass *G* (Fig. 5).

A dial gauge gave the initial deflexion due to the stop *M* (Fig. 5), and also the deflexion for "Southwell plot" static tests. For these latter, the dial gauge had to be electrically loaded so that when its plunger was moved in and out by hand, the reading at which contact with the strut was just made could be determined. This arrangement prevented the dial gauge spring from moving the strut. Dial gauges were also used to give the spring compression during static tests.

A "plane table" system was employed to give the vertical rise of the striking mass, two large machined bars clamped to the main frame, on either side of the strut, forming the table. A flat cross bar, resting on both machined bars, carried a dial gauge which was thus constrained to move in a horizontal plane. Its plunger, travelling vertically, rested on the hook *Q* (Fig. 5), the gauge reading then giving the vertical movement of the cage weight *G*.

(iii) *Experiments and Results*

The cage weight was used as a time base in finding the first natural frequency of the strut. A rigid stop was fixed to contact the crossbar *E* (Fig. 5) when the weight *G* was hanging in its lowest position. The weight then swung against the stop as a simple pendulum, giving to the paper recorder, via the strain gauge on *E*, pulses whose frequency could be accurately timed,

and compared with vibrations from the gauges on the strut when this was vibrating freely in its first mode.

A static loading test was carried out to determine simultaneously the strut Euler load and initial curvature from a "Southwell plot," and also the stiffness of the coil springs F.

The "Southwell plot" gave P_E between 121 and 126 lbs. while the measured natural frequency 31·7 c.p.s. corresponds with $P_E = 125{\cdot}6$ lbs. and the value $P_E = 125$ lbs. was used in comparison with theory.

To get $G_s = 0{\cdot}00122$ as in Table II, a central strut deflexion of 0·053 was required, and since the calculated self weight deflexion was 0·012 in. (the Southwell plot gave 0·010 in.) the total upward movement on the stop M (Fig. 5) was 0·065 in. j was made 2·0 by adjusting the cage weight mass to 20·6 lbs., giving $M/m = 42{\cdot}6$. Various values of Q_s were obtained by varying the drop height of the cage weight, and Fig. 6 is the resulting graph of maximum strut deflexion against Q, compared with the theoretical results from Table III. At each drop height, an impact with the strut held straight gave strain gauge readings of strut load. These readings were compared with the corresponding readings when the strut deflected, and confirmed the results of Table III in giving a negligible change of peak load δp due to coupling.

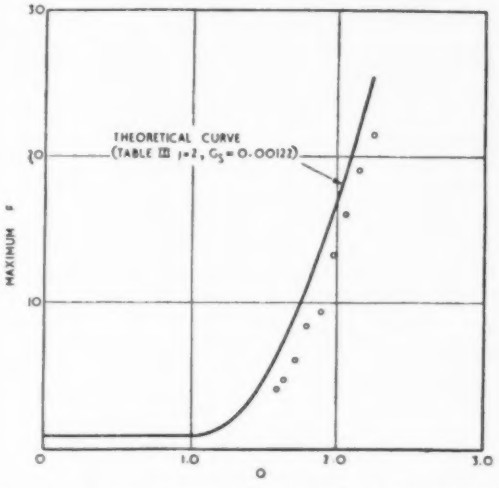

Fig. 6. Maximum strut deflexion F (non-dimensional) against applied load $Q = (1 + (Q_S{}^2))^{\frac{1}{2}}$. Q would give (P/P_E) max without coupling. Initially straight strut. Experimental points O.

4. Practical Application

The results of the foregoing sections can be applied to the design of compression members subjected to *single* impacts such as cranes and railway carriage or air frame components.

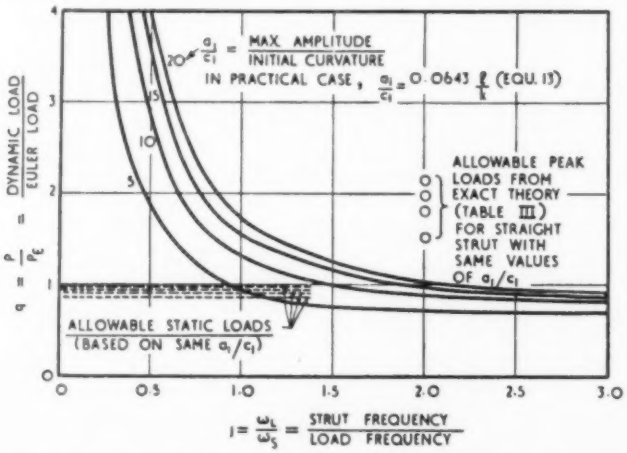

Fig. 7. Full curves give allowable constant strut load q when applied for time π/w_s to naturally curved strut. Dotted lines give allowable static load for same final amplitude.

It we accept the conclusions of Section 2, then in practical cases : (i) The effect of stress waves is negligible, so that the axial load in the strut is always constant. (ii) The effect on strut load of strut shortening due to curvature is negligible if $M/m < 50$. This means negligible coupling so that the load-time graph is a half sine wave. Then the curves shown in Fig. 7 may be applied. Each full curve shows the constant load which may be applied for time π/ω_s at the given value of a_1/c_1. The points obtained from the theory of Table III show that a much higher peak load can be applied when the load-time graph is sinusoidal rather than rectangular. The static load which may be applied is given by $a_1/c_1 = q\ (1 - q)$, and for a particular q, is half the maximum dynamic deflexion from (12). But the reduction in dynamic load to make the two deflexions equal is small. Hence for *large* a_1/c_1 *the allowable static and dynamic loads are nearly equal.*

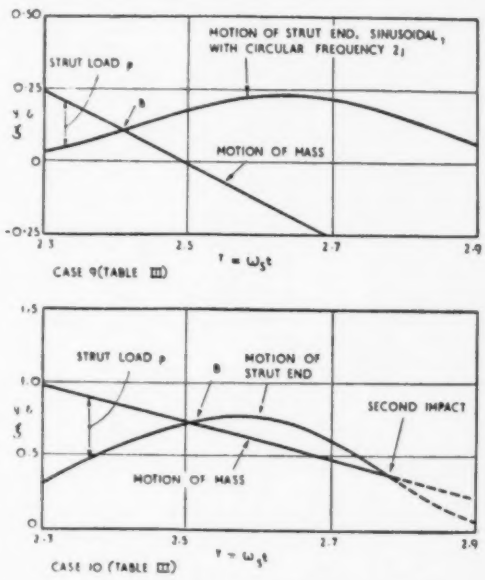

Fig. 8. Behaviour of strut and mass immediately after zero strut load. See Fig. 4 for previous motion.

It must be understood that the above theory can be applied only to the *single impact case.* If the axial load is oscillatory, as for example, when a mass bounces on a crane rope, the problem is completely altered. The possibility of resonance between the periodic axial load and the strut then exists. When the axial load is a continuous sine wave, the resonant frequencies can be found from the theory given by Einaudi (1935 and 1936), Utida and Sezawa (1940), Lubkin and Stoker (1943) and McLachlan (1947). This latter theory is not applicable to the crane problem, where the load is essentially a *transient* vibration. It is felt that further work with this problem should begin with an experimental investigation of the nature of the transient load.

Acknowledgment

The work described in this paper was carried out in the Engineering Laboratory, Cambridge University, and the author wishes to thank Professor J. F. Baker for his encouragement. He wishes to acknowledge also the sponsorship of the Aluminium Development Association and the assistance of Mr. S. Gill of the Mathematical Laboratory Cambridge, who carried out the programming on the electronic calculating machine Edsac.

APPENDIX

Double impact

To find out whether a double impact will occur, we consider the motion of the end of the strut, whose displacement is $\zeta = G_s F_1^2$. When the load is zero, F_1 is a harmonic oscillation $F_1 = (a_1/d) \sin(jT + \phi)$ so that ζ will be harmonic and of circular frequency $2j$. The values of a_1/d and ϕ are found from the values of F_1 and F_1' at point B (Figs. 4 and 8) when the load is zero. The motion of the mass after point B is given by a straight line determined by the velocity at B.

It is evident from the results of Fig. 8 that a high degree of coupling is necessary to give double impact.

REFERENCES

DAVIDSON, T. and MEIER, J. H.	1946	*Proc. Soc. Exp. Stress Analysis*, **4**, 88.
EINAUDI, R.	1935	*Atti. d. Accad. Gioenia, Catania*, vol. 1, mem. 20.
	1936	*Ibid.*, vol. 2, mem. 5.
GOLDENBLAT, I. I.	1950	*Izvestia Acad. Nauk. U.S.S.R.*, **6**, 819.
HOFF, N. J.	1949	*Colston Res. Papers*, p. 121 (London : Butterworth)
	1950	*Estratto da "La Ricerca Scientifica,"* A 20, n. 12.
	1951	*J. Appl. Mech.*, **18**, 68.
HOFF, N. J., NARDO, S. V. and ERICKSON, B.	1951	*Pol. Inst. Brooklyn, N.Y.* PIBAL Rept. No. 185.
	1951	*Proc. Soc. Exp. Stress Analysis* **9**, 201.
KONING, C. and TAUB, J.	1934	*N.A.C.A. Tech. Mem.*, No. 748.
LAVRENTIEV, M. A. and ISHLINSKY, A. V.	1949	*Doklady Acad. Sci. U.S.S.R.*, **64**, 779.
LUBKIN, S. and STOKER, J. J.	1943	*Q. Appl. Math.*, **1**, 215.
MCLACHLAN, N. W.	1947	*Mathieu Functions*, p. 292 (Oxford University Press).
MEIER, J. H.	1945	*J. Aero. Sci.* **12**, 433.
ŌI, K.	1949	*Ōyō Sugaku* 2, No. 1, 13-4 (This has not been located, see *Appl. Mech. Rev.* **3** (No. 5), 1950).
PIAN, T. H. H. and SIDDALL, J. N.	1950	*Navy Report*, Mass. Inst. Tech.
TAUB, J.	1934	*N.A.C.A. Tech. Mem.* No. 749.
UTIDA, I. and SEZAWA, K.	1940	*Aero. Res. Inst. Tokyo*, Rept. No. 193.

Vol 2 1953

Journal of the Mechanics and Physics of Solids, 1953, Vol. 1, pp. 67 and 68. Pergamon Press Ltd., London.

CORRIGENDA : THE AUTOFRETTAGE OF THICK TUBES WITH FREE ENDS

By D. G. B. Thomas

(*Received* 17*th July*, 1953)

Dr. Koiter, of the Technische Hogeschool, Delft, has pointed out (private communication) that the writer's solution (Thomas 1953) does not satisfy the condition

$$\left(\frac{\partial \sigma_z}{\partial c}\right)_{r=c=a} = \frac{4-26\nu}{13-2\nu}\cdot\frac{Y}{a}$$

which he obtained by substituting derivatives from equations (2), (3) and (12) in equation (11) (where the numbers refer to the original paper). Investigation has revealed an error in the solution of equations (18) and (19). Corrected results, which satisfy Koiter's condition at the origin, have now been calculated and are discussed below.

The most significant changes are in the axial stress. In the curves of axial stress against position, the maxima are flatter than in Fig. 3 and, for $c = 1{\cdot}5a$, the corrected curve lies between the T and A-S curves of Fig. 4. The values of q now lie between $-0{\cdot}021$ and $-0{\cdot}472$, and are uniformly more positive, so that the Tresca yield criterion is nowhere violated. The mean m value mentioned in Section 4 is unchanged, but the maximum local relative error in using the stated approximation to the Mises yield criterion is reduced from 17 per cent to 12 per cent at $c = b = 2a$, decreasing rapidly with c and r as before.

Smaller changes occur in the strains. The corrected curves of axial strain and external expansion against c now differ from the A-S curves of Figs. 5 and 6 by only $+3\frac{1}{2}$ per cent and $+\frac{1}{2}$ per cent respectively at $c = b$. The internal expansion is descreased by less than 1 per cent.

It is now possible to improve the approximation (26) for the axial strain. If the axial stress in the elastic region is represented by a linear function of c,

$$\frac{E\epsilon_z}{Y} = -\frac{\nu c^2}{b^2} + 0{\cdot}035\left(\frac{c}{a} - 1\right)$$

with a maximum error of 3 per cent.

The revised table of computed quantities is given below.

c/a	$(E\epsilon_\theta/Y)_a$	$(E\epsilon_\theta/Y)_b$	$-E\epsilon_z/Y$	$(\sigma_z/Y)_e$
1·0	0·738	0·250	0·075	0·000
1·1	0·897	0·302	0·090	0·001
1·2	1·078	0·359	0·104	0·004
1·3	1·282	0·420	0·119	0·008
1·4	1·507	0·486	0·134	0·013
1·5	1·753	0·557	0·150	0·019
1·6	2·019	0·633	0·168	0·024
1·7	2·306	0·714	0·188	0·029
1·8	2·612	0·800	0·211	0·032
1·9	2·937	0·893	0·238	0·032
2·0	3·281	0·992	0·272	0·028

Certain misprints in the previous paper should be noted. In equations (13) and (27), a factor of $\frac{1}{2}$ should multiply c^2/b^2, while in equation (19), the coefficient of $\Delta c/b^2$ should be negative.

Since the writer's paper was published KOITER (1953) has obtained an analytical solution of the problem using the Tresca yield criterion and Tresca plastic potential. A feature of this solution is that the axial stress increases until, at the bore, it is equal to the circumferential stress, and violation of the yield criterion is imminent. This differs from the results for a Mises potential, for which the criterion is violated, if at all, when the axial stress at the outer surface becomes equal to the radial stress there.

REFERENCES

KOITER, W. T. 1953 *Biezeno Anniversary Volume* (Stam, Haarlem).

THOMAS, D. G. B. 1953 *J. Mech. Phys. Solids*, **1**, 124.

Vol 2 1953

BOOK REVIEWS

A. H. Cottrell: **Dislocations and Plastic Flow in Crystals.** Clarendon Press, Oxford. 1953. x + 223 pp. with 93 illustrations and diagrams. 25s.

It was recognized in 1926 that if a crystal was perfect, then the stress necessary to cause plastic flow would be some thousand times greater than is observed experimentally. To explain the weakness of crystals some defect in their structure must be supposed, and about 1934 a particular form of defect, the dislocation, was postulated. In the last twenty years much research, both theoretical and experimental, has been undertaken to explore the properties of dislocations, and the results have been published in papers scattered among many journals. Until the welcome appearance of this book, there was no comprehensive account of all these developments and, since progress in dislocation research is still rapid, there must be a natural reluctance to undertake the great labour of writing a book because of the possibility of it rapidly becoming obsolescent. However, such a book was very desirable at this time and the author is therefore to be congratulated for having the courage to write this apposite account, while the publishers should be commended for making the book available so speedily. In general, all important contributions to the topic up to the end of 1952 are covered and a very full series of references is given.

The essential purpose of the book is to present an account of contemporary dislocation theory as far as it has been developed. Throughout, only those experimental observations are discussed that are relevant to the various aspects of dislocation theory, and the book does not purport to cover all the experimental details of the various aspects of plastic deformation. The engineer, for instance, may be disappointed to find but a few lines relating to the fatigue of metals; this omission is deliberate, since dislocation theory has, at present, little to say about fatigue behaviour. The author, who has himself made both theoretical and experimental contributions to the field, has generally managed to preserve a good balance between them, although occasionally there is a tendency to discuss the experimental evidence in insufficient detail. There is no doubt that the zealots in various experimental branches will complain that particular aspects have not been given the prominence they deserve.

Vol. 2 53/54

Chapter I is concerned with the basic features of slip in crystals, the necessity of supposing defects in crystals, and the general features of dislocations. Chapter II is devoted to an analysis of the stress and strain fields around dislocations. In Chapter III the properties of dislocations in particular types of crystal structure are discussed and the explanation of certain basic facts of plastic deformation examined. These three chapters occupy rather less than half the book and this part is likely to remain unchanged by any future developments.

The remainder is concerned with the application of the basic knowledge so far gained to various phenomena. Chapter IV deals with the factors influencing the yield strength, interpreted in its broadest sense, and involves a discussion of age-hardening alloys, alloys with a sharp yield such as steel, and the relation between polycrystal and single crystal properties. The theory here is fairly well established and a clear-cut treatment is possible. In Chapter V, the discussion turns to work-hardening, annealing and creep. In these branches, as the author himself points out in the Preface, questions are still far from settled and in places the theoretical treatment is necessarily somewhat speculative, although the author has succeeded in his attempt "to present a fairly coherent story based substantially upon the main stream of present-day opinion."

Dislocation theory was born out of a quantitative discrepancy between earlier theories and experiment, and its continued place in the field must depend on its success in explaining experimental phenomena in a quantitative manner. Any worth-while book on dislocation theory must therefore contain a certain amount of mathematical treatment. In this field, where a precise formal treatment is impossible, some arbitrary level of mathematics must be selected and the problems simplified so that they can be tackled at that level. The author has chosen to derive formulae by using fairly simple physical concepts, thereby avoiding the more difficult mathematics, and where the formulae so derived differ from those given by more advanced treatments the results of the latter are quoted. The reader is not expected to possess any great mathematical gifts, and there is nothing more difficult than, say, simple elasticity theory. This treatment will

disappoint the mathematical physicist, who would prefer the more formal treatment, and will not enlighten the type of metallurgist to whom any mathematics is an affliction, but is well chosen to suit the majority of readers.

Although the author has succeeded in his attempt to keep the mathematical treatment simple, it cannot be said that the first three chapters of the book will be found very readable by those who must take their mathematics slowly and in small doses. The two later chapters, where specific problems concerned with the deformation of crystals are considered, are much more readable and the less mathematical reader would be well advised to start his reading here, preferably selecting the topic in which he is most interested. An excellent series of cross references is carried on throughout the book, and the reader is thereby referred to the appropriate earlier parts of the book, an understanding of which is essential to the particular aspect of the theory he is studying. This would be a very convenient way of breaking the essential preliminary mathematics into easily assimilated small doses.

It must be emphasized, however, that many readers will wish to read the book in the order it is presented and there can be no suggestion that the present lay-out is other than the best possible. With the proviso that a little more space could have been devoted to experimental evidence, the length of the book appears to be adequate, and the writing is always to the point without becoming so terse as to be incomprehensible.

This book, then, is extremely welcome not only because it is the first to cover all aspects of dislocation theory, but because it follows adequately the difficult course between the excessively theoretical and the purely descriptive. The book will appeal to all connected with research on the plastic flow of crystalline solids and, since the price is very reasonable, can well be recommended for their personal library.

G. B. GREENOUGH

Vol 2 1953

The Cold Working of Non-ferrous Metals and Alloys. Institute of Metals Monograph and Report Series No. 12, London 1952. 15s. 0d.

THE subtitle of the monograph is misleading : of five papers only the first is strictly confined to " metallurgical aspects of the subject," the second is about lubricants, the third deals with the engineering aspects of rolling, and the fourth and fifth are reviews of wire drawing and deep drawing practice in the widest technological sense. Undoubtedly, the Institute of Metals has been wise to interpret the terms of reference of this symposium with discretion, for in this field, more than any other, it is often impossible and always undesirable to stick rigidly to only one of the many technological disciplines involved. The cold working processes here considered depend just as much on the geometry of tools, machine design, and lubrication, as on the metallurgical properties of the stock, and all factors are closely interrelated.

While the originators of the symposium were thus right to cast their net wide, it is debatable whether they have caught the right fish. The first paper by COOK and RICHARDS is an excellent survey of its kind, but it covers only the structural aspect of the ' fundamentals ' of cold working, and it is a pity that the subsequent technological papers were not further backed by a companion survey of the fundamental mechanics of cold working. The second paper, on lubrication, is out of tune with its companions ; its point of view and its level of scholarship are more appropriate to technical or trade journals than to publications of a learned Institution. Admittedly, our knowledge of lubrication in metal working lags behind knowledge of its other aspects, but we *have* outgrown the metaphysics of " lubricity " and " tackiness " ; The reviewer can think of three symposia by learned Institutions on the chemical and physical aspects of boundary and thin film lubrication, which would have provided ample material for a review of up-to-date knowledge in this field and served as a unifying background to some of the author's shrewd observations on specific practical problems. The remaining three papers are excellent surveys of

existing practice and of technological knowledge and contain many stimulating ideas about future developments.

Symposia are fashionable, but do they fill a real need? Technical and scientific knowledge is proceeding at such a pace that it is imperative to take stock at frequent intervals. Treatises take so long to write and date so quickly, that monographs are claiming an increasing share of our personal libraries, – not least because of their moderate price. Among these " Penguins " of technical and scientific literature the Institute of Metals monographs are second to none, in standard of scholarship and of publishing. The present one, though uneven in the level of its papers and perhaps a little uncertain in its choice of topics, is nevertheless a most informative book to read and to refer to, not least because of the well-edited discussion which – making allowance for the smaller print – occupies more than half as much space as the papers, and which most worthily supports and supplements them.

J. G. WISTREICH.

F. B. SEELY and J. O. SMITH : **Advanced Mechanics of Materials.** John Wiley & Sons Inc., New York, Chapman & Hall, London. 1952. xvii + 680 pp. $8.50 or £3 8s. 0d.

Vol. 2 53/54

THIS second edition of a volume first published in 1932 is essentially a new book, as a result of considerable revision and additions made necessary by advances in methods of analysis and by altered emphasis on the importance of certain topics. The Authors set themselves the formidable task of producing a book of value both to advanced undergraduate and to first year graduate students, which might in addition prove useful in engineering offices. While the simplified methods and graphical results may well be of assistance to a designer, the advanced material is too condensed to satisfy the needs of most graduate students. As a textbook for use in degree courses in Great Britain, however, this edition contains many chapters that will cover the subjects taught during the second and following years. The fundamentals are discussed lucidly, and the limitations of methods of analysis are clearly defined. Illustrative problems and the selected bibliography enhance the value of the book.

The subject matter is divided into six parts, the first of which is relevant to a first course in Strength of Materials. This contains a discussion of modes of failure of members and of design procedure which is not to be found in other textbooks. The second part, nearly half the book, is devoted to the study of special problems of strength and stiffness of members under static loading. In addition to the analysis of a number of flexural and torsional problems, an exhaustive treatment of thick-walled cylinders is included. The chapters on the bending of flat plates and contact stresses are marred by lack of detail and over simplification, and might mislead the average student. Following a short section on stress concentrations, the methods of strain energy are presented. Their application in the field of indeterminate structures is illustrated, but no indication is given of methods useful in solving instability problems. The section dealing with the effects of small inelastic strains provides an introduction to limit design methods, and is a worthwhile addition to the orginal text. The remaining additional section, ' Introduction to Instability,' discusses the buckling of columns, cylinders and plates. Thoretical treatment of the elastic buckling of struts is limited to a statement of Euler's solution ; on the other hand, the tangent and reduced modulus approaches to plastic instability problems are defined and their significance is discussed rationally. Cylinders collapsing under external pressure provide a better exercise in analysis, but the section leaves the reader ill equipped to tackle the many problems of instability.

The shortcomings of this book may chiefly be attributed to the Authors' assumptions that differential equations and the elementary theory of elasticity are hurdles as yet uncrossed by its readers. The technique of teaching by repetition of facts is also better tolerated in the lecture room than in print. Despite these criticisms, this revised edition may claim a high place among the many textbooks that serve this field of study.

A. R. FLINT

C. S. BARRETT: **Structure of Metals.** 2nd. Edition. McGraw-Hill Book Company Inc. 1952. pp. xvi + 661. 10$ or 72s. 6d.

IN this second edition of his invaluable and immensely impressive book, Prof. BARRETT has made extensive additions of material, amounting in all to about one hundred pages. Much of the rest has been re-written and brought up-to-date. There are also certain important changes of emphasis; for example, the chapter on X-ray measurement of stress in crystalline aggregates now concludes with a word of caution. The chapters chiefly expanded are those entitled: Laue and Fixed Crystal Methods; Powder Method; Superlattices; Age Hardening and Transformations; Diffraction of Electrons, Atoms and Neutrons; and Dislocation Theory. The latter replaces the original title: Theories of Slip – a change that epitomises the major development in metal physics since the first edition appeared in 1943.

R. HILL.

Vo
2
1953

Journal of the Mechanics and Physics of Solids, 1954, Vol. 2, pp. 73 to 80. Pergamon Press Ltd., London.

ON THE USE OF HODOGRAPHS IN PROBLEMS OF PLANE PLASTIC STRAIN

By A. P. Green
The British Iron and Steel Research Association, Sheffield

(*Received* 10*th July*, 1953)

Summary

The paper describes the properties and uses of the hodograph of the velocity distribution in an ideal plastic-rigid body undergoing plane plastic deformation. The network in the hodograph plane corresponding to the slip-line field in the physical plane has the same distinctive geometrical properties as a slip-line field. The method, which was first developed by the writer in 1951 to help to solve the problem of strip compression between two smooth parallel dies, assists the solution of mixed boundary value problems ; it is useful for checking whether the rate of plastic work is everywhere positive ; and it enables rapid graphical calculations to be made of velocity distributions. It is applied to the problem of the compression of a block between rough parallel dies, and Nadai's limiting distribution of velocity is justified. Its use in the solution of problems for which the configuration is geometrically similar at all stages of the deformation is also briefly discussed.

Vol. 2 953/54

1. Introduction

The purpose of this paper is to draw attention to a method of representing graphically, by means of a " transformed velocity field," the velocity distribution in an ideal plastic-rigid body undergoing plane plastic deformation.* The method was proposed by the writer in 1951, but does not seem to be widely known. The transformed velocity field is in fact a hodograph, and this term, which was first used in this connection by Prager at a Summer School on Plasticity at the Imperial College, London, July 1952, will henceforward be used instead of " transformed field."

After an account of the properties of hodographs, some applications are discussed. In certain exceptional problems the slip-line field and hodograph are identical. One such example which is examined here is the problem of compression of a wide block between rough parallel dies. The approach to a limiting distribution of velocity at a sufficiently great distance from the centre of the block is investigated by means of the hodograph.

Finally, it is observed that the " unit diagram " method (Hill 1950, p. 213) of analysing the deformation, in problems where the configuration is geometrically similar at all stages, makes implicit use of the hodograph. The condition for continuing geometrical similarity of the surface is formulated as a relationship between the hodograph and the curve representing the free surface in the unit diagram.

* For an account of the theory of plane plastic strain, see R. Hill, *The Mathematical Theory of Plasticity*, Ch. VI (Clarendon Press 1950).

2. GEOMETRICAL PROPERTIES

Following the usual notation, the two sets of orthogonal slip lines in a plastic region are labelled α-and β-lines. By convention, if the α-and β-lines are regarded as a pair of right-handed curvilinear axes, the line of action of the algebraically greater principal stress falls in the first and third quadrants. The velocity components at any point P referred to α and β directions are denoted by u and v respectively. The anti-clockwise angular rotation of an α-line from some fixed direction is denoted by ϕ.

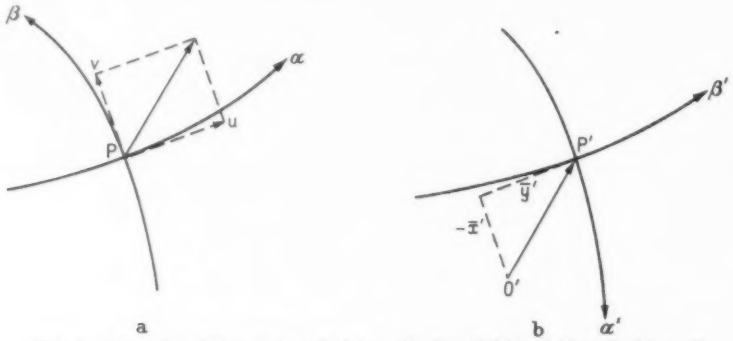

Fig. 1. Corresponding points in (a) a slip-line field and (b) a hodograph.

The resultant velocity at P is represented in the hodograph by the vector $O'P'$, where O' is a fixed origin and the vector is equal in magnitude and parallel in direction to the velocity at P (Fig. 1). Let α' and β' be a right-handed pair of orthogonal directions taken through P', which are oriented so that their clockwise angular rotation from the α and β directions respectively through P is $\pi/2$; i.e. $\phi' = \phi - \pi/2$, where ϕ' is defined in a similar manner to ϕ. The co-ordinates $(\bar{x}', \bar{y}')$ of P' with respect to O' and referred to axes through O' parallel to the α' and β' directions at P' are

$$\bar{x}' = -v, \qquad \bar{y}' = u. \tag{1}$$

Then, as the writer has shown (GREEN 1951), the network traced by P' in the hodograph plane, that corresponds to the slip-line field network traced by P, consists of the orthogonal α'-and β'-lines, where $\alpha \rightarrow \alpha'$ and $\beta \rightarrow \beta'$ (if P is traced in the positive α direction, P' may move in either the positive of the negative α' direction). Thus, the hodograph has the distinctive geometrical properties of a slip-line field, since the angular variations between corresponding points are identical in the two networks.* GEIRINGER's (1930) velocity relations in the slip-line field, viz :—

$$du - vd\phi = 0 \quad \text{along an } \alpha\text{-line},$$

$$\text{and } dv + ud\phi = 0 \quad \text{along a } \beta\text{-line}, \tag{2}$$

* An alternative proof of the essential geometrical properties of the hodograph has since been given by PRAGER (July 1952, Summer School on Plasticity at Imperial College, London). The proof is derived directly from the fact that the rate of extension is zero in the slip-line directions. It follows that the line element between two adjacent points P_1, P_2, on a slipline is perpendicular to the vector representing the increment in velocity between the two points, which is in turn parallel to $P_1'P_2'$ in the hodograph plane.

become

$$d\bar{y}' + \bar{x}'d\phi' = 0 \text{ along an } \alpha'\text{-line},$$

$$\text{and } d\bar{x}' - \bar{y}'d\phi' = 0 \text{ along a } \beta'\text{-line}, \tag{3}$$

in the hodograph.

A velocity discontinuity, say of magnitude Δu across an α-line, is always constant along the length of the slipline. In the hodograph the velocities on either side of such an α-line are mapped as two parallel α'-lines connected by straight β'-lines of equal length $\Delta u = |\Delta\bar{y}'|$. A non-rotating rigid *region* becomes a single *point* in the hodograph. In practice a velocity discontinuity often occurs across a slip line that separates a rigid from a deforming region. The velocities on the deforming side of such a slip line are mapped as a circular arc, with the point representing the rigid region as its centre of curvature, and with radius equal to the velocity discontinuity. If, however, a rigid region is rotating, the velocities along any curve in that region (including for example a slip line bounding the region) are mapped as a geometrically similar curve rotated through an angle $\pi/2$ in the same direction as that of the rigid body rotation. Points representing the velocities of deforming material in contact with a flat rigid die (rough or smooth) lie on a straight line.

Vol. 2 53/54

The radii of curvature R, S, R', and S' of the α-and β-lines through P and the α'-and β'-lines through P' are defined by the equations

$$\frac{1}{R} = \frac{\partial\phi}{\partial s_\alpha}, \qquad \frac{1}{S} = -\frac{\partial\phi}{\partial s_\beta}, \tag{4}$$

(and similarly for R' and S') where ds_α and ds_β are a right-handed pair of elemental arc lengths measured along the slip lines. The effect of superimposing a uniform velocity of translation on the deforming body is only to move the origin of the hodograph, while its shape remains unaltered, (i.e. R' and S' are not affected). The shape is changed, however, if a uniform rotation about any fixed point is superimposed. An angular velocity ω in the clockwise direction changes the radii of curvature at P' from R', S', to

$$R_1' = R' + \omega R, \qquad S_1' = S' + \omega S. \tag{5}$$

3. Plastic Work

The rate of plastic work per unit volume at P, expressed in terms of the radii of curvature in the slip-line field and hodograph (Green 1952 and 1953), is

$$k\dot{\gamma} = k\left(\frac{S'}{S} - \frac{R'}{R}\right), \tag{6}$$

where k is the constant maximum shear stress in the plastic region, and $\dot{\gamma}$ is the maximum shear strain-rate at P (twice the tensor component). If the signs of the terms S'/S and $-R'/R$ in (6) are found to be the same merely by examining the general form of the two networks, laborious calculation of the radii is not necessary in order to ascertain whether the rate of plastic work is positive throughout a slip-line field with a certain associated velocity distribution. The sign of the work of instantaneous shear done as an element crosses a velocity discontinuity must, however, be checked separately since (6) provides no information about this.

4. The Identity of Slip-line Field and Hodograph in Certain Problems

In the particular problems of symmetrical compression of a strip between smooth parallel dies and of sheet-drawing through a smooth wedge-shaped die, it was observed (GREEN 1951) that the slip-line field and its corresponding networks in the hodograph plane are *identical* geometrical configurations (with certain boundaries interchanged). This enabled the exact solution of the compression problem to be obtained for (die-breadth)/(strip-thickness) ratios greater than one, and the form of the slip-line field in sheet-drawing to be found qualitatively in certain ranges of die-angle and reduction for which it was not previously known. If the compressing dies are rough, a similar identity holds between hodograph and slip-line field in all the solutions described by HILL (1950 pp. 228-234). This problem is discussed further in the following section.

In general, however, such identity does not occur, and when it does it is a fortuitous product of simple boundary conditions. The hodograph and slip-line field are different, for example, in the problem of extrusion through a square die if the walls of the container are rough (HILL 1947). Consider also the hodograph for the expansion of a semi-cylindrical cavity in the surface of a semi-infinite block (HILL 1948); it is a single circular arc, since at any instant the magnitude of the velocity is the same at all points in the deforming regions. This differs of course, from the slip-line field*.

5. Compression between Rough Parallel Dies

Consider a rectangular block of material compressed in plain strain between two rough parallel dies that do not overlap the ends of the block. The breadth of the dies and the thickness of the block are denoted by $2w$ and $2h$ respectively. Solutions for which the slip-line field and hodograph are identical are :—

(1) $1 \leqslant w/h \leqslant 3{\cdot}64$ (HILL 1950, p. 230); the material in contact with the dies is rigid; the range of frictional conditions for which the solution is valid is not known.

(ii) $3{\cdot}64 \leqslant w/h$ (HILL, LEE, and TUPPER 1945 and 1951); the dies are so rough that the frictional stress, τ_F, which is induced over the plastically deforming regions, is equal to k, the yield stress of the material in shear, and hence one family of slip lines meets each die orthogonally.

(iii) Solution (ii) modified for partially rough dies (HILL 1950, p. 231); τ_F has some constant value mk ($m < 1$) so that the slip lines intersect the dies at constant angles. This is an artificial condition, chosen for simplicity. If the coefficient of friction were constant, the angle of intersection would vary with normal pressure along the dies, and the slip-line field would not then be identical to the hodograph.

The solution (ii) for perfectly rough dies ($m = 1$) and that for perfectly smooth dies ($m = 0$) are, clearly, limiting cases of solution (iii). Corresponding quadrants of the slip-line field and the hodograph of solution (iii) for $w/h \sim 6{\cdot}9$ and $m \sim 0{\cdot}91$ are shown in Fig. 2. They are drawn here to the same scale but the actual ratio of their dimensions is U/h, where U is the speed of the dies. The solution is only valid for those values of w/h for which the velocity discontinuities (shown by

* It was previously stated incorrectly by the writer (GREEN 1951) that this was an example of indentical networks.

thickened lines in Fig. 2a) initiated at the block centre, T, terminate at the edges of the dies and not on the exit slip lines. In comparing the shapes of the networks, it can be seen that certain boundaries are interchanged. The velocity of the rigid wedge at the centre corresponds to the singularity in the slip-line field at the edge of the die, and, vice-versa, the velocities at this singularity correspond to the plastic-rigid boundary at the centre.

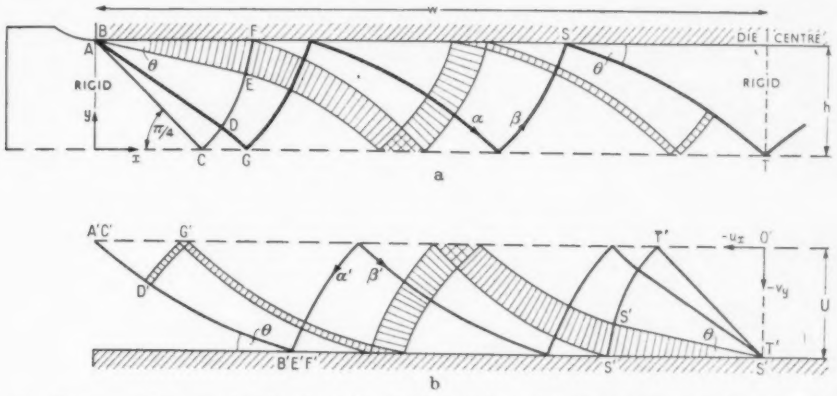

Fig. 2. Corresponding quadrants of (a) the slip-line field and (b) the hodograph for compression between partially rough dies ($w/h \sim 6{\cdot}9$, $m \sim 0{\cdot}91$).

The magnitude of each velocity discontinuity propagated from the centre is multiplied at each reflection at the dies by the factor $\tan\theta$, where $\theta\,(\leqslant \pi/4)$ is the angle at which the α — lines in Fig. 2a meet the die, and $m = \cos 2\theta$. Hence the discontinuities are progressively diminished toward the edge, unless the die is smooth. Correspondingly, the straight line regions in the slip-line field are reduced in length towards the centre by the same factor at each reflection from the die. If w/h is very large it might be expected that the field of slip lines approaches PRANDTL's (1923) cycloid solution. This limiting field consists of that part of two orthogonal families of cycloids which is contained between the two parallel lines that meet the sliplines at the angles θ and $\pi/2 - \theta\,(0 \leqslant \theta \leqslant \pi/4)$, where $\cos 2\theta = m$. Fig. 3a shows the top half of such a field on the left-hand side of the block. It has been shown (HILL et. al 1945) that, when $m = 1$, such a configuration is in fact approached in a quasi-oscillatory manner. It seems reasonable to suppose that, when $m < 1$, a similar approach is made, though probably more slowly the smaller the value of m. The identical hodograph, of course, approaches the same limiting configuration at a sufficiently great distance from the *centre*.

Let (x, y) axes of reference be taken such that the axis of x coincides with the horizontal axis of symmetry, and the axis of y passes through the left-hand edges of the dies (Fig. 2a). If, at a large distance from both the centre and the edge, *both* the slip-line field *and* the hodograph approximate to PRANDTL's field, the strain-rate in that region is independent of x. The distribution of velocity can be deduced from the two cycloidal networks (Fig. 3). Suppose that through any point $P\,(x, y)$ the β — line and the perpendicular to the x-axis cut this axis at the points

Q and N respectively, and that the magnitudes of x and of the velocity at an arbitrarily chosen point Q_0 on the horizontal axis of symmetry in the uniform region are x_θ and u_0 respectively. Then the Cartesian components of velocity at P are

$$u_x = -u_0 + Q_0'Q' + Q'N', \qquad v_y = -P'N'. \tag{7}$$

Since the networks are similar,

$$Q_0'Q' = (U/h)\,Q_0Q = U(x - x_0 - QN)/h, \tag{8}$$

and their cycloidal form leads to the expressions

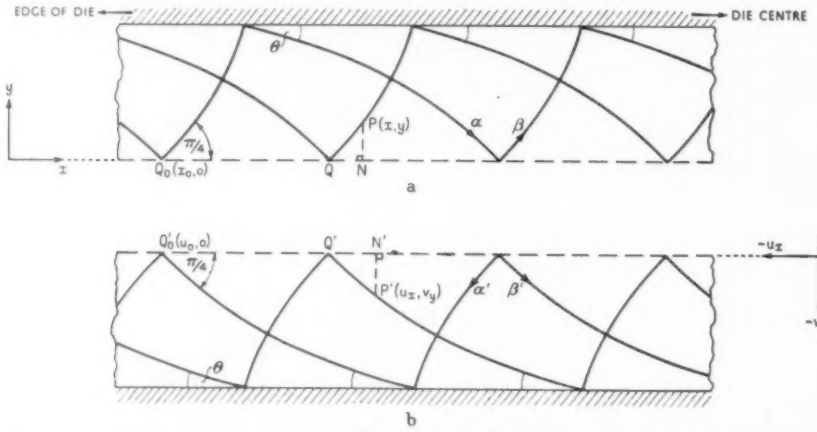

Fig. 3. Corresponding regions of (a) the limiting slip-line field and (b) the limiting hodograph, for compression between partially rough dies.

$$\left.\begin{aligned} QN &= h(2\lambda - 1 + \cos 2\lambda)/m, \\ Q'N' &= U(2\lambda + 1 - \cos 2\lambda)/m, \\ PN = y &= h(\sin 2\lambda)/m = (h/U)\,P'N', \end{aligned}\right\} \tag{9}$$

where λ is the angle turned through by the β-line between Q and P and by the β'-line between Q' and P'. Hence from (7), (8) and (9),

$$\frac{u_x}{U} = \frac{x}{h} - \frac{2}{m}\sqrt{\left(1 - \frac{m^2y^2}{h^2}\right)} + C, \qquad \frac{v_y}{U} = -\frac{y}{h}, \tag{10}$$

where C is a constant. These expressions are the same as those due to NADAI, who suggested them as a *possible* limiting velocity distribution. The present analysis demonstrates their *uniqueness* for the *boundary conditions of this problem* and shows that they are approached in regions where not only the slip-line field but also the hodograph tends to PRANDTL'S cycloid solution. The constant C is determined, as HILL shows, by the condition that the horizontal flow across a vertical section is equal to the rate at which material to the right is displaced by the dies. This gives

$$C = -\frac{w}{h} + \frac{\sin^{-1} m}{m^2} + \frac{1}{m}\sqrt{(1 - m^2)}.$$

6. Problems involving Geometrical Similarity

In the simplest kind of non-steady motion problem the configuration remains geometrically similar as deformation proceeds. Two such problems for which solutions exist are the indenting of the plane surface of a semi-infinite block by a wedge (Hill, Lee, and Tupper 1947), and the expansion of a semi-cylindrical cavity in a similar surface (Hill 1948). It is interesting to observe that the ' unit diagram ' method, which was developed in the wedge-indentation solution, for determining the history of deformation of any particular element, implicitly involved the construction of the hodograph.

To obtain this unit diagram, the slip-line field at any stage of the deformation is scaled down to the same size by reducing to unity a characteristic length, c, defining the stage (e.g. c might be the depth of penetration of a wedge). The hodograph of the velocity distribution corresponding to the slip-line field is constructed with its origin at the origin of distortion, and the velocities are referred to c as the scale of " time," so that this network also is fixed in size and shape as deformation proceeds. Then, in the unit diagram, a point P moves towards P', its corresponding point in the hodograph, with a speed equal to PP'/c. Thus the path of an element in actual space is represented by some trajectory in the unit diagram. In particular, the curve in the unit diagram corresponding to the free surface θ must be the trajectory for surface elements. Hence the tangent at any point P on this curve must pass through its associated point P' in the hodograph.

Vol. 2 53/54

This condition enables the surface corresponding to a tentative velocity distribution to be constructed. For example, if the surface is rigid and moves without rotating, it must be straight (as in the solutions quoted); if, however, it rotates with angular velocity ω, it must take the form of an equiangular spiral whose tangent at any point makes an angle $\tan^{-1}\omega$ with the radius vector. If the surface is deforming it must be the envelope of straight lines drawn through associated points in the hodograph to bisect the angles between the α' and β' directions.

7. Conclusions

The hodograph has proved most useful where, in certain problems with particularly simple boundary conditions, it has been found to be indentical with the slip-line field. Such identity does not generally occur, and it must be emphasized that the hodograph does not provide a general method for solving mixed boundary value problems that eliminates the element of trial and error. It does, however, assist the process of solution by enabling various conditions to be expressed in geometrical form. Velocity boundary conditions impose geometrical conditions on the hodograph just as stress boundary conditions often impose geometrical conditions on the slip-line field. The condition of geometrical similarity is conveniently expressed as a geometrical relationship between the hodograph and the free surface. By means of the hodograph tentative solutions may be rapidly investigated to check whether the rate of plastic work is everywhere positive. A given velocity distribution may be calculated quickly and easily by mapping the hodograph network on a drawing board, thus avoiding lengthy analysis or numerical

computation. Alternatively, it may be found that the hodograph is a standard network which has already been computed such as, for example, the field defined by two circular arcs.

ACKNOWLEDGMENTS

I am grateful to Prof. R. HILL for suggesting the investigations described in Sections 5 and 6. This paper is B.I.S.R.A. Report No. MW/B/43/53.

REFERENCES

GEIRINGER, H.	1930	*Proc. 3rd. Int. Cong. Appl. Mech.* (Stockholm), **2**, 185.
GREEN, A. P.	1951	*Phil. Mag.*, **42**, 900.
	1952	British Iron and Steel Research Association Report MW/B/85/51.
	1953	*J. Mech. Appl. Maths.*, **6**, 223.
HILL, R.	1947	*J. Iron and Steel Inst.*, **158**, 177.
	1948	*Proc. 7th Int. Cong. Appl. Mech.* (London).
	1950	*Mathematical Theory of Plasticity* (Clarendon Press).
HILL, R., LEE, E. H., and TUPPER, S. J.	1945	Ministry of Supply, Armament Research Dept., Theoretical Research Report. 28/45.
	1947	*Proc. Roy. Soc.* A, **188**, 273.
	1951	*J. Appl. Mech.* **18**, 46.
PRANDTL, L.	1923	*Zeits. ang. Math. Mech.*, **3**, 401.

VO
2
1953

Journal of the Mechanics and Physics of Solids, 1954, Vol. 2, pp. 81 to 86. Pergamon Press Ltd., London.

CALCULATIONS AND MEASUREMENTS ON WEDGE-INDENTATION

By J. GRUNZWEIG,* I. M. LONGMAN† and N. J. PETCH*

(*Received 27th August*, 1953)

SUMMARY

THE penetration, contact pressure and slip-line field dimensions in plastic indentation by a rough wedge are calculated by the HILL, LEE and TUPPER theory, and the results are compared with some experimental measurements.

Vol. 2 953/54

1. CALCULATIONS FOR A ROUGH WEDGE

THE slip-line field in a semi-infinite block of plastic-rigid material penetrated normally by a smooth, rigid wedge has been established by HILL, LEE and TUPPER (1947). When the wedge is rough, the corresponding field differs only in that the slip lines no longer meet the wedge face at 45° (Fig. 1), provided AC remains straight. To make calculations for the rough wedge we follow HILL, LEE and TUPPER.

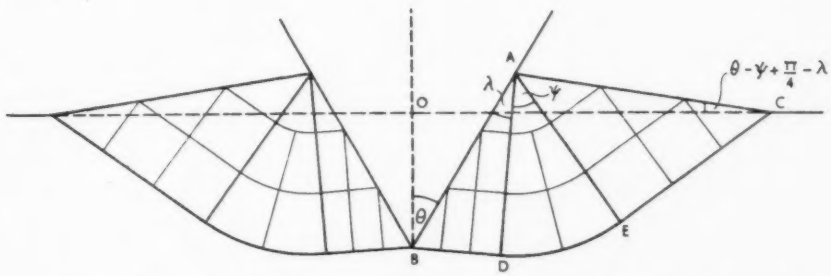

Fig. 1. Slip-line field for the indentation of a plane surface by a rough wedge.

From the height of A (Fig. 1) above the original surface,

$$h \cos \theta - c = \sqrt{2}h \cos \lambda \sin \left(\theta - \psi + \frac{\pi}{4} - \lambda \right) \tag{1}$$

where h is the length AB of the contact surface, c is the depth of penetration beneath the original surface, θ is the semi-angle of the wedge and λ, ψ are the angles BAD and DAE.

From the displacement velocities and the condition for geometric similarity,

* Metallurgy Laboratory, University of Leeds.
† British Iron and Steel Research Association, now at the Hebrew Institute of Technology, Haifa.

$$h\cos\left(\psi+\lambda-\frac{\pi}{4}\right)-c\cos\left(\theta-\psi+\frac{\pi}{4}-\lambda\right)=\frac{c\sin\theta}{\sqrt{2}\cos\lambda} \tag{2}$$

At the contact surface the normal stress on the wedge is $p + k\sin 2\lambda$ and the frictional stress in the direction BA is $k\cos 2\lambda$, where k is the shear yield stress of the block and p is the hydrostatic pressure in the zone ABD. By Hencky's theorem, $p = k(1 + 2\psi)$. Hence, the pressure P on the wedge is

$$P = k(1 + 2\psi + \sin 2\lambda) \tag{3}$$

and

$$\cos 2\lambda = \mu(1 + 2\psi + \sin 2\lambda) \tag{4}$$

where μ is the coefficient of friction.

As a preliminary to the calculation of h/c, P/k, λ and ψ from (1)-(4), we choose values of λ and ψ and calculate θ and h/c from (1) and (2) and μ from (4). Then, for given θ and μ, we guess a value of λ from the preliminary calculation, obtain ψ from (4) and h/c from (1) and from (2). Comparison of the two h/c values gives a guide to the next guess for λ.

With increase of μ, one or other of two limiting cases occur. For the sharper wedges, the frictional stress reaches the shear yield stress k and λ becomes zero. For the blunter wedges, the limit occurs when BD is inclined at 45° to the downward vertical; the indenter then becomes covered with a 90° wedge-shaped cap of dead metal (HILL 1950, p. 220).

The results are shown in Table I. P/k and h/c are accurate to $\frac{1}{4}\%$, λ to 1′ and ψ to 5′.

TABLE I.

θ	μ	h/c	P/k	λ	ψ	ck/L
0°	0·0	1·00	2·00	45°0′	0°	∞
	0·05	1·00	2·10	41°59′	3°1′	4·76
	0·10	1·00	2·20	38°39′	6°21′	2·28
	0·15	1·00	2·29	34°58′	10°2′	1·46
	0·20	1·00	2·38	30°49′	14°11′	1·05
	0·25	1·00	2·45	26°7′	18°53′	0·816
	0·30	1·00	2·51	20°34′	24°26′	0·664
	0·35	1·00	2·55	13°18′	31°42′	0·559
	*0·389	1·00	2·57	0°	45°	0·500
10°	0·0	1·17	2·09	45°0′	2°40′	1·179
	0·05	1·16	2·22	41°49′	6°21′	0·873
	0·10	1·15	2·35	38°13′	10°42′	0·679
	0·15	1·15	2·46	34°9′	15°21′	0·550
	0·20	1·14	2·57	29°32′	20°25′	0·460
	0·25	1·14	2·66	24°10′	26°8′	0·394
	0·30	1·13	2·73	17°29′	33°12′	0·345
	0·35	1·13	2·78	6°46′	44°14′	0·308
	*0·359	1·13	2·78	0°	51°3′	0·302

* frictional stress = k. † dead-metal cap.

TABLE I.—*continued.*

θ	μ	h/c	P/k	λ	ψ	ck/L
20°	0·0	1·34	2·31	45°0′	8°52′	0·473
	0·05	1·33	2·46	41°28′	13°24′	0·394
	0·10	1·32	2·60	37°27′	18°20′	0·335
	0·15	1·30	2·74	32°51′	23°50′	0·289
	0·20	1·29	2·86	27°33′	29°48′	0·255
	0·25	1·28	2·96	21°9′	36°50′	0·228
	0·30	1·28	3·03	12°22′	46°6′	0·207
	*0·328	1·27	3·05	0°	58°45′	0·198
30°	0·0	1·55	2·60	45°0′	17°20′	0·248
	0·05	1·53	2·77	41°1′	22°32′	0·217
	0·10	1·51	2·94	36°27′	28°12′	0·192
	0·15	1·50	3·08	31°13′	34°20′	0·172
	0·20	1·48	3·21	25°0′	41°29′	0·156
	0·25	1·47	3·31	17°6′	50°2′	0·144
	*0·297	1·46	3·36	0°	67°40′	0·135
40°	0·0	1·82	2·96	45°0′	27°25′	0·144
	0·05	1·80	3·15	40°28′	33°15′	0·130
	0·10	1·78	3·32	35°18′	39°30′	0·118
	0·15	1·76	3·48	29°17′	46°31′	0·108
	0·20	1·74	3·60	21°57′	54°42′	0·100
	0·25	1·72	3·69	11°23′	65°56′	0·094
	*0·270	1·72	3·71	0°	77°33′	0·093
50°	0·0	2·24	3·35	45°0′	38°42′	0·0871
	0·05	2·21	3·56	39°53′	45°4′	0·0799
	0·10	2·17	3·74	34°1′	51°57′	0·0741
	0·15	2·15	3·90	27°6′	59°50′	0·0692
	0·20	2·12	4·02	18°17′	69°20′	0·0655
	†0·242	2·11	4·08	5°0′	83°10′	0·0626
60°	0·0	2·93	3·77	45°0′	50°50′	0·0521
	0·05	2·88	3·99	39°15′	57°42′	0·0488
	0·10	2·85	4·18	32°38′	65°12′	0·0458
	0·15	2·81	4·34	24°42′	73°53′	0·0436
	†0·195	2·78	4·44	15°0′	84°7′	0·0421
70°	0·0	4·34	4·22	45°0′	63°34′	0·0290
	0·05	4·27	4·45	38°35′	70°50′	0·0275
	0·10	4·21	4·64	31°11′	78°50′	0·0263
	†0·135	4·16	4·75	25°0′	85°27′	0·0256
80°	0·0	8·61	4·68	45°0′	76°41′	0·0126
	0·05	8·46	4·91	37°54′	84°15′	0·0121
	†0·069	8·41	4·99	35°0′	87°18′	0·0120
90°	0·0	∞	5·14	45°0′	90°0′	—

* frictional stress = k. † dead-metal cap.

Vol. 2 53/54

The load L per unit length of the wedge is $2\,Ph \sin\theta + 2\mu\,Ph\cos\theta$; calculated values of the penetration, expressed as ck/L, are also in Table 1. The influence of friction on the penetration is much greater at small, than at large, wedge angles.

2. EXPERIMENTAL

These calculations have been compared with some measurements on the indentation of lead and polytetrafluoroethylene (" Fluon ") by small-angle steel wedges under various frictional conditions.

In one set of measurements, the wedges were pressed into lead blocks of approximately 1" square section in a small Hounsfield testing machine. The load was measured by the machine and the penetration, which did not exceed 1 mm, was obtained from the relative movement of points on the wedge and on the lead using a measuring microscope. The lead had previously been strained by a 60% reduction in thickness to decrease the strain-hardening rate and two alloys containing 0·05% tellurium and 2·5% silver were used, which do not recover at room temperature. The indentation extended right across the block, but it was thought that the error due to end effects would be small, and, in agreement with this, the load-penetration relationship was linear.

Measurements were made with both dry and lubricated wedges. In the second case, small increments rof penetration were used and, afte each of them, the wedge was lifted slightly out of the indentation and lubricated with white spirit + 5% stearic acid.

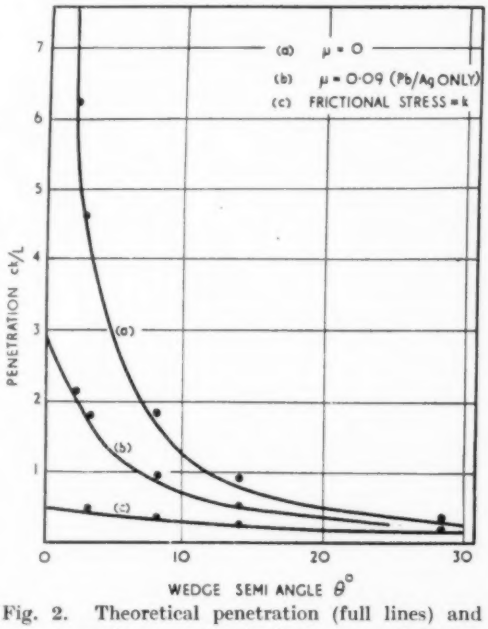

Fig. 2. Theoretical penetration (full lines) and experimental points for lead (average of *Pb/Ag* and *Pb/Te* results).

In another set of experiments, the wedge was lubricated and, in addition, it was driven to-and-fro in its own plane of symmetry by an arm attached to an accurately-guided cross-head driven by a geared-down electric motor. Direct loading by weights on the wedge holder was used in this case. Since the longitudinal force applied to the wedge overcomes the residual friction with the lead, this arrangement approximately simulated frictionless penetration, although the longitudinal force meant some departure from the conditions in the theoretical calculation.

Measurements of the shear yield stress k were made by compression of cylindrical samples with grooved, lubricated ends, assuming that the yield stress in compression is $\sqrt{3}k$; the results were Pb/Te : 97 kg/cm², Pb/Ag : 208 kg/cm². The coefficients of friction relevant to these experiments were obtained using the

apparatus with the to-and-fro movement. A wedge was pressed into the lead block, which was fixed in a carriage supported on balls, and the displacing force when the wedge was moved was measured by the deflection of a light steel beam to which the carriage was attached. With a lubricated wedge, $\mu = 0{\cdot}09$ for the Pb/Ag alloy, but the shear yield stress was attained for both the lead alloys with a dry wedge and metal was dragged out of the groove.

The results of the indentation experiments are in Fig. 2. The observed penetrations for given loads are higher than the theoretical values. At $\mu = 0$, the agreement is fairly close for small wedge angles, but the divergence from the theory increases to 11% at the largest angle. At $\mu = 0{\cdot}09$, the divergence ranges from 8% at the smallest angle to 21% at the largest angle, and the corresponding range for the dry wedge is 12%-25%.

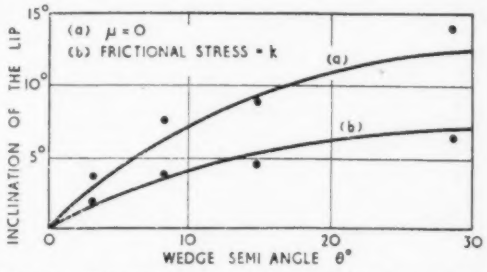

Fig. 3. Theoretical lip inclination (full lines) and experimental points for lead.

The ratio h/c was also measured, Table II. For this purpose, the lead blocks were cut in half and then firmly clamped together during the indentation, so that a section free from end-effects was obtained. The lip departed from its theoretical form by a rounding of the apex in the manner that has already been described by HILL, LEE and TUPPER. Observed h/c values were lower than the theoretical ones by an amount that increased with the wedge angle and was greatest for the dry wedges. The inclination of the lip was also measured; and, although the results were rather uncertain, they agreed fairly closely with the theoretical values (Fig. 3).

TABLE II.

$\theta°$	h/c (*Pb*)						h/c (*Fluon*)	
	Dry Wedge		*Lubricated Wedge, stationary*		*Lubricated Wedge, moved to-and-fro*		*Dry Wedge, stationary*	
	Obs.	*Calc.*	*Obs.*	*Calc.*	*Obs.*	*Calc.*	*Obs.*	*Calc.*
3·2	1·00	1·04	1·00	1·05	1·08	1·05	1·00	1·05
8·2	1·00	1·10	1·00	1·12	1·12	1·14	0·97	1·13
14·8	1·06	1·20	1·09	1·23	1·15	1·25	0·96	1·24
28·5	1·16	1·43	1·22	1·48	1·30	1·52	0·90	1·50

HILL, LEE and TUPPER have shown that the formation of a lip with a plane surface involves a relative movement of the lead and the wedge at their contact surface, and interference with this movement by friction will be one cause of the rounded lip. Strain-hardening may also contribute, but presumably friction is

more important in the present case. The h/c figures indicate that the reduction of contact area due to this rounding is sufficient to account for the main part of the excess of the observed, over the calculated, penetrations.

3. The Indentation of Fluon

Measurements were also made with polytetrafluoroethylene (Fluon), which has a low coefficient of friction; $\mu = 0{\cdot}06$ was observed with the steel wedges. This material strain-hardens considerably ($k \sim 43$ kg/cm^2); consequently, the experimental results were expressed at each wedge angle as the ratio of the penetration ck/L of a dry wedge in the Hounsfield machine to the penetration of the same dry wedge in the to-and-fro apparatus. The slip-line fields compared are then nearly geometrically similar, so the deformation and strain-hardening are approximately the same and the penetration ratio is approximately independent of strain-hardening. These experiments were primarily intended merely to demonstrate that the increase in penetration from the to-and-fro movement is small when the coefficient of friction is small, and this is shown by the results in Fig. 4.

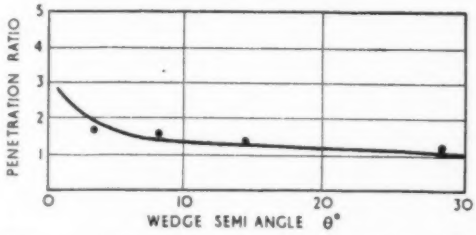

Fig. 4. Theoretical curve for the ratio of the penetration ck/L at $\mu = 0$ to that at $\mu = 0{\cdot}05$, with experimental points for polytetrafluoroethylene.

There was very little lip with this strain-hardening material; the top corners of the impression were again rounded and h/c was less than unity. On unloading, the impression closed up until its angle was only about half that of the wedge, indicating considerable elastic strain. The h/c values were measured on the recovered impression.

Acknowledgment

We are grateful to the British Iron and Steel Research Association for a grant and for permission to quote from reports.

References

Hill, R. 1950 Mathematical Theory of Plasticity (Clarendon Press, Oxford).

Hill, R., Lee, E. H. and Tupper, S. J. 1947 *Proc. Roy. Soc.* A **188**, 273.

Journal of the Mechanics and Physics of Solids, 1954, Vol. 2, pp. 87 to 91. Pergamon Press Ltd., London.

THE PLASTIC TORSION OF ANISOTROPIC BARS

By R. Hill
Department of Mathematics, University of Nottingham

(*Received* 21*st October*, 1953)

Summary

The fully plastic state of stress is examined in an anisotropic prismatic bar twisted by terminal couples. The only restriction imposed on the anisotropy is that it should be orthotropic everywhere, with one principal axis parallel to the generators. It is shown how the distributions of shearing stress and warping displacement can be calculated without difficulty for any shape of section. Explicit formulae are obtained for the torque when the section is circular or rectangular and when the anisotropy is of a kind probably occurring in a torsion specimen cut from a rolled slab.

Vol.
2
53/54

1. Statement of the Problem

Consider a prismatic metal bar of arbitrary section twisted by terminal couples about an axis parallel to the generators. The heat treatment and d stortion received by the bar while being formed leave it in general with a preferred crystal orientation. The resultant state of plastic anisotropy is assumed to be the same in any section and orthotropic at each point, with one principal axis parallel to the generators. This restriction rules out the consideration of a preferred orientation arising from previous torsion of the bar, where the principal axes of anisotropy are probably all inclined to the generators (Barrett 1952, p. 481) ; some discussion of this case for a thin-walled tube has been given by Hill (1950, pp. 325-8).

In the present analysis the material is treated as plastic-rigid, and the torque and mode of warping are calculated at the yield point of the fully plastic bar. Experimental data showing the significance of the yield point of the hypothetical plastic-rigid body in regard to the behaviour of a metal has recently been obtained by Hill and Siebel (1953) and by Crossland and Hill (1953).

2. Distribution of Shearing Stress

Let (x, y) axes by taken in some transverse section, so that the z axis is parallel to the generators. The state of stress in each element is to be a pure shear acting over the section. We denote its (x, y) components by (p, q). When the bar is fully plastic these satisfy some relation

$$f(p^2, q^2, x, y) = 0 \tag{1}$$

where f, the yield function, depends on the anisotropy at each point. Only the squares of p and q are involved, by virtue of the assumed orthotropic symmetry. We have also the equation of equilibrium

$$\frac{\partial p}{\partial x} + \frac{\partial q}{\partial y} = 0 \tag{2}$$

and the boundary condition

$$q/p = dy/dx \tag{3}$$

on the external contour C of the section.

The directions of the characteristic curves of equations (1) and (2), together with the variations of p and q along them, are given by

$$dp \Big/ \frac{\partial f}{\partial y} = -dq \Big/ \frac{\partial f}{\partial x} = dx \Big/ \frac{\partial f}{\partial q} = -dy \Big/ \frac{\partial f}{\partial p}. \tag{4}$$

In particular, when the anisotropy does not vary across the section, $\frac{\partial f}{\partial x} = 0 = \frac{\partial f}{\partial y}$ and so $dp = 0 = dq$. The characteristics are therefore straight, and along any one of them the resultant shear stress is uniform and parallel to the associated tangent to C. The magnitude of the shear stress can be obtained from (1) and (3). When the bar is isotropic (1) reduces to

$$p^2 + q^2 = k^2 \tag{5}$$

where k is the shear yield stress; as is well known, the characteristics are then the normals to C since the directions defined by (3) and (4) are orthogonal. When the bar is anisotropic, however, the characteristics cut C at varying angles.

Within the contour there will be a certain curve Γ (possibly having several branches) which is the locus of intersections of characteristics from different parts of C. In general the shear stress is discontinuous across this curve; the component normal to it is, however, continuous for reasons of equilibrium (this indeed is the defining property of Γ). Any projecting sharp corner on C is the source of one of the branches of Γ. A re-entrant sharp corner, on the other hand, is a point singularity from which radiates a fan of characteristics*.

3. Mode of Warping

Consider, now, the calculation of the warping displacements. It is supposed that the relation between the applied stress and the associated plastic strain-increment is such that a reversal of the stress would merely produce a strain of opposite sign but equal magnitude. Hence, having regard to the considered state of anisotropy, the strain in any element must be a simple shear parallel to the section (though not, of course, necessarily in the direction of the shear stress). We thus ignore changes in length of the bar due to residual microscopic internal stresses (c.f. HILL 1950, pp. 37 and 328). Since such stresses are mainly effective only while the crystal grains in an element are not yet all plastic, the length change is of an elastic order of magnitude and its neglect is consistent with the plastic-rigid treatment.

For the velocity (u, v, w) of an element we assume, then, the expressions

* The indeterminacy of the characteristic field around such a corner, if only the stress equations are considered, is resolved by requiring the co-existence of a *continuous* warping displacement. Equivalently, in conformity with the maximum work principle, the field must be chosen to give the greatest possible torque, or, in terms of the stress function 'roof,' the greatest volume under the roof.

$$u = -yz, \qquad v = xz, \qquad w \equiv w(x, y), \tag{6}$$

where the rate of twist per unit length is taken as unity. If the yield function f is also the plastic potential, the ratio of the shear strain-rate components is

$$\left(\frac{\partial w}{\partial x} - y\right) \Big/ \left(\frac{\partial w}{\partial y} + x\right) = \frac{\partial f}{\partial p} \Big/ \frac{\partial f}{\partial q}. \tag{7}$$

The characteristics of this equation have at any point the direction given by

$$\frac{\partial f}{\partial p}\, dx + \frac{\partial f}{\partial q}\, dy = 0, \tag{8}$$

which is identical with that in (4). Equation (8) states that the component of shear strain-rate in the characteristic direction is zero.

Now the part of this component due to the relative rotation of neighbouring sections is of amount t, where t is the perpendicular distance from the origin to the tangent at the point under consideration. The sense of this shear along the tangent is such that its direction has a positive (right-handed) moment about the z axis, in conformity with (6). The remaining part of the component of shear strain-rate is due to the warping and is of amount $\partial w/\partial s$, where s is the arc-length along the characteristic in the prescribed sense. Since the two parts have zero resultant,

$$\frac{\partial w}{\partial s} = -t \qquad \text{or} \qquad w = -\int t\, ds = \int (y\, dx - x\, dy). \tag{9}$$

This equation specifies the variation of w along a characteristic. The present method of derivation appears to be new and is more direct than methods hitherto used in the isotropic case.

The integration of (9) is begun from the point of intersection of a characteristic with the stress discontinuity Γ. It may be proved (c.f. Hill 1952, p. 26) that the shear strain-rate vanishes on Γ, provided f is a convex function* ; hence equation (9) holds also on Γ. The rate of warping is thus determined on Γ, and hence everywhere in the section, to within an immaterial additive constant. Note that the selection of the origin, hitherto arbitrary, effects (u, v, w) only to the extent of a rigid-body motion.

4. A Particular Type of Anisotropy

A simple form of yield function is

$$\frac{p^2}{{p_0}^2} + \frac{q^2}{{q_0}^2} = 1 \tag{10}$$

where p_0 and q_0 are the yield stresses in pure shear in the x and y directions respectively. We suppose that this holds at every point. Equation (10) probably represents fairly well the anisotropy in a specimen cut from the central portion of a rolled slab.

From (4) the inclination θ of a characteristic to the positive x axis is such that

* The same conclusion follows if we regard Γ as the limit approached by the elastic core as the rigidity modulus tends to infinity, for a given angle of twist (Mandel 1946 ; Prager and Hodge 1951, p. 84). It is, however, then necessary to prove first the existence, and uniqueness, of a plastic-elastic solution under certain conditions on the yield function and plastic potential.

$$\tan\theta = -pq_0^2/qp_0^2. \tag{11}$$

Hence, if ψ is the inclination of the contour tangent to the negative x axis,

$$\tan\theta \tan\psi = q_0^2/p_0^2. \tag{12}$$

When evaluating the torque it is convenient to introduce a stress function Φ such that

$$p = \frac{\partial\Phi}{\partial y}, \qquad q = -\frac{\partial\Phi}{\partial x}, \tag{13}$$

so satisfying the equilibrium equation (2). Equation (10) becomes

$$\left(\frac{1}{p_0}\frac{\partial\Phi}{\partial y}\right)^2 + \left(\frac{1}{q_0}\frac{\partial\Phi}{\partial x}\right)^2 = 1. \tag{14}$$

The contours of Φ in the (x, y) plane are the shearing stress trajectories; in particular, the boundary condition (3) is satisfied by arbitrarily choosing $\Phi = 0$ on C. As is well known, the torque can then be expressed as

$$T = \iint (xq - py)\,dx\,dy = 2\iint \Phi\,dx\,dy. \tag{15}$$

To find Φ at any point we note from (11), (13) and (14) that its inward rate of increase along a characteristic is

$$\sqrt{(p_0^2\sin^2\theta + q_0^2\cos^2\theta)}. \tag{16}$$

Alternatively, we may proceed as follows. Put

$$q_0 x = k\xi, \qquad p_0 y = k\eta, \tag{17}$$

where k is an arbitrary constant with the dimensions of stress. In terms of the new coordinates (14) becomes

$$\left(\frac{\partial\Phi}{\partial\xi}\right)^2 + \left(\frac{\partial\Phi}{\partial\eta}\right)^2 = k^2. \tag{18}$$

This is just the equation satisfied by the stress function for a bar of isotropic material with a shear yield stress k (c.f. equation (5)); the Φ surface has the constant slope k. In the (ξ, η) plane the characteristics are the normals to the transformed contour and correspond to the characteristics in the (x, y) plane; the stress trajectories also correspond. If T^* is the yield point torque of this isotropic bar,

$$\left.\begin{aligned} T^* &= 2\iint \Phi\,d\xi\,d\eta \\ \text{and} \qquad T &= \frac{k^2}{p_0 q_0}.\,T^*. \end{aligned}\right\} \tag{19}$$

5. An Elliptical Section

Consider the particular elliptical contour

$$\left(\frac{x}{a}\right)^2 + \left(\frac{y}{b}\right)^2 = 1 \qquad \text{where} \qquad \frac{a}{b} = \frac{p_0}{q_0}.$$

Introduce a length r such that

$$kr = q_0 a = p_0 b.$$

Then the corresponding contour in the (ξ, η) plane is the circle

$$\xi^2 + \eta^2 = r^2.$$

Hence, from (19)

$$T = \frac{k^2}{p_0 q_0} \times \tfrac{2}{3} \pi k r^3 = \tfrac{2}{3} \pi a^2 b q_0 = \tfrac{2}{3} \pi a b^2 p_0.$$

Since the stress trajectories in the (ξ, η) plane are concentric circles, the trajectories in the (x, y) plane are similar concentric ellipses. Again, since the characteristics in the (ξ, η) plane are radii, so are those in the (x, y) plane (since the two origins correspond). It follows from (9) that there is no warping.

6. Circular Section

If the actual contour is a circle of radius a, the transformed contour is an ellipse with semi-axes $\alpha = aq_0/k$, $\beta = ap_0/k$. A stress discontinuity extends over a length $2\beta(1 - \alpha^2/\beta^2)$ of the η axis (supposing that $p_0 > q_0$) and hence over a length $2a(1 - q_0^2/p_0^2)$ of the y axis. From (9) and the general configuration of the characteristic field it is evident that the warping is antisymmetric, w being positive in the first and third quadrants and negative in the others.

Vol. 2 53/54

Suppose, now, that the degree of anisotropy is small. Then, to a good approximation, the yield point torque of the transformed section is midway between the torques for circular sections whose radii are respectively equal to the semi-axes of the ellipse. Hence

$$T = \frac{k^2}{p_0 q_0} \times \tfrac{2}{3} \pi k a^3 \times \frac{(p_0^3 + q_0^3)}{2k^3} = \tfrac{1}{3} \pi a^3 . \frac{(p_0^3 + q_0^3)}{p_0 q_0}.$$

7. Rectangular Section

Let the rectangle have sides a, b parallel respectively to the x, y axes. The transformed contour is a rectangle with sides $\alpha = aq_0/k$, $\beta = bp_0/k$, parallel to the ξ, η axes. From (19),

$$T = \frac{k^2}{p_0 q_0} \times \tfrac{1}{6} k\alpha^2 (3\beta - \alpha) = \tfrac{1}{6} a^3 q_0 \left(\frac{3b}{a} - \frac{q_0}{p_0}\right) \quad \text{if} \quad \frac{a}{b} \leqslant \frac{p_0}{q_0},$$

$$\text{or} \quad \frac{k^2}{p_0 q_0} \times \tfrac{1}{6} k\beta^2 (3\alpha - \beta) = \tfrac{1}{6} b^3 p_0 \left(\frac{3a}{b} - \frac{p_0}{q_0}\right) \quad \text{if} \quad \frac{a}{b} \geqslant \frac{p_0}{q_0}.$$

References

Barrett, C. S.	1952	*Structure of Metals*, 2nd Ed. (McGraw-Hill Book Co.)
Crossland, B. and Hill, R.	1953	*J. Mech. Phys. Solids* **2**, 27.
Hill, R.	1950	*Mathematical Theory of Plasticity* (Clarendon Press).
	1952	*J. Mech. Phys. Solids* **1**, 19.
Hill, R. and Siebel, M. P. L.	1953	*J. Mech. Phys. Solids* **1**, 207.
Mandel, J.	1946	*C. R. Acad. Sci.* (Paris) **222**, 1205.
Prager, W. and Hodge, P. G.	1951	*Theory of Perfectly Plastic Solids* (Wiley and Sons, Inc.).

Journal of the Mechanics and Physics of Solids, 1954, Vol. 2, pp. 92 to 102. Pergamon Press Ltd., London.

IMPACT OF FINITE BEAMS OF DUCTILE METAL

By P. S. Symonds and C. F. A. Leth
Brown University

(*Received 1st August*, 1953)

Summary

An analysis is here presented of the large plastic deformations of a beam under impact such as that due to a blow of a massive hammer, in which one cross-section is suddenly forced to move with a given velocity. The analysis treats both the case in which the velocity of the struck section is maintained constant until the total permanent deformation is acquired and cases of interrupted impacts in which the force at the struck section is suddenly removed after an arbitrary contact time. A complete solution in general non-dimensional form is obtained in a simple manner by basing the analysis on the assumption of " plastic-rigid " behaviour and results can be expected to be valid when the plastic deformations are large enough. Criteria for the validity of the present results are discussed, based on the major assumptions of the analysis.

1. Introduction

We consider the problem of a uniform beam of arbitrary length, initially at rest, which is subjected to a concentrated impact load at its mid-point such that the mid-section of the beam instantaneously acquires a velocity V which is then maintained constant. Duwez, Clark and Bohnenblust (1950) treated the corresponding problem for an infinitely long beam, in general terms for an arbitrary moment-curvature relation. It was recently discussed again by Conroy (1952), who investigated the simplifications obtainable by neglecting the elastic part of the deformations, and took, in particular, moment-curvature relations of the two types shown in Fig. 1; again only infinitely long beams were considered.

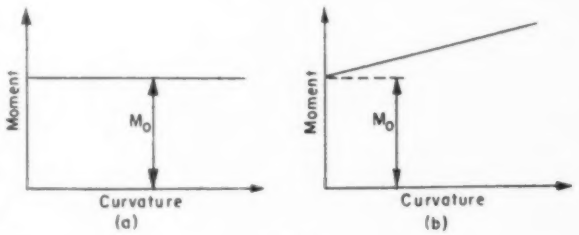

Fig. 1.

The solution presented here is another example of the analysis of large plastic deformations in a finite structure subjected to a dynamic load, on the basis of the moment-curvature relation of Fig. 1 (a). In this " plastic-rigid " type of analysis it is assumed that infinitely large curvatures can occur at cross-sections where the bending moment maintains the magnitude M_0, the " limit moment " or " fully plastic moment " used in limit analysis of structures under static loads. The

concept of localization of deformations at such " plastic hinge " sections is assumed to be applicable to problems of dynamic loading of structures of ductile metal provided the energy absorbed in plastic deformations greatly exceeds that which could be absorbed in a wholly elastic manner. Based on this hypothesis criteria were given in a previous paper (LEE and SYMONDS 1952) for the validity of the solutions obtained, and similar criteria are given in the present paper for the new solution presented here.

Earlier papers (LEE and SYMONDS 1952, SYMONDS 1953, SEILER and SYMONDS 1953) dealt with finite beams subjected to force pulses with specified magnitudes and shape. Our main purpose in treating the present problem was to obtain a solution that could be treated more easily experientally than solutions obtained previously; the imposition of a known velocity involves fewer experimental difficulties than the application and measurement of a specified force-time curve. The present problem was emphasized by VIGNESS (1953) as of interest in experimental verification of the general method.

2. ANALYSIS

For simplicity we treat the problem of a beam moving initially with velocity V normal to its length. At time $t = 0$ the mid-section is instantaneously brought to rest by contact with a rigid stop. It is obvious that the subsequent deformations will be identical with those that would be produced if the bar, initially at rest, were struck so that the mid-section suddenly acquires and maintains the velocity V. The beam is taken to have uniform mass per unit length m, limit moment M_0, and length $2l$. A typical cross-section will be specified by its distance x from the centre of the beam (Fig. 2).

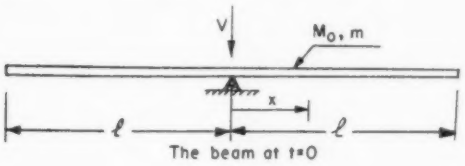

Fig. 2.

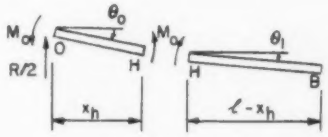

Fig. 3.

For a sufficiently small time interval after the bar strikes the stop, the deformation is indistinguishable from that of the infinite beam treated by CONROY (1952). Hence it is to be expected that the force on the beam varies initially as $1/\sqrt{t}$, and that plastic hinges will occur at the mid-section and at two cross-sections each at a distance x_h from the centre; x_h is to be expected to increase initially in proportion to $\sqrt{t}$. The analysis of the present problem is therefore based on the diagrams of Fig. 3. From the symmetry of the problem it is obviously enough to consider either half of the beam. The segments OH and HB are subjected to end moments as shown. At the centre of the beam there is a reaction force R exerted by the stop so that a shear force $R/2$ acts as shown on the one segment. However, there is no shear force at cross-section $x = x_h$, where the travelling hinge is located at a given instant, since this is a cross-section where the bending moment has a relative maximum; thus $dM/dx = Q = 0$. The loading on the segments includes

also the distributed inertia forces due to the accelerations. It can be verified that, although they are changing in length, at any instant the two segments move as rigid bodies (hinged together as shown) since at any instant the complete set of loads is such that the bending moment reaches the magnitude M_0 only at the sections $x = 0$ and $x = x_h$. The lateral hinge moves outward (i.e., x_h increases with time) so that the segment OH acquires a permanent deformation, but since the moment in the interior of the segment HB is always less than M_0 in magnitude the segment to the right of the travelling hinge at any instant is undeformed.

Let the angular velocities of the segments OH and HB be ω_0 and ω_1, respectively. Writing moment-angular acceleration equations with respect to the fixed point O in one case and the mass centre of the segment in the other, we obtain*

$$\tfrac{1}{3} m x_h^3 \frac{d\omega_0}{dt} = -2M_0, \tag{1}$$

$$\tfrac{1}{12} m (l - x_h)^3 \frac{d\omega_1}{dt} = M_0. \tag{2}$$

The following equation expresses the fact that the change of moment of momentum of the half-beam OB with respect to an axis at O is equal to the angular impulse of the moment M_0 acting during the time t:

$$-M_0 t = \left[\tfrac{1}{6} m (\omega_0 - \omega_1)(3l^2 x_h - x_h^3) + \tfrac{1}{3} m l^3 \omega_1\right] - \tfrac{1}{2} m l^2 V. \tag{3}$$

The expression in square brackets is the moment of momentum at any time t, while the last term is the initial moment of momentum of the half-beam.

(1), (2) and (3) are the basic equations of the analysis from which, together with appropriate initial conditions, the three unknowns x_h, ω_0, ω_1 are to be found. It is now convenient to rewrite the equations in terms of new dimensionless variables defined as follows:

$$\Omega = \frac{l}{V}\omega_0; \qquad \psi = \frac{l}{V}\omega_1, \tag{4}$$

$$\eta = \frac{M_0 t}{m l^2 V}; \qquad \xi = \frac{x_h}{l}. \tag{5}$$

Equations (1) (2), and (3) become

$$\Omega' \equiv \frac{d\Omega}{d\eta} = -\frac{6}{\xi^3}, \tag{6a}$$

$$\psi' \equiv \frac{d\psi}{d\eta} = \frac{12}{(1-\xi)^3}, \tag{6b}$$

$$3 - 6\eta = (\Omega - \psi)(3\xi - \xi^3) + 2\psi. \tag{6c}$$

Henceforth a dash is used to denote differentiation with respect to η. The initial conditions may be taken as

$$\eta = 0; \qquad \xi = 0; \qquad \psi = 0. \tag{7}$$

* These equations are correct despite the fact that x_h is a function of time, because the velocities of elements just to the left and just to the right of the travelling hinge are equal at any instant. Thus, although the segment of length x_h is increasing in length, the element joining it in time dt comes in with the same velocity as the end of the segment, and there is no impulsive contribution to the momentum.

From equation (6c) this implies that $(\Omega\xi)_0 = 1$, so that in this type of impact there is initially a singularity in the angular velocity at the point of impact.

We begin the solution of equation (6) by differentiating (6c) with respect to η, making use of (6a) and (6b) and simplifying to obtain the relation

$$\Omega - \psi = \frac{6}{\xi'}\left[\frac{1}{\xi^2} - \frac{1}{(1-\xi)^2}\right]. \tag{8}$$

For completeness, we note that the above result may be derived from a quite different viewpoint, namely by differentiating the equation which expresses the fact (as shown by LEE and SYMONDS) that velocities are continuous at the hinge section. Equation (8) can thus be identified as expressing the fact that accelerations are discontinuous across the moving hinge section.

A second differentiation of (8), substitution again of Ω' and ψ' from (6a) and (6b), and rearrangement leads to the following equation for ξ :

$$\left[\frac{1-2\xi}{(1-\xi)^2}\right]\xi\xi'' + \xi'^2 = 0, \tag{9}$$

which is to be solved subject to the initial conditions (7). A first integration of (9) can easily be performed since the independent variable does not appear explicitly. Let $\xi' = p(\xi)$; then

$$\xi'' = \frac{dp(\xi)}{d\xi}\frac{d\xi}{d\eta} = \xi'\frac{dp}{d\xi} = p\frac{dp}{d\xi}.$$

With this substitution (9) becomes

$$\left[\frac{1-2\xi}{(1-\xi)^2}\right]\xi\frac{dp}{d\xi} + p = 0$$

if it is assumed that $p \neq 0$. Integration of the above yields

$$p = \frac{d\xi}{d\eta} = \frac{1}{A}\cdot\frac{e^{\xi/2}(1-2\xi)^{1/4}}{\xi}.$$

Thus the general solution of (9) can be written in the form

$$\eta = A\int_0^{\xi}\frac{ze^{-z/2}\,dz}{(1-2z)^{1/4}} + B \tag{10}$$

where A and B are constants to be evaluated by means of the initial conditions (7). The numerical evaluation of the integral in (10) is speeded by making the substitution $(1-2z) = 4s$. Integration by parts and rearrangement then leads to the following form :

$$\eta = A\left[e^{-\xi/2}(1-2\xi)^{3/4} + 2F(\xi)\right] + B \tag{11}$$

where

$$F(\xi) = \sqrt{2}\,e^{-1/4}\int_{\frac{1}{4}(1-2\xi)}^{1/4} s^{-1/4}e^{s}\,ds - \tfrac{1}{2}.$$

The advantage of this form appears when the integrand in (11) is expanded in a power series ; term by term integration then leads to the following rapidly converging series for $F(\xi)$:

$$F(\xi) = 0{\cdot}07952 - 2e^{-1/4}(1-2\xi)^{3/4} \sum_{n=0}^{\infty} \frac{(1-2\xi)^n}{n!\,(3+4n)\,4^n}.$$

Equations (6) and (8) can now be integrated to give the dimensionless angular velocities as follows :

$$\Omega = \tfrac{3}{2} + 6A\left[\frac{1}{\xi}(1-2\xi)^{3/4}\,e^{-\xi/2} - F\right] - 3B, \tag{12a}$$

$$\psi = \tfrac{3}{2} - 6A\left[\frac{(2-\xi)(1-2\xi)^{3/4}\,e^{-\xi/2}}{(1-\xi)^2} + F\right] - 3B. \tag{12b}$$

After applying the initial conditions (7) to (10) and (12b) we find that A and B must have values $B = 0$, $A = 1/6$. Thus ξ and η are related by

$$6\eta = e^{-\xi/2}(1-2\xi)^{3/4} + 2\sqrt{2}\,e^{-1/4}\int_{\frac{1}{4}(1-2\xi)}^{1/4} s^{-1/4}\,e^{s}\,ds - 1. \tag{13}$$

It can be seen from the denominator in (10) that the above solution is valid only for $0 < \xi < \frac{1}{2}$. This is the range we are interested in, as will appear shortly.

3. Numerical Results

The deformations of main interest are the angles θ_0 and θ_1 at mid-point and tip, respectively, and the permanent curvature κ of the part of the bar through which the lateral hinge has travelled. We have the following general formulas for the angles

$$\theta_0 = \int_0^t \omega_0\,dt = \frac{mlV^2}{M_0}\int_0^{\xi}\frac{\Omega}{\xi'}\,d\xi, \tag{14}$$

$$\theta_1 = \int_0^t \omega_1\,dt = \frac{mlV^2}{M_0}\int_0^{\xi}\frac{\psi}{\xi'}\,d\xi. \tag{15}$$

The change $d\theta$ of the angle of the beam across the lateral hinge has the value

$$d\theta = (\omega_0 - \omega_1)\,dt.$$

Then

$$\kappa = \frac{d\theta}{dx} = (\omega_0 - \omega_1)\frac{dt}{dx} = \frac{mV^2}{M_0}\frac{\Omega - \psi}{\xi'} = \frac{mV^2}{6M_0}\frac{(1-2\xi)^{1/2}\,e^{-\xi}}{(1-\xi)^2}. \tag{16}$$

Numerical results are given in Table 1.

The previous analysis is based on the configuration of Fig. 3. This type of motion continues until the angular velocities of the inner and outer segments become equal, i.e., until $\Omega = \psi$. From (8) this happens when

$$\frac{1}{\xi_s^2} - \frac{1}{(1-\xi_s)^2} = 0 \qquad \text{or} \qquad \xi_s = \tfrac{1}{2} \tag{17a}$$

where ξ_s denotes the final value of the hinge coordinate. The corresponding value of the dimensionless time is

$$\eta_s = 0{\cdot}0265. \tag{17b}$$

For later times, $\eta \geqslant \eta_s$ there is a plastic hinge at the mid-section only, and the

two halves rotate as rigid bars pinned at one end. The equation of angular acceleration of the right-hand half, in dimensionless variables, is

$$\frac{d\Omega}{d\eta} = -3. \tag{18}$$

Hence in this final phase of the motion we have

$$\Omega = -3\eta + c_1, \qquad \frac{M_0}{mlV^2}\theta_0 = -\tfrac{3}{2}\eta^2 + c_1\eta + c_2.$$

TABLE 1.

ξ	η	Ω	ψ	$\frac{M_0}{mlV^2}\theta_0$	$\frac{M_0}{mlV^2}\theta_1$	$\frac{M_0}{mV^2}\kappa$
0	0	∞	0	0	0	0·1667
0·05	0·0002	19·524	0·003	0·0083	0·0000	0·1667
0·10	0·0008	9·045	0·012	0·0167	0·0000	0·1665
0·15	0·0019	6·583	0·031	0·0250	0·0000	0·1661
0·20	0·0034	5·883	0·063	0·0334	0·0001	0·1652
0·25	0·0053	3·845	0·114	0·0418	0·0003	0·1632
0·30	0·0078	3·136	0·191	0·0502	0·0007	0·1594
0·35	0·0108	2·610	0·309	0·0588	0·0013	0·1523
0·40	0·0144	2·191	0·491	0·0676	0·0029	0·1388
0·45	0·0191	1·829	0·786	0·0769	0·0059	0·1111
0·50	0·0265	1·421	1·421	0·0888	0·0138	0·0000

Making use of the conditions $\eta_s = 0{\cdot}0265$, $\Omega_s = 1{\cdot}421$, $M_0/mlV^2\,\theta_{0s} = 0{\cdot}0888$, as given in Table 1, we obtain

$$\Omega = 1{\cdot}500 - 3\eta, \tag{19a}$$

$$\frac{M_0}{mlV^2}\theta_0 = 0{\cdot}0500 + 1{\cdot}5\eta - 1{\cdot}5\eta^2. \tag{19b}$$

These hold until $\Omega = O$, or, from (19a), until $\eta = \eta_f$, where

$$\eta_f \equiv \frac{M_0 t_f}{ml^2 V} = 0{\cdot}500. \tag{20a}$$

The corresponding final value of the angle θ_0 is

$$\theta_0 = 0{\cdot}425\,\frac{mlV^2}{M_0}. \tag{20b}$$

The growth of the deformations with time as shown in Fig. 4.

Some simple checks on the above results are of interest. First, we note that the momentum relation (6c), evaluated at the time η_s, becomes

$$3 - 6\eta_s = 2\psi_s.$$

Taking values from the last line of Table 1 the two sides of the equation have values

$$3 - 0{\cdot}1590 = 2{\cdot}841\,; \qquad 2 \times 1{\cdot}421 = 2{\cdot}842$$

which is a satisfactory check. Again, from (6c) the time η_f at which the deformation is completed is given by

$$3 - 6\eta_f = 0, \qquad \eta_f = \tfrac{1}{2}.$$

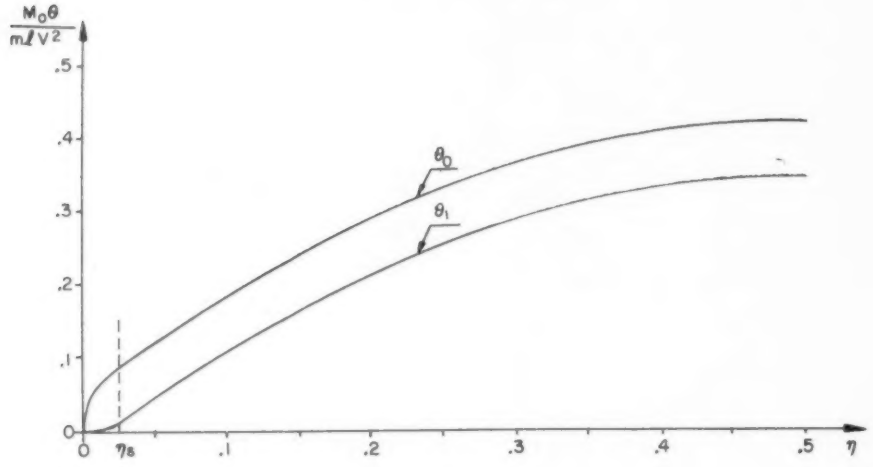

Fig. 4.

which verifies the value (20a) computed from the tabulated values.

Finally, the energy relations may be examined. Before the beam hits the rigid stop it has the kinetic energy $E = m\,l\,V^2$. When the motion has ceased, this energy has been spent in work at plastic hinges. The total energy absorbed in plastic deformations is W, where

$$W = 2M_0\,\theta_{0f} + 2\,(\theta_{0f} - \theta_{1f})\,M_0.$$

Inserting values from (20b) and Table 1 this becomes

$$W = 2M_0\left(0{\cdot}425\,\frac{mlV^2}{M_0}\right) + 2M_0\left(0{\cdot}0750\,\frac{mlV^2}{M_0}\right) = 1{\cdot}000\,mlV^2.$$

Thus the necessary energy balance is checked.

We may also compare the results obtained here with those obtained by CONROY (1952). It is there shown by equations (2) and (20) that $12\eta = \xi^2$ for an infinitely long beam. Our result should converge to this value for small ξ. We expand the right-hand side of (13) as a power series in ξ :

$$e^{-\xi/2}\,(1 - 2\xi)^{3/4} = 1 - 2\xi + \tfrac{1}{2}\,\xi^2 + O\,(\xi^3),$$

$$\int_{\frac{1}{4}\,(1-2\xi)}^{1/4} \frac{e^s\,ds}{s^{1/4}} = \frac{\sqrt{2}}{2}\,e^{1/4}\,\xi + O\,(\xi^3).$$

Hence (13) reduces, for small ξ, to

$$\eta = \frac{1}{12}\xi^2 + O(\xi^3). \tag{21}$$

Furthermore CONROY shows by (20) and (26) that the shear force at the centre varies as $\frac{1}{2}\sqrt{\frac{3}{\eta}}\frac{M_0}{l}$. The moment equilibrium for the inner part of the beam around its mass centre requires

$$\tfrac{1}{4} R x_h - 2M_0 = \frac{m x_h^3}{12}\dot{\omega}_0.$$

Transforming this into dimensionless coordinates we obtain

$$\mu\xi = 8 + \tfrac{1}{3}\xi^3 \Omega' \tag{22}$$

where $\mu = \dfrac{Rl}{M_0}$. With the use of (6a) we obtain

$$\mu = \frac{6}{\xi}. \tag{23}$$

In the limit for small ξ we have $\xi = \sqrt{12\eta}$. Hence in the limit $\mu = \sqrt{(3/\eta)}$, which agrees with CONROY's result.

For completeness we finish the analysis with the calculation for the motion of the beam if the support is removed at a time $t = \tau < (ml^2 V/M_0)\eta_f$. The subsequent motion ($t > \tau$) is to be determined by analysis appropriate to a beam acted on by no external loads. Such an analysis is described by SYMONDS (1953). There it is shown that, when lateral hinges are present at the instant the central force is reduced to zero, the lateral hinges then move with constant velocity until the angular velocities become equalized. By simple calculations, using equations (20)-(29) of SYMOND's paper, one can find the increments in angular velocities and displacements which occur after removal of the force at arbitrary times τ, corresponding to dimensionless times $\eta_\tau = (M_0\,\tau/ml^2\,V) < 0{\cdot}5$. Fig. 6 shows a curve of final deformation angles resulting from " interrupted impacts " of various durations, plotting $M_0\,\theta_{0f}/mlV^2$ against $M_0\,\tau/ml^2\,V$. The shape of the force-time curve concerned here is indicated in Fig. 5.

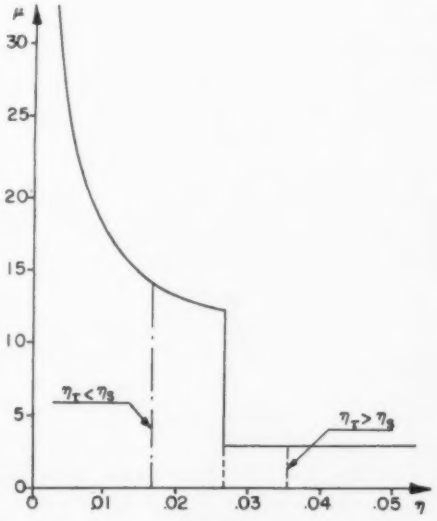

Fig. 5.

4. CRITERIA FOR VALIDITY OF RESULTS

We consider now the implications for experimental comparisons of two major assumptions involved : namely, the neglect of all elastic deformations by com-

parison with plastic ones, and the neglect of shape changes throughout the analysis.

The first assumption can be expected to be valid (LEE and SYMONDS 1952) if the total energy absorbed in plastic deformations greatly exceeds the maximum possible amount of *elastic* strain energy that could be stored in the beam. In the present case this implies that

$$2M_0\,\theta_{0f} = mlV^2 \gg M_0^2\,l/EI$$

where EI is the elastic flexural rigidity. Thus, for the present results to be good approximations, one requirement is that

$$V^2 \gg M_0^2/mEI. \tag{24a}$$

Alternatively the above requirement may be expressed as

$$V^2 \geqslant n\,M_0^2/mEI \tag{24b}$$

where n is a number which presumably is of the order of 10.

A further requirement is set by the assumption of negligible shape changes, i.e., the use of coordinates referring to the undeformed rather than to the actual beam. This assumption actually restricts the magnitude of the central angle θ_0 attained only during that part of the response in which deformations are occurring at lateral hinges; when only the central hinge is present the equations apply to deformation angles of unrestricted magnitude. From Table 1 the maximum value of θ_0 obtained while the lateral hinges are present is $0{\cdot}0888\,mlV^2/M_0$; if we assume that this does not exceed about 0·15 radians, we have the additional inequality

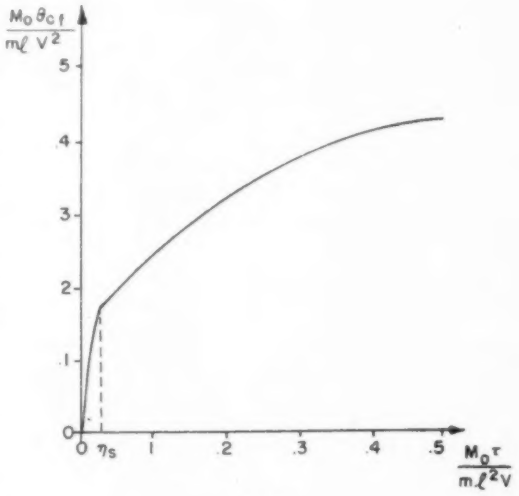

Fig. 6.

$$0{\cdot}0888\,mlV^2/M_0 < 0{\cdot}15 \tag{25}$$

This imposes a limitation on the length-depth ratio of the beam, if the requirements of inequalities (24) is taken into account. Let (24b) be taken as an *equation* and combined with the inequality (25). We obtain

$$n\,.\,\frac{lM_0}{EI} < \frac{0{\cdot}15}{0{\cdot}0888} \cong 1{\cdot}7. \tag{26a}$$

But the limit moment M_0 can be computed (SYMONDS and NEAL 1951) as

$$M_0 = \alpha\sigma_y Z = \alpha\sigma_y\left(\frac{2I}{h}\right) \tag{27}$$

where the " shape factor " α is a number of the order of unity which depends on the shape of the cross-section and has the value 1·5 for a rectangular cross-section ; σ_y is the yield stress ; $Z = 2I/h$ is the elastic section modulus, i.e., quotient of moment of inertia I and half-depth $h/2$. With this formula for M_0, the inequality (26a) can be written as

$$\frac{h}{2l} > \frac{1}{1{\cdot}7}\, n\alpha\, \frac{\sigma_y}{E}. \tag{26b}$$

Since σ_y/E is of the order of 10^{-3} for steel, and α probably about 1·5, it is seen that the restriction of small shape changes requires only that $h/2l$ should exceed about 1/100 for $n = 10$. Hence it is clear that this restriction would introduce no experimental difficulties.

Finally, the order of magnitude of V demanded by inequality (24b) is of interest. We use (27) and write also $m = \rho A$, $I = Ai^2$, $E/\rho = c_0^2$, and obtain

$$V \geqslant \sqrt{n}\, c_0 \left(\frac{\sigma_y}{E}\right) \left(\frac{i\alpha}{h/2}\right) \tag{24c}$$

where $c_0 = \sqrt{E/\rho}$ = speed of longitudinal elastic waves, ρ = mass density, A = cross-sectional area, i = radius of gyration, h = depth of beam, α = shape factor (defined in connection with (27)). Thus, for steel with $c_0 = 16{,}000$ ft/sec, $\sigma_y/E = 10^{-3}$, a rectangular cross-section, and $n = 10$, we find that V must exceed about 45 ft/sec.

Vol. 2 53/54

The main purpose of a laboratory test would be to determine under what circumstances, if any, the plastic-rigid analysis yields satisfactory results for the major plastic deformations. The fundamental assumption is that elastic deformations are negligible. To find the range of usefulness of this assumption, a series of tests could be made to determine the value of the number n used in (24b), above which the present analysis predicts deformation in good agreement with that observed. If the elastic deformations are the only important physical effect which is ignored, such a series of tests should yield a definite value of n, such that when the total energy absorbed is at least n times the maximum possible elastic energy the beam could carry, the present type of analysis is suitable. A value of n determined for the present case of velocity impact would probably have significance for other types of problems of dynamic loading.

In any experiments other physical effects will occur which have been neglected here, and these might turn out to be so important that the present type of analysis does not yield accurate results even though the criterion based on elastic energy is satisfied. Among the physical phenomena which have been ignored are :

(a) *Strain-hardening*

Strain-hardening at cross-sections where plastic hinge action occurs.

(b) *Speed of loading*

Speed of loading effect on the yield-stress and post-yield properties, as, for example, reported by Manjoine (1944) and Nadai and Manjoine (1941).

(c) *Effect of transverse shear forces*

Effect of transverse shear forces which are known to reduce the limit moment below that which can be reached in pure bending (in the present problem the shear force at the struck section has large values in the initial instants of the impact).

d) *Finite contact area of the hammer or stop*

The study in SEILER and SYMONDS (1953) of distributed, as compared with concentrated, loads showed that even a very small degree of spreading of the load over a finite segment may appreciably reduce the magnitude of the final deformations.

e) *Finite time of acceleration*

It was assumed that the hammer or stop is perfectly rigid and that the velocity of the struck section is instantaneously acquired or annihilated; since any physical hammer or stop has finite rigidity there is a finite time of acceleration. In fact the contact will probably be *intermittent* during the initial instants of the impact, as is known to be the case in the elastic impact of a mass on a beam.

All but one of the foregoing effects, if taken into account, would tend to reduce the deformations below those given by the present analysis. The single exception is the effect of transverse shear forces, which tend to weaken the beam and hence if properly taken into account would cause the analysis to predict larger deformations than those of the present theory. If the transverse shear effect is minimized by use of compact sections and fairly large ratios of span to depth, the other effects would presumably predominate, and cause the present analysis to over-estimate the deformations.

Finally, it should be re-emphasized that a fundamental pre-supposition throughout the paper is that the material has sufficient ductility under dynamic conditions so that rupture does not occur before the predicted final deformations are attained. The present type of analysis should be regarded as a basic one, particularly attractive for its simplicity and generality, but which may have to be refined in particular cases. Carefully planned and interpreted tests are needed. They will be an invaluable aid in assessing the range of usefulness of the present type of analysis and in showing the directions in which refinements are most urgent.

ACKNOWLEDGMENT

The results in this paper were obtained in the course of research conducted under Contract N7-onr-35810 between the Office of Naval Research and Brown University.

REFERENCES

CONROY, M. F.	1952	*J. Appl. Mech.*, **19**, 465.
DUWEZ, P. E., D. S. CLARK and H. F. BOHNENBLUST	1950	*J. Appl. Mech., Trans. ASME*, **72**, 27.
LEE, E. H. and SYMONDS, P. S.	1952	*J. Appl. Mech.*, **19**, 308.
MANJOINE, M. J.	1944	*J. Appl. Mech.*, **11**, 211.
NADAI, A. and MANJOINE, M. J.	1941	*J. Appl. Mech.*, **8**, 77.
SEILER, J. A. and SYMONDS, P. S.	1953	*Technical Report No.* 13, *Brown University to Office of Naval Research.*
SYMONDS, P. S.	1953	*National Conference Applied Mechanics Division, ASME, Minneapolis, Minn.*, Paper No. 53-APM-26.
SYMONDS, P. S. and NEAL, B. G.	1951	*J. Franklin Institute*, **252**, 383.
VIGNESS, I.	1953	*J. Appl. Mech.*, **20**, 151.

Journal of the Mechanics and Physics of Solids, 1954, Vol. 2, pp. 103 to 109. Pergamon Press Ltd., London

ON EULERIAN CO-ORDINATES IN ELASTIC WAVE PROPAGATION

By R. E. D. Bishop* and J. N. Goodier†

(*Received* 23*rd November*, 1953)

Summary

When a stress wave passes through an elastic solid, it is usual to treat the problem of analysis as it occurs : i.e. with the wave moving through the stationary solid. Under certain circumstances however, it is possible to invert the problem by imagining the disturbance to be stationary and the solid to flow through it. The equations of motion are found for this scheme and they are illustrated by reference to non-dispersive propagation of waves in plane strain.

Vol. 2 53/54

1. Introduction

The equations of motion of a fluid may be obtained in two different forms which correspond to the two ways in which a flow may be viewed. In the ' Lagrangian ' scheme, attention is focussed upon the particles of fluid and the history of each is the object of analysis. The ' Eulerian ' scheme (which is usually the more profitable in hydrodynamics) has, as the object of investigation, the conditions of pressure, velocity, etc. at all points in the flow at any instant. The relevant equations are derived by Lamb (1932).

When treating the propagation of elastic waves, it is usual to think of problems as they actually occur : i.e. of disturbances passing through elastic media. This is comparable, in a sense, to the Lagrangian scheme of fluid flow and will be referred to, hereafter, as the ' orthodox ' scheme. This paper deals with the alternative (' Eulerian ') point of view. That is, the conditions will be examined under which an elastic solid " flows through " a disturbance so that the wave is brought to rest.

The Eulerian treatment introduces nothing that is fundamentally new to elasticity theory. However, it is sometimes helpful in visualizing the mechanism of wave propagation and a great deal of the standard theory of elastic waves can be derived equally well from either standpoint. It is thought to be worthwhile, therefore, to record the salient points of the technique.

2. Waves on Taut Elastic Strings

In order to fix ideas, the elementary problem of transverse motion of a long, flexible, taut string may be considered. Associating the undeflected line of the string with the x axis, the string is supposed to have a constant velocity V in

*The Engineering Laboratory, Cambridge
†Stanford University, California

the x-direction and to be passed through a system of lateral deflection y such that its tension S is constant. Let $f(x, t)$ be an applied force per unit length and $q(x, t)$ the body force per unit length, both acting in the plane of the deflection.

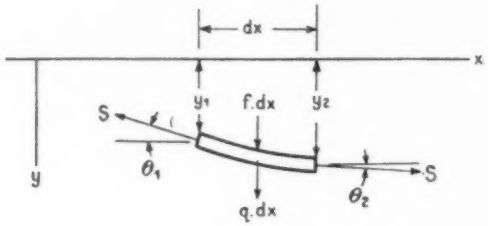

Fig. 1.

In passing from x to $x + dx$, the change of deflection of a particle is $y_2 - y_1 = dy$ (see Fig. 1) and this is achieved in time dt.

Now

$$dy = \frac{\partial y}{\partial x}\,dx + \frac{\partial y}{\partial t}\,dt$$

where $dx = V\,dt$, so that the average vertical velocity of a particle is

$$v = \left(V\frac{\partial}{\partial x} + \frac{\partial}{\partial t}\right) y.$$

The acceleration is evidently

$$a = \left(V\frac{\partial}{\partial x} + \frac{\partial}{\partial t}\right)^2 y.$$

Thus, if the only body force is that of inertia,

$$q = -\,m\left(V\frac{\partial}{\partial x} + \frac{\partial}{\partial t}\right)^2 y$$

where m is the uniform mass per unit length. For dynamic equilibrium of the element shown in Fig. 1,

$$S(\sin\theta_2 - \sin\theta_1) + f\,.\,dx + q\,.\,dx = 0.$$

On dividing by dx and proceeding to the limit as $dx \to 0$, this yields

$$S\frac{\partial^2 y}{\partial x^2} + f = m\left(V\frac{\partial}{\partial x} + \frac{\partial}{\partial t}\right)^2 y, \tag{1}$$

which is the equation of motion.

The steady-state deflection is such that f and y are functions of x alone, so that

$$(S - mV^2)\frac{d^2 y}{dx^2} = -f. \tag{2}$$

If the transverse pressure f is zero, either

$$V^2 = S/m \quad \text{or} \quad \frac{d^2 y}{dx^2} = 0. \tag{3}$$

These results conform to the well-known, simple theory of non-dispersive propagation of free waves on a string.

3. Waves in a Homogeneous Elastic Solid

Let axes $Oxyz$ be fixed in space and suppose that the infinite elastic solid has a constant velocity V in the x direction. The solid will be distorted as it is passed through a system of deflection which is fixed with respect to the axes but not with respect to time.

Particle displacements may be defined by letting

$$u = u(x, y, z, t), \qquad v = v(x, y, z, t), \qquad w = w(x, y, z, t),$$

be the displacements in the x, y, z directions of a particle that would have been at (x, y, z) at time t in the absence of the deformation. In a short interval of time dt,

$$du = \frac{\partial u}{\partial x}\,dx + \frac{\partial u}{\partial t}\,dt = \left(V\frac{\partial u}{\partial x} + \frac{\partial u}{\partial t}\right)dt,$$

$$dv = \frac{\partial v}{\partial x}\,dx + \frac{\partial v}{\partial t}\,dt = \left(V\frac{\partial v}{\partial x} + \frac{\partial v}{\partial t}\right)dt,$$

$$dw = \frac{\partial w}{\partial x}\,dx + \frac{\partial w}{\partial t}\,dt = \left(V\frac{\partial w}{\partial x} + \frac{\partial w}{\partial t}\right)dt.$$

The x, y, z components of particle velocity are therefore

$$V + \left(V\frac{\partial}{\partial x} + \frac{\partial}{\partial t}\right)u, \qquad \left(V\frac{\partial}{\partial x} + \frac{\partial}{\partial t}\right)v, \qquad \left(V\frac{\partial}{\partial x} + \frac{\partial}{\partial t}\right)w,$$

respectively. The corresponding components of the particle acceleration are given by another application of the operator $\left(V\frac{\partial}{\partial x} + \frac{\partial}{\partial t}\right)$; they are, respectively,

$$\left(V\frac{\partial}{\partial x} + \frac{\partial}{\partial t}\right)^2 u, \qquad \left(V\frac{\partial}{\partial x} + \frac{\partial}{\partial t}\right)^2 v, \qquad \left(V\frac{\partial}{\partial x} + \frac{\partial}{\partial t}\right)^2 w.$$

In the usual notation, the equations of equilibrium are

$$\frac{\partial \sigma_x}{\partial x} + \frac{\partial \tau_{xy}}{\partial y} + \frac{\partial \tau_{xz}}{\partial z} + X = 0,$$

$$\frac{\partial \tau_{xy}}{\partial x} + \frac{\partial \sigma_y}{\partial y} + \frac{\partial \tau_{yz}}{\partial z} + Y = 0,$$

$$\frac{\partial \tau_{xz}}{\partial z} + \frac{\partial \tau_{yz}}{\partial y} + \frac{\partial \sigma_z}{\partial z} + Z = 0,$$

where X, Y and Z denote body forces per unit volume (e.g., see Timoshenko and Goodier (1951), art. 76). In the absence of body forces other than that of inertia,

Vol. 2 53/54

$$X = -\rho\left(V\frac{\partial}{\partial x} + \frac{\partial}{\partial t}\right)^2 u,$$

$$Y = -\rho\left(V\frac{\partial}{\partial x} + \frac{\partial}{\partial t}\right)^2 v,$$

$$Z = -\rho\left(V\frac{\partial}{\partial x} + \frac{\partial}{\partial t}\right)^2 w,$$

where ρ is the mass density. Now the equations of equilibrium may be written in terms of the displacements u, v and w by virtue of Hooke's Law (Timoshenko and Goodier (1951), art. 79) and, if this is done and the above values are assigned to X, Y and Z, the following equations of motion arise :

$$\begin{aligned}(\lambda+\mu)\frac{\partial\Delta}{\partial x} + \mu\nabla^2 u &= \rho\left(V\frac{\partial}{\partial x} + \frac{\partial}{\partial t}\right)^2 u,\\ (\lambda+\mu)\frac{\partial\Delta}{\partial y} + \mu\nabla^2 v &= \rho\left(V\frac{\partial}{\partial x} + \frac{\partial}{\partial t}\right)^2 v,\\ (\lambda+\mu)\frac{\partial\Delta}{\partial z} + \mu\nabla^2 w &= \rho\left(V\frac{\partial}{\partial x} + \frac{\partial}{\partial t}\right)^2 w.\end{aligned} \tag{4}$$

λ and μ are Lamé's constants, Δ is the dilatation given by

$$\frac{\partial u}{\partial x} + \frac{\partial v}{\partial y} + \frac{\partial w}{\partial z},$$

and ∇^2 is the Laplacian operator

$$\frac{\partial^2}{\partial x^2} + \frac{\partial^2}{\partial y^2} + \frac{\partial^2}{\partial z^2}.$$

When $V = 0$, (4) assumes the orthodox form for propagation within the stationary solid (e.g., see Timoshenko and Goodier (1951), art. 144).

Boundaries may be introduced into the infinite solid provided that those stresses are applied at the surface which would otherwise be supplied by the solid cut away. It is understood that the boundaries are such that the geometrical picture does not alter as the solid moves ; for instance, a slab of varying thickness cannot be discussed in this way.

4. Steady-State Distortion Patterns

For non-dispersive propagation of elastic waves u, v and w in (4) are all independent of t so that

$$\begin{aligned}(\lambda+\mu)\frac{\partial\Delta}{\partial x} + \mu\nabla^2 u &= \rho V^2\frac{\partial^2 u}{\partial x^2},\\ (\lambda+\mu)\frac{\partial\Delta}{\partial y} + \mu\nabla^2 v &= \rho V^2\frac{\partial^2 v}{\partial x^2},\\ (\lambda+\mu)\frac{\partial\Delta}{\partial z} + \mu\nabla^2 w &= \rho V^2\frac{\partial^2 w}{\partial x^2}.\end{aligned} \tag{5}$$

As before, boundaries may be introduced into the solid so that, translating back to the orthodox point of view, (5) governs the motions of an elastic body which is subjected to *constant* boundary tractions that travel with constant speed V in the negative x direction. This may be thought of as the condition of ' forced wave propagation.'

Now (5) may easily be derived from the orthodox equations of motion,

$$(\lambda + \mu)\left[\frac{\partial}{\partial x}, \frac{\partial}{\partial y}, \frac{\partial}{\partial z}\right]\Delta + \mu\nabla^2\left[u, v, w\right] = \rho\frac{\partial^2}{\partial t^2}\left[u, v, w\right]. \tag{6}$$

If propagation is to have the speed V in the negative direction of x, the displacements will be of the form

$$u = u(x + Vt, y, z), \quad v = v(x + Vt, y, z), \quad w = w(x + Vt, y, z).$$

Letting $\xi = x + Vt$, it is seen that

$$\frac{\partial^2 u}{\partial t^2} = \frac{\partial^2}{\partial \xi^2}\left[u(\xi, y, t)\right],$$

$$\frac{\partial^2 u}{\partial t^2} = V^2\frac{\partial^2 u}{\partial \xi^2} = V^2\frac{\partial^2 u}{\partial x^2}.$$

Similar relations hold for v and w so that (6) are brought into coincidence with (5). Although the displacements u, v, w are now functions of t, there is no derivative with respect to that parameter. Provided that the only dependence of the boundary conditions upon time is through the variable ξ, it is only necessary to consider the displacements when $t = 0$; the values of u, v, w at time t are then found by writing $x + Vt$ in place of x.

Returning to (5), solutions may be found either directly or, more conveniently, by the use of potential functions. These functions are associated with the division of the (now static) displacement pattern into irrotational and equivoluminal components (e.g., see BISHOP (1953)). The potential functions will now be functions of x, y and z only.

5. Steady-State, Plane Strain Patterns

Steady-state, plane strain patterns are governed by a special form of (5); u and v are now independent of z and t, while w is everywhere zero, so that

$$\begin{aligned}(\lambda + \mu)\frac{\partial \Delta}{\partial x} + \mu\nabla^2 u &= \rho V^2\frac{\partial^2 u}{\partial x^2},\\ (\lambda + \mu)\frac{\partial \Delta}{\partial y} + \mu\nabla^2 v &= \rho V^2\frac{\partial^2 v}{\partial x^2}.\end{aligned} \tag{7}$$

It is now necessary to postulate that, if a boundary is contemplated, the surface tractions must also be independent of z and t. A few simple results will now be derived from (7).

If $V = c_1 = \sqrt{[(\lambda + 2\mu)/\rho]}$, it is found that

$$(\lambda+\mu)\frac{\partial^2 v}{\partial x\,\partial y}+\mu\frac{\partial^2 u}{\partial y^2}=0,$$
$$-(\lambda+\mu)\frac{\partial^2 v}{\partial x^2}+(\lambda+\mu)\frac{\partial^2 u}{\partial x\,\partial y}+(\lambda+2\mu)\frac{\partial^2 v}{\partial y^2}=0. \tag{8}$$

These equations do not amount to a demand that the displacements shall be irrotational because the analysis admits forced, as well as free, waves. If u and v do constitute an irrotational strain system, so that the extra restriction

$$\frac{\partial u}{\partial y}-\frac{\partial v}{\partial x}=0$$

is placed upon (8), it is found that

$$\frac{\partial^2 v}{\partial x\,\partial y}=\frac{\partial^2 u}{\partial y^2}=0\,;\qquad \frac{\partial^2 v}{\partial y^2}=0. \tag{9}$$

On the other hand if u and v are such that, at all points, the dilatation is zero so that

$$\frac{\partial u}{\partial x}+\frac{\partial v}{\partial y}=0,$$

(8) requires that

$$(\lambda+\mu)\frac{\partial^2 u}{\partial x^2}-\mu\frac{\partial^2 u}{\partial y^2}=0,$$
$$(\lambda+\mu)\frac{\partial^2 v}{\partial x^2}-\mu\frac{\partial^2 v}{\partial y^2}=0. \tag{10}$$

If $V=c_2=\sqrt{(\mu/\rho)}$, (7) yields

$$(\lambda+\mu)\frac{\partial^2 u}{\partial x^2}+(\lambda+\mu)\frac{\partial^2 v}{\partial x\,\partial y}+\mu\frac{\partial^2 u}{\partial y^2}=0,$$
$$(\lambda+\mu)\frac{\partial^2 u}{\partial x\,\partial y}+(\lambda+2\mu)\frac{\partial^2 v}{\partial y^2}=0. \tag{11}$$

If, further, the strain is equivoluminal (i.e. the dilatation is zero) these become

$$\frac{\partial^2 u}{\partial y^2}=0\,;\qquad \frac{\partial^2 u}{\partial x\,\partial y}=\frac{\partial^2 v}{\partial y^2}=0. \tag{12}$$

But if c_2 is treated as a particular speed of forcing irrotational waves, it is found that

$$(\lambda+\mu)\frac{\partial^2 u}{\partial x^2}+(\lambda+2\mu)\frac{\partial^2 u}{\partial y^2}=0,$$
$$(\lambda+\mu)\frac{\partial^2 v}{\partial x^2}+(\lambda+2\mu)\frac{\partial^2 v}{\partial y^2}=0. \tag{13}$$

It is of interest to examine (9) more closely. Evidently, the most general irrotational strain system that is propagated at the speed c_1 is

$$u=A(x)+y\,.\,\frac{d\,B(x)}{dx},\qquad v=B(x)+Cy. \tag{14}$$

The system $A(x)$ is simply a plane longitudinal wave. The terms containing $B(x)$ represent a type of wave whose existence has been pointed out by GOODIER and BISHOP (1952). The term containing the constant C has no apparent significance.

Again, (12) indicates that the most general equivoluminal wave (within the ambit of non-dispersive systems in plane strain) is

$$u = -E(x) + Fy, \qquad v = y \cdot \frac{dE(x)}{dx} + G(x). \tag{13}$$

The system $G(x)$ is a plane transverse wave, that containing $E(x)$ is of the type discussed by GOODIER and BISHOP (1952) and the distortion Fy is probably of no importance.

REFERENCES

BISHOP, R. E. D.	1952	*Quart. J. Mech. Appl. Math.*, **6**, 250.
GOODIER, J. N. and BISHOP, R. E. D.	1952	*J. Appl. Phys.*, **23**, 124.
LAMB, H.	1932	*Hydrodynamics*, Cambridge University Press.
TIMOSHENKO, S. P. and GOODIER, J. N.	1951	*Theory of Elasticity*, McGraw-Hill.

Vol. 2 53/54

Journal of the Mechanics and Physics of Solids, 1954, Vol. 2, pp. 110 to 116. Pergamon Press Ltd., London.

ON INOUE'S HYDRODYNAMICAL ANALOGY FOR THE STATE OF STRESS IN A PLASTIC SOLID

By R. Hill
Department of Mathematics, University of Nottingham

(*Received* 14*th December*, 1953)

Summary

An interesting correspondence has recently been pointed out by Inoue between the variables characterizing the steady flow of an inviscid compressible fluid and those characterizing the equilibrium state of stress in an ideal fully-plastic solid. The basic equations of transformation are, however, stated by Inoue only in an implicit differential form, and not all details of the derivation are given. In the present note the matter is re-examined along different lines, and the correspondence is obtained in a more useful explicit form. The inherent restrictions in the analogy are also clarified, and some additional features are discussed.

1. Introduction

In a recent series of papers, Inoue (1952 a, b, c) has developed an interesting formal analogy between the steady flow of a compressible fluid and the equilibrium state of stress in a plastic solid. The analogy consists of certain equations of transformation that link the variables characterizing a field of fluid flow (pressure, density, velocity) with those characterizing a plastic state (components of stress). These equations enable one to pass from a known flow pattern for a fluid with a certain pressure-density relation to a plastic stress distribution over the whole or a part of a solid with a certain yield criterion, and vice versa. By this means, known solutions and methods of analysis in one field become, in principle, available in the other. The correspondence does not, however, extend to the non-plastic (or elastic) part of the solid.

The equations of transformation are stated by Inoue only in implicit differential form (equations (10) and (11) below). Full details of the derivation are lacking, and the restrictions inherent in the analogy are not apparent. The present note is intended to clarify the situation and to show that the correspondence between the two fields can actually be stated in a simple and explicit way (equation (4) below).

2. Transformation Equations

(i) Consider the steady flow of an inviscid fluid under no body forces. The equations of continuity and motion are

$$\frac{\partial}{\partial x_i}(\rho u_i) = 0, \qquad \frac{\partial p}{\partial x_i} + \rho u_j \frac{\partial u_i}{\partial x_j} = 0, \tag{1}*$$

*The summation convention is implied.

where ρ is the density, p the pressure, and u_i $(i = 1, 2, 3)$ the components of velocity at a point whose coordinates are x_i. If each element undergoes adiabatic changes of state, there is in addition Bernoulli's relation

$$\tfrac{1}{2}q^2 + \int \frac{dp}{\rho} = h, \tag{2}$$

where q is the velocity magnitude; the integral is taken along the streamline through the point considered, and h is a constant for that streamline. It is now supposed that h has the same value everywhere (homenergic flow); this would be so, for instance, if each fluid element came from a region in which conditions were uniform. It is supposed also that the entropy of every element is the same (homentropic flow), so that the pressure is a universal one-valued function of the density:

$$p \equiv p(\rho). \tag{3}$$

It then follows, as is well known, that the vorticity vector is in the stream-direction at each point. For the existence of the transformation it is not essential that the vorticity should vanish (as INOUE assumes). However, in two-dimensional or axially symmetric flow, curl u_i is perpendicular to the planes of motion and so the vorticity is *automatically* zero.

New variables σ_{ij}, having the dimensions of stress, are now introduced:

$$\sigma_{ij} = \pm\left[(p - p_0)\,\delta_{ij} + \rho u_i\, u_j\right] \tag{4}$$

where p_0 is an arbitrary constant and δ_{ij} is the delta symbol ($\delta_{ij} = 1$ *if* $i = j$, 0 *if* $i \neq j$); the same choice of sign must be made throughout. It is evident that the σ_{ij} constitute a symmetric second-order tensor (since the u_i form a vector) and are therefore capable of representing stress at a point. The components for *any* set of axes are given by (4) when the corresponding components of velocity are taken. In particular, if the axis 1 is in the stream-direction (so that $u_1 = q$, $u_2 = u_3 = 0$), it may be seen that one principal axis of stress coincides with the stream-direction and that the principal values of stress are

$$\sigma_1 = \pm\left[(p - p_0) + \rho q^2\right], \qquad \sigma_2 = \sigma_3 = \pm\,(p - p_0). \tag{5}$$

The state of stress is thus a very special one: a uniaxial stress combined with a hydrostatic pressure or tension. Equations (4) and (5) do not appear in INOUE's papers (at least, in those known to the writer).

That the distribution of stress defined by (4) is in equilibrium follows at once from (1) and (2):

$$\pm\frac{\partial \sigma_{ij}}{\partial x_j} = \frac{\partial}{\partial x_j}(p\delta_{ij} + \rho u_i\, u_j) = \left(\frac{\partial p}{\partial x_i} + \rho u_j \frac{\partial u_i}{\partial x_j}\right) + u_i \frac{\partial}{\partial x_j}(\rho u_j) = 0.$$

The same choice of sign must be made throughout the whole of the field, or any considered part of it.

Finally, the elimination of p, ρ, and q between (2), (3) and (5) leads to a relation between σ_1 and σ_2, involving the arbitrary parameters p_0 and h. This may be interpreted as a plastic yield condition for an isotropic non-hardening solid under stress states in which two principal stresses are equal. However, the stress distribution obtained by the transformation (4) is still not a possible plastic state unless

it may also be related to displacement-increments through the stress-strain relations. This is in fact a severe restriction. Indeed, non-trivial three-dimensional plastic states can only be derived in this way from a fluid flow pattern in the particular case where the plastic potential surface is *singular* (i.e. has no determinate normal) whenever two principal stresses are equal (e.g. the Tresca potential). The transformation will not furnish possible three-dimensional states of stress associated with the regular part of the potential surface. INOUE does not remark on these limitations.

The situation is quite different for two-dimensional flows and plastic states. In this case it is not necessary that the stress normal to a plane of motion should be equal to one of the other two principal values : equation (4) is to be regarded as specifying just the three stress components in a plane of motion. The only equations to be satisfied by these components are the yield criterion and two equilibrium relations ; no additional compatibility condition must be satisfied to ensure the existence of displacement-increments. It appears, therefore, that two-dimensional problems are likely to be the main field of application of INOUE's analogy.

(ii) Consider, now, the converse transformation where we begin with a known equilibrium distribution of stress satisfying some yield criterion, $\sigma_1 - \sigma_2 = f(\sigma_2)$ say, and (if three-dimensional) such that two principal values are equal at each point. We take the σ_1 direction as the stream-direction and calculate the local values of $(p - p_0)$ and ρq^2 from (5), arbitrarily choosing the sign. These values satisfy $\pm \rho q^2 = f\{\pm (p - p_0)\}$, and this in conjunction with (2) determines a pressure-density relation involving the parameter p_0 and an arbitrary constant of integration. We now have p, ρ, and u_i satisfying (1), (2) and (3). Since the stresses are in equilibrium,

$$0 = \pm \frac{\partial \sigma_{ij}}{\partial x_j} = \left(\frac{\partial p}{\partial x_i} + \rho u_j \frac{\partial u_i}{\partial x_j}\right) + u_i \frac{\partial}{\partial x_j}(\rho u_j).$$

Differentiation of (2) gives

$$\frac{\partial p}{\partial x_i} + \rho u_j \frac{\partial u_j}{\partial x_i} = 0$$

in view of (3). Combining these two equations :

$$\rho u_j \left(\frac{\partial u_j}{\partial x_i} - \frac{\partial u_i}{\partial x_j}\right) = u_i \frac{\partial}{\partial x_j}(\rho u_j).$$

Now multiply by u_i and sum over i. The resulting left-hand side vanishes identically, and we recover the equation of continuity, and hence also the equations of motion. (The consequent vanishing of the left-hand side of the last equation above for $i = 1, 2, 3$ proves the result previously quoted, namely that the vorticity and velocity vectors are parallel).

It should be noted that there is a restriction on the possible yield criteria that can be admitted if we require the derived p (ρ) relation to have a positive gradient $dp/d\rho$ as in any actual fluid. This is the condition that there should be a real local velocity of sound, $a = \sqrt{(dp/d\rho)}$. From (2) and (5),

$$\pm d\sigma_1 = -dp + q^2\, d\rho, \qquad \pm d\sigma_2 = dp.$$

Hence

$$\frac{d\sigma_1}{d\sigma_2} = M^2 - 1 \tag{6}$$

where $M = q/a$ is the local Mach number. Thus the curve in (σ_1, σ_2) space representing the yield criterion, or the admissible part of it, must satisfy

$$\frac{d\sigma_1}{d\sigma_2} \geqslant -1. \tag{7}$$

Another obvious restriction is that $p_0 \pm \sigma_2 > 0$ everywhere, if p is to be positive.

3. Shock Waves and Stress Discontinuities

It seems to be implied by Inoue (1952b) that the analogy is still valid when the fluid flow contains shock waves. This, however, is only true in a very limited sense. For the flow through a shock wave is not isentropic. Each streamline behind a curved shock wave is a different adiabatic, having its own separate p (ρ) relation. Even when the wave is plane and the incident flow uniform, the common adiabatic behind the wave differs from that in front. Thus, the analogy cannot apply downstream of a shock wave.

A shock wave does, however, correspond to a stress discontinuity in the sense that both occur together. Moreover, the Rankine-Hugoniot equations relating to the transfer of mass and momentum through the wave correspond to the conditions for the continuity of the stress vector acting on the discontinuity surface

4. Inoue's Equations

We introduce now the maximum shear stress

$$\tau = \tfrac{1}{2}\,|\sigma_1 - \sigma_2| = \tfrac{1}{2}\,\rho q^2 = \rho\left(h - \int\frac{dp}{\rho}\right) \tag{8}$$

from (2) and (5), and also

$$\sigma = \tfrac{1}{2}\,(\sigma_1 + \sigma_2) = \pm\,[(p - p_0) + \tau]. \tag{9}$$

The yield criterion for a state of plane strain or plane stress is expressible as a relation between τ and σ. Then

$$\pm\, d\sigma = dp + d\tau = \tau d\rho/\rho, \tag{10}$$

and

$$\frac{dq}{q} = -\frac{dp}{\rho q^2} = -\frac{dp}{2\tau} = \left(\frac{d\tau}{d\sigma} \mp 1\right)\frac{d\sigma}{2\tau}, \tag{11}$$

from (2).

From (7) it is seen that the admissible part of the yield curve is such that $d\tau/d\sigma < 1$ if the upper sign is taken in (4) and elsewhere (so that $\sigma_1 \geqslant \sigma_2$), or $d\tau/d\sigma > -1$ if the lower sign is taken $(\sigma_1 \leqslant \sigma_2)$. In fact

$$M^2 = q^2\Big/\frac{dp}{d\rho} = 2\Big/\left(1 \mp \frac{d\tau}{d\sigma}\right) \tag{12}$$

from (10) and (11). The flow is thus supersonic if $-1 < d\tau/d\sigma < 1$. It is subsonic

when $d\tau/d\sigma < -1$ if the upper sign is taken, and when $d\tau/d\sigma > 1$ if the lower sign is taken. The supersonic and subsonic regions in the fluid flow correspond to the parts of the plastic zone where the stress equations are hyperbolic and elliptic respectively (*not* to the plastic and non-plastic parts of the body).

Equations (10) and (11), together with the stipulation that a principal axis should be in the stream-direction, constitute INOUE's point of departure. He considers also the axially symmetric case, where two principal stresses are equal, but not the general three-dimensional correspondence.

5. SOME PARTICULAR CORRESPONDENCES

(i) $p = \lambda \rho^\gamma$; λ and $\gamma > 0$, $\gamma \neq 1$. Consider, first, the adiabatic pressure-density relation for a perfect gas. From (8) and (9):

$$\tau = h\rho - \frac{\lambda\gamma}{\gamma - 1} \cdot \rho^\gamma, \qquad \pm\sigma = -p_0 + h\rho - \frac{\lambda}{\gamma - 1} \cdot \rho^\gamma, \tag{13}$$

where the arbitrary constant of integration is absorbed in h.

Suppose, for instance, the flow is such that $h = 0$, and hence supersonic with a constant Mach number $M = \sqrt{\{2/(1-\gamma)\}}$ if $\gamma < 1$ (a case considered by INOUE). The corresponding plastic solid has a yield criterion

$$\tau = \gamma(p_0 \pm \sigma). \tag{14}$$

In actual solids, τ increases as σ becomes more negative under plane *strain* conditions. To reproduce this type of behaviour the lower sign in (14) and elsewhere must be chosen. Such a solid can not sustain a hydrostatic tension exceeding p_0 (whose value is still disposable). This type of linear relation is often assumed in soil mechanics (the restriction $\gamma < 1$ parallels the physical requirement that the slope, $-d\tau/d\sigma$, should be less than unity if the envelope of Mohr's circles is to be real).

If the fluid is such that h is positive, the flow is supersonic where

$$h > \frac{\gamma(\gamma+1)}{2(\gamma-1)} \cdot \frac{p}{\rho}$$

and subsonic where the reverse inequality is true. The corresponding yield relation, parametrically expressed by (13), is now a curve. By suitably choosing p_0, λ, and γ we can approximate to, say, a *portion* of the plane stress ellipse for the Mises yield criterion. INOUE (1952b) remarks that the *whole* ellipse can be approximated if the upper sign in (13) is taken where $\sigma < 0$ and the lower sign where $\sigma > 0$. However, this possibility does not appear to offer any real advantage since we are not at liberty to take different signs in two adjoining parts of *one and the same stress field*; the stress vector acting on the interface would generally be discontinuous.

(ii) $p_0 - p = m^2(1/\rho - 1/\rho_0)$. This is not considered by INOUE. From (8) and (9), taking the upper sign,

$$\tau = h\rho + m^2/2\rho, \qquad \sigma + m^2/\rho_0 = -h\rho + m^2/2\rho, \tag{15}$$

h being supposed *negative* (the flow is then subsonic). Eliminating ρ,

Vol 2 1953/

$$\tau^2 - (\sigma + m^2/\rho_0)^2 = 2m^2 h. \tag{16}$$

This is a rectangular hyperbola, of which only the branch symmetric about the negative σ axis is here relevant. If the greatest possible value of σ is to be positive (as in most actual materials) ρ_0 must be sufficiently large and negative ; p_0, ρ_0 are then to be regarded, of course, as parameters in the pressure-density relation, not as an actually attainable fluid state.

It is well known that this (p, ρ) relation is the only one for which a steady, homentropic, non-uniform, one-dimensional flow is possible. This flow is such that $h = 0$, while $\rho q = m$ is the rate of transfer of mass per unit sectional area. The corresponding yield criterion is $\sigma_1 = m^2/\rho_0$, $\sigma_2 \leqslant m^2/\rho_0$. A non-uniform distribution of p, ρ, and q in a straight channel corresponds to a rectangular solid specimen under a uniform longitudinal stress and a non-uniform lateral one. In particular, this is the only (p, ρ) relation for which the analogy is valid on both sides of a shock-wave, provided also that h is zero and the rate at which mass crosses unit area is equal to m.

(iii) $p - p_0 = k \log(\rho/\rho_0)$; $k > 0$. From (8) and (9) :

$$\tau = k - h\rho, \qquad \pm \sigma = k(1 + \log \rho/\rho_0) - h\rho. \tag{17}$$

Inoue gives special attention to flows such that $h = 0$; the Mach number is equal to $\sqrt{2}$ everywhere, the Mach lines being orthogonal. The corresponding solid is such that yielding occurs under a constant maximum shearing stress k. In this case the choice of sign does not affect the yield criterion or the stress magnitudes, only their signs.

6. Applications

Consider the flow pattern produced by a stream of Mach number M and pressure np_0 $(n > 1)$ issuing uniformly from an orifice into a fluid at rest at pressure p_0. Particular examples of such a flow have been calculated by Pack (1948) for a perfect gas with $\gamma = 1{\cdot}3$, $M = 1{\cdot}5$, and $n = 2{\cdot}0$ and $5{\cdot}7$. The corresponding plastic solid has the yield criterion (13) with the appropriate value of h, p_0 being arbitrary. According to (5), with the lower sign, the part of the boundary of the solid corresponding to the orifice is a straight section under a normal pressure $\{(1 + \gamma M^2) n - 1\} p_0$ since the velocity of sound is expressible as $\sqrt{(\gamma p/\rho)}$. The part of the boundary corresponding to the streamline on which the fluid pressure is p_0 is free from stress. Such a plastic state is produced at the yield point of a body of this shape when indented by a flat die. Bishop (1953) has calculated the field of slip-lines (characteristics) when the yield criterion is $\tau = k$ and the applied pressure is $2k(1 + \frac{1}{2}\pi)$. The general resemblance of these two fields is very marked, despite the fact that the p (ρ) and τ (σ) relations do not correspond. In particular, the fields involve a shock wave and stress discontinuity, respectively, where the Mach lines or slip-lines run together. Either solution can, of course, be transformed to give another solution in the other field.

The calculations for the fluid were carried out by approximate integration of the Temple-Guderley-Steichen relations along a network of Mach lines, and, for the solid, by approximate integration of the Hencky relations along a network of slip-lines. A detailed comparison of the respective methods, and of the various

refinements that can be introduced for greater accuracy, is both interesting and profitable. An account of this is beyond the scope of the present note ; the reader is referred to HOWARTH (1953, pp. 84-7), HILL (1950, pp. 132-148), and PRAGER and HODGE (1951, pp. 134-143). The properties and structure of various types of singularity (branch, and limit, lines) seem to have been studied more thoroughly for fluid flow.

The equations along the characteristics in supersonic flow of a fluid with a *general* p (ρ) relation are due to MASSAU and BUSEMANN (given by HOWARTH, op. cit., pp. 80-1), and in the hyperbolic region in a plastic solid with a general τ (σ) yield criterion are due to MANDEL (given by HILL, op. cit., 297-9). The correspondence of the respective equations can, of course, be demonstrated by means of (4), (8) and (9). In particular, the Prandtl-Meyer equations for the expansion of a supersonic stream round a corner (HOWARTH, op. cit., pp. 164 et seq.) correspond to those for a plastic state centred on a point singularity (e.g. HILL, 1952, for plane stress with the Mises criterion).

Subsonic flow corresponds to the elliptic part of the plastic zone. There is here a striking contrast between the respective available methods, which are very much more developed in fluid flow. Whether these can be taken over and applied in the plastic field is a matter for further study (INOUE gives some discussion of the hodograph method). It is likely, however, that only a rather limited application will be practicable. This is partly due to the different kinds of problem that occur *in practice*, but still more to the additional complexities arising from the presence of a non-plastic zone and from the fact that the boundary conditions are generally *mixed* (involving displacements as well as stresses).

Vol 2 1953

REFERENCES

BISHOP, J. F. W.	1953	*J. Mech. Phys. Solids* **2**, 43.
HILL, R.	1950	*Mathematical Theory of Plasticity* (Clarendon Press).
	1952	*J. Mech. Phys. Solids* **1**, 19.
HOWARTH, L.	1953	*Modern Developments in Fluid Dynamics ; High Speed Flow*, I (Clarendon Press).
INOUE, N.	1952a	*J. Phys. Soc. Japan* **7**, 119 and 518.
	b	*J. Aero. Sci.* **19**, 783.
	c	*Doshisha Engineering Review*, Special Paper No. 1.
PACK, D. C.	1948	*Qu. J. Mech. Appl. Math.* **1**, 1.
PRAGER, W. and HODGE, P. G.	1951	*Theory of Perfectly Plastic Solids* (Wiley).

Journal of the Mechanics and Physics of Solids, 1954, Vol. 2, pp. 117 to 126. Pergamon Press Ltd., London.

SHELLS WITH ZERO BENDING STRESSES

By M. R. Horne
Department of Engineering, University of Cambridge

(*Received 30th November*, 1953)

Summary

Shells in general, when subjected to external loads, develop bending as well as membrane stresses. If the middle plane of the shell is a surface of revolution and the applied loads are radially symmetrical about the axis, the membrane stresses are readily calculated provided the bending stresses are small enough to be ignored. When the bending stresses are taken into account, the problem becomes very much more complicated. It may, however, be relatively easy to design the shell in such a way that bending stresses are entirely absent. The paper describes shells which will be free from bending stresses when the applied load is any uniform axial force. Consideration is given to shells of varying thickness, but particular attention is paid to shells whose thickness is uniform. The possibilities of providing boundary rings to prevent local bending stresses in the vicinity of the end sections is also investigated.

Vol. 2 53/54

1. Introduction

When calculating stresses in thin shells, it is usual to assume that external loads produce membrane stresses only, except in the close vicinity of point loads. This is a sufficiently close approximation provided the thickness of a shell is small compared with the minimum radius of curvature, and also provided buckling does not occur. When the thickness is not small, membrane stress theory gives approximate results only due to the influence of bending stresses. Unfortunately, the general elastic theory of shells is involved, and solutions to problems in which bending stresses are of some importance have usually to be

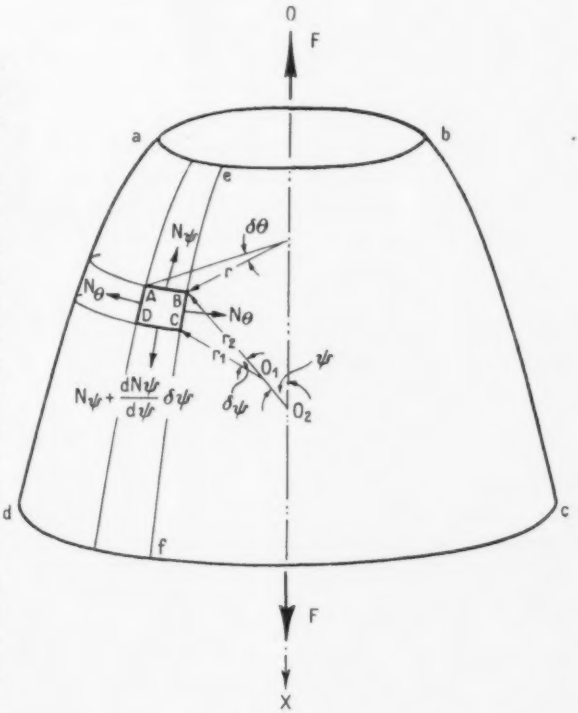

Fig. 1.

obtained by a process of successive approximations (TIMOSHENKO 1940).

In view of the difficulty of calculating bending stresses in shells, it is worth investigating shells in which no bending stresses whatsoever will be induced by given loads. In certain cases, this inverse problem may be solved, and does not appear to have been treated in the literature. The present paper contains a discussion of such a problem, which may be described as follows.

The shell *abcd* in Fig. 1 has the form of a surface of revolution about the axis OX. The shell is bounded by planes at right-angles to OX, and is required to transmit a force F with line of action along OX. The force may be taken to be uniformly distributed, tangentially to the shell, at the end sections. It is required to determine the possible forms which the shell may take, the shell being either of uniform or of varying thickness, with the stipulation that membrane stresses only shall be induced.

NOTATION

x = distance along the axis of the shell.
r = radius of shell.
h = thickness of shell.
ψ = angle between normal to shell and longitudinal axis.
η = cosec ψ.
r_0, h_0, ψ_0, η_0 = coincident values of r, h, ψ and η respectively.
r_1 = radius of curvature in meridian plane.
r_2 = radius of curvature in plane perpendicular to meridian.
θ = angle subtended by two meridians on axis OX.
w = displacement of shell in normal direction.
v = displacement of shell along a meridian.
ϵ_ψ = strain parallel to meridian
ϵ_θ = strain perpendicular to meridian.
N_ψ = membrane force per unit length acting parallel to meridian.
N_θ = membrane force per unit length acting perpendicular to meridian.
σ_ψ, σ_θ = stresses corresponding to N_ψ and N_θ respectively.
$\sigma_{\psi 0}$ = value of σ_ψ when $r = r_0$.
F = longitudinal force transmitted by shell.
E = modulus of elasticity.
ν = Poisson's ratio.

2. THE GENERAL SOLUTION

The geometry of the shell and the forces acting on an element are shown in Fig. 1. The element $ABCD$ is contained between two meridian planes intersecting at an angle $\delta\theta$ and two planes at rightangles to the longitudinal axis. The centre of curvature of the element in the plane containing the meridian ef is 0_1, and the radius of curvature r_1. The side BC of the element $ABCD$ subtends an angle $\delta\psi$ at O_1, the normal to the shell making an angle ψ with the axis OX. The centre of curvature in a plane peroendicular to the meridian *ef* is at O_2, and the corresponding radius of curvature is denoted by r_2. The radius of the shell at AB is r.

The only forces acting on the element are membrane stresses, since no bending

stresses or distributed external loads are present. The forces per unit length of shell are N_ψ in the direction of tangents to the meridians and N_θ perpendicular to the meridians. The corresponding stresses are denoted by σ_ψ and σ_θ, so that if h is the thickness of the shell, $N_\psi = h\sigma_\psi$ and $N_\theta = h\sigma_\theta$.

The displacements of the arc BC of the shell are shown in Fig. 2. As a result of the application of the longitudinal force F, BC is displaced to $B'C'$. The point B is displaced w towards the centre of curvature O_1 and v in the tangential direction.

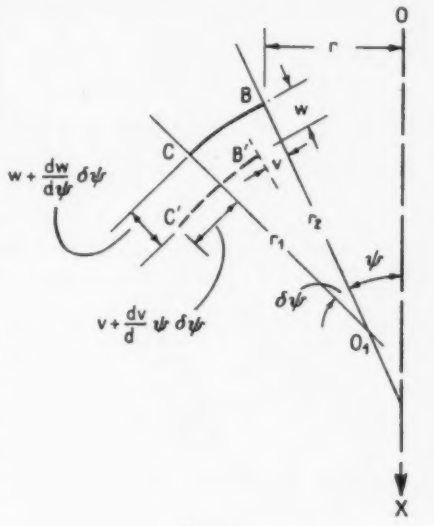

Fig. 2.

Two equations of equillibrium are obtained. The first is most conveniently derived by resolving parallel to OX for the forces acting on the shell at the cross section containing the arc AB, and the second by resolving for the forces acting on the element $ABCD$ in a direction perpendicular to the element. Hence it is found that

$$N_\psi = \frac{F}{2\pi r} \operatorname{cosec} \psi, \tag{1}$$

$$N_\theta = -\frac{F}{2\pi r_1} \operatorname{cosec}^2 \psi. \tag{2}$$

The strains ϵ_ψ in the direction of a meridian and ϵ_θ perpendicular to a meridian are readily shown (Timoshenko 1940) to have the values

$$\epsilon_\psi = \frac{1}{r_1}\frac{dv}{d\psi} - \frac{w}{r_1}, \tag{3}$$

$$\epsilon_\theta = \frac{v}{r_2} \cot \psi - \frac{w}{r_2}. \tag{4}$$

The strains ϵ_ψ and ϵ_θ are related to the membrane forces N_ψ and N_θ by the equations

$$\epsilon_\psi = \frac{1}{Eh}(N_\psi - \nu N_\theta), \tag{5}$$

$$\epsilon_\theta = \frac{1}{Eh}(N_\theta - \nu N_\psi). \tag{6}$$

Finally, two equations are obtained from the fact that, since no bending stresses are induced, there must be no change of curvature in either the meridian plane or in a plane at rightangles to the meridian. Hence (Timoshenko 1940)

$$\frac{1}{r_1}\frac{d}{d\psi}\left(\frac{v}{r_1} + \frac{1}{r_1}\frac{dw}{d\psi}\right) = 0, \tag{7}$$

Vol. 2 53/54

$$\frac{\cot\psi}{r_2}\left(\frac{v}{r_1}+\frac{1}{r_1}\frac{dw}{d\psi}\right)=0. \tag{8}$$

Equations (7) and (8) are both satisfied when

$$v+\frac{dw}{d\psi}=0. \tag{9}$$

The values of r_1 and r_2 are related to r and ψ as follows :

$$\frac{1}{r_1}=\frac{d}{dr}(\sin\psi), \qquad \frac{1}{r_2}=\frac{1}{r}(\sin\psi). \tag{10}$$

Upon eliminating ϵ_ψ and ϵ_θ between equations (3) to (6), and substituting for the values of r_1 and r_2 from (10), it is found that

$$\cos\psi\frac{dv}{dr}-w\frac{d(\sin\psi)}{dr}=\frac{1}{Eh}(N_\psi-\nu N_\theta), \tag{11}$$

$$\frac{1}{r}(v\cos\psi-w\sin\psi)=\frac{1}{Eh}(N_\theta-\nu N_\psi). \tag{12}$$

Equations (9) and (11) give

$$\frac{d}{dr}(v\cos\psi-w\sin\psi)=\frac{1}{Eh}(N_\psi-\nu N_\theta). \tag{13}$$

Hence from equations (12) and (13)

$$N_\psi-\nu N_\theta=h\frac{d}{dr}\left\{\frac{r}{h}(N_\theta-\nu N_\psi)\right\}. \tag{14}$$

Substituting the values of N_ψ and N_θ from equations (1) and (2) in equation (14), it is found that if $\eta=\operatorname{cosec}\psi$,

$$\frac{\eta}{r}-\nu\frac{d\eta}{dr}=h\frac{d}{dr}\left\{\frac{r}{h}\frac{d\eta}{dr}-\frac{\nu}{h}\eta\right\} \tag{15}$$

The value of h may be expressed generally in the form $h=f(r)$. Equation (15) then becomes

$$r^2\frac{d^2\eta}{dr^2}+\left(1-r\frac{f'(r)}{f(r)}\right)r\frac{d\eta}{dr}-\left(1-\nu r\frac{f'(r)}{f(r)}\right)\eta=0. \tag{16}$$

All shells which fulfil the conditions which have been imposed are required to satisfy equation (16).

3. General Solution when $h \propto r^n$

If it is assumed that

$$\frac{h}{h_0}=\left(\frac{r}{r_0}\right)^n \tag{17}$$

where r_0 and h_0 are coincident values of r and h respectively and n is real (positive or negative), then equation (16) becomes

$$r^2\frac{d^2\eta}{dr^2}+(1-n)r\frac{d\eta}{dr}-(1-\nu n)\eta=0. \tag{18}$$

The general solution is

$$\eta = Ar^{m_1} + Br^{m_2} \tag{19}$$

where

$$m_1, m_2 = \tfrac{1}{2}\{n \pm \sqrt{n^2 + 4(1 - n\nu)}\}. \tag{20}$$

and A and B are constants. If x denotes distance along the axis of revolution, then a relationship between r and x may be obtained by integrating the equation

$$\frac{dr}{dx} = \sqrt{\eta^2 - 1}. \tag{21}$$

The values of the membrane forces N_ψ and N_θ may be derived from equations (1). (2), (10) and (19). Remembering that $\eta = \operatorname{cosec} \psi$, it follows that

$$N_\psi = \frac{F}{2\pi r}\eta, \qquad N_\theta = \frac{F}{2\pi}\frac{d\eta}{dr}. \tag{22}$$

The general shapes of shell obtainable from equations (19) and (21) are illustrated in Fig. 3. When $n < \frac{1}{\nu}$, m_1 is positive and m_2 negative. When $n = \frac{1}{\nu}$, m_1 is positive and m_2 zero, while if $n > \frac{1}{\nu}$, both m_1 and m_2 are positive. The type of curve obtained depends on the signs of m_1, m_2, A and B, and on the number of real positive roots resulting when $|\eta| = 1$ in equation (19). The types of curve (Fig. 3) obtainable in each case are shown in Table 1.

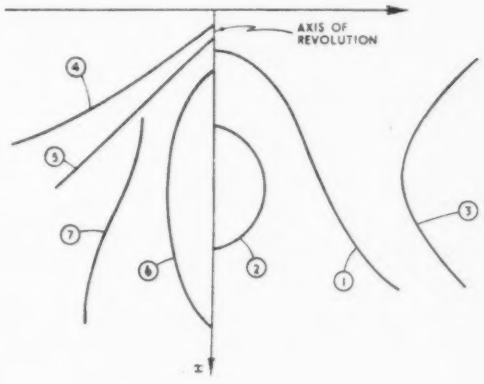

Fig. 3.

TABLE 1

Types of shell obtained when $h \propto r^n$ (see Fig. 3)

n	Real positive roots for $\lvert\eta\rvert = 1$	$AB > 0$	$A = 0$	$B = 0$	$AB < 0$
Less than	0	1	—	—	—
$\frac{1}{\nu}$	1	—	2	3	—
	2	2 and 3	—	—	2 and 3
Equal to	0	4	5	—	—
$\frac{1}{\nu}$	1	3	—	3	3
	2	—	—	—	3 and 6
Greater than	1	3	3	3	3
$\frac{1}{\nu}$	2	—	—	—	—
	3	—	—	—	3 and 7

4. Special Case of Conical Shell

When $n = \frac{1}{\nu}$, $A = 0$ and $B > 1$, a conical shell with half angle $\sec^{-1} B$ is obtained. The thickness, membrane forces and membrane stresses are then as follows

$$\frac{h}{h_0} = \left(\frac{r}{r_0}\right)^{\frac{1}{\nu}},$$

$$N_\psi = \frac{F}{2\pi}\frac{B}{r}, \qquad \sigma_\psi = \frac{F}{2\pi}\frac{B}{h_0 r_0}\left(\frac{r_0}{r}\right)^{\frac{1+\nu}{\nu}},$$

$$N_\theta = 0 \qquad \sigma_\theta = 0.$$

5. General Solutions for Shells of Uniform Thickness

The remainder of the paper is concerned with shells of uniform thickness. Equations (18) to (22) are applicable with $n = 0$, whence

$$\eta = Ar + \frac{B}{r}. \tag{23}$$

Since $n < \frac{1}{\nu}$, the shells obtained are confined to types 1, 2 and 3 (see Fig. 3 and Table 1).

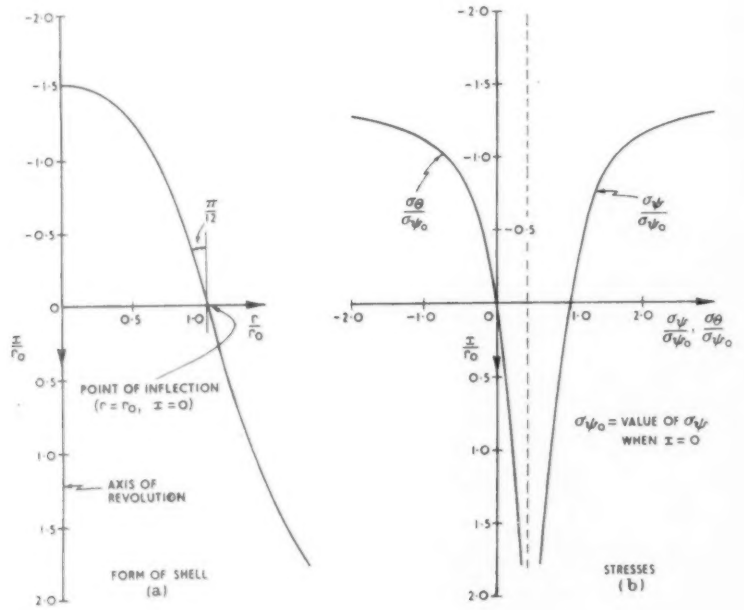

Fig. 4.

(i) *Case* $AB > \frac{1}{4}$

When this condition is satisfied, equation (23) has no real roots with $|\eta| = 1$, and all shells are formed from curves of type 1. Since each curve has a point of

inflection, it is convenient to establish the constants A and B by defining the radius and slope of the curve at this point. If r_0 and ψ_0 denote the radius and angle of slope $\cot^{-1}(dr/dx)$ at the point of inflection, then it is found that

$$\frac{\eta}{\eta_0} = \frac{r^2 + {r_0}^2}{2rr_0},$$

$$\frac{x}{r_0} = \left\{\sinh^{-1}\left(\frac{r^2 + {r_0}^2 \cos 2\psi_0}{{r_0}^2 \sin 2\psi_0}\right) - \sinh^{-1}(\cot\psi_0)\right\} \sin\psi_0. \tag{24}$$

The constant of integration is chosen such that $x = 0$ when $r = r_0$. The membrane forces and stresses are given by

$$\left.\begin{aligned} N_\psi = h\sigma_\psi &= \frac{F\eta_0}{2\pi r_0}\left(\frac{r^2 + {r^2}_0}{2r^2}\right), \\ N_\theta = h\sigma_\theta &= \frac{F\eta_0}{2\pi r_0}\left(\frac{r^2 - {r_0}^2}{2r^2}\right), \end{aligned}\right\} \tag{25}$$

where $\eta_0 = \operatorname{cosec}\psi_0$. Hence both stresses increase rapidly as $r \to 0$, but as r becomes large compared with r_0, the stresses both approach asymptotically to the value $F\eta_0/4\pi r_0 h$. The sum of the stresses is constant and equal to $F\eta_0/2\pi r_0 h$.

An example of this type of shell is given in Fig. 4, which shows the form of shell and stresses when $\psi_0 = \frac{5}{12}\pi$.

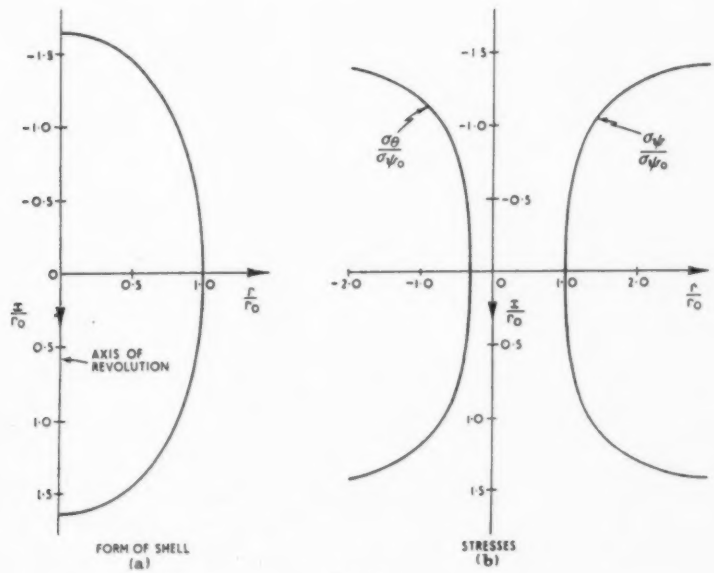

Fig. 5.

(ii) *Case* $AB < \frac{1}{4}$

All the shells obtained are of types 2 and 3. If r_0 denotes the maximum radius in the case of a curve of type 2 and the minimum radius when the curve is of type 3, then

$$\left.\begin{aligned} \eta &= \frac{1}{1+\mu}\left(\frac{\mu r^2 + r_0^2}{r r_0}\right), \\ \frac{x}{r_0} &= \frac{1+\mu}{2\mu}\cosh^{-1}\left\{\frac{(1+\mu^2)\,r_0^2 - 2\mu^2 r^2}{(1-\mu^2)\,r_0^2}\right\}, \end{aligned}\right\} \tag{26}$$

$$\left.\begin{aligned} N_\psi = h\sigma_\psi &= \frac{F}{2\pi r_0}\left(\frac{\mu r^2 + r_0^2}{(1+\mu)\,r^2}\right), \\ N_\theta = h\sigma_\theta &= \frac{F}{2\pi r_0}\left(\frac{\mu r^2 - r_0^2}{(1+\mu)\,r^2}\right). \end{aligned}\right\} \tag{27}$$

The constant of integration is chosen so that $x = 0$ when $r = r_0$. When the curve is of type 2, $-1 < \mu < 1$ and $r \leqslant r_0$. When type (3) is required, $-1 < 1/\mu < 1$ and $r \geqslant r_0$.

Examples of shells of types 2 and 3 are given in Figs. 5 and 6 respectively. Fig. 5 shows a shell of type 2 for which $\mu = \frac{1}{2}$, and Fig. 6 a shell of type 3 with $\mu = 2{\cdot}0$.

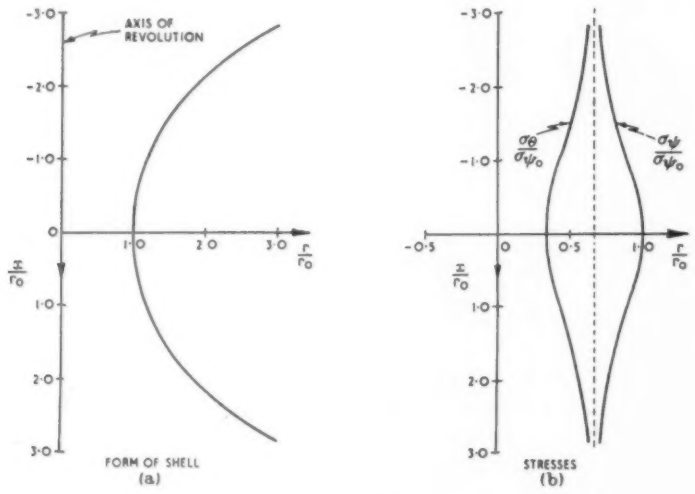

Fig. 6.

(iii) *Special Cases*

A plane disc is obtained if $\psi_0 = 0$ is substituted in (24), or if $\mu = -1$ is substituted in (26). A circular cylinder is obtained if $\psi_0 = \frac{1}{2}\pi$ or $\mu = 1$. When $\mu = 0$ in (26) and (27), the case of a spherical shell is obtained, viz :—

$$r^2 + x^2 = r_0^2,$$

$$N_\psi = -N_\theta = h\sigma_\psi = -h\sigma_\theta = \frac{F r_0}{2\pi r^2}.$$

When $\mu = \infty$, (26) and (27) give

$$\frac{x}{r_0} = \cosh^{-1}\frac{r}{r_0},$$

$$N_\psi = N_\theta = h\sigma_\psi = h\sigma_\theta = \frac{F}{2\pi r_0}.$$

6. Boundary Rings

Sections of the shells which have been derived above may be used to transmit an axial force F from one body to another. Bending stresses will be absent from the main part of the shell, but will be induced in the vicinity of the boundaries unless the force F is distributed in such a way as to balance exactly the membrane forces. The condition may be difficult to achieve, but may be much facilitated by introducing boundary rings of suitable rigidity.

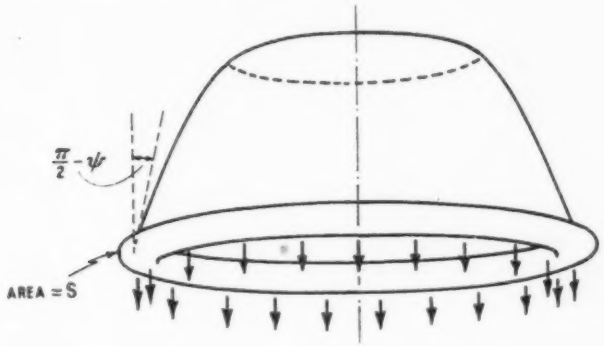

Fig. 7.

Consider a ring forming an outer boundary to a shell, as shown in Fig. 7. The force F is applied to the ring as a uniformly distributed axial load, and the ring is required to develop the same circumferential strain as the shell at that section. Hence if σ_θ' is the circumferential stress in the ring, and the ring and shell have the same modulus of elasticity,

$$\sigma_\theta' = \sigma_\theta - \nu\sigma_\psi. \tag{28}$$

If the cross-sectional area of the ring is S, the equation of equilibrium for a small arc of the ring in a radial direction is

$$S\sigma_\theta' + h\sigma_\psi r \cos\psi = 0. \tag{29}$$

When the ring forms an inner boundary to the shell, (28) still applies, but in place of (29) we have

$$S\sigma_\theta' - h\sigma_\psi r \cos\psi = 0. \tag{30}$$

Considering uniform shells of type 1 ((24) and (25)) it is found that boundary rings must have areas given by

$$S = \pm \frac{hr\sqrt{r^4 + r_0^4 + 2r^2 r_0^2 \cos 2\psi_0}}{(1+\nu)r_0^2 - (1-\nu)r^2} \tag{31}$$

where the positive sign is appropriate for outer boundary rings and the negative sign for rings forming inner boundaries. Since S is essentially positive, outer

boundary rings loaded as shown in Fig. 7 can only be used when r is less than $r_0\sqrt{\frac{1+\nu}{1-\nu}}$, while inner boundary rings can only be used when r is greater than this quantity.

When the shell is of type (2) or (3), the areas of boundary rings may be obtained from equations (26) to (30), and are given by

$$S = \pm \frac{hr\sqrt{(r_0^2 - r^2)(r_0^2 - \mu^2 r^2)}}{(1+\nu)r_0^2 - \mu(1-\nu)r^2} \tag{32}$$

where the positive and negative signs again refer to outer and inner boundaries respectively. An outer boundary ring is possible for a shell with positive value of μ provided r is less than $r_0\sqrt{\frac{1}{\mu}\left(\frac{1+\nu}{1-\nu}\right)}$, and is always possible for a shell with negative μ. It is possible to find an inner boundary ring for a shell with positive μ provided r is greater than $r_0\sqrt{\frac{1}{\mu}\left(\frac{1+\nu}{1-\nu}\right)}$, but never when the value of μ is negative.

It will be seen from the above discussion that if bending stresses are to be completely avoided, it is impossible to provide the same shell with both an inner and an outer boundary ring, although it may be possible to form the boundaries of type 2 shells with two inside rings or of type 3 shells with two outside rings, by using shells which go through the maximum or minimum radius r_0.

REFERENCE

TIMOSHENKO, S. 1940 *Theory of Plates and Shells.* (McGraw Hill) Chapters 10 and 12.

Journal of the Mechanics and Physics of Solids, 1954, Vol. 1, pp. 127 to 136. Pergamon Press Ltd., London.

ON THE STRESS DISTRIBUTION IN THE WALLS OF PRESSURE VESSELS

By H. Fessler and R. T. Rose
Departments of Civil and Mechanical Engineering, University of Nottingham

(*Received 9th December*, 1953)

Summary

The stresses in and near the hemispherical end of a pressure vessel of uniform wall thickness and mean diameter to thickness ratio of 10 were determined by the frozen stress photoelastic method. The meridional and circumferential stresses at the inner and outer surface are compared with values calculated by Watts and Burrows' (1949) method of evaluation of the Love-Meissner equations. The distribution of meridional, circumferential and radial stresses across the wall thickness at three sections was determined by a procedure based on Frocht's shear difference method of separation of principal stresses. The integration of the meridional stress and the surface value of the radial stress satisfies the equilibrium of all sections investigated. The shear stress at the head to shell juncture is also compared with the calculated value.

Vol. 2 53/54

1. Frozen Stress Method

The frozen stress method of photelasticity (Hetenyi, 1938 ; Fessler, 1953, etc.) is based on the property of some plastics to retain the strain and birefringence caused by stressing at an elevated temperature. If the stressing loads are removed after cooling to room temperature, the strains and associated birefringence of every part of the model remain substantially unaltered. Parallel slices can be cut from the model for analysis in the polariscope.

The isochromatics or fringes visible in such slices are proportional to the difference of the principal stresses in the plane of the slice. These stresses are called secondary principal stresses because they are only the components of the actual principal stresses in the plane of the slice at any point in the model. The isoclinics visible in the slice indicate the directions of the secondary principal stresses. The shear stress and the difference of the direct stresses in any arbitrary direction are readily calculated from a Mohr circle at the point considered.

Because one secondary principal stress (the hydrostatic pressure) is always known in magnitude and direction at the free boundary of any frozen stress slice, the surface stress is obtained directly from the fringe pattern. The individual direct stresses within a three dimensional model can be obtained by calculation as follows.

(i) *Cartesian co-ordinates.*

The equation of equilibrium of an element in a solid (on which no body forces are acting) may be written in cartesian co-ordinates (x, y, z) as

$$\frac{\partial \sigma_x}{\partial x} + \frac{\partial \tau_{xy}}{\partial y} + \frac{\partial \tau_{xz}}{\partial z} = 0$$

where σ_x is the direct stress in the x direction, τ_{xy} the shear stress acting in the x direction on the plane $y = \text{const.}$, etc. In finite difference form, the above equation becomes

$$\frac{\Delta \sigma_x}{\Delta x} = -\frac{\tau_1 - \tau_3}{\Delta y} - \frac{\tau_2 - \tau_4}{\Delta z}$$

where τ_1 and τ_3 are the values of τ_{xy} along the lines $y = +\frac{1}{2}\Delta y$, $z = 0$ and $y = -\frac{1}{2}\Delta y$, $z = 0$ respectively, as obtained from a frozen stress slice cut in the xy plane and τ_2 and τ_4 are the corresponding values in the xz plane. If the origin is taken at a free boundary so that σ_{x_m} is known, σ_x along $y = 0$, $z = 0$ can be determined by summation of the shear differences in two orthogonal slices because

$$\sigma_{x_n} = \sigma_{x_m} - \Sigma_m^n (\tau_1 - \tau_3)\frac{\Delta x}{\Delta y} - \Sigma_m^n (\tau_2 - \tau_4)\frac{\Delta x}{\Delta z}. \tag{1}$$

FROCHT suggested this extension of his two dimensional shear difference method to three dimensional problems (FROCHT 1952).

(ii) *Cylindrical polar co-ordinates.*

For solids of revolution it is more convenient to use polar co-ordinates. The radial equilibrium equation in cylindrical polar co-ordinates (r, θ, z) is

$$\frac{\partial \sigma_r}{\partial r} + \frac{1}{r}\frac{\partial \tau_{r\theta}}{\partial \theta} + \frac{\partial \tau_{rz}}{\partial z} + \frac{\sigma_r - \sigma_\theta}{r} = 0.$$

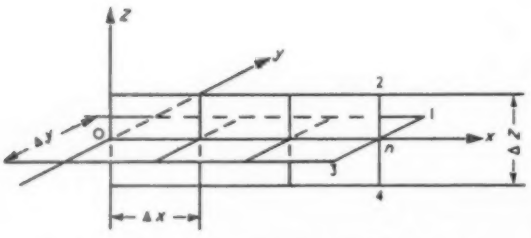

Fig 1. Cartesian system for determination of σ_x.

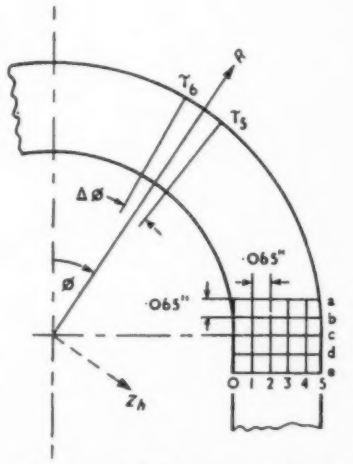

Fig. 2. Spherical polar co-ordinates for determination of σ_R ("z_h" axis would only be required if cylindrical co-ordinates were used). Not to scale.

Due to rotational symmetry $\tau_{r\theta} = 0$, so that in finite difference form

$$\frac{\Delta \sigma_r}{\Delta r} = -\frac{\sigma_r - \sigma_\theta}{r} - \frac{\tau_2 - \tau_4}{\Delta z}$$

and

$$\sigma_{r_n} = \sigma_{r_m} - \Sigma_m^n (\sigma_r - \sigma_\theta)\frac{\Delta r}{r} - \Sigma_m^n (\tau_2 - \tau_4)\frac{\Delta r}{\Delta z}. \tag{2}$$

The last term is obtained from a meridional slice (in the rz plane) as for the cartesian system. Because $\tau_{r\theta} = 0$, σ_r and σ_θ are the secondary principal stresses in a slice in the $r\theta$ plane. Thus $(\sigma_r - \sigma_\theta)$ is proportional to the fringe orders observed in a circumferential slice. All circumferential slices were cut normal to the meridional plane and normal to the shell surface. The meridional slice contains the axis of symmetry and thus lies in the meridional plane.

(iii) *Spherical polar co-ordinates.*

Whenever possible, slices are cut normal to the surface of models to facilitate the accurate determination of the (usually important) surface stresses. When analyzing the "head" it would therefore be necessary to set up a different set of cylindrical co-ordinates for each circumferential slice, replacing "R" by "r" in Fig. 2 and setting up a "z_h" axis as shown by the dotted line. Because such systems are not rotationally symmetrical about the z axis, $\Delta\tau_{r\theta}$ must be calculated in the same manner as $\Delta\tau_{rz}$. It is therefore less laborious to use spherical polar co-ordinates (R, θ, ϕ).

$$\frac{\partial\sigma_R}{\partial R} + \frac{\sigma_R - \sigma_\theta}{R} + \frac{\sigma_R - \sigma_\phi}{R} + \frac{\partial\tau_{R\theta}}{R\sin\phi\partial\theta} + \frac{\partial\tau_{R\phi}}{R\partial\phi} + \frac{\tau_{R\phi}\cot\phi}{R} = 0$$

is the appropriate equilibrium equation and again $\tau_{R\theta} = 0$ due to symmetry, so that the finite difference form is

$$\frac{\Delta\sigma_R}{\Delta R} = -\frac{\sigma_R - \sigma_\vartheta}{R} - \frac{\sigma_R - \sigma_\phi}{R} - \frac{\tau_5 - \tau_6}{R\Delta\phi} - \frac{\tau_{R\phi}\cot\phi}{R}$$

where τ_5 and τ_6 are the values of $\tau_{R\phi}$ on the lines $\phi = \phi + \frac{1}{2}\Delta\phi$, $\theta = 0$ and $\phi = \phi - \frac{1}{2}\Delta\phi$, $\theta = 0$ respectively, as obtained from a meridional slice (Fig. 2). The values of $(\sigma_R - \sigma_\theta)$ are proportional to the fringe order in the circumferential slice along the required line $\theta = 0$ because this line lies in the conical surface $\phi = \text{const}$ (i.e. it is the axis of symmetry of the circumferential slice).

The values of $(\sigma_R - \sigma_\phi)$ are determined from the fringe orders and isoclinics along the line $\phi = \phi$ in the meridional slice. Thus

$$\begin{aligned}\sigma_{R_n} = \sigma_{R_m} &- \Sigma_m^n(\sigma_R - \sigma_\theta)\frac{\Delta R}{R} - \Sigma_m^n(\sigma_R - \sigma_\phi)\frac{\Delta R}{R} \\ &- \Sigma_m^n(\tau_5 - \tau_6)\frac{\Delta R}{R\Delta\phi} - \cot_\phi\,\Sigma_m^n\,\tau_{R\phi}\frac{\Delta R}{R}\end{aligned} \tag{3}$$

2. Evaluation of Individual Stresses

In the previous Section it has been shown how the radial stress σ_r or σ_R can be determined from the fringe orders in the circumferential slice and from the fringe orders and isoclinics in the meridional slice for any part of the shell.

If F is the material fringe value expressed as the difference of principal stresses/(fringe order/inch) in lb/fr. $\times$ in., and N is the fringe order per inch thickness, the circumferential stress σ_θ is obtained from the circumferential slices :

$$\sigma_\theta = \sigma_r + FN \qquad \text{or} \qquad \sigma_\theta = \sigma_R + FN \tag{4}$$

because σ_θ, σ_r and σ_R are secondary principal stresses in these slices. The meridional stresses are obtained from the meridional slices

$$\sigma_z = \sigma_r + FN \cos 2\alpha \qquad \text{or} \qquad \sigma_\phi = \sigma_R + FN \cos 2\alpha \tag{5}$$

where α is the isoclinic angle at the point considered.

3. Calculation of Surface Stresses

LOVE's theoretical analysis of rotationally symmetrical shells considers the equilibrium of elements under the action of circumferential and meridional bending moments, shearing forces and direct stresses. Consideration of the forces in radial and meridional directions and of moments in the meridional plane gives three equations relating the shape and external loading of the shell to the above five unknowns (the circumferential shearing force is zero due to symmetry). LOVE expressed the bending moments and direct stresses in terms of the meridional and radial displacements.

MEISSNER replaced these equilibrium equations by two second-order differential equations in terms of a displacement function and a shear force function. This is known as the LOVE-MEISSNER analysis. An exact solution of this approximate analysis was produced by BOLLE for spherical shells.

BARTKY and BURROWS improved the convergence of BOLLE's hypergeometric series and extended the solution to hemispheres. The calculations in this paper were based on this solution as given by WATTS and BURROWS (1949) and by WATTS and LANG (1953). This analysis ignores radial stresses and is therefore only strictly applicable to thin shells where the radial stress is small compared with the meridional and circumferential stresses. WATTS and BURROWS' analysis is simplified by the assumption that the internal pressure acts on the middle surface of the shell. This would lead to serious errors for the shell under consideration, the wall thickness t of which was 0·1 × mean diameter D. The theoretical solution was therefore modified to consider the pressure acting on the inner surface. This was done by reducing the meridional membrane stresses in cylinder and hemisphere and the circumferential membrane stress in the hemisphere to $(1 - t/D)^2 = 0{\cdot}81$ of their original value. The circumferential membrane stress in the cylinder was multiplied by $1 - (t/D) = 0{\cdot}90$ and all discontinuity stresses were multiplied by $1 - (t/D)^2 = 0{\cdot}99$.

The surface stresses calculated in this manner (to six significant figures) for a value of Poisson's ratio of 0·5 are shown by the full lines in Figs. 4 and 5.

4. Material

The model material was Araldite casting resin *B*, an ethoxylene resin (SPOONER and MCCONNEL 1953). 30 parts of hardener No. 901 were mixed into 100 parts of molten resin ; the mixture was poured into a cast iron mould, cured in 4 hours at 160°C and cooled slowly. To reduce the machining time of the model, an Araldite core was used which was removed after the gelling of the cast. Mould and core had to be coated with a silicone separator to prevent adhesion of the casting. The material fringe value (using light of 5460 A wavelength) was 1·315 lb/fr. × in.,

and the effective modulus was 1,878 lb/sq. in. These quantities were calculated from the radial stress and deformation at the " infinite " cylinder. The material is subject to edge stresses which are avoided by storage of models and slices in dessicators.

5. The Model

Fig. 3 shows the finished (unstressed) dimensions of the model. The open end was closed by a similarly shaped dummy, the head of which was reduced in thickness to minimize discontinuity stresses at this end. A spigot ensured concentricity of the two shells, which were joined by a small quantity of araldite cured at 135°C.

It was estimated that the shape of the (unstressed) model, which was determined by the " formers " of a " profiling attachment " on the lathe, was accurate to $\pm$ 0·002 in.

An oil pressure of 8·07 lb/sq. in. was applied for 1 hour at 135°C before the model was allowed to cool under pressure at 7° C/hour.

Slicing was carried out with a liquid cooled $\frac{1}{16}$ in. thick abrasive cut-off wheel. Slices varied in thickness from 0·095 in. to 0·097 in. but the maximum variation of thickness of any slice was 0·0005 in.

Integral fringe orders were measured with a wedge compensator while fractional fringe orders were determined by Tardy's (1929) method to $\pm$ 0·03 fr. Isoclinics were estimated to $\pm 1°$. Deformations were measured by dial gauge to $\pm$ 0·0001 in.

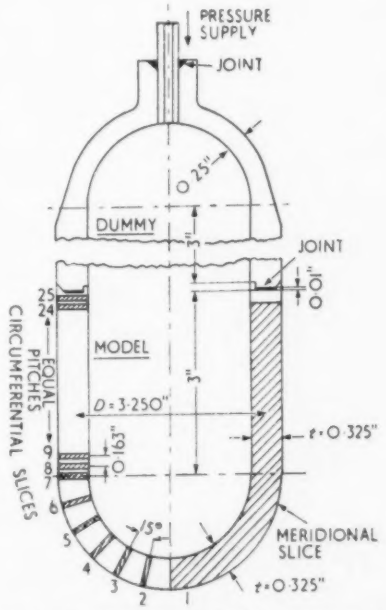

Fig 3. Dimensions of model, showing also position of slices. (Not to scale).

6. Surface Stresses

The stresses at the outer surface are equal to the material fringe value $\times$ fringe order/inch. The fringe order at the inner surface is proportional to the difference between the meridional or circumferential stress and the hydrostatic pressure p. The fringe order corresponding to the latter ($-$ 10·6 fr/in.) has therefore to be added to the measured value to obtain the inner surface stresses.

The material fringe value was calculated from the radial stress at the inside surface of the " infinite " part of the cylinder. The latter was considered to exist where the isoclinic angle was zero and the meridional stress at the inner and outer surface had the same value (indicated on Fig. 4). The stresses set up by the contraction of the joint material, during polymerisation of the joint, locally disturbed the simple state of stress.

The results are shown on Figs. 4 and 5 in terms of the " stress index," as proposed by WATTS and BURROWS (1949), that is as fractions of the equivalent hoop stress in a thin cylinder ($pD/2t$). Each pair of points in Fig. 5 was obtained from the corresponding slice shown in Fig. 3. The radial deformation of the cylindrical part of the shell was also measured and recorded in Fig. 5 to make possible the comparison of deformations with stresses.

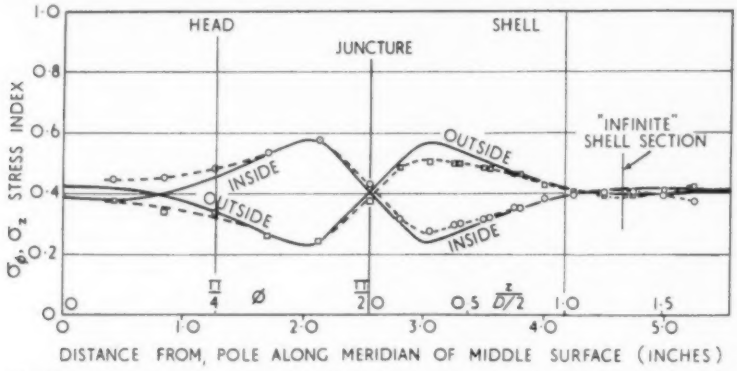

Fig. 4. Meridional surface stresses. The full lines represent the calculated values of stress.

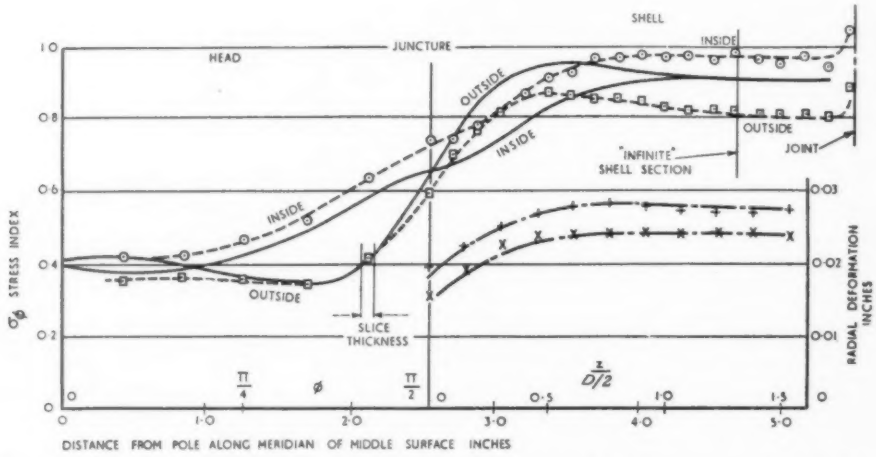

Fig. 5. Circumferential surface stresses and deformations. The full lines represent the calculated values of stress. The chain dotted lines indicate the measured deformations.

○ (photoelastic) stress at inside surface.
⊡ (photoelastic) stress at outside surface.
\+ - inside deformation from measured stresses.
× outside deformation from measured stresses.

7. THE " INFINITE " CYLINDER

At a section in the infinite cylinder $\tau_{rz} = 0$ so that σ_z and σ_r are principal stresses. To calculate σ_r a radial line in circumferential slice No. 20 was divided by four nodes into five equal sections of length Δr ($\simeq 0{\cdot}065$ in.). The fringe

order at each node was measured, divided by the thickness of the slice and by the corresponding radius r, and multiplied by Δr. Summing the mean values of this quantity across the section gave a fringe order proportional to the change in radial stress from the inner to the outer surface. The difference in radial stress between the surfaces must be equal to the (known) internal pressure. The material fringe value F was therefore calculated as the pressure / (the above fringe order/inch) and found to be 1·315 lb./fr. × in.

The radial stress at each node was calculated by subtracting the negative values of $\Delta\sigma_r$ from the known negative value of σ_r at the inner surface. σ_θ and σ_z at each node were calculated from equations (4) and (5) ($\alpha = 0$ throughout). These stresses are plotted in Fig. 6 and compared with the radial and circumferential stresses calculated from Lamé's thick cylinder equations.

The meridional stresses σ_z were integrated over the cross-section to check the accuracy of the measurements by comparing the total meridional tensile force with the force due to the internal pressure. Thus using the mean values of r and σ_z for each section,

$$\Sigma_i^o 2\pi r\sigma_z \Delta r = k \times p\pi r_i^2 \tag{6}$$

where " o " refers to outer surface, " i " refers to inner surface and k is a measure of the overall accuracy. All values of k are recorded in Table 2.

Vol. 2 53/54

TABLE 1

Values of actual fringe orders " n " and isoclinic angles " α " for nodes shown in Fig. 2.

	a		*b*		*c*		*d*		*e*	
	n	α	n	α	n	α	n	α	n	α
0	2·17	4°	2·00	2°	1·86	0°	1·67	− 1°	1·56	− 1°
1	1·86	5°	1·81	4°	1·73	4°	1·64	3°	1·59	2°
2	1·62	9°	1·62	7°	1·59	6°	1·59	5°	1·56	4°
3	1·33	11°	1·39	9°	1·45	8°	1·45	7°	1·45	6°
4	1·17	12°	1·22	10°	1·28	9°	1·31	6°	1·39	4°
5	0·78	3°	0·89	1°	1·09	0°	1·22	− 1°	1·28	− 1°

8. THE CYLINDER-HEMISPHERE JUNCTION ($\phi = \pi/2$)

The determination of σ_r from equation (2) was not attempted because the small changes of the isoclinic angle near the juncture would have made the direct determination of τ_2 and τ_4 liable to large errors in this case. The network shown in Fig. 2 was therefore set up based on the line $z = c$ at $\phi = \pi/2$. The values of fringe order and isoclinic angle, as measured at each node, are recorded in Table 1. From these the values of $\tau_{rz} = \frac{1}{2} FN \sin 2\alpha$ were calculated and plotted in Fig. 9 (a). Along the lines a, b, d and e, τ_{rz} at the free surfaces is not zero because these lines are not normal to the surfaces due to the shape and deformations of the shell. $\partial\tau_{rz}/\partial z$ (Fig. 9 (b)), when obtained from the slopes at c of the cross-plots of Fig. 9 (a), was less influenced by errors in individual measurements than $(\tau_2 - \tau_4)/\Delta z$.

Equation 2 was therefore modified to

$$\sigma_{r_n} = p + \Sigma FN \frac{\Delta r}{r} - \Sigma \frac{\partial \tau_{rz}}{\partial z} \Delta r$$

where N is the fringe order at the mid-points between the nodes in the circumferential slice. Because the radial stress at the outer surface is zero, the radial stress at the inner surface can be calculated from $\sigma_{ri} = p - \sigma_{r0}$ where the last term is the final value of the above summation. Thus a value of the accuracy factor k was obtained.

The circumferential and meridional stresses were obtained by use of equations (4) and (5).

The results are recorded in Fig. 7 and the radial stress is compared to the stress given by Lamé's cylinder equations. Another value of the accuracy factor was obtained by the application of equation (6) to this section.

The actual distribution of shear stress across the junction, as given by the "c" curve of Fig. 9 (a) can be compared with the parabolic distribution assumed in thin shell theory. The theoretical shear force Q (WATTS and BURROWS, 1949) was calculated as 0·0748 (lb./inch of middle surface)/pressure. This is in good agreement with the experimental value

$$\frac{1}{p\pi D} \Sigma 2\pi r \tau_{rz} \Delta r = 0{\cdot}0754 \text{ in.},$$

although the distribution is only approximately parabolic.

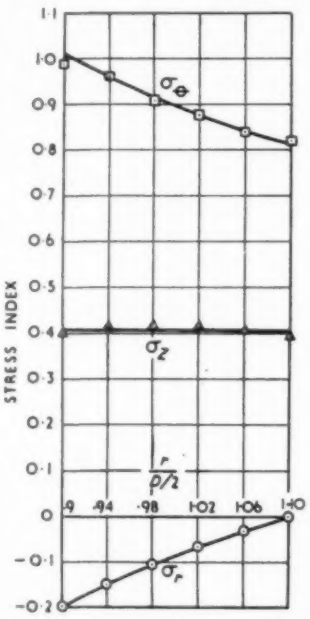

Fig. 6. Stresses in a radial section of an "infinitely long" cylinder. The full lines are calculated from Lamé's thick cylinder equations.

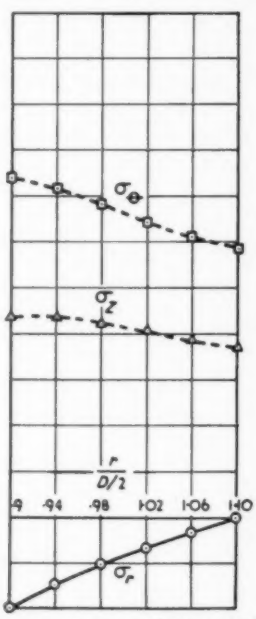

Fig. 7. Stresses in the radial section at the junction of head to shell. The full line is calculated from Lamé's thick cylinder equations.

Note: The symbols on the top curves should read σ_ϕ.

9. THE HEMISPHERE SECTION $\phi = \pi/4$

This section was analyzed in spherical polar-co-ordinates. As the isoclinic angle in both slices was constant across this section, there were no shear stresses. Therefore σ_R and σ_ϕ are principal stresses and (3) reduces to the summation of the fringe order in the meridional and circumferential slices. σ_θ and σ_ϕ were calculated from (4) and (5), where $\alpha = 0$, and the results were recorded in Fig. 8 and compared with the stresses in a (complete) thick sphere under the same pressure.

The accuracy factor in the radial direction was determined as for the juncture of hemisphere to cylinder. The meridional accuracy factor was determined by consideration of the axial equilibrium of the section,

$$\sin\phi\ \Sigma_i^0\ 2\pi\,(R\sin\phi)\,\sigma_\phi\,\Delta R = kp\pi\,(R_i\sin\phi)^2.$$

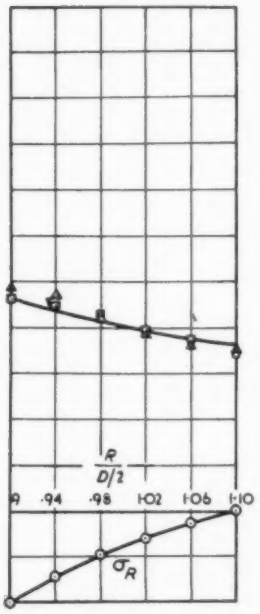

Fig. 8. Stresses in the radial section of the head $\phi = \pi/4$. The full lines are calculated for a (complete) thick sphere. △ values of σ_ϕ, ⊡ values of σ_θ.

10. Conclusions

The good agreement of the total forces at different sections, as shown by the accuracy factors, together with the smooth curves obtained for the different stresses shows the

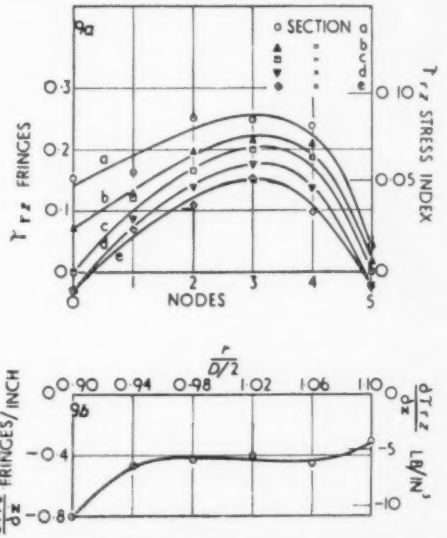

Fig. 9. Distribution of shear stress across radial section near junction and $\partial\tau_{rz}/\partial z$.

Table 2

Overall accuracy of measurements

Section	*Direction of equilibrium*	*Accuracy factor k*	*% error*
" Infinite " cylinder	radial	1·0000	0
	meridional	0·9911	0·9
Junction	radial	1·0042	0·4
	meridional	0·9929	0·7
$\phi = \pi/4$	radial	1·0085	0·9
	meridional	1·0183	1·8

methods to be accurate and reliable.

The surface stresses and the shear force at the juncture are in fair agreement with the modified calculations by WATTS and BURROWS' method. It should be pointed out that experimental and calculated results apply for a Poisson's ratio of 0·5. Calculation shows that the calculated stresses for Poisson's ratio 0·25 are slightly smaller than the above, the maximum meridional stress being reduced to 97 per cent. of the calculated value shown in Fig. 4.

The results have been calculated for the loaded, i.e. deformed, shell. As the maximum strain (of the cylinder) was 1·9 per cent., slightly different values would have been obtained for the individual stresses and the accuracy factors if the unstressed dimension had been used. For instance the (fictitious) material fringe value, based on the original dimensions was 1·285 instead of 1·315 lb./fr. × in.

The methods described are applicable to any solid of revolution and can therefore be used for any shape of head. Furthermore, they may be used for thicker vessels for which no satisfactory methods of calculation are known at present.

ACKNOWLEDGMENT

The authors wish to express their thanks to Professor J. A. POPE, Head of the Departments of Civil and Mechanical Engineering at Nottingham University, who provided all necessary facilities for this work.

REFERENCES

FESSLER, H.	1953	*Proc. I. Mech. E.*, 1B, No. 12.
FROCHT, M. M.	1952	*Proc. 1st. U.S. Nat. Congress of Appl. Mech.*, 301.
HETENYI, M.	1938	*J. Appl. Mech.* **5**, A-149.
SPOONER, H. and McCONNEL, L. D.	1953	*Brit. J. Appl. Phys.* **4**, 181.
TARDY, H. L.	1929	*Revue d'optique*, **8**, 59.
WATTS, G. W. and BURROWS, W. R.	1949	*Trans. A.S.M.E.* **71**, 55.
WATTS, G. W. and LANG, H. A.	1953	*Trans. A.S.M.E.* **75**, 83.

Vol 2 1953

BOOK REVIEWS

Advances in Applied Mechanics : Vol. III. Edited by TH. VON KÁRMÁN and R. VON MISES. Academic Press, New York. 1953, x + 324 pp. $9.0.

IT seems appropriate in reviewing a volume of this kind to make some general comments on the type of material which could most profitably be included and how such material should be handled. In a preface to the first volume the Editors, TH. VON KÁRMÁN and R. VON MISES, suggest that ' perhaps the research worker will not need our surveys in the proper field in which he is himself active, but he might be interested in summaries of related topics.' This intention is admirable and recognizes a very real need. It is implicit in this policy that, having regard to the diversity of training of potential readers, the emphasis should be on *what* has been achieved and *why* rather than on the details of *how*. This presents a difficult but by no means impossible task to those writers whose topics depend on subtleties of mathematical reasoning. The considerably widened interest of such a treatment should more than compensate the specialist for the qualms he might perhaps feel in presenting his subject with an unwonted lack of rigour and esoteric appeal.

The first article is an interesting essay of nineteen pages by G. F. CARRIER on ' Boundary Layer Problems in Applied Mechanics.' The author discusses the type of equation which can give rise to boundary-layer phenomena and illustrates his remarks with a few examples. The main thread of the argument is clearly maintained in a readable article. A discussion of thirty-nine pages on ' The One-Dimensional Isentropic Fluid Flow ' by OTHAR ZALDASTANI follows. The article is confined to analytical solutions of the continuous motion problem. The presentation is concise and logical and admirable from a mathematical viewpoint. The next contribution, a forty-seven page article on ' Turbulent Diffusion : Mean Concentration Distribution in a Flow Field of Homogeneous Turbulence ' is by F. N. FRENKIEL. The author presents the statistical ideas associated with a turbulent field and considers examples relevant to a homogeneous, isotropic and stationary field. In a final section the author shows that Fick's Law of Turbulent Diffusion is valid only for dispersion times which are large compared with the Lagrangian scale of turbulence. This polished and lucid article will appeal principally to readers with a mathematical background, but it is by no means inaccessible to those with a lesser degree of mathematical facility. H. F. LUDLOFF's article, ' On Aerodynamics of Blasts,' of thirty-six pages, follows. The author considers the problem of shocks of varying strengths encountering obstacles ranging from slight variations in near-planar surfaces to an almost perpendicular wall. This article is clearly intended for those with more than popular knowledge in the field. The development is logical, attractive and balanced. A forty-page contribution from G. GUDERLEY, ' On the Presence of Shocks in Mixed Subsonic-Supersonic Flow Patterns,' follows. The theme of the article is the assertion that potential flows are in general not possible over a contour in a transonic flow field. This is a very readable article in which the development is lucid and the arguments well expressed. The author's handling of a topic which is very far from cut and dried is commendable and provides a good example of how quite involved points can be presented and argued without excessive recourse to detailed mathematics. The shortest contribution with, incidentally, the longest list of references follows. It is an eleven page article by L. ROSENHEAD, ' Vortex Systems in Wakes.' It is rather surprising to find this topic in a current volume of Advances in Applied Mechanics, but according to the author there has been a renewal of interest in the field. The paper summarizes well-known work, comments on its deficiencies, and makes suggestions for future work. It is a useful although perhaps rather too brief survey which will be readily assimilated by all readers. The following article of ninety-eight pages is by HILDA GEIRINGER and is entitled ' Some recent Results in the Theory of an Ideal Plastic Body.' A rather more detailed criticism of this article is undertaken, not because the reviewer feels that it falls below the high standard of the volume, but because it is by far the longest article and because the reviewer's chief interest embrace this topic.

The governing equations in three-dimensions for a material obeying von Mises criterion are given and particularized to the plane stress and plane strain problems. The three-dimensional problem with a general yield function and differing plastic potential is then formulated and particularized

Vol.
2
53/54

to the general plane problem with similar yield and potential functions. The general plane problem and various yield functions are discussed and a mathematical treatment of general methods for solving the relevant equations given. Initial value problems are then considered followed by a discussion of simple waves. A final section deals with specific plane strain solutions which are all chosen to exemplify specific mathematical points. If Dr. GEIRINGER's choice of material and approach is accepted, the development is logical and consistent. The reviewer would have preferred to see an approach of this type commencing with the general three-dimensional problem with an arbitrary yield and differing potential function. Dr. GEIRINGER considered this approach as her remark on p. 211 shows. The theorem of p. 256 to the effect that in the non-orthogonal case the plastic-rigid boundary is a straight characteristic if the tangential velocity component is discontinuous across the boundary, and the remark at the bottom of p. 256 that the normal velocity component across a plastic-rigid boundary is continuous require some comment. In plasticity theory velocity discontinuities are conceived as vanishingly narrow zones undergoing very high strain-rates, with all velocity components continuous. There is therefore in *general* no objection to a 'discontinuity' in both the normal and tangential velocity components across a narrow transition region; in *particular* the normal component may be continuous as under plane strain conditions at non-singular points. Since the theorem quoted above relies on the partial derivative of the normal velocity component across a plastic-rigid boundary being *finite* with respect to the normal direction when it may in fact tend to infinity, the theorem established appears to be in error. It should perhaps be remarked that the indentation solutions of p. 290 are only upper bounds to the yield-point problems in the given configurations since no provision is made for material forced out at the surface, and the stress solution does not include the rigid regions. The reviewer would have preferred to see an article much more broadly based and in keeping with the remarks in the preface. However, as the author says, the choice of material is naturally very subjective. Dr. GEIRINGER is to be congratulated on a comprehensive treatment of the aspects considered. The article is definitely for the mathematical specialist.

The final article is a twenty-six page paper, 'Non-autonomous Systems,' by A. I. BELLIN. This is chiefly concerned with the existence and stability of periodic solutions to non-linear second-order differential equations. Articles of this type perform a very valuable service for the applied worker.

The Editors are to be congratulated on presenting this volume in spite of the difficulties mentioned in their preface. It is to be hoped that the loss to the scientific world of one of the Editors will not impair the standard of the series. In any event, this volume cannot be regarded as in any way inconsistent with the deservedly high reputations which both the Editors enjoy.

J. F. W. BISHOP

S. P. TIMOSHENKO: **History of Strength of Materials.** McGraw-Hill Book Co., Inc. 1953. 452 pp. with 245 illustrations and diagrams. 71s. 6d.

THE debt that all students of engineering owe to Professor TIMOSHENKO grows prodigiously with every new work of his. This latest book describes the progress of civil engineering as a science from antiquity to the present day. It is a remarkable tour-de-force: imposing in its scholarship, authoritative, well-balanced, thoroughly documented, finely illustrated, and very readable.

It is not merely a general history of personalities and achievements, but a detailed record of each important contribution to the theory of elasticity and strength of materials on the one hand, and to railway engineering, ship construction, building methods and analysis of structures on the other. In addition there are critical appraisals of teaching methods at various periods, and informative accounts of the growth of centres of research in European countries and in Russia.

The book has appeared at an opportune moment, and very probably marks a distinct stage in the growth of its subject. The developments of recent years portend that a future historian of strength of materials will need to be a metal physicist as well as an elastician in the tradition of LAMÉ, KELVIN and SAINT-VENANT.

R. HILL.

R. E. PETERSON : **Stress Concentration Design Factors.** Wiley and Sons, Inc., New York, 1953, x + 153 pp. $8.50.

THIS is a design handbook covering the effects on a wide variety of stress concentrations written by an experienced and accomplished journeyman in the field of engineering. Great care has been lavished on its preparation not only by the author but by various referees, editorial policy committees, and friends. All of this care is reflected in the finished product which is certainly of the highest calibre.

A paragraph from the preface describes the book well : " It is the purpose of this book to place in the designer's hands information which will enable him to improve his design calculations to the end that failure will be less prevalent and better-balanced designs will be achieved. The book should be regarded primarily as a working tool ; it is not intended to be a textbook in the usual sense, and therefore only enough background and references are given to enable the reader to explore the subject further if he so desires. Features have been incorporated into the book to increase its usefulness to designers – the " edge finder," the helical binding, and the large, full-grid charts." And to the last might be added a list of symbols.

From the technical standpoint it might be pointed out that insufficient explanation is made of the ductile to brittle transition behaviour of steels (and other non-face-centred cubic metals, of course) and its role in design. To be sure little enough *can* be said, but its importance is so great that whatever could have been said should have been. The reviewer, for example, would hate to design buckets for a jet engine from some of the alloys contemplated now, on the basis of this handbook, unless he adopted the view that the material were *completely* brittle. But then that isn't the best design.

For all this, the reviewer knows of no better book of this type.

W. M. BALDWIN.

Vol. 2 53/54

R. CAZAUD : **Fatigue of Metals.** Chapman and Hall, London, 1953. xiv + 334 pp., with numerous illustrations. 60s.

THE literature relating to the fatigue of metals is remarkable in that, while the volume of published work in the form of research papers is enormous, the number of comprehensive surveys in textbook form is extremely small. The reasons are not hard to find : the phenomena associated with fatigue have yet to be satisfactorily correlated by any complete physical explanation. The behaviour of a specific material in a specific state and subjected to specific cycles of stress or strain can therefore be studied and described phenomeno-logically, but the task of presenting the results in a concise and logical form is one of the most extreme difficulty.

In Dr. CAZAUD's book, one short chapter of nineteen pages is devoted to a discussion of the theories that have been advanced " regarding the nature of the mechanism of failure by fatigue." Although it is convenient to have these theories grouped together and supported by a bibliography containing some fifty references, the discussion of them makes little or no contribution to the topic and serves merely to illustrate how painfully inadequate is our understanding of the subject. The rest of the book deals with the characteristics of fatigue cracks and their detection ; with testing techniques and machines ; with the fatigue strength of various metals and alloys and the influence on the fatigue strength of the multitude of factors that affect it ; with the strength of structural joints ; and with methods of improving resistance to fatigue. Altogether the book contains an immense amount of information, no small proportion being original, and the bibliography is excellent. It is a book which will be of great value to those whose chief interest is in the strength of materials, but of even greater value to those whose main concern is engineering design and development.

The translator has taken the opportunity of adding to the original (1948) text some recent material. The translation is so outstandingly good that it would be unfair to cavil at the very few slips which have been made. It would serve as a pattern for many translators of literary works.

J. L. M. MORRISON

NOTICE OF MEETINGS

Conference on the Physics of Particle Size Analysis

At The Institute of Physics' Conference on "The Physics of Particle Size Analysis," to be held in Nottingham from 6-9 April, 1954, the following sessions have been arranged: The motion of particles in fluids; the scattering of light by particles; the general phenomena encountered in particles size analysis: the comparison of methods and the automatised methods of particle counting and sizing.

Preprints of the papers to be presented to the Conference will be available beforehand and, together with a summary of the discussion, will, in due course, be issued as a supplement to the *British Journal of Applied Physics*. Further particulars may be obtained from the Secreatry, The Institute of Physics, 47 Belgrave Square, London, S.W.1.

16 *December*, 1953.

International Conference on Semiconductors

The Netherlands Physical Society, with the support of the International Union of Pure and Applied Physics and U.N.E.S.C.O. will organize an *International Conference on Semiconductors*, to be held at Amsterdam from June 29th-July 3rd, 1954.

The following scientists (two of them with some reserve) will deliver lectures: J. Bardeen, W. H. Brattain, H. B. G. Casimir, F. A. Kröger, D. Polder, M. Schön, W. Shockley, R. A. Smith, H. J. Vink, H. Welker on subjects such as bulk recombination; surface conductivity; surface trapping; surface recombination; intermetallic compounds, the band picture in polar and non-polar semiconductors; photoconductivity in semiconductors like PbS, PbTe, PbSe, ZnS, CdS; the application of general physical and chemical laws for the preparation of semiconductors with specific properties.

Discussions will be held in connection with these main lectures and there will be opportunity to discuss problems in more detail in sectional meetings. In these sectional meetings short communications of about 15 minutes can be given.

Scientists who would like to participate in the conference or want to give a scientific contribution should communicate this to the secretary (Dr. H. J. Vink, Floralaan 142, Eindhoven, Holland) as soon as possible. They will receive a detailed programme in due course.

Vo
2
1953

Journal of the Mechanics and Physics of Solids, 1954, Vol. 2, pp. 141 to 155. Pergamon Press Ltd., London.

THE FUNDAMENTAL ACTION OF EARTH PRESSURE CELLS

By K. R. Peattie and R. W. Sparrow
Departments of Civil and Mechanical Engineering, The University of Nottingham

(*Received 15th December*, 1953)

Summary

The measurement of earth pressures by pressure cells is complicated by the disturbance of the pressure distribution in the soil by the introduction of a cell whose stress-deformation characteristics are radically different from those of the soil. Predictions have been made of the cell characteristics which are likely to affect these errors in the light of theoretical considerations and of previous experimental work.

A number of cells have been constructed in which the following properties can be varied: diameter-thickness ratio; ratio of the sensitive area of the cell face to the total facial area; cell compressibility. Tests have been carried out with these cells in sands and clays under different conditions. The results of these tests show that for the size of cell used in the tests it is possible to construct a cell which will record pressures to within $\pm$ 3 per cent irrespective of the type or condition of the soil.

Vol. 2 53/54

1. Introduction

Many of the methods of design in soil mechanics are based on theoretical stress distributions in the soil which it has not been possible to check because of the lack of suitable earth pressure recording devices. The necessity for such devices is shown by the large number which have been produced and used in the past but in many cases the results have been rather inconclusive.

Some of the difficulties in earth pressure measurement are caused by the non-homogeneous nature of the soil, but the cell itself also causes difficulties. Basically, an earth pressure cell is a device that will provide an indication, at a remote point, of the pressure in the soil at the point of installation. This however involves the introduction into the earth mass of a body whose stress-deformation characteristics are radically different from that of the soil with a consequent redistribution of pressure in the vicinity of the inclusion, so that the cell does not indicate the true stress existing at the point of its installation.

The purpose of this work has been to investigate the effect of various cell properties on these inherent errors, and to develop a rational basis for the design of cells which will minimize the errors and reduce them to predictable proportions. The work is not concerned with the design of mechanical and electrical details for cells suitable for field use.

A perusal of the literature on earth pressure cells shows that in the past very little consideration has been given in the design of cells to the errors that will accompany their use. The design of such devices has been largely controlled by

the size and shape of the internal pressure measuring system. KÖGLER and SCHEIDIG (1927) first called attention to the inherent difficulties in measuring earth pressures accurately with a pressure cell. They pointed out that a cell which was more rigid than the surrounding soil would indicate pressures in excess of those existing in the soil before the introduction of the cell, and conversely, a cell less rigid than the soil would indicate lower pressures than those existing. Thus it is seen that only if the cell has the same stress-deformation characteristics under pressure as the surrounding soil will its use be free from error.

This latter condition would appear at first sight to be the obvious solution to the problem but there are further difficulties in attempting to construct such a cell. Owing to the non-homogeneous nature of soil, its stress-deformation characteristics (hereafter referred to as the modulus) are by no means constant in a given location, neither does the modulus remain constant over different ranges of pressure and there are obvious difficulties in constructing a cell whose modulus could be made to match that of any given soil. Further, as will be shown later, although the error is zero when the modular ratio is unity, the rate of change of error with change in modular ratio is then a maximum. Therefore, unless the pressure cell is to be used in a material of constant known modulus, it is highly undesirable to construct it so that it has nearly the same modulus as the material. These conditions are unlikely to be found in soils.

An early investigation into the problem of cell action was carried out by BENKELMAN and LANCASTER (1941) who used modified Goldbeck pneumatic cells of various diameters. The cells were buried in a soil mass contained in a cylindrical vessel and the load was applied through a concrete bearing block to the surface of the soil. Further experimental work was carried out by the U.S. Waterways Experiment Station (1944) in order to determine the effect of the projection of a cell from a rigid wall; cell compressibility in a cell mounted flush with a rigid wall; and cell dimensions and compressibility in cells embedded in a soil mass on the pressures indicated. Flat cylindrical cells designed by the Station were used in this work and their diameters ranged from 3 inches to 12 inches. The cells were tested in sand in a pressure chamber and the load was applied by air pressure acting on a rubber diaphragm in contact with the top surface of the sand. The sand used throughout the tests was Ottawa standard sand and the following conclusions were drawn. Flat cylindrical cells embedded in rigid materials would indicate true pressures provided that the diameter-projection ratio exceeded 30 and the diameter-deflection ratio exceeded 1,000. For cells embedded in the soil mass the diameter-thickness ratio should exceed 5 and the diameter-deflection ratio should exceed 2,000.

Both these experimental investigations were of limited value because of the unrepresentative nature of the soils and the fact that the soil masses were small in regard to the size of the cells.

2. THEORETICAL ANALYSES

A theoretical analysis of the soil pressure cell problem was carried out by TAYLOR (1947) in which the following relationship between cell error and dimensions was derived for a compressible cell embedded in a soil mass :

$$\frac{p_e}{p} = \frac{\frac{B}{D}\left(\frac{N}{M} - \frac{N}{M_c}\right)}{1 + \frac{B}{D} \cdot \frac{N}{M_c}} \tag{1}$$

where

p_e = additional pressure recorded by the cell owing to its relative rigidity
p = field pressure existing at the plane of the cell in the absence of the cell
M = stress-strain modulus of soil
M_c = stress-strain modulus of cell
N = property of the soil, such that N/D is analogous to the coefficient of subgrade reaction
B = half thickness of cell
D = diameter of cell.

This expression may be considerably simplified without introducing serious error. If it is assumed that, for a given condition of the soil, the ratio N/M has a constant value, say K, then equation (1) becomes

$$\frac{p_e}{p} = \left[\frac{K\left(1 - \frac{M}{M_c}\right)}{1 + \frac{B}{D} \cdot \frac{M}{M_c} K}\right] \cdot \frac{B}{D} \tag{2}$$

where the expression in square brackets tends towards K as the value of M_c/M tends towards infinity, and is approximately independent of the value of B/D provided that both B/D and M/M_c are small. Hence, under these conditions, this expression may be replaced by a constant C_A which has been called the Cell Action Factor and whose value depends solely on the value of M_c/M. The relation between cell errors and dimensions can now be written in the form :

$$\frac{p_e}{p} = C_A \cdot \frac{B}{D}. \tag{3}$$

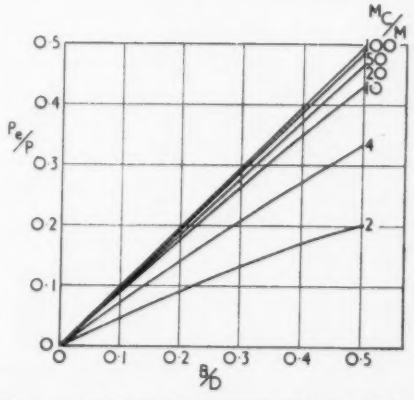

Fig. 1. Variation of cell error with cell thickness and compressibility for $N/M = 1$.

To illustrate the magnitude of the error introduced by these assumptions in the simplification of equation (1), Fig. 1 has been plotted. This shows the relation between p_e/p and B/D for different values of the ratio M_c/M, the value of N/M being assumed to be unity. It is seen that for values of B/D less than 0·5, which is as large a value as is likely to be encountered in practice, the relation between p_e/p and B/D is very nearly linear and the error involved in assuming this linear relation decreases as the value of the ratio M_c/M increases.

A more rigorous analysis of the influence of a cell on the pressure distribution in and near a cell embedded in an infinite homogeneous solid was made by Monfore (1950). In this analysis a cell is considered to be embedded in an infinite

elastic mass and a section is taken through the mass and cell on the plane of symmetry. This plane is assumed to remain plane after the application of pressure to the mass. The cell and the surrounding mass are then considered to be divided into a number of concentric ring areas and, in order to keep the plane of symmetry plane, additional loads over and above the field stress must be applied to each of these ring areas. The Boussinesq equations for the surface deflections of a semi-infinite mass under normal loads are then used to develop expressions for the deflections of the ring areas in terms of the loads applied to them. These expressions are then solved simultaneously to determine the loads on the ring areas.

If these ring loads are plotted across the plane of symmetry the resulting pressure distribution curve shows the additional pressure acting over the face of the cell and the relief of pressure occurring in the adjoining soil. The actual values of the ring loads are dependent on the modulus of the solid E_s, the modulus of the cell E_g, Poisson's ratio for the solid and the thickness of the cell. MONFORE computed results for a solid having a modulus of 4×10^6 lb./sq.in., a Poisson's ratio of 0·2, and the following variations of cell dimensions and properties : for a fixed value of B/D of 0·1, cells of different moduli are considered so as to give the modular ratio E_g/E_s values of $\frac{1}{4}$, $\frac{1}{2}$, 2 and 4; for a fixed value of modular ratio of 2 the (half-thickness)/(diameter) ratio B/D is varied to have values of 0·05, 0·1 and 0·2.

Using the same values of E_s, Poisson's ratio and B/D as MONFORE, the results have been extended to include values of modular ratio E_g/E_s of 10, 20, 50 and ∞; the resulting pressure distributions are shown in Fig. 2. In order to determine the probable behaviour of cells used in soil, further computations were carried out for an infinite modular ratio E_g/E_s, Poisson's ratio $= (0{\cdot}1)^{\frac{1}{2}}$ and $B/D = 0{\cdot}177$. This latter value is the (half-thickness)/(diameter) ratio of the basic type of cell used in the experimental work.

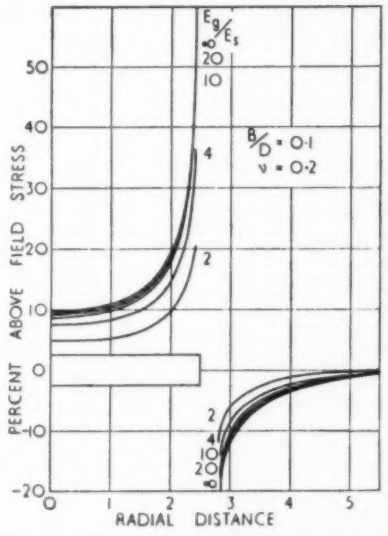

Fig. 2. Effect of Modular Ratio on Stress Distribution.

From the theoretical analyses of TAYLOR and MONFORE the following conclusions can be drawn :

(*a*) For a given set of conditions the cell errors are directly proportional to the (half-thickness)/(diameter) ratio and may be expressed in the form

$$\frac{p_g}{p} = C_A \cdot \frac{B}{D}$$

where C_A is defined as the cell action factor.

(*b*) The cell action factor C_A is a function of the modular ratio E_g/E_s and its value increases with increasing values of this modular ratio. But, as is seen from Fig. 3, provided that the modular ratio exceeds 10, C_A can be

considered to be approximately constant and independent of the value of the ratio, for a given value of the ratio of sensitive area to total facial area.

(*c*) For a given value of modular ratio, C_A is a function of the ratio of the sensitive area of the cell face to the total area of the face. This effect is caused by the non-uniform pressure distribution over the face of a cell. For a rigid cell, the value of C_A varies from unity (when the ratio of sensitive cell area to total cell area is about 0·1) to about 1·5 (when the ratio of the areas is about 0·8). The value of C_A thereafter increases rapidly towards infinity as the area ratio approaches unity. This is shown in Fig. 4.

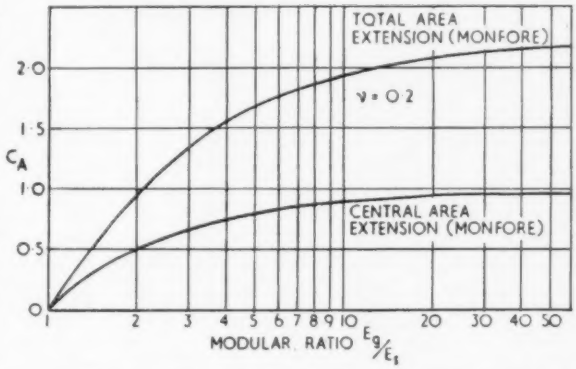

Fig. 3. Variation of C_A with modular ratio.

(*d*) The cell action factor depends on the value of Poisson's ratio for the material in which the cell is embedded, but only in the term $(1 - \nu^2)$ where ν is Poisson's ratio. Thus, provided Poisson's ratio is less than 0·3 or 0·4, its effect on the value of C_A is small.

(*e*) Since the analyses have been carried out for a material which has been assumed to be elastic, homogeneous and isotropic, and capable of developing infinite edge stresses the results of the analyses are independent of the magnitude of the field stresses and the time for which they are applied.

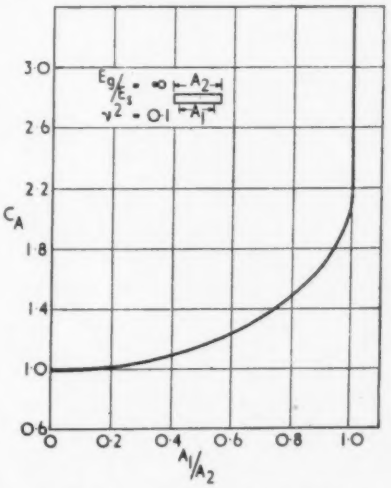

Fig. 4. Variation of C_A with sensitive area.

3. Experimental Investigation of Cell Action

Since most soils are heterogeneous and possess stress-deformation characteristics that are only very approximately those of an ideal elastic solid, the application of the results of the theoretical analyses to cells embedded in soils must be made with caution. A valuable contribution of the theoretical analyses to the problem is, however, the indication they give of the factors most likely to affect cell action. Consequently it is possible to devise an experimental programme which will provide a large amount of information on cell action in an expeditious manner.

(i) *The Cells*

At the start of the experimental work it was decided to construct a basic cell which would be simple in construction and operation, rugged, and have a constant sensitive area on the cell face. By varying the thickness of this cell the effect of thickness-diameter ratio on cell action could be investigated. A second type of cell was constructed which had the same diameter and thickness as the basic cell but whose sensitive area of face could be varied so that the effect of the ratio of sensitive area to total facial area on cell action could also be investigated.

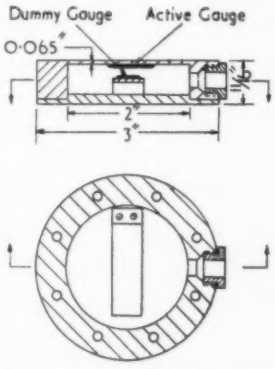

Fig. 5. Standard Earth Pressure cell.

The basic or standard cell used in the work is shown in Figs. 5 and 6. It consists of a cylindrical brass body 3 inches in diameter which is bored out to form a thin diaphragm 0·065 inches thick and 2 inches in diameter and the chamber so formed is closed by a back plate $\frac{1}{8}$ in. thick. The diametral tensile strain at the centre of the diaphragm is measured by an electrical resistance strain gauge, and temperature compensation for the strain gauge is obtained from a similar gauge mounted on a brass bracket attached to the back plate of the cell. A P.V.C. covered three-cored cable leaves the cell via a gland nut and makes connection with the recording apparatus. The thickness of the cell is altered by attaching additional brass plates to the backing plate.

An improved model of this type of cell is shown in Fig. 7. The thickness of this cell has been reduced to $\frac{3}{8}$ in. by dispensing with the bracket used for carrying the compensating strain gauge, and mounting this gauge radially at the edge of the diaphragm where it is subjected to compressive strains. This method of construction has the incidental advantage of approximately doubling the sensitivity of the cell.

The variation in sensitive area of a cell face is not so easy to obtain. It was achieved by constructing cells of the type shown in Fig. 8. These cells have added to the sensitive face an additional plate which has a groove turned in it so that the additional piece acts as a piston

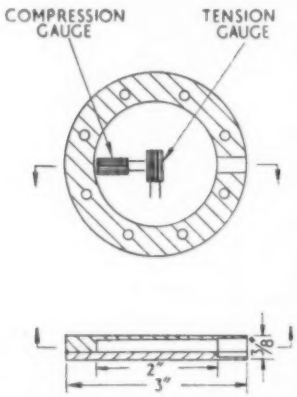

Fig. 7. Improved Earth Pressure cell.

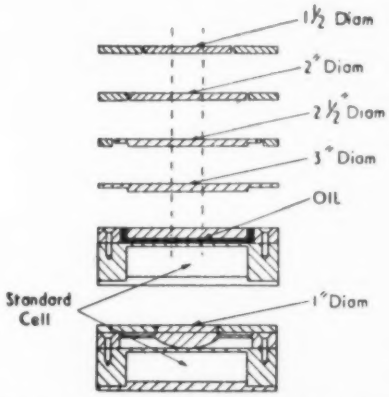

Fig. 8. Cell with variable sensitive areas.

attached to a rim by a thin flexible web. The space between the piston and the original cell face is filled with oil so that the piston load is transmitted to the sensitive face of the cell. Additional brass plates of various diameters can be attached to the piston and where necessary extra rims can be fixed to the rim of the cell, thus varying the ratio of the sensitive area of the cell to its total facial area. This type of cell is satisfactory for its purpose but it possesses the disadvantage that as the area of the piston extension is reduced so also is the overall sensitivity of

Vol.
2
53/54

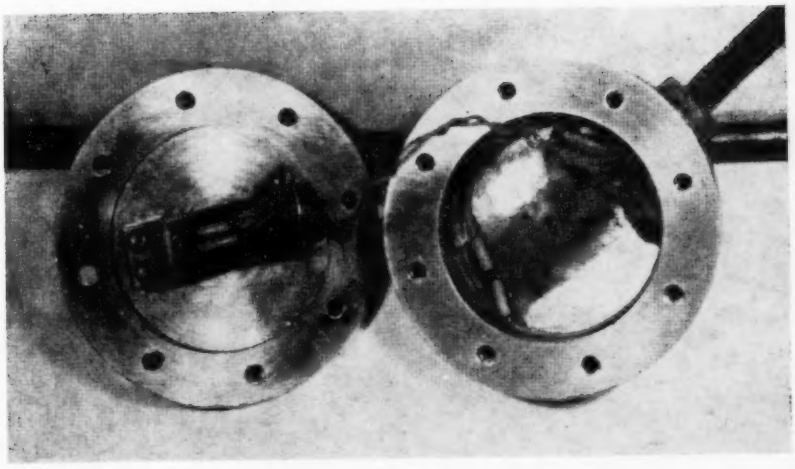

Fig. 6. Standard Earth Pressure cell.

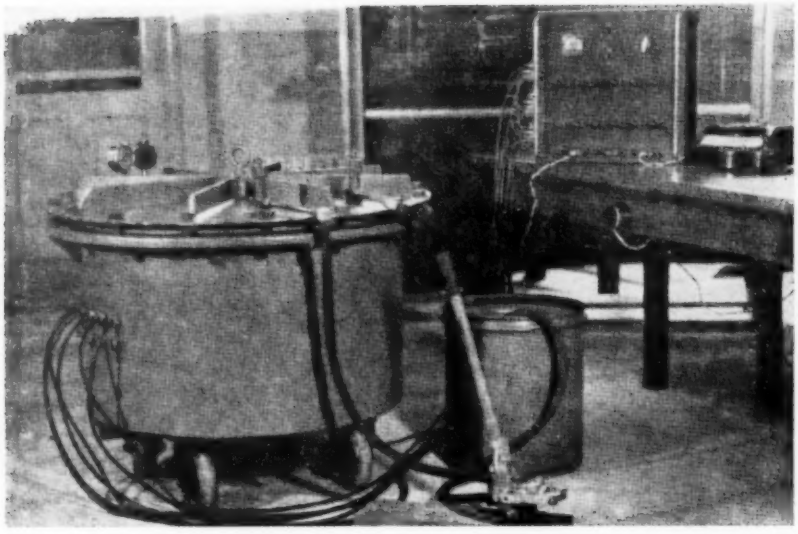

Fig. 10. General view of apparatus.

Vo
2
1953

the cell. For this reason when a sensitive area having a diameter of 1 in. is required a different form of construction is used so that the piston load in this case is applied approximately as a point load to the centre of the diaphragm of the sensitive part of the cell.

Each cell, irrespective of type, was calibrated by fluid pressure. Over the working range the calibrations were found to be linear and stable.

In order to investigate the effect of modular ratio E_g/E_s on cell action, cells of different compressibilities had to be constructed. Composite back plates of brass and rubber are fitted to the back of the standard cell in place of the different brass plates used to vary the cell thickness. The compressibility is controlled by the thickness of rubber used and in all cases the total thickness of rubber plus brass is kept constant.

The measuring equipment is basically a multi-channel Wheatstone bridge in which two of the arms are composed of the two strain gauges in the cell and the other two arms in each channel consist of similar strain gauges mounted on opposite sides of cantilever beams. Initially, balance is obtained in each channel by applying a deflection to the cantilever, subsequent changes in the balance caused by the application of pressure to the cell are recorded by galvanometer.

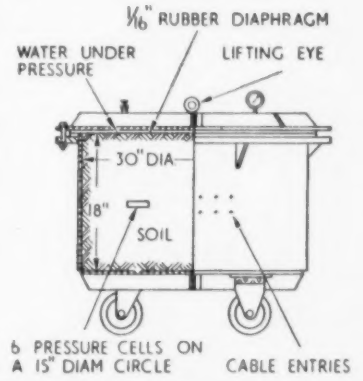

Fig. 9. Diagram of pressure chamber.

(ii) *The Pressure Chamber*

The pressure chamber in which the cells and soils were tested is shown in Figs. 9 and 10. The top cover plate could be removed without breaking the seal between the diaphragm and the top cover plate.

Difficulty was encountered in determining the field pressure at the plane of the cell since this was less than the applied hydraulic pressure at the surface due to frictional effects on the sides of the chamber. These effects could not be satisfactorily eliminated in the chamber and the following method was employed. From equation (3),

$$\frac{p_c}{p} = C_A \cdot \frac{B}{D} + 1$$

where $p_c = p + p_e$ is the recorded cell pressure. Then, if p_0 is the pressure applied at the surface of the soil,

$$\frac{p_c}{p_0} = \left(C_A \cdot \frac{B}{D} + 1\right)\frac{p}{p_0}. \tag{4}$$

If it is assumed that p is directly proportional to p_0, equation (4) is a straight line, and since p_c/p_0 is known for various values of B/D, the curve may be drawn. The intercept of this curve is a measure of the amount of friction taking place and, by dividing the slope of the line by this intercept, C_A may be found.

In practice it was found that p_c/p_0 varied with the applied pressure, indicating either a variation in C_A with pressure or that p is not proportional to p_0, or a combination of both. By plotting p_c/p_0 against B/D for various applied pressures, it was found that a series of straight lines resulted with various slopes and intercepts. In order to find if C_A varied with pressure, it was necessary to plot a number of curves. Considerable effort may be saved by substituting p_{c_1}, the reading of the thinnest cell, for p_0 in equation (4); this eliminates any variations introduced in assuming p to be proportional to p_0, and any variation in C_A with pressure may be detected at once as a variation in p_c/p_{c_1} with pressure. Hence, if p_c/p_{c_1} is independent of pressure, an average value may be taken and only one plot is necessary to determine C_A.

This method proved very satisfactory and the actual field pressure existing at the plane of the cell may be found. Equation (4) becomes

$$\frac{p_c}{p_{c_1}} = \left(C_A \cdot \frac{B}{D} + 1\right)\frac{p}{p_{c_1}}. \tag{5}$$

p_c/p_{c_1} is plotted against B/D. The slope of this plot divided by the intercept is C_A and the intercept is p/p_{c_1}, hence the field pressure p is Intercept $\times p_{c_1}$.

(iii) *Experimental technique*

For the first part of the procedure six standard cells were used with back plate additions giving half thickness to diameter ratios of 0·062, 0·135, 0·219, 0·302, 0·386 and 0·470. For the second part five standard cells with modifications giving sensitive areas of 1, 1½, 2, 2½ and 3 inches in diameter were used, with one standard cell to read lateral pressures. In all cases the cells were placed on the mid-plane of the tank on a circle of 15 inches diameter.

The procedure was to fill the tank to the half-way mark and strike it off level, and then place the cells in position with their sensitive faces upward using a strickle and marks on the lip of the tank to position the cells in the correct place and at the correct radial distance. With cells of various thicknesses it was arranged that the mid-plane of the cell coincided with the mid-plane of the tank. The cells with the various sensitive areas were placed on the levelled surface of the soil and the lateral cell was placed with a diameter on the mid-plane of the tank.

In all cases after the cells had been placed in position, they were levelled with a small spirit level, their positions finally checked and the tank was filled to the top, the excess soil was struck off and the lid placed in position.

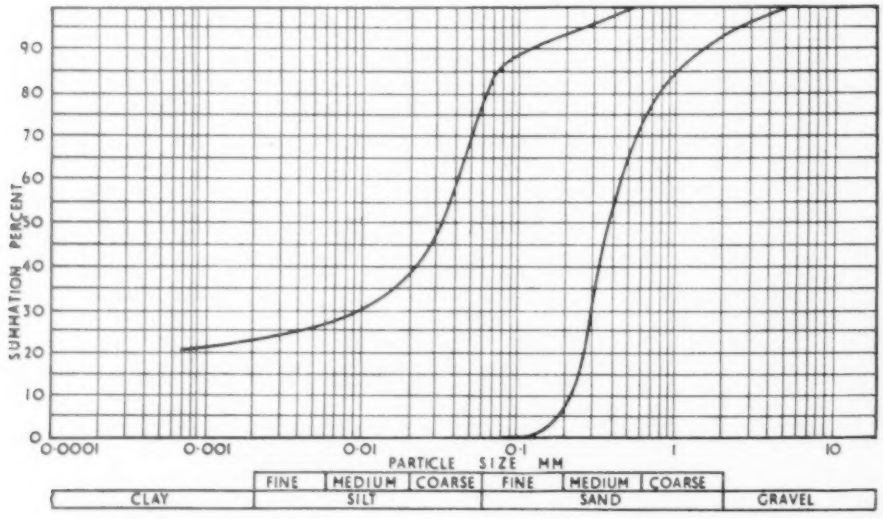

Fig. 11. Particle size distributions of soils used.

The cells were connected to the bridge and were allowed to warm up whilst the lid was bolted down and the pump connected to the tank ; the bridge channels were then balanced and when it had been ascertained that the cell readings were steady, pressure was applied to the tank in 10 p.s.i. intervals up to a maximum of 60 p.s.i., the cell readings being taken at each interval, the pressure was released in the same intervals, cell readings being taken again. The loading cycle was repeated, and the pressure released. Each test was repeated three or four times completely, the tank being unloaded and the cells removed each time.

Before the above installation technique was standardized, the effect of the mode of installation on the pressures recorded was investigated. Six cells were placed at the mid-depth of the pressure chamber at the same radial distance from the centre. Two of the cells were placed on the levelled surface of the soil, two were forced into the soil until they were half buried and the remaining two cells were forced into the soil till their top surfaces were flush with the soil surface. The chamber was then filled and the pressure applied and it was found that the first two pairs of

cells agreed closely while the third pair recorded pressures which were about 15 per cent higher than the other pairs.

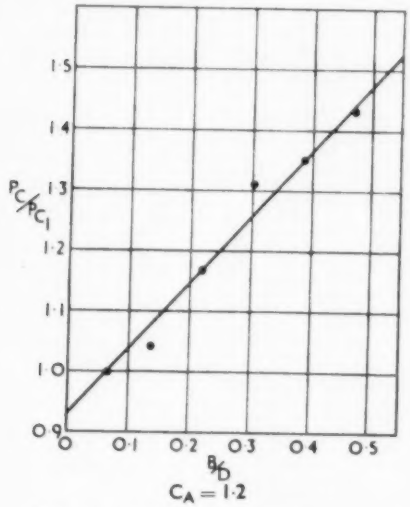

Fig. 12. Variation with B/D. Loose moist sand.

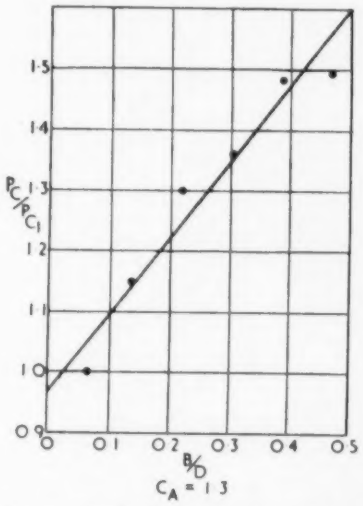

Fig. 13. Variation with B/D. Dense moist sand.

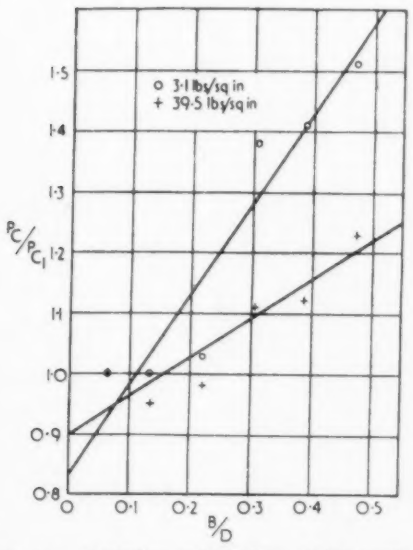

Fig. 14. Variation with B/D. Brick earth at 13·5 per cent moisture content.

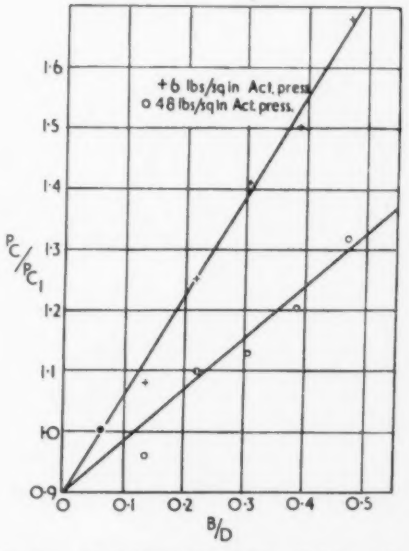

Fig. 15. Variation with B/D. Brick earth at 16 per cent moisture content.

4. Results of Experimental Investigation

(i) *Variation of cell errors with B/D*

Tests were carried out on two different soils each in different conditions and their grading curves are shown in Fig. 11.

Loose sand : water content 1·7 per cent, dry density 101 lb./cu.ft.
Dense sand : water content 1·6 per cent, dry density 104 lb./cu.ft.
Harmondsworth Brick Earth : Liquid Limit $L_L = 31$ per cent, Plastic Limit $P_L = 18$ per cent, tested at water contents of 13·5 per cent, 16 per cent and 18 per cent and corresponding densities of 117 lb./cu.ft., 110 lb./cu.ft. and 111 lb./cu.ft.

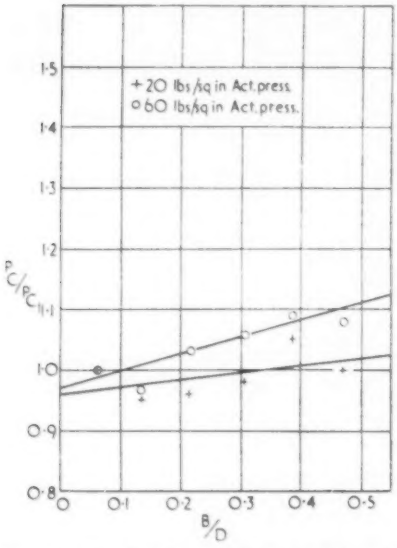

Fig. 16. Variation with B/D. Brick earth at 18 per cent moisture content.

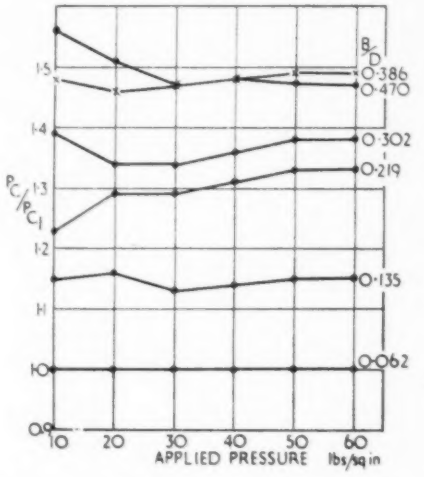

Fig. 17. Variation with applied pressure. Dense moist sand.

The results for the sands are shown in Figs. 12 and 13 and those for the brick earth in Figs. 14, 15 and 16. These results indicate that, as predicted, the cell error is directly proportional to the value of B/D. The graphs have different slopes, which indicates that the value of C_A is not constant.

The second series of tests was designed to investigate the factors that might affect the value of C_A. The factors considered were :

The value of the applied load pressure p_0.
The ratio of the sensitive area of the cell to its total area.
The value of the modular ratio E_g/E_s.
The effect of the time for which the load was allowed to act.

(ii) *The effect of pressure*

(a) *Sands.* The values of p_c/p_{c_1} are plotted against the applied pressure p_0 in Fig. 17. The different lines correspond to different values of B/D and in all cases the sensitive area of the cell was constant. The results show a fair scatter, but there is no definite trend of p_c/p_{c_1} with pressure. Similar results were obtained with the loose sand.

Hence, for cells with the sensitive areas used in these tests in sands, C_A may be considered independent of pressure. Subsequent tests with different sensitive

areas show that for the loose sand C_A is independent of pressure for all the areas tested. However, with the dense sand, it was found that when the sensitive area exceeded 1½ inches in diameter there was a variation of C_A with pressure.

(b) *Brick Earth.* It is obvious from Figs. 14, 15 and 16 that p_c/p_{c_1} is varying with the value of the applied pressure. The value of C_A was calculated for each value of pressure at the plane of the cell and the results for three values of water content are shown in Fig. 18.

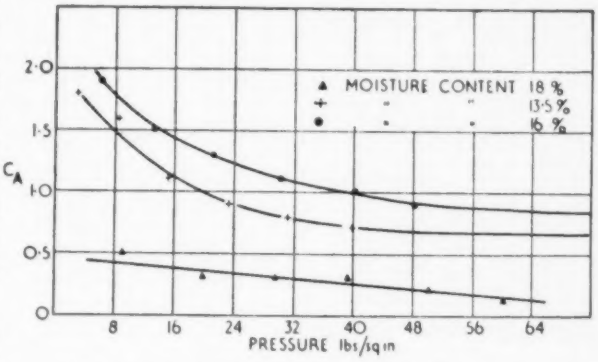

Fig. 18. Effect of pressure on C_A. Brick earth.

The value of C_A is seen to be relatively independent of pressure when the soil is at a water content of 18 per cent; the maximum dependence on pressure occurs when the water content is 16 per cent, which is the Optimum Water Content for this soil.

When different sensitive areas are taken into account it is found that at a water content of 18 per cent C_A is relatively independent of pressure at all the sensitive areas tested. As the water content decreases, C_A becomes more dependent on pressure for different sensitive areas. It is also found that as the pressure is increased the dependence of C_A on it decreases. This trend is also shown in Fig. 18.

(iii) *The effect of the ratio of sensitive area to total area of the cell*

The pressure distribution over the face of the cell for sands is shown in Fig. 19. The curve marked "Theory" was computed on the basis of MONFORE's analysis for the value of B/D employed in the tests.

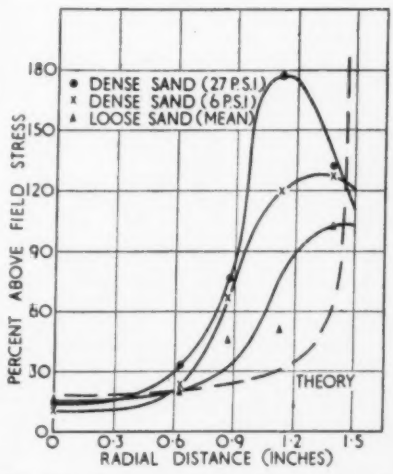

Fig. 19. Pressure distribution over cell face. Sand.

The results for the tests on brick-earth at water contents of 18 per cent and 16 per cent are shown in Figs. 20 and 21 respectively. The results for the test at 13·5 per cent water content were of a similar shape to those for the test at 16 per cent but showed an even greater deviation from the theoretical value.

The general trend of these results is that high pressures are developed towards the edges of the cell face and to minimize cell errors the cell should not be sensitive to the edges. For the 3 in. diameter cells used in these tests it is considered that the optimum sensitive diameter is 1½ in., and the so-called "standard cell"

Vol. 2 53/54

behaves as if its sensitive diameter was about this value.

The question of sensitive areas is of primary importance in the design of earth pressure cells since the selection of unsuitable sensitive areas will make the cell

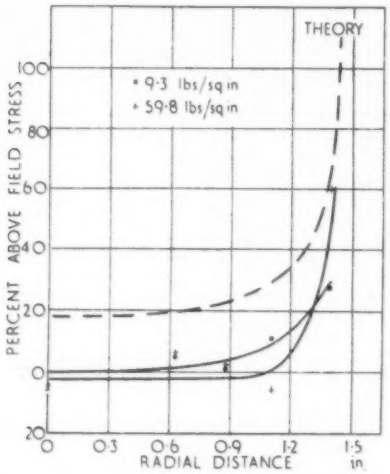

Fig. 20. Pressure distribution over cell face. Brick earth. 18 per cent moisture content.

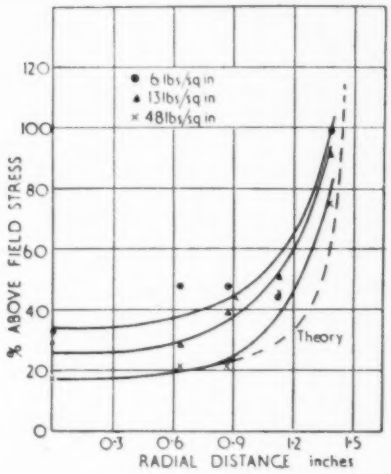

Fig. 21. Pressure distribution over cell face. Brick earth. 16 per cent moisture content.

sensitive to the high edge pressures, with consequently large cell errors. If considerably larger cells were employed it is not known whether the region of high pressures would be restricted to a small distance in from the circumference of the cell, in which case the ratio of sensitive area to total area would be of minor importance, or whether the region would extend in for a proportionally greater distance. It has not been possible to investigate this effect because the pressure chamber available will not accommodate cells of a greater diameter than 3 in. without danger of the pressure bulbs due to the cells interfering with the top and bottom surfaces of the chamber. There are considerable practical difficulties in constructing and working with cells smaller than 3 in. in diameter.

(iv) *The value of the modular ratio* E_g/E_s

As described earlier, cells of different compressibility were tested in loose moist sand. Values for E_s for the sand over the range of pressures used in the tests were obtained from tests in a " shear-cell " apparatus. The sensitive areas and thickness-diameter ratios of all the compressible cells were the same.

The results are shown in Fig. 22. The theoretical curve is computed from MONFORE's type of analysis for the given B/D and sensitive area values. The cell error is independent of E_g/E_s when the value of this ratio exceeds 9 or 10. It should be noted that the cells whose results are shown in Fig. 22 are all considerably more compressible than the cells used in all the other tests described in this paper.

It is preferable to construct cells which give a value of E_g/E_s in excess of 10 because, although the error is then a maximum, it is independent of the value of

the ratio and variations in E_s will not affect the value of the error obtained. As stated at the beginning it is seen that, if an attempt is made to construct a cell so that E_g/E_s is unity, the error will be a minimum but its value will be greatly affected by small variations in E_s and it would not be possible to predict the error with any accuracy.

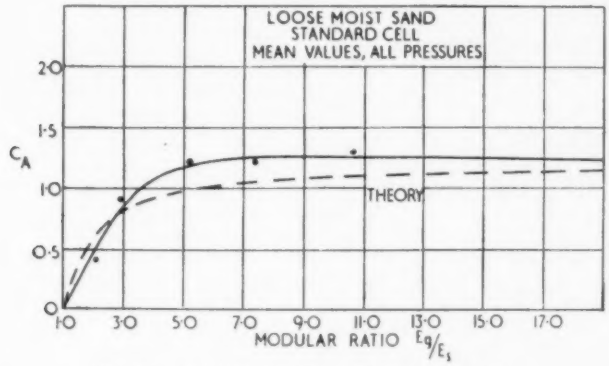

Fig. 22. Variation of C_A with modular ratio.

Vol. 2 53/54

(v) *The effect of the time for which the load was allowed to act*

The readings of all cells when embedded in sand were independent of the time for which the load was allowed to act. Cells embedded in the brick earth at 18·5 per cent water content were also independent of time effects.

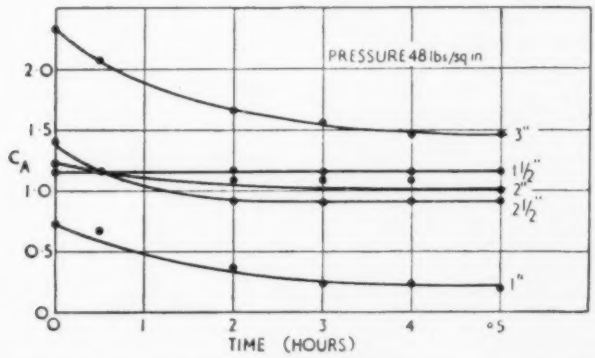

Fig. 23. Effect of time for which load acts, on C_A. Brick earth. 16 per cent moisture content.

When the brick earth was tested at 16 per cent water content C_A was found to vary with time in the manner shown in Fig. 23. It is seen that for sensitive areas of 1½ in. and 2 in. diameter C_A is independent of time. Tests were not carried out on the brick earth at 18 per cent water content since in any case the magnitude of the cell errors for this condition is very small.

(vi) *Magnitude and Variation of Errors*

To give an idea of the magnitude of the errors involved in this type of work and the factors affecting them, Fig. 24 has been drawn. This shows the cell error for different soils and different conditions of these soils. The two curves relate to 3 in. diameter cells, one of which is fully sensitive and the other is sensitive over an area whose approximate diameter is $1\frac{1}{2}$ in. Both cells have a B/D of 0·062.

It is seen that for the "standard" cell the error is about 8 per cent, the limits being 11 per cent and 2 per cent. The dotted line is a plot of the error involved in an assumption of a constant value of C_A of 1·2 and the deviations from this line are about $\pm$ 3 per cent. The only large deviations from these figures are for the clay at 18 per cent water content and in that case the errors themselves are very small.

For the fully sensitive cell the magnitude of the errors is much greater and the dependence on soil type and condition is much more pronounced. Errors of up to 50 per cent are possible.

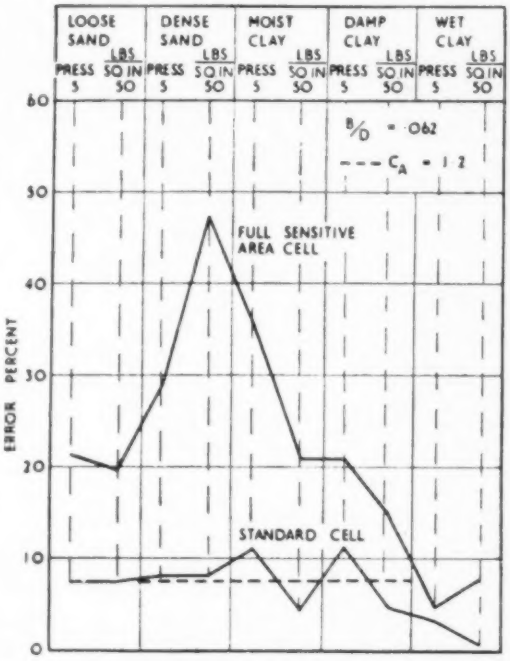

Fig. 24. Effect of soil type and condition on cell errors.

5. General Conclusions and Design Criteria

No design for a cell will eliminate errors completely, except in the unlikely case where the cell modulus exactly matches that of the soil and the latter remains constant. However, the errors can be reduced to small and predictable proportions by fulfilling the following criteria :

(*a*) The error has been shown to be directly proportional to the thickness-diameter ratio of the cell, and hence this should be kept as small as possible.

(*b*) The error is dependent on the ratio of the sensitive area of the cell face to the total facial area. For cells of diameters up to 4 inches the following proposals are made. If the cell design is such that the pressure is averaged over the responsive area the ratio of sensitive area to total facial area should be less than about 0·25. If the cell has a pressure responsive diaphragm such as the "standard" cell this ratio should be less than about 0·45.

(*c*) Errors caused by the modular ratio E_g/E_s are not very large and it is variations in the value of the ratio which are more liable to be trouble-

some. The cell should be as incompressible as possible with a modular ratio in excess of about 10. Most cell designs would appear to be incompressible when compared with the compressibility of soils.

If these criteria are fulfilled, the general equation for cell action becomes

$$\frac{p_e}{p} = 1{\cdot}2\,\frac{B}{D}, \tag{6}$$

and so the correction for cell action can be incorporated into the calibration curve for the cell.

Provided the above criteria have been fulfilled the variations in the errors produced by changes in field pressure are unlikely to be important. It seems most probable that when cells are used in cohesive soils which are at water contents above their plastic limits the cell errors will be so small that they can be entirely neglected. The criterion stated in Section 5 (b) should not be extended to cover cells larger than 4 inches in diameter without further experimental work having been carried out. However, it is considered that cells of this size are very suitable for most classes of work. The results on which these conclusions are based were obtained for static loads but very probably they are valid for use where the soils are under dynamic loading, since under these conditions most soils approximate more closely to an elastic solid.

Vol. 2 53/54

Acknowledgments

The work described in this paper has been carried out in the Laboratories of the Civil and Mechanical Engineering Department of the University of Nottingham. The Authors would like to thank the Authorities of the University for permission to publish the results and Professor J. A. Pope, Head of the Department, for providing the laboratory and workshop facilities.

The junior Author would like to acknowledge the receipt of a D.S.I.R. Maintenance Allowance for the duration of the work.

References

Benkelman, A. C. and Lancaster, R. J. 1941 *Proc. Highway Res. Board*, **20**, 299.

Kögler, F. and Scheidig, A. 1927 *Die Bautechnik*, **31**, July 15.

Monfore, G. E. 1950 U.S. Dept. of Interior, Bureau of Reclam. (Res. and Geol. Div.) Struct., Res. Lab. Report No. S.P. 26.

Taylor, D. W. 1947 *Pressure distribution theories, earth pressure cell investigations and pressure distribution data*, U.S. Waterways Exp. Station, Vicksburg, Miss.

U.S. Waterways Experiment Station 1944 Soil Pressure Cell Investigation.

Journal of the Mechanics and Physics of Solids, 1954, Vol. 2, pp. 156 to 169. Pergamon Press Ltd., London.

A THEORETICAL INVESTIGATION OF THE YIELD POINT LOADING OF A SQUARE PLATE WITH A CENTRAL CIRCULAR HOLE

By F. A. GAYDON* and A. W. MCCRUM†

(*Received* 21*st December*, 1953)

SUMMARY

THE mathematical theory of plasticity is applied to the problem of a thin square plate, with a central circular hole, yielding under loads applied at its outside edges. Upper and lower bounds to the external loads at the yield point are determined for all values of the ratio between the diameter of the hole and the length of the side of the plate.

Vol 2 1953

1. INTRODUCTION

THE purpose of this paper is to determine the yield point loading of a thin square plate with a central circular hole. HODGE (1952) and GAYDON (1954) have examined this problem using the Tresca yield criterion and potential function. In this paper the Mises yield criterion and potential are employed.

The plate $ABB'A'$ has sides of length 2 and a circular hole of radius a ($0 \leqslant a \leqslant 1$) in its centre. Uniform normal stresses are applied along the outside edges in the plane of the plate, and the edge of the hole is unstressed. The problem is therefore one of plane stress, with all stress and strain components assumed constant through the thickness of the plate. The plate is assumed to be constrained to prevent its buckling out of plane when the external loads are compressive.

The material of the plate is assumed to be plastic rigid. Experiment shows (HILL and SIEBEL 1953) that, provided the plastic region is not unduly constrained, the loads on a real body attain values within a few per cent of the corresponding plastic-rigid yield-point loads whilst the overall deformation is still of an elastic order of magnitude.

The ratio λ of the stresses on the sides AB and BB' is kept constant as they are increased to their respective yield point values S and λS. Three loading states are examined in detail : equal biaxial stressing ($\lambda = 1$) ; uniaxial stressing ($\lambda = 0$) ; and equal, opposite biaxial stressing ($\lambda = -1$). The yield-point loads are either evaluated exactly, or upper and lower bounds are obtained by means of the extremum principles for a plastic-rigid body. From these solutions upper and lower bounds to the yield-point loads are obtained for a general loading state.

* Department of Theoretical Mechanics, University of Bristol.
† British Iron and Steel Research Association, Sheffield.

2. The Mises Yield Criterion and Potential Function

In plane stress the Mises yield criterion is

$$\sigma_1^2 - \sigma_1 \sigma_2 + \sigma_2^2 = Y^2, \tag{1}$$

where σ_1 and σ_2 are principal stresses in the plane and Y is the yield stress in uniaxial tension.

In the plastic region the characteristics of the differential equations of stress are two families of curves inclined at angles $\pm(\frac{1}{4}\pi + \frac{1}{2}\psi)$ to the direction of the algebraically greater principal stress (Hill 1950) where

$$\sin\psi = \frac{\sigma_1 + \sigma_2}{3(\sigma_1 - \sigma_2)} \qquad (\sigma_1 \geqslant \sigma_2).$$

Hence the characteristics are real if, and only if,

$$|\sigma_1 + \sigma_2| \leqslant 3|\sigma_1 - \sigma_2|.$$

The relation between stress and strain-rate for a material with a Mises plastic potential function is

$$\frac{\dot{\epsilon}_1}{\dot{\epsilon}_2} = \frac{2\sigma_1 - \sigma_2}{2\sigma_2 - \sigma_1}, \tag{2}$$

where $\dot{\epsilon}_1$ and $\dot{\epsilon}_2$ are the principal components of strain-rate in the directions of σ_1 and σ_2 respectively.

The directions of zero strain-rate (velocity characteristics) coincide with the characteristics of stress (Hill 1950). If local necking occurs the neck coincides with a velocity characteristic (Hill 1952), since at least one side of the neck must be rigid.

3. Extremum Principles

It has been shown by Hill (1950 and 1951) and by Drucker, Greenberg and Prager (1951) that any equilibrium stress distribution satisfying the given stress boundary conditions and nowhere violating the yield criterion will correspond to external boundary loads which are less than or equal to the actual yield point loads. Similarly they have shown that the internal rate of plastic working W_I calculated from any mode of deformation compatible with the velocity boundary conditions, is greater than the rate of plastic working W_E of the actual boundary stresses in the same mode. Any postulated deformation mode therefore leads to an upper bound to the yield point boundary loads.

In particular, the internal rate of working in a local neck is

$$\int \frac{Y}{\sqrt{3}} v \sqrt{(1 + 3\sin^2\psi)}\, ds$$

per unit thickness, where v, the velocity of one side of the neck relative to the other, is inclined at an angle ψ to the neck and the integral is evaluated along the neck (Hill 1952).

4. Equal Biaxial Stressing

(a) *Lower bound.* A lower bound applicable to all values of the radius of the hole a, is given by the stress distribution of Fig. 1. In the annulus between the

hole and the circle touching the sides the stress state is axially symmetric, and the plate is plastic. The radial and circumferential stress components at a radius r in this region are given parametrically by the equations

$$\sigma_r = \frac{2}{\sqrt{3}} Y \sin\left(\gamma - \frac{\pi}{6}\right); \qquad \sigma_\theta = \frac{2}{\sqrt{3}} Y \sin\left(\gamma + \frac{\pi}{6}\right); \qquad \left(\frac{\pi}{6} \leqslant \gamma\right)$$

where

$$\frac{r^2}{a^2} = \frac{\sqrt{3}}{2} \sec\gamma \exp\left\{\sqrt{3}\left(\gamma - \frac{\pi}{6}\right)\right\}.$$

Across the circle the normal stress is continuous but the tangential stress is discontinuous. The remainder of the plate is uniformly stressed below the yield point in equal biaxial stressing. Hence in these regions

$$\sigma_1 = \sigma_2 = \frac{2}{\sqrt{3}} Y \sin\left(\alpha - \frac{\pi}{6}\right),$$

where

$$\frac{1}{a^2} = \frac{\sqrt{3}}{2} \sec\alpha \exp\left\{\sqrt{3}\left(\alpha - \frac{\pi}{6}\right)\right\}.$$

By the extremum principle, therefore,

$$\frac{S}{Y} \geqslant \frac{2}{\sqrt{3}} \sin\left(\alpha - \frac{\pi}{6}\right). \tag{8}$$

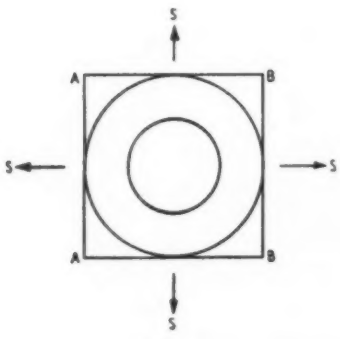

Fig. 1.

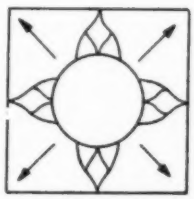

Fig. 2.

(b) *Upper bounds.* If $\alpha \leqslant \frac{1}{2}\pi$ (i.e. $0{\cdot}483 \leqslant a \leqslant 1$) the characteristics of stress and velocity exist over the whole of the plastic annulus, and the characteristic field of Fig. 2 gives an upper bound to the yield point loading. This coincides with the lower bound previously determined since, in the deforming region, the associated stress distribution is identical with that of the lower bound. Hence it is the exact solution .

Over the remainder of the range of values of a, three deformation modes are used to derive upper bounds. In the first of these (Fig. 3) deformation occurs only in the necks, and ψ and v are constant along them. Hence, with the notation of the Figure,

$$W_I = \frac{8}{\sqrt{3}} Yv (1 + 3 \sin^2 \psi)^{\frac{1}{2}} (1 - a \cos \theta) \operatorname{cosec} \beta ;$$

whilst

$$W_E = 8Sv \{\sin \psi + a \sin (\beta - \psi) \cos (\beta + \theta)\} \operatorname{cosec} \beta.$$

Thus

$$\frac{S}{Y} \leqslant \frac{(1 + 3 \sin^2 \psi)^{\frac{1}{2}} (1 - a \cos \theta)}{\{\sin \psi + a \sin (\beta - \psi) \cos (\beta + \theta)\} \sqrt{3}}.$$

All possible configurations are included if $0 \leqslant \theta \leqslant \frac{\pi}{2}$, $\beta \leqslant \pi - \theta$, and

$$\frac{1 - a \sin \theta}{1 - a \cos \theta} \geqslant \cot \beta \geqslant \frac{-1 - a \sin \theta}{1 - a \cos \theta}.$$

Within these limits θ, β, and ψ can be chosen arbitrarily. By differentiation with respect to θ, β, and ψ in turn it is found that the least upper bound occurs when

$$\theta = \tfrac{1}{2}\pi + \psi - 2\beta, \qquad \sin \psi = \frac{1}{3a}, \qquad \text{and} \qquad \tan \beta = 4 \tan \psi.$$

Vol. 2 53/54

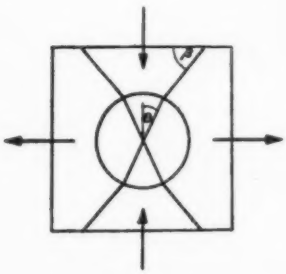

Fig. 3.

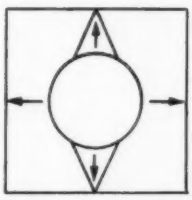

Fig. 4.

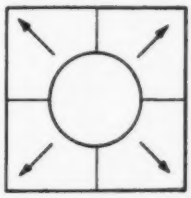

Fig. 5.

Putting this set of values in the inequality for S above, we obtain

$$\frac{S}{Y} \leqslant \frac{(1 - a^2)}{\sqrt{(1 + 3a^2)}}. \tag{4}$$

This is an upper bound for all values of λ, since the necks meet at the edge of the plate (Fig. 4) and thus the stress λS does no work.

For ψ to be real it is necessary that $a \geqslant 0{\cdot}33$; otherwise the best configuration is that with $\psi = \beta = \frac{1}{2}\pi$, $\theta = 0$ (Fig. 5), and

$$\frac{S}{Y} \leqslant \frac{2}{\sqrt{3}} (1 - a). \tag{5}$$

For $a \leqslant 0{\cdot}15$ a better upper bound is provided by the uniform deformation of the plate. The internal rate of working per unit thickness is

$$W_I = 2YU (4 - \pi a^2),$$

where U is the normal velocity of each edge.

Since $W_E = 8SU$, we have

$$\frac{S}{Y} \leqslant \left(1 - \frac{\pi a^2}{4}\right). \tag{6}$$

The upper and lower bounds are shown in Fig. 6. The difference between the bounds is less than 5 per cent for all values of a.

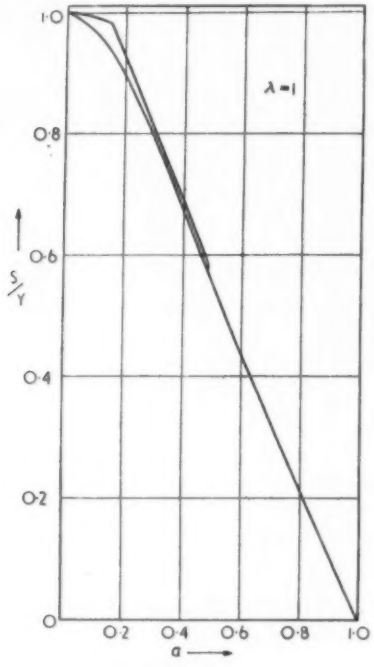

Fig. 6.

5. UNIAXIAL STRESSING

(a) *Lower bounds.* Two lower bounds have been derived for this loading state. The first, which is the greater in the range $0 \leqslant a \leqslant 0{\cdot}434$ is obtained from the stress distribution of Fig. 7. A similar configuration was used by HODGE (1952) in his examination of this problem with the Tresca yield criterion. The stress state is uniform within each region and there are

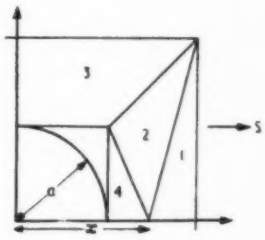

Fig. 7.

discontinuities in the tangential stress across the regional boundaries. The principal components of stress (σ_1, σ_2) in each region are

(1) $\sigma_1 = S$, $\qquad \sigma_2 = \dfrac{Sa}{(1-a)(1-x)}$;

(2) $\sigma_1 = \dfrac{S\{x - 2a + \sqrt{(x^2 + 4a^2)}\}}{2x(1-a)}$, $\qquad \sigma_2 = \dfrac{S\{x - 2a - \sqrt{(x^2 + 4a^2)}\}}{2x(1-a)}$;

(3) $\sigma_1 = \dfrac{S}{(1-a)}$, $\qquad \sigma_2 = 0$;

(4) $\sigma_1 = 0$, $\qquad \sigma_2 = \dfrac{-Sa}{(1-a)(x-a)}$.

Substitution in the yield criterion (equation (1)) gives four inequalities which S must satisfy :

$$S \leqslant \frac{Y(1-a)(1-x)}{\sqrt{\{(1-x)^2(1-a)^2 - a(1-a)(1-x) + a^2\}}} \quad \ldots \quad (I_1)$$

$$S \leqslant \frac{Y(1-a)x}{\sqrt{(x^2 - ax + 4a^2)}} \quad \ldots \ldots \ldots \ldots \ldots \quad (I_2)$$

$$S \leqslant Y(1-a) \quad \ldots \ldots \ldots \ldots \ldots \quad (I_3)$$

$$S \leqslant \frac{Y(1-a)(x-a)}{a} \quad \ldots \ldots \ldots \ldots \ldots \quad (I_4)$$

The value of x in the inequalities can be chosen arbitrarily in the interval $a \leqslant x \leqslant 1$. It is required to choose x such that the inequalities admit the largest possible value of S. The righthand sides of the four inequalities can be plotted as functions of x for fixed a, and the largest admissible value of S is then the maximum ordinate of the area below all four curves. It is found that for $0 \leqslant a \leqslant 0{\cdot}204$ the highest value of s admitted by the four inequalities is

$$S = Y(1-a). \tag{7}$$

For $0{\cdot}204 \leqslant a \leqslant 0{\cdot}412$ the highest value of S is the join of I_1 and I_2, which can be accurately and rapidly determined by interpolation. For $a \geqslant 0{\cdot}412$ the highest value of S is the join of I_1 and I_4 and is again obtainable by interpolation.

In the range $0{\cdot}434 \leqslant a \leqslant 1$ a greater lower bound is obtained from the two lower bounds derived in Sections 4 and 6. It follows from the maximum plastic work principle for a finite body that the yield locus of a plastic rigid body must be concave to the origin (Fig. 8). Hence, if two points on the locus are known, either exactly or as lower bounds, then any point lying between the two and on the line joining them, is a lower bound to the yield locus.

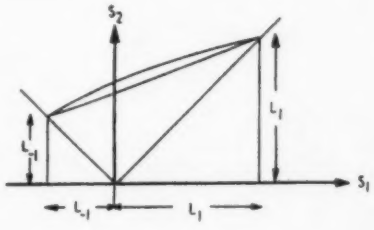

Fig. 8.

From the geometry of the Figure we have

$$S \geqslant \frac{2L_1 L_{-1}}{(L_1 + L_{-1})}, \tag{8}$$

where L_λ is the solution (or lower bound) for the yield point stresses in the loading state $(S, \lambda S)$ $(\lambda = \pm 1)$.

(b) *Upper bounds.* For $a < 0{\cdot}42$ an upper bound to the yield point stresses is derived from the velocity field of Fig. 9. A pair of straight necks run from the unstressed edge of the plate and meet on the edge of the hole. The remainder of the plate remains rigid, and hence

$$W_I = \frac{4}{\sqrt{3}} Yv(1 + 3\sin^2\psi)^{\frac{1}{2}}(1-a)\operatorname{cosec}\beta,$$

whilst

$$W_E = 4Sv\cos(\beta - \psi).$$

Hence

$$\frac{S}{Y} \leqslant \frac{(1 + 3\sin^2\psi)^{\frac{1}{2}}(1-a)\operatorname{cosec}\beta}{\sqrt{3}\cos(\beta - \psi)}.$$

This bound has a minimum value when $\psi = \sin^{-1}(\frac{1}{3})$, $\beta = \frac{1}{4}\pi + \frac{1}{2}\psi$, and

$$\frac{S}{Y} \leqslant (1 - a). \tag{9}$$

This is the exact solution in the range $0 \leqslant a \leqslant 0{\cdot}2044$ since the upper and lower bounds coincide.

The second upper bound is derived from the hypothetical deformation mode in which the four quarters of the plate rotate with angular velocity ω about points whose co-ordinates are $(\pm c, \pm d)$ relative to cartesian axes through the centre

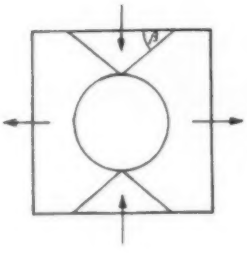

Fig. 9.

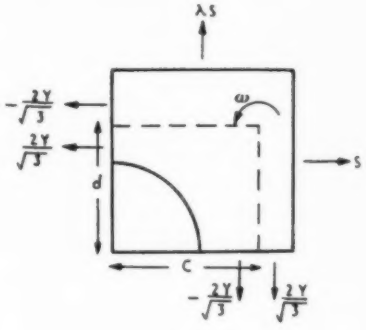

Fig. 10.

of the plate and parallel to its sides, with local necking or bulging along the axes. Thus there is a normal discontinuity of velocity whose magnitude is $2\omega(x - c)$ and $2\omega(y - d)$, at the points $(x, 0)$ and $(0, y)$. The remainder of the plate is rigid. The associated stress normal to the axis is $\pm 2Y/\sqrt{3}$ at each point in the deforming region (Fig. 10) and

$$W_I = \frac{2}{\sqrt{3}} Y\omega \{a^2 + c^2 + d^2 + 1 - (a + 1)(c + d)\}.$$

Further,

$$W_E = S\omega \{(d - \lambda c) - \tfrac{1}{2}(1 - \lambda)\}.$$

Hence

$$\frac{S}{Y} \leqslant \frac{2\{a^2 + c^2 + d^2 + 1 - (a + 1)(c + d)\}}{\sqrt{3}\{(d - \lambda c) - \frac{1}{2}(1 - \lambda)\}} = \frac{S^*}{Y} \text{(say)}.$$

By differentiating S^* with respect to c and d in turn it is found that its minimum value occurs when associated stresses along the boundary of the deforming region are in equilibrium with the stresses S^*, λS^* at the edges; i.e.

$$\frac{\lambda S^*}{Y} = \frac{2.}{\sqrt{3}}(2c - 1 - a), \qquad \frac{S^*}{Y} = \frac{2}{\sqrt{3}}.(a + 1 - 2d),$$

and

$$\frac{S^*}{Y}(1 - \lambda) = \frac{4}{\sqrt{3}}\{c^2 + d^2 - (1 + a^2)\}.$$

Eliminating c and d from the equations we obtain

$$\frac{S^*}{Y} = \frac{2\left[\sqrt{\{(1-\lambda)^2 a^2 + 2(1-a)^2(1+\lambda^2)\}} - (1-\lambda)a\right]}{\sqrt{3}(1+\lambda^2)}, \tag{10}$$

which, in the particular case $\lambda = 0$, becomes

$$\frac{S^*}{Y} = \frac{2}{\sqrt{3}}\{\sqrt{(2 - 4a + 3a^2)} - a\}. \tag{11}$$

There is a better upper bound for $a > 0{\cdot}45$. It is obtained from the characteristic field of Fig. 11. As in Fig. 10 the four quarters of the plate rotate about the points $(\pm c, \pm d)$. The strain rate distribution, and hence the associated stress state, in the regions DF and CE along the axes of the plate, is identical with that of Fig. 10. In the regions CMN and DKL the characteristics are defined by the circular edge of the hole, and the associated stress state is axially symmetric. The remainder of the plate is rigid.

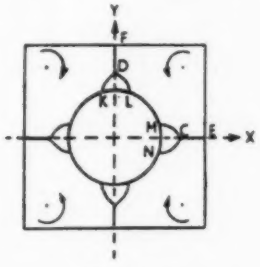

Fig. 11.

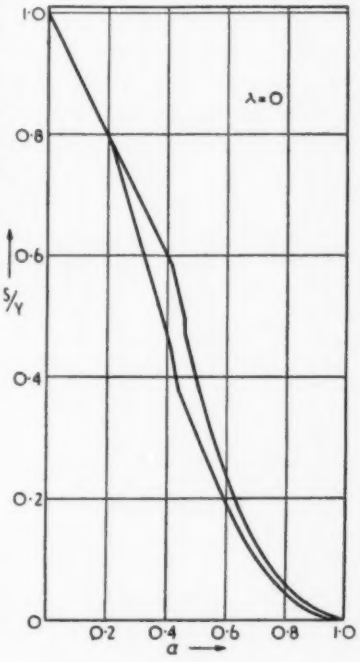

Fig. 12.

The associated stress states are in internal equilibrium and again it can be shown that the minimal upper bound S^* is obtained by satisfying the equilibrium equations for a quarter of the plate. Resolving parallel to the x-axis,

$$S^* = \int_a^d \sigma_\theta \, dr - \frac{2}{\sqrt{3}} Y(1-d), \tag{a}$$

and parallel to the y-axis,

$$0 = \int_a^c \sigma_\theta \, dr + \frac{2}{\sqrt{3}} Y(1-c), \tag{b}$$

and, taking moments about the centre,

$$S^* = \int_a^d r\sigma_\theta \, dr - \int_a^c r\sigma_\theta \, dr - \frac{2Y}{\sqrt{3}}(2 - d^2 - c^2). \tag{c}$$

(12)

The stresses in the regions of axial symmetry are given parametrically in Section 4. When S is a tensile stress the regions CMN and DKL are stressed in compression and in tension respectively.

The equations cannot be solved directly as the integral $\int r\sigma_\theta \, dr$ cannot be evaluated analytically. A graphical method of solution was used and is believed to be accurate to within 2 per cent.

For $a \leqslant 0{\cdot}45$ (approx.) it was found that $c \geqslant 2{\cdot}071a$. Since the velocity characteristics in the axially symmetric region do not exist beyond this radius, for $a < 0{\cdot}45$ this bound is not applicable and we must fall back on that given by equation (11).

The upper and lower bounds are shown in Fig. 12. The two bounds differ by less than 25 per cent except for $0{\cdot}35 \leqslant a \leqslant 0{\cdot}5$ where the difference rises to a maximum of almost 40 per cent of the lower bound.

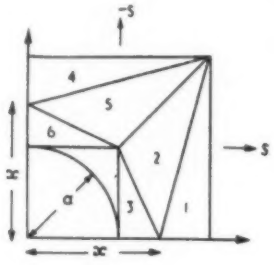

Fig. 13.

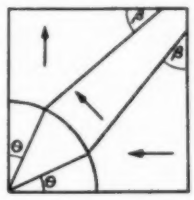

Fig. 14

6. EQUAL OPPOSITE BIAXIAL STRESSING

(a) *Lower bound.* A lower bound for all values of a is obtained from the stress distribution of Fig. 13. As in Fig. 7 within each region the stress distribution is uniform and there are discontinuities in the tangential stress across the regional boundaries. The principal components of stress (σ_1, σ_2) in each region are

(1) $\sigma_1 = S$, $\qquad \sigma_2 = \dfrac{S(x + a - 1)}{(1 - x)(1 - a)}$;

(2) $\sigma_1 = \dfrac{S\{\sqrt{(a^2 + x^2)} - a\}}{x(1 - a)}$, $\qquad \sigma_2 = \dfrac{-S\{\sqrt{(a^2 + x^2)} + a\}}{x(1 - a)}$;

(3) $\sigma_1 = \dfrac{Sx}{(1 - a)(x - a)}$, $\qquad \sigma_2 = 0$;

(4) $\sigma_2 = \dfrac{S(1 - a - x)}{(1 - x)(1 - a)}$, $\qquad \sigma_2 = -S$;

(5) $\sigma_1 = \dfrac{S\{\sqrt{(a^2 + x^2)} + a\}}{x(1 - a)}$, $\qquad \sigma_2 = \dfrac{-S\{\sqrt{(a^2 + x^2)} - a\}}{x(1 - a)}$;

(6) $\sigma_1 = 0$, $\qquad \sigma_2 = \dfrac{-Sx}{(1 - a)(x - a)}$.

Apart from a change of sign the stress state in the regions 4, 5 and 6 is identical with that in regions 1, 2 and 3 respectively. Hence, on substitution in the yield criterion only three inequalities are obtained. They are

$$S \leqslant \frac{Y(1-a)(1-x)}{\sqrt{\{(3-6a+3a^2)-x(6-9a+3a^2)+x^2(3-3a+a^2)\}}}, \qquad (I_1)$$

$$S \leqslant \frac{Y(1-a)x}{\sqrt{(4a^2+3x^2)}}, \qquad (I_2)$$

$$S \leqslant \frac{Y(1-a)(x-a)}{x}. \qquad (I_3)$$

For $0 \leqslant a \leqslant 0{\cdot}433$ the highest admissible value of S occurs when $I_1 = I_2$, and for $0{\cdot}433 \leqslant a \leqslant 1$ when $I_1 = I_3$.

(b) *Upper bounds.* Three upper bounds to the yield-point loading have been calculated. The first, which is closest to the upper bound for $a \leqslant 0{\cdot}37$ is derived from the deformation mode of Fig. 14. In each quarter of the plate there are two straight lines, across which the tangential velocity is discontinuous. Hence, with the notation of the figure

$$W_I = \frac{8}{\sqrt{3}} Yv(1 - a\cos\theta)\operatorname{cosec}\beta,$$

where v is the magnitude of the velocity discontinuity.

Further

$$W_E = 8Sv\{2\cos\beta - a\cos(\beta + \theta)\}.$$

and therefore,

$$\frac{S}{Y} \leqslant \frac{1 - a\cos\theta}{\{\sin 2\beta - a\sin\beta\cos(\beta+\theta)\}}. \qquad (13)$$

By differentiation with respect to θ and β in turn it is found that the minimum value of this bound occurs when

$$\tan\beta = \frac{\sin\theta}{\cos\theta - a}, \qquad \tan 2\beta = \frac{a\cos\theta - 2}{a\sin\theta}. \qquad (14)$$

Eliminating β from these equations we obtain a cubic equation for $\cos\theta$:

$$4a\cos^3\theta - 4\cos\theta(1+a^2) + a\cos\theta(1+a^2) + 2 = 0.$$

This equation can be solved numerically for each value of a and the appropriate value of $\cos\theta$ substituted in (14) and (13) to obtain the upper bound to S.

For $0{\cdot}37 \leqslant a \leqslant 0{\cdot}45$ the deformation mode of Fig. 10 gives an upper bound. Putting $\lambda = -1$ in equation (10), we have

$$\frac{S^*}{Y} = \frac{2}{\sqrt{3}}\{\sqrt{(1-2a+2a^2)} - a\}. \qquad (15)$$

For $0{\cdot}45 \leqslant a \leqslant 1$ a better upper bound is obtained from a characteristic solution similar to Fig. (11). In this case the three equations obtained by resolving the forces and taking moments about the centre, for one quarter of the plate, are

Vol. 2 53/54

$$
\left.
\begin{aligned}
S^* &= \int_a^d \sigma_\theta \, dr - \frac{2}{\sqrt{3}} Y (1 - d), && \text{(a)} \\
-S^* &= \int_a^c \sigma_\theta \, dr + \frac{2}{\sqrt{3}} Y (1 - c), && \text{(b)} \\
S^* &= \int_a^d r\sigma_\theta \, dr - \int_a^c r\sigma_\theta \, dr - \frac{2}{\sqrt{3}} Y (2 - d^2 - c^2). && \text{(c)}
\end{aligned}
\right\} \quad (16)
$$

Since the stress σ_θ is compressive and tensile in the regions *CMN* and *DKL* respectively, the equations (a) and (b) are identical and S^* and c are the only two unknown quantities. A graphical method of solution was again used to evaluate S^*. The upper and lower bounds are shown in Fig. 15 plotted as fractions of the maximum shear stress. The difference between the bounds is less than 10 per cent of the lower bound except for $0{\cdot}2 \leqslant a \leqslant 0{\cdot}5$ where it rises to a maximum value of 26 per cent at $a = 0{\cdot}37$.

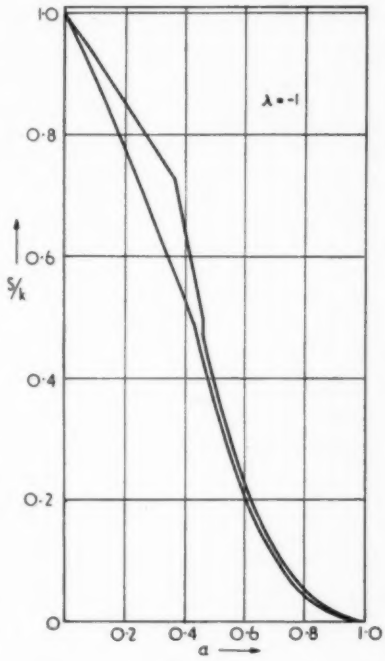

Fig. 15.

7. The Yield Locus of the Plate

The yield locus of the plate is the graphical representation in stress-space of the relation between the yield point stresses on the two pairs of opposite sides. From this locus the yield point stresses in any loading state can be quickly obtained. In this problem the yield locus cannot be determined exactly but upper and lower bounds to the locus can be established by using the information obtained for the three loading states which have been examined, and certain essential properties of the yield locus.

Since the material is assumed to be isotropic it follows that the yield locus must be symmetrical about the origin. Further the symmetry of the plate requires that if $(S, \lambda S)$, is a yield point loading state, so is $(\lambda S, S)$. Hence the locus is symmetrical about the two lines through the origin at 45° to the stress axes *i.e.* the lines along which $\lambda = 1$ and $\lambda = -1$. This is also true for an upper or lower bound to the yield locus and henceforward attention is restricted to the quadrant between two axes of symmetry.

In Section 5 the convexity of the yield locus was used to obtain a lower bound to the yield-point stresses. Since the locus is symmetrical as well as convex it follows that the yield locus lies inside the perpendiculars to the lines $\lambda = 1$ and $\lambda = -1$ at the points representing upper bounds in the appropriate loading state.

A lower bound to the yield locus is simply constructed by drawing straight lines between the points representing lower bounds to the yield-point stresses

in the three loading states examined in detail. An upper bound is obtained by generalizing the upper bounds previously obtained.

The bending mode of Fig. 11 can be solved graphically for any value of λ provided $a \geqslant 0{\cdot}45$ (approx.), but for some values of λ the accuracy decreases considerably as a increases.

Similarly, there are characteristic solutions (Fig. 16) similar to that of Fig. 2 which define upper bounds for $0 \leqslant \lambda S \leqslant Y/\sqrt{3}$. The parametric expressions for the bounds are

$$\left.\begin{aligned} S \leqslant S^* &= \frac{2}{\sqrt{3}}\, Y \left[\sin\left(\alpha + \frac{\pi}{6}\right) - a\sqrt{\left\{\frac{\sqrt{3}}{2}\cos\alpha\right\}\exp\left\{\frac{\sqrt{3}}{2}\left(\alpha - \frac{\pi}{6}\right)\right\}}\right], \\ \text{where} \quad \lambda S^* &= \frac{2}{\sqrt{3}}\, Y \sin\left(\alpha - \frac{\pi}{6}\right), \qquad \text{and} \qquad \frac{\pi}{6} \leqslant \alpha \leqslant \frac{\pi}{3}. \end{aligned}\right\} \tag{17}$$

For $a \geqslant 0{\cdot}483$ the bending mode and the characteristic solution define an upper bound to the yield locus for all values of λ. When $a \leqslant 0{\cdot}483$ there is no characteristic solution for values of $\lambda \geqslant 1/(2 - 2{\cdot}071\, a)$ and the best upper bound for such values of is precisely that of equation 4.

When $a \leqslant 0{\cdot}45$ the solution of Fig. 11 is inapplicable for certain values of λ and the best upper bound is that of equation (10).

For $a \leqslant 0{\cdot}42$ the value of S^* from (10) is greater than that from (17) at $\lambda = 0$. Accordingly a better bound is required over some of the area between $\lambda = 0$ and $\lambda = 1$. This is provided by a generalisation of Fig. 3. With the notation of the figure we have, as before,

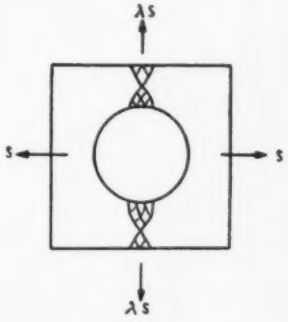

Fig. 16.

$$W_I = \frac{Y}{\sqrt{3}}\, v\,(1 + 3\sin^2\psi)^{\frac{1}{2}}\,(1 - a)\operatorname{cosec}\beta.$$

In the general loading state, however,

$$W_E = Sv\,\{\cos(\beta - \psi) - \lambda\,(1 - a)\cot\beta\sin(\beta - \psi)\}.$$

Hence

$$\frac{S}{Y} \leqslant \frac{(1 + 3\sin^2\psi)^{\frac{1}{2}}\,(1 - a)}{\sqrt{3}\,\{\sin\beta\cos(\beta - \psi) - \lambda\,(1 - a)\cos\beta\sin(\beta - \psi)\}} = \frac{S^*}{Y}.$$

It is found that the minimum value of S^* occurs when $\beta = \frac{1}{4}\pi + \frac{1}{2}\psi$ and

$$\sin\psi = \frac{1 + \lambda\,(1 - a)}{3\,\{1 - \lambda\,(1 - a)\}}.$$

Substitution of these values in the original expression gives

$$\frac{S}{Y} \leqslant \frac{(1 - a)}{\sqrt{\{1 - (1 - a)\,\lambda + (1 - a)^2\,\lambda^2\}}}. \tag{18}$$

The upper bounds given by (17) and (18) coincide at $\lambda = 0$.

For $a \leqslant 0{\cdot}87$ the upper bounds of (17), (4) and (18) are closer to the lower bounds than the solution of (10) for all values of λ and the upper bound to the yield locus is composed of arcs which are defined by the first three equations.

When $a \leqslant 0{\cdot}33$ the best (or least) upper bound (4) involves an imaginary value of ψ and the best upper bound is precisely that in (5).

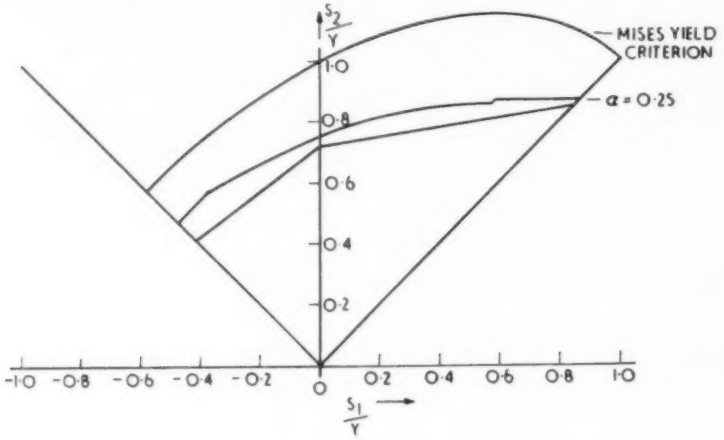

Fig. 17a.

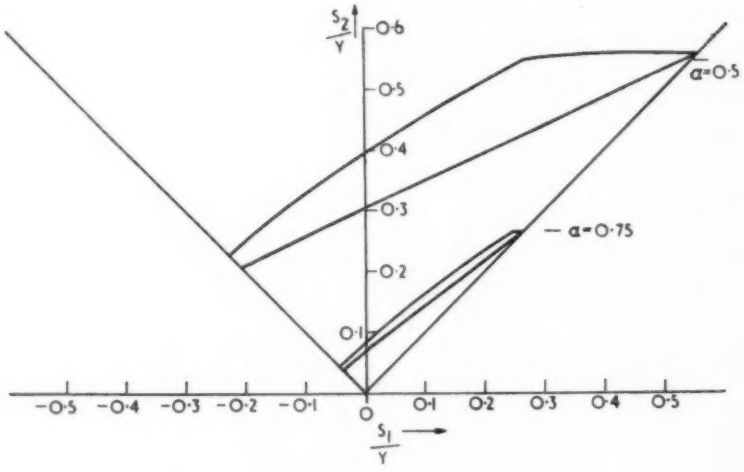

Fig. 17b.

Finally, when $a \leqslant 0{\cdot}15$, a generalisation of (6) is a better upper bound to the yield locus, first at $\lambda = 1$, and then, with further decrease in a, over an increasing range of loading states. The principal direction of stress and strain-rate are parallel to the edges of the plate and the rate of straining and stress state are uniform.

For a plate without a hole therefore

$$S = Y/\sqrt{(1 - \lambda + \lambda^2)},$$

and for a plate with hole of radius a, since the internal work is proportional to the area, we have

$$\frac{S}{Y} \leqslant \frac{(1 - \frac{1}{4}\pi a^2)}{\sqrt{(1 - \lambda + \lambda^2)}}. \tag{19}$$

Representative quadrants of the yield loci for $a = 0{\cdot}25$, $0{\cdot}5$ and $0{\cdot}75$, are shown in Fig. 17 together with the Mises yield criterion (the locus for $a = 0$) for comparison.

Acknowledgments

The authors wish to thank Professor R. Hill and Mr. A. P. Green for their valuable advice and help in the preparation of this paper. This paper is report number MW/B/84/53 of the British Iron and Steel Research Association.

References

Drucker, D. C., Greenberg, H. J. and Prager, W. 1951 *J. Appl. Mech.*, **18**, 371.

Gaydon, F. A. 1954 *J. Mech. Phys. Solids*, **2**, This number.

Hill, R. and Siebel, M. P. L. 1953 *J. Mech. Phys. Solids*, **1**, 207.

Hill, R. 1950 *The Mathematical Theory of Plasticity* (Oxford, Clarendon Press).

1951 *Phil. Mag.*, **42**, 868.

1952 *J. Mech. Phys. Solids*, **1**, 19.

Hodge, P. G. 1952 *Tech. Rep.* B11-7, N7onr-35810, Brown University.

Vol. 2 53/54

Journal of the Mechanics and Physics of Solids, 1954, Vol. 2, pp. 170 to 176. Pergamon Press Ltd., London.

ON THE YIELD-POINT LOADING OF A SQUARE PLATE WITH CONCENTRIC CIRCULAR HOLE

By F. A. Gaydon
Department of Theoretical Mechanics, University of Bristol

(*Received 21st January*, 1954)

Summary

The problem discussed in this paper is that of determining upper and lower bounds to the yield locus of a square plate, with concentric circular hole, under certain loading of the edges. The loads on opposite edges are equal, those on adjacent edges are held in a fixed proportion during each loading programme. The loads are supposed to be uniformly distributed and normal to the edges over which they act and the edge of the hole is stress free. The Tresca yield criterion and potential function are used throughout. It is found that the methods of Hill (1950 and 1951) and of Drucker, Greenberg and Prager (1951 and 1952) give reasonably close upper and lower bounds to the yield locus.

Vol 2 1953

1. Introduction

Upper and lower bounds are determined for the yield point loading of a thin square plate with a concentric circular hole. The two cases (*a*) uniaxial tension, (*b*) simultaneous equal biaxial tension and compression, are examined in detail using the Tresca yield criterion and plastic potential. Hodge (1952) has obtained upper and lower bounds for uniaxial tension and the exact solution for uniform equal biaxial tension.

The plate $ABCD$ (Fig. 1) has sides of length, 2, thickness h and the concentric circular hole is of radius a $(0 \leqslant a \leqslant 1)$. Uniform stresses are applied in the plane of the plate normal to the edges. The edge of the hole is stress free. The problem is considered to be one of plane stress, with the stresses and strains regarded as functions of coordinates in the plane only. The material of the plate is assumed to be plastic-rigid, incompressible and isotropic.

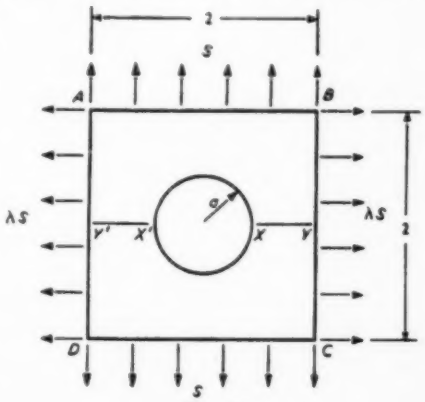

Fig. 1.

The stresses over the sides AB, CD are S, those over BC, DA are λS $(-1 \leqslant \lambda \leqslant 1)$. S is then supposed to increase uniformly until its yield point value is reached.

2. The Tresca Yield Criterion

If σ_1, σ_2 are principal stresses at any point of the plate they must satisfy the relations

$$|\sigma_1| \leqslant 2k, \qquad |\sigma_2| \leqslant 2k \qquad \text{and} \qquad |\sigma_1 - \sigma_2| \leqslant 2k, \tag{1}$$

where k is the yield stress in pure shear. The yield locus in (σ_1, σ_2) space is a hexagon.

The curve representing the potential function is taken to be a similar and similarly situated hexagon. It then follows that the strain-rate vector corresponding to a given stress-state represented by a point on one of the sides of the yield locus is normal to that side. If the stress-state corresponds to a vertex of the hexagon then the strain-rate vector is not uniquely determined; however, it must lie between the normals to the locus on each side of the vertex. This indeterminacy only affects the actual deformation mode; we are not concerned with this here, only with the loads at the yield point.

Vol. 2 53/54

3. Extremum Principles

It has been shown by Hill (1950 and 1951) and by Drucker, Greenberg and Prager (1951 and 1952), that any equilibrium stress distribution satisfying the given stress boundary conditions and nowhere violating the yield criterion, will give rise to external boundary loads which are less than or equal to the actual yield point loads. They have shown also that the internal rate of plastic working calculated (via the plastic potential), from any mode of deformation compatible with the velocity boundary conditions, is greater than or equal to the rate of working of the actual boundary stresses. Any postulated deformation mode therefore gives rise to an upper bound to the yield point boundary loads.

In particular, the internal rate of working in a localized neck is $\int kvh\,(1+\sin\psi)ds$ where v is the velocity of a point just on one side of the neck relative to the adjacent point just on the other side and this velocity vector is inclined at angle ψ to the neck (Hill 1952).

4. Equal Biaxial Tension (or Compression)

Hodge and Prager (1951) have shown that an upper and lower bound for S is $2k\,(1-a)$; that is, the yield point loading is exactly $2k\,(1-a)$ in this case.

5. Equal and Opposite Biaxial Loading

(a) *Lower bound.* The plate is divided into areas of constant stress (one quarter of the plate is shown in Fig. 2).* It is assumed that the stress is zero in zone 7. For the plate to be in equilibrium the principal stresses (r, s) in zones 1 to 6 are given by

* Subsequent to completing this work the author has seen a report by Hodge (1958) in which a similar constant stress lay-out is used for the equal biaxial tension case.

$$
\left.\begin{aligned}
r_1 &= \frac{S\left[\lambda(1-x)+a\right]}{(1-a)(1-x)}, & s_1 &= S.\\
r_2 &= \frac{S\left[\lambda(x-a)-a\right]}{(1-a)(x-a)}, & s_2 &= 0\\
(r_3, s_3) &\equiv \frac{S}{2x(1-a)}\left[x(\lambda+1)-2a \mp \sqrt{(1-\lambda)^2x^2+4a^2}\right].\\
r_4 &= \lambda S, & s_4 &= \frac{S(1-h+\lambda a)}{(1-a)(1-h)}.\\
r_5 &= 0, & s_5 &= \frac{S(h-a-a\lambda)}{(1-a)(h-a)}.\\
(r_6, s_6) &\equiv \frac{S}{2h(1-a)}\left[h(\lambda+1)-2a\lambda \mp \sqrt{(1-\lambda)^2h^2+4\lambda^2a^2}\right].
\end{aligned}\right\} \quad (2)
$$

These stresses must not violate the yield criterion (1).

In this particular case $\lambda = -1$ and zones 1, 2, 3 give rise to the same inequalities as zones 4, 5, 6 respectively; one set involves x, the other h. The inequalities that must not be violated are then

$$S \leqslant 2k, \quad (3)$$

$$\left|\frac{S(1-x-a)}{(1-x)(1-a)}\right| \leqslant 2k, \quad (4)$$

$$\left|S + \frac{S(1-x-a)}{(1-x)(1-a)}\right| \leqslant 2k, \quad (5)$$

$$\frac{2S\sqrt{a^2+x^2}}{x(1-a)} \leqslant 2k, \quad (6)$$

$$\frac{Sx}{(x-a)(1-a)} \leqslant 2k. \quad (7)$$

Clearly (4) is more stringent than (5) when $x + a > 1$. In order to obtain the largest lower bound for this particular distribution x must be so chosen that all the inequalities are satisfied and the permissible value of S is as large as possible. It is found that the optimum value of x is such that $x + a$ is always greater than unity. The inequalities to be satisfied may then be written

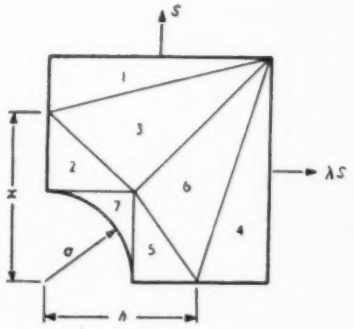

Fig. 2.

$$S \leqslant 2k, \quad (8)$$

$$S \leqslant \frac{2k(1-x)(1-a)}{x+a-1}, \quad (9)$$

$$S \leqslant \frac{kx(1-a)}{\sqrt{a^2+x^2}}, \quad (10)$$

$$S \leqslant \frac{2k\,(x - a)\,(1 - a)}{x}. \tag{11}$$

If the right-hand sides of the above inequalities are plotted as functions of x for discrete values of a, it is found that the best value of x is given by

$$\frac{2\,(1 - x)\,(1 - a)}{x + a - 1} = \frac{x\,(1 - a)}{\sqrt{a^2 + x^2}} \qquad \text{when} \qquad 0 \leqslant a \leqslant 0{\cdot}482, \tag{12}$$

and by

$$\frac{2\,(1 - x)\,(1 - a)}{x + a - 1} = \frac{2\,(x - a)\,(1 - a)}{x} \qquad \text{when} \qquad 0{\cdot}482 \leqslant a \leqslant 1. \tag{13}$$

The latter equation gives

$$x = \frac{1 + \sqrt{a^2 + (1 - a)^2}}{2},$$

and then the best value of S is given by

$$\frac{S}{2k} = -a + \sqrt{a^2 + (1 - a)^2}, \qquad 0{\cdot}482 \leqslant a \leqslant 1. \tag{14}$$

The values of S which follow from (12) are found graphically.

(b) *Upper bound.* The plate is supposed to have a velocity discontinuity v at an angle ψ to XY in the quarter plate of Fig. 3, with similarly placed necks in the other three quarters. The material is rigid on each side of the neck. In the general case it follows that the external work-rate

$$= Svh \cos(\beta - \psi) - \lambda S\,(XY)\,vh \sin(\beta - \psi),$$

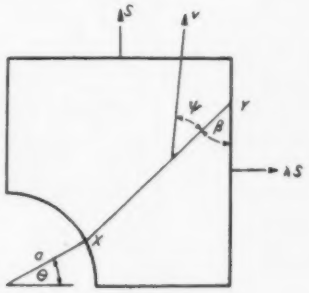

Fig. 3.

where

$$XY = a \sin\theta + (1 - a\cos\theta)\cot\beta,$$

and the internal work-rate

$$= kvh \operatorname{cosec}\beta\,(1 - a\cos\theta).$$

The value of S for which these work-rates are equal is an upper bound. Therefore

$$\frac{S}{k} \leqslant \frac{(1 + \sin\psi)\,(1 - a\cos\theta)}{\sin\beta\cos(\beta - \psi) - \lambda\sin(\beta - \psi)\left[\cos\beta - a\cos(\beta + \theta)\right]}. \tag{15}$$

In the present case $\lambda = -1$ and

$$\frac{S}{k} \leqslant \frac{(1 + \sin\psi)\,(1 - a\cos\theta)}{\sin(2\beta - \psi) - a\cos(\beta + \theta)\sin(\beta - \psi)}. \tag{16}$$

It is thought that the right-hand side of equation (16) does not possess a true analytic minimum value. In order to avoid the numerical work involved in finding its *least* value, ψ is taken as zero. It is certain that the consequent upper bound is very close to the best that can be obtained from equation (16). With

$\psi = 0$ the best upper bound (GAYDON and MCCRUM 1954) is given by values of β and θ satisfying the relations

$$\tan \beta = \frac{\sin \theta}{\cos \theta - a}, \qquad \tan 2\beta = \frac{a \cos \theta - 2}{a \sin \theta}.$$

These equations give rise to the following cubic in $\cos \theta$:

$$4a \cos^3 \theta - 4(1 + a^2) \cos^2 \theta + a(1 + a^2) \cos \theta + 2 = 0. \tag{17}$$

This has been solved for $a = 0{\cdot}1$, $0{\cdot}2$, $0{\cdot}3$, $0{\cdot}4$. The resulting upper bound is the best obtained for $0 \leqslant a \leqslant 0{\cdot}37$.

For $0{\cdot}37 \leqslant a \leqslant 1$, consider the hypothetical deformation mode in which the four quarters of the plate rotate rigidly with necking and bulging along the sections of least width. The quarter plate shown in Fig. 4

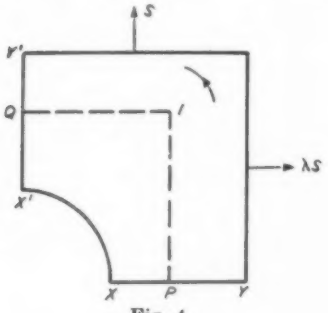

Fig. 4.

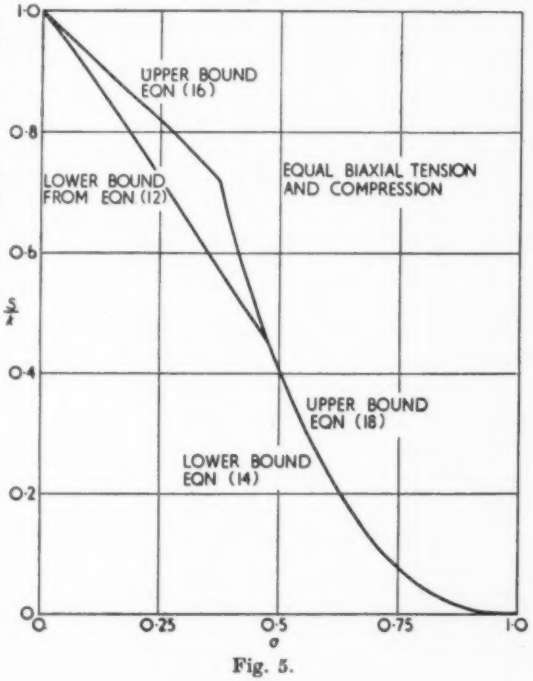

Fig. 5.

rotates about I, necks along PY, QX' and bulges along XP, QY'. It is easily shown that the least value of the upper bound occurs when the plate is in equilibrium. The stress along PY, QX' is $2k$, that along XP, QY' is $-2k$.

For equilibrium it is found that

$$\left(\frac{S}{2k}\right)^2 + \left(\frac{\lambda S}{2k}\right)^2 + \frac{2S(1 - \lambda)a}{2k} = 2(1 - a)^2. \tag{18}$$

In the present case $\lambda = -1$ and therefore

$$\frac{S}{2k} = -a \pm \sqrt{a^2 + (1 - a)^2};$$

that is to say, as S is positive,

$$\frac{S}{2k} = -a + \sqrt{a^2 + (1 - a)^2}. \tag{19}$$

• Communicated to the author by R. HILL.

Equations (14) and (19) are identical. The exact yield point loading is then that given by (19) or (14) in the range $0{\cdot}482 \leqslant a \leqslant 1$. The bounds are plotted in Fig. 5.

6. Uniaxial Tension

(a) *Lower bound.* When $\lambda = 0$ the stress distribution of Fig. 2 reduces to that of Hodge (1952), the zones 4, 5, 6 become one zone, and $h = 1$. The inequalities that arise are

$$\frac{S}{2k} \leqslant 1\,; \quad \frac{S}{2k} \leqslant \frac{(1-a)\,x}{\sqrt{x^2+4a^2}}\,; \quad \frac{S}{2k} \leqslant \frac{(1-a)\,(1-x)}{a}\,; \quad \frac{S}{2k} \leqslant \frac{(1-a)\,(x-a)}{a}\,.$$

For a in the range $0{\cdot}443 \leqslant a \leqslant 1$, the lower bound is $k\,(1-a)^2/a$. For $0 \leqslant a \leqslant 0{\cdot}443$, S is found graphically.

However, for 0·45 (approx.) $\leqslant a \leqslant 1$, a better lower bound is obtained from the lower bound of equation (14) and the exact solution of Section 4. It follows from the maximum work principle that the yield locus of a plastic rigid body must be concave to the origin. Therefore the chord joining any two points representing lower bounds lies entirely inside the locus. The point in which this chord meets the line through the origin with slope $1/\lambda$ represents a lower bound for the case $(S, \lambda S)$.

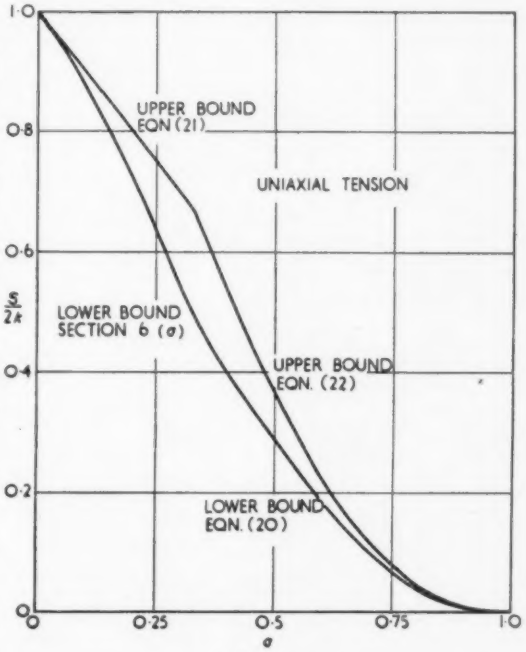

Fig. 6.

In the case under consideration a lower bound is obtained from the coordinates of the intersection of the chord joining the points representing the lower bound of the cases (S, S), $(S, -S)$, and the line $\lambda = 0$. In the range $0{\cdot}482 \leqslant a \leqslant 1$ the lower bound is

$$S = \frac{2k\,(1-a)\,(1-\sqrt{a^2+(1-a)^2})}{a}. \tag{20}$$

In the range $0{\cdot}45 \leqslant a \leqslant 0{\cdot}482$ the lower bound is found graphically.

(b) *Upper bound.* In the range $0 \leqslant a \leqslant \frac{1}{3}$, the best upper bound is obtained from (15) after putting $\lambda = 0$. This gives

$$S = 2k\,(1-a) \tag{21}$$

and the mode corresponds to necking along XY, $X'Y'$ (Fig. 1), the two halves of the plate moving apart as rigid bodies.

For $\frac{1}{3} \leqslant a \leqslant 1$, the upper bound obtained from equation (18) is

$$S = 2k\left[-a + [a^2 + 2(1-a)^2]^{\frac{1}{2}}\right]. \qquad *(22)$$

The bounds are plotted in Fig. 6.

7. The Yield Locus

Since the material is assumed to be isotropic the yield locus is symmetrical about the origin. The symmetry of the plate requires that if $(S, \lambda S)$ is a yield state, so is $(\lambda S, S)$. The locus is therefore symmetrical about the lines $\lambda = 1$, $\lambda = -1$, at 45° to the stress-axes and passing through the origin. It is thus only necessary to consider one quadrant between the axes of symmetry.

If a is small a simple upper bound, with λ in the range $-1 \leqslant \lambda \leqslant 0$, is obtained by taking $\psi = \theta = 0$, $\beta = \frac{1}{2}\pi$ in equation (15), then

$$\frac{S}{2k} = \frac{1-a}{1-\lambda+\lambda a}. \qquad (23)$$

Equation (23) is represented by the line AB $(a = 0{\cdot}2)$ in Fig. 7. When $\lambda = -1$ this bound is slightly greater than that derived from (17). Similarly if λ lies in the range $0 \leqslant \lambda \leqslant 1$ equation (21) is a good upper bound. It is obtained from (15) by taking $\psi = \beta = \frac{1}{2}\pi$, $\theta = 0$. This is represented by the line BC $(a = 0{\cdot}2)$ in Fig. 7.

For $a \geqslant 0{\cdot}45$ (approx.) and for all λ, equation (18) provides good upper bounds.

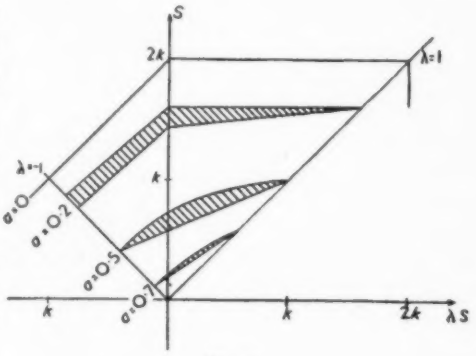

Fig. 7.

The results for $a = 0{\cdot}2$, $0{\cdot}5$, $0{\cdot}7$ are shown in Fig. 7, which represents one quarter of the yield locus diagram. The actual yield loci for these values of a lie in the corresponding shaded areas.

Acknowledgments

The author wishes to thank Professor R. Hill for many helpful suggestions and criticisms. He also wishes to acknowledge considerable help from work of Professor P. G. Hodge which has appeared in reports issued by Brown University.

References

Drucker, D. C., Greenberg, H. J. and Prager, W.	1951	*J. Appl. Mech.*, **18**, 371.
Gaydon, F. A. and McCrum, A. W.	1954	*J. Mech. Phys. Solids*, **2**, 156.
Hill, R.	1950	*The Mathematical Theory of Plasticity* (Oxford, Clarendon Press).
	1951	*Phil. Mag.*, **42**, 868.
	1952	*J. Mech. Phys. Solids*, **1**, 19.
Hodge, P. G. and Prager, W.	1951	*Tech. Rep.* B11-22, Brown University.
Hodge, P. G.	1952	*Tech. Rep.* B11-7, Brown University.
	1953	*Final Rep.* B11-22, Brown University.

* Hodge (1952) has also obtained this expression but mistakenly calls it a lower bound.

Journal of the Mechanics and Physics of Solids, 1954, Vol. 2, pp. 177 to 196. Pergamon Press Ltd., London.

LOW TEMPERATURE EMBRITTLEMENT MECHANICS DEDUCED FROM ZINC SINGLE CRYSTAL FRACTURE STUDIES

By P. H. Morton,* R. Treon and W. M. Baldwin, Jr.
Department of Metallurgical Engineering, Case Institute of Technology

(*Received 6th January*, 1954)

Summary

The most important conclusion of this work is that low temperature brittleness in zinc single crystals is not due to the cessation of slip below a certain temperature. On the contrary slip is quite active, and it is its activity that induces low temperature brittleness : slip causes rotation of the lattice which in turn sets up orientation gradients adjacent to constricted and unslipped regions. At high temperatures these orientation gradients are accommodated by bend-planes, at low temperatures, by cleavage.

Vol. 2 53/54

1. Introduction

At present writing there is virtually no understanding of the events leading to fracture in metal single crystals, much less polycrystalline aggregates, although there are two popular, if vague, trends in thought along these lines. One stems originally from O'Neill's (1926) observation that brittleness is found in those metals and under those testing conditions where twinning is prevalent. An imposing Russian school (Davidenkov 1938 ; Yakutovich and Yakovleva 1950 ; Shevandin 1940 ; Vitman and Stepanov 1939 ; Lifshits 1948, *et al.*) have pressed this parallel to the point of proposing a direct cause-and-effect relationship between twinning and brittle fracture, though recent observations of Low and Feustel (1953) have discredited this extreme view. The other stems originally from the observations of Barrett, Ansel and Mehl (1937) that slip in some ferritic materials, while occurring indiscriminately at room temperature on a number of crystallographic systems – (011) [11$\bar{1}$], (112) [11$\bar{1}$], (123) [11$\bar{1}$] – is restricted as temperature is lowered to successively fewer systems and ultimately to only one – (011) [11$\bar{1}$]. The rationalizations of low temperature brittleness based on either of these two observations have in a sense been particularizations of the theories of Kuntze (1928), McAdam (1942), Fridman (1946) *et al.* ; to wit, that low temperatures repress slip by increasing the critical stresses for it at such a rapid rate that alternative processes presumed not to be so sensitively affected by temperature – *e.g.* twinning or cleavage – set in.†

* At present at Imperial Chemical Industries, Ltd., Metals Division, Birmingham, England.

† Yakutovich and Yakovleva's proposal is different. They suggested that metal twin boundaries have a high concentration of Rose (1868) canals as mineral twin boundaries do, and these, like the perforations of a postage stamp, lead to ready fracture.

The present investigation sought to clarify some of this vagueness, and specifically inquired into the effects of temperature, orientation, and specimen shape on the mode of fracture and the ductility accompanying fracture of zinc single crystals.

(i) *Flow of Zinc Single Crystals*

Zinc single crystals commonly slip on the system (001) [11$\bar{2}$0], (MARK, POLANYI and SCHMID 1923)*, and twin on the 10$\bar{1}$2 plane by shear in the direction perpendicular to [1$\bar{2}$10].

In a tensile test, crystals whose (0001) basal poles lie less than 70 to 75° to the tensile axis ($\phi_0 < 70$-75°) (see Fig. 1 (*a*)) deform by slip (primary slip), the crystal rotating thereby such that in a standard stereographic projection the tensile axis

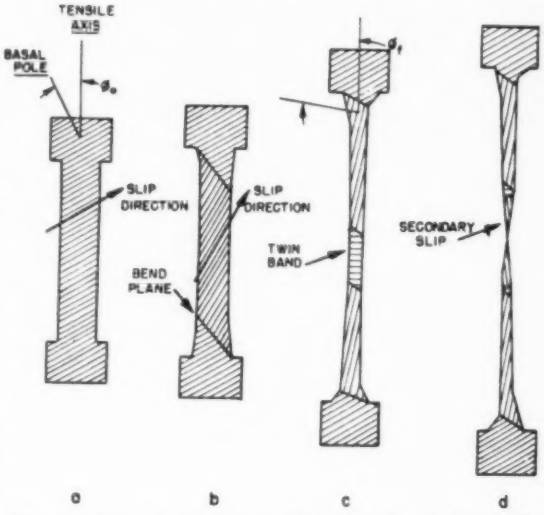

Fig. 1. Steps in the flow and fracture of a zinc crystal.

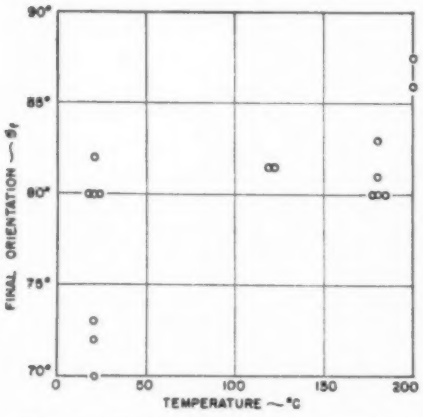

Fig. 2. Effect of temperature on the orientation just before twinning (MARK, POLANYI and and SCHMID, 1923).

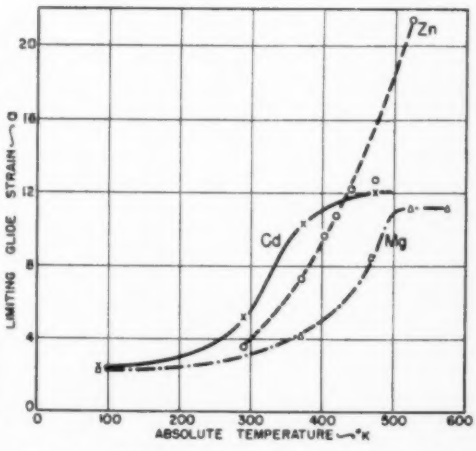

Fig. 3. Effect of temperature on the total shear, *a* before twinning occurs (SCHMID and BOAS 1935).

migrates along the great circle toward a [11$\bar{2}$0] slip direction (Fig. 1 (*b*)). Because the crystal rotates during a tensile test and because it is constrained from rotating

* Other slip systems must also act at high temperatures. Crystals strained at 100 to 200°C show markings that could not be explained on the basis of (0001) [11$\bar{2}$0] (BOAS and SCHMID 1930). KOLESNIKOV (1938) on rather weak evidence, it is true, suggests the slip system (1100) [11$\bar{2}$0] to operate in crystals having the (0001) basal plane nearly parallel to the tensile axis when tested above 300°C. WASHBURN (1951) finds good evidence for the slip system (1$\bar{1}$0X) [11$\bar{2}$0] for crystals of similar orientation tested at 400°C. All of these slip systems (including the usual system) involve a common slip direction [11$\bar{2}$0] but different planes zonal to this direction.

in the grips, there must be a change in orientation somewhere between the gripped and free portions of the specimen. This change was observed (MARK, POLANYI, and SCHMID 1923; MILLER 1934), as a sharp bend in the crystal lattice (see Fig. 1 (*b*)). HESS and BARRETT (1949), demonstrated that these bends were the same as OROWAN's (1942) kink-planes. Rotation of the crystal proceeds until at a critical point the crystal twins (Fig. 1 (*c*)) yielding bands of a different orientation in which further secondary slip occurs (Fig. 1 (*d*)). There is some confusion as to the criterion setting the critical point at which primary slip terminates. In early work (MARK, POLANYI and SCHMID 1923; BOAS and SCHMID 1929), it was reported that both zinc and cadmium twinned when the angle between normal to

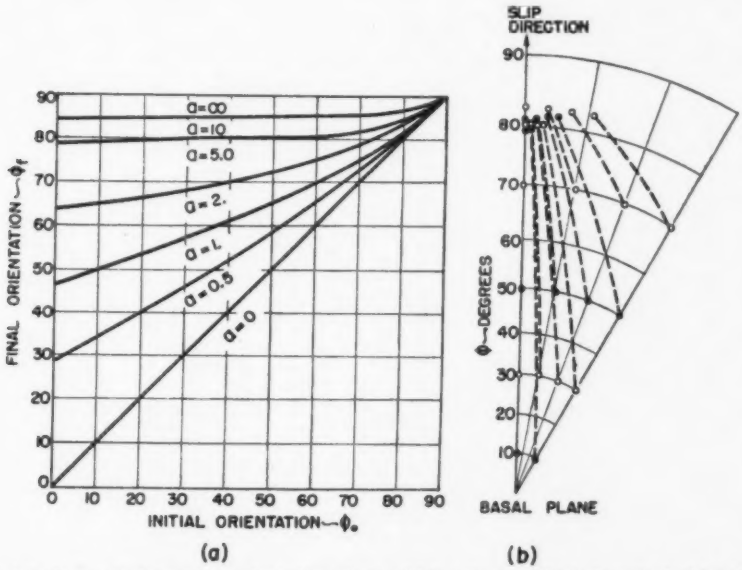

Fig. 4. (*a*) This graph shows the orientation ϕ_f at which primary slip is terminated by twinning for any starting orientation ϕ_0, presuming that the criterion for termination of primary slip is a constant value of resolved shear train, a. For high values of a the value of ϕ_f is almost constant for any value of ϕ_0 less than 70 to 75, the range over which the criterion is supposed to hold. For $a = 5$, for example, ϕ_p runs from 79° when ϕ_0 is 0 up to 82° when ϕ_0 is 70° this small difference is about equal to the accuracy of orientation determination whence it is easy to see the difficulty in deciding whether twinning occurs at a constant value of ϕ_f under these conditions, or a constant value of a.

(*b*) This is a stereographic plot of the final orientations of crystals just before twinning of crystals with various initial orientations assuming that the criterion for termination of primary slip is a resolved shear strain of 5.

the (0001) basal plane and the tensile axis reached a critical value, ϕ_f (see Fig. 1 (*c*)), dependent upon temperature (Fig. 2). In subsequent work (SCHMID and BOAS 1935) it was reported that both metals twinned when the shear strain resolved on the slip plane reached a critical value a, also dependent upon temperature (Fig. 3). Actually, for $\phi_0 < 70\text{-}75°$ and for high values of a (such as were reported, cf. Fig. 3) the two criteria are very much the same (cf. Fig. 4), It is of interest to note moreover that the values of resolved shear strain reported as critical for

zinc by SCHMID and BOAS (1935) convert to the same range of values of ϕ_f reported as critical for zinc by MARK, POLANYI and SCHMID (1923) as shown in Fig. 5.

GILMAN and READ (1952) note that crystals in which $\phi_0 > 80°$ deformed at room temperature by twinning " mostly " and when $\phi_0 > 85°$ by twinning only, *i.e.*, crystals which were originally in the condition of Fig. 1 (*c*) twinned without primary slip.

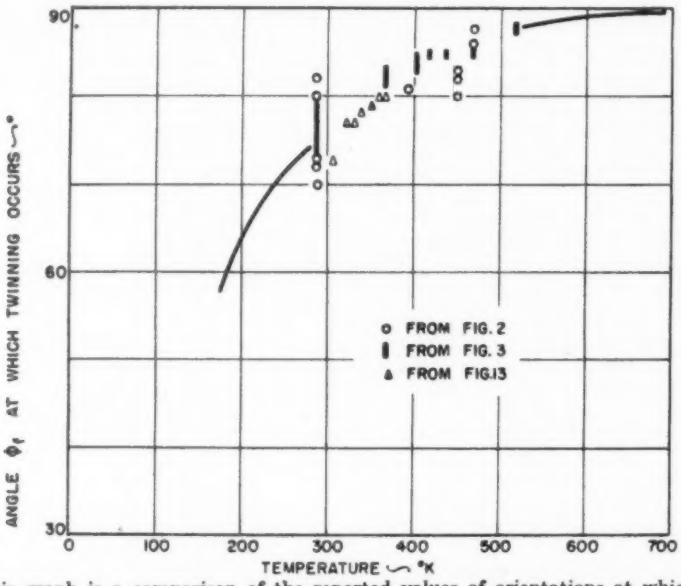

Fig. 5. This graph is a comparison of the reported values of orientations at which twinning terminates primary slip. The circles are retained directly from Fig. 2. The bars represent the range of values of ϕ_f for all values of ϕ_0 from 0 to 70° for the values of a given in Fig. 3. The conversion being made by means of Fig. 4. The triangles are values obtained in the present report (*cf.* Fig. 13).

(ii) *The Fracture of Zinc Single Crystals*

At temperatures of 18°C and over, zinc is ductile ; secondary slip within the twinned lamella " leads to a marked necking of the crystal ribbon and to final rupture " (Fig. 1 (*d*)) (SCHMID and BOAS 1935).

At temperatures of − 80°C and lower, FAHRENHORST and SCHMID (1930) found that single crystals of zinc fractured by cleavage. For low values of ϕ_0, cleavage was on the basal plane and it is of interest that one crystal underwent a total shear of 200 per cent at − 185°C. For crystals with high values of ϕ_0 cleavage occurred only after twinning had taken place (MARK, POLANYI and SCHMID 1923 ; WASHBURN 1951).*

Since apparently all crystals tested at 100°C parted after localized necking whereas at − 80°C they failed by cleavage, it is evident that a transition temperature exists. SCHMID and BOAS (1935) state that at 20°C zinc crystals did not " as a rule " fracture by cleavage, so that the transition temperature (as

* The early workers described the fracture as prismatic cleavage, but it has since been shown by MATHEWSON and PHILLIPS (1927) to be in fact cleavage on the basal plane in the twinned crystal.

evidenced by a change in the type of fracture) is presumably near but below room temperature.

2. Material and Procedure

The zinc was three-quarter inch extruded rod from the *National Lead Company*. The nominal purity was 99·99 per cent Zn.

A polycrystalline zinc specimen of the shape required for the single crystal was used as the pattern in an investment mould, which was heated at 1,000°F until the zinc melted.* The mould was removed from the furnace and directional cooling was produced by a quenched copper rod acting as a chill. A single crystal nucleated at the point of contact of zinc with copper, and grew into the rest of the melt.

The crystal was given an acid polish in a 10 per cent solution of HNO_3 and then etched for five to ten seconds in a 50-50 solution of HCl. Any grain boundaries were clearly revealed. The crystals were made in batches of eight to twelve, and the yield varied, but an average of about 80 per cent of the investment gave good single crystals.

The orientation of each crystal was determined by means of an X-ray back-reflection photograph using the Greninger method.

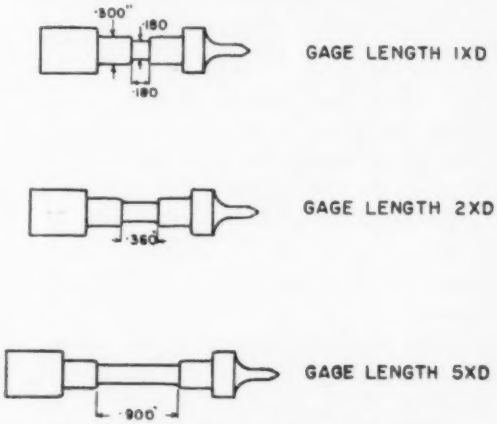

Fig. 6. Shape of single crystal specimens.

From the measurement of the film, three angles representing the orientation of a crystal were determined. These were ϕ_0, λ_0, and α_0 as shown in Fig. 7. (The λ_0 used here is the same as that used by Schmid and Boas (1935). The angle, χ, which they used is $90° - \phi_0$, and their angle κ is the same as α_0.)

Extreme care was required in the handling of the crystals as some even deformed under their own weight at room temperature. Damage during handling was revealed by an overall bending of the crystal or by blurred spots on the Greninger photograph. If an overall bend was observed, the crystal was not tested.

Handling of the crystal was reduced to a minimum by inserting the specimen in the test rig before putting the rig into the temperature bath. The temperature medium used was water from 5°C to 95°C and a transparent mineral oil at 105° and 115°C. The different environment appeared to have no effect on fracture properties. Thus the crystal could be observed directly throughout the test.

Although the rate of movement of the tensile machine head was kept constant at about 0·2 in. per min., the rate of straining was different for the three series

* Preliminary experiments had shown that the manner in which the specimen was gripped was of pronounced influence on the ductility of the specimen, fracture frequently being caused by, and located at, the orientation difference at the juncture of the free test length (which had rotated during testing) and the shoulder or head of the specimen (which had not rotated). The double shoulder on the three specimen shapes finally adopted (gauge length one, two, and five times the diameter of the specimen, see Fig. 6) placed a reasonably reproducible restraint on the ends of the free test length, and at the same time insured fracture at a point not concealed by the grip.

Vol. 2 53/54

of specimens (because of their different free length) and also changed as soon as slip became localized by necking or by the opening of a cleavage crack. The rate of shear, resolved in the slip direction on the slip plane, was of course different for different orientations.

3. Results and Discussion

A comprehensive presentation of the dependence of ductility (as measured by reduction in area) on temperature and orientation* is given in Fig. 8. Each of the surfaces in this model are discussed below :

(i) *The Ductile Plateau* (*Surface* A *in Fig.* 8)

At 95°C, for example, all crystals showed 100 per cent contraction in area irrespective of their starting orientation, although the elongation values were sharply dependent upon this variable (cf. Fig. 9 (*h*)). This behaviour is a result of the various processes by which zinc deforms from its initial orientation.

In the region of $\phi_0 = 80$ to 90°, specimens twinned with little or no preceding slip, and twinning and secondary slip (slip within the twinned region) led to a highly necked specimen having a low elongation and high contraction in area.

Crystals with starting orientation about 30° to 80° deformed first by primary slip and thereby elongated. Twin bands finally appeared and secondary slip within the twin band led immediately to necking and rupture. The contribution which the necked band made toward the elongation was minor and elongation data therefore may be taken as a first approximation to decide what is the proper criterion for the termination of primary slip. The shear strain, a, resolved on the slip plane, and the final orientation ϕ_f, corresponding to these elongation values, δ, re computed using equations (26/3) and (26/2) respectively of Schmid and Boas (1935)

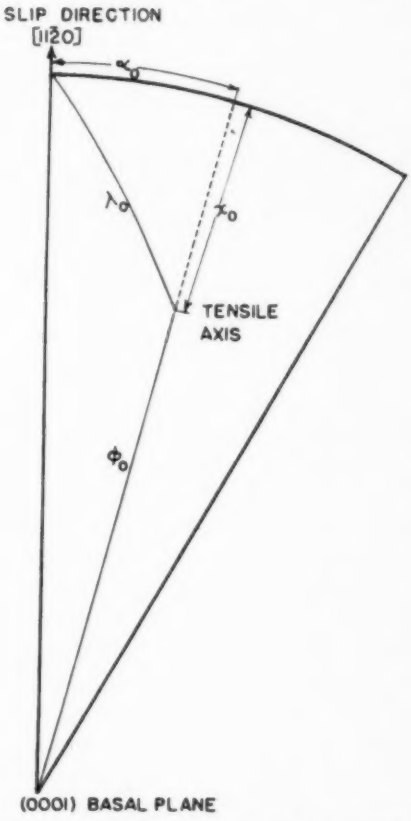

Fig. 7. Standard projection showing angles used in orientation determinations.

$$a = \frac{1}{\cos \phi_0}\left[(1+\delta)^2 - \sin^2 \lambda_0 - \cos \lambda_0\right]^{\frac{1}{2}} \qquad (1)$$

* In no case was any consistent variation of ductility with α_0 observed. Therefore in most of the following discussion orientation will be treated as if it were governed by ϕ_0 alone.

$$\cos \phi_f = \frac{\cos \phi_0}{1 + \delta} \tag{2}$$

and are plotted in Fig. 12 (*a*) and (*b*). The data clearly favour the constancy-of-final-orientation criterion. If that small portion of the elongation due to secondary slip and necking were subtracted from the total elongation values that were used, the decision would be even more clearcut, for the values of a would drop con-

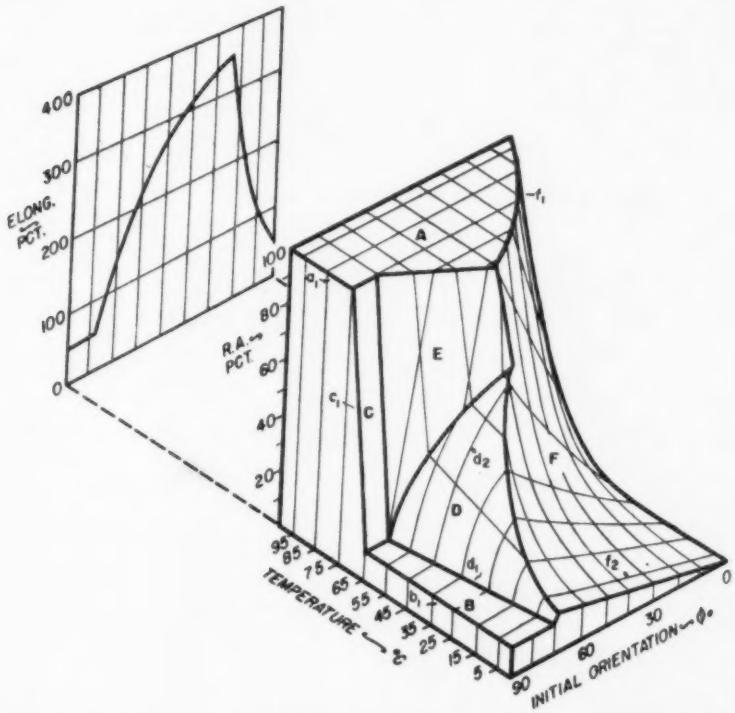

Fig. 8. Simplified representation of ductility (reduction in area) as a function of orientation and temperature for 5*D* specimens. Each surface *A*, *B* . . . *F*, is discussed in detail in the text. Section a_1, c_1, b_1, is taken from Fig. 19. Line d from Fig. 5, lines d_2 from Fig. 9, lines f_2 from Fig. 21.

siderably in the range of $60° < \phi < 80°$, whereas the values of ϕ_f would drop only a degree or two at high values of ϕ_0. All other elongation data reported in this paper give plots similar to Fig. 12, but are not reproduced here in the interest of economy.*

A more precise determination of the value of ϕ_f can be made from the ratio of the cross-sectional area when primary slip ceases, a_f, to the initial cross-sectional

* The choice between the two criteria considered here is of more importance than merely the choice between two criteria that in the manner in which they are observed are closely similar. The implication of a constancy-of-slip criterion is that twinning is set by a single standard: twinning occurs at a constant value of resolved shear stain or relatedly (because of the invariance of the resolved shear stress-resolved shear strain diagram) at a constant value of resolved shear stress or at a constant value of deformational energy (cf. MILLER 1936; THOMPSON and MILLARD 1952). The constancy-of-final-orientation implies that twinning is set by a comparative standard: twinning occurs when the ratio of streases on two different deformation systems is critical or is brought into a critical state by virtue of the particular final orientation (cf. BURKE and HIBBARD 1952).

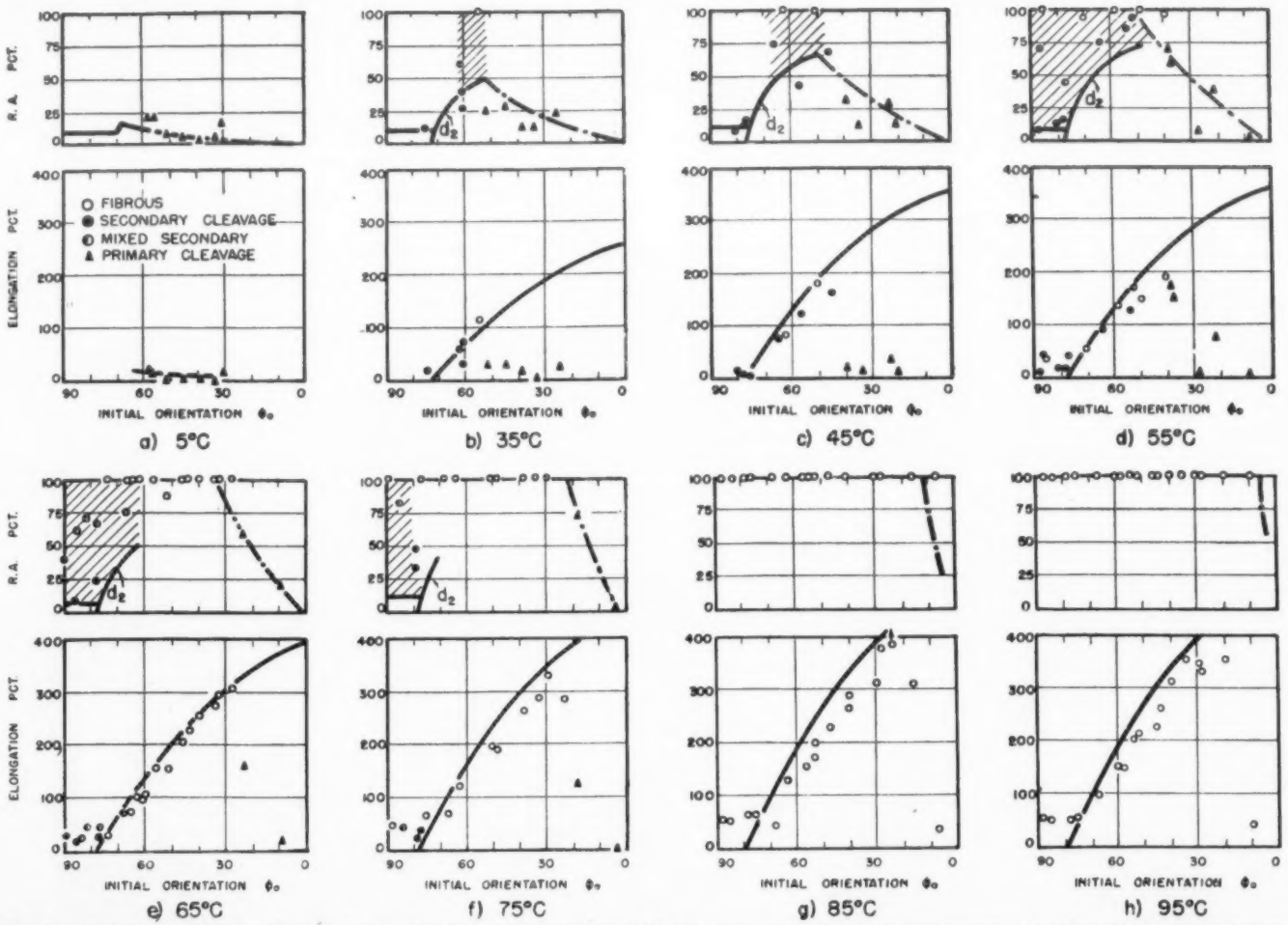

Fig. 9. Ductility (reduction in area and elongation) as a function of initial orientation, ϕ_0 at the temperatures indicated for $5D$ specimens. Solid lines represent ideal ductilities as computed by equations (2 or 3) of the text. In the case of elongations data conform to these curves whether fracture was brittle or ductile since localized neck of ductile fracture contributed little to elongation values. In the case of reduction in area only the brittle fractures conform to these curves, the ductile fractures falling above the curve to as high as 100 per cent. Shaded areas represent transition temperature zone where fractures may be either ductile or brittle and reduction in area values will fall between

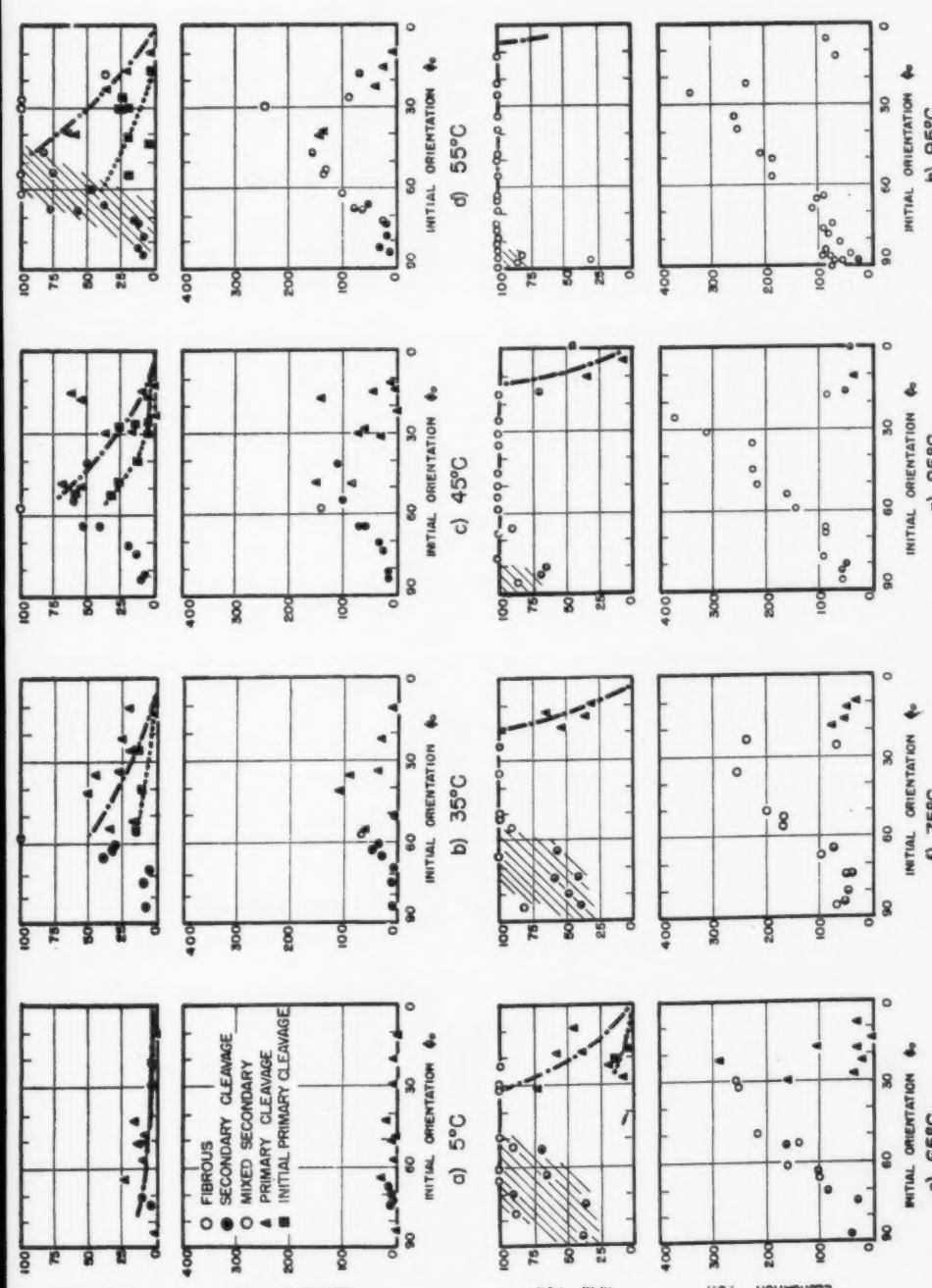

Fig. 10. Ductility (reduction in area and elongation) as a function of initial orientation, ϕ_0, at the temperatures indicated for $2D$ specimens. (Dot-dash curves are taken from Fig. 21, represent primary cleavage. Dotted curves indicate initial primary cleavage.)

Vol. 2 53/54

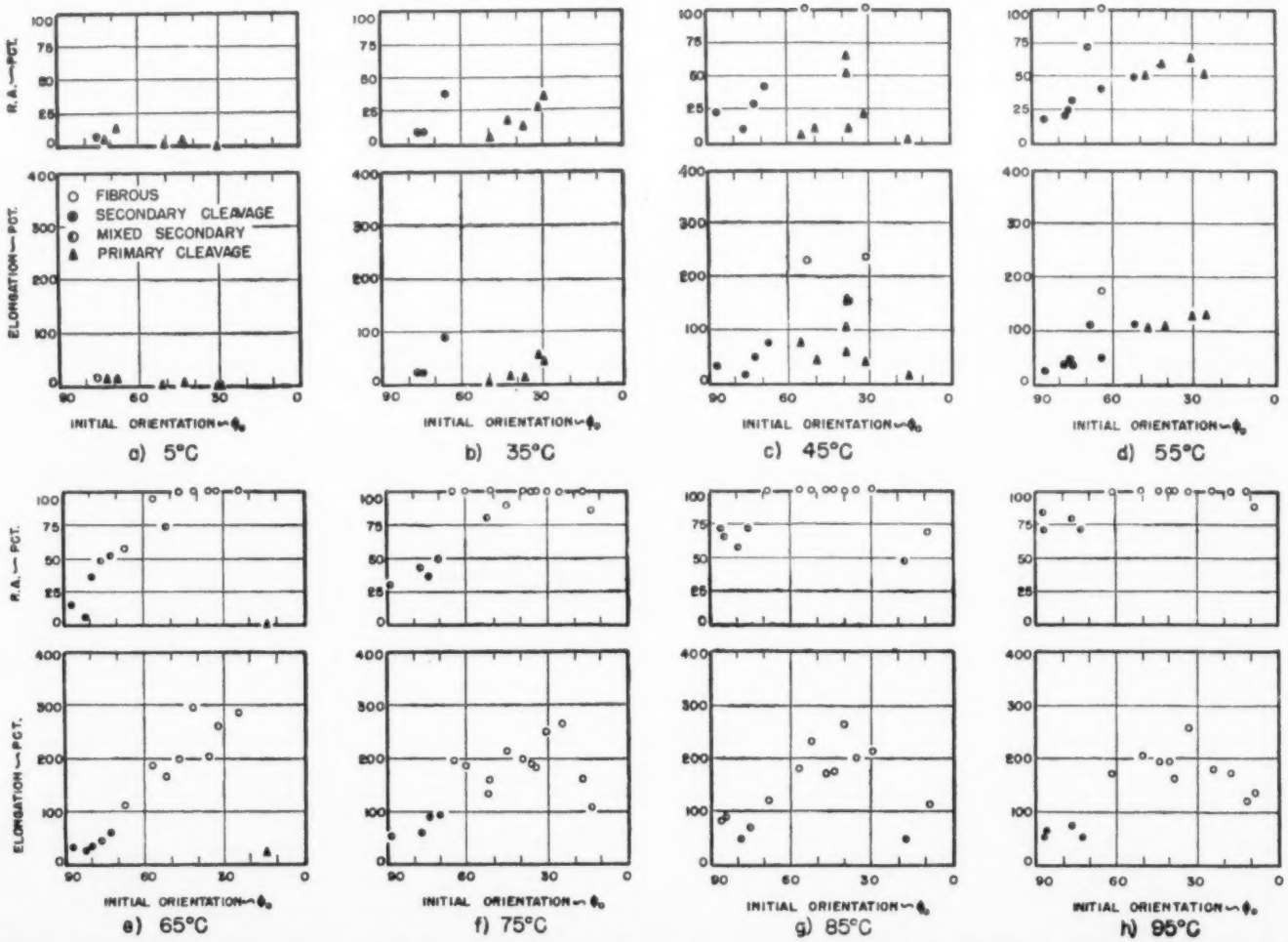

Fig. 11. Ductility (reduction in area and elongation) as a function of orientation ϕ_0, at the temperatures indicated for 1D specimens.

area, a_0, through the equation

$$\frac{a_0}{a_f} = \frac{\cos \phi_0}{\cos \phi_f} \tag{3}$$

(which follows directly from equation (2) under the assumption of constancy of volume). In the present case in place of the ratio of areas, the minor axis of the elliptical section of the uniformly deformed portion adjacent to the necked twin band was divided by the original diameter. Although this is not strictly proper unless $\alpha_0 = 0$, the error involved was less than half a degree in the majority of cases and in no case exceeded two degrees. The values of ϕ_f so determined are plotted on a standard stereographic projection of Fig. 13, where it has been assumed that the tensile axis rotated along a great circle as demanded by simple slip.

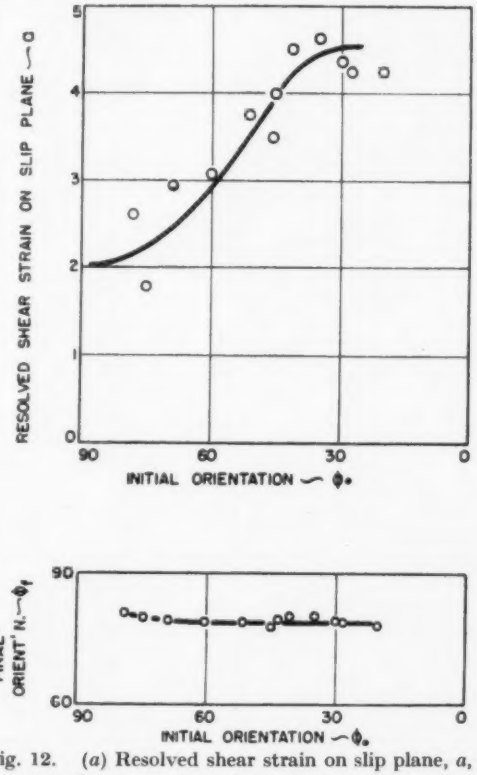

Fig. 12. (*a*) Resolved shear strain on slip plane, *a*, corresponding to the elongation values given in Fig. 9 (*h*) as computed by Equation (1) of the text. (*b*) Final orientation ϕ_f, computed from same elongation values by equation (2) of the text.

The shorter crystals – $2D$ and $1D$ gauge lengths – of this orientation range, $\phi_0 = 30$ to 80°, behaved in a similar way to the longer ones just described. They deformed by primary slip up to a constant final angle ϕ_f. Here the reduction due to necking however, occupied a greater proportion of the gauge-length and it was difficult to determine the amount of deformation due to slip alone, but measurements were taken and the values of ϕ_f calculated were slightly lower for the $2D$ and $1D$ crystals than for the $5D$ crystals.

In the range of initial orientations $\phi_0 = 0$ to 30°, crystals with a gauge-length five times their diameter deformed by primary slip up to a constant angle ϕ_f of 80°, twinned and failed by fibrous fracture with 100 per cent reduction in area. However, in these crystals the deformation was usually localized to a quite short length of the crystal.

During deformation of the shorter crystals ($1D$ and $2D$) in the orientation range, $\phi_0 = 0$ to 30°, longitudinal ridges near the shoulders were seen as shown in Fig. 14. Fig. 15 shows diagrammatically the slip lines visible before necking commenced. The upper set of ridges are those shown in Fig. 14. This specimen was cleaved by inserting a razor blade parallel to the slip planes at the temperature

of liquid nitrogen, and the sections obtained are shown in Fig. 16. It is seen that the ridges produced a number of " gable roofs " on these slip planes.

These ridges apparently form as a consequence of the following chain of events. Deformation takes place largely in the two regions, P and R in Fig. 15. Prior to

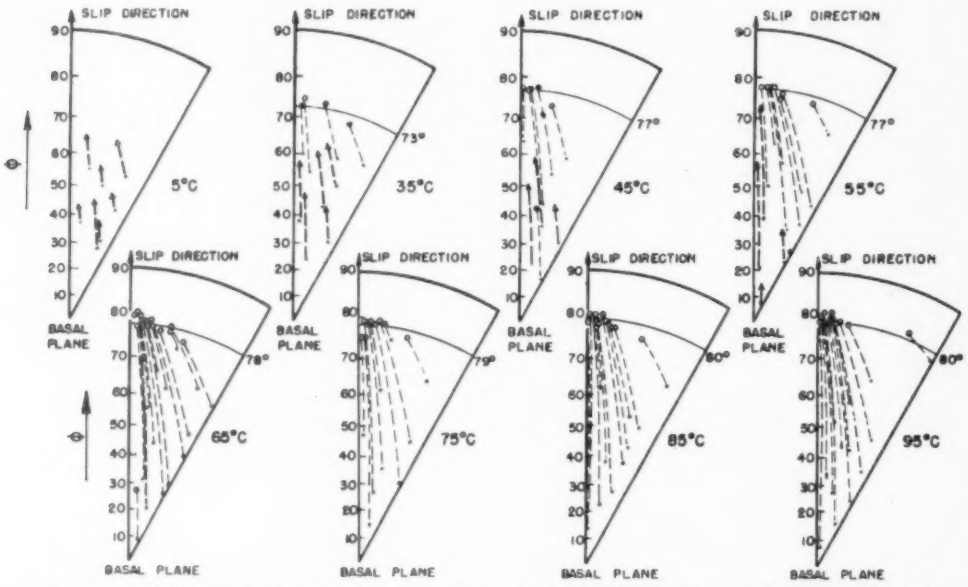

Fig. 13. Initial and final orientations of $5D$ specimens pulled at the temperatures indicated. Starting orientations are given by the dots. Final orientations given by open circles indicate specimens twinned and necked to give ductile fracture. Minor axis of cross-sectional ellipse of specimen next to twin (as at point A in Fig. 1 (d)) was used in equation (3) of text to determine final orientation. Final orientations given by solid circles indicate specimen twinned and cleaved and here minor axis of cross-sectional ellipse next to fracture was used to determine final orientation. Final orientations given by solid triangle indicate specimen failed by primary cleavage. Minor axis of cross-section ellipse was taken midway along test length.

the ridge formation a section near the top of the deformed region is as in Fig. 17 (a). The plane $ABCD$ is a kink-band boundary or bend-plane. If it assumes the position of lowest energy it bisects the angle between the slip-planes on either side of it (HESS and BARRETT 1949). As further slip takes place, the bend-plane tends to rotate in a clockwise direction (Figs. 15 and 17). The appearance of the sections in Fig. 16 seems to indicate that this movement is resisted at the surface of the crystal; the points A and C are effectively anchored,* so that the movement of B which is comparatively free gives rise to a curved bend-plane as shown in Figs. 16 (b), (c) and in Fig. 17 (b). But such a curved bend-plane is in a fairly high energy state, so that B will also reach a limit of movement dependent on the magnitude of the force tending to straighten $AB'C$. Then line $B'E'$ is unable to rotate further (clockwise about the fixed point B') as a result of slip, without shortening the length $E'C$ on the surface of the crystal. This shortening can only be accommodated by means of a buckling process as shown in Fig. 17 (c).

* HESS and BARRETT (1949) report a similar effect in the compression of zinc single crystals.

Vol.
2
53/54

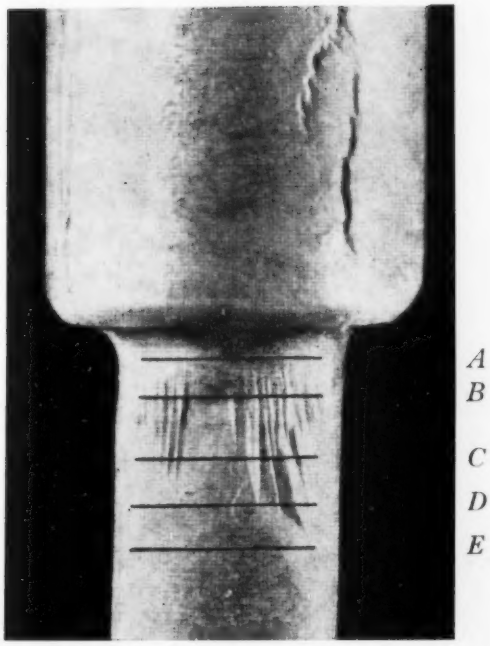

Fig. 14. Ridges formed at high temperature on $2D$ specimen with low orientation angle $\varphi_0 = 25°$, when pulled at 75°C magnification about 7 ×. Letters $a, b \ldots e$ represent the sections shown in Fig. 16 (a-e).

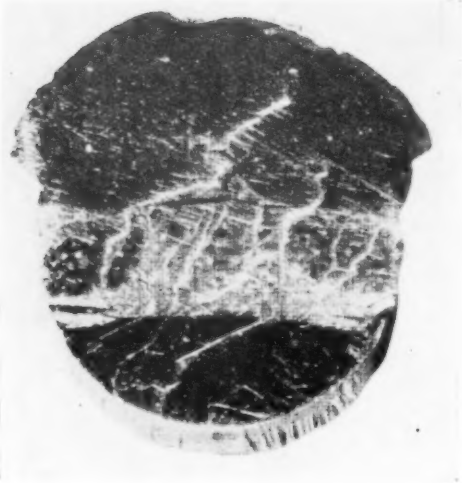

(a)

(b)

(c)

(d)

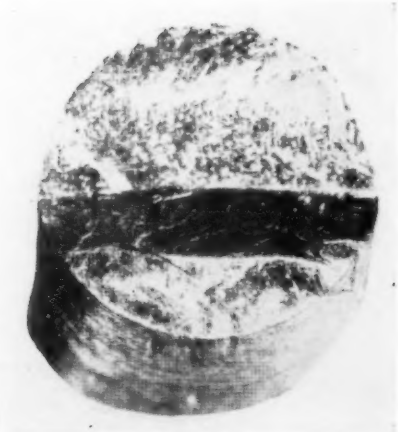

(e)

Fig. 16. Cleaved sections through ridged region of specimen shown in Fig. 14.

Vo
2
1953

The fact that ridges were observed only where the bend-plane was curved (cf. Fig. 16) is consistent with this theory. The buckling process need involve only basal slip (though in directions other than that of the primary operative slip). In that case the edge ***FGH*** should lie in a plane perpendicular to the surface ***FHJ***. The ridges in Figs. 16 (*b*) and (*c*) were examined under a binocular microscope and such appeared to be the case.

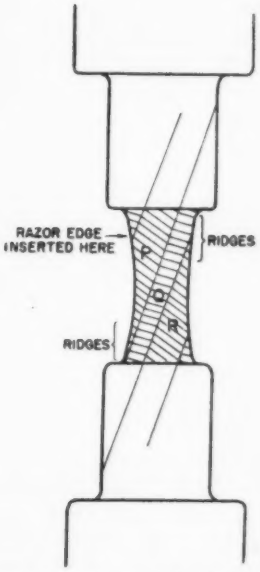

Fig. 15. Schematic drawings of slip lines visible on specimen shown in Fig. 14 before necking to fracture. Upper set of ridges are ridges visible in Fig. 14. Razor was inserted parallel to slip lines to give sections shown in Fig. 16.

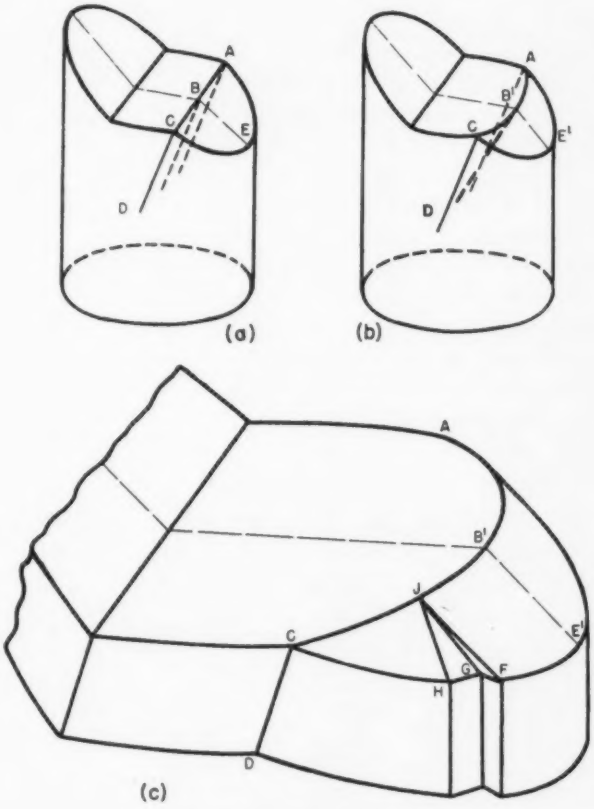

Fig. 17. The formation of a ridge.

(ii) *The Brittle Floor due to Secondary Cleavage* (*Surface* **B** *in Fig.* 8)

As test temperature was lowered, all of the above phenomena underwent changes. As may be seen in Figs. 9 to 11, the crystals with initial orientation $\phi_0 = 80$ to $90°$ became embrittled in the sense that their contraction in area dropped from 100 per cent to about 10 per cent. These crystals, which at higher temperatures necked by twinning and secondary slip, at lower temperatures simply twinned and cleaved on the basal plane of the twinned metal, generally midway along the gauge-length (Fig. 18). Cleavage in a crystal which has twinned will be designated as " secondary cleavage " as distinguished from " primary " basal cleavage which occurs in untwinned material.

(iii) *The Transition Cliff* (*Surface* C *in Fig.* 8)

The cliff (C) in Fig. 8 which denotes a transition between ductile and brittle behaviour for crystals with $\phi_0 > 80°$ is a simplification of the facts. From the plots of actual contraction in area data for $5D$ specimens in Fig. 9, for example, it is seen that secondary cleavage can occur at a temperature as high as 75°C, while in a statistical manner typical of transition behaviour in general, ductile fractures can occur at temperatures as low as 55°C. In this temperature range the fracture was often mixed secondary cleavage and fibrous.

Fig. 19 shows the contraction in area as a function of temperature for crystals with $\phi_0 > 80°$. The transition for crystals with $5D$ gauge-length was sharp covering the range 75 to 55°C, whereas for the $2D$ crystals it was more gradual, and for gauge-length $1D$ even more so, covering the range about 95 to 60°C.

(iv) *The Brittle Zone* D *in Fig.* 8

In this region of temperature and orientation the crystals would deform by primary slip to a critical terminating orientation, ϕ_f, twin, and then fracture by secondary cleavage.

Fig. 18. Schematic cross-section of crystal that failed by secondary cleavage.

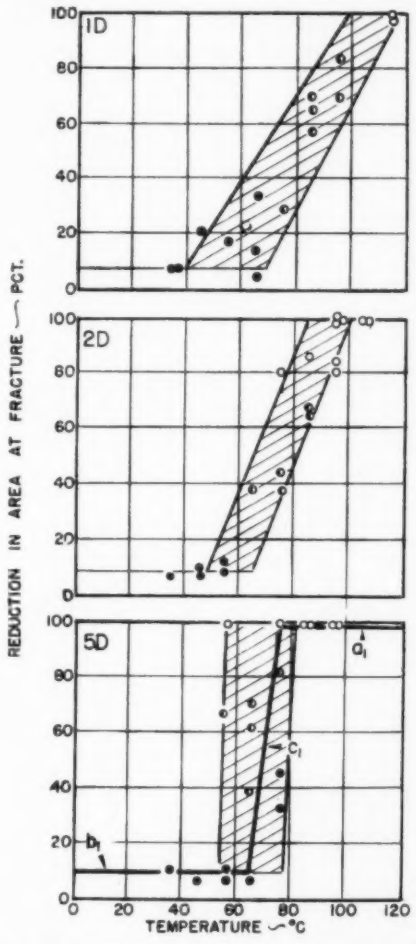

Fig. 19. Reduction in area as a function of temperature for specimens with initial orientation $\phi_0 \geqq 80°$. These data are cross plots of the data (for specimens $\phi_0 \geqq 80°$) given in Figs. 9, 10 and 11. Line a_1, b_1, c_1, drawn as a trend curve through the data points for $5D$ specimens is the same as Figs. a_1, c_1, b_1, in Fig. 8. The shaded areas correspond to the shaded areas at $\phi_0 \geqq 80°$ in Figs. 9, 10 and 11.

The critical orientation, ϕ_f, at which primary slip ended, though constant for a given temperature, decreased slightly with decreasing temperature as indicated by the skew course to line d_1 in Fig. 8. The experimentally determined values of

ϕ_f are shown in the stereographic projections in Figs. 13 and the mean values which were obtained are plotted as a function of temperature in Fig. 5 together with those of MARK, POLANYI and SCHMID (1923) and BOAS and SCHMID (1935).

Since specimens that broke in secondary cleavage showed no necking, equation (3) may be used to relate the reduction in area with initial orientation. Lines d_2 in Figs. 8 and 9 are computed by this equation using the average values of ϕ_f given in Fig. 13.

(v) *Transition Cliff* (*Surface* E *of Fig.* 8)

As in the case of crystals with $\phi_0 = 80$ to $90°$ there was a considerable temperature range where failure could be either ductile or brittle, but in the present case this range was displaced downward as ϕ_0 decreased. This trend can be seen in Fig. 9, for example, where crystals with orientations $\phi_0 > 80°$ have started to embrittle at 75°C whereas crystals with orientations $\phi_0 < 80°$ are still ductile ; and again at 45°C where crystals with high ϕ_0 are all brittle, while crystals with lower ϕ_0 ($\sim 60°$) are by and large relatively ductile. This is an interesting point ; it means that while a crystal whose orientation, ϕ_0, was initially greater than 80° would be brittle at a given temperature, one that rotated by primary slip from a lower value of ϕ_0 into the range $\phi > 80°$ remained ductile. In other words primary slip or some concomitant of primary slip allayed embrittlement due to secondary cleavage.

vol.
2
53/54

(vi) *Primary Cleavage Slope* (*Surface* F *of Fig.* 8)

The crystals in this region would commence to rotate by primary slip, the orientation gradient developed at the shoulder would be accommodated at first by bend planes, but soon the crystal would cleave on its basal plane in the vicinity of the bend plane as shown in Fig. 20 (*c*). The type of crack shown in Fig. 20 (*c*) at "*g*" would result when a bend-plane becomes fixed in one position. To maintain the position of lowest energy the bend-plane should rotate during extension of the crystal so as to bisect the slip planes on either side of it.* Should it fail to do so, large stresses will be developed as slip proceeds on one side of it (cf. KOEHLER 1952). Evidence of such stresses can be judged, not only from considerations of geometry, but also from BURKE and HIBBARD's (1952) work on magnesium single crystals. These authors found bend-planes near the grips of a tensile specimen where constraint was greatest and further observed twins on the relatively unslipped side of the bend-plane, which twins terminated at the bend-plane precisely. Magnesium can only form twins if there is extension in the direction normal to the basal plane. This indicates that, on the unslipped side of the boundary, there is a tensile stress perpendicular to the basal plane which can cleave the sample as shown in Fig. 20 (*c*).

Thus it appears that the accommodation of orientation gradients by bend-planes involves not only the formation of the planes but their ability to rotate also.

The reduction in area of the test specimen was taken at the moment of the initial primary cleavage of the crystal and is a measure of the amount of rotation

* A large number of bend planes were found, however, that did not always lie so disposed.

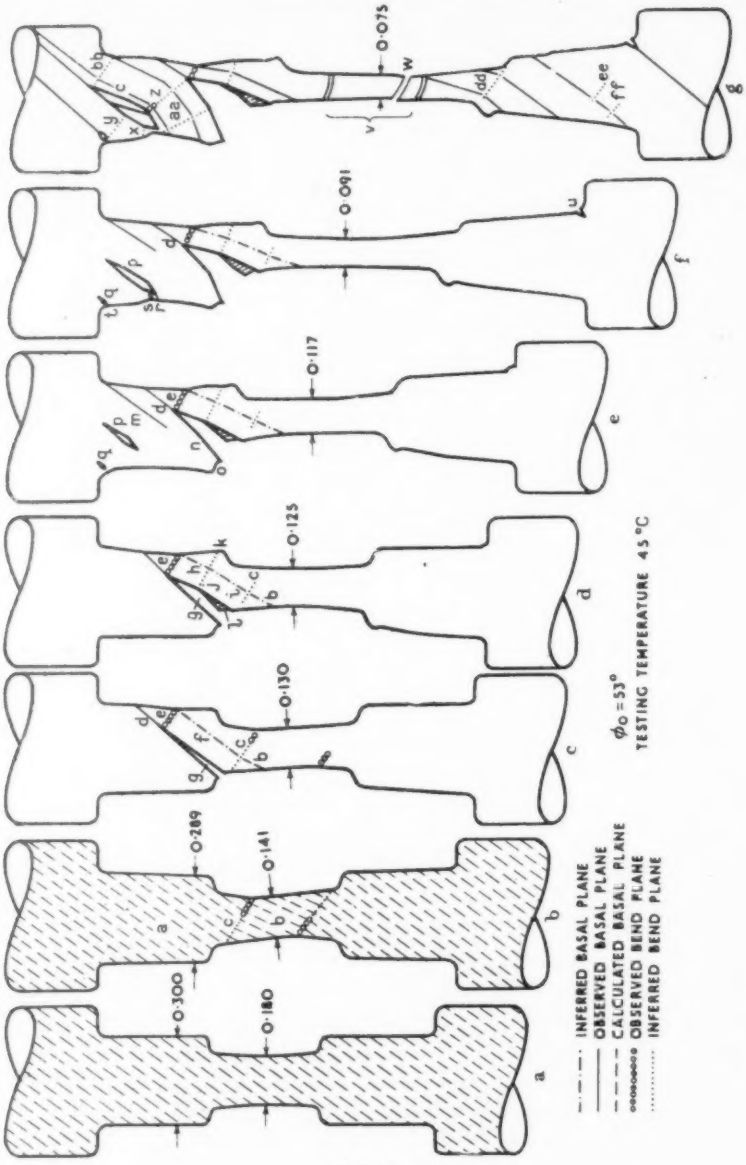

Fig. 20.

(*a*) This is the undeformed crystal of original orientation $\phi_0 = 53°$ before being tested at 45°C.
(*b*) The slip lines (a) were calculated from the original orientation and the reduction in diameter of the shoulder from 0·300 to 0·289 in. by equation (3). In a similar manner, slip lines (b) were calculated for the test section which was reduced in diameter from 0·180 to 0 141 in. Bend plane (c) was directly observed in part (as shown by the circles) and then extrapolated (as shown by the dots). The lower half of the specimen was offset from the upper in respect to the longitudinal axis.

(*c*) A crack (g) appeared in the upper shoulder. Slip line (d) was a projection of the crack and directly visible. Slip line (f) was drawn parallel to crack (g). Slip line (b) was calculated in a way similar to those in (*b*).

(*continued on opposite page*)

which the test length suffered before cleavage appeared. These values are shown in Fig. 10 for the $2D$ specimens.

Once the primary cleavage commenced, one of three courses would be followed to complete fracture of the specimen.

(*a*) On further elongation of the specimen cleavage would continue as an extension of the original crack. The reduction in area value was again taken on the test section (even though the fracture was in the shoulder) and is a measure of the amount of rotation which the test length suffered before cleavage completely severed the crystal. These values are plotted in Figs. 9, 10 and 11 and form surface F in Fig. 8, and the curves shown in Fig. 21. The latter plots show that primary cleavage is not affected by the length-to-diameter ratio of the test specimen.

(*b*) On further extension of the specimen, the orientation gradients would be accommodated by bend planes or systems of bend planes forming in the now reduced cross-section near the partial fracture to such an extent that the test section rotated until it reached the critical value of ϕ_f, twinned and fractured by secondary cleavage (see Fig. 20 (*g*)). Reduction in area values in this case form surfaces D and E near their intersection with surface F in Fig. 8.

(*c*) Events would proceed as in (*b*) except that, having twinned, the metal would not suffer secondary cleavage, but rather would undergo secondary slip giving a completely ductile neck, *i.e.*, 100 per cent fracture. Reduction in area values in this case form surfaces A and E near surface F in Fig. 8.

It is felt that in the absence of primary cleavage (*i.e.*, in tensile tests in which

Vol. 2 53/54

Fig. 20 continued.

(*d*) The section of the specimen immediately below the bend plane (e) rotated and slipped causing the observed bend plane (e) to pivot, toward the slip line (d). During the pivotting it was inferred that slip line (f) bent into two segments (h) and (i). These were obtained by drawing lines parallel to the bottom face of crack (g). Lines (h) and (i) were divided by bend plane (j) which was constructed from the discontinuity in the lower face of crack (g) to bisect the angle made by (h) and (i). Bend plane (e) disappeared from view which was consistent with the lessening of inferred angular difference between slip planes (b) and (i). The shoulder protruded at (k) as a result of these events. A lip (l) (shown by the shading) was produced where the shoulder meets the lower face of crack (g).

(*e*) As the processes of (*d*) continued, slip line (d) was observed to rotate counterclockwise, indicating deformation and rotation in the shoulder above the crack. Slip line (m) parallel to (d) became visible. The upper face of crack (g) bent at (n). At (o) the shoulder moved upwardly and outwardly. Cracks (p) and (q) appeared.

(*f*) As the processes in (*d*) and (*e*) continued,crack (p) extended toward the surface and propagated a slip line (r) and a small bend plane (s). The small crack (q) developed a tiny bend plane (t). A small crack (u) appeared in the lower head.

(*g*) Further deformation produced twinning in the region (v) and finally secondary cleavage on the basal plane (w) of the twinned metal. The specimen was cooled in liquid nitrogen and cleaved with a razor blade. The silhouettes of the cleft basal planes were traced and are drawn in as light weight solid lines. These revealed the bend planes (x), (y), and (z) meeting crack (p) at points of discontinuity. Bend plane (aa) accounted for the change at (n) in the upper face of crack (g). Bend planes (aa) and (z) permitted shoulder (o) to peel back. Lip (cc) on the lower face of crack (p) was similar to lip (l). Bend planes (dd), (ee), and (ff) appeared in the lower shoulder. The total reduction in area was 54 per cent. It is seen that the original crack (g) never grew in length once it had been formed.

rotation in the grips is not prevented) surface *F* would not appear in Fig. 8 and surfaces *A*, *E* and *D* would be extended to lower temperatures as suggested in Fig. 22.

The inability of bend-planes to accommodate orientation gradients in zinc as temperature is lowered and the appearance of primary cleavage is of enormous importance, for it at once gives a clue to why secondary cleavage appears. Second-

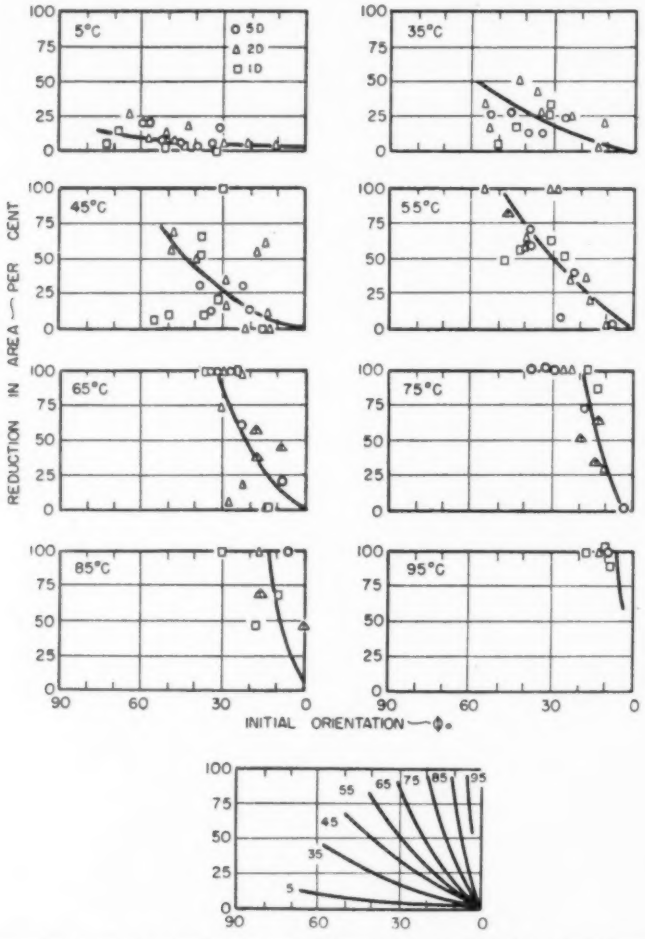

Fig. 21. A composite plot of reduction in area values for 5*D*, 2*D* and 1*D* specimens which failed by primary cleavage. The data taken from Figs. 9, 10 and 11. show the negligible effect of gauge length on values obtained.

ary and primary cleavage both occur on the basal plane. They both occur in regions adjacent to orientation gradients : primary cleavage in the shoulder where slip is restricted in the broader portion of the crystal, secondary cleavage in a twin band where orientation gradients must develop adjacent to the twin boundaries to maintain compatibility (PRATT and PUGH 1951, 1952). It is proposed therefore that secondary cleavage is fundamentally the same as primary cleavage,

the only difference being the manner in which the orientation gradient which induces basal cleavage is developed.

The inability of bend planes to accommodate orientation gradients as temperature is lowered is of importance, too, in the case of polycrystalline specimens, since here orientation gradients are as numerous as the grains of the sample at hand, being a common mode by which compatibility between the grains is effected (KAWADA 1951; BARRETT and LEVINSON 1940; WOODWARD 1949; HONEYCOMBE 1950; LAURENT and EUDIER 1950; KING and CHALMERS 1948; CHALMERS 1937; WASHBURN and PARKER 1951). If these gradients cannot be accommodated by kinking, cleavage may be expected to result. It is to be expected that the conditions for cleavage in different grains will be reached at different stages in a polycrystalline aggregate. HOMES and GOUZOU (1950) have shown by direct observation of the process of fracture that this is the case for zinc below the transition temperature. It was not until a large number of "premature" cracks had formed that rapid cleavage cut through the remaining grains.

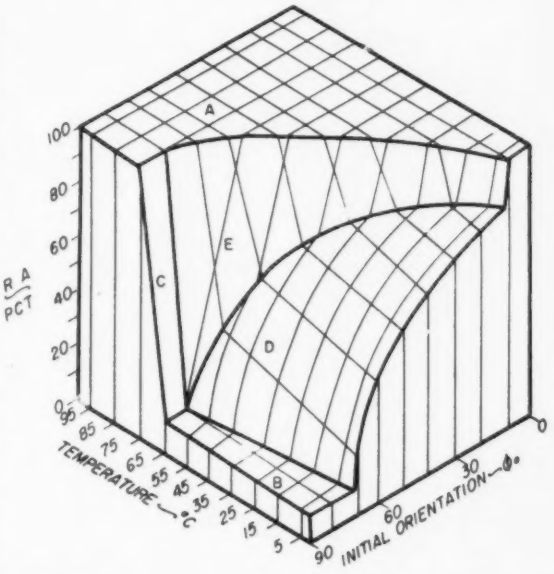

Fig. 22. Suggested course to Fig. 8 in the absence of primary cleavage induced by constraint of shoulders or grips.

Vol. 2 53/54

ACKNOWLEDGMENTS

This investigation was sponsored by the Ship Structure Committee through a Bureau of Ships United States Navy Department contract and was conducted with the advice of the Committee on Ship Steel of the National Academy of Sciences – National Research Council. The opinions expressed are those of the authors and do not necessarily represent the opinions of the Committee on Ship Steel, the Ship Structure Committee or any of its member agencies.

The authors thank F. KARPOFF, I. ROZALSKY and C. A. PHALNIKAR for assistance in the preparation and testing of specimens.

REFERENCES

BARRETT, C. S., ANSEL, G. and MEHL, R. F. 1937 *Trans. A.S.M.*, **25**, 702.

BARRETT, C. S. and LEVENSON, L. H. 1940 *Trans. A.I.M.E.*, **137**, 112.

BURKE, E. C. and HIBBARD, W. R. 1952 *Trans. A.I.M.E.*, ,**194** 295.

BOAS, W. and SCHMID, E. 1929 *Z: Physik*, **54**, 16.

BOAS, W. and SCHMID, E.	1930	*Z. Physik*, **61**, 767.
CHALMERS, B.	1937	*Proc. Roy. Soc.*, **A162**, 120.
DAVIDENKOV, N. N.	1938	*Problems in Impact*, Izdatel 'stro Akademii Nauk SSSR, Moscow and Leningrad, 16.
FAHRENHORST, W. and SCHMID, E.	1930	*Z. Physik*, **64**, 845.
FRIDMAN, Y. B.	1946	*Zhur. Tekh. Fiz.*, **11**, 985.
GILMAN, J. J. and READ, T. A.	1952	*Trans. A.I.M.E.*, **194**, 875.
HESS, J. B. and BARRETT, C. S.	1949	*Trans. A.I.M.E.*, **185**, 599.
HONEYCOMBE, R. W. K.	1950	*Proc. Phys. Soc.*, **A63**, 672.
HOMES, G. A. and GOUZOU, J.	1950	*Revue de Metallurgie*, **47**, 678.
KAWADA, T.	1951	*Proc. First World Metallurgical Congress A.S.M.*, 591.
KING, R. and CHALMERS, B.	1949	*Progress in Metal Physics, Vol. I*, Chapter 3 (Pergamon Press Ltd.).
KOEHLER, J. S.	1952	*Phys. Rev.*, **85**, 3.
KOLESNIKOV, A. F.	1938	*Zhur. Eksp. i Teort. Fiz.*, **8**, 1031.
KUNTZE, W.	1928	*Arch. Eisenhüttenwesen*, **2**, 109.
LAURENT, R. and EUDIER, M.	1950	*Revue de Metallurgie*, **47**, 582.
LOW, J. R., Jr. and FEUSTEL, R. G.	1953	*Acta Metallurgica*, **1**, No. 2, 185.
LIFSHITS, I. M.	1948	*Zhur. Eksp. i Teort. Fiz.*, **18**, 1135.
MARK, H., POLANYI, M. and SCHMID, E.	1923	*Z. Physik*, **12**, 58.
MATHEWSON, C. H. and PHILLIPS, A. J.	1927	*Proc. Inst. Met. Div. A.I.M.E.*, 143.
MCADAM, D. J.	1942	*Trans. A.I.M.E.*, **150**, 311.
MILLER, R. F.	1934	*Trans. A.I.M.E.*, **111**, 135.
MILLER, R. F.	1936	*Trans. A.I.M.E.*, **122**, 176.
O'NEILL, H.	1926	*J. Iron and Steel Inst.*, **113**, 417.
OROWAN, E.	1942	*Nature*, **149**, 643.
PRATT, P. L. and PUGH, S. F.	1951	*J. Inst. Metals*, **80**, 653.
ROSE, G.	1868	*Abhandl. d. Konigl. Akad.* 1 Wissenschaft, 57.
SCHMID, E. and BOAS, W.	1935	" Kristallplastizitat mit besonderer Berücksichtigung der Metalle " (Julius Springer, Berlin) ; " Plasticity of Crystals with Special Reference to Metals " (Translation by F. A. Hughes and Company Ltd., London, 1950).
SHEVANDIN, E.	1940	*Zhur. Tekh. Fiz.*, **10**, 396.
THOMPSON, N. and MILLARD, D. J.	1952	*Phil. Mag.*, **43**, 422.
VITMAN, F. and STEPANOV, V.	1939	*Zhur. Eksp. i Teort. Fiz.*, **9**, 1070.
WOODWARD, D. H.	1949	*Trans. A.I.M.E.*, **185**, 722.
WASHBURN, J. and PARKER, E. R.	1952	*Trans. A.I.M.E.*, **194**, 1076.
YAKUTOVICH, M. T. and YAKOVLEVA, Y. S.	1950	*Zhur. Tekh. Fiz.*, **20**, 16.

Vol 2 1953

Journal of the Mechanics and Physics of Solids, 1954, Vol. 2, pp. 197 to 211. Pergamon Press Ltd., London.

THE PLASTIC YIELDING OF METAL JUNCTIONS DUE TO COMBINED SHEAR AND PRESSURE

By A. P. Green
British Iron and Steel Research Association, Sheffield

(*Received* 10*th February*, 1954)

Summary

Plane strain and plane stress solutions are obtained for the plastic yielding of a junction connecting two relatively massive blocks of plastic-rigid metal. The work is part of a detailed analysis (Green 1954a) of the Bowden-Tabor junction model for sliding between unlubricated metals. The aim of this paper is to estimate the forces exerted through junctions during sliding. Various simple shapes of junctions are considered and the effect of a plane of weakness across the centre of the junction is discussed. The theoretical modes of deformation are confirmed experimentally in various cases.

Vol. 2 53/54

1. Introduction

According to Bowden, Moore and Tabor (1943), friction between unlubricated metals is primarily due to the plastic deformation of minute asperities on the sliding surfaces. Junctions are formed between the two metals wherever these asperities engage and adhere more or less strongly under the intense local stresses. Each junction goes through a " life-cycle " of formation, plastic deformation, and fracture, new junctions being formed as fast as the old ones are broken. The present theoretical investigation was undertaken in order to obtain an estimate of the forces exerted through such junctions at various stages of their life-cycles. It is part of a detailed analysis of the junction model which is fully described elsewhere (Green 1954a).

It is assumed for simplicity that the metal is rigid up to a sharp yield-point after which it deforms plastically without hardening. Solutions are obtained under the following two extreme conditions :

(i) *Plane Strain*

The strain is assumed to be zero in the width direction, perpendicular to the direction of relative motion of the two sliding blocks of metal and parallel to their surfaces (Fig. 1). A good approximation to this condition is obtained if the cross-section of the junction in the plane of flow is uniform across its width, and if the width is large in comparison to the dimensions in this plane.

(ii) *Plane Stress*

The stress in the width direction is assumed to be zero and the width uniform. This condition is only achieved if the width is small compared with the other

dimensions of the junction. Uniformity of width could not, of course, be maintained in practice since the deformation would cause thickening in some parts and thinning in others.

The problem, therefore, consists of constructing fields of characteristics* in the junctions to satisfy the various stress and boundary conditions which depend on :

(a) *The shape of the junction.* There is at present no method of calculating the changing external shape of a junction as it deforms. Therefore, separate plastic yield-point solutions are found for certain simple shapes, from which an overall picture of the life-cycle of the junction can be deduced. Only those shapes are considered for which yielding takes place in a *single* continuous zone extending across the minimum section of the junction. If the junctions are sufficiently long and thin there may be *two* zones of deformation separated by a rigid central region. Solutions of this kind are described by the writer in an analysis of the plastic yielding of cantilevers (GREEN 1954b).

(b) *The strength of adhesion.* A junction is regarded as strong or weak according to whether or not the adhesion is strong enough to prevent relative sliding at the interface. Solutions are obtained for both strong and weak junctions.

(c) *The relative motion of the two blocks of metal which the junction connects.* It is assumed that there is no relative rotation of the blocks, such as occurs in rolling contact. Two situations are examined. First, during the initiation of sliding the direction of relative translation of the two blocks is inclined to their surfaces at a finite angle, γ say (Fig. 1). Second, when a steady state of sliding is reached the blocks move parallel to their surfaces, *i.e.* $\gamma = 0$.

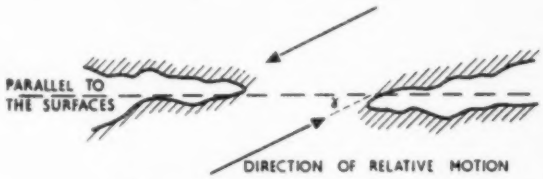

Fig. 1. Diagram of a junction.

In all the following solutions it has been checked that the rate of plastic work is positive throughout the deforming regions defined by the fields of characteristics. The state of stress outside these regions, however, has not been examined. It is possible, therefore, that the total rate of plastic work is overestimated (HILL 1951), *i.e.* the forces exerted through the junction in the direction of relative motion of the two blocks may be overestimated, while the force perpendicular to this direction, which does no work, may be over- or under-estimated. The possibility of error is diminished by the fairly good agreement between theory and experiment for some of the solutions, and it seems unlikely that any of the solutions that satisfy all the boundary conditions are seriously in error.

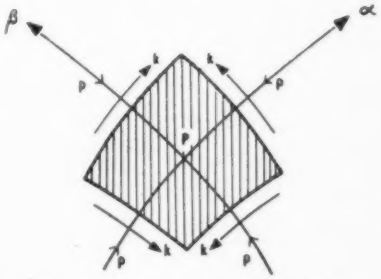

Fig. 2. Curvilinear element in a slip-line field.

* For an account of the theories of plane strain and plane stress see R. HILL, "The Mathematical Theory of Plasticity," Chapters VI and IX (Clarendon Press, Oxford).

2. Plane Strain Solutions

In the plastically deforming regions the state of stress in any element is a pure shear stress, k combined with a hydrostatic pressure p; this maximum shear stress, k, is constant and the distribution of p is defined by the slip-line field. Following the usual notation, the two sets of orthogonal slip lines (the lines of maximum shear stress), are labelled α- and β-lines, the α and β sets being distinguished by the directions of the maximum shear stress acting on a curvilinear element bounded by slip lines (Fig. 2). Let ϕ be the anti-clockwise angular rotation of an α-line from some fixed direction. The variation of p along a slip line is governed by the Hencky relations,

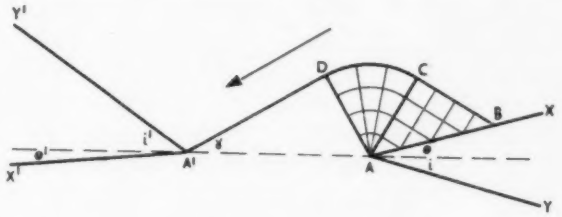

Fig. 3a. Slip-line fields for a strong junction with wedge-shaped sides.

$$\left.\begin{aligned} p + 2k\phi &= \text{constant along an } \alpha\text{-line} \\ p - 2k\phi &= \text{constant along a } \beta\text{-line} \end{aligned}\right\} \qquad (1)$$

The mode of deformation can be calculated with the aid of Geiringer's equations for the components of velocity along the slip lines (Hill 1950, p. 136).

(a) *Strong junction with wedge-shaped sides*

Consider a junction whose shape in the plane of flow is defined by wedge-shaped sides XAY and $X'A'Y'$ (Fig. 3a). The acute angles which the sides XA, YA, $X'A'$ and $Y'A'$ make with AA' are denoted by θ, i, θ', and i' respectively. We suppose, for the moment that AA' is parallel to the surfaces of the sliding blocks.

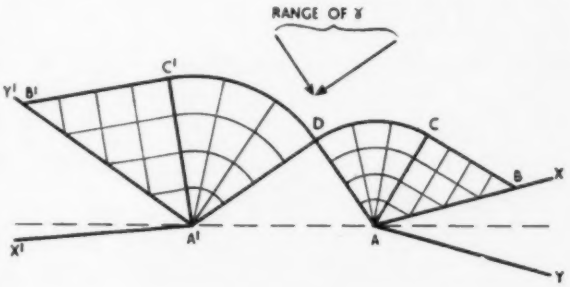

Fig. 3b. Slip-line fields for a strong junction with wedge-shaped sides.

If $\theta > \theta'$ the slip-line field shown in Fig. 3a is a possible yield-point solution. A similar field with part of $A'X'$ instead of AX plastic would certainly be invalid since the yield-point loads would be higher for any value of γ. In ABC the field, which is determined by the straight stress free edge AB, consists of straight lines inclined at angles $\frac{1}{4}\pi$ to AB. It is extended round the singularity at A to form the region ACD consisting of straight lines and circular arcs, and is completed by the straight slip line $A'D$ which is perpendicular to AD. If the lower block is regarded as fixed, the upper block moves parallel to $A'D$ and there is a

velocity discontinuity across $A'DCB$. If the direction of motion is from D to A', as shown in the figure, $A'D$ is a β-line and $p = k$ in ABC (reversing the direction of motion merely reverses the signs of all the stresses and velocities in the deforming regions, so that α-lines become β-lines and vice-versa). Using the Hencky relations (1) along CD, it is found that on $A'D$ and AD

$$p = k\,(1 + \tfrac{1}{2}\pi + 2\gamma - 2\theta). \tag{2}$$

By resolving the forces acting across these latter two slip lines, it is found that the mean stresses, p_1 and s_1 normal (compressive) and tangential to AA', exerted through the junction across its breadth t (AA'), are

$$p_1 = k\,(\sin 2\gamma + 1 + \tfrac{1}{2}\pi - 2\theta + 2\gamma), \qquad s_1 = k \cos 2\gamma. \tag{3}$$

The range of values of γ over which this solution is valid depends on the geometry of the junction. Since the angle CAD must be positive, γ must be greater than $\theta - \frac{1}{4}\pi$. This is the lower limit for γ if $\theta > \frac{1}{4}\pi$; otherwise the lower limit is $\gamma = 0$, when the slip-line field degenerates into the single straight line AA'. This degenerate solution may be expected to be valid for values of p_1 between $k\,(1 + \frac{1}{2}\pi - \theta)$ and zero (also, of coures, for negative values of p_1 over a range depending on the value of i or i'). The upper limit occurs when the field can first be extended to one of the sides AY or $A'Y'$, (Figs. 3b and 3c), *i.e.* when

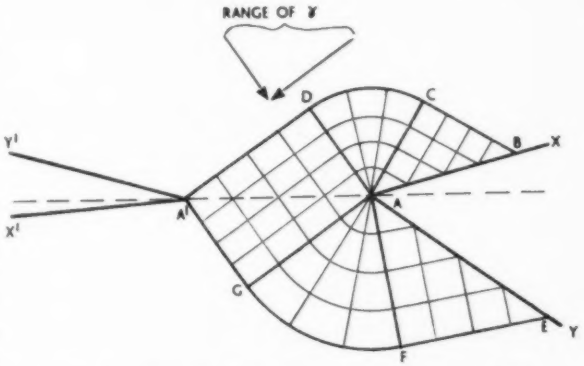

Fig. 3c. Slip-line fields for a strong junction with wedge-shaped sides.

$$\left.\begin{aligned} \gamma &= \tfrac{1}{4}\pi + (\theta - i) \quad \text{if} \quad i > i', \\ \text{or} \quad \gamma &= \tfrac{1}{4}\pi + (\theta - i') \quad \text{if} \quad i > i'. \end{aligned}\right\} \tag{4}$$

If s_1 and p_1 are plotted from a fixed origin 0, to the same scale and parallel to the directions in which they act, the end point p of their resultant vector represents a possible yield-point state. The curve traced out by P representing all possible yield-point states may be regarded as the yield locus of the given junction. A typical yield locus is shown in Fig. 4 for a junction with $\theta = 5° \geqslant \theta'$ and $i = 10° \geqslant i'$.

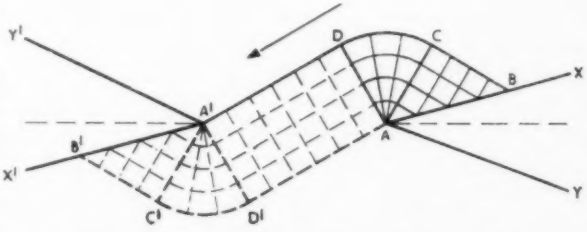

Fig. 3d. Slip-line fields for a strong junction with wedge-shaped sides.

The locus is symmetrical about the origin 0, since the material is assumed to be isotropic. It can be shown, by differentiating equations (3) with respect to γ, that the direction of motion of the upper block corresponding to a yield-point state P, is normal to the locus at P and directed outwards. According to the maximum work principle for a finite plastic-rigid body this property of the yield locus would be true for a set of *actual* yield-point states. This does not prove, however, that the solutions found are the actual ones since it is possible (though unlikely) that the yield criterion is violated in the rigid regions where no stress distribution has been constructed.

When $\theta > \frac{1}{4}\pi$, the solutions for $\gamma < \theta - \frac{1}{4}\pi$ are not known except for certain symmetrical junctions when $\gamma = p_1 = 0$ and $\theta \geqslant 75°$ (see Section 2b). However, an upper bound* to the relation between p_1 and s_1 is provided by the fictitious deformation consisting of the sliding of the two halves of the junction over a single straight slip line through A' which is inclined at the angle γ ($< \theta - \frac{1}{4}\pi$) to $A'A$. The least upper bound for a given value of p_1/s_1 is obtained by putting $2\gamma = \tan^{-1}(p_1/s_1) + \theta - \frac{1}{4}\pi$. The corresponding overestimates of p_1 and s_1 are

$$\left.\begin{aligned} p_1{}^x &= \frac{k \sin\theta \cos(\theta - 2\gamma)}{\sin^2(\theta - \gamma)} \\ \text{and} \quad s_1{}^x &= \frac{k \sin\theta \sin(\theta - 2\gamma)}{\sin^2(\theta - \gamma)} \end{aligned}\right\} \quad (5)$$

The larger θ and the smaller p_1/s_1 the worse these estimates may be expected to be.

According as i is less than or greater than i', the slip-line field shown in either Fig. 3b or Fig. 3c is valid, for a range of γ extending $\frac{1}{2}\pi$ above the appropriate limit given by (4). As γ varies in this range, p_1 and s_1 remain constant, though the velocity solution naturally depends on γ. Over the remaining range of γ up to $\gamma = \pi$ the solution is of the same type as that shown in Fig. 3a, but it extends to AY or $A'Y'$ instead of to AX.

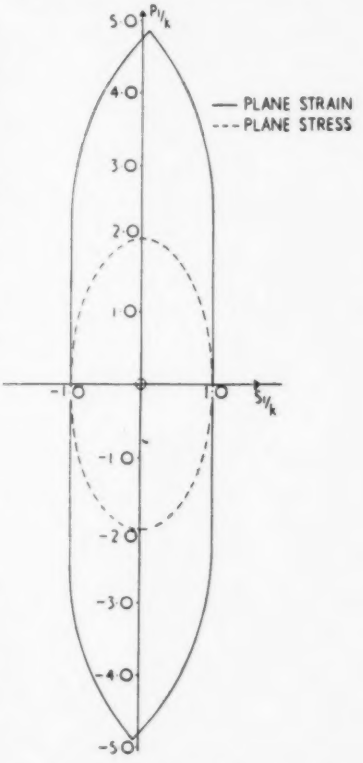

Fig. 4. Yield loci for a strong junction with wedge-shaped sides ($\theta = 5° \geqslant \theta'$ and $i = 10° \geqslant i'$).

The velocity solutions associated with the slip-line fields discussed so far are uniquely defined by Geiringer's equations and the condition that the velocities normal to the slip lines defining the plastic-rigid boundaries are continuous across them. Deformation occurs only along the velocity discontinuities and in the regions where the slip lines are curved; the regions where both families of slip lines are straight move as rigid blocks. If, however, $\theta = \theta'$ fields which extend to XA can also be extended to the side $X'A'$ (Fig. 3d), and the associated velocity solutions

* See R. Hill (1951, *Phil. Mag.* 42, 868) for an account of the method of calculating upper and lower bounds to the yield-point loads for a plastic-rigid body.

are then no longer uniquely defined (and similarly if $i = i'$). It seems likely that in a work-hardening material deformation would rapidly spread over the whole of this extended region, even if it were momentarily localized in some part of it when yielding began. It should be emphasized that the theoretical ambiguity of the velocity solution is removed if there is the smallest difference between θ and θ' or if one of the sides is not perfectly straight.

If the junction were formed between two metals of unequal hardness, with AA' as the interface between them the solutions are similar. Yielding would most likely be confined to the softer half and the loads would then be governed by slopes of the edges on this side only. There would be no ambiguity about the velocity solutions.

(b) *Strong Symmetrical Junctions*

Let us now consider solutions for junctions which are symmetrical about axes parallel and perpendicular respectively to the surfaces of the blocks. When

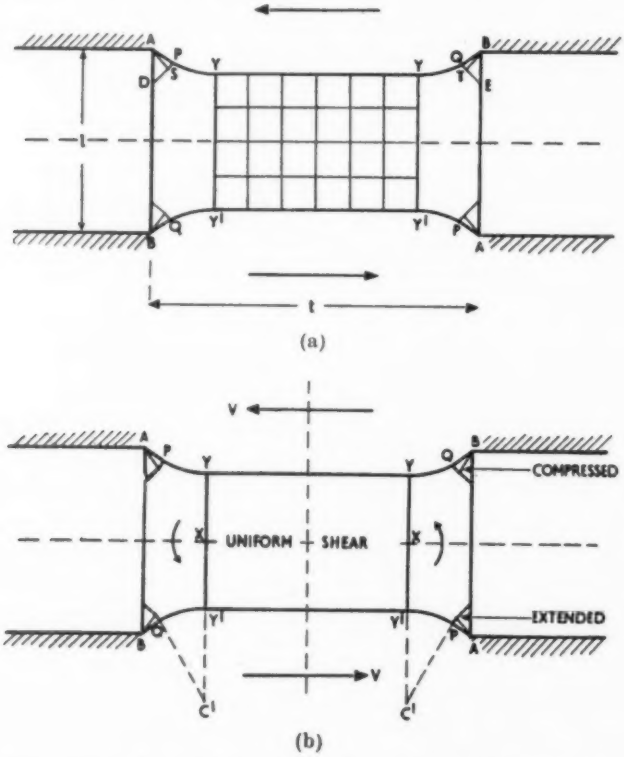

Fig. 5. Strong symmetrical plane-sided junction in plane strain with $\gamma = 0$; (*a*) slip-line field ; (*b*) mode of deformation.

$\gamma = 0$, by symmetry there is always a solution for which $p_1 = 0$ and in general this value of p_1 is likely to be unique (although for the wedge-shaped junction discussed above this is not so since the solution is degenerate).

If the junction has plane sides AB of length l, and its breadth is t, then a possible slip-line field for $\gamma = 0$ and $t/l > 0{\cdot}68$ is shown in Fig. 5a. The form of the field in the regions $APSD$ and $BQTE$ at the corners of the junction is defined in the usual manner by the straight stress-free edges AB and the singularities at A and B. PY and QY' are equal circular arcs, and in then central region $YYY'Y'$ the slip lines are all straight and parallel to the respective axes Ox and Oy. The slip line $APYYQB$ is continuous. With the direction of motion of the blocks as shown, the material around A is in tension and around B in compression, so that $p = -k$ in ASD and $p = k$ in BTE. The whole field is symmetrical and hence $p_1 = 0$, and in $YYY'Y'$ $p = 0$. Along $DSPY$ p varies from k to zero and by applying the Hencky relations we find that angles SAP and TBQ are both equal to $\frac{1}{8}\pi - \frac{1}{4}$ and the angular span of the arc PQ is $\frac{1}{8}\pi + \frac{1}{4}$.

Let us denote the length $AS\ (= BT)$ by d, YY' by y, and the radius of curvature of the arcs PY and QY' by R. These unknown dimensions are found by considering the region $APYY'QB$. The total projected length of the slip lines APY, YY' and $Y'QB$ on AB is l. Since the region must be in equilibrium the resultant force parallel to AB and the resultant couple, acting on its boundaries, must both be zero (the resultant force perpendicular to AB is automatically zero by symmetry). From these three equations we find that

$$d/l = 0{\cdot}052, \qquad R/l = 1{\cdot}076, \qquad \text{and} \qquad y/l = 0{\cdot}739. \tag{6}$$

The breadth YY of the central region depends on the breadth of the junction. It is zero when $t/l = 0{\cdot}68$ which is, therefore, the minimum ratio for which this solution is valid.* By integrating the forces acting across $APYYQB$, the means shear stress exerted through the junctions is found to be

$$s_1 = k\,(1 - 0{\cdot}249\,l/t) \tag{7}$$

which tends to k as $l/t \to 0$.

The mode of deformation associated with this slip-line field is illustrated by Fig. 5b. Let V be the equal and opposite velocities of the lower and upper blocks and U be the equal velocity discontinuities across $AY'Y'B$ and $AYYB$ (the velocity from right to left increases by this amount as one crosses these lines travelling from the lower to the upper block). The rigid regions on either side of the junction rotate in the anti-clockwise direction with angular velocity ω, about the instantaneously stationary points X, the midpoints of YY'. Relative to the lower block, however, these regions rotate about the respective centres of curvature C' of the circular arcs QY' and $Y'P$, so that the rigid material on either side of these arcs maintains contact. This relative motion is made up of the two components, the angular velocity ω about X and the velocity V from right to left. Hence

$$\omega = V/R, \text{ and } V = U\,(1 + y/2R) = 1{\cdot}34\,U. \tag{8}$$

The motion of these two rigid regions relative to the upper block is similar. Their rotation demands a linear variation along each of the lines YY' of the velocity perpendicular to YY'. Hence the whole of the central region $YYY'Y'$

* If $t/l > 0{\cdot}68$ the solution is of the type mentioned in Section 1 (a) with a deforming zone at each end of the junction and a rigid zone between.

undergoes uniform shear as it slides relative to the upper and lower blocks. The regions $APSD$ are compressed and $BQTE$ extended.

Similar solutions with $\gamma = p_1 = 0$ have been obtained for other symmetrical shapes of junctions (GREEN 1953). The plane-sided junction is a particular example ($\theta = 90°$) of the junction with wedge-shaped sides, for which such solutions exist if the angle between the sides $2\theta > 150°$. Results for $\theta = 85°$ and $80°$ are

$$\left.\begin{array}{ll} \theta = 85° & \\ t/l > 0{\cdot}57 & \end{array}\right\} \quad d/l = 0{\cdot}094, \quad R/l = 0{\cdot}446, \quad y/l = 0{\cdot}739, \quad s_1 = k\,(1 - 0{\cdot}163\,l/t);$$

$$\left.\begin{array}{ll} \theta = 80° & \\ t/l > 0{\cdot}48 & \end{array}\right\} \quad d/l = 0{\cdot}155, \quad R/l = 0{\cdot}324, \quad y/l = 0{\cdot}739, \quad s_1 = k\,(1 - 0{\cdot}0077\,l/t), \tag{9}$$

where t is now the breadth of the minimum section. It is interesting to observe that y/l appears to be independent of θ. The reason for this is not known. When $2\theta \leqslant 150°$ the solution degenerates to a single line of shear across the minimum section and $s_1 = k$ for all values of t/l (cf. Section 2a).

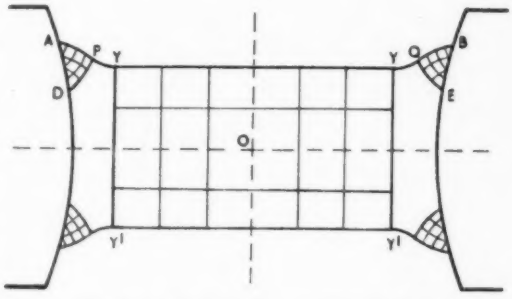

Fig. 6. Slip-line field for a strong symmetrical junction with circular sides and $\gamma = 0$.

The solution for a symmetrical junction with concave circular sides is shown in Fig. 6. This type of slip-line field is valid for all values of $t/r > 0{\cdot}23$, where t is again the breadth of the minimum section and r is the radius of curvature of the sides (provided, of course, that the angular span of these sides is large enough to contain the field). It is found that $R/r = 0{\cdot}117$ and.

$$s_1 = k\,(1 - 0{\cdot}066\,r/t), \tag{10}$$

so that $s_1 \to k$ as $r/t \to 0$.

One might expect that these symmetrical solutions could be modified for γ and p_1 slightly greater than zero, merely by upsetting the symmetry of the slip-line fields. Unfortunately the answer does not appear to be so simple as this. Consider a junction with plane sides. Each rigid region on either side of the junction must rotate at the same rate relative to the upper and lower blocks. Since the velocity discontinuity across $AYYB$ is constant along its length, it follows that even if the slip-line field were made unsymmetrical (*i.e.* region $APSD$ region $BQTE$), the radii of curvature of the arcs PY and YQ *would have to be equal*. With this condition it can be shown that, except for the symmetrical solution already described, there is one too few independent variables to satisfy the geometrical conditions, the threel equilibrium equations for rotating rigid regions, and the Hencky relation along $SPYYQT$. So the solution is not known in the range $0 < \gamma < \tan^{-1}(l/t)$. For greater values of γ the slip-line fields are easily constructed by connecting the regions defined by the stress-free edges with a straight slip-line (Fig. 7a). If

$t/l > 3{\cdot}64$ it is necessary to extend the field round the corners A to the surface of the blocks (Fig. 7b). No calculations of p_1 and s_1 have been made for these solutions.

(c) *Weak Junctions*

The simple model chosen (Fig. 8) is similar to that shown in Fig. 3a except that adhesion is not strong enough to prevent relative sliding at the interface. The interface AA', and the back edges AB of the upper asperity, are assumed to be straight. The angles of inclination of AA' and AB to the surfaces of the blocks are denoted by δ and θ respectively. Solutions are obtained only for the condition $\gamma = 0$.

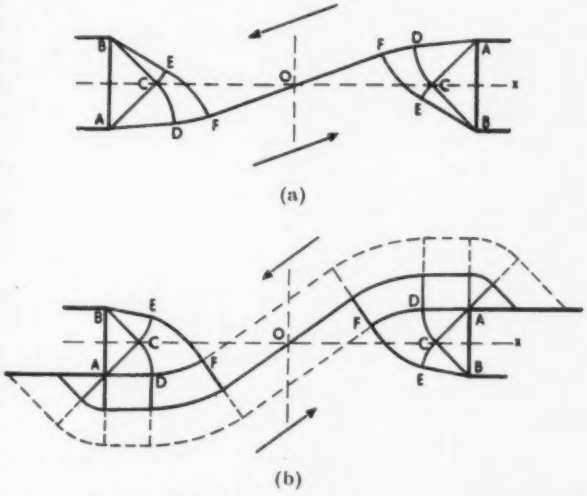

Fig. 7. Slip-line fields for a strong symmetrical plane-sided junction with $\gamma > \tan^{-1} l/t$; (*a*) $t/l < 3{\cdot}64$; (*b*) $t/l > 3{\cdot}64$.

Suppose that the upper asperity deforms plastically and that the shear stress s_1^* that can be supported across the interface is uniform over this plane surface. Thus s_1^* represents the strength of adhesion, which is weaker than the bulk strength of the metal. The lower asperity may or may not deform also depending on its shape and relative hardness. Let p_1^* be the mean pressure perpendicular to the interface.

Since s_1^* is constant along the straight line AA', the directions of the slip lines where they cut AA' are also constant and depend only on the value of s_1^*/k, where k is the yield stress in shear of the upper asperity. With the direction of motion of the top block as shown in Fig. 8, s_1^* acts from A' to A on the upper asperity, and the angle of inclination, ϵ, of the β-lines to $A'A$ is given by

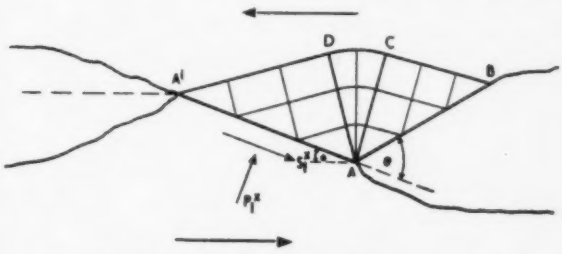

Fig. 8. Slip-line field for a weak junction with wedge-shaped sides.

$$\cos 2\epsilon = s_1^*/k. \tag{11}$$

If the junction were strong ϵ would be equal to δ.

The slip-line field shown in Fig. 8 is a possible solution if angle $DAC \geqslant 0$, *i.e.* if $\theta \leqslant \frac{1}{4}\pi + \epsilon$. The field is compatible with the stress conditions at the interface

and at the straight stress-free edge AB, and a velocity solution can be constructed starting in $A'DC$ which involves relative sliding across $A'A$. Applying the Hencky relation along $BCDA$, $p = 1 + \frac{1}{2}\pi + 2\epsilon - 2\theta$ on AA', and hence

$$p_1^*/k = 1 + \tfrac{1}{2}\pi + 2\epsilon - 2\theta + \sin 2\epsilon \tag{12}$$

It is apparent from (11) and (12) that the weaker the adhesion the greater is ϵ and hence the greater is p_1^* for a given shape of junction.

3. Plane Stress Solutions

It is a good approximation for most metals to assume that they obey the Mises yield criterion and plastic potential. Expressing this in terms of the principal stresses (σ_1, σ_2) and the principal strain-rates $(\dot{\epsilon}_1, \dot{\epsilon}_2)$ in the plane of the junction:

$$\sigma_1^2 - \sigma_1\sigma_2 + \sigma_2^2 = 3k^2 = Y^2, \tag{13}$$

and

$$\frac{\dot{\epsilon}_1}{\dot{\epsilon}_2} = \frac{2\sigma_1 - \sigma_2}{2\sigma_2 - \sigma_1}, \tag{14}$$

where Y is the tensile yield stress.

In the following solutions it is only necessary to consider states of stress and strain-rate in the deforming regions for which the stress and velocity characteristics are real. The velocity characteristics are directions of zero-rate of extension and, since the yield criterion and plastic potential are the same, they are identical with the stress characteristics. At any point in the plastic region there are two such directions, which we label by the parameters α and β, and they define the state of stress and strain-rate. By convention α and β are a right-handed pair of directions, and the line of action of the algebraically greatest principal stress, which bisects the angle $\frac{1}{2}\pi + \psi$ between them, lies in the first and third quadrants (Fig. 9). Let the stress components referred to the directions tangential and normal to a characteristic at any point be denoted by P, Q, and R. Then,

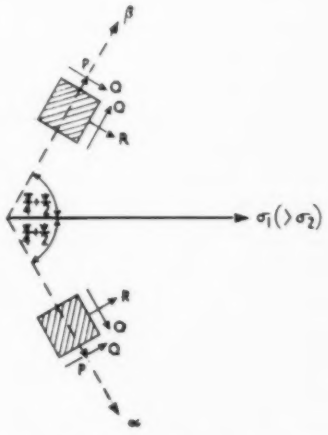

Fig. 9. Stress components in plane stress referred to the characteristic directions.

$$\frac{R}{k} = \frac{2P}{k} = \frac{4\sin\psi}{\sqrt{(1 + 3\sin^2\psi)}}, \qquad \frac{Q}{k} = \frac{\cos\psi}{\sqrt{(1 + 3\sin^2\psi)}}, \tag{15}$$

and

$$\sin\psi = (\sigma_1 + \sigma_2)/3(\sigma_1 - \sigma_2).$$

Let ϕ_α, ϕ_β and ω be the anticlockwise orientations of the α and β curves and the greatest principal stress direction respectively from some fixed direction. Since it is assumed that the width of the junction is uniform, the stress relations along the characteristics are,

$$d(\lambda - \omega) = 0 \quad \text{along an} \quad \alpha\text{-line},$$
$$\text{and} \qquad d(\lambda + \omega) = 0 \quad \text{along a} \quad \beta\text{-line}, \tag{16}$$

where $\lambda = \tan^{-1}(2\tan\psi - \frac{1}{2}\psi)$ defines the state of stress, and $d\omega = d(\phi_\alpha + \frac{1}{2}\psi) = d(\phi_\beta - \frac{1}{2}\psi)$.

As HILL (1952) has shown, local necking can only occur along a characteristic, and the vector representing the relative velocity of the material on either side of the neck is perpendicular to the other characteristic (*i.e.* it is inclined at an angle ψ to the neck). Some of the solutions which follow involve local bulging as well as local necking. Such bulging can only occur with a strain softening material or with a metal like annealed mild steel which has a sharp drop in yield stress after the initial yield-point. However, whether or not bulging is possible, such a solution provides an upper bound to the rate of work at the yield-point (HILL, 1951).

(a) *Strong Junction with Wedge-shaped Sides*

We consider a junction with the same shape and notation as in Fig. 3a and construct fields of characteristics analagous to the slip-line fields already described.

If $\theta > \theta'$, the field shown in Fig. 10 is a possible yield-point solution. In ABC the field is determined by the straight stress-free edge AB and consists of straight lines inclined to AB at the constant angle $\beta = \tan^{-1}\sqrt{2} = 54°\,44'$; the state of stress is either uniaxial tension or uniaxial compression parallel to AB. Let us assume the latter, which implies that the blocks are moving together, that BC is a $\beta =$ line, and that ψ is negative throughout the field. HILL (1952) has shown that the extension of the field round the singularity at A consists of straight lines through A and curves whose polar equations are $r^2 \sin\phi =$ constant, and along which,

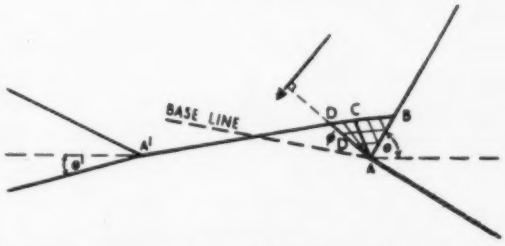

Fig. 10. Characteristic field in a strong junction with wedge-shaped sides (plane stress).

$$\tan\psi = -\tfrac{1}{2}\cot\phi, \qquad R = -2k\cos\phi, \qquad \text{and} \qquad Q = k\sin\phi, \tag{17}$$

where the polar angle ϕ is measured from the base line indicated in Fig. 10, which is inclined at the angle β to AC. The straight characteristic DA' which completes the field is tangential at D to the curved characteristic CD. Along DA' there is local bulging and the direction of relative motion of the rigid material on either side is perpendicular to AD. Hence on AD

$$\phi = \phi_D = 19°\,28' - \gamma + \theta. \tag{18}$$

Resolving the forces acting across AD and DA', it is found with the aid of equations (17) and (18) that

$$p_1/k = 2\cos\phi_D + 2\sin\phi_D/[\cot(\gamma + \psi_D) + \tan\gamma]$$
$$s_1/k = \sin\phi_D\,[\cot(\gamma + \psi_D) - \tan\gamma]/[\cot(\gamma + \psi_D) + \tan\gamma] \qquad (19)$$

where $\tan\psi_D = -\frac{1}{2}\cot\phi_D$.

The limits of validity of this solution are somewhat more complex than those for the plane strain solution because there is an inflexion in the curve CD when $\phi = \frac{1}{2}\pi - \beta$, and the characteristics run together when $\phi = 0$. Because of the inflexion, the angle between $A'D$ and AB cannot be less than $\frac{3}{2}\pi - 4\beta = 51° 4'$, and hence if θ is less than this value the solution degenerates to the single characteristic AA' for all values of γ. Then $\gamma = \psi$ and from (15)

$$p_1/k = 4\sin\gamma/\sqrt{(1 + 3\sin^2\gamma)}, \qquad s_1/k = \cos\gamma/\sqrt{(1 + 3\sin^2\gamma)}. \qquad (20)$$

Using these equations, the yield locus for a thin junction with $\theta = 5° \geqslant \theta'$ and $\psi = 10° \geqslant \psi'$ is plotted in Fig. 4. It can be seen that p_1 is considerably less than it is for the similar junction in plane strain.

If $\theta > 51° 4'$, the solution (19) is valid only over the range of ϕ_D greater than zero for which angles $DA'A$ and CAD are positive, *i.e.*

$$\phi_D + \tan^{-1}(\tfrac{1}{2}\cot\phi_D) \leqslant \theta + 19° 28', \qquad (21a)$$

and

$$\phi_D \leqslant \beta. \qquad (21b)$$

If $51° 4' < \theta < 54° 44'$, (21a) gives both the upper and lower limits of ϕ_D. If $54° 44' < \theta < 70° 32'$ the upper limit is (22b). If $\theta > 70° 32'$ the full range of ϕ_D, $0 \leqslant \phi_D \leqslant \beta$ is valid.

The corresponding upper and lower limits of γ can be calculated with the aid of (18). Above the upper limit of the degenerate solution (19) may be used. Below the lower limit the solution is unknown, except for certain symmetrical junctions when $\gamma = p_1 = 0$ (see Section 3b). An upper bound could be constructed, similar to (6) for plane strain, consisting of a single straight local bulge (or neck).

The range of the above solutions is also limited by the possibility of extending the field to one of the sides AY or $A'Y'$ at a sufficiently high value of γ. If a field of the type shown in Fig. 10 is so extended, the resultant field is analagous to one of those shown in Figs. 3b or 3c.

Velocity distributions can be calculated with the aid of equations given by HILL (1950, p. 306). However, the extent of the diffuse modes of deformation that must occur in compression, and when the rate of hardening is high, are not known.

(b) *Strong Symmetrical Junctions*

Solutions are presented only for short junctions with plane sides with $\gamma = p_1 = 0$. Here again the field of characteristics (Fig. 12b) is analagous to that in plane strain. At the corners A and B, the field defined by the straight stress-free edge and the singularity has the same form as that described above.* PY and QY' are single arcs, curved but not circular. In the central region $YYY'Y'$, the characteristics are straight and $\psi = R = P = 0$ *i.e.* the state of stress and strain rate is pure shear in the plane of the junction. Using equations (16), the change in ψ between the central region and a free edge (where $\psi = 19° 28'$) determines that angles PAS and QBT are equal to $19° 20'$.

* These regions are too small to be seen in Fig. 12b, which is drawn to scale.

As in the plane-strain solution the mode of deformation involves uniform shear in the central region and rotation of the rigid regions on either side. Relative to the lower block these side regions rotate about points C' which lie on the continuation of YY', so that there is local necking along QY' and local bulging along PY'. At any point on either of these arcs the direction of relative motion of the rigid material on either side of the arc is inclined to it at the angle ψ, which is found from equations (16) and the condition that $\psi = 0$ at Y. This direction must be perpendicular to the radius vector through the appropriate centre of rotation C'. Hence, the polar equation of the arc referred to the origin C' is $r^2 \cos \phi'$ the polar angle ϕ' being measured from the base-line $C'Y'$. It will be noticed that this is the same type of curve as that round the singularities at A and B. The dimensions of the field are finally determined by considering the equilibrium of $APYY'QB$. It is found that

$$AS = BT = 0{\cdot}006\, l, \qquad C'Y' = 0{\cdot}393\, l, \qquad \text{and} \qquad YY' = 0{\cdot}832\, l, \quad (22)$$

and that $YY = 0$ when $t/l = 0{\cdot}79$ which is, therefore, the minimum ratio of t/l for which this solution is valid. Also

$$s_1 = k\,(1 - 0{\cdot}300\, l/t). \quad (23)$$

Vol. 2 53/54

4. Formulae for Steady Sliding

The simple shape of junction used by the writer (Green 1954a) in analysing steady sliding is shown in Fig. 11. The junction has wedge-shaped sides as in Fig. 3 and 9, but AA' is now inclined to the surfaces of the blocks at a finite angle, δ say. The solutions already obtained for wedge-shaped junctions apply, of course, to this junction also. The breadth of the junction is redefined as $t' = t \cos \delta$ and the new mean stresses, p_1' and s_1' normal and tangential to the surfaces, exerted through the junction across this breadth, are

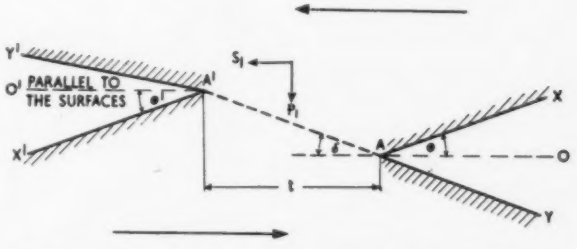

Fig. 11. Shape of junction for analysis of steady sliding between metals.

$$p_1' = p_1 - s_1 \tan \delta, \quad \text{and} \quad s_1' = p_1 \tan \delta + s_1. \quad (24)$$

The relative direction of motion of the two blocks is now inclined at the angle $\gamma' = \gamma - \delta$ to the surfaces. Let us redefine θ and θ' as the angles that XA and $X'A'$ make with the surfaces of the sliding blocks (instead of with AA'). Then, in steady sliding (*i.e.* $\gamma' = 0$), the expressions for p_1' and s_1' obtained either by applying equations (24) to equations (3), (19) and (20), or directly from the fields, are :

Plane Strain (if $\theta' \leqslant \theta \leqslant \frac{1}{4}\pi$) :

$$p_1'/k = 1 + \tfrac{1}{2}\pi - 2\theta + \tan \delta, \qquad s_1'/k = 1 + \tan \delta\,(1 + \tfrac{1}{2}\pi - 2\theta); \quad (25)$$

Plane Stress (if $\theta' \leqslant \theta \leqslant \tan^{-1}(1/\sqrt{2}) = 35° 16'$) :

$$\left.\begin{aligned} p_1'/k &= (2 \sin \delta_0 + \cos \delta_0 \tan \delta)/\sqrt{(1 + 3 \sin^2 \delta_0)}, \\ s_1'/k &= (4 \sin \delta_0 \tan \delta + \cos \delta_0)/\sqrt{(1 + 3 \sin^2 \delta_0)}, \end{aligned}\right\} \quad \text{if } \delta > \delta_0 ; \quad (26)$$

and

$$\left.\begin{aligned} p_1'/k &= 3 \sin \delta/\sqrt{(1 + 3 \sin^2 \delta)}, \\ s_1'/k &= (4 \sin \delta \tan \delta + \cos \delta)/\sqrt{(1 + 3 \sin^2 \delta)}, \end{aligned}\right\} \quad \text{if } \delta < \delta_0 ; \quad (27)$$

where $\delta_0 = -\psi_D = \tan^{-1}(\frac{1}{2} \cot \phi_D)$, and $\phi_D = \theta + 19° 28'$.

5. Experiments on Symmetrical Junctions

The mode of deformation for a plane sided symmetrical junction when $\gamma = 0$ has been demonstrated in experiments with both mild steel and with plasticine.

Each steel specimen was annealed, deformed just past the yield-point in the manner specified, aged at 250°C for about half an hour, and finally etched with Wazeau's reagent (Hundy 1954). The etching revealed the regions where plastic deformation had taken place. To obtain plane strain conditions a wide specimen was used; after deformation it was cut in half so that the central section could be polished and etched.

The comparison between theory and experiment under conditions of both plane strain and plane stress, shown in Fig. 12, clearly demonstrates the validity of the assumed regions of deformation. Yielding was allowed to continue slightly too far, however, with the result that work-hardening caused the deformation to spread beyond the regions predicted by the theory (it is difficult to judge the precise moment for comparison). The striated pattern of yielding is characteristic of mild steel. Yielding does not occur instantaneously over the whole theoretical region; it begins along narrow bands and, as it proceeds, these bands broaden

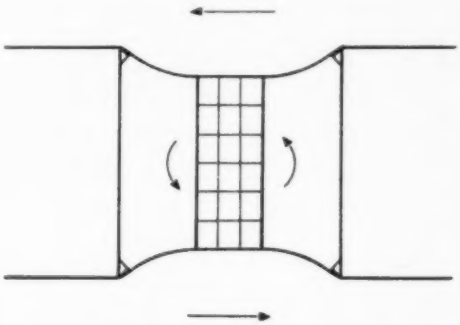

(*a*) plane strain, $l/t = 1{\cdot}04$;

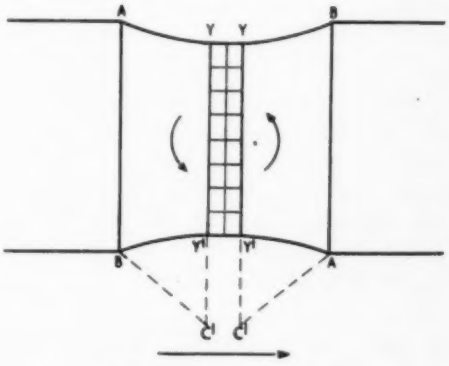

(*b*) plane stress, $l/t = 1{\cdot}08$.

Fig. 12. Theoretical and experimental regions of plastic deformation in symmetrical plane-sided junctions with $\gamma = p_1 = 0$.

Vol.
2
53/54

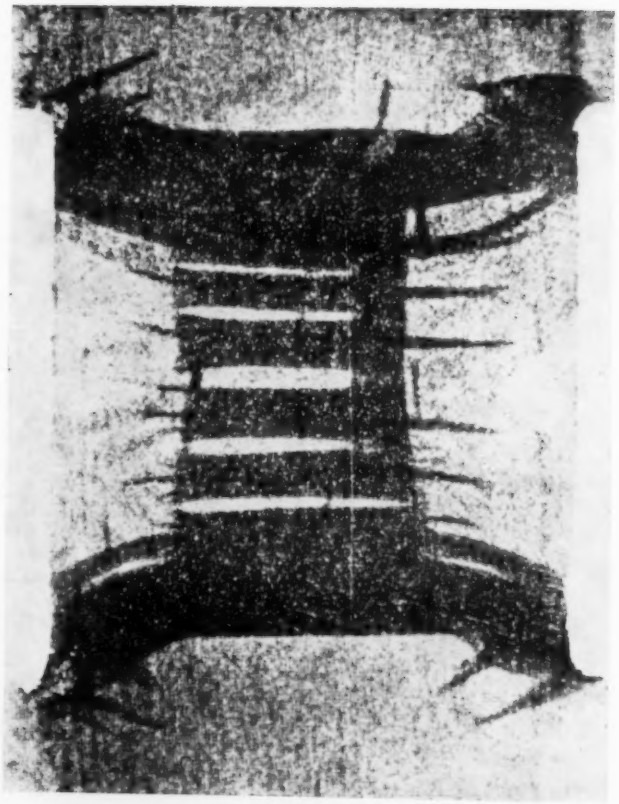

Fig. 12b.

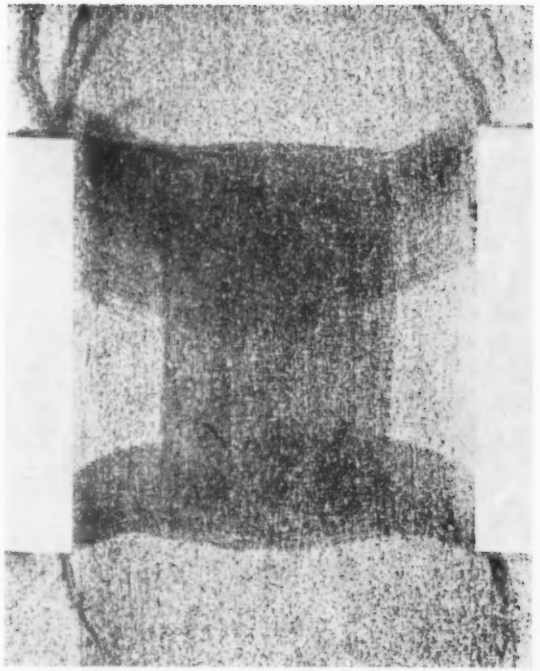

Fig. 12a.

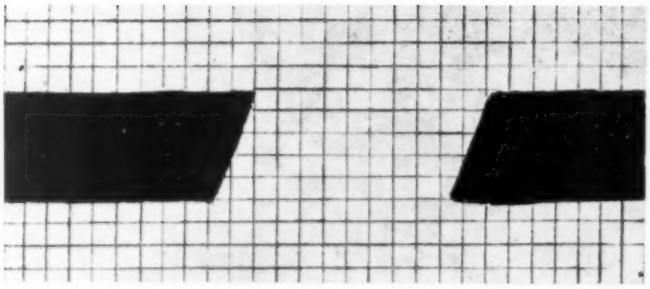

(a)

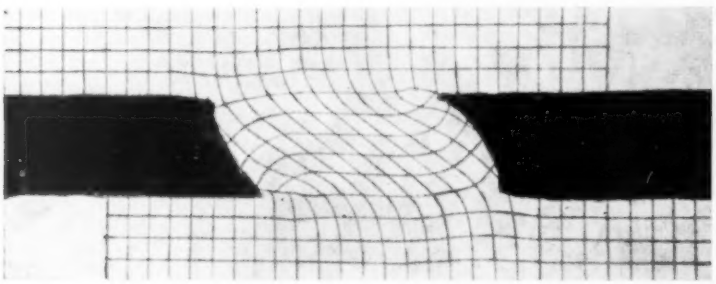

(b)

Fig. 13. Deformation of a plasticine junction with $\gamma = 0$. (*a*) initially; (*b*) after deformation.

out and new bands are formed. It is interesting that the bands appear to run approximately parallel to characteristic directions. The reason for this is not clear but it may be because the boundary of a ' rigid ' zone must coincide with a direction of zero rate of strain, at least in the initial stages of yielding.

The general mode of deformation was also confirmed by the plasticine experiment shown in Fig. 13. As the writer has shown (GREEN 1951) plasticine deforms in plane strain in a similar manner to an ideal non-hardening metal. The theoretical solution is, of course, only instantaneously valid when the junction is symmetrical, but the plasticine model had to be deformed a finite amount through this position in order to produce a finite deformation of the grid stamped on the surface. The specimen was cut from one piece of plasticine and was constrained by lubricated glass plates which ensured plane-strain conditions except over the small regions at the two diagonally opposite corners where thinning occurred. The region of uniform shear in the centre is quite clear, and the regions on either side rotated without deforming much, in reasonably close agreement with the theory.

ACKNOWLEDGMENTS

I am grateful to my colleagues, Dr. B. HUNDY, for the experimental results shown in Fig. 12, and to Mr. D. SPENCELY, for his assistance in calculating the results and drawing the diagrams for this paper.

Vol. 2 53/54

REFERENCES

BOWDEN, F. P., MOORE, A. J. W. and TABOR, D. 1943 *J. Appl. Phys.*, **14**, 80.

GREEN, A. P. 1951 *Phil. Mag.*, **42**, 365.

1953 *B.I.S.R.A. Report* MW/B/14/53.

1954a *B.I.S.R.A. Report* MW/B/7/54 ; *Proc. Roy. Soc.* A. (to be published).

1954b *B.I.S.R.A. Report* MW/B/9/54.

HILL, R. 1950 *Mathematical Theory of Plasticity* (Clarendon Press, Oxford).

1951 *Phil. Mag.*, **42**, 868.

1952 *J. Mech. Phys. Solids*, **1**, 19.

HUNDY, B. 1954 *B.I.S.R.A. Report* MW/B/5/54 ; *Metallurgia* (to be published).

BOOK REVIEWS

Progress in Metal Physics: Vol. 4. Edited by BRUCE CHALMERS. Pergamon Press Ltd., London 1953. 9¾ x 6¼ in. Pp. viii + 403, with numerous illustrations. 60s.

WHEN the first volume of this series was published some years ago, it was felt that there was a need for authoritative reviews of specific fields in fundamental physical metallurgy to enable the research worker to keep abreast of developments which were possibly not included within his own sphere of activity. The undoubted popularity of the previous volumes has confirmed that this need existed, and is being notably met by this series of books. The student of physical metallurgy has also found them useful as a supplement to his formal studies. The present volume carries on the tradition. There are seven review articles, two of which are devoted to further developments in fields already treated in earlier volumes. The article on "Theory of Dislocations" by A. H. COTTRELL carries the subject a great deal farther than was possible when Volume I was prepared, and summarizes recent progress. In particular, the evidence obtained from crystal growth phenomena for the existence of dislocations is stressed, and, following a clear discussion of the dynamic properties of dislocations, there is a section on dislocations in the typical metallic structures. The remainder of the article is chiefly concerned with progress in the application of the dislocation theory to various problems, such as creep, work-hardening, and the creation of lattice vacancies, which are of importance in studying the deformation of metals. The whole article forms a critical appraisement of the situation which will be read with profit by all interested in the physics of the mechanical properties of metals. The article entitled "Diffusion in Metals" by A. D. LECLAIRE is of much the same general character. It takes up the story of diffusion from the point reached in Volume I, and summarizes recent progress. It is in five main sections, of which the first three deal with further evidence on the Kirkendall Effect and grain boundary and surface diffusion, and with current ideas on the mechanism of diffusion. After a brief discussion of experimental methods for studying diffusion, the final section deals with the thermodynamics of diffusion.

The remaining five articles break new ground, and are in general of the high standard now expected for this publication. A. S. NOWICK writes on "Internal Friction in Metals," mainly from the point of view of the use which can be made of damping in studying the details of the atomic arrangement in metals and alloys. The subject is introduced attractively, and the possible sources of non-elastic behaviour are fully discussed, with particular reference to stress-induced ordering, internal friction originating in grain boundaries, and the effects of cold-work, annealing and other treatments. A brief discussion of internal friction in terms of dislocation theory is given. This article is a most competent review.

"The Mechanism of Oxidation of Metals," by KARL HAUFFE, deals essentially with high-temperature oxidation, and gives a good picture of the present degree of understanding of this subject in terms of diffusion in the oxide layer; Wagner's theory is presented in some detail, both in relation to pure metals and to alloys. The somewhat related subject of "Gases in Metals" forms the subject of a review by C. R. CUPP, in which the more important experimental facts are summarized, and their significance discussed. The effects of dissolved gases on such physical and mechanical properties as internal friction, lattice expansion, magnetic properties and electrical properties are fully treated.

A welcome contribution to "The Theory of Sintering" is made by G. A. GEACH. This is a short article, but nevertheless the main considerations are clearly summarized, and the fact that our ignorance of several features of the mechanism is stressed may stimulate further work on this important subject.

The book concludes with a long article on "Nucleation" by J. H. HOLLOMON and D. TURNBULL. The work of these two experts on this subject is well known among the specialists, and the appearance of a connected account not only of their own ideas but of the subject in general is to be widely welcomed.

All the articles are well illustrated, and carry long lists of references which will be useful to those who wish to follow up the subjects discussed in greater detail. In conversation with his

Vol 2 1953

friends, the reviewer has heard the view expressed that the articles are becoming too specialized and of too high a standard to appeal to, or be of much use to, the non-specialist reader ; they are becoming little monographs, rather than reviews. To a certain extent, this is true, but it must be remembered that keeping up with progress over a wide field in these days of increasing specialization can never be a painless process. The difficulty the non-specialist reader may have over some of the articles in this book is surely matched by the difficulty the writers of the articles have in trying to eliminate from their accounts the more difficult theoretical conceptions, or to express what is essentially a mathematical argument in words. The non-specialist reader should be willing to meet the writer half-way, and to settle down to these articles as he would to serious study, rather than to treat them as light reading. However, the Editor might bear in mind the developing opinion in some quarters that the Series is getting tough.

The price (60s.) is high, but the book is worth it.

G. V. RAYNOR.

C. KITTEL : **Introduction to Solid State Physics.** Chapman & Hall, 1953. pp. 396. 56s.

IN his preface, Professor KITTEL stresses that the book is intended ' as an introductory text book in solid state physics for senior and beginning graduate students in physics, chemistry and engineering.' With this aim, the accounts of the selected topics have been commenced at a reasonably elementary level, and the knowledge of mathematics assumed should certainly have been acquired during most honours physics courses. In the writer's opinion, the author has admirably achieved his purpose and the excellent basic account provided should considerably assist the study of more specialized monographs in the solid state field.

Vol. 2 53/54

In sixteen chapters, the subjects include crystal forms and their properties, lattice vibrations, dielectric properties and ferroelectricity, magnetic properties, superconductivity, the free electron and band theories of metals, semi-conductors and a brief account of imperfections in solids. The author acknowledges that many possible topics are omitted entirely, and almost every reader will regret that some subject is missing or dealt with only very briefly. However, further reading is aided by the inclusion of over 250 references to original works – many dated 1952 – and to other relevant books and reviews. Three features make the book attractive to the reader. Firstly, in spite of the considerable condensation of the material, the unsatisfactory words ' It can be shown that . . . ' appear infrequently. Secondly, the more difficult mathematical points are removed to a series of 21 appendices, and, finally, there is a plentiful accumulation of data in the form of tables and graphs.

The book is based in part upon a teaching course at the University of California and there is no doubt of its value to the undergraduate and to the post-graduate research worker as well as to his more senior colleagues who find it necesary to make even a brief incursion into solid state theory. It is perhaps not out of place once more to record one's regret that the price of a book may well place it out of the reach of many for whom it was specifically written.

K. J. STANDLEY.

CHI-TEH WANG : **Applied Elasticity.** McGraw-Hill Publishing Co., 1953. ix + 357 pp. 57/6d.

THE feature that distinguishes this book from any other single work on Elasticity is the treatment of a wide range of subjects up to a fairly advanced level, combined with an exposition of approximate methods of solution. The adjective 'Applied ' in the title emphasizes that the book is mainly for engineers and that the author's intention is to show how solutions to problems may be obtained, first in implicit analytical form, and afterwards in numerical terms as well. This aspect he treats in some detail by means of examples and, so far as the reviewer is able to judge, in a clear and helpful way for engineers.

The main approximation methods treated are those of relaxation and Rayleigh-Ritz, primarily in relation to torsion and buckling of columns, strips and plates. Other subjects given prominence are two-dimensional problems (*e.g.* rotating discs, thermal stresses in cylinders, stress concentrations) ; the theory of thin shells and curved plates ; and the method of complex potentials.

No previous knowledge of Elasticity is assumed, and the preliminary analysis of stress and strain is sufficiently thorough.

Occasionally, heavy weather is made of parts of the basic theory : *e.g.* the derivation of the expression for strain energy on pp. 36-7 ; the principle of minimum energy on pp. 152-4 ; and Rayleigh's principle on pp. 263-7. This rather suggests that another method might have been included for the benefit of engineers, namely the use of a summation sign and, in places, the use of the summation convention. This not only saves time and space, but throws the structure of a proof into relief.

In all important respects the book can be strongly recommended.

R. HILL.

S. P. TIMOSHENKO : **Collected Papers.** McGraw-Hill Publishing Co., 1953. pp. xxv + 642. £7.

MOST of the published work of Professor STEPHEN TIMOSHENKO is to be found here, including many of his early Russian papers which were later translated. About one half of the book is in French or German, the rest in English. A very interesting biography is contributed by Professor D. H. YOUNG.

The subject common to all the papers is the engineering applications of the theory of elasticity. One main theme runs throughout : the avoidance, wherever possible, of a complicated exact analysis by a simple and sufficient approximation. Two procedures are used for this purpose : the minimum energy principle for ordinary statical problems, and Rayleigh's principle for the gravest frequency of a vibrating system or for the first buckling mode of an unstable structure. Professor TIMOSHENKO's most important paper will be considered by many to be that in which he shows for the first time that Rayleigh's principle, originally enunciated for vibrations, can be taken over and used with good effect in a stability problem. This paper is also the longest (133 pages) and one of his earliest (1910).

Collected works of scientists are often notable for other things beside their positive and lasting contributions to knowledge (which are indeed often only a small part by volume of the whole). Many impress or (it may be) repel by their sheer bulk. A few are distinguished by their felicity of style. Others are a model of lucidity and conciseness ; among these, Professor TIMOSHENKO's writings will surely be rated highly.

R. HILL

F. S. SHAW : **An Introduction to Relaxation Methods.** 1953. pp. 396. Dover Publications, Inc. $5.50.

IN his preface the author writes : ' The intention is to present a simple detailed account of the computational processes (known as relaxation methods) and little more.' He thus expressly excludes the mechanical and physical analogues used to good effect by R. V. SOUTHWELL who, with his collaborators (the author being one), has done so much to develop and systematize this type of iteration procedure for numerical solution of algebraic and differential equations. It is indeed possible that (to a mathematician at least) an introductory exposition in which pin-jointed frame-works and screw-jacks are prominent seems a little unrefined and is something of a hindrance to a clear understanding of an essentially simple technique. Once the crude mechanics have been mastered, however, much is lost by not drawing on all possible analogies to stimulate the reader's interest as well as his intuition. Not to do so makes for very arid reading.

A second intentional omission is a discussion of the limitations of relaxation methods or the demarcation of their sphere of usefulness. For example, though the enormous practical difficulties involved in handling the important biharmonic equation will be apparent to the reader of the chapter on this topic, no guide is given as to the degree of accuracy obtainable with a grid of practicable fineness or the man-hours of computation required. In the reviewer's opinion, treatment by relaxation is by no means a specific for this particular equation. It is also not

Vol 2 1953

made sufficiently clear why relaxation is definitely unsuitable for almost all boundary-value problems of wave motion and hyperbolic equations in general. Again, in the solution of characteristic (algebraic) equations there is no comparison with alternative iterative procedures, such as the widely-used one of Stodola (which in the reviewer's opinion is often superior).

Within these self-imposed limits, however, the author has written a book that should be extremely useful as a compendium of tricks of the trade and refinements of computing technique.

R. HILL

O. HOFFMAN and G. SACHS : Introduction to the Theory of Plasticity for Engineers, McGraw-Hill Publishing Co. 1953. 52s.

TEXTS on Mathematical Plasticity, have of late, been appearing at such short intervals, that the student can afford to be discerning in the choice of a book, while the writer has to choose and present his material with especial care to justify the publication of yet another book. Professors HOFFMAN and SACHS have evidently had this point in mind when deciding to address themselves to engineers, whose ta tes and needs have not been particularly well catered for.

The engineer expects three things from a textbook on a subject in Applied Mathematics, which is written specifically for his benefit : simple mathematics at the expense of rigorous proof (usually with a preference for graphical methods), presentation keyed to physical reality, and solutions of practical interest. The authors have tried to meet these requirements, but only with partial success. The mathematics is on an elementary level throughout, extensive use is made of Mohr's diagram and geometric concepts are stressed ; fundamental questions of the theory, *e.g.* the problem of uniqueness, are wisely left to the mathematicians. This, however, exhausts the list of ' positive ' achievements.

Many important engineering applications of the theory are ignored. Among them, the absence of any reference to limit design is all the more surprisping since Professor HOFFMAN is in charge of a Civil Engineering Department. That the theory of metal forming processes occupies the greater part of the book is understandable in view of Professor SACH's long and well-known standing in this field. It is a pity, however, that problems of drawing through stationary and rotating dies predominate, and no space was allotted to the theory of machining, to piercing, to stretch forming, to residual stresses and so on. All these omissions are bound to influence adversely the prospective buyer, that is the engineer who wishes to apply an elementary working knowledge of mathematical plasticity to problems within his purview.

More serious than the one-sided selection of technological problems, is the restriction to an elementary treatment of them. Although the authors present an account of the theory of slip-line fields for plane strain deformation, they do not make use of it in the solution of metal forming problems. They advance two reasons for this. First, they argue that elementary solutions are much simpler than the rigorous ones and in practice yield surprisingly good results, whenever the actual conditions are closely represented by the assumptions of the analysis. Second, they say that no attempt has yet been made to investigate experimentally the validity of relations resulting from the use of slip-line fields (p. 127), or that some features of the solutions based on the slip-line field theory are not supported by experimental evidence, *e.g.* dead metal regions (p. 161).

As to the first argument, there are many instances of practical interest, when the assumptions used by the authors do not apply. Moreover, there are instances where, at first sight, the authors' solutions are applicable, and yet fail in practice (BARON and THOMPSON, whose paper on wire drawing is quoted in the book, experienced this). Alternatively, the elementary solution may not be of practical interest ; this is the case with the authors' solution for extrusion through conical or tapered dies : in practice the die angle is always substantially larger than admissible by the elementary solution.

As for the second argument, neither the first nor the second above-quoted variant of it should have appeared in print in the year in which the book was published. By expressing this sort of opinion the authors shake one's confidence in those solutions advanced by them, which have not, in fact, been checked experimentally.

J. G. WISTREICH.

Vol. 2 53/54

W. FLUGGE: **Four-place Tables of Transcendental Functions.** Pergamon Press Ltd., London, 1954. 186 pp. 25s.

THE avowed aim of this book is to provide the engineer and physicist with a set of tables, for use with slide-rule calculation, of the most common functions of mathematical physics that can be presented in compact form. The following functions are tabulated to four significant figures for the ranges indicated.

ELEMENTARY FUNCTIONS

$\sin x$, $\cos x$, $\tan x$, $\cot x$: $x = 0\ (0{\cdot}1^\circ)\ 90{\cdot}0^\circ$.

$\sin x$, $\cos x$, $\tan x$: 0 (0·01) 10·09 radians.

$\sinh x$, $\cosh x$: 0 (0·01) 10·09 ; $\tanh x$: 0 (0·01) 5·09.

$e^x - 1$, $1 - e^{-x}$: 0 (0·001) 0·209 ; e^x, e^{-x} : 0 (0·01) 10·09 ; $\ln x\ (= \log_e x)$; 1 (0·01) 10·09.

HIGHER FUNCTIONS

Bessel functions J_0, J_1, Y_0, Y_1, I_0, I_1, K_0, K_1. Thomson functions (Bessel functions with argument $x\sqrt{i}$) ber, bei, ker, kei and their first derivatives : 0 (0·01) 10·09.

Incomplete elliptic integrals $F(x, y)$ (first kind) and $E(x, y)$ (second kind) : $y = 0\ (1^\circ)\ 90^\circ$, $x = 0\ (2^\circ)\ 90^\circ$.

Error function $\operatorname{erf} x$: 0 (0·001) 1·009 ; 1 − $\operatorname{erf} x$: 1 (0·01) 3·09.

Fresnel integrals $S(x)$ and $C(x)$ $(= \int^x J_{\pm\frac{1}{2}}\, dt)$: 0 (0·01) 10·09.

Exponential, Sine and Cosine Integrals : 0 (0·01) 10·09.

Factorial or Gamma Function, $\Gamma(x) = y!$: $x = 1\ (0{\cdot}001)\ 2{\cdot}009$, $y = x - 1$.

Each table is preceded by an introduction which gives the mathematical definition and a valuable collection of formulae including where relevant the ascending series, asymptotic series, differential equations, periodic properties, recurrence relations, derivatives, integrals and other properties, a note on extension of the tables beyond the given range, and a short list of other relevant tables. A final page gives four-figure values of a few functions of the transcendental constants, e, π and $\ln \gamma$ (the latter is not the usual definition of Euler's constant). Linear interpolation can be used almost everywhere, but there is no indication of the position and extent of exceptional regions.

The elementary functions need no justification, and in modern physics a working knowledge of the higher functions is almost essential. Bessel functions, through their connexion with Laplace's equation in cylindrical coordinates, occur in all problems in hydrodynamics, heat conduction, electricity and magnetism, elasticity, etc., involving potential flow or its various analogies. Thomson functions arise in alternating current theory, Fresnel integrals in optics, while differential equations in many physical contexts are soluble in terms of the various Bessel functions. The other transcendental functions, defined as definite integrals rather than as solutions of differential equations, also arise directly in many physical problems and are necessary for evaluating integrals not expressible in terms of elementary functions.

Here then is a wealth of material for the physicist, and there can be little quarrel with the author's choice, some obvious omissions requiring much more space for effective tabulation.

The arrangement of the tables is less happy. The argument increases horizontally so that, for example, values for $x = 0\ (0{\cdot}01)\ 0{\cdot}09$ appear in one row, those for $0{\cdot}10\ (0{\cdot}01)\ 0{\cdot}19$ in the next. This is perhaps essential in tables of this kind, but requires the use of asterisks to indicate changes of sign, leading figures, and transition from say three decimals to four. The arrangement of the first column is then very important and the suppression, at all except change points, of signs, decimal points, leading figures and even the first one or two figures after the decimal point (if the leading figure is 0) does not lead to easy and accurate reading. Change points in the number of decimals might also with advantage have been confined to the first column.

The printing, however, is clear in good " heads and tails " type, a random sampling test suggests that errors are few, and at 25s. the book is a sound investment.

L. Fox

Vo. 2 1953

Journal of the Mechanics and Physics of Solids, 1954, Vol. 2, pp. 217 to 237. Pergamon Press Ltd., London.

THE STRENGTH OF SHORT CYLINDERS UNDER INTERNAL PRESSURE

By D. G. Christopherson and G. R. Higginson
Department of Mechanical Engineering, University of Leeds

(*Received 25th February*, 1954)

Summary

This paper provides a method of estimating the internal pressure required to cause plastic expansion of a uniform circular tube under internal pressure, when the ends of the tube are constrained. Both 'simple support' and 'clamped' conditions at the ends are considered. The method is based on work considerations. The results obtained are shown to agree reasonably well with experiment, the form of the deformation being predicted very accurately and the magnitude of the pressure required to cause failure with fair accuracy. With some additional trouble the method can be extended to cover the effect of work-hardening.

It is shown that the end effect is small unless the tube is very short.

Vol. 2 53/54

1. Introduction

Much work has been done in recent years on the strength of long tubes of circular cross-section stressed into the plastic range by internal pressure. Indeed this is one of the comparatively few problems in plasticity for which a complete treatment is available (summarized by Hodge and White 1950).

It would also be of value, however, to be able to calculate the limiting strength under internal pressure of a tube which is not long compared with its diameter. It is no doubt to be expected that if the length exceeds the diameter the conditions of constraint at the ends will be without important effect on the strength, but some cases occur in practice in which the length is only a fraction of the diameter and end effects have an important effect on the strength.

It seems at the present time to be out of the question to attempt an exact solution of this problem, even with some simplifying assumptions about the stress-strain relations for the material. But it may be worth while to enquire whether an approximate treatment based on known general theorems in plasticity could not provide a solution whose accuracy would be adequate for most practical purposes. In outlining such an approximate treatment, a high place must be given to simplicity. A method of calculation that can be rapidly applied to give a result of reasonable accuracy in a given case, provided that it is fundamentally sound, is likely to be of greater practical value than a more lengthy method leading to far greater accuracy.

In the field of elasticity many such approximate methods based on energy considerations are well-known, for example, Rayleigh's method for determining vibration frequencies. In this paper an analogous energy or work method is employed which is proving to have applications to a considerable range of problems

(HILL 1950 a and b, 1951 ; ONAT and PRAGER 1952 ; HILL and SIEBEL 1953). In RAYLEIGH's method, it is customary to make an assumption about the mode of vibration of a particular system, and hence to estimate the frequency. The starting point of this investigation is a similar assumption about the *mode of distortion* of the plastic tube, and work considerations are enlisted to deduce the internal pressure sustained.

One of the difficulties of analytical work in the plastic range is, of course, that the fundamental equations relate not to the total strain but to the increments of strain taking place at any given stage. As is well known, the results can only be applied to total strains or deformations if the ratio of the principal stresses and hence of the strain increments remain constant throughout the deformation.

The present work is restricted to cylinders constrained radially at the ends, and loaded by internal pressure. However, the ratios of the principal stresses and consequently the strain ratios will only remain constant in certain conditions. One such condition is that in which the tube is entirely elastic. A second is that in which the tube consists of a plastic-rigid material which does not work harden ; in such a specimen the stresses will remain constant throughout the deformation until the distortion becomes so great that the whole geometry of the problem is changed. A third such condition occurs in many ductile materials when plastic strains are large compared with elastic strains but still not large anough to make the effect of work hardening appreciable. In this case it is legitimate to employ the "total strain" theory instead of the theoretically correct "incremental strain" theory in determining the displacement since for this condition the theories are identical.

A special feature of the problem studied here is to be found in the fact that no large deformation can take place until the whole of the material has become plastic. It is perhaps possible to conceive a tube which is plastic over part of its length only ; since elastic strains are neglected, such a part would be equivalent to a shorter tube, and it will be seen that in all cases a short tube is stronger than a long one. Thus the yield criterion must be satisfied over all the material, and the determination of the elastic-plastic boundary, which forms so large a part of some problems, does not arise.

2. OUTLINE OF THE ENERGY THEORY

In a solid material deformed by forces which set up a system of principal stresses $(\sigma_1, \sigma_2, \sigma_3)$ the work done per unit volume is given by the integral

$$\int (\sigma_1 \, d\epsilon_1 + \sigma_2 \, d\epsilon_2 + \sigma_3 \, d\epsilon_3) \tag{1}$$

through the changes of the principal strains $(\epsilon_1, \epsilon_2, \epsilon_3)$. It is easily shown that for an incompressible material deformed in such a way that the ratios of stress and strain remain constant and satisfy the LÉVY-MISES relation, expression (1) is equal to

$$\int_0^R S \, dR \tag{2}$$

where

$$S = \frac{1}{\sqrt{2}} \sqrt{(\sigma_1 - \sigma_2)^2 + (\sigma_2 - \sigma_3)^2 + (\sigma_3 - \sigma_1)^2},$$

$$R = \frac{\sqrt{2}}{3}\sqrt{(\epsilon_1 - \epsilon_2)^2 + (\epsilon_2 - \epsilon_3)^2 + (\epsilon_3 - \epsilon_1)^2}.$$

For an elastic material this is the strain energy of distortion per unit volume while for a plastic-rigid material it is equal to the total work done per unit volume for those deformations where the strain ratios are constant. For a plastic material deforming according to the yield criterion of VON MISES, $S = Y$ where Y is the yield stress in simple tension or compression. Thus, for a material which undergoes plastic flow at a constant value of the yield criterion, equation (2) reduces to an integral involving only the strain function.

In the present problem the tube sustains an internal pressure p with end conditions as yet unspecified. The length is l, the mean radius a, and the wall thickness h. The radial deflection, which varies along the length is denoted by the symbol U. Cylindrical co-ordinates (r, θ, z) having axis along the axis of the tube are used. Transforming the co-ordinates and employing the incompressibility condition of plastic flow we obtain :

$$R = \frac{2}{\sqrt{3}}\sqrt{\epsilon_\theta^2 + \epsilon_\theta \epsilon_z + \epsilon_z^2 + \tfrac{1}{4}\epsilon_{rz}^2} \tag{3}$$

since, by symmetry, shear strains other than ϵ_{rz} are zero.

Further analysis requires some relationship between the strains ϵ_r, ϵ_θ, ϵ_z. It is known that

$$\epsilon_r + \epsilon_\theta + \epsilon_z = 0$$

and it is proposed to assume that the neutral surface about which bending occurs coincides with the geometrical central surface of the tube. This will be almost exactly true for relatively thin tubes.

Consider now the central surface. Over most of the length this is subjected to a large circumferential stress and relatively small radial and longitudinal stresses. Thus it is effectively subject to simple tension only, and in these circumstances the strains in the two directions perpendicular to the tension may be assumed to be equal. Hence, on the central surface

$$\epsilon_r = \epsilon_z = -\tfrac{1}{2}\epsilon_\theta. \tag{4}$$

It can be shown that the adoption of any other linear relation between ϵ_z and ϵ_θ independent of z leads to an increase in the theoretical value of the work done.

The variation of ϵ_z through the wall thickness is assumed to be linear,

$$\epsilon_z = -\tfrac{1}{2}\epsilon_\theta - x\frac{d^2 U_b}{dz^2} \tag{5}$$

where U_b is the radial deflection due to bending and x is measured radially from the central surface. Also :

$$\epsilon_{rz} = \frac{dU_s}{dz} \tag{6}$$

where U_s is that part of the radial deflection due to shear.

From (5) and (6), expression (3) becomes

$$R = \sqrt{\epsilon_\theta^2 + \tfrac{4}{3}x^2\left(\frac{d^2 U_b}{dz^2}\right) + \tfrac{1}{3}\left(\frac{dU_s}{dz}\right)^2}. \tag{7}$$

ϵ_θ is treated as independent of x, and is simply U/a.

This strain function is still not in an integrable form. The next step can be envisaged if the tube is regarded as being made up of a large number of longitudinal elements each in effect forming a similar small beam spanning between the end supports. The mode of failure of such elementary beams is obvious. Either they will fail in bending in which case the shear deflections will be relatively trivial, $U_b \gg U_s$, or if the beams are very short and thick the failure will be by shear and the converse will be true, $U_s \gg U_b$. There will doubtless be a transition range in which both shear and bending failures take place nearly simultaneously, but we may hope that this condition will seldom arise in practice. Thus the strain function R has been expressed solely in terms of the radial displacement U.

Now, if Y is constant, the total work done in plastic deformation in the whole tube is

$$W = \int^V \int_0^R S\,dR\,dV = Y \int^V R\,dV = 4\pi a Y \int_0^l \int_{-\frac{h}{2}}^{\frac{h}{2}} R\,dx\,dz \tag{8}$$

Thus, if with a specified form of the radial displacement U, the function R can be integrated, the plastic work done is known, and hence the internal pressure sustained is obtained. In fact, we obtain two different values corresponding respectively to the pressure required to cause a bending failure and that required to cause a shear failure at the ends. The smaller of these values is, of course, the one required in practice.

3. Application to a Cylinder Simply Supported at the Ends

We consider first tubes which are constrained radially but not clamped (i.e. free to rotate) at the ends and in which shear deformation is unimportant. It seems likely that the form of deflection of a bending failure will be represented fairly well by a half-cosine wave, except perhaps when the tube is so long that the middle section behaves in the same way as a tube without constraint. We assume, therefore, a form which differs slightly from a cosine, while still satisfying the known conditions at the ends and the middle of the tube. Thus :

$$U_b = U = U_1 \cos\frac{\pi z}{l} + U_3 \cos\frac{3\pi z}{l}, \qquad U_s = 0, \tag{9}$$

where $U_1 + U_3 = U_c$, the radial deflection at the middle. The work done by the internal pressure is

$$W' = 4alU_1 p\,\{1 - \tfrac{1}{3}\xi\}^* \tag{10}$$

to the 1st order, where $\xi = U_3/U_1$. The aim now is to find that value of the parameter ξ which corresponds to the smallest value of the limiting pressure p.

The work done in plastic deformation is given by expression (8), where

$$R = \frac{U_1}{a}\cos\frac{\pi z}{l}\left\{\left(1 + \xi\,\frac{\cos\frac{3\pi z}{l}}{\cos\frac{\pi z}{l}}\right)^2 + \left(\frac{x}{b}\right)^2\left(1 + 9\,\xi\,\frac{\cos\frac{3\pi z}{l}}{\cos\frac{\pi z}{l}}\right)^2\right\}^{\frac{1}{2}}, \qquad b = \frac{\sqrt{3}\,l^2}{2\pi^2 a} \tag{11}$$

Equating W, the energy absorbed in deforming the material, and W', the work done by the

* Strictly the internal radius should be used in this expression but assumptions already introduced into the analysis restrict the application of the theory to relatively thin tubes. Any error in the assumptions as to strain will cause an overestimate in the yield pressure, the discrepancy becoming greater as the tube thickness increases and this will in part be compensated by using the mean radius in the expression above.

internal pressure, we obtain

$$\frac{p}{Y} = \frac{\pi}{al}\int_0^{\frac{l}{2}}\int_{-\frac{h}{2}}^{\frac{h}{2}} \cos\frac{\pi z}{l}\,\frac{1}{(1-\frac{1}{3}\xi)}\left\{\left(1+\xi\,\frac{\cos\frac{3\pi z}{l}}{\cos\frac{\pi z}{l}}\right)^2+\left(\frac{x}{b}\right)^2\left(1+9\,\xi\,\frac{\cos\frac{3\pi z}{l}}{\cos\frac{\pi z}{l}}\right)^2\right\}^{\frac{1}{2}} dx\,dz.$$

Integrating this with respect to x and changing the other variable to $\mathbf{z} = \pi z/l$ leads to

$$\frac{pa}{Yh} = \frac{1}{2(1-\frac{1}{3}\xi)}\int_0^{\frac{\pi}{2}}\left(1+\xi\,\frac{\cos 3\,\mathbf{z}}{\cos\mathbf{z}}\right)\cos\mathbf{z}\left\{\sqrt{1+\left(\frac{h}{2A}\right)^2}+\frac{2A}{h}\sinh^{-1}\left(\frac{h}{2A}\right)\right\}d\mathbf{z} \qquad (12)$$

where

$$\frac{h}{2A} = \frac{h}{2b}\left\{\frac{1+9\,\xi\,\frac{\cos 3\mathbf{z}}{\cos\mathbf{z}}}{1+\xi\,\frac{\cos 3\mathbf{z}}{\cos\mathbf{z}}}\right\}$$

is a non-dimensional ratio.

For the special case when $\xi = 0$, we have then a comparatively simple expression for the strength :

$$\frac{pa}{Yh} = \tfrac{1}{2}\left\{\sqrt{1+\left(\frac{h}{2b}\right)^2}+\frac{2b}{h}\sinh^{-1}\left(\frac{h}{2b}\right)\right\}. \qquad (13)$$

However, the correct procedure is to select that value of the parameter ξ which leads to the smallest value of the ratio p/Y for a given h/b. If this value of ξ is small compared with unity it might be permissible to use the simpler expression (13) for determination of the yield pressure. Fig. 1 shows the variation of the optimum value of ξ with $h/2b$ while Fig. 2 shows the variation of pressure with ξ for $h/2b = 2$; and the shape of deformation for minimum pressure.

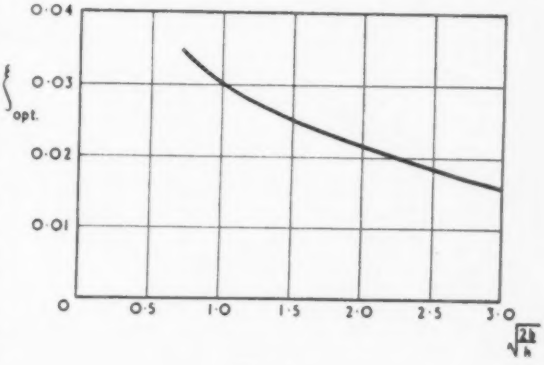

Fig. 1.

It will be seen that for an ideal plastic material having a constant yield stress Y the shape of deformation differs very little from the simple cosine form ; indeed, as the length increases the ratio ξ tends towards zero so that for a very long tube simply supported at the ends the form of deflection is a half-cosine wave and the strength is the same as that of a tube without end support.

An interesting conclusion is derived from minimizing the expression for the work done in plastic deformation (8) ; this gives the optimum shape and the minimum expenditure of energy in deforming a cylinder in the plastic range without specifying the conditions of loading (see Fig. 2). To achieve this state of affairs the work done by the applied load should be independent of ξ, a condition which is satisfied by a central circumferential line load, among other loading systems.

It can be concluded that in order to obtain an accurate estimate of the form of deformation of an expanded tube it is necessary to use expression (12), but in computing the yield pressure, which in most practical cases will be the important factor, only a small discrepancy arises if the simpler expression (13) is used.

Considering now those tubes which are likely to fail in shear, it is clear that they will be very short and the deflection due to bending will be very small ; it will be assumed, therefore, that

the deformation consists of a large shear deflection near the ends accompanied only by circumferential strain along the remainder of the tube. Now $U_b = 0$, $U_s = U = U_c$ (constant),

$$R = \sqrt{\left(\frac{U}{a}\right)^2 + \frac{1}{3}\left(\frac{dU}{dz}\right)^2}$$

where, from 0 to $\frac{l}{2} - \delta z$, $\frac{dU}{dz} = 0$; and, from $\frac{l}{2} - \delta z$ to $\frac{l}{2}$, $\frac{U}{a} < \frac{dU}{dz}$.

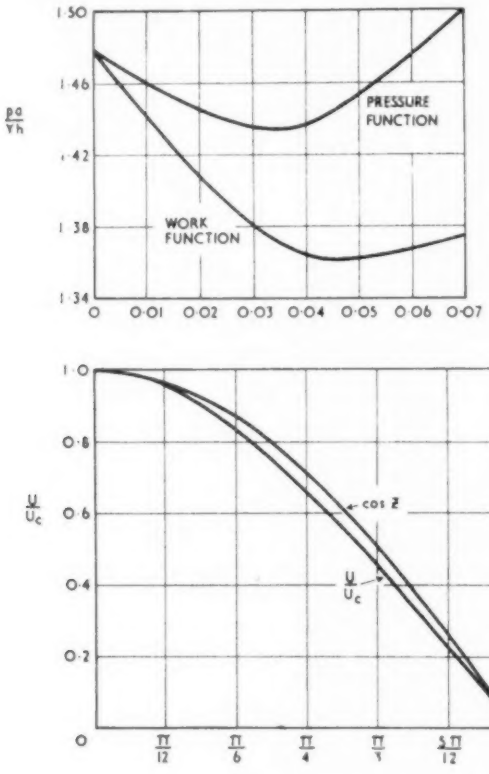

Fig. 2. Theoretical yield pressure and shape of deformation for $\frac{h}{2b} = 2$ (simple support).

So

$$\int_0^{\frac{l}{2}} R\,dz = \int_0^{\frac{l}{2}-\delta z} \frac{U}{a}\,dz + \int_{\frac{l}{2}-\delta z}^{\frac{l}{2}} \frac{1}{\sqrt{3}} \sqrt{\left(\frac{dU}{dz}\right)^2}\,dz = U_c\left(\frac{l}{d_0} + \frac{1}{\sqrt{3}}\right)$$

where $d_0 = 2a$, the mean diameter of tube. Thus

$$W = 4\pi\, Ya\, h\, U_c\left(\frac{l}{d_0} + \frac{1}{\sqrt{3}}\right).$$

The work done by the internal pressure is $W' = 2\pi\, la\, p\, U_c$.
Putting $W = W'$ we obtain

$$\frac{pa}{Yh} = \left(1 + \frac{1}{\sqrt{3}}\frac{l}{d_0}\right). \qquad (14)$$

4. Application to a Cylinder Completely Constrained at the Ends

For a simply supported cylinder the only condition imposed is that of zero radial displacement at the ends. When the cylinder is clamped – or " built-in " – at the ends a further condition imposed is that the bending rotation at the ends is zero. Since shear deformation will once again be neglected, except when failure is primarily due to shear, the latter condition implies that the total rotation at the ends is zero. A symmetrical form of deformation satisfying this condition can be represented by a series involving the terms $\cos(2\pi z/l)$, $\cos(4\pi z/l)$, $\cos(6\pi z/l)$, etc.

It is assumed that the form taken by a tube with clamped ends expanded by internal pressure is given by

$$U = \tfrac{1}{2} U_1 \left(1 + \cos \frac{2\pi z}{l}\right) + \tfrac{1}{2} U_2 \left(1 - \cos \frac{4\pi z}{l}\right). \qquad (15)$$

and we shall write $\mathbf{z} = \pi z/l$ and $\eta = U_2/U_1$.

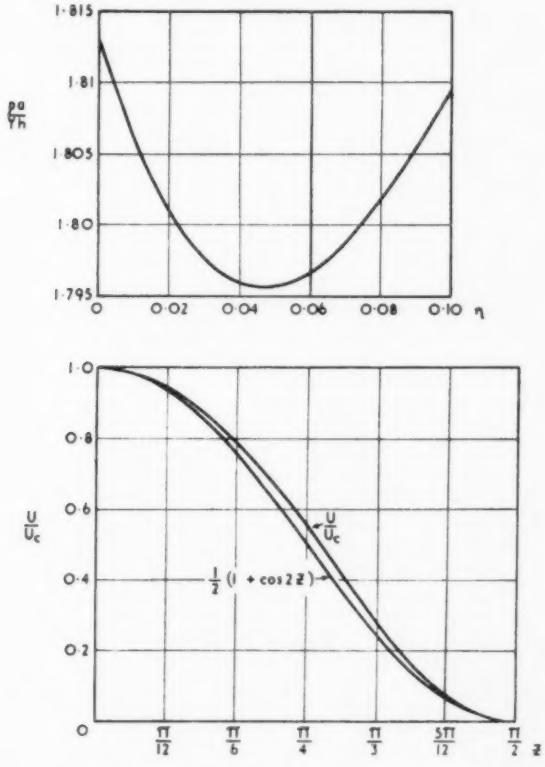

Fig. 3. Theoretical yield pressure and shape of deformation for $\dfrac{h}{2b} = 1$ (built-in ends).

The pressure required to yield a rigid-plastic cylinder will be minimized with respect to the parameter η. If it is found that η is small then the form of deformation can be adequately represented by expression (15).

Proceeding as in the last paragraph, we obtain

$$\frac{p}{Y} = \frac{8}{\pi} \int_0^{\frac{\pi}{2}} \int_0^{\frac{h}{2}} \left\{ \frac{1}{a^2} \left[\tfrac{1}{2} + \frac{1}{2(1+\eta)} (1 - v) \cos 2z \right]^2 + \frac{16}{3(1+\eta)^2} \frac{\pi^4}{l^4} (1 - 4v)^2 \cos^2 2z \, . \, x^2 \right\}^{\frac{1}{2}} dx \, dz.$$

where

$$v = \eta \frac{\cos 4\mathbf{z}}{\cos 2\mathbf{z}}.$$

Integrating with respect to x and writing $b = \sqrt{3}\, l^2/2\pi^2 a$ as before, and

$$\frac{h}{2B} = \frac{h}{2b}\left\{\frac{4(\cos 2\mathbf{z} - 4\eta \cos 4\mathbf{z})}{1 + \cos 2\mathbf{z} + \eta(1 - \cos 4\mathbf{z})}\right\} \tag{16}$$

we obtain

$$\frac{pa}{Yh} = \frac{1}{\pi}\int_0^{\frac{\pi}{2}} \frac{(1 + \cos 2\mathbf{z}) + \eta(1 - \cos 4\mathbf{z})}{1 + \eta}\left\{\sqrt{1 + \left(\frac{h}{2B}\right)^2} + \frac{2B}{h}\sinh^{-1}\left(\frac{h}{2B}\right)\right\} d\mathbf{z}. \tag{17}$$

This must be integrated numerically with respect to $\mathbf{z}$. In the special case $\eta = 0$,

$$\frac{pa}{Yh} = \frac{1}{\pi}\int_0^{\frac{\pi}{2}} (1 + \cos 2\mathbf{z})\left\{\sqrt{1 + \left(\frac{h}{2B}\right)^2} + \frac{2B}{h}\sinh^{-1}\left(\frac{h}{2B}\right)\right\} d\mathbf{z}. \tag{18}$$

When the tube is so short that failure is due to shear at the ends, it is assumed that the deflection due to bending is negligible and so the type of constraint at the ends is of little consequence. Thus for failures of this kind the analysis is the same as that for simply supported tubes.

Values of the pressure integral over a range of values of η are shown in Fig. 3 for $h/2b = 1$; also shown is the form of deformation, which differs only slightly from a complete cosine wave. The variation in the pressure integral with η is so small over the range examined that the yield pressure can quite well be found by integrating the simpler expression (18) which assumes that the form of deformation is an exact cosine. It might be noted here that extraction of the optimum values of ξ and η from equations (12) and (17) requires accurate computation, but of course this accuracy is not required in evaluating the simpler pressure expressions.

5. Application to a Cylinder Completely Constrained at One End

It is possible that in certain design problems it will be convenient to constrain a cylinder completely at one end while the other end can only be simply supported. In view of the foregoing results we can obtain an indication of the effect of such a system of constraints on the strength of a tube by assuming that the deformation takes the form of a half complete cosine wave between the built-in end and the point of maximum deflection and a quarter cosine wave for the remainder of the tube. This leads to the result

$$\frac{pa}{Yh} = \frac{f_1\left(\frac{h}{2B_1}\right) + \sqrt{2}\, f_2\left(\frac{h}{2b_2}\right)}{\pi + 2\sqrt{2}} \tag{19}$$

where

$$f_1\left(\frac{h}{2B_1}\right) = \int_0^{\frac{\pi}{2}} (1 + \cos 2\mathbf{z})\left\{\sqrt{1 + \left(\frac{h}{2B_1}\right)^2} + \frac{2B_1}{h}\sinh^{-1}\frac{h}{2B_1}\right\} d\mathbf{z},$$

$$f_2\left(\frac{h}{2b_2}\right) = \left\{\sqrt{1 + \left(\frac{h}{2b_2}\right)^2} + \frac{2b_2}{h}\sinh^{-1}\frac{h}{2b_2}\right\},$$

$$\frac{h}{2B_1} = \frac{h}{2b}\frac{(3 + 2\sqrt{2})\cos 2\mathbf{z}}{2(1 + \cos 2\mathbf{z})}, \quad \text{and} \quad \frac{h}{2b_2} = \frac{h}{2b}\left(\frac{3 + 2\sqrt{2}}{4}\right).$$

$h/2b$ is the same ratio as before.

The position of maximum deflection has been found from the condition that there must be no discontinuity in the curvature.

6. Numerical Results

The values of yield pressure for the three end conditions computed from (13), (18) and (19) are shown in Fig. 4 plotted against the general variable $2b/h$ and

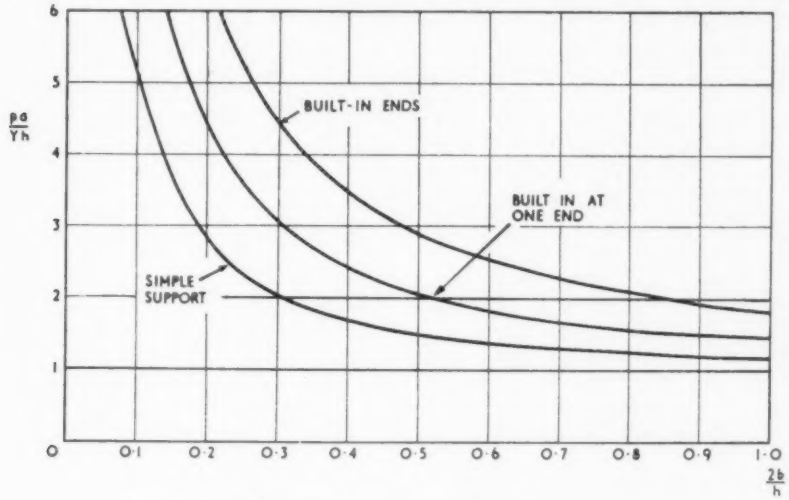

Fig. 4. Theoretical yield pressure (bending failure).

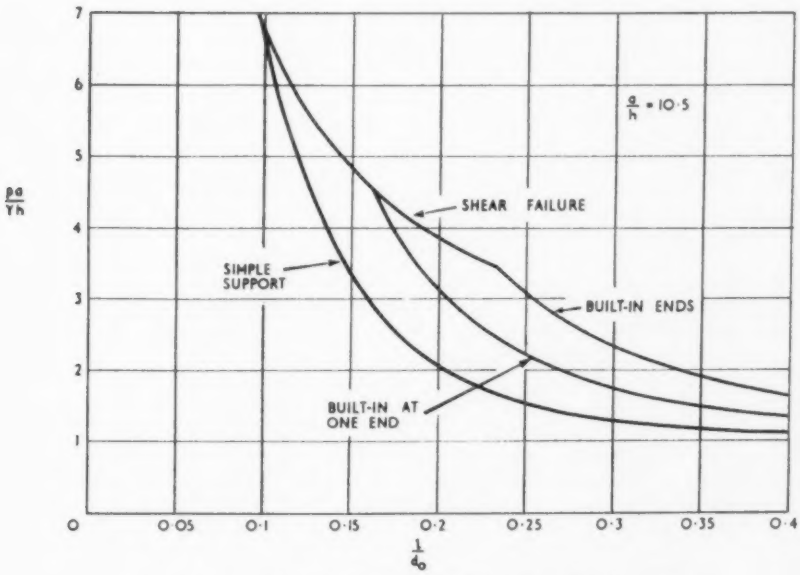

Fig. 5. Theoretical yield pressure for three end conditions.

in Fig. 5 against l/d_0 for the value of $a/h = 10{\cdot}5$; in the latter figure the limitation imposed by the shear failure condition (14) is shown. The forms of deformation have appeared in previous paragraphs.

The treatment outlined above produces results whose numerical values are

easily computed, particularly for a tube simply supported at the ends where only a slide-rule calculation is necessary. A further advantage is that the strength of a tube of any dimensions can be represented in terms of one non-dimensional variable $h/2b$, within the limitation imposed by the shear failure condition. Shear failures should be very rare as the specimen would be so short that a better description would be " ring " rather than " tube."

On the other hand, the energy theory is essentially an approximate one and in view of the assumptions made it seems probable that the results will be in error for thick tubes. It seems unlikely, however, that applications will arise where the effect of end support is of importance in thick tubes which in general will be fairly long and undergo only partial yielding. Thus the energy treatment will probably satisfy all those design problems where the end support is significant.

7. Application to a Work Hardening Material

The expressions already derived for the yield pressure of a cylinder of ideal plastic material serve as an indication of the yield pressure for specimens of all ductile materials with a well defined yield point, but they give no indication of the behaviour of such specimens beyond this stage. To proceed further the effect of work hardening must be considered. It is assumed that there exists a unique relation between equivalent shear stress and equivalent shear strain (Morrison and Shepherd 1950).

As a cylinder of work hardening material is expanded, it loses the uniformity of equivalent shear stress possessed by an ideal plastic specimen ; we might expect, therefore, that the shape of deformation will vary during straining. In such a situation, the deformation must be considered on the basis of an " incremental " type strain theory. Such an approach, with the assumption that there exists a unique relation between equivalent shear stress and equivalent shear strain, shows that for a simply supported tube the variation in shape is extremely small ; only a small discrepancy is introduced in the pressure prediction if it is assumed that the shape remains an exact cosine throughout deformation and the work is integrated according to the total strain theory.

As an example of an actual material the steel which is used for most of the experiments will be considered. An expression which fits quite closely the tensile stress/strain curve is of the type

$$\sigma = Y + \frac{\alpha\epsilon}{1 + \beta\epsilon}$$

where the line of elastic deformation is taken as the axis of stress ; α and β are constants.

Since it is assumed that the form of deformation is an exact cosine throughout the expansion, the work done by the internal pressure is given by

$$W' = \int_0^v p\,dv = 4a^2 l \int_0^{\epsilon_{\theta_c}} p\,d\epsilon_{\theta_c}$$

where ϵ_{θ_c} is the circumferential strain at the middle of the tube. The work done in plastic deformation is given by the total integration

$$W = 4\pi a \int_0^{\frac{l}{2}} \int_{-\frac{h}{2}}^{\frac{h}{2}} \int_0^R S\,dR\,dx\,dz.$$

Now

$$S = Y + \frac{\alpha R}{1 + \beta R}$$

So

$$W = 4\pi a \int_0^{\frac{l}{2}} \int_{-\frac{h}{2}}^{\frac{h}{2}} \left\{ \left(Y + \frac{\alpha}{\beta} \right) R - \frac{\alpha}{\beta^2} \log_e (1 + \beta R) \right\} dx\,dz.$$

Equating W and W', differentiating with respect to ϵ_{θ_c} and integrating with respect to x and z we obtain

$$p = \left(Y + \frac{\alpha}{\beta}\right)\frac{h}{2a} \cdot J - \frac{\alpha}{\beta^2} \cdot \frac{1}{a\epsilon_{\theta_c}} \left\{\frac{h\pi}{2} - \int_{-\frac{h}{2}}^{\frac{h}{2}} f(B_0)\, dx\right\}$$

where

$$J = \left\{\sqrt{1 + \left(\frac{h}{2b}\right)^2} + \frac{2b}{h} \sinh^{-1}\left(\frac{h}{2b}\right)\right\}, \qquad B_0 = \beta\epsilon_{\theta_c}\sqrt{1 + \left(\frac{x}{b}\right)^2}$$

and

$$f(B_0) = \begin{cases} \dfrac{\cos^{-1} B_0}{\sqrt{1 - B_0^2}} & \text{when} \quad B_0^2 < 1 \\ 1 & \text{when} \quad B_0 = 1 \\ \dfrac{\cosh^{-1} B_0}{\sqrt{B_0^2 - 1}} & \text{when} \quad B_0^2 > 1. \end{cases}$$

The integration with respect to x in the second term must be performed numerically.

In the special case of a material which exhibits linear work hardening the stress-strain curve can be represented by

$$\sigma = Y + \mu\epsilon$$

Then, for a simply supported tube

$$\frac{pa}{Yh} = \frac{J}{2} + \frac{\mu}{Y} \cdot \frac{K}{4} \cdot \epsilon_{\theta_c}, \qquad \text{where} \qquad K = \pi\left\{1 + \tfrac{1}{3}\left(\frac{h}{2b}\right)^2\right\}.$$

Vol. 2 53/54

8. Experimental Work

A number of steel tubes having a fixed external diameter, but various lengths and thicknesses, have been tested to destruction by hydraulic pressure to check the accuracy of the foregoing theory. The apparatus is shown in Fig. 6.

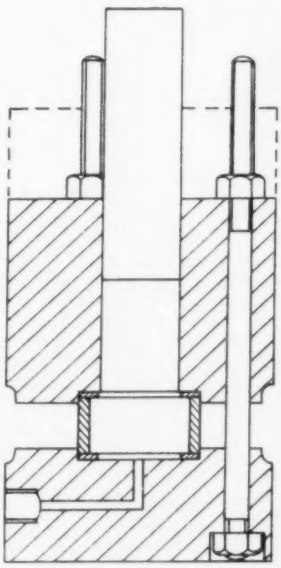

Fig. 6. Internal pressure apparatus.

The specimen was held in recesses between two cylindrical end-pieces held together by bolts, which were kept just tight so that they did not exert any appreciable direct compression on the specimen. The upper end-piece had a cylindrical hole through which passed a well-fitting plunger. The lower one had a small hole to which could be attached a Budenberg pressure gauge reading up to 12 tons per sq. in. The internal space was filled with oil and the whole was placed in an Avery 50 ton Universal testing machine on the compression side. The load on the plunger and hence the internal pressure could be read direct as the load imposed by the machine, and this could be checked against the Budenberg gauge. In the earlier tests no special sealing devices were employed; the tubes by yielding very slightly radially at the points of support sealed themselves effectively into the recesses. A slow leakage past the plunger took place but this was regarded as advantageous as it tended to reduce friction. Since some

of the tests lasted several hours, it meant that the load had to be removed and the oil replenished several times during a test, as is indicated in Fig. 7. These unloading periods seemed to be without effect on the stress-strain curves as a whole. After somehigh pressure tests had been carried out, however, some slight yielding of the upper end-piece took place, so that the plunger became a rather

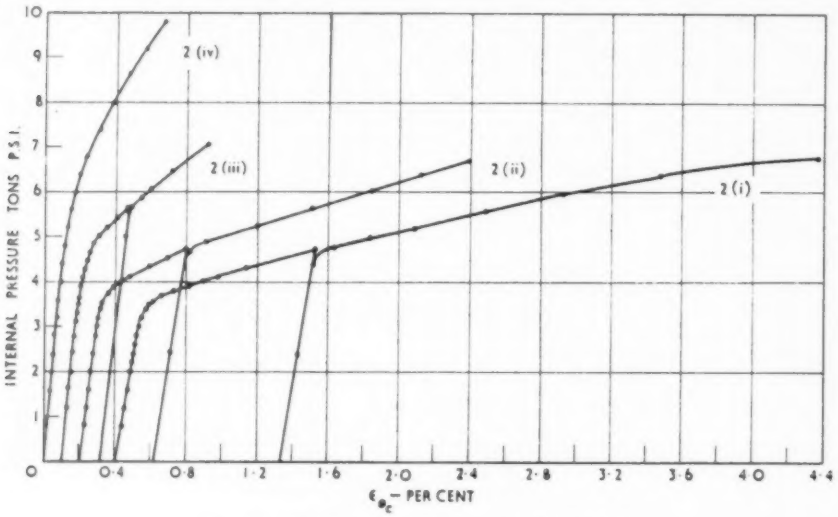

Fig. 7. Pressure-deflection curves (Series A2).

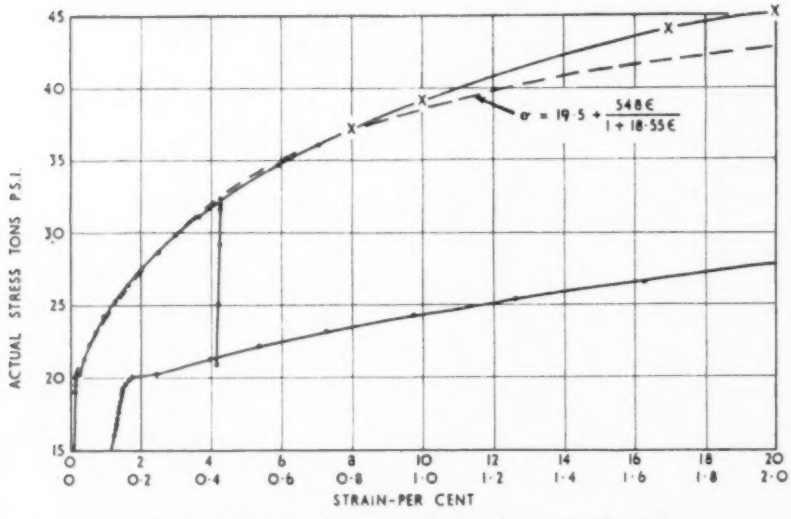

Fig. 8. Plastic stress-strain curve for Steel A in simple tension.

looser fit and an ordinary fibre sealing ring had to be employed. Agreement between the measured pressure and that deduced from the load on the machine, however, remained satisfactory indicating that no large friction had been introduced.

The expansion of the tubes under internal pressure was measured either directly

by micrometer observation or by employing as a resistance strain gauge a single strand of annealed copper-nickel wire of diameter 0·002 in., wound round the circumference of the tube. The gauge factor of this arrangement was found to be constant up to strains of at least 5%. The shape of permanent deformation was measured in a two-way travelling microscope.

TABLE 1.

Results of Preliminary Tension and Compression Tests (Steel A)

No.	*Test*	*Yield Stress Tons p.s.i.*
Aa	Tension	19·8
Ab	Tension	19·78
Ac	Tension	19·8
Ad	Compression	19·89
Ae	Compression	20·18
Af	Compression	19·84

Ad cut at right angles to axis of billet ;
Ae cut at right angles to axis of billet and to Ad ;
Af cut parallel to axis of billet.

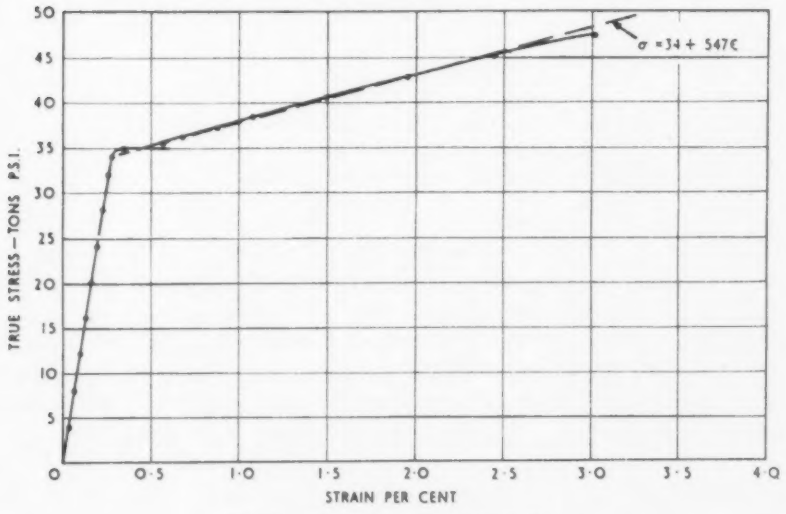

Fig. 9. Tensil test on specimen Ba.

Two steels were used in the tests. The first, Steel A (0·26-0·28% C, 0·08-0·11% Si, 1·4-1·8% Mn ; 20 tons p.s.i. yield stress) was used in the majority of the specimens. A few of Steel B (0·54-0·56% C, 0·13-0·17% Si, 0·26-0·28% Mn ; 35 tons p.s.i. yield stress) were supplied when the tests on Steel A were under way.

The homogeneity and isotropy of the material employed were checked by direct tension and compression tests on solid specimens made from billets of the appropriate materials. Results are shown in Tables 1 and 2 and Figs. 8 and 9; both materials were shown to be isotropic.

In order to obtain comparable results for the stress-strain properties of the material in the exact condition found in the tubes, it was thought desirable to use identical specimens for test in direct compression. The difficulty in doing so is, of course, to ensure that the load is imposed exactly along the axis of the tube so that the compression stress is the same at all points on the circumference

TABLE 2.

Results of Tension and Compression Tests (Steel B)

No.	*Test*	*Yield Stress Tons p.s.i.*
Ba	Tension	35·0
Bc	Compression (Solid)	35·18
Bd	Compression (Solid)	35·18
Be	Compression (Cylinder)	34·9
Bf	Compression (Cylinder)	34·8

Bc cut parallel to axis of billet;
Bd cut at right angles to axis of billet.

(MORRISON 1940). A device believed to be original was employed in this connection. The specimen was loaded through spherical seats, and also through small cylindrical blocks which were located so that their centres exactly coincided with the axis of the test tube as in Plate 1. Four ordinary strain gauges were affixed to the surface of each of these blocks at equally spaced points on the circumference. A small load was imposed first. If the strains recorded by the strain gauges were not identical, a small adjustment could be made by tapping the spherical seats. It was usually possible without much difficulty to adjust to the position in which this load was purely axial, and it was found to remain so when full load was imposed. The strain in the specimen itself was measured by three Huggenburger extensometers.

Results of compression tests carried out in this way are shown in Table 3. It will be seen that work hardening due to machining stresses has raised the yield point of material A appreciably. This effect is naturally most marked in the thinner specimens Ag and Ah; and least marked in the specimen Aj in which

Vol.
2
53/54

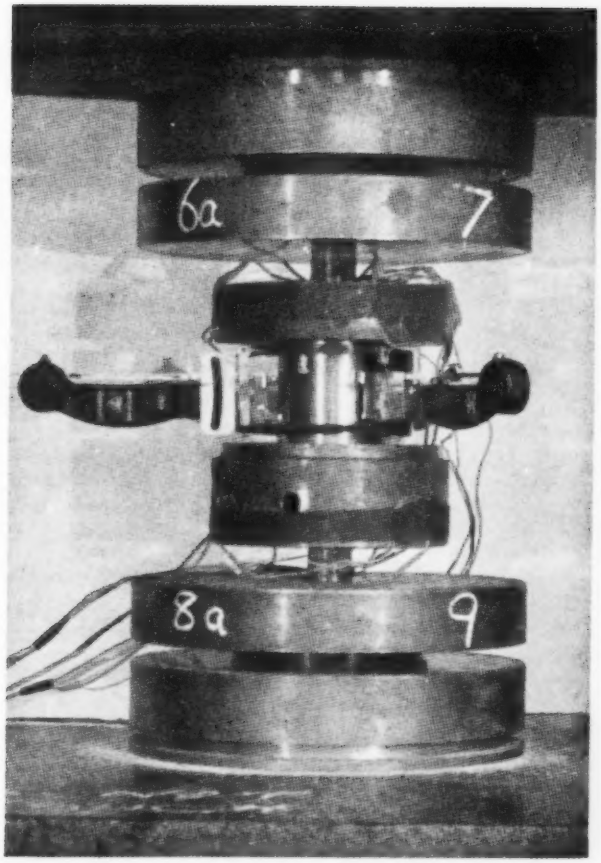

Plate 1.

Vol
2
1953/

particular care was taken to approach the final condition by a series of " fine cuts." These tests were in fact performed late in the programme, and the extent to which machining had modified the specimens was not appreciated until most of the internal pressure tests had been completed. No machining effect was observed with material B.

The series of experiments on tubes subject to internal pressure was designed to check the accuracy of the theoretical work and so the specimen dimensions were dictated by the computed results of the theory. The curves shown in the theoretical section show that radial constraint at the ends has a significant effect on the strength only if the tube is very short and all the tubes tested were in this range.

TABLE 3.

Results of Compression Tests on Tubes (Steel A)

No.	*Wall thickness in.*	*O.D. in.*	*Yield Stress Tons p.s.i.*
Ag	0·125	2·75	21·74
Ah	0·125	2·75	21·78
Ai	0·25	2·75	21·2
Aj	0·25	2·625	20·6

Vol. 2 53/54

The chief aim throughout the investigation was to obtain a suitable criterion for design which would estimate the pressure at which major permanent deformation commenced. Thus the experiments were designed primarily as a measure of the validity of the limit design theory, the secondary object being to discover as much as possible about the behaviour of the specimens in the hardening range.

Most of the experiments were done on simply supported tubes and these will be described first.

Steel A.
- Series 1 – wall thickness 0·125 in. (7 tubes)
- Series 2 – wall thickness 0·1875 in. (4 tubes)
- Series 3 – wall thickness 0·25 in. (3 tubes)

Steel B. Series 1 – wall thickness 0·125 in. (4 tubes)

The only feature of the experimental technique which requires elaboration is the way in which the effective lengths of the tubes were determined. Plainly, it is impossible to support the ends of a cylinder on a circle in the mathematical sense. There are two limitations on an attempt to do so when the tube is subject to internal pressure. The first is that there must be an " overhang " of the tube beyond the effective circle of support. The second is that the end of the tube cannot be supported by a line contact only, but must have an area of contact. (The recesses in the heads were 0·0625 in. deep for Series A1 and B1 and 0·125 in. deep for series A2 and A3.)

It can be shown analytically that with the present experimental set-up the first limitation is of no importance; the second is of more consequence. After the first test a slight deformation of the edges of the recesses in the heads was observed; this increased during each subsequent test. Although this deformation was at first very small, it was clear that the edge of the recess could not be taken as the effective end of the tube, since the tube was expanding for a small distance inside the recess. It was decided, therefore, to measure the shape contour of the tube soon after yield and take as the effective length that length over which expansion had occurred. That this is satisfactory as far as yielding and early deformation are concerned can be shown by computing the work dissipated in

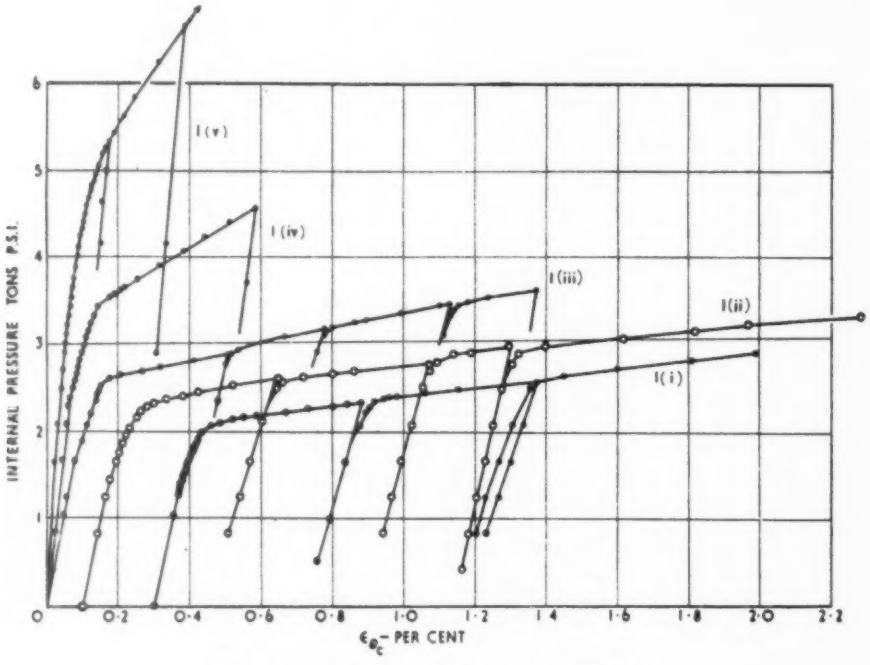

Fig. 10. Pressure-deflection curves (Series A1).

deforming the material in the heads round the recesses; it is trivial compared with the work done on the tubes. However, when the tube is very short the support given by the recesses is significant at large deformations, the tube becoming effectively shorter as expansion proceeds.

Typical curves of internal pressure against central circumferential strain for the simply supported tubes are shown in Figs. 7 and 10. In most of the tests there were two points of significance on the loading curve in the range of small strains; the first a departure from near-linearity, indicating presumably the first yielding at the middle plane of the tube, the second a distinct " yield " point for the tube as a whole, beyond which any remaining elastic region exerted no apparent restraint on the subsequent plastic distortion. A summary of the main

results appears in Table 4. The yield pressure was determined by fitting to the loading curve two straight lines, one immediately before and one immediately after yield.

TABLE 4.

Results of Internal Pressures Tests (Simple Support, Bending Failures)

Specimen		l	l/d_0	$2b/h$	pa/Yh
A1	(i)	0·977	0·372	1·021	1·10
	(ii)	0·820	0·312	0·719	1·20
	(iii)	0·725	0·276	0·562	1·38
	(iv)	0·55	0·209	0·323	1·83
	(v)	0·45	0·171	0·216	2·52
A2	(i)	0·94	0·367	0·645	1·243
	(ii)	0·87	8·339	0·553	1·34
	(iii)	0·77	0·300	0·433	1·575
	(iv)	0·66	0·258	0·318	—
A3	(i)	1·36	0·544	1·042	1·05
	(ii)	1·25	0·5	0·877	1·13
	(iii)	0·905	0·362	0·460	1·47
B1	(i)	0·912	0·347	0·887	1·13
	(ii)	0·792	0·302	0·672	1·33
	(iii)	0·640	0·244	0·439	1·50
	(iv)	0·535	0·211	0·328	1·87

Only one result was recorded for a tube with built-in ends. The specimen was machined from a tube of Steel A, 3 in. long, 2·75 in. O.D. and 2 in. I.D. In order to produce approximately built-in conditions it was found necessary to reduce the wall thickness of the effective tube to 0·05 in.; the length was 0·54 in. ($h/2b = 1$). The shape of the deformation is shown in Fig. 11.

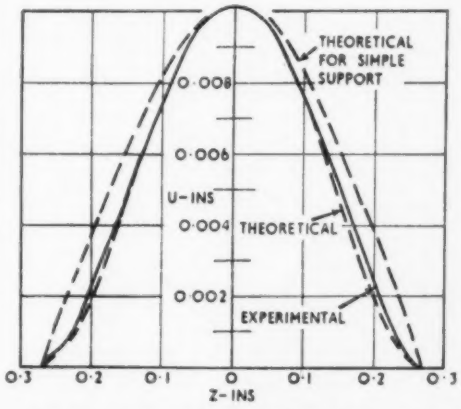

Fig. 11. Shape of deformation of tube with built-in ends.

9. Discussion

The feature of the work on which agreement between theory and experiment is most accurate is considered first. This is the shape of permanent deformation. Figs. 12 and 13 show the state of deformation after testing some of the tubes which failed in bending; these figures illustrate that in this quantity the discrepancy between theory and

experiment is barely measurable, and amply justify the omission of shear deflection in bending failures from the analysis.

Before the pressures sustained by the tubes are considered, attention must be paid to the high values of yield stress obtained in the compression tests on cylinders

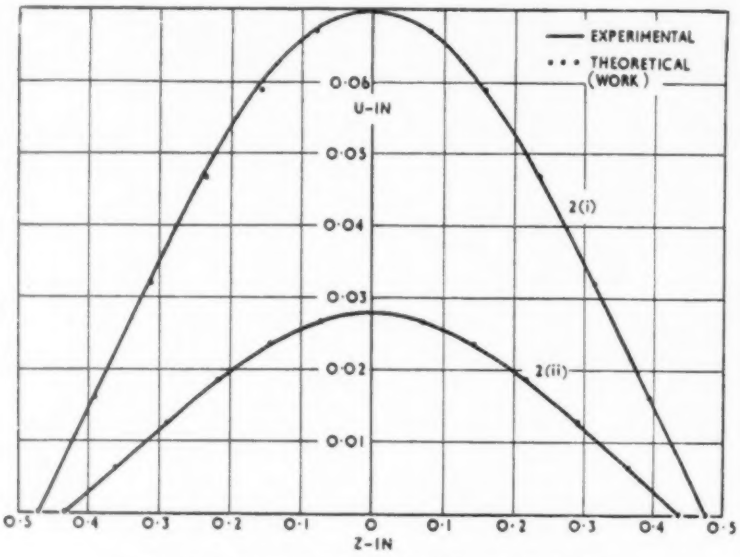

Fig. 12. Shape of deformation (Steel A, Series 2).

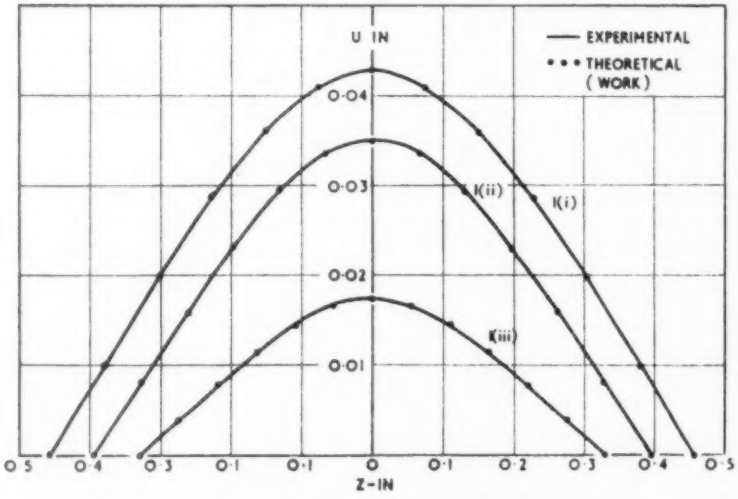

Fig. 13. Shape of deformation (Steel B, Series 1).

of Steel A. A correction could be made by using for each tube thickness the appropriate mean compressive yield stress, but this arrangement seems far from satisfactory; it will be seen that the results of internal pressure tests on Steel B indicate that the machining effect on Steel A is not nearly so serious as might be expected.

Turning now to the consideration of the internal pressure results in detail, some of the pressure-expansion curves are reproduced without experimental points and unloading curves in Figs. 14 and 15. On these diagrams have been

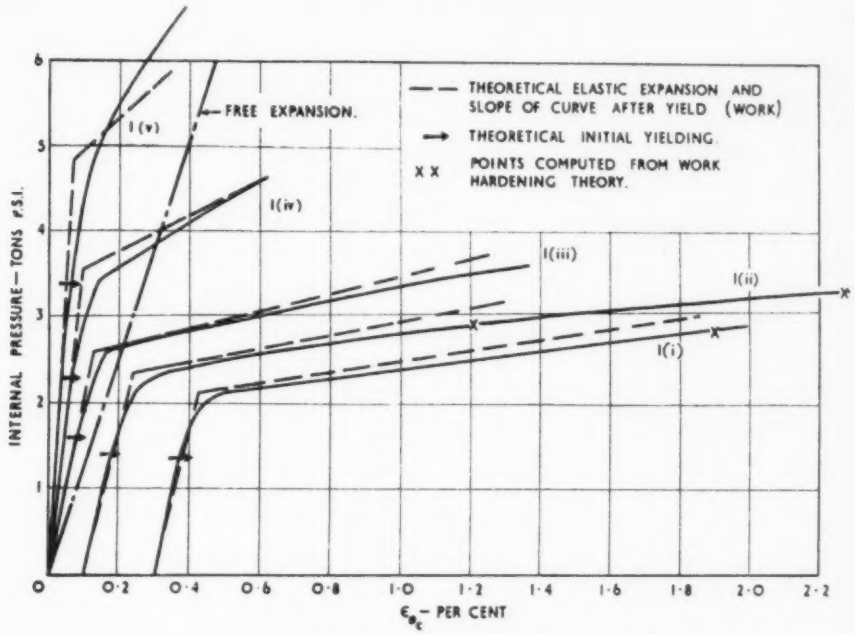

Fig. 14. Pressure-deflation curves (Series A1).

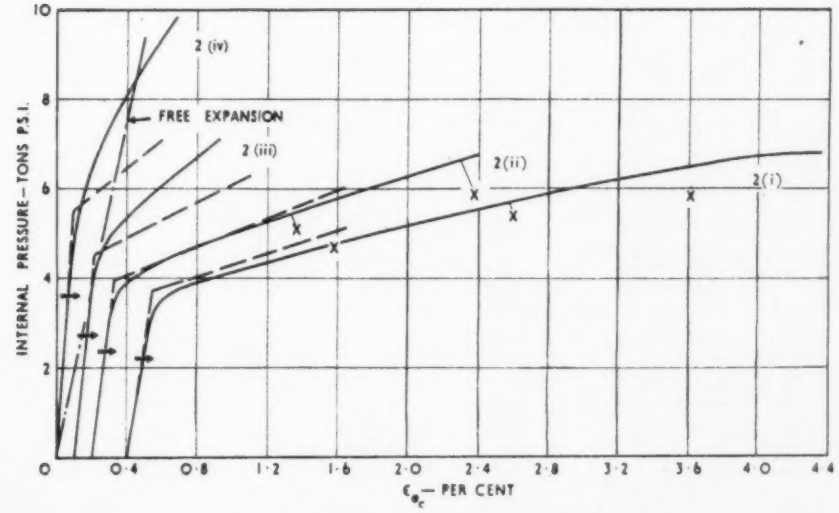

Fig. 15. Pressure-deflection curves (Series A2).

drawn (i) the theoretical expansion in the elastic range, (ii) the slope of the pressure-deflection curves after yield according to the simple work-hardening theory with a linear stress-strain relation for both materials as in Section 7. The discontinuities

in these broken lines represent the yield pressures predicted by the theory of Section 6 and the chain-dotted line on each diagram represents the elastic expansion of a similar tube without end support. The bold crosses stand for points computed according to the work hardening theory using an approximation to the true stress-strain curve of Steel A as in Section 7, and the arrows crossing the curves indicate the points of initial yielding according to simple elastic theory.

The pressures at which major permanent deformation began agree within a few per cent with the work theory in all those cases where the points on the loading curves can be distinctly located. In some of the shortest tubes such obvious discontinuities did not occur but in all except one, A2 (iv), the simple construction previously described could be easily applied. The yield pressures are plotted against $2b/h$ in Fig. 16.

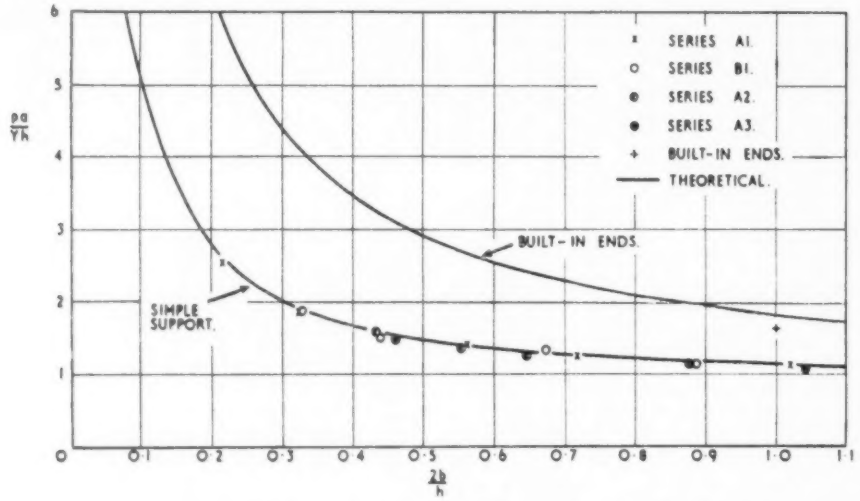

Fig. 16. Theoretical and experimental yield pressures (bending failures).

While for the longer tubes the agreement between theory and experiment is satisfactory over the whole range, for the short ones like 2 (iii) and 2 (iv) in Fig. 15, the internal pressure sustained increases more rapidly than is predicted. It is believed that this is due solely to the imperfection of the end supports. Some yielding of the lip of the recess in which the tubes fitted unavoidably took place. This meant that in the later higher-pressure tests there was a tendency for the unsupported length to become less as the deformation proceeded, so that the tube apparently became stronger. This effect was more marked in the case of a short tube than in a long one for two reasons: first, because any given reduction in length makes a larger proportionate change when the overall length is small, and, second, because a given radial expansion implies a larger terminal slope when the length is short, and hence a given modification in the point of support takes place at a smaller value of ϵ_θ.

The last test to be considered is that on a tube with built-in ends. The experimental shape of permanent deformation at an internal pressure of 2 tons p.s.i. is shown in Fig. 11 where it is compared with the corresponding theoretical shape

and the theoretical shape for a simply supported tube. The agreement with theory is quite good, a small discrepancy arising near the ends. The explanation of this is most probably that complete " built-in " conditions could not be obtained, the inside of the specimen having the same diameter before deformation as the thick end sections of the cylinder; shear deformation is unlikely to account for the difference with this relatively large span to thickness ratio (about 11 : 1). The yield pressure for $2b/h = 1$ was found to be 8% below the theoretical value, which might also be due to incomplete building-in. The experimental results thus indicate the approximate validity of the work theory, despite the fact that the experimental arrangement could not comply with all the conditions set out in the analysis. The treatment is particularly suitable as a criterion of design, which is the ultimate object of all such investigations, since its lack of precision is amply compensated by its simplicity of application. The inaccuracies in the simplifying assumptions in the analysis have been shown not to introduce large errors in the final result. One of the advantages of methods of this kind is that the solution involves the integration of the strain functions and serious local errors need not necessarily have a correspondingly serious effect on the overall result.

Vol.
2
53/54

Acknowledgments

We wish to express our thanks to the Ministry of Supply for a grant which enabled this work to be carried out. We are particularly grateful to the Armament Design Establishment, which not only provided nearly all the material tested, but also made in their own workshops a large number of the test specimens.

References

Hill, R.	1950a	*Mathematical Theory of Plasticity*, p. 67.
	1950b	*J. Appl. Mech.*, **17**, 64.
	1951	*Phil. Mag.*, **42**, 868.
Hill, R. and Siebel, M. P. L.	1953	*J. Mech. Phys. Solids*, **1**, 207.
Hodge, P. G. and White, G. N.	1950	*J. Appl. Mech.*, **72**, 180.
Morrison, J. L. M.	1940	*Proc. I. Mech. E.*, **142**, 193.
Morrison, J. L. M. and Shepherd, W. M.	1950	*Proc. I. Mech. E.* (*App. Mech.*), **163**, 1.
Onat, E. T. and Prager, W.	1953	*J. Mech. Phys. Solids*, **1**, 77.

Journal of the Mechanics and Physics of Solids, 1954, Vol. 2, pp. 238 to 258. Pergamon Press Ltd., London.

AN EXPERIMENTAL INVESTIGATION OF RESIDUAL STRESSES IN HOLLOW CYLINDERS DUE TO THE CREEP PRODUCED BY THERMAL STRESSES

By Y. G. Attia, D. Fitzgeorge and J. A. Pope
Departments of Civil & Mechanical Engineering, University of Nottingham

(*Received 1st March*, 1954)

Summary

The paper describes an investigation into the residual stresses produced in cast iron cylinders by the creep-relaxation of thermal stresses. The connexion of the work with failures of combustion chamber parts in large internal combustion engines is discussed.

A series of thick-hollow cylinders were subjected to a radial flow of heat by heating the bore and water-cooling the outer diameter for a chosen period of time, during which the thermal stresses were relaxed by creep. The residual stresses due to relaxation were determined by slitting the cylinder and subsequently boring out concentric layers from the inside, the resulting changes in strain at the outside diameter being measured.

The creep strains are confined to the inner layers of the wall and result in a steep residual stress gradient within those layers. The residual stress at the bore (in the extreme case) is $4\frac{1}{2}$ times that at the outside diameter. Creep in compression at the bore is the predominating factor in causing residual stresses on cooling.

1. Introduction

In internal combustion engines above a certain size it is necessary to introduce cooling fluids to prevent the temperatures of the cylinder liner, cylinder cover and piston crown rising to a value which would prohibit satisfactory operation. This results in a flow of heat across those parts. The heat flow gives rise to a temperature gradient across the walls, which in turn creates a tendency for the walls to bend. The rigidity of the component, however, partially suppresses this flexure and thermal stresses are set up.

At the working temperatures which exist in combustion chamber parts the phenomenon of creep takes place, causing a relaxation of the thermal stresses. While in one sense this may be considered an advantage, it is undesirable inasmuch as when the engine is shut down and the combustion chamber parts become cool, a state of residual stress exists within them. The layers of material nearest to the burning cylinder gases operate under compressive stresses when the engine is running and, on cooling, contain residual tensile stresses.

The maximum thermal compressive stress occurring within the hot regions of the part at the first heating is much higher than the corresponding maximum tensile stress within the cooler regions. This is fortunate, as cast iron is commonly used in these components and is much stronger in compression than in tension.

Furthermore, design evolution has long ago eliminated failures which occurred on the first heating due to tensile fracture. On cooling down, however, the stresses are reversed and the regions affected by creep under compressive stresses have residual tensions. If the initial thermal stress is sufficiently high, the residual tension may be sufficient to cause a crack, in spite of its value being numerically smaller than the initial compression.

The object of the present experiments was to determine the magnitude of the residual tensions in relation to the initial compressions.

It was decided to use hollow cylinders heated on the inside and cooled on the outside, thus promoting a radial flow of heat. This system had the following advantages :

(a) The initial thermal stresses were readily calculable from existing formulae.
(b) A symmetrical distribution of temperature and stress could be obtained.
(c) No external forces need be used to constrain the cylinders.
(d) The cylinders would be readily adaptable to residual stress measurements.
(e) The test would simulate the steady-state thermal conditions in cylinder walls.

Vol. 2 53/54

The problem of determining a suitable shape and size of hollow cylinder can be appreciated by the following data. Consider a cylinder 2 ft. 4 in. o.d. × 2 ft. 0 in. i.d. × 5 ft. 0 in. long, the dimensions of a typical cylinder liner, with a temperature at the bore 250°C higher than that at the outside diameter. Such conditions of temperature and stress would approximate to those obtaining in a cylinder liner of similar size. The compressive stress at the bore would be about $12\frac{1}{2}$-ton/sq. in. The power required to maintain the temperature difference would be approximately 800 kW. This prohibits a full scale laboratory test.

The relations between power expended, temperature difference, cylinder proportions to size were studied and the final size of the test cylinder was fixed at 13 in. o.d. × $4\frac{1}{2}$ in. i.d. × $4\frac{3}{4}$ in. long. The $4\frac{1}{2}$ in. diameter bore was the smallest size inside which it was estimated that the necessary power could be developed with the highest possible winding temperature. The required temperatures and stresses could have been realized with ease in a cylinder double the size, but the maximum outside diameter was limited by the cost of the specimen and the available handling and boring facilities. A further factor limiting the diameter of the heating element (and hence the cylinder bore) is the expansion of the coils. The power estimated to establish a temperature difference of 200°C across the chosen cylinders is $7\frac{1}{4}$ kW. The tangential compressive stress under these conditions, using the formula (2a) for short cylinders, is $12\frac{1}{2}$ tons/sq. in. at the bore, which is of the same order as estimated values for cylinder liners in published literature. The bore temperature also approximates to recorded values of liner temperature measurements.

(i) *The temperature distribution in hollow cylinders*

In a hollow cylinder in which heat flows uniformly in radial directions, the isothermals are cylindrical surfaces concentric with the cylinder axis. If the thermal conductivity may be regarded as remaining constant regardless of temperature, the temperature at any radius of the wall is given by

$$\theta = \theta_D \frac{\log (k/n)}{\log k}, \tag{1}$$

where θ_D is the temperature difference between the inner and outer radii, k is the ratio of the outer radius to the inner radius and n is the ratio of the radius considered to the inner radius.

The temperature has therefore a logarithmic distribution along the radius, the general form of which is shown in Fig. 3a.

(ii) *Thermal stresses in hollow cylinders*

The tangential, radial and axial thermal stresses in infinitely long hollow cylinders with a concentric temperature distribution defined by equation (1) are given by the following equations (Timoshenko 1951) :

$$\sigma_t = \frac{E \alpha \theta_D}{2(1-\nu)} \left[\frac{1 - \log (k/n)}{\log k} - \frac{k^2 + n^2}{n^2 (k^2 - 1)} \right], \tag{2}$$

$$\sigma_r = \frac{E \alpha \theta_D}{2 (1-\nu)} \left[\frac{k^2 - n^2}{n^2 (k^2 - 1)} - \frac{\log (k/n)}{\log k} \right], \tag{3}$$

$$\sigma_a = \frac{E \alpha \theta_D}{2 (1-\nu)} \left[\frac{1 - 2 \log (k/n)}{\log k} - \frac{2}{k^2 - 1} \right], \tag{4}$$

where E is Young's modulus, α is the coefficient of linear expansion, and ν is Poisson's ratio.

In the case of a hollow cylinder of negligible length, the stress in the axial direction is non-existent, and the above relations become

$$\sigma_t = \frac{E \alpha \theta_D}{2} \left[\frac{1 - \log (k/n)}{\log k} - \frac{k^2 + n^2}{n^2 (k^2 - 1)} \right], \tag{2a}$$

$$\sigma_r = \frac{E \alpha \theta_D}{2} \left[\frac{k^2 - n^2}{n^2 (k^2 - 1)} - \frac{\log (k/n)}{\log k} \right], \tag{3a}$$

$$\sigma_a = 0. \tag{4a}$$

The difference between equations (2) and (2a) and between (3) and (3a) is the factor $1/(1-\nu)$. The stresses within a cylinder of finite length will vary along the length. If the cylinder is sufficeintly long the stresses at mid-length will approach the values given by equations 2, 3 and 4. The cylinders used in the present series of tests were very short and the expressions (2a) and (4a) are therefore more applicable than (2) to (4). Any small error resulting from the use of the second set of equations will be that the calculated values of the tangential and radial stress will be less than those actually present.

(iii) *The relaxation of stress within a heated bar*

Consider a bar of unit length (Fig. 1a) at a datum temperature. After heating through $\theta°$ the length will increase by $\alpha \theta$ units if the bar is free to expand (Fig. 1b). If this expansion is totally suppressed (Fig. 1c) a compressive force Q will be needed, the elastic strain ϵ_0 being equal to the thermal expansion $\alpha \theta$. If the heating takes place within a short period of time, it is unimportant whether

the expansion is continuously suppressed during the heating or the heating and stressing are considered as two separate steps as in Figs. 1b and 1c.

With the length of the bar maintained constant at the temperature θ, and the temperature sufficiently high to allow creep to take place, the force required to keep the length constant will diminish, that is, there will be a relaxation of the

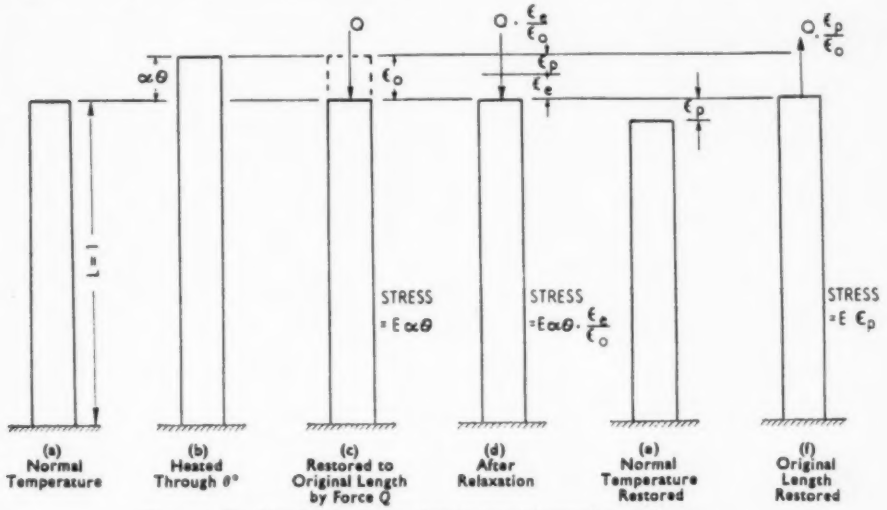

Fig. 1. Residual stress in a simple bar (thermal stressing).

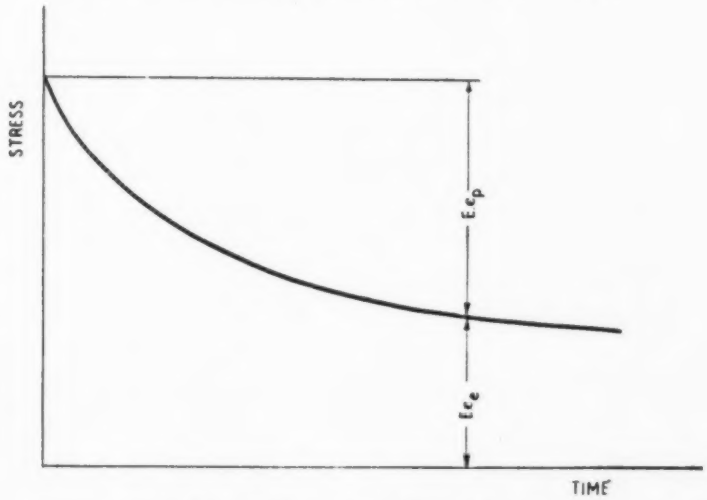

Fig. 2. Typical stress relaxation curve.

stress. Fig. 2 shows a typical relaxation curve. At any instant, $\epsilon_0 = \epsilon_p + \epsilon_e$, where ϵ_0 is the initial elastic strain, ϵ_e and ϵ_p are the elastic and creep strains respectively at the time considered.

On cooling to its initial temperature, the bar would have a free length $(1 - \epsilon_p)$ as in Fig. 1e. Suppressing the contraction produces a tensile stress $E\,\epsilon_p$ within the bar.

The process just described is similar to that which produces residual stresses in bodies after non-uniform heating. In practical cases the thermal expansions are only partly suppressed, due to the elasticity of the constraints. Similarly, on cooling, the plastic strains are only partially suppressed, and the resulting residual stress is less than $E\,\epsilon_p$.

(iv) *Residual stresses in hollow cylinders*

Having considered the establishment of residual stresses in simple bar, the corresponding phenomenon in hollow cylinders will be considered with reference to Fig. 3.

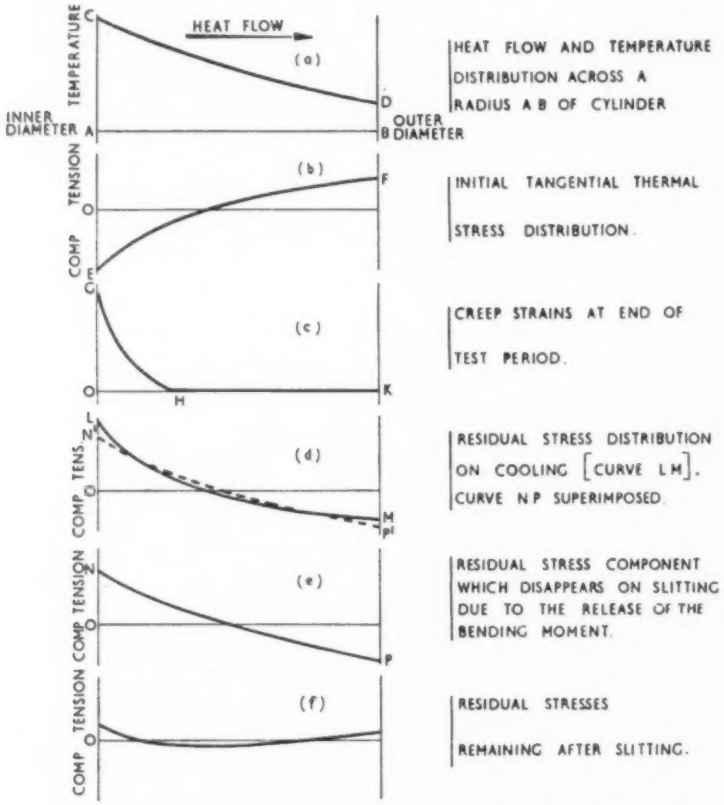

Fig. 3. Residual stresses in the wall of a hollow cylinder (diagrammatic).

Diagram (a) shows a radius AB of the cylinder, the direction of heat flow and the form of the resulting thermal gradient. The tangential stress distribution along the radius is depicted at (b). It will be noted that the maximum temperature and the maximum stress occur together at the inner radius, thus the inner radius will be the position of greatest creep strain after a given time. Temperature and stress decrease rapidly as the radius increases, thus at a certain distance within the wall creep will not take place, since the stress will be too low at

that particular temperature to cause it. These conditions hold for the intermediate region of the cylinder wall. Approaching the outer wall, the tensile stress becomes considerable once more. In the present test cylinders, the maximum tensile stress (at the outside diameter) is limited to about a half of the compressive stress at the bore. The temperatures in this outer zone are much less than near the bore and probably low enough to exclude the possibility of creep. The creep strains will therefore be either zero or very small compared with those at the bore.

Fig. 3c shows the probable distribution of creep strains after a period of time.

On cooling down to a uniform temperature, a residual stress system is set up (see Fig. 3d), the maximum value of stress (tensile) occurring at the bore. This maximum value is necessarily less than the numerical value of the initial compressive stress, since

(a) All the thermal stresses (and therefore the elastic strains) cannot be relieved by creep within a finite running time.

(b) On cooling, all the plastic (creep) strain cannot be converted into elastic strain, because of the elasticity of the remainder of the cylinder.

The residual stress distribution is similar in form to the stress distribution in a thick curved beam subjected to end couples. Fig. 3e shows such a distribution, the curve being superimposed on Fig. 3d to show the difference. Use is made of the above fact in the method used here for determining the residual stresses in the test cylinders. In this method, suggested by DAVIDENKOV (1932), a radial-axial slit is cut in the cylinder wall to destroy the residual bending moment (see Fig. 4). Before slitting, the sum of the tangential forces along any radius is zero, but the sum of the moments of the tangential forces has a definite value. This moment disappears on slitting, thus after slitting the sum of the tangential forces and the sum of their moments are both equal to zero.

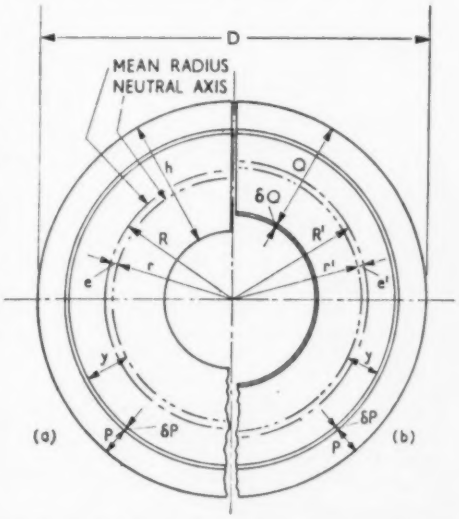

Fig. 4. Test cylinder during machining operations.

Fig. 3f shows the stresses remaining in the cylinder after the slitting operation. These stresses obey the conditions of equilibrium, and are detected by the boring out of successive layers of material from the inside of the cylinder. The slitting and boring operations cause diameter changes which are measured by electrical resistance strain gauges fixed to the outside diameter of the cylinder. The relationship between the diameter changes and the relieved stresses is given in Appendix I.

Some residual stress will be present which is not due to creep, but to the plastic component of the deformation of the material, cast iron being inelastic even at small loads.

2. Apparatus

The apparatus designed to subject the test specimens to a radial flow of heat is shown in section in Fig. 5.

The two test cylinders (1) are 13 in. o.d. × 4½ in. i.d. × 1½ in. thick and are separated by a ¾ in. thick dummy cylinder (3). This is used for temperature measurements since it is not permissible to drill holes in the test cylinders. The test cylinders are sandwiched between two ½ in. thick guard discs (2). The total length of the cylinders thus built up is 4¾ in.

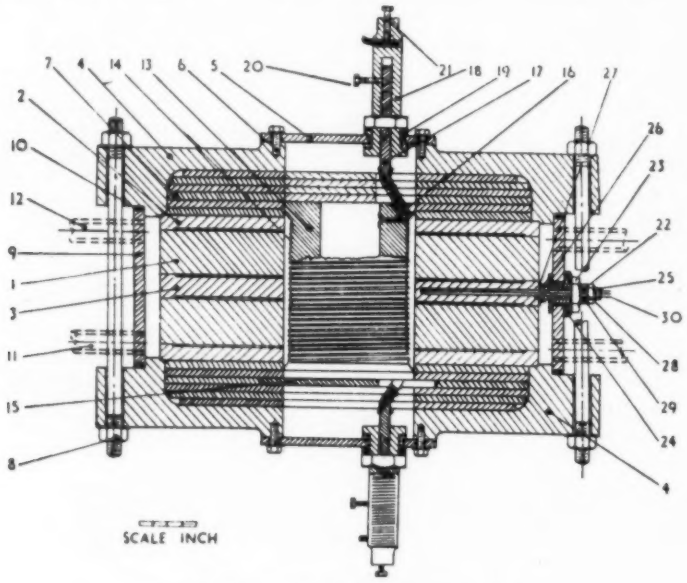

Fig. 5. Section of relaxation apparatus.

The heating element (14) is Kanthal A.1 resistance wire (14 s.w.g.) wound on a former of alumina cement (13). The end connections (17) are made of heavy section so that the heat generated within them will be reasonably small and will be conducted away. The outer casing consists of the iron castings (4) and the water jacket wall (9). The space between the guard rings and the cast covers (4) is filled by discs of ¼ in. thick asbestos millboard and sindanyo packed alternately. These are to limit the axial heat flow from the guard rings. Clearances (0·010 in.) are machined on the faces of the dummy and guard cylinders which adjoin the test cylinders. They have two purposes; (a) to provide a barrier to axial heat flow and (b) to ensure that the axial expansion of the test cylinders is unrestricted, thus preserving standard conditions and also maintaining water-tightness at the outer edge of the cylinders. Mains water is circulated through the jacket to cool the outer surfaces.

It was initially intended to charge the apparatus with inert gas under pressure. Argon was chosen for this purpose. The objects were to suppress oxidation and evaporation of the wire and also to increase the quantity of heat transferred to the cylinders by conduction, since pressure increases the density and thermal conducitivity of the gas. Difficulty was experienced, however, in achieving gas-tightness. It was found that oxidation and evaporation of the wire were not the main causes of the trouble and the inert gas atmosphere was dispensed with.

Measurement of temperatures across the cylinder wall was by a traversible thermocouple (30) situated within a radial hole in the dummy cylinder.

Trouble during the development stages of the apparatus was experienced with the winding coming out of the grooves in the former. The winding temperature (estimated at about 1,300°C) involves a considerable expansion. The grooves were made sufficiently deep to allow for the

radial expansion on the assumption that it was everywhere uniform. This, however, did not happen in practice and matters were made worse by the on-off periods of the current being of the order of 20 seconds, resulting in large amplitudes of element temperature. This caused the resistance element to be continuously on the move, with the wires drooping from the grooves at places and on some occasions earthing on the test cylinders. The trouble was largely eliminated by an improved method of temperature control which reduced the on-off periods to 2 to 3 seconds.

Temperature control was relatively simple during the present experiments due to the high stability of the apparatus. The proportion of heat stored in the apparatus to that transferred to the cooling water is very low. It was considered undesirable to insert a thermocouple either within the element former or within the gap between the winding and the cylinders. The insertion of a controlling thermocouple within the dummy ring was ruled out because of the low temperatures and the anticipated thermal lag. The method chosen was the connection of a small simplified model of the apparatus in parallel with it. A thermocouple made from 32 s.w.g. chromel-alumel wire was inserted in the air gap of the model so that the hot junction was almost in contact with the winding. The thermocouple operated an electronic temperature controller. The low heat capacity of the thermocouple and the electric element of the model, coupled with the high heat losses, made the switching period very short. The bore temperature of the test cylinders was maintained to within $\pm \frac{1}{2}$°C.

3. Test Procedure

The apparatus was assembled with the test cylinders in position, jointing compound being applied to the appropriate surfaces to ensure water-tightness. The water supply was turned on and then the electric power at a reduced value of current. The full heating current was not used at the outset so as to avoid too high thermal gradients within the refractory former. The current was then gradually increased to full rate, and the specimen temperature allowed to rise slowly until the desired value was attained, the controller then being brought into operation. This instant was taken to be the start of the relaxation period. Minor temperature adjustments were made during the subsequent hour and as necessary during the remainder of the period. Thermal equilibrium was attained very rapidly (with negligible "overshoot") due to the high stability of the apparatus.

At the end of the required period the test cylinders were removed and electrical resistance strain gauges were affixed to the outer cylindrical surface to detect the circumferential strains during the machining operations. Three gauges spaced at 120° were used on each cylinder. The leads were waterproofed with pitch and brought out to an 11-pin plug, which was incorporated to dispense with repeated soldering and un-soldering of connections. After the zero readings on the resistance bridge had been taken a $\frac{1}{8}$ in. wide slit was milled in the cylinder. As with all subsequent machining operations the cylinder was kept overnight in close proximity with the cylinder bearing the dummy gauge, thus ensuring temperature equality when the resistance measurements were made the following morning.

The layers bored out were as follows :

3 layers	0·050 in. thick
1 layer	0·100 in. thick
2 layers	0·250 in. thick
6 layers	0·500 in. thick

The layers were made thin at the bore because the tangential strains changed rapidly as the innermost layers were removed. After the removal of each layer the tangential strains were re-measured.

4. Test Programme and Results

The present series of tests were confined to cast iron cylinders. The composition of the iron was T.C. 2·97, G.C. 2·18, C.C. 0·79, Si 1·19, S 0·115, P 0·28, Mn 0·8 and Ni 0·11, all per cent. The average tensile strength determined from tests on three $\frac{1}{2}$ in. diameter specimens was 15 tons/sq. in. The Brinell hardness

number was 206 using a load of 3,000 kg. and a 10 mm. diameter ball. Microexamination of the structure of the iron showed the matrix to be fully pearlitic with the exception of occasional minute indications of ferrite. Some phosphide eutectic was present. The graphite flakes were observed to be short and thick generally, but the form of distribution varied slightly throughout the castings.

The test cylinders were subjected to a stress relief treatment before being treated in the relaxation apparatus.

The relaxation tests were arranged to involve variation of both temperature and time. The temperature of the relaxation treatment is denoted by the temperature of the bore.

The heating periods were as follows :

Test No.	1	2	3	4	5	6	7
Bore temperature (°C)	200	200	200	200	225	250	275
Time of heating (hrs.)	50	100	250	400	100	100	100
Initial compressive stress at bore (tons/sq. in.)	8·2	8·2	8·2	8·2	9·6	11·0	12·4
Residual tensile stress at bore (tons/sq. in.)	1·3	1·8	2·5	2·6	2·2	2·7	3·0

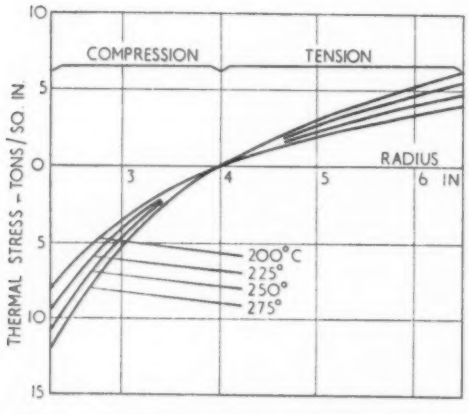

Fig. 6. Initial thermal stress distributions in test cylinders.

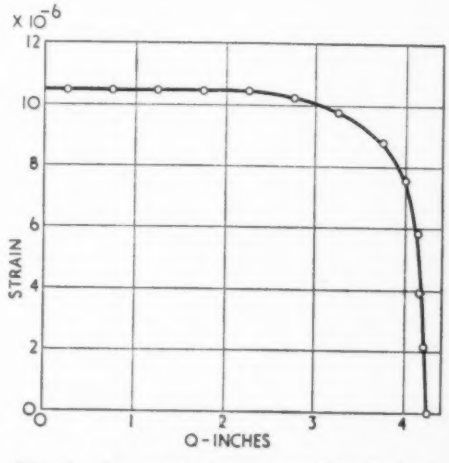

Fig. 7. Aggregate strains caused by boring.

The residual tensile stress at the bore has been included in the above table, the figures having been determined from the strain measurements (recorded during the slitting and boring operations) used in conjunction with the theory outlined in Appendices I and II.

The complete stress distribution along a radius has been determined and that for the test No. 7 is shown in Fig. 8.

The results of tests in which an earlier apparatus was used have been reported by ATTIA (1953).

5. DISCUSSION OF RESULTS

Fig. 6 shows the distribution of initial tangential thermal stress across the cylinder wall for the four test temperatures. Fig. 7 is a plot of the aggregate strain changes which occurred as the cylinders used in test 4 were bored out. It will be noted that almost all the total change took place during the removal of the first inch of material.

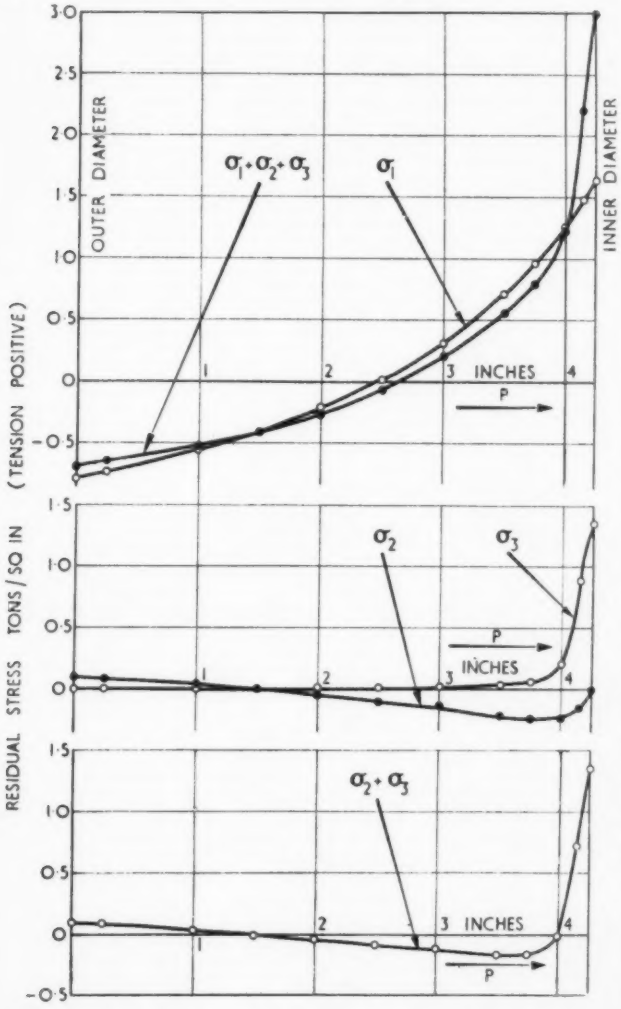

Fig. 8. Residual stress distributions in test cylinder (Test 7).

Fig. 8 refers to test 7 and shows the distribution of the total and component residual tangential stresses with respect to the position within the wall. General compliance with the distributions anticipated (see Fig. 3) is found. (The curve of σ_1 agrees perfectly with the calculated points. This is because the curve is actually a theoretical form of curve representing one strain change only (i.e. that occurring on slitting) each ordinate being proportional to this change).

σ_2 is the most difficult stress to calculate, being derived by graphical or tabular integration. It is worthy of note, however, that this component si zero at the bore. This follows from the definition of the component, viz., if no previous boring out has been done, no stress can have been released. σ_1 and σ_3 are very easily calculated from the appropriate formulae, thus the value of $(\sigma_1 + \sigma_3)$ representing the total residual stress at the bore is easily derived.

The σ_3 curve shows that the most rapid release of that stress component occurs within the first half-inch of boring, indicating that creep strains of any appreciable

magnitude are confined to this region. The remainder of the changes in σ_3 are small and must be due, in the main, to inelasticity of the cast iron (distinct from creep). Loading to the stress values denoted by the 275°C curve in Fig. 6 would certainly produce some residual strains in the material.

The $(\sigma_2 + \sigma_3)$ curve agrees in form with that of Fig. 3f.

The total residual stress curve, given by $(\sigma_1 + \sigma_2 + \sigma_3)$ shows that the residual tensile stress at the bore is $4\frac{1}{2}$ times the residual compression at the outer radius. The stress gradient is very steep near the bore.

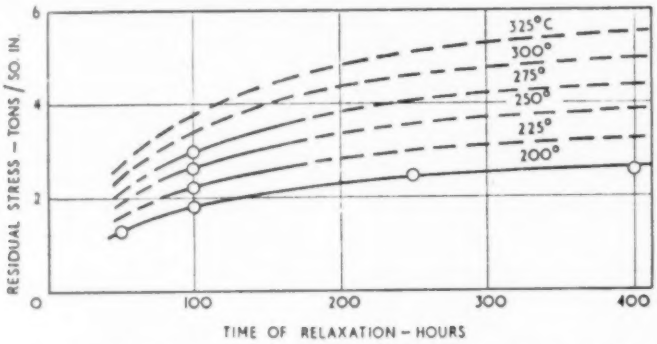

Fig. 9. Residual tangential stresses (tensile) at the inner diameter of the test cylinders.

The maximum values of residual stress are of particular interest in this discussion. As in the case of initial thermal stress, the maximum values of residual stress occurred at the bore. This was actually foreseen and was the principal reason for heating the cylinders from the inside in preference to the outside, which could have been accomplished with much less practical difficulty. The values determined for the residual tensile stress at the bore are plotted in Fig. 9

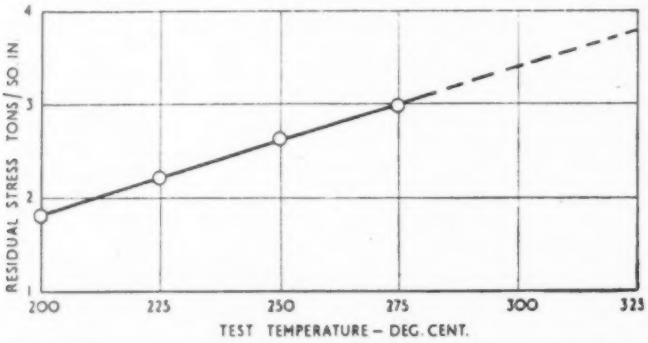

Fig. 10. Extrapolation of residual stresses at the bore of the test cylinders after 100 hours relaxation (Tests 2, 5, 6 and 7).

in which the 200°C curve is fully experimental. In the absence of further experimental points it is considered to be of interest to estimate by extrapolation the residual stresses due to treatment at temperatures and times greater than those which were actually achieved.

First, to determine the residual stresses which might be expected to occur after 100 hours treatment at 300° and 325°, a linear extrapolation of the four experimentally derived stresses plotted on a temperature base was made (see Fig. 10). The points so derived were inserted on the 100 hour ordinate (Fig. 9). In view of the fact that initial thermal stress and temperature difference across the wall increase in proportion to each other it is to be expected that the actual rate of increase of residual stress with test temperature will be greater than the linear rate used for extrapolation. Thus the extrapolated values may be regarded as conservative.

Having estimated the residual stress values for 100 hours treatment it is necessary to assume a form for the curve. The most suitable assumption appears to be that the residual stress curve for each temperature has each ordinate a fixed multiple of the corresponding ordinate in the 200°C curve. The curves of Fig. 9 are drawn in on this basis, which is again considered to yield conservative values.

Fig. 11 is a logarithmic plot of Fig. 9, the curves being extrapolated to 1,000 hours. As time increases beyond the limit of the graph each curve must become asymptotic with a value of residual stress which is equal to or less than the initial compressive stress. The trend of the 325°C curve (which represents an initia

Vol. 2 53/54

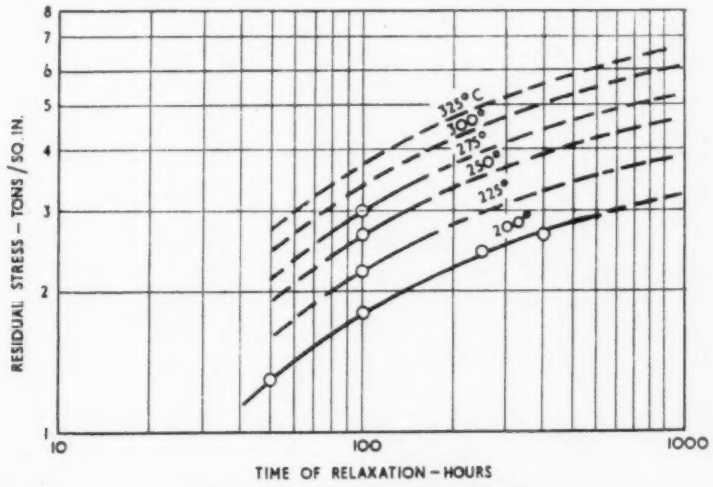

Fig. 11. Logarithmic plot of Fig. 9.

compressive stress at the bore of 14·9 tons/sq. in.) shows that under the implied temperature conditions, a residual stress of more than 8 tons/sq. in. could be established if the heating time were sufficiently prolonged. Failure resulting from the residual loads could never be expected at this temperature since the initial stress is only numerically equal to the strength of the material. At some higher value of temperature, not evident from the present results, fracture would occur after a finite period of relaxation. This is also shown by Fig. 12. For thin walled cylinders where the thermal stress distribution across the wall is almost linear the temperatures required for fracture would be higher than in the case of the

present experimental cylinders. In thin cylinders the danger of fracture at the outside surface due to the initial thermal (tensile) stress would therefore be more likely than failure by residual stress on cooling. In cylinders made from steel the initial thermal stresses, which are proportional to Young's modulus, would be higher. In this case, however, the short-time deformation characteristics of the steel become important since the yield stress may be exceeded. In mild

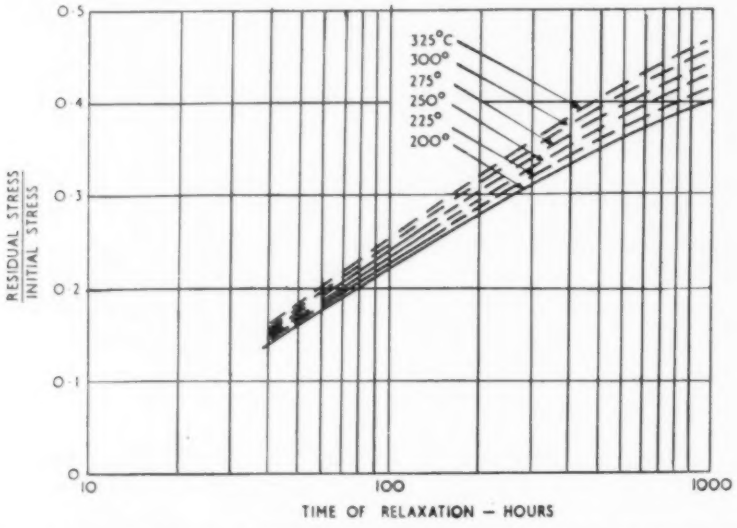

Fig. 12. Residual stress at the bore as a function of the initial stress at the bore.

steel, where the strain at yield may be many times the imposed thermal expansion, the maximum thermal stress is limited to the yield stress. Similarly, on cooling the residual stress is limited by plastic deformation in the reverse direction. Thus failure of mild steel cylinders would not be likely on the first cooling, but would be a possibility, due to fatigue, if the heating and cooling process were repeated sufficiently often.

In very long hollow cylinders the axial stress must be considered. At the inner and outer surfaces the axial stress is equal to and of the same sign as the tangential stress. The radial stress is zero at both faces and has its maximum value (compressive, in the case of radially outward heat flow) near the middle of the wall. The radial stress is the difference between the axial and tangential stresses and becomes smaller as the wall thickness diminishes, thus in a hollow cylinder of the proportions of the cylinder liner in a large diesel engine, the axial and tangential thermal stresses may be considered equal and the radial stress negligible. Defining an equivalent simple stress σ as that which will produce the same rate of dissipation of shear strain energy by creep as the combined stress system σ_t, σ_a and σ_r, we have (see Marin 1942):

$$\sigma = \sqrt{\tfrac{1}{2}\{(\sigma_t - \sigma_a)^2 + (\sigma_a - \sigma_r)^2 + (\sigma_r - \sigma_t)^2\}}, \qquad (5)$$

and, for the principal creep strains,

$$\left.\begin{aligned}\epsilon_t &= \frac{\epsilon}{2\sigma}\left[(\sigma_t - \sigma_a) - (\sigma_r - \sigma_t)\right],\\ \epsilon_a &= \frac{\epsilon}{2\sigma}\left[(\sigma_a - \sigma_r) - (\sigma_t - \sigma_a)\right],\\ \epsilon_r &= \frac{\epsilon}{2\sigma}\left[(\sigma_r - \sigma_t) - (\sigma_a - \sigma_r)\right],\end{aligned}\right\} \tag{6}$$

where ϵ is the creep strain corresponding to the simple stress σ. Writing $\sigma_t = \sigma_a$ and $\sigma_r = 0$ we have, from (5),

$$\sigma = \sigma_t = \sigma_a, \tag{7}$$

and, from (6),

$$\epsilon_t = \epsilon_a = \epsilon/2, \qquad \epsilon_r = -\epsilon. \tag{8}$$

Thus, under an equal biaxial stress system such as exists at the inside surface of a long cylinder, the axial and tangential creep strains would be equal, and a half that in a simple system such as that in a very short cylinder. However, the initial stresses in a long cylinder would be greater, for the same temperature conditions, in the ratio $1/(1-\nu)$, i.e. 1·33 when $\nu = 0{\cdot}25$. Thus, for the same temperatures, the tangential creep strain in a long cylinder would be at least $(\frac{1}{2} \times 1{\cdot}33)$ times that in a short cylinder. It can be shown that for a given state of initial strain within two hollow cylinders, one of which is very short and the other very long, the ratio of the resulting axial and tangential stresses in the long cylinder to those in the short cylinder is $1/(1-\nu^2)$, this factor being 1·07 for $\nu = 0{\cdot}25$. Combining the above relationships we have that the residual tangential stress in a long cylinder is equal to or greater than $1/2\left\{(1-\nu)(1-\nu^2)\right\}$ of the residual tangential stress in a short cylinder, the value of the factor being 0·711. It was shown above that a thin-walled short cylinder made of cast iron would be vulnerable to fracture at the outside surface on the first heating, whilst not being very susceptible to the residual stresess. In the long cylinder the residual stresses are less likely to cause failure.

The stress at any point within a thermally or residually stressed body is dependent on what might be termed a " constraint factor " for that point. This factor may be defined as follows. Consider an elementary volume of metal at the point in question and suppose that it tends to undergo a length change (such as might be caused by thermal expansion or plastic deformation) in one direction. Now suppose that the rigidity of the remainder of the body suppresses part of the length change ; then the constraint factor for that point and direction would be defined as the elastic deformation of the element due to the surrounding constraints divided by the change of free length.

Consideration of a small cubical element subjected to a temperature rise θ and fully restrained from expanding in all directions shows that the thermal stresses in all directions are compressive and equal to $E\,\alpha\,\theta/(1-2\,\nu)$. If the constraint is in two directions only, the stresses in those directions are $E\,\alpha\,\theta/(1-\nu)$, whilst if the constraint is in one direction the stress in that direction is $E\,\alpha\,\theta$. Points at a free surface must have zero constraint in the direction normal to the surface and are therefore stressed biaxially or uniaxially.

A body which is thermally stressed is an aggregate of such elements. In the

absence of external forces the condition of complete restraint will not hold, since the restraint must be generated by the elastic deformation of other elements. This may only occur if the considered element is allowed to follow partly its tendency to deform. The thermal stress at a point within a body may be written in the following general form :*

$$\sigma = E \alpha \theta \times \frac{\text{Constraint Factor}}{\text{Stress System Factor}}, \tag{9}$$

where the Stress System Factor is 1, $1 - \nu$ or $1 - 2\nu$, the Constraint Factor is a pure number between 0 and 1 defined as above, and θ is the temperature of the element above that at which it is stress free. The formula is useful if the body has a shape which prohibits exact calculation of the thermal stresses, in which case it may be possible to make a reasonable estimate of the constraint factor and so derive a direct estimate of the thermal stress at a given point. The method

	Ratio, outside diameter/ inside diameter	*Stress System Factor*	*Constraint Factor*	
1. Thick hollow cylinder (long)	3	$1 - \nu$	0·67	See equations (2) and (3)
2. Thick hollow cylinder (short)	3	1	0·67	See equations (2a) and (3a)
3. Thin hollow cylinder (long)	1·1	$1 - \nu$	0·52	See equations (2) and (3)
4. Thin hollow cylinder (short)	1·1	1	0·52	See equations (2a) and (3a)
5. Rectangular bar. Free to extend ; prevented from bending		1	0·5	—
6. Rectangular bar. Prevented from bending ; prevented from extending		1	1·0	—
7. Flat plate. Free to expand in plane of plate ; prevented from bending		$1 - \nu$	0·5	—
8. Flat plate. Prevented from expanding in plane of plate ; prevented from bending		$1 - \nu$	1·0	—

* This equation applies for
(a) the general three-dimensional case where the constraint factors are equal in all three directions, i.e. constraint factor $= c = c_1 = c_2 = c_3$,
(b) the two dimensional case where the constraint factors are equal in both directions, i.e. $c = c_1 = c_2$,
(c) the simple linear case,
(d) hollow cylinders subjected to a radial flow of heat (see equations (2) to (4a)).

In the more general cases where the constraint factors are unequal we have for the thermal stresses in three dimensions

$$\sigma_1 = E \alpha \theta \left\{ \frac{c_1}{1 + \nu} + \frac{\nu (c_1 + c_2 + c_3)}{(1 + \nu)(1 - 2\nu)} \right\} \tag{9a}$$

and for biaxial stresses,

$$\sigma_1 = E \alpha \theta \left\{ \frac{c_1 + \nu c_2}{1 - \nu^2} \right\} \tag{9b}$$

In both cases the suffixes may be interchanged cyclicly to derive the remaining stresses.

It should be noted that the constraint factors are not only dependent on the geometry of the body but also on its temperature distribution.

Vol.
2
53/54

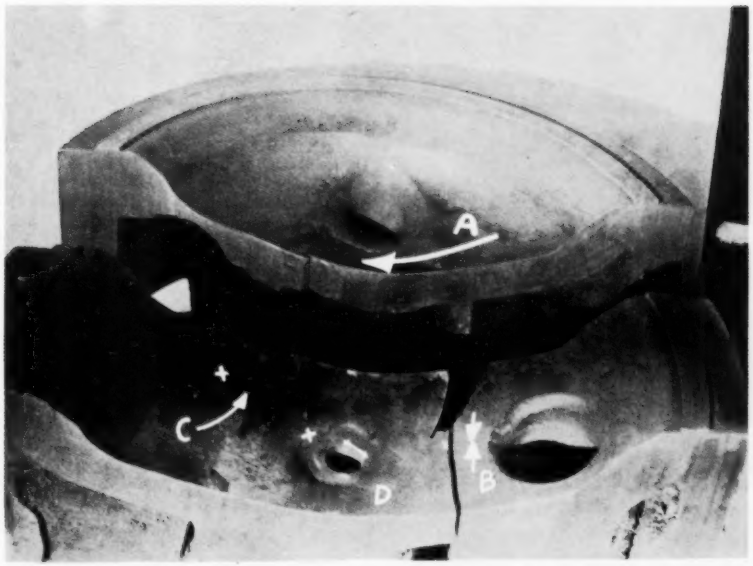

PLATE I. Residual stress cracks in the cylinder cover of a large diesel engine.

Vol
2
1953/

has been used by FITZGEORGE and POPE (1954) for estimating stresses in cylinder covers. The following table gives stress system factors and constraint factors for some hollow cylinders and flat bars and plates. In cylinders the heat flows radially outwards; in bars and plates the heat flow is directly across the thickness. The constraint factors refer to the points in the hot surface, where the stress is compressive.

The concept of a constraint factor is useful also in considering residual stresses. A point which has a high constraint factor in relation to thermal expansion will sustain a high stress as a result of a given temperature change. It will also sustain a high residual stress as a result of a given plastic strain. An example of such a condition is given in Plate 1 which shows a large cylinder cover which failed in four places due to residual stress cracks. Here, the expansion of the hot surface of the cover was restrained by the cooled metal parts attached to it and possibly by interactions at the spigot.

Thus the avoidance of high constraint factors in bodies subjected to unequal temperatures will alleviate the thermal stresses and the likelihood of subsequent failure by residual stresses. Young's modulus has a double effect on the residual stresses; high modulus leads to high initial thermal stresses and large creep strains (i.e. in comparing materials whose creep properties may be regarded as equal), while the residual stresses produced by the creep strains are also proportional to the modulus.

Vol. 2 53/54

ACKNOWLEDGMENTS

The work described in this paper has been carried out in the Civil & Mechanical Engineering Department of Nottingham University. The authors acknowledge the help of Mr. K. R. PEATTIE in connection with strain gauges and of Mr. R. T. ROSE in checking the Appendices.

REFERENCES

TIMOSHENKO, S.	1951	*Strength of Materials*, Pt. II (D. Van Nostrand Co., Inc., New York).
DAVIDENKOV, N.	1932	*Z. Metallkunde*, **24**, 25.
MARIN, J.	1942	*Mechanical Properties of Materials and Design* (McGraw-Hill Book Co. Inc., New York).
FITZGEORGE, D., and POPE, J. A.	1954	Report No. 123, British Shipbuilding Research Association, London (restricted circulation).
ATTIA, Y. G.	1953	Thesis, University of Nottingham.

APPENDIX I

The evaluation of the tangential residual stress distribution by the slitting and boring method

The residual stress distribution in the test cylinders was determined by measurement of the strains which occurred on machining away parts of the cylinders. The machining process adopted consisted of (a) the cutting of a radial slit and (b) boring out successive layers of metal from the inside surface of the cylinder. Strain measurements were made after the slitting and subsequently after each boring operation. The method of manipulation of the measured strain changes to deter-

mine the initial residual stress distribution follows closely that of Davidenkov (1932), the basic difference being that Davidenkov's method applies to long cylinders (involving expressions for the flexure of a curved plate) whereas the method used here applies to very short cylinders and is based on the flexure of a thick curved beam.

For the purpose of the analysis the following assumptions are necessary :

(a) The changes in deformation occurring during the slitting and boring operations involve elastic strains only, allowing the use of Hooke's law.
(b) Radial and axial stresses are negligible, the tangential stresses only being considered.
(c) No additional residual stresses are induced in the cylinder by the slitting and boring operations.

Fig. 4a shows a cylinder after slitting but before boring ; Fig. 4b shows a later stage, during the boring operations. The analysis aims at finding the initial residual stress state, that is, the state which existed before the commencement of the slitting.

The analysis relates to the residual stress within an elementary ring of thickness δP and distant P from the outer surface (see Fig. 4). The initial residual stress within this layer consists of three components :

(a) that relieved by the slitting operation ;
(b) that relieved by the removal of all the layers of metal up to the inner radius of the layer ; and
(c) that relieved when the layer itself is removed.

In the following analysis a prescribed machining operation is deemed to be performed on the residually stressed cylinder. A certain deformation will result, this being measured in a convenient way. To ensure that the calculated stress components have their correct signs, a convention is necessary. Tensile stresses and strains are taken as positive. The dimension y is taken positive towards the centre of curvature. Deformations due to machining are taken negative since they correspond to the relief of a stress ; positive deformations are those which occur if the necessary forces and couples are applied to the slit cylinder to restore its shape to that prior to the considered machining operation. Couples acting on the slit cylinder must therefore be positive when tending to increase its diameter.

1. *Evaluation of the tangential residual stress component relieved by slitting*

Consideration of any radius of the cylinder before slitting from the viewpoint of static equilibrium shows that the sum of the tangential forces is zero and their total effect to be equivalent to a couple.

To determine the relation between the change in diameter on slitting and the corresponding change in tangential strain at the outside diameter, consider a curved beam (see Timoshenko 1951) which subtends an angle θ at its centre of curvature and has a radius r to its neutral axis when free from external forces and couples. Let positive couples now be applied to the ends of the beam causing the radius r to change by δr and the angle θ to change by $\delta\theta$.

Since the neutral axis of the beam carries no stress, its length will be unchanged by the application of the couple, therefore $r\theta = (r + \delta r)(\theta + \delta\theta)$, which becomes, on transposing,

$$\frac{\delta r}{r} = -\frac{\delta\theta}{\theta}. \tag{1}$$

The strain at the outside diameter due to a positive moment

$$= \frac{-([h/2] + e)(-\delta\theta)}{[D/2] \cdot \theta} = -\frac{([h/2] + e)\,\delta r}{[D/2] \cdot r}. \tag{2}$$

For a cylinder of known dimensions, the values of h, D, e and r may be substituted. For the cylinders used in this work the relation becomes

$$\delta D = -21{\cdot}2 \times (\text{tangential strain at o.d.}) \tag{3}$$

The relation applies only to the changes due to slitting. Separate consideration is given later to the changes which occur as a result of boring. In deriving (3) use has been made of the basic

assumption that the radial pressures (and therefore the deformations along a radius) are negligible. This enables δD to be substituted for $2\delta r$.

The relation between the applied couple M and the deformation of the beam is

$$M = -E \,.\, h \,.\, e \,.\, \delta\theta/\theta = E \,.\, h \,.\, e \,.\, \delta D/2r \tag{4}$$

per unit length of cylinder.

The tangential stress at the layer distant y from the neutral axis is

$$\sigma_1 = \frac{M}{h \,.\, e} \cdot \frac{y}{r - y} = \frac{E}{2r} \cdot \frac{y}{r - y} \cdot \delta D, \tag{5}$$

after substitution for M from (4). Substituting $y = P - ([h/2] + e)$, $r = R - e$, and $e = h^2/12R$ in (5), we have

$$\sigma_1 = \frac{E}{2r}\left[\frac{P - (h/2) - (h^2/12R)}{R - P + (h/2)}\right] \delta D, \tag{6}$$

which for convenience may be written

$$\sigma_1 = \left(\frac{R}{r}\right)\frac{E}{2R}\left[\frac{P - (h/2) - (h^2/12R)}{R - P + (h/2)}\right] \delta D \tag{6a}$$

for the stress at any layer δP due to the reinstatement of the moment M relieved by the slitting operation. The use of the formulae $e = h^2/12R$ in place of the more exact expression $(h^2/12R)[1 + (4/15)(h/2R)^2]$ results in an inaccuracy of approximately $1\frac{1}{2}\%$ in the value of e. In the present cylinders the neutral axis is thus located to within 0·005 in.

Vol. 2 953/54

2. *Evaluation of the tangential residual stress component relieved by the removal of all the metal up to the inner radius of the layer δP*

Fig. 4b shows the cylinder after some boring has taken place. The radial thickness of the cylinder is now Q. It is required to find the stress within the layer δP due to the residual stress in the layer δQ adjacent to the present bore.

Suppose that just prior to removal, the layer δQ carries a tangential stress σ corresponding to a force $\sigma \,.\, \delta Q$. The action of this force on the remainder of the cylinder may be represented by a normal force $-\sigma \,.\, \delta Q$ uniformly distributed over a radial section, and a couple $-\sigma.Q.\delta Q/2$.

Consider firstly the couple, which is the incremental moment due to the residual stress within the layer δQ. The curved beam is now of different depth from the original. It is therefore necessary to rewrite certain relations as follows :

$$\left.\begin{aligned} y &= P - [(Q/2) + e'], \qquad r' = [(D - Q)/2] - e', \\ e' &= Q^2/[6\,(D - Q)], \qquad R' = (D - Q)/2. \end{aligned}\right\} \tag{7}$$

Substituting (7) in (5) we have, for the stress in the layer δP due to the couple,

$$\delta\sigma_2' = \frac{E}{D - Q - 2e'} \cdot \frac{P - [(Q/2) + e']}{(D/2) - P} \cdot \delta D \tag{8}$$

$$= \frac{E}{D - 2P} \cdot \frac{3\,(2P - Q)\,(D - Q) - Q^2}{3\,(D - Q)^2 - Q^2} \cdot \delta D. \tag{9}$$

Consider now the uniformly distributed stress $-\sigma.\delta Q/Q$ acting circumferentially on the beam. The circumferential deformation at any radius will be proportional to the circumference, which in turn is proportional to the radius. There will therefore be no change in curvature (and hence diameter) due to the action of the direct stress. It is necessary to determine the stress in the layer δP (let it be denoted by $\delta\sigma_2''$) due to the direct force. This is possible even though the diameter undergoes no change. Now $\delta\sigma_2'' = -\sigma \,.\, \delta Q/Q$. Proceeding to determine the value of σ in terms of the change in diameter, we have from (4)

$$-\sigma \,.\, \delta Q \,.\, \frac{Q}{2} = \frac{EQe'}{D - Q - 2e'} \cdot \delta D. \tag{10}$$

By transposition of (10)

$$\sigma = -\frac{2Ee'}{D - Q - 2e'} \cdot \frac{\delta D}{\delta Q}. \tag{11}$$

Substituting (7) in (11)

$$\sigma = -\frac{EQ^2}{3(D - Q)^2 - Q^2} \cdot \frac{\delta D}{\delta Q}. \tag{12}$$

Then

$$\delta\sigma_2'' = -\frac{\sigma \,.\, \delta Q}{Q} = \frac{EQ \,.\, \delta D}{3(D - Q)^2 - Q^2}, \tag{13}$$

giving the value of the stress component in terms of the diameter change cause by the couple $-\sigma \,.\, Q \,.\, \delta D/2$.

The residual stresses $\delta\sigma_2'$ and $\delta\sigma_2''$ given by (9) and (13) are those connected with the removal of one layer of material. The total stress relieved by boring out the material between the original bore and the layer δP will be given by a summation. Allowing the thickness of the layers δP and δQ to diminish without limit, we may write from (9) and (13)

$$\sigma_2 = \frac{E}{D - 2P}\int_{Q=h}^{Q=P} \frac{3(2P - Q)(D - Q) - Q^2}{3(D - Q)^2 - Q^2} \cdot dD + E\int_{Q=h}^{Q=P} \frac{Q}{3(D - Q)^2 - Q^2} \cdot dD. \tag{14}$$

To simply the evaluation of these integrals the following method is adopted. It will be noted from (8) that $\delta\sigma_2'$ is inversely proportional to $(D - Q - 2e')$ which is the equivalent of $2r'$ (see 7) but

$$\frac{1}{2r'} = \left(\frac{R'}{r'}\right)\left(\frac{1}{2R'}\right), \tag{15}$$

enabling (8) to be written in the more convenient form,

$$\delta\sigma_2' = \left(\frac{R'}{r'}\right)\frac{E}{D - Q} \cdot \frac{P - (Q/2) - e'}{(D/2) - P}\,\delta D. \tag{8a}$$

Equation (11) may be treated similarly. (9) and (13) then become

$$\delta\sigma_2' = \left(\frac{R'}{r'}\right)\frac{E}{D - 2P}\left[\frac{2P - Q}{D - Q} - \frac{Q^2}{3(D - Q)^2}\right]\delta D \tag{9a}$$

and

$$\delta\sigma_2'' = -\left(\frac{R'}{r'}\right)\frac{EQ}{3(D - Q)^2} \cdot \delta D. \tag{13a}$$

Rewriting (14) and adding, we have

$$\sigma_2 = \frac{2E}{3(D - 2P)}\int_{Q=h}^{Q=P} \frac{R'}{r'}\left[\frac{Q^2 - 2PQ - 2DQ + 3DP}{(D - Q)^2}\right]\frac{dD}{dQ} \cdot dQ \tag{15}$$

which may be evaluated graphically.
Writing $p = Q/D$ the ratio R'/r' can be written

$$\frac{R'}{r'} = \frac{3(1 - p)^2}{3(1 - p)^2 - p^2}, \tag{16}$$

which yields the following numerical values :

p	0·875	0·25	0·125	0·0625
R'/r'	1·136	1·038	1·007	1·001

If p is less than 0·025 the quantity R'/r' may be considered sufficiently near to unity to justify its omission, and some numerical work avoided. If σ_2 is known to be a small fraction of the total residual stress, the justification for omitting the term R'/r' is improved. In the present case the maximum value of R'/r' is 1·086 and the ratio is not considered to be negligible.

If the ratio p is sufficiently small it will be permissible to use the method of integration given by DAVIDENKOV (1932) in which (15) is manipulated to give

$$\sigma_2 = \frac{2E}{3(D-2P)} \int_{Q=h}^{Q=P} \left[\frac{4P-Q}{D-Q} - \frac{PD}{(D-Q)^2} \right] dD. \tag{17}$$

The binomial theorem is then used to expand the quantities $(D-Q)^{-1}$ and $(D-Q)^{-2}$. The first three terms of each expansion are used for substitution in (17) yielding a form suitable for graphical integration. For this method the ratio p must be small enough to justify the use of the first three terms only of the binomial expansion. In the present cylinders the first three terms represent only 81 % of the value of $(D-Q)^{-1}$ and 89¼ % of $(D-Q)^{-2}$.

3. *Evaluation of the tangential residual stress component relieved in the layer δP when the layer itself is removed*

When all the layers interior to δP have been removed, P and Q become identical and the layer δQ superimposed on δP. The case corresponds to that considered in the above paragraph when determining the residual stress component $\delta\sigma_2''$. We can therefore write directly from (12)

$$\sigma_3 = -\left(\frac{R'}{r'}\right) \frac{EP^2}{3(D-P)^2} \left(\frac{dD}{dQ}\right)_P \tag{18}$$

the term $(\mathrm{d}D/\mathrm{d}Q)_P$ being determined from the slope of the graph of D plotted against Q. Equation (18) is derived from consideration of the couple $-\sigma_3 P.\delta P/2$ acting on a radial section of the beam of thickness P. The equation fully defines the relation between σ_3 and δD since, as has already been explained, the direct force $-\sigma_3.\delta P/P$ does not cause any change in diameter of the cylinder.

4. *Consideration of the effect of the finite thickness of the bored-out layers*

The finite thickness of the bored-out layers has no effect on the accuracy of the residual stress determinations, providing sufficient readings are made to allow an accurate plot of diameter change with respect to Q to be made. It is emphasised that the thickness of the bored-out layers should not be associated with the layer δQ used in the analysis.

APPENDIX II

Modification of the theory of Appendix I to suit the case when strain gauges are mounted on the outside diameter

1. *Evaluation of σ_1*

When the change of diameter occurring on slitting is known, the distribution of the component σ_1 along a radial section may be quickly determined by using either (5), (6) or (6a). When the change of tangential strain at the outside diameter is measured, it is possible to convert the measurements into diameter changes by the relation (2).

2. *Evaluation of σ_2*

Considering a curved beam and using the same notation as previously we have, as a general relation for the strain in a fibre distant y from the neutral axis due to the couple M,

$$\epsilon = \frac{y}{(r-y)} \cdot \frac{M}{Ehe}. \tag{19}$$

It has been shown previously that the effect on the slit cylinder of the stress σ in the layer δQ is equivalent to a uniformly distributed normal stress $-\sigma.\delta Q/Q$ and a couple $-\sigma.Q.\delta Q/2$ acting at any radial section. The strain at the outside diameter due to the direct stress is given by $-\sigma.\delta Q/EQ$ and the diameter undergoes no change. The strain at the outside diameter due to the couple is, from (19),

$$\delta\epsilon' = \frac{[(Q/2)+e']}{R'+(Q/2)} \cdot \frac{\sigma \cdot \delta Q}{2Ee'}.$$

Substituting the value of σ from (11), we have

$$\delta\epsilon' = \frac{Q + \{Q^2/(3\,[D-Q])\}}{D\,(D-Q)} \cdot \frac{R'}{r'} \cdot \delta D. \tag{20}$$

The strain at the outside diameter, due to the direct stress,

$$\delta\epsilon'' = -\frac{\sigma}{E}\frac{\delta Q}{Q}.$$

Substituting for σ from (11), we have

$$\delta\epsilon'' = \left(\frac{R'}{r'}\right)\frac{Q}{3\,(D-Q)^2} \cdot \delta D. \tag{21}$$

The total strain at the outside diameter due to the stress within the layer δQ is equal to $d\epsilon' + d\epsilon''$. Adding these and transposing gives

$$\delta D = -\frac{3}{2}\left(\frac{r'}{R'}\right)\frac{D\,(D-Q)}{Q}\,\delta\epsilon. \tag{22}$$

Substituting (22) in (9a)

$$\delta\sigma_2' = -\frac{3}{2}\frac{ED}{D-2P}\left[\frac{2P}{Q} - 1 - \frac{Q}{3\,(D-Q)}\right]\delta\epsilon. \tag{23}$$

Substituting (22) in (13a)

$$\delta\sigma_2'' = -\frac{3}{2}\frac{ED}{3\,(D-Q)}\delta\epsilon. \tag{24}$$

Adding (23) and (24) and integrating :

$$\sigma_2 = \frac{3}{2} \cdot \frac{ED}{D-2P}\int_{Q=h}^{Q=P}\left[\frac{2P+Q-D}{3\,(D-Q)} - \frac{2P}{Q} + 1\right]\frac{d\epsilon}{dQ}\,dQ, \tag{25}$$

which may be integrated graphically.

3. *Evaluation of* σ_3

From (18),

$$\sigma_3 = -\left(\frac{R'}{r'}\right)\frac{EP^2}{3\,(D-P)^2}\left(\frac{\delta D}{\delta Q}\right)_P.$$

Substituting for δD from (22),

$$\sigma_3 = \frac{EPD}{2\,(D-P)}\left(\frac{d\epsilon}{dQ}\right)_P.$$

In the present investigation σ_2 and σ_3 were calculated using (25) and (26).

Journal of the Mechanics and Physics of Solids, 1954, Vol. 2, pp. 259 to 264. Pergamon Press Ltd., London.

YIELD CRITERIA AND THE BENDING OF WIDE BEAMS

By D. A. Barlow
Aluminium Laboratories Limited, Banbury

(*Received 5th March*, 1954)

Summary

The ductility of aluminium alloys in bending is discussed. The ductility at fracture of a wide beam in bending is dependent on both yield and fracture criteria and the relation between the amount of hardening and the amount of strain. It is shown that the minimum bend radius of a wide beam is very sensitive to the yield criterion, so that bend tests can be used to distinguish between different yield criteria, if the other stress-strain relations are known. In a practical case, a yield criterion about halfway between those of Tresca and von Mises was obtained.

Vol. 2 53/54

1. Introduction

In the plastic bending of beams, fracture can occur either in compression or in tension. In aluminium alloys the ductility in compression is generally greater than that in tension, so that failure in bending takes place in tension in the outer fibre of the beam. If the beam is narrow, the material is practically free from laterial restraint so that the outer fibres of the beam are in almost pure tension and the familiar anticlastic curvature takes place. Under these conditions the outer fibres may be stressed to well beyond their maximum load in simple tension while the load on other fibres of the beam is still increasing, so that the bending moment as a whole is still increasing. Local necking of the outer fibres is in this case prevented for a time by the support of the remainder of the beam, and what is normally known as local elongation in a tensile test occurs uniformly in the outer fibres along the whole of the bend surface. The bending moment eventually reaches a maximum when, if the beam is unsupported by a former, local instability sets in, giving local necking followed by fracture of the outer fibres, or if the local ductility of the outer fibres in simple tension is exhausted before the bending moment reaches a maximum, fracture of the outer fibres at this value will take place without necking. The point at which the maximum bending moment is reached depends of course on the rate of work hardening, but for most aluminium alloys it can be shown that this occurs at high values of outer fibre extension, 100-200% (Dorn and Jelinek 1944), so that fracture most often occurs due to exhaustion of local ductility in simple tension. Further, at an outer fibre extension of about 100%, the material is bent flat on itself and further bending is impossible. If the beam is bent by wrapping over a former, local collapse or 'peaking' after the maximum bending moment is reached is prevented by the former in any case, and fracture occurs only when the local ductility in simple tension is exhausted. This limiting value is slightly greater than the reduction of area measured in a

conventional tensile test, as in the latter case the presence of triaxial tension in the neck no doubt tends to reduce the ductility. Dorn, Jelinek, Thomsen and Putnam (1944) have shown for a variety of aluminium alloys that tensile and bend test results do, in fact, agree in this way with a fair degree of accuracy.

In the bending of wide beams, lateral strain is prevented except at the edges. For an infinitely wide beam, plane strain conditions are thus obtained and in practice with a width/thickness ratio of greater than about 10 the centre of the beam may be considered as being under plane strain conditions.

2. Ductility in plane strain

Dorn *et al.* (1944) have shown that under plane strain conditions the outer fibre strain at fracture in bending can be estimated briefly as follows.

It can be easily shown that in any fibre in plane strain the tranverse stress $\sigma_2 = \frac{1}{2}\sigma_1$, where σ_1 is the longitudinal stress : the thickness stress σ_3 is sufficiently small to be ignored. Taking the maximum principal stress criterion for fracture, and supposing that the stresses satisfy von Mises' criterion for yielding at any stage of the preceding flow, the longitudinal fracture strain in plane strain is

$$\phi'_{cr} = \frac{\sqrt{3}}{2} F\left(\frac{\sqrt{3}}{2}\sigma_{cr}\right)$$

where σ_{cr} is the true failing stress in simple tension and F is the function relating true stress to true plastic strain for simple tension (or compression). It is assumed that the material is isotropic and that the Ros-Eichinger equation relating true stress to true plastic strain holds good, as in this case the principal axes of successive strain increments do not rotate, the principal stress ratios and principal strain ratios are constant, and elastic strains can be ignored. The only other alternative hypothesis is that the degree of hardening is a function only of the total plastic work, and this gives the same result in this case. Another fracture criterion which is generally considered to show good agreement with observation for many aluminium alloys is that of maximum shear stress (this is analogous to Tresca's yield criterion). Under plane strain conditions this gives the same results as the maximum principal stress criterion. In a later paper Dorn (1948) lists various further suggested fracture criteria. The hydrostatic tension criterion ($\frac{1}{3}(\sigma_1 + \sigma_2 + \sigma_3)$ reaches a critical value) gives results widely different from the previous two criteria, and is not in agreement with combined loading test results on aluminium alloys in the biaxial tension range ; in any case, it predicts zero ductility in plane strain for many aluminium alloys using any reasonable yield criterion. The cubic invariant $\sigma_1\,\sigma_2\,\sigma_3$ is obviously inapplicable to biaxial tension, since σ_3 is zero. The material may fracture according to a general function of stresses and strains and previous strain history, but such a function has yet to be formulated. The remaining fracture criterion is the so-called equivalent or effective stress :

$$\sqrt{\frac{(\sigma_1 - \sigma_2)^2 + (\sigma_2 - \sigma_3)^2 + (\sigma_3 - \sigma_1)^2}{2}}$$

(this is similar to the expression in von Mises' criterion for yielding). Although experimental results on aluminium alloys agree more closely with the maximum

Vol.
2
53/54

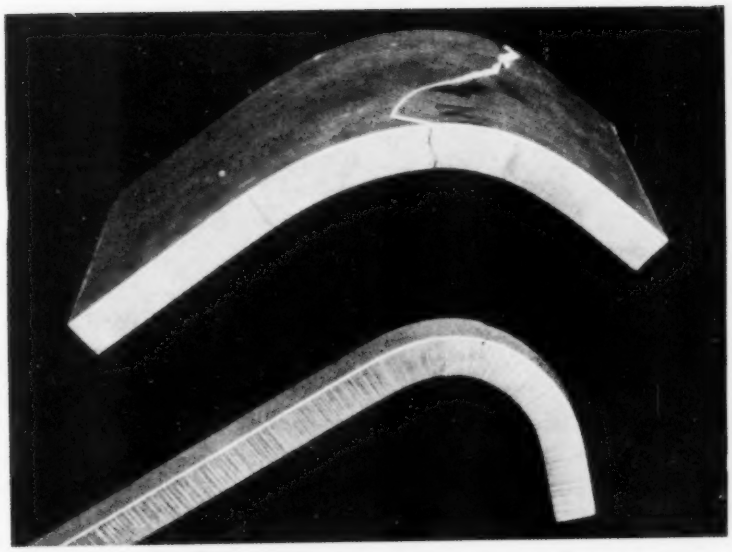

Fig. 1. Wide and narrow bend test specimens in HP15WP plate.

Vol
2
1953/

shear stress criterion, the effective stress criterion is not entirely ruled out. We thus have four possible combinations of yield and fracture criteria (assuming either of the above hypotheses of strain hardening) which may be summarized as follows :—

(1) Maximum shear stress yield criterion (TRESCA) + maximum shear stress or maximum principal stress fracture criterion. This gives $\phi'_{cr} = \phi_{cr}$, the longitudinal fracture strain in simple tension.

(2) Maximum shear stress yield criterion + effective stress fracture criterion. This gives $\phi'_{cr} = F\left(\frac{2}{\sqrt{3}}\,\sigma_{cr}\right)$.

(3) Effective stress yield criterion (VON MISES) + maximum shear stress or maximum principal stress fracture criterion. This gives $\phi'_{cr} = \frac{\sqrt{3}}{2}\,F\left(\frac{\sqrt{3}}{2}\,\sigma_{cr}\right)$ — DORN's formula.

(4) Effective stress yield criterion + effective stress fracture criterion. This gives $\phi'_{cr} = \frac{\sqrt{3}}{2}\,\phi_{cr}$.

The difference between values thus obtained from (1) and (4) is not very great. (2) and (3) give very different values from (1) and (4) and from each other; the differences depend on the shape of the stress-strain curve and are of the order of from 2 : 1 to 4 : 1 for aluminium alloys. It will be noted that (2) is an unlikely combination, as it gives values of ductility in plane strain greater than in simple tension. With the exception of (1) versus (4), bend tests are a sensitive method for distinguishing between the different criteria. In the usual type of combined loading tests for distinguishing between different yield criteria, only small differences have to be detected, so that not only must measurements be accurate, but any slight anisotropy of the material of, say, a few percent difference in the stress-strain curves is sufficient to destroy the value of the tests. In the present case, it is difficult to imagine that even an appreciable amount of anisotropy would mask an effect as large as from 2 : 1 to 4 : 1.

3. PRACTICAL TESTS

For aluminium alloys it is known that the minimum bend radii for narrow beams are much smaller than those for wide beams of the same material and thickness, and this is true for both longitudinal and transverse directions of commercially rolled materials showing some anisotropy; this rules out (1) and (2) and throws considerable doubt on (4). For the present purpose, bend tests on $\frac{1}{2}$ inch thick aluminium alloy plate conforming to B.S. 1477, HP15WP, were carried out on a "wrap" type bending machine, using specimens with width/thickness ratios of 1 and 8. The outer fibre strains at fracture were approximately 27% and 10% respectively. The specimens are shown in Fig. 1.

If stress-strain curves for comparison are taken in tension, uniaxial stress is not obtained during necking, although for many aluminium alloys with a relatively small amount of necking the errors involved are small. Compression stress-strain curves were therefore taken for both longitudinal and transverse directions using cylinders of 0·424 inch diameter and $\frac{3}{8}$ inch length (this short length was necessary

to avoid end-slip buckling). The specimens were unloaded at every 2% compression and re-lubricated with grease containing molybdenum disulphide, as previous work had shown that this technique gave very little barrelling, while the increments of 2% were sufficiently large to surmount the knee of the stress-strain curve for each increment. The envelope curve thus obtained is believed to be an accurate representation of the true stress-strain curve in pure compression. It was found that the compressive stress-strain curve in the longitudinal direction coincided with the tensile stress-strain curve in the transverse direction (i.e. the bend direction), and that the transverse compression curve was slightly higher, with a maximum difference of 2%. This suggests that the slight anisotropy thus exhibited was due to the Bauschinger effect, no doubt arising from the flattening operation on the plate.

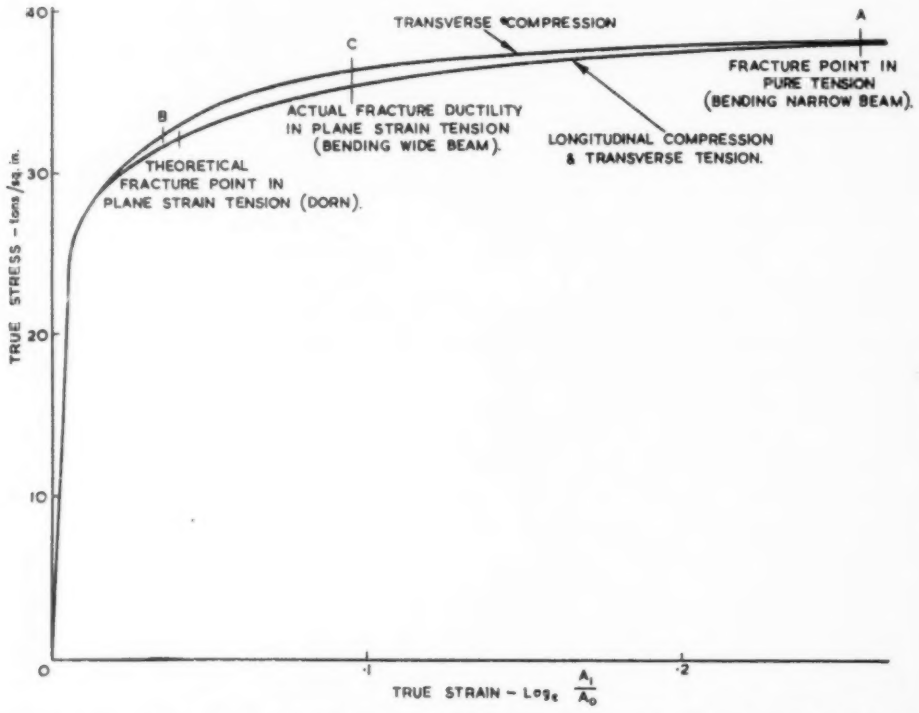

Fig. 2. Stress-strain curves in longitudinal and transverse directions-HP15WP plate ½ in. thick.

For the local ductility in simple tension at fracture, the reduction of area values from conventional tensile tests were taken in the bend direction (transverse to the rolling direction). The values of local elongation were 26% and 32% compared with 27% obtained in bending the narrow beam. (This latter value was obtained by simple geometry, as check tests with grids scribed on the outer fibre had shown that the measured and geometric values agreed : it can be shown that the shift of the neutral surface at this amount of deformation can be ignored.) Fig. 2 shows the compressive stress-strain curves in the two directions with the local ductility in tension given by point A. On the hypothesis (3) (VON MISES' yield criterion

and the maximum shear stress fracture criterion), the corresponding ductility in plane strain is given by points B, equivalent to about 4% extension. This compares with 10% (point C) obtained on wide plate and gives better agreement than do the three other cases. The plate was rather narrower than desirable, but even so this would not be expected to explain the relatively large difference obtained.

It seems, therefore, that the yield criterion is not accurate. If we assume that either the total plastic work or Ros-Eichinger strain hardening hypothesis is correct and that the maximum shear or principal stress fracture criterion is correct (and combined loading tests give good agreement with these criteria under plane strain conditions), it suggests that the true yield criterion is between those of TRESCA and VON MISES. This is further illustrated in Fig. 3. If the TRESCA

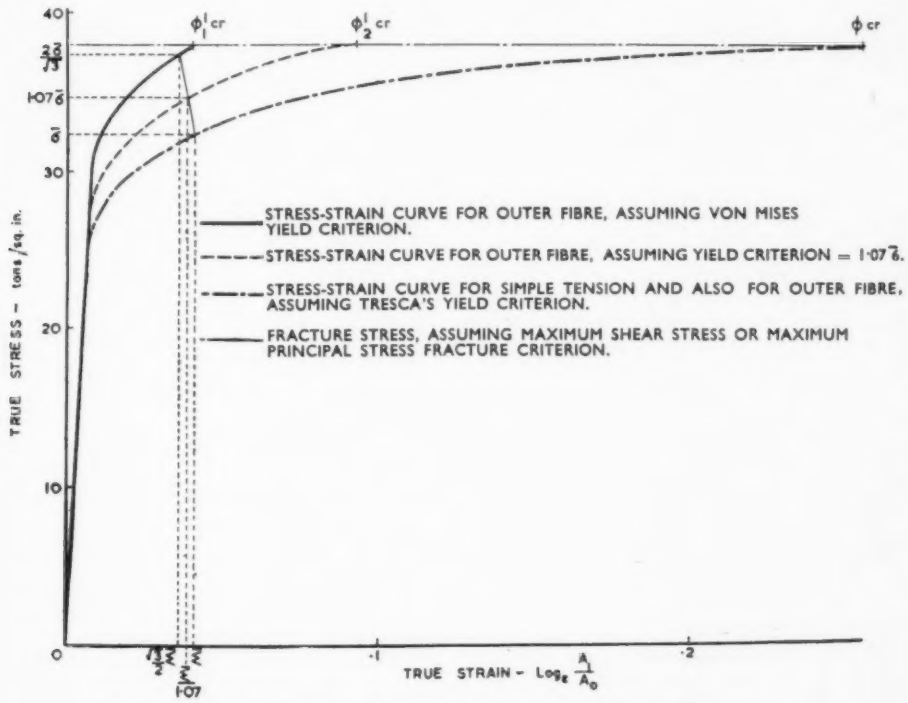
40
30
20
10
0
TRUE STRESS – tons/sq. in.
TRUE STRAIN – $\log_e \frac{A_1}{A_0}$
·1
·2
1·07
STRESS-STRAIN CURVE FOR OUTER FIBRE, ASSUMING VON MISES YIELD CRITERION.
STRESS-STRAIN CURVE FOR OUTER FIBRE, ASSUMING YIELD CRITERION = 1·07 $\bar{\sigma}$.
STRESS-STRAIN CURVE FOR SIMPLE TENSION AND ALSO FOR OUTER FIBRE, ASSUMING TRESCA'S YIELD CRITERION.
FRACTURE STRESS, ASSUMING MAXIMUM SHEAR STRESS OR MAXIMUM PRINCIPAL STRESS FRACTURE CRITERION.

Fig. 3. Stress-strain curves for outer fibre in bending wide beam.

NOTE: The total plastic work or Ros-Eichinger hypothesis of strain-hardening is assumed throughout.

criterion of yielding is adopted, the stress-strain curve for the outer fibres of the wide beam coincides with the stress-strain curve for simple tension. If the VON MISES criterion for yielding is adopted, however, the tensile stress in the outer fibres of the material is 1·155 × the simple tensile yield stress of the material. The corresponding true strain required to work harden the outer fibres of the beam to this extent is therefore 0·866 × the true strain in simple tension. The maximum shear or principal stress fracture criterion together with the VON MISES yield criterion gives the value ϕ'_{1cr} (Fig. 3) since at this value of outer fibre strain the critical

maximum shear or principal stress is attained. In order to satisfy the stress-strain curve for transverse tension (or longitudinal compression) and the bend tests results (also in the transverse direction), a modified yield criterion is used, such that the tensile stress $= 1{\cdot}07\,\bar{\sigma}$, where $\bar{\sigma}$ is the simple tensile (or compressive) yield stress; this is indicated by the dotted curve in Fig. 3, giving a correct fracture ductility of ϕ'_{2cr}. This is in good agreement with the value of $1{\cdot}08\,\bar{\sigma}$ for plane strain, predicted by BISHOP and HILL's (1951) theoretically derived yield criterion for a polycrystalline face-centered cubic metal. If the stress-strain curve for transverse compression is taken, a value of 1·05 is obtained for the constant, but as it is being compared with bend test results at right angles to it, the real value of the constant should be higher than this, nearer to 1·07. The experimental stress-strain curves obtained in the two directions represent the extremes between which the stress-strain curve (and the corresponding yield criterion) of the equivalent isotropic material would lie. As an alternative to these yield criteria it is possible that the material has similar yield and fracture criteria, in which case values of $2{\cdot}7\bar{\sigma}$ and $2{\cdot}7\sigma_{cr}$ are required, which is highly unlikely.

A rough check on published values of minimum bend radii for aluminium alloys in sheet form suggests that for heat-treated alloys, such as that used here, DORN's formula underestimates the fracture ductility in plane strain. The fracture ductility for the cold-worked tempers of Al-Mg alloys is overestimated and for all other alloys good agreement with DORN's formula is obtained. This suggests that the yield and fracture criteria may be different for the various alloys, although a more accurate check is required before this can be stated with certainty.

REFERENCES

DORN, J. E. and JELINEK, J. J.	1944	OPRD Research Report, Serial No. W-175.
DORN, J. E., JELINEK, J. J., THOMSEN, E. G. and PUTNAM, J. A.	1944	OPRD Research Report, Serial No. W-115
DORN, J. E.	1948	*Trans. Amer. Soc. Metals*, **40 A**, 32.
BISHOP, J. F. W. and HILL, R.	1951	*Phil. Mag.*, **42**, 1298.

Journal of the Mechanics and Physics of Solids, 1954, Vol. 2, pp. 265 to 277. Pergamon Press Ltd., London.

CONE INDENTATION EXPERIMENTS

By D. S. Dugdale
Department of Mechanical Engineering, University of Bristol

(*Received* 11*th March*, 1954)

Summary

Indentations were made in three cold-worked metals, namely mild steel, copper and aluminium, using indenting tools of cone angles between 10° and 140°. The indenting tools were lubricated to reduce the coefficient of friction to a low value. Minimum permissible sizes of indentation specimens were determined. The shear yield stress of the materials was found from torsion tests. Precautions were taken that non-uniformity and anisotropy should not vitiate the results. The ratio between mean indentation pressure and shear yield stress was found to be approximately the same for the three materials, and the variation of indentation pressure with cone angle is shown. Measurements of the volume of the raised lip and shape of the impression are given. The possible influence of plastic-elastic effects on the observed indentation pressures is discussed.

Vol. 2 53/54

1. Introduction

When an indentation is made in a solid body the displaced material may diffuse inwards, or it may form a ridge raised above the original surface. It is well known that with cold-worked metals an elevated ridge is formed around the indenting tool, but that with annealed metals this ridge is often absent. Hill (1950a, p. 259) put forward the qualitative explanation that local flow outwards to the surface necessitates severe distortion, and that with a work-hardening material a mainly inward displacement accommodated by the resilience of the whole body of material may occur first. This disappearance of the displaced volume of material in the case of annealed metals is to some extent illusory, for the surface around the impression is slightly raised over a wide area. It can be seen from the experiments of Ichihara (1931) with ball indenters and of Dugdale (1953) with wedge indenters that for materials of various small rates of work-hardening the shape of the raised lip varied greatly while the ratio of lip volume to displaced volume remained near to a value of unity. It appears, therefore, that impressions made in materials having different rates of work-hardening can be of different shapes due to a changed mode of flow, or to the elasticity of the material, or to both conjointly. From the point of view of hardness testing it is of interest to know what material properties are being measured when an indentation test is made, and whether the indentation hardness is defined uniquely by the plastic stress-strain relation or not. For investigating this problem, conical indenters have an advantage over spherical indenters in that impressions made under different loads are always geometrically similar in shape, so that absolute magnitudes of mpression size and load are not of primary importance. Also it is desirable to

use, in the first instance, materials whose behaviour is not complicated by high rates of work-hardening. Cold-worked metals usually possess a fairly distinct initial yield stress and subsequent straining produces little further hardening. Unfortunately some unwanted properties such as non-uniformity and directionality also appear in these materials and consequently a greater number of tests must be carried out to obtain reliable experimental values.

It appears that the problem of cone indentation has not been worked out theoretically. Some of the mathematical difficulties have been discussed by HILL (1950a, p. 280). Regarding experimental work, HANKINS (1926) reported a comprehensive series of tests with conical indenters of various cone angles. However, these results were not related to any other material tests, and friction coefficients were derived by assuming that in frictionless indentation the mean pressure on the projected area of impression was the same for all cone angles. BISHOP, HILL and MOTT (1945) found that for lubricated cones the mean pressure decreased slightly with increasing cone angle, but it seems that their experiments were too few in number to be reliable. In the present work it was found that for cones of angle greater than 30° the mean indentation pressure increased with increasing cone angle.

2. MATERIALS

Materials not too remote from engineering practice were chosen. The copper was from a slab of high-conductivity (electrolytic) copper of dimensions 5 × 1½ × 36 in. The aluminium slab (nominally pure) was of dimensions 8 × 1½ × 36 in.

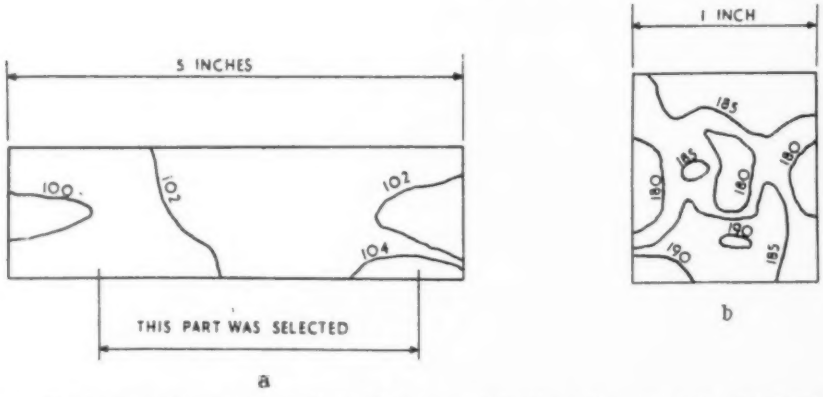

Fig. 1. Hardness contours over sections of bars. (a) Section of copper bar; (b) Section of steel bar.

Both slabs had been reduced in thickness by about 25% by cold rolling. The "bright-drawn" steel bar was of 1 × 1⅛ in. section and about 9 ft. long, and from a micro-section it was deduced that the carbon content was about 0·15%.

The steel and copper had average crystal sizes 0·03 mm and 0·06 mm. Hardness variations were investigated by taking large numbers of Vickers Pyramid Hardness readings over sections cut from the bars. It was found that a certain minimum size of diamond impression relative to the grain size must be used if small variations

in macroscopic hardness were to be determined with certainty. Satisfactory results were obtained when the impression diagonal length was 15 times the mean grain dimension. Three equally spaced sections were taken from the copper slab, and the distributions of hardness over each section were similar in that the material near the edges of the bar was below average in hardness. The results for the central section are shown in Fig. 1a. The part which appeared to be abnormally soft was discarded.

The section of the steel bar was not large enough to allow of any selection of material. It was arranged that both cone indentations and torsion test specimens involved material from the centre of the section. The hardness distribution shown in Fig. 1b was typical of distributions obtained from sections taken at various positions along the bar. It can be seen that the non-uniformity must necessarily produce some random variations in the measured values of the mean indentation pressure, since tests made in different directions cannot involve deformation of material from precisely the same regions. The method by which the diagrams of Fig. 1 were constructed was to take as many Vickers hardness readings as possible (100 on the steel section and 250 on the copper section) and then to average all possible groups of four contiguous readings. This procedure reduced the random variations due to finite crystal size. From these averages the contours were drawn.

Vol. 2 53/54

The mean grain size of the aluminium was much larger, about 1·0 mm. Reproducible maps of hardness could not be obtained, but irregular areas of hardness numbers 35 to 38 seemed to exist. An etched section showed that the grain size did not vary greatly, though the crystals were slightly larger towards the centre of the section. About half an inch from each edge of the slab was discarded.

Some convention must be adopted for describing the orientation of specimens cut from these bars. The orientation of a cone indentation specimen is defined by the direction of the cone axis relative to the bar, and the orientation of a torsion specimen by the direction of its longitudinal axis. The direction of the greater dimension of the cross-section of the bar is designated x, the direction of the lesser dimension y, and the longitudinal direction z.

The plastic anisotropy of these materials is well illustrated by the apparent ellipticity of the cone impressions. These diameter ratios are shown in Table 1.

TABLE 1.

Impression axis : *Diameter ratio* :	x d_y/d_z	y d_z/d_x	z d_x/d_y
STEEL	1·00	1·01	0·99
COPPER	1·02	1·01	0·96
ALUMINIUM	1·05	1·04	0·90

They were obtained by plotting one principal diameter against the other throughout the indentation test, the gradient of the curve giving the mean diameter ratio. Values for the 120° cone angle only need be given. It can be seen that the aluminium shows marked anisotropy while the steel is almost isotropic.

3. TORSION TESTS

Longitudinal specimens only were taken from the steel bar, but copper and aluminium specimens were taken from each of the three principal directions of the bars. The specimens were solid, of diameter 0·3 in. over a gauge length of $1\frac{1}{4}$ in. The torsion machine permitted the specimen to expand axially during the test. A calibrated optical torque-meter was used, and the twist over the gauge length was indicated by pointers clamped to the specimen registering on a circular graduated scale. The procedure was to apply quickly a fairly large strain increment (about 0·2) to the specimen, and then to wait 2 minutes before taking the torque reading. The shear yield stresses k were derived from the torque-twist curves by the usual NADAI construction. These stresses were determined over the range of shear strain γ (engineering definition) that is likely to be found in material deformed by indentation, i.e. strains of the order of unity. They are shown in Table 2, the units being tons per square inch.

TABLE 2.

	Orientation of specimen	Engineering shear strain 0·2	0·5	0·7	1·0	1·5
STEEL	z	19·1	20·2	20·7	21·2	21·8
		19·4	20·3	20·9	21·5	22·3
		19·2	20·2	20·8	21·3	21·8
	Average :	19·2	20·2	20·8	21·3	22·0
COPPER	x	10·05	10·40	10·65	10·90	11·00
		10·30	10·65	10·85	10·95	11·00
	y	9·90	10·20	10·30	10·50	—
		9·90	10·45	10·55	10·75	—
	z	10·25	10·55	10·60	10·60	10·65
		10·10	10·40	10·45	10·53	10·60
	Average :	10·10	10·45	10·60	10·70	10·80
ALUMINIUM	x	3·52	3·67	3·80	3·84	3·82
		3·35	3·59	3·64	3·66	3·64
	y	3·42	3·49	3·54	3·61	3·68
		3·41	3·54	3·62	3·68	3·76
	z	3·32	3·41	3·46	3·49	3·48
		3·37	3·50	3·55	3·58	3·56
	Average :	3·40	3·53	3·60	3·64	3·66

This method for determining the shear yield stress has certain shortcomings. The final surfaces of the torsion specimens were more or less rough, but measurement showed that the mean diameters had diminished by amounts up to 0·001 in. for the steel specimens and up to 0·002 in. for the copper specimens. The aluminium

specimens were too rough to be measured accurately, the surface irregularities being about 0·005 in. in height. As a correction for this effect would be very uncertain, none has been applied, but it is clear that the stresses at the larger strains must be slightly under-estimated (by 1 or 2%) on this account. Another difficulty is that the so-called generalized, or equivalent, shear stress need not be exactly the same function of the integral of equivalent shear strain increments for different deformations if these deformations induce different kinds of preferred crystal orientation. The orientations that may result from the torsion of a cylinder and from the flow around a penetrating cone are likely to be different. Further, the yield locus (cf. HILL 1950a, p. 18) for these materials need not be a circle. The stress in a torsion specimen remains on the same point of the yield locus, while the stress in a particle of a body deformed by a cone indenter must traverse some arc of the yield locus during its strain history. However, it is assumed in the sequel that the MISES criterion of yielding is applicable.

Further torsion tests were carried out to investigate the behaviour of the materials at small plastic strains. The stress-strain diagrams are shown in Fig. 2. They show that the copper and aluminium reached an almost constant flow stress after quite a small strain (about 0·01). For the steel, however, there was a considerable range of plastic strain over which the rate of strain-hardening was comparatively rapid.

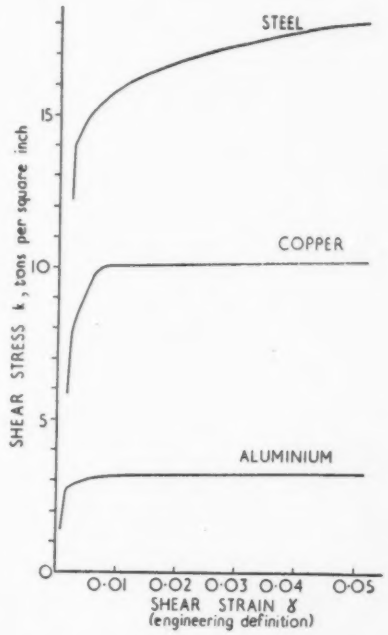

Fig. 2. Shear yield stresses at small plastic strains.

4. INDENTING TECHNIQUE

Cones of hardened carbon steel were employed. The cone was rigidly fixed to the upper platen of a Buckton testing machine in such a manner that the axis of the cone was accurately perpendicular to the surface of the lower platen and parallel to the vertical guiding surfaces of the machine. The specimens were machined to a cylindrical shape, with flat parallel faces. They were not constrained or located in any way, but were free to assume a central position as the cone entered the impression. For all tests calcium oleate was used as a lubricant. A pellet of this substance was shaped into a pointed cone and introduced into the impression so as to completely fill it before introducing the indenting tool for the next loading. The cones were finished by grinding to give a cone angle accurate to within 3 minutes of arc, and to give a surface finish of about $\pm$ 10 micro-inches. Coefficients of friction were measured by a method described by HILL (1950b) which depends on the unequal lateral expansions of a lamina of the material when compressed between parallel lubricated anvils. The coefficients found

Vol. 2 53/54

were : steel 0·030 ; copper 0·020 ; aluminium 0·025. The cones became blunted to a certain extent during the tests, but the bluntness never exceeded 0·001 in. measured axially. They were re-ground before commencing tests on each material. The area of the impression as viewed from above, i.e. the projected area, was taken to be that of an ellipse of the same principal diameters, and these were measured by means of a travelling microscope reading to 0·001 cm. The edge of the impression was always clearly defined, but it was noted that for the indentations in copper with cones of cone angle 60° and less, the rim of the impression contained deep radial fissures. This may explain why these values of mean pressure appeared to be erratic. Care was taken to ensure that the testing machine was correctly adjusted and well lubricated, and that the load was applied without shock. The load was applied for 2 minutes on all occasions.

5. Size of Specimen

It is of great importance that the indentation specimen should behave in the same way as a semi-infinite block of material. Preliminary tests were made to determine the critical size of impression : that is, the size beyond which the mode of deformation changes due to the finite size of the specimen. One set of specimens had a large depth (1·0 in.) and small diameter (0·5 in.), and another set had large diameter (1·0 in.) and small depth (0·1 in.). For each specimen about 10 uniformly increasing loads were applied so that the critical size of impression was exceeded. By plotting the impression area against load, the point at which the readings departed from a straight-line relation was found. The limiting ratios of specimen outside diameter s and specimen depth t to mean impression diameter d are shown in Fig. 3.

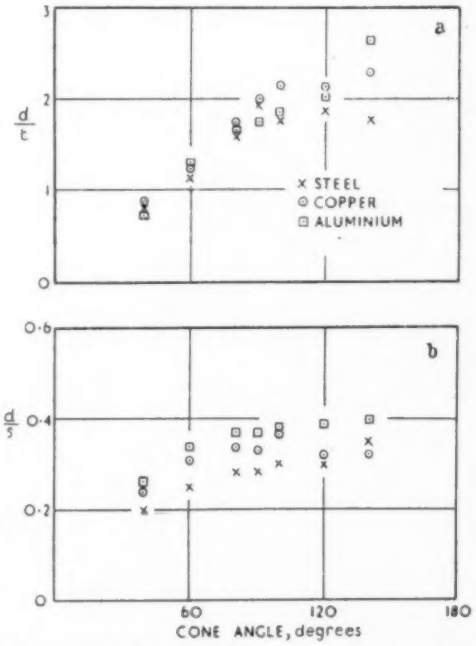

Fig. 3. Critical dimensions of indentation specimen. (a) Ratio of impression diameter d to specimen thickness t ; (b) Ratio of impression diameter d to specimen outside diameter s.

From this information it was decided that the specimens should be 1·0 in. in diameter and 0·6 in. in depth for a maximum impression diameter of 0·2 in. It should be noted that the critical ratios do not hold good when both diameter and depth are simultaneously made small. To make quite certain that no overall expansion took place, the outside diameter of the specimen was measured to within 0·0001 in. after each loading.

6. Indentation Tests

Load values were applied which gave equal increments of penetration, so that the peculiar friction effects that must exist at the extreme point of the cone should remain constant at all stages of the penetration. Thirteen applications of load were sufficient to give a satisfactory graph of impression area applied against load. A typical example is shown in Fig. 4. A graph such as this was carefully drawn for each specimen. The curve does not pass exactly through the origin because of the small additional load required to overcome the high friction at the extreme point of the cone, but this is of no consequence as only the gradient of the curve is relevant. This gradient defines the mean indentation pressure acting on the lubricated surface of the cone. For each material, specimens oriented relative to the bar in each of the three possible ways were prepared, 63 specimens in all. It was considered that the average values thus obtained would be free from the grosser errors that might arise from anisotropy and non-uniformity. The observed values are shown in Table 3, the units being tons per square inch.

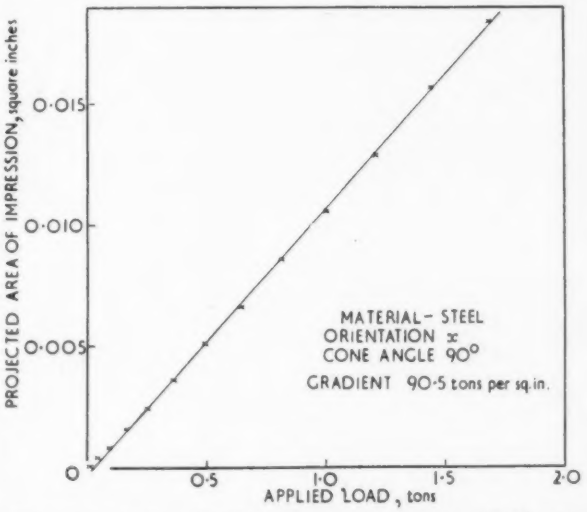

Fig. 4. Typical graph of impression area against applied load. All the points except the first few lie on a straight line.

The pressure p_c corrected for friction was found from the average of the observed pressures p by applying the usual formula

$$p_c = p/(1 + \mu \cot \theta) \tag{1}$$

where μ is the friction coefficient and θ is the semi-angle of the cone. Friction must also have an effect on the slip-line field. This effect could not be evaluated, but the analogous effect for wedge indentation (Dugdale 1953) may give some guide as to its probable magnitude; the mean pressure is there increased by a factor $1/(1 - \mu)$ on this account irrespective of wedge angle (if μ is small).

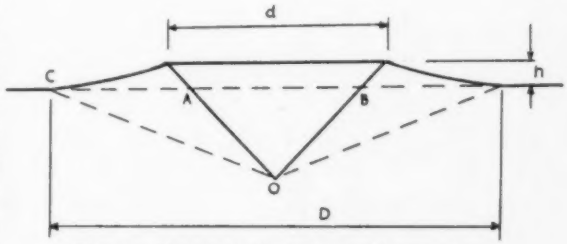

Fig. 5. Measured dimensions of impression.

Before an indentation was begun, the upper surface of the specimen was polished,

the aluminium and copper specimens with alumina and the steel ones with chromium oxide. The specimen was tilted so as to give a strong reflection of light into the microscope, and the mean diameter D of the plastically strained area (Fig. 5) was recorded after each loading. On plotting these values against mean impression diameter d for each specimen the mean ratio D/d was found. These were averaged for the x, y and z specimens, and are shown in Fig. 6a.

TABLE 3.

	Cone angle (degrees)	*Observed pressure*			*Corrected pressure (average)*
		x	y	z	
STEEL	40	78·5	83·0	81·0	75·0
	60	84·0	85·0	84·5	80·5
	80	90·0	92·5	90·5	88·0
	90	90·5	97·0	92·5	91·0
	100	93·0	101·0	94·5	93·5
	120	95·0	101·5	95·5	96·0
	140	96·0	98·0	96·0	95·5
COPPER	40	40·1	40·8	41·5	38·7
	60	40·7	41·9	41·5	40·0
	80	46·4	46·8	47·4	45·8
	90	47·9	47·9	49·4	47·5
	100	50·6	49·5	51·0	49·5
	120	54·8	53·4	53·7	53·4
	140	57·7	55·9	56·9	56·4
ALUMINIUM	40	13·15	13·10	13·00	12·25
	60	14·75	13·15	13·90	13·35
	80	15·65	14·50	15·75	14·85
	90	16·50	15·80	15·90	15·65
	100	17·50	16·05	16·65	16·40
	120	18·60	17·05	17·85	17·60
	140	18·85	18·40	18·85	18·55

The height of the raised lip was determined by taking the overall measurement with a micrometer and deducting the original thickness of the specimen. This measurement was taken at four points on the circumference of the impression after each loading. Plotting the mean height of the lip h against the mean impression diameter gave an average ratio h/d for each specimen. These are shown in Fig. 6b, the value shown being the average for the x, y and z specimens.

Although the individual readings were subject to a small uncertainty due to irregularity in the height of the lip and to difficulty in deciding the exact limit of the distorted area, it can be seen that each value shown in Fig. 6 was obtained by averaging large numbers of these readings. These are therefore considered to be trustworthy.

7. Volume of Raised Lip

After the indentation tests were completed each specimen was cut away to leave a diametral section of the impression. This section was made very thin (about 0·02 in.) to avoid effects of curvature, and was taken at 45° to the principal diameters of the impression so that any lack of axial symmetry of the impression would introduce a minimum of error. With the specimen mounted in a projector giving a magnification of about 50 times, the profile of the disturbed surface was traced on a sheet of paper. From the known cone angle and the measured length of the line in the original surface AB (Fig. 5), the displaced volume was calculated. The volume of the raised lip was found by integrating numerically, assuming it to be a body of revolution. Dividing the lip volume by the displaced volume gave the ratios shown in Table 4. Elastic recovery of the impression would presumably reduce the length of the line AB and would therefore make the value of the calculated ratio greater than the correct value, but the effect is assumed to be negligible.

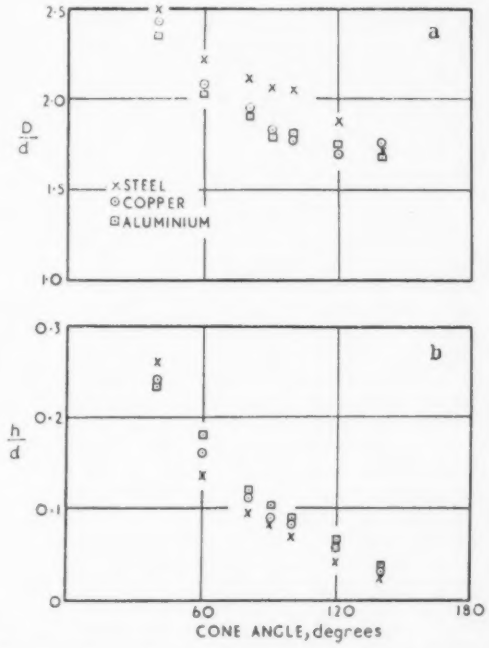

Fig. 6. Proportions of impression in terms of mean diameter d. (a) Diameter of plastically deformed area D; (b) Height of lip above original surface h.

8. Mean Strain

In order to relate the indentation pressures to the shear yield stresses found from torsion tests it is necessary to know the magnitude of the mean strain in the deformed material around the indentation. It is conceivable that this problem might be avoided by analysing the indentation results in terms of an initial yield stress and an assumed constant rate of strain-hardening, but unfortunately it is impossible to decide upon values for either of these, since the stress-strain curves have continually varying slopes. In any attempt to calculate the mean strain, the difficulty immediately arises that the distorted volume is not known. Here an approximation is made by assuming that the distorted region is bounded by the surface of the cone generated by the line OC (Fig. 5). This assumption has no particular virtue other than its simplicity. By equating the work done by the applied force to the work dissipated in straining this volume of material of mean shear yield stress k to a mean value of equivalent shear strain γ it is found that

Vol. 2 53/54

$$\gamma = \frac{p_c}{k}\left(\frac{d}{D}\right)^2. \qquad (2)$$

The p_c values were taken from Table 3 and the D/d values from Fig. 6a. A brief iterative method was required, taking a trial value of k and then verifying that it corresponded with the strain value γ in Table 2. The strains thus found varied from 0·6 for the 40° cone angle to 1·75 for the 140° cone angle. The latter is unlikely to be correct, for the assumption made becomes unreasonable at large cone angles, but it can be seen that even if the assumed volumes of the distorted region are doubled the resulting k values will only be reduced by amounts up to 5%.

TABLE 4.

	Cone angle (degrees)	*Observed volume ratio*			*Average*
STEEL	40	0·87	0·79	0·82	0·8
	60	0·90	1·03	0·90	0·9
	80	0·74	0·87	0·87	0·8
	90	0·93	0·85	0·96	0·9
	100	0·96	0·90	0·89	0·9
	120	0·66	0·79	0·77	0·7
	140	0·49	0·75	0·76	0·7
COPPER	40	0·98	0·87	0·86	0·9
	60	1·01	1·01	0·99	1·0
	80	0·95	1·03	0·90	1·0
	90	0·94	1·01	0·92	1·0
	100	1·07	0·89	0·82	0·9
	120	0·90	0·78	0·77	0·8
	140	0·90	0·77	0·69	0·8
ALUMINIUM	40	1·13	0·73	1·06	1·0
	60	1·10	0·67	1·12	1·0
	80	1·00	1·24	0·91	1·0
	90	0·84	1·09	0·97	1·0
	100	0·94	0·92	0·98	0·9
	120	1·00	0·76	1·08	0·9
	140	0·62	0·96	0·74	0·8

9. TESTS WITH CONES OF SMALL ANGLE

Because of the experimental difficulties this work is less accurate than the work with cones of larger angles. The aim was to determine approximately the cone angle for minimum mean pressure. In general, the procedure was the same. Two specimens only were made for each material and each cone angle. The 10° cone was made from a tough alloy steel, but when used with copper, the tip repeatedly broke off to the extent of 0·02 in. measured axially. The greatest impression diameter was 0·05 in. The results are shown in Table 5 (in units of tons per square inch).

Vol 2 1953/

10. Discussion of Results

An ideal plastic-rigid material must give a unique value of the ratio of mean indentation pressure to shear yield stress (p_c/k) for a cone of any given angle, since such a material is completely defined by its flow stress. From the pressure

Table 5.

	Cone angle (degrees)	*Observed pressure*	*Corrected pressure (average)*	*Volume ratio*
Copper	10	57·5		0·92
		54·9	45·8	0·73
	20	47·7		0·76
		44·8	41·6	0·76
	30	40·0		0·91
		38·8	36·6	0·86
Aluminium	10	18·2		0·70
		18·9	14·3	0·95
	20	15·4		0·92
		15·6	13·5	0·89
	30	14·2		0·80
		14·0	12·9	1·06

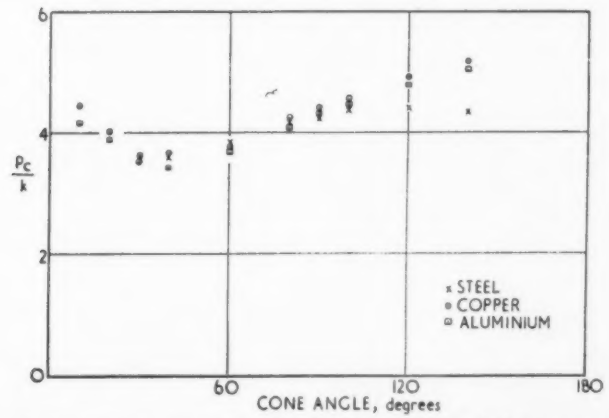

Fig. 7. Mean indentation pressure p_c expressed as a multiple of the appropriate shear yield stress k.

p_c from Table 3, and the mean shear stress k from Table 2 using mean strains given by equation (2), these ratios were calculated. They are shown in Fig. 7. The ratios for copper and aluminium agree fairly closely and, subject to an allowance for the various sources of error that have been mentioned, they should represent the ratios for an ideal plastic-rigid material. The ratios for steel also agree with those for copper and aluminium except for the obtuse cone angles. The ratios of lip volume to displaced volume (Table 4) for the copper and aluminium

are approximately equal to unity. The proportions of the impression (Fig. 6) show fair agreement between copper and aluminium, and it is likely that the values lie close to those for the idealized material.

The experimental results for cones of small angle (Table 5) show that the mean indentation pressure rises for very small angles. The volume ratios show that even for the 10° cone most of the displaced material escapes to the surface, so a rapid rise in pressure might be expected as the angle is further decreased. It may be mentioned that BISHOP, HILL and MOTT (1945) gave a theoretical pressure of 71 tons per square inch for cold-worked copper for a cone of zero angle. The angle giving the lowest mean pressure (Fig. 7) is probably between 30° and 40°.

11. BEHAVIOUR OF STEEL

The results for steel for cone angles of 120° and 140° were at variance with those for copper and aluminium and inconsistent with the values for smaller cone angles (see Figs. 3a, 6a, 7 and Table 4). As these variations were considered to be significant, an attempt has been made to explain them.

BISHOP, HILL and MOTT (1945) suggested that the pressure beneath the head of a punch could not exceed the pressure p_s required to enlarge indefinitely a small spherical cavity in an infinite block of material. By following their method it was found that

$$p_s = \frac{2}{\sqrt{3}} k_0 + 2\sqrt{3} \int_1^{c/a} \frac{k}{(r/a)}\, d\,(r/a)$$

$$k = f(\gamma)$$

$$\gamma = \frac{2}{\sqrt{3}} \ln \frac{(r/a)^3}{(r/a)^3 - 1}$$

where a and c are the current radii of the cavity and the plastic region, and

$$\left(\frac{c}{a}\right)^3 = \frac{2G}{\sqrt{3}\, k_0}$$

TABLE 6.

	STEEL	COPPER	ALUMINIUM
G tons per sq. in.	5,240	2,930	1,725
k_0 tons per sq. in.	14·0	8·0	2·75
c/a	7·56	7·51	8·98
p_s tons per sq. in.	139·0	78·6	27·1
p_c (140°) tons per sq. in.	95·5	56·4	18·55
p_c/p_s	0·69	0·72	0·68

where G is the modulus of shear and k_0 the initial yield stress (see also HILL 1950a, pp. 104-106). From these equations p_s was found by numerical integration using k values from Fig. 2 and Table 2. This integration showed that p_s depends largely on the stresses at small plastic strains.

Table 6 shows the shear moduli that were taken and the calculated values of p_s. The greatest observed indentation pressures p_c (for the 140° cone) were then selected from Table 3, and the ratios p_c/p_s were found. On the basis of these calculations the following discussion of the indentation pressures is offered. The pressure acting on the surface of the cone is not uniform, but increases towards the tip, where the material is most confined. The mean pressure increases with cone angle (Fig. 7) so that the pressure at the point of the cone must also increase. At some cone angle, the pressure acting on the part of the cone near to the point will become sufficiently great to initiate a flow inwards into the body of the material. It is supposed that this pressure is nearly equal to, but not greater than, p_s, the pressure required for expanding a spherical cavity. Meanwhile, the material around the edge of the impression can escape to the surface more readily. Therefore, the mean pressure acting on the cone when this mixed flow is occurring need not be equal to p_s, but will be equal to some fraction of it. This fraction must be a function of the material and cone angle. However, the experimental results (Table 3) show that the mean indentation pressure p_c for steel reaches an almost constant value of about 95 tons per square inch for cone angles of 100°, 120° and 140°, which suggests that the fraction does not vary greatly with cone angle, but assumes a value of about 0·7 (Table 6) for this material. Further, if the assumption that this fraction will not vary greatly for the three materials is admissible, then inward flow should not develop for the copper and aluminium until the ratio p_c/p_s reaches a similar value of 0·7, which does not occur until the cone angle reaches 140° (Table 6). This argument is supported by the evidence of Table 4 which shows that the apparent loss of displaced volume for the cone angles 120° and 140° was greater for steel than it was for copper and aluminium. Therefore, it is suggested that the lower indentation pressures for steel with cones of these angles were brought about by plastic-elastic effects resulting in an inward flow of some of the displaced material, and that these effects occurred for steel to a greater extent than for copper and aluminium because of the greater curvature of the stress-strain diagram.

Vol. 2 53/54

Acknowledgments

The author has been assisted by many valuable discussions with Professor J. L. M. Morrison of Bristol University and Professor R. Hill of Nottingham University.

References

Bishop, R. F., Hill, R. and Mott, N. F.	1945	*Proc. Phys. Soc.*, **57**, 147.
Dugdale, D. S.	1953	*J. Mech. Phys. Solids*, **2**, 14.
Hankins, G. A.	1926	*Proc. Inst. Mech. Eng.*, Vol. II, 823.
Hill, R.	1950a	*Mathematical Theory of Plasticity* (Clarendon Press).
	1950b	*Phil. Mag.*, **41**, 733.
Ichihara, M.	1931	*Tech. Rep. Tohoku Univ.*, **10**, 25.

Journal of the Mechanics and Physics of Solids, 1954, Vol. 2, pp. 278 to 285. Pergamon Press Ltd., London.

ON THE LIMITS SET BY PLASTIC YIELDING TO THE INTENSITY OF SINGULARITIES OF STRESS

By R. Hill
Department of Mathematics, University of Nottingham

(*Received 5th May*, 1954)

Summary

The following general problem is considered: Elements of a solid body deform appreciably only when the local stresses satisfy a certain relation; the material properties are otherwise arbitrary. What combinations of loads over some given part of the surface would definitely produce significant deformation, irrespective of forces and constraints elsewhere?

Attention is given mainly to the loading of an angle in the surface where there is necessarily a singularity of stress. An important application occurs in the theory of the yield point of a plastic-rigid body under given loads, where it is often necessary to decide whether non-deforming zones proposed in a solution are overstressed or not. Several examples are discussed.

1. Stress States in an Angle

Consider a two-dimensional wedge of vertex angle α with curved boundaries over which act given distributions of stress, continuous and tending to finite limits as the vertex is approached. If the stress at an internal point with polar coordinates (r, θ) has components $(\sigma_r, \sigma_\theta, \tau_{r\theta})$ the equations of equilibrium in the absence of body forces are

$$r\frac{\partial \sigma_r}{\partial r} + \frac{\partial \tau_{r\theta}}{\partial \theta} + \sigma_r - \sigma_\theta = 0, \qquad r\frac{\partial \tau_{r\theta}}{\partial r} + \frac{\partial \sigma_\theta}{\partial \theta} + 2\tau_{r\theta} = 0.$$

Since the boundary conditions exclude the possibility of infinities, the stresses at the vertex ($r = 0$) are functions of θ only and satisfy

$$\frac{d\tau_{r\theta}}{d\theta} + \sigma_r - \sigma_\theta = 0, \qquad \frac{d\sigma_\theta}{d\theta} + 2\tau_{r\theta} = 0, \tag{1}$$

together with the boundary values at $r = 0$, say

$$\sigma_\theta(0) = -p_1, \qquad \sigma_\theta(\alpha) = -p_2, \qquad \tau_{r\theta}(0) = q_1, \qquad \tau_{r\theta}(\alpha) = q_2 \qquad \text{(Fig. 1)}.$$

In general, for arbitrary p_1, p_2, q_1, q_2, the vertex is a singularity of stress, i.e. $\tau_{r\theta}$ is not a simple harmonic function of 2θ. Its precise functional dependence can naturally be determined only in terms of the properties of the material and the distribution of surface forces elsewhere. However, irrespective of what these may be, it will be shown that definite restrictions are imposed on p_1, p_2, q_1, q_2 by the condition that the maximum shear stress at any point must not exceed a critical value k, namely

$$\tfrac{1}{4}(\sigma_\theta - \sigma_r)^2 + \tau_{r\theta}^2 \leqslant k^2 \qquad \text{or} \qquad \tfrac{1}{4}\left(\frac{d\tau_{r\theta}}{d\theta}\right)^2 + \tau_{r\theta}^2 \leqslant k^2. \tag{2}$$

A state of stress violating this condition is regarded as being necessarily accompanied by deformations large enough to alter significantly the geometry of the wedge. It is immaterial whether this is due specifically to plastic yielding, as in a ductile metal with a sharply-defined elastic limit, or to failure in some other sense. For convenience, however, and since the applications to be described all concern the ideal plastic solid, an element will be said to be 'plastic' when the maximum shearing stress is equal to k.

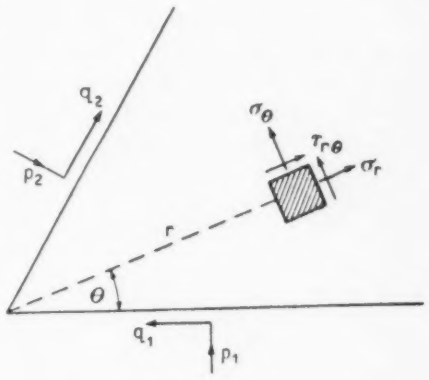

Fig. 1.

We make now the substitution

$$\tau_{r\theta} = k \sin 2\phi \tag{3}$$

where, to be definite, ϕ is always chosen in the closed interval $(-\frac{1}{4}\pi, \frac{1}{4}\pi)$. The boundary values ϕ_1 and ϕ_2 are defined by

$$q_1 = k \sin 2\phi_1, \qquad q_2 = k \sin 2\phi_2.$$

The inequality (2) reduces to

$$\left|\frac{d\phi}{d\theta}\right| \leqslant 1, \tag{4}$$

while the second of (1) becomes

$$\int_0^\alpha \sin 2\phi \, d\theta = (p_2 - p_1)/2k. \tag{5}$$

Note that the maximum shear stress is equal to k either when $|d\phi/d\theta| = 1$ for any value of ϕ, or when $|\phi| = \frac{1}{4}\pi$ for any value of $d\phi/d\theta$. Also, since σ_r (though not σ_θ and $\tau_{r\theta}$) can be a discontinuous function of θ so can $d\tau_{r\theta}/d\theta$ and $d\phi/d\theta$.

For some given loading of the vertex, specified by the four quantities p_1, p_2, q_1 and q_2, consider all continuous functions $\phi(\theta)$ passing through the terminal values ϕ_1, ϕ_2, and with gradients nowhere exceeding unity and not necessarily continuous. If none of these functions satisfies (5) we conclude that the condition (2) is definitely violated throughout a certain range of θ; the wedge could therefore not maintain its supposed shape under such loads applied at the vertex. For any given ratios of p_1, p_2, q_1, and q_2, we can determine in this way the stress magnitude above which (4) is always violated and below which equilibrium states can be found satisfying (4) and the boundary conditions. That there is such a unique value follows from the remark that if a satisfactory equilibrium state can be associated with any particular stress magnitude so can one with any lesser magnitude.* The totality of critical magnitudes for arbitrary stress ratios is representable

* For we can construct it by diminishing the former stress distribution in the ratio of the two magnitudes, (2) being satisfied *a fortiori*.

by a surface with $p_1 - p_2$, q_1, and q_2 as coordinates.* Any load combination represented by a point outside this surface would produce significant deformation of the vertex even under the most favourable attendant circumstances; in other words, the limited strength of the body does not allow of stress singularities above a certain intensity. On the other hand, without further investigation nothing can be concluded about the effect of a load combination represented by a point within the surface; whether or not significant deformation would occur (at the vertex or elsewhere) depends on the material properties, on the geometry of the whole body, and on the other applied forces and constraints.

To calculate this 'failure' surface it is convenient to regard ϕ_1 and ϕ_2 as given and to seek the algebraically least and greatest values of $p_1 - p_2$ allowed by (5) for all permissible $\phi(\theta)$. An over-riding restriction on ϕ_1 and ϕ_2 must first be noted: this is

$$|\phi_1 - \phi_2| \leqslant \alpha; \tag{6}$$

otherwise it is impossible to join the terminal values by any permissible function whatsoever. Suppose now that points P_1 and P_2 in Fig. 2 represent ϕ_1 and ϕ_2 and that $\phi_1 + \phi_2 \leqslant \frac{1}{2}\pi - \alpha$. Then the greatest value of the integral in (5) is given by the function represented by P_1QP_2, where P_1Q and P_2Q are straight segments of unit slope. If, however, the terminal values are P_1', P_2' such that $\phi_1 + \phi_2 > \frac{1}{2}\pi - \alpha$, the required function is represented by $P_1'Q_1'Q_2'P_2'$ where the slope of $P_1'Q_1'$ and $P_2'Q_2'$ is unity and $\phi = \frac{1}{4}\pi$ on $Q_1'Q_2'$. Thus

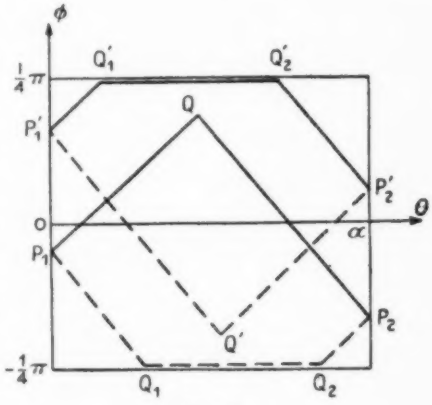

Fig. 2.

$$\left(\frac{p_2 - p_1}{2k}\right)_{\max} = \begin{cases} \frac{1}{2}(\cos 2\phi_1 + \cos 2\phi_2) - \cos(\alpha + \phi_1 + \phi_2), \\ \alpha + \phi_1 + \phi_2 \leqslant \frac{1}{2}\pi. \\ \frac{1}{2}(\cos 2\phi_1 + \cos 2\phi_2) + (\alpha + \phi_1 + \phi_2 - \frac{1}{2}\pi), \\ \alpha + \phi_1 + \phi_2 \geqslant \frac{1}{2}\pi. \end{cases} \tag{7}$$

Similarly, by considering functions such as $P_1'Q'P_2'$ and $P_1Q_1Q_2P_2$,

$$\left(\frac{p_2 - p_1}{2k}\right)_{\min} = \begin{cases} -\frac{1}{2}(\cos 2\phi_1 + \cos 2\phi_2) + \cos(\alpha - \phi_1 - \phi_2), \\ \alpha - \phi_1 - \phi_2 \leqslant \frac{1}{2}\pi. \\ -\frac{1}{2}(\cos 2\phi_1 + \cos 2\phi_2) - (\alpha - \phi_1 - \phi_2 - \frac{1}{2}\pi), \\ \alpha - \phi_1 - \phi_2 \geqslant \frac{1}{2}\pi. \end{cases} \tag{8}$$

Permissible functions can clearly be found for all values of $p_2 - p_1$ between these limits.

* It is evident from (5) that only the difference of p_1 and p_2 is relevant. This was to be expected *a priori* since any uniform distribution of hydrostatic stress can be super-imposed without affecting equilibrium or the condition (2).

It will be observed that P_1QP_2 and $P_1'Q'P_2'$ each represent a fully plastic state in which two uniformly stressed zones are separated by a stress discontinuity, while $P_1Q_1Q_2P_2$ and $P_1'Q_1'Q_2'P_2'$ each represent a fully plastic state in which two uniformly stressed zones are separated by one in which the slip-lines are radii and concentric circular arcs. These fields are similar to those obtained by PRAGER and PRANDTL respectively in another context ; namely, at the yield point of a triangular wedge of plastic-rigid material indented along one side by a smooth rigid die.

Discussion of the full significance of this similarity is left to Section 3. Meanwhile we consider some particular singularities, corresponding to certain sections of the 'failure' surface.

2. SOME PARTICULAR SINGULARITIES

(i) $q_1 = q_2 = 0$

Only normal pressures p_1 and p_2 are applied. Substitution of $\phi_1 = \phi_2 = 0$ in (7) and (8) leads to

$$\left|\frac{p_2 - p_1}{2k}\right| \leqslant \begin{cases} 1 - \cos\alpha, & \alpha \leqslant \tfrac{1}{2}\pi. \\ 1 + \alpha - \tfrac{1}{2}\pi, & \alpha \geqslant \tfrac{1}{2}\pi. \end{cases} \tag{9}$$

Whatever the circumstances elsewhere, the vertex cannot sustain a greater pressure difference than this. Of course, the elastic limit is reached locally at a smaller pressure difference (except for $\alpha = \frac{1}{2}\pi$, when there is no singularity). It is of some interest to mention that the elastic limit is reached first on the two sides of the vertex when $\alpha < \frac{1}{2}\pi$, and on the median plane $\theta = \frac{1}{2}\alpha$ when $\alpha > \frac{1}{2}\pi$.

(ii) $q_1 = -q_2 = \pm k$.

The shearing stresses are the largest possible and are both directed either towards or away from the vertex. According to (6), since $\phi_1 = -\phi_2 = \pm \frac{1}{2}\pi$, it is first necessary that $\alpha \geqslant \frac{1}{2}\pi$, and then from (7) and (8)

$$\left|\frac{p_2 - p_1}{2k}\right| \leqslant \alpha - \tfrac{1}{2}\pi. \tag{10}$$

An application occurs in the theory of indentation by a rough wedge (GRUNZWEIG, LONGMAN and PETCH, 1954). The proposed solution is invalid whenever the two slip-lines from the tip of the indenter enclose an angle less than $\frac{1}{2}\pi$; this confirms what has hitherto been only a conjecture. The argument due to LEE (1952) is inadequate since the possibility of a permissible singularity of stress is not ruled out.

(iii) $q_1 = q_2 = k$.

One shear stress (q_1) is directed towards, and the other (q_2) away from, the vertex. Since $\phi_1 = \phi_2 = \frac{1}{4}\pi$ (6) is satisfied for all α, and the allowed range is

$$\alpha \geqslant \frac{p_2 - p_1}{2k} \geqslant \begin{cases} \sin\alpha, & \alpha \leqslant \pi. \\ -(\alpha - \pi), & \alpha \geqslant \pi. \end{cases} \tag{11}$$

Applications occur in the theories of the yield point of a notched bar and of a built-in beam in plane-strain bending (GREEN 1953 and 1954). For certain dimensions the zones of deformation separate two rigid regions which have a single point in common (about which they rotate). The vertex of each region is bounded by a pair of orthogonal slip-lines of the same family. Equation (11) with $\alpha = \frac{1}{2}\pi$ shows that, as GREEN rightly conjectured, the vertices could not sustain a pressure difference outside the range $2k$ to πk.

(iv) $q_1 = 0,\ q_2 = k.$

On one side there is no shearing stress, but on the other the maximum possible. With $\phi_1 = 0$ and $\phi_2 = \frac{1}{4}\pi$, (6) requires $\alpha \geqslant \frac{1}{4}\pi$ while (7) and (8) give

$$1 + 2(\alpha - \tfrac{1}{4}\pi) \geqslant \frac{p_2 - p_1}{k} \geqslant \begin{cases} 2\cos(\alpha - \frac{1}{4}\pi) - 1, & \frac{1}{4}\pi \leqslant \alpha \leqslant \frac{3}{4}\pi. \\ -2(\alpha - \frac{3}{4}\pi) - 1, & \alpha \geqslant \frac{3}{4}\pi. \end{cases} \tag{12}$$

This result is relevant wherever the free surface of a plastic-rigid solid is met by the slip-line boundary of a zone of deformation in the proposed solution. In order that this should be valid it is necessary at least that (12) should be satisfied at the vertex of the rigid material between the slip-line and the free surface. Here $p_1 = 0$ while p_2 is known from the calculated distribution of stress in the zone of deformation. For example, as the present writer shows elsewhere (HILL 1954), this consideration suffices to disprove the steady-state configurations proposed for the machining problem by ERNST and MERCHANT (1941) and by LEE and SHAFFER (1951). Again, this result establishes the necessity for the 'standing-wave' solution in the problem of sheet drawing when the die pressure is sufficiently large (HILL 1948).

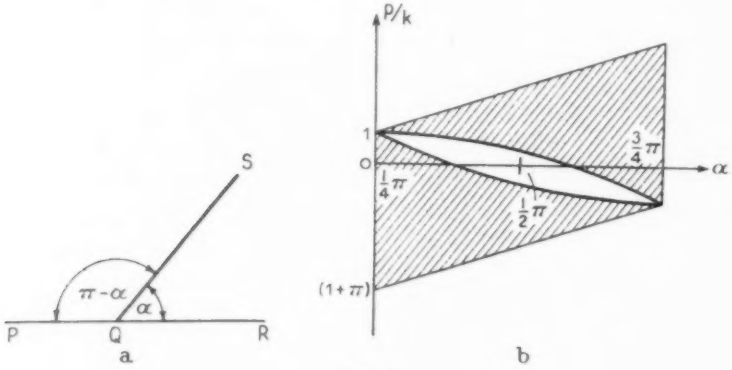

Fig. 3.

An important consequence of (12) is that a slip-line, SQ say in Fig. 3a, cannot intersect a free surface PR with a *continuous* slope at an acute angle other than $\frac{1}{4}\pi$. Suppose the shearing stress k along SQ, acting on the vertex SQR, is directed away from Q; then the shearing stress k along SQ, acting on the vertex SQP, is directed towards Q. From (6) both α and $\pi - \alpha$ must exceed $\frac{1}{4}\pi$, while from (12) applied in turn to each vertex

$$\left.\begin{aligned} 1 + 2\,(\alpha - \tfrac{1}{4}\pi) &\geqslant p/k \geqslant 2\cos(\alpha - \tfrac{1}{4}\pi) - 1 \\ 1 + 2\,(\tfrac{3}{4}\pi - \alpha) &\geqslant -p/k \geqslant 2\cos(\tfrac{3}{4}\pi - \alpha) - 1 \end{aligned}\right\} \quad (\tfrac{1}{4}\pi \leqslant \alpha \leqslant \tfrac{3}{4}\pi)$$

where p is the pressure across SQ at Q. The ranges of p/k allowed by the respective inequalities are shown shaded in Fig. 3b. The only value for α for which there exists a pressure common to both ranges is $\frac{1}{4}\pi$ (or equivalently $\frac{3}{4}\pi$) as stated. Of course, other values are allowable in conformity with (12) when the surface PR is not straight but has an angle at Q (as at the outer boundary of the raised lip in the well-known solution of the problem of wedge indentation).

3. A General Approach

We now describe a general method for deciding when certain proposed surface forces could under no circumstances be sustained by a body of given shape.

Suppose that significant deformation of an element would be produced by any stress represented by a point outside a certain surface Σ in stress space, but not by a point within it. Σ is assumed to contain the origin (zero stress) and to be convex everywhere. Let S denote that part of the surface of the body which consists of the points of application of the proposed forces. Let their ratios and the sign of one of them be regarded as given, and denote by m the numerical magnitude specifying the absolute value. The surface forces and constraints elsewhere are of no concern. If, for some value m_1 of m, an equilibrium distribution of stress can be found, within Σ at every point of the body and compatible with the forces on S, then so can one for any lesser value m_0 : it is constructed by reducing the original distribution in the ratio m_0/m_1. On the other hand, if for some value m_1 no such stress state can be found, then neither can one for any greater value m_2 ; for otherwise one could be found corresponding to m_1 by a reduction in the ratio m_1/m_2. It follows that there exists a unique magnitude, f say (f for failure), with the property that at least one such stress state can always be found for any lesser value of m, but none for any greater value. We emphasize that f depends only on the ratios of the considered forces and on the constraining surface Σ, but not on any other material properties.

However, the method suggested here for calculating f is such that the formal analytical procedure can advantageously be expressed in terms associated with the yield point of an ideal plastic-rigid solid (Hill 1951).* Thus, the function defining Σ is regarded as the yield function of an element of the solid, and also as its plastic potential. The following theorem may then be enunciated : *f is equal to the stress magnitude y at the yield point of a geometrically-similar plastic-rigid body when loaded by the forces on S in the given ratios and rigidly constrained over the remainder of its surface.* For, according to the maximum work principle (Hill 1950), valid when the yield function and plastic potential are identical, no equilibrium state of stress compatible with the condition Σ can do work at a greater rate in a yield-point deformation mode than is done by the actual state of stress associated with this mode ; since work is done only by the forces on S and the ratios of these are given, we see that f is certainly not greater than y. On the other hand, since the actual state at the yield point is in equilibrium, satisfies the

* The yield point of such a solid is the instant when deformation can first occur under a given loading programme.

conditions on S and does not violate Σ, f cannot be less than y. It is therefore identical with it. For the sake of underlining previous remarks, it may be mentioned in passing that, for a material with these particular properties, deformation modes can be obtained for values of y less than f by variously relaxing the rigid constraints.

As an example of the application of this theorem we re-derive equations (7) and (8). Consider a two-dimensional body whose shape is arbitrary except that its surface contains two straight segments U_1V, U_2V including at V an angle α (Fig. 4). Along U_1V, U_2V are applied uniform distributions of normal stresses p_1, p_2 and shearing stresses q_1, q_2, while the remainder of the surface is rigidly constrained. We seek the relation between q_1, q_2 and $p_1 - p_2$ at the yield point in

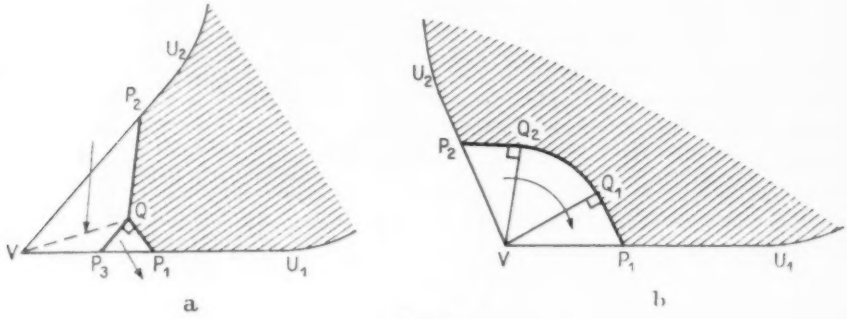

Fig. 4.

plane strain if any element yields when the maximum shearing stress attains the value k. There are two possible deformation modes, depending on the ratios and signs of the applied stresses. In Fig. 4 (a) a stress discontinuity VQ separates two uniformly stressed zones bounded by slip-lines P_1Q and P_2Q. Regions P_2QP_3V and P_1QP_3 slide as rigid blocks parallel to P_2Q and QP_1 respectively; there is a tangential velocity discontinuity across the slip-line QP_3. In Fig. 4 (b) the uniformly stressed zones P_1VQ_1 and P_2VQ_2 are separated by the zone Q_1VQ_2 in which the slip-lines are radii and circular arcs. The stream-lines coincide with slip-lines of the same family as $P_1Q_1Q_2P_2$. The same stress fields may be extended indefinitely throughout the remainder of the body, which is rigid (shaded in Fig. 4).

Since these fields are exactly those discussed in connexion with Fig. 2. the required yield-point relation is given (implicitly) by (7) and (8). When the angle is bounded by curved sides the result follows from a limiting argument, U_1 and U_2 being allowed to approach indefinitely near to V. By the above theorem, equations (7) and (8) also define the 'failure surface' for other materials whose only common property is the restriction (2).

REFERENCES

ERNST, H. and MERCHANT, M. E. 1941 *Trans. Amer. Soc. Metals*, **29**, 299.

GREEN, A. P. 1953 *Quart. J. Mech. Appl. Math.*, **6**, 223.

1954 *J. Mech. Phys. Solids*, **2**, p. 000.

GRUNZWEIG, J., LONGMAN, I. M. and PETCH, N. J. 1954 *J. Mech. Phys. Solids*, **2**, 81.

HILL, R.	1948	*Dissertations* (Cambridge) issued by A.R.E., Min. of Supply, as Survey 1/48.
	1950	*Mathematical Theory of Plasticity* (Clarendon Press) p. 66.
	1951	*Phil. Mag.*, **42**, 868.
	1954	*J. Mech. Phys. Solids*, in press.
LEE, E. H.	1952	*J. Appl. Mech.*, **74**, 97.
LEE, E. H. and SHAFFER, B. W.	1951	*J. Appl. Mech.*, **73**, 405.

Vol.
2
953/54

Journal of the Mechanics and Physics of Solids, 1954, Vol. 2, pp. 286 to 295. Pergamon Press Ltd., London

WAVE MOTION IN PLASTIC-ELASTIC STRINGS

By J. W. Craggs
King's College, Newcastle-upon-Tyne

(*Received 22nd March*, 1954)

Summary

The equations of motion of an extensible string are obtained for transverse motions sufficiently large to alter the tension. Examples are given to show how particular problems may be solved, either by the method of characteristics or by a general numerical technique.

1. Introduction

The classical theory of wave motions in strings is concerned with two distinct types of wave. Longitudinal elastic waves are discussed under the assumption that no transverse displacement occurs, and discussion of transverse waves is restricted to waves of amplitude so small that the tension remains constant.

The non-linear problem involved in the discussion of transverse waves of amplitude large enough to affect the tension has been treated by Taylor (1942) for an elastic-plastic wire and by Cole, Dougherty and Huth (1953) for an elastic wire, but in each case only simple-wave solutions (in which the waves travel along the wire in only one direction) are given. In the present paper a general theory of waves in strings is derived in characteristic form, and a simple numerical technique for the solution of special problems is proposed.

2. The Equations of Motion

Consider the plane motion of a thin, perfectly flexible string of uniform mass m per unit length (in the unstretched state). Suppose that initially the string is unstretched, but just taut, and lies along the axis $y = 0$, $x \geqslant 0$ in rectangular Cartesian coordinates. Let the displacement, at time t, of the point of the string initially at $(x, 0)$ be (u, v), and use Lagrange-type equations of motion.

Define r as the ratio of the stretched to the unstretched length of an element of the string, and ψ as the inclination of the string, in its strained state, to the axis $y = 0$. Then

$$1 + \partial u/\partial x = r \cos \psi, \tag{1}$$

$$\partial v/\partial x = r \sin \psi. \tag{2}$$

Let T be the local tension in the strained state, and suppose that a load-extension law

$$T = f(r) \tag{3}$$

is known and holds independently of rate of strain. Note that $r - 1$ is the "engineering strain" and T is proportional to the "engineering stress," so that (3) is an "engineering stress-strain curve."

The equations of motion of an element are

$$m \frac{\partial^2 u}{\partial t^2} = \frac{\partial}{\partial x}(T \cos \psi) \tag{4}$$

and

$$m \frac{\partial^2 v}{\partial t^2} = \frac{\partial}{\partial x}(T \sin \psi) \tag{5}$$

Differentiate these equations with respect to x, substitute for $\partial u/\partial x$, $\partial v/\partial x$ from (1) and (2), and eliminate the trigonometric terms. Then

$$\frac{m \partial^2 r}{\partial t^2} - mr \left(\frac{\partial \psi}{\partial t}\right)^2 = \frac{\partial^2 T}{\partial x^2} - T \left(\frac{\partial \psi}{\partial x}\right)^2, \tag{6}$$

$$mr \frac{\partial^2 \psi}{\partial t^2} + 2m \frac{\partial r}{\partial t} \cdot \frac{\partial \psi}{\partial t} = T \frac{\partial^2 \psi}{\partial x^2} + 2 \frac{\partial T}{\partial x} \frac{\partial \psi}{\partial x}. \tag{7}$$

Equation (6) is a quasi-linear hyperbolic equation for r or T, and has two real characteristic directions at every point, corresponding to stress waves with velocity of propagation

$$c = \left(\frac{1}{m} \frac{dT}{dr}\right)^{\frac{1}{2}}. \tag{8}$$

(7) is a similar equation for the slope, and shows that infinitesimal transverse waves travel with velocity

$$\lambda = (T/mr)^{\frac{1}{2}}. \tag{9}$$

3. Solution by the Method of Characteristics

Write

$$U = \partial u/\partial t, \qquad V = \partial v/\partial t. \qquad \mu = \partial u/\partial x \qquad \text{and} \qquad \nu = \partial v/\partial x. \tag{10}$$

Then equations (4) and (5) may be rewritten in the forms

$$\frac{\partial U}{\partial t} = c^2 \frac{\partial r}{\partial x} \cos \psi - \lambda^2 r \frac{\partial \psi}{\partial x} \sin \psi$$

and

$$\frac{\partial V}{\partial t} = c^2 \frac{\partial r}{\partial x} \sin \psi + \lambda^2 r \frac{\partial \psi}{\partial x} \cos \psi,$$

where c, λ are given by (8) and (9). Use of (1), (2), and (10) then leads to

$$\frac{\partial U}{\partial t} \cos \psi + \frac{\partial V}{\partial t} \sin \psi = c^2 \left(\frac{\partial \mu}{\partial x} \cos \psi + \frac{\partial \nu}{\partial x} \sin \psi\right) \tag{11}$$

and

$$-\frac{\partial U}{\partial t} \sin \psi + \frac{\partial V}{\partial t} \cos \psi = \lambda^2 \left(-\frac{\partial \mu}{\partial x} \sin \psi + \frac{\partial \nu}{\partial x} \cos \psi\right). \tag{12}$$

Now introduce characteristic variables α_1, β_1, such that

$$\frac{\partial \alpha_1}{\partial t} + c\frac{\partial \alpha_1}{\partial x} = \frac{\partial \beta_1}{\partial t} - c\frac{\partial \beta_1}{\partial x} = 0 \tag{13}$$

and use the equations $\partial U/\partial x = \partial \mu/\partial t$, $\partial V/\partial x = \partial \nu/\partial t$. Then

$$\frac{\partial U}{\partial \alpha_1}\cos\psi + \frac{\partial V}{\partial \alpha_1}\sin\psi + c\left(\frac{\partial \mu}{\partial \alpha_1}\cos\psi + \frac{\partial \nu}{\partial \alpha_1}\sin\psi\right) = 0, \tag{14}$$

and

$$\frac{\partial U}{\partial \beta_1}\cos\psi + \frac{\partial V}{\partial \beta_1}\sin\psi - c\left(\frac{\partial \mu}{\partial \beta_1}\cos\psi + \frac{\partial \nu}{\partial \beta_1}\sin\psi\right) = 0. \tag{15}$$

Again, define α_2, β_2 by

$$\frac{\partial \alpha_2}{\partial t} + \lambda\frac{\partial \alpha_2}{\partial x} = \frac{\partial \beta_2}{\partial t} - \lambda\frac{\partial \beta_2}{\partial x} = 0. \tag{16}$$

Then

$$-\frac{\partial U}{\partial \alpha_2}\sin\psi + \frac{\partial V}{\partial \alpha_2}\cos\psi + \lambda\left(-\frac{\partial \mu}{\partial \alpha_2}\sin\psi + \frac{\partial \nu}{\partial \alpha_2}\cos\psi\right) = 0 \tag{17}$$

and

$$-\frac{\partial U}{\partial \beta_2}\sin\psi + \frac{\partial V}{\partial \beta_2}\cos\psi - \lambda\left(-\frac{\partial \mu}{\partial \beta_2}\sin\psi + \frac{\partial \nu}{\partial \beta_2}\cos\psi\right) = 0. \tag{18}$$

A numerical method for the solution of special problems follows from (14), (15), (17) and (18). Suppose, for example, a curve L is given in the (x, t) plane, such that it nowhere touches a characteristic line, and suppose U, V, μ, ν are given on L. Choose a point P near to L and draw characteristic arcs through P to meet L in A, B, C and D. Then the values of the dependent variables at P may be deduced from those at A, B, C and D. The extension of this method to other types of boundary problem, and the refinement of the accuracy by successive approximations, presents no difficulty.

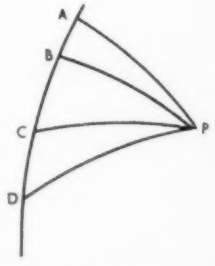

Fig. 1.

4. Discontinuous Solutions

The method indicated above has two drawbacks in practice. First, as Lee (1953) has pointed out in the case of uniaxial compression, the intersections of the characteristics must be calculated to a high degree of accuracy, and the computation is not easily reduced to a routine suitable for unskilled or mechanical computation. The second difficulty arises when the boundary or initial conditions of a problem involve discontinuities of velocity, tension or slope. In a non-linear problem such discontinuities do not necessarily propagate with the characteristic velocity, and the problem must be re-examined.

Now White and Griffis (1948) have shown that, in uniaxial compression of a cylinder, there can be no shock wave unless the load-compression curve is concave upwards (or straight, as a limiting case). The corresponding result for tension is that a shock wave involving a discontinuity of stress can occur only if dT/dr,

the so-called tangent modulus, is either constant or an increasing function of r. The latter possibility may be discounted in practice, but the former, that of a straight portion of the load-extension curve, may occur in any elastic region, including any region where the tension is less than a value previously reached. In any such case, however, the shock wave propagates with the characteristic velocity, so the use of the characteristics method is still possible.

The velocity of propagation of a wave involving a discontinuity of slope may be obtained by using the conditions of continuity of displacement and of conservation of momentum. The velocity is found to be the characteristic velocity for transverse waves, as might be expected since the velocity of a transverse wave is independent of the slope and depends only on the tension.

It remains to show how shock waves may be fitted in to a characteristics type of solution. It is sufficient to show how shock waves interact with each other, as any continuous change of stress, for example, may be regarded as a sequence of small discontinuous changes. Since longitudinal shocks can arise, in general, only in elastic regions, and since the extension to plastic regions with linear strain-hardening (if such regions do exist) is easy, it suffices to consider only elastic strings.

Vol. 2 53/54

5. Elastic Strings

Define an elastic string as one for which the load-extension curve is straight and of slope E. (This definition gives a Hookeian elastic material only when the strains are everywhere small.) Then all longitudinal waves travel with velocity $c_0 = (E/m)^{\frac{1}{2}}$. The tension is small compared to the modulus E, and the velocities of transverse waves are therefore very much smaller than the velocities of longitudinal waves.

Consider, for example, the interaction of a longitudinal wave and a transverse wave, meeting head-on. Let the slope behind the transverse wave be ψ_2 and in front of it ψ_0. Let the tension behind the longitudinal wave be T_2 and behind it T_0 (see Fig. 2a). After the intersection of the waves, longitudinal and transverse waves may be expected to spread out in both directions, and since the longitudinal waves travel faster the configuration will be as shown in Fig. 2b, where T_1 and ψ_1 are the intermediate values of the tension and slope. Let λ_0, λ_1 be the wave velocities appropriate to tensions T_0 and T_1, and let U_0, U_1, U_2 be the x-components of velocity reading from left to right, in the three regions of Fig. 2a. Let the components, reading from left to right in Fig. 2b be U_0, U_a, U_b, U_c, U_2. Then the equations of momentum at the various wave fronts give

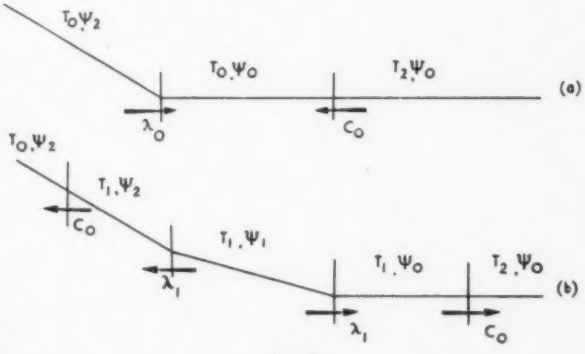

Fig. 2.

$$m(U_0 - U_1) = (T_0/\lambda_0)(\cos\psi_0 - \cos\psi_2),$$
$$m(U_1 - U_2) = -(T_2/c_0)\cos\psi_0 + (T_0/c_0)\cos\psi_0,$$

and

$$m(U_0 - U_a) = -(T_1/c_0)\cos\psi_2 + (T_0/c_0)\cos\psi_2,$$
$$m(U_a - U_b) = -(T_1/\lambda_1)(\cos\psi_1 - \cos\psi_2),$$
$$m(U_b - U_c) = (T_1/\lambda_1)(\cos\psi_0 - \cos\psi_1),$$
$$m(U_c - U_0) = (T_2/c_0)\cos\psi_0 - (T_1/c_0)\cos\psi_0.$$

Eliminate the velocity components from these six equations, and from the corresponding equations for the transverse velocity components (which differ only in having sines for cosines). Then the resulting equations for T_1 and ψ_1 may be written in the symmetrical form

$$\frac{\dfrac{T_1 - 2T_2 + T_0}{c_0} + \dfrac{T_0}{\lambda_0} - \dfrac{T_1}{\lambda_1}}{\sin(\psi_1 - \psi_2)} = \frac{\dfrac{2T_1}{\lambda_1}}{\sin(\psi_2 - \psi_0)} = \frac{\dfrac{T_1 - T_0}{c_0} - \dfrac{T_0}{\lambda_0} - \dfrac{T_1}{\lambda_1}}{\sin(\psi_0 - \psi_1)}. \tag{19}$$

Similar equations may be derived for the case in which a transverse wave is overtaken by a longitudinal wave travelling in the same direction. Finally, consider the case in which two transverse waves meet in a string of tension T_0. Let the slope between the incident waves be ψ_1, and the slopes behind them ψ_2 and ψ_0. Then, after the intersection, there will in general be longitudinal waves and transverse waves spreading from the point of intersection. The tension T_3 between the longitudinal waves and the slope ψ_3 between the transverse waves are then given by

$$\frac{\dfrac{T_0}{\lambda_0} - \dfrac{T_1}{c_0} + \dfrac{T_1}{\lambda_1}}{\dfrac{T_0}{\lambda_0}\sin(\psi_2 - \psi_0) + \dfrac{T_1}{\lambda_1}\sin(\psi_2 - \psi_3)}$$
$$= \frac{\dfrac{T_0}{\lambda_0} + \dfrac{T_1}{\lambda_1} + \dfrac{T_0 - T_1}{c}}{\dfrac{T_0}{\lambda_0}\sin(\psi_0 - \psi_1) + \dfrac{T_1}{\lambda_1}\sin(\psi_3 - \psi_1)} = \frac{2}{\sin(\psi_2 - \psi_1)}. \tag{20}$$

Consider, for example, an elastic string of length $2L$, initially straight, unstretched and with fixed ends $x = \pm L$. Suppose the midpoint is suddenly constrained to move with a uniform velocity W in the direction of the y-axis. Then the initial motion for $x \geqslant 0$ consists of a longitudinal wave followed by a transverse wave. In Fig. 3, which shows an (x, t) plane, these waves are represented by OA, OB, respectively. When the longitudinal wave reaches the fixed end, it is reflected, the tension being doubled, and a longitudinal wave AB travels back into the string. At B this wave meets the transverse wave, and is partially transmitted (BD) and partially reflected with change of sign (BC). The transverse wave is also split into two waves (BE and BF). The tension between the waves BC and BD, and the slope between BE and BF follow from (17). In subsequent motion, the longitudinal waves are reflected backwards and forwards by the

fixed boundaries and there are also interactions whenever two waves meet, so that the picture becomes more and more complicated. At some stage, however, a serious difficulty arises. For example, as the wave BF approaches the fixed end, a longitudinal wave is reflected alternately from the transverse wave and the end; since at each intersection it modifies the transverse wave the actual instant at which the transverse wave reaches the wall can be obtained only by some sort of limiting procedure. The same trouble arises as two transverse waves approach each other. In view of this difficulty it is better, for any actual problem, to use the numerical method developed below.

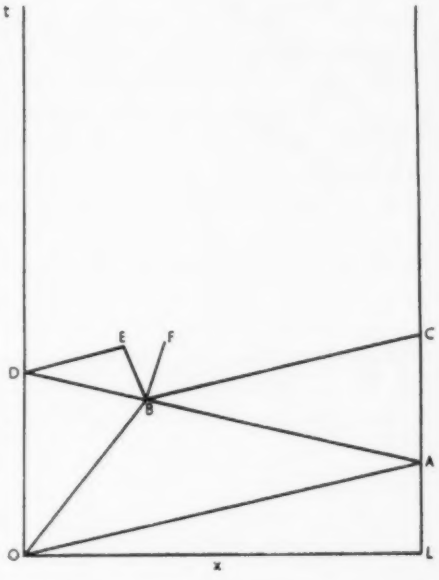

Fig. 3.

6. Plastic-elastic Materials

For plastic-elastic wires with strain-hardening, longitudinal shock waves can occur only in elastic regions, and in many problems will not appear at all. Transverse shocks, however, may still exist. The general characteristics method is still available, but a further difficulty arises. In a metal, as Lee has pointed out, the characteristic velocities for longitudinal waves differ according to whether or not the waves cause loading above a previously reached elastic limit. This causes considerable complications, and necessitates a very high order of accuracy in numerical work.

These difficulties make it advisable to look for an entirely different method when numerical results are required for particular problem. The simplest technique is that due to Richardson (1910) where the equations of motion are replaced by difference equations, which may then be solved successively to give numerical values for the stresses, slopes and velocities.

Suppose the (x, t) plane to be covered by a rectangular mesh of lines,

$$x = x_i = i\Delta x, \qquad t = t_j = j\Delta t,$$

where i, j are integers and Δx, Δt are suitably chosen small intervals. Write u_{ij} for $u(x_i, t_j)$ and v_{ij} for $v(x_i, t_j)$. Then the length ratio r and the slope ψ at a point $x = x_{i+\frac{1}{2}} = (i + \frac{1}{2})\,\Delta x$ at time t_j are given, to a first approximation, by

$$(r \cos \psi)_{i+\frac{1}{2},j} = 1 + (u_{i+1,j} - u_{i,j})/\Delta x \tag{19}$$

and

$$(r \sin \psi)_{i+\frac{1}{2},j} = (v_{i+1,j} - v_{i,j})/\Delta x. \tag{20}$$

The equations of motion may be replaced to the same degree of accuracy by

$$\frac{(u_{i,j+1} - 2u_{i,j} + u_{i,j-1})}{(\Delta t)^2} = \frac{(T \cos \psi)_{i+\frac{1}{2},j} - (T \cos \psi)_{i-\frac{1}{2},j}}{\Delta x} \tag{21}$$

and

$$\frac{v_{i,j+1} - 2v_{i,j} + v_{i,j-1}}{(\Delta t)^2} = \frac{(T \sin \psi)_{i+\frac{1}{2},j} - (T \sin \psi)_{i-\frac{1}{2},j}}{\Delta x} \tag{22}$$

where $T_{i+\frac{1}{2},j} = f(r_{i+\frac{1}{2},j})$.

Now suppose that the values of u, v are known for all i at the values of t given by j, $j-1$, then the values at t_{j+1} follow from equations (19) to (22). The values for all t can therefore be calculated successively, provided that suitable boundary and initial conditions are given.

The validity of this method has been established by COURANT, FRIEDRICHS and LEWY (1928) and his associates (see also O'BRIEN, HYMAN and KAPLAN 1951) provided that $\Delta t/\Delta x$ is less than the reciprocal of the greatest characteristic velocity in the problem, in this case c_0.

This method has one great advantage, that it puts the numerical work into a very simple and systematic form, which can be used by an unskilled computor, or put on to a machine. It has a disadvantage, that it assumes continuity of the stress and velocity, and smoothes out any discontinuity which may be present in the initial or boundary conditions. Two examples will be given showing the limitation and the power of the method by applying it to pure longitudinal motion.

Example (*i*)

Consider first a plastic-elastic material with modulus of elasticity E, yield stress $0{\cdot}0250\,E$, and linear strain-hardening with gradient $0{\cdot}04\,E$. Plastic shock waves are possible with velocity $c_0/5$. Consider a string ($-\infty < x \leqslant 0$) initially unstretched, and let an elastic wave, changing the tension from zero to the yield tension, move along the string from left to right, and be reflected at the end $x = 0$. Then the accurate solution gives a plastic wave from right to left, with velocity $c_0/5$, the tension behind the wave being $0{\cdot}0300\,E$. The approximate solution, with $\Delta t = \Delta x/c_0$ gives the following stresses at times t after the reflection,

TABLE 1. *Values of* $10^4 T/E$.

$c_0 t/x$	0·05	0·15	0·25	0·35	0·45	0·55	0·65	0·75	0·85	0·95	1·00
1·0	304	287	258	251	250	250	250	250	250	250	250
2·0	298	290	301	281	259	252	252	250	250	250	250
3·0	302	302	294	294	299	278	260	252	250	250	250
4·0	296	297	302	301	301	294	296	276	260	252	250
5·0	301	297	299	296	298	301	301	299	294	276	260
Max.	306	302	302	302	301	301	301	301	–	–	–
Min.	291	294	294	292	293	294	292	–	–	–	–

at coordinates x. It will be seen that the shape of the wavefront is fairly constant. At any point of the string after the wave-front has passed, the stress oscillates. The figures appearing in the last two lines of the table are the maximum stress occurring over the interval and the minimum stress occurring after the first

maximum. The asymmetry of these values about 300 is due to the different velocities of elastic and plastic waves. Note that the stress is only seriously overestimated in the first column, the interval in which the discontinuity first appears. Over the rest of the string the errors in the maximum stress are much smaller.

Example (ii)

As an example of the power of the method an example due to LEE has been re-computed. Consider the compressive stresses in a cylinder of finite length L when it is constrained to move by a varying pressure over one end, in such a manner that the velocity of that end is uniform. Then, according to LEE's solution, there is an elastic wave, followed by a plastic wave, emanating from the constrained end. The elastic wave is reflected from the free end as a tension wave, and immediately behind the reflected wave the stress is below the yield value. There is, however, a secondary plastic region which starts at a point in the interior of the cylinder and causes renewed plastic flow for a short time.

For the numerical method the length was split up into ten intervals, and the time interval was chosen to make $\Delta t/\Delta x = 1/2c_0$. The secondary flow region appeared in the intervals between $x = 0{\cdot}2\,L$ and $0{\cdot}5\,L$, in agreement with LEE's results. The values for the residual plastic strain (expressed as a percentage) are compared in the following table with the values read off from the curve in LEE's paper. The first line gives $10\,x/L$, the second line the computed strain and the last line LEE's value.

Vol. 2 53/54

TABLE 2.

0·5	1·5	2·5	3·5	4·5	5·5	6·5	7·5	8·5	9·5
0·741	0·708	0·352	0·106	0·039	0·015	0·006	0·003	0·000	0·000
0·700	0·700	0·400	0·100	0·056	0·013	0·006	0·003	0·000	0·000

In comparing these values two points should be borne in mind. First, because the computation was started from the moment of first motion, there is a discontinuity in the boundary condition at $x = 0$, $t = 0$. Thus, as in the last example, the values in the first space interval may be expected to be somewhat in error. However, if the computation had been done for shorter space intervals, the error would still have occurred only in the first one, and a little experience enables one to estimate its magnitude fairly accurately. Secondly, it should be remembered that the computed values are averages (e.g. the value printed for $10\,x/L = 0{\cdot}5$ is really the mean over the interval $0 < 10\,x/L < 1{\cdot}0$) so disagreement with LEE's more accurate figures may be expected to be greatest where the curvature of the residual strain graph is largest.

In spite of these effects, the computed values would probably be sufficiently accurate for most practical purposes. It should perhaps be emphasized that the work involved took only about ten hours, with no mechanical aid but a slide rule.

7. TRANSVERSE WAVES

In applying the numerical method to problems involving transverse waves a slight difficulty was encountered. It was found that to ignore the discontinuity in slope at a transverse shock wave introduced gross errors in the computed values of the tension. The method of treating this difficulty is to calculate, in each line of the work, the position of the transverse shock (in most practical problems with plastic-elastic wires there will be only one such). Suppose at a given stage the shock has reached a point $(i_0 + \theta)\,\Delta x$, $0 \leqslant \theta < 1$. Then the values of the tension and slope in all the space intervals except i_0 *to* i_1 may be calculated from (19), (20), and the load-extension curve. For the interval containing the shock wave, two values of r and ψ, are obtainable, r_0, ψ_0 to the left and r_1, ψ_1 to the right of the shock, where, from the momentum conditions,

$$r_1 \cos\psi_1 = 1 + u_{i_0+1,j} - u_{i_0,j} + (\theta\Delta x/\lambda)\,(u_{i_0,j} - u_{i_0,j-1} - u_{i_0+1,j} + u_{i_0+1,j-1})$$

$$r_0 \cos\psi_0 = 1 + u_{i_0+1,j} - u_{i_0,j} - (1-\theta)\,(\Delta x/\lambda)\,(u_{i_0,j} - u_{i_0,j-1} - u_{i_0+1,j} + u_{i_0+1,j-1})$$

$$r_1 \sin\psi_1 = v_{i_0+1,j} - v_{i_0,j} + (\theta\Delta x/\lambda)\,(v_{i_0,j} - v_{i_0,j-1} - v_{i_0+1,j} + v_{i_0+1,j-1})$$

$$r_0 \sin\psi_0 = v_{i_0+1,j} - v_{i_0,j} - (1-\theta)\,(\Delta x/\lambda)\,(v_{i_0,j} - v_{i_0,j-1} - v_{i_0+1,j} + v_{i_0+1,j-1}).$$

When the wave velocity λ is assumed these equations enable the values of r, ψ, to be calculated. In fact, it was found advisable, in view of the known continuity of T through the shock wave, to use a mean tension deduced from

$$r = r_0\,\theta + r_1\,(1-\theta)$$

for the whole interval, using ψ_0 and ψ_1 for the slopes. The value of θ for a line was found by successive approximation. First it was assumed that the wave speed for the previous time interval was that appropriate to the last complete line of the work, then a second approximation was taken using the mean of the stresses at the beginning and end of the time interval.

The method was tested by applying it to the head-on intersection of a transverse wave and a longitudinal wave in an elastic wire. In the notation of equation (17) the values assumed were

$$T_0 = 0{\cdot}025\,E, \qquad T_2 = 0{\cdot}030\,E, \qquad \tan\psi_2 = 0{\cdot}6360, \qquad \tan\psi_0 = 0.$$

The computed values of T_1, ψ_1, just behind the shock, at successive time intervals with $\Delta t/\Delta x = 1/c_0$ were

$10^4\,T/E$	250	275	299	283	296	284	284	286	295	284
$10^3 \tan\psi_1$	636	600	569	578	583	586	588	587	594	588

which should be compared with the correct values, deduced from (17) of $T_1 = 0{\cdot}0290$ and $\tan\psi_1 = 0{\cdot}586$.

It will be seen that, after the passing of the longitudinal wave front, there is a periodic error in the tension, which shows no sign of decreasing. This is to be expected since with the present choice of $\Delta t/\Delta x$, the method is just stable. On the other hand the mean tension and the slope are in good agreement with the accurate values, and the method can be applied with confidence to any given problem.

ACKNOWLEDGMENTS

The author is indebted to Prof. E. H. LEE for a copy of the load-extension curve used in his paper, and to Mr. J. L. KING for an advance copy of his London University Ph.D. thesis. in which he obtained independently equations equivalent to those of the first part of this paper.

REFERENCES

COLE, J. D., DOUGHERTY, C. B. and HUTH, J. H.	1953	*J. Appl. Mech.*, **20**, 519.
COURANT, R., FRIEDRICHS, K. and LEWY, H.	1928	*Math. Annalen*, **100**, 32.
LEE, E. H.	1953	*Quart. J. Appl. Math.*, **10**, 335.
O'BRIEN, G., HYMAN, M. A. and KAPLAN, S.	1951	*J. Math. and Phys.*, **29**, 223.
RICHARDSON, L. F.	1910	*Phil. Trans. Roy. Soc.* A **210**, 307.
TAYLOR, G. I.	1942	Unpublished.
WHITE, M. P. and GRIFFIS, L.	1948	*J. Appl. Mech.*, **15**, 251.

Vol.
2
53/54

Journal of the Mechanics and Physics of Solids, 1954, Vol. 2, p. 296. Pergamon Press Ltd., London.

HODOGRAPHS IN PROBLEMS OF PLANE PLASTIC STRESS

By A. P. GREEN
The British Iron and Steel Research Association, Metal Working Laboratory, Sheffield.

(*Received 29th April*, 1954)

THE writer has recently shown that, for an ideal plastic-rigid body undergoing plane plastic deformation, there is a certain geometrical similarity between the slip-line field in the physical plane and the corresponding network of lines in the hodograph of the velocity distribution (GREEN 1951, 1954). The aim of this brief note is to show that this result can be extended to problems of plane plastic stress.

The simplest proof of the property in plane strain (PRAGER 1953) derives directly from the fact that the rate of extension is zero in a slip-line direction. It follows that a line element between two adjacent points P_1, P_2, on a slip-line is perpendicular to the vector representing the increment of velocity between the two points, which is in turn parallel to the corresponding line element $P_1'\ P_2'$ in the hodograph plane. That is, $P_1\ P_2$ is perpendicular to $P_1'\ P_2'$.

In plane stress the velocity characteristics are also directions of zero rate of extension. Hence, the same argument applies and any line element of a velocity characteristic is perpendicular to its corresponding line element in the hodograph plane. The two families of velocity characteristics in plane stress are not in general orthogonal, as they are in plane strain, and therefore neither is the corresponding hodograph an orthogonal network.

REFERENCES

GREEN, A. P.	1951	*Phil. Mag.*, **42**, 900.
	1954	*J. Mech. Phys. Solids*, **2**, 73.
PRAGER, W.	1953	*Trans. Royal Inst. Tech. Stockholm*, No. 65.

END OF VOL.

Vol.
2
53/54